AD-A070 009 AIR WEATHER SERVICE SCOTT AFB IL F/G 4/2
PROCEEDINGS OF THE TECHNICAL EXCHANGE CONFERENCE 8TH AIR FORCE --ETC(U)
MAY 79

UNCLASSIFIED AWS/TR-79/001 NL

1 OF 3

AD A070009

AWS/TR-79/001

LEVEL II

PROCEEDINGS OF THE 8th TECHNICAL EXCHANGE CONFERENCE, AIR FORCE ACADEMY, COLORADO 28 November – 1 December 1978

MAY 1979

AIR WEATHER SERVICE (MAC)
Scott AFB, Illinois 62225

REVIEW AND APPROVAL STATEMENT

This publication is approved for public release. There is no objection to unlimited distribution of this publication to the public at large, or by DDC to the National Technical Information Service (NTIS).

This report has been review and is approved for publication.

Gary D. Atkinson

GARY D. ATKINSON, Colonel, USAF
Reviewing Officer

FOR THE COMMANDER

Robert M. Gottuso

ROBERT M. GOTTUSO, Colonel, USAF
DCS/Aerospace Sciences

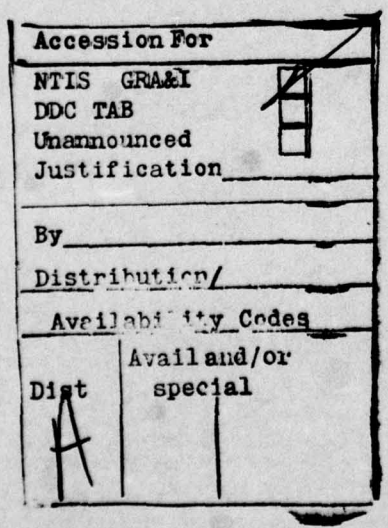

REPORT DOCUMENTATION PAGE	READ INSTRUCTIONS BEFORE COMPLETING FORM
1. REPORT NUMBER: AWS/TR-79/001 (84)	2. GOVT ACCESSION NO. / 3. RECIPIENT'S CATALOG NUMBER
4. TITLE (and Subtitle): PROCEEDINGS OF THE 8th TECHNICAL EXCHANGE CONFERENCE, AIR FORCE ACADEMY, Colorado, 28 November - 1 December 1978	5. TYPE OF REPORT & PERIOD COVERED: Conference Proceedings
	6. PERFORMING ORG. REPORT NUMBER
7. AUTHOR(s)	8. CONTRACT OR GRANT NUMBER(s)
9. PERFORMING ORGANIZATION NAME AND ADDRESS: Air Weather Service, Scott Air Force Base, Illinois 62225	10. PROGRAM ELEMENT, PROJECT, TASK AREA & WORK UNIT NUMBERS: 12 271p.
11. CONTROLLING OFFICE NAME AND ADDRESS: Air Weather Service, Scott Air Force Base, Illinois 62225	12. REPORT DATE: 11 May 1979
	13. NUMBER OF PAGES: 271
14. MONITORING AGENCY NAME & ADDRESS(if different from Controlling Office)	15. SECURITY CLASS. (of this report): Unclassified
	15a. DECLASSIFICATION/DOWNGRADING SCHEDULE

16. DISTRIBUTION STATEMENT (of this Report)

Approved for public release; distribution unlimited

17. DISTRIBUTION STATEMENT (of the abstract entered in Block 20, if different from Report)

18. SUPPLEMENTARY NOTES

19. KEY WORDS (Continue on reverse side if necessary and identify by block number)

Meteorology
Automated Observing and Forecasting
Atmospheric Propagation
Climatological Modeling
Tailored Environmental Support

20. ABSTRACT (Continue on reverse side if necessary and identify by block number)

Full length or abbreviated reports of 48 presentations at the Eighth Technical Exchange Conference, held at the USAF Academy, Colorado, 28 November through 1 December 1978 are presented. Session topics were Automated Observing and Forecasting, Atmospheric Propagation, Climatological Modeling, Tailored Environmental Support and Scientific Surveys.

014 670 JOB

DD FORM 1 JAN 73 1473

FOREWARD

The Air Weather Service is pleased to distribute this report of the proceedings of the Eighth Technical Exchange Conference, held at the U.S. Air Force Academy, Colorado, during 28 November through 1 December 1978. This publication provides a record for conferees and makes the presentations available to a much wider audience than the approximately 150 people able to attend.

The purpose of the conference is to bring together operational specialists and scientists from the research community which have project results that may be applied to operational support.

The conference was opened by Colonel Salvatore Lemole, Vice Commander Air Weather Service. The conferees were welcomed to the Academy by Brigadier General William A. Orth, Dean of Faculty. Dr. Kenneth Hare provided an interesting, stimulating, and entertaining banquet address. The conference was closed by Colonel Albert J. Kaehn, Jr., Commander Air Weather Service. These four presentations are included in the proceedings.

All presentations at the conference were invited. The conference was partitioned into sessions. Session topics were Automated Observing and Forecasting, Atmospheric Propagation, Climatological Modeling, Tailored Environmental Support and Scientific Surveys. In the survey papers, selected experts apprised conferees of the status of particular areas of specialization in the atmospheric sciences.

Conferences such as this require a lot of backstage support and it is appropriate that the hard work of the Steering Committee with members from Air Weather Service, Naval Oceanographic Command, National Weather Service, Air Force Geophysics Laboratory, and the Army's Atmospheric Sciences Laboratory be publicly acknowledged. Deepest appreciation is also acknowledged to the Directorate of Conferences at the Academy. They did a superb job of making all the tedious physical arrangements for the conference. Gratitude is also expressed to all speakers, session chairmen, and participants who contributed to making this a beneficial and enjoyable conference.

TABLE OF CONTENTS

(In Order of Agenda for the Conference)

* Paper Not Available (Abstract)

* Paper Not Available (Abstract)

* Paper Not Available (Abstract)

ATTENDEES OF 1978 TECHNICAL EXCHANGE CONFERENCE

Mr. H. Appleman
Maj C. P. Arnold, USAF/AWS/AFGWC
Col G. D. Atkinson, USAF/AWS
Capt R. R. Babcock, Jr., USAF/AWS
Mr. W. Baginsky, USAF/AFGL
Mr. B. Bailin, NOAA/EM
Capt W. H. Balsterholt, USAF/AWS/7WW
Dr. M. L. Barad, USAF/AFGL
Mr. J. M. Beck, USA/DAMI
Mr. W. J. Becker, TRACOR, Inc.
Dr. D. W. Beran, NOAA/ERL/WPL
Mr. R. J. Bergemann, USA/Night Vision Laboratory
Maj R. Borkowski, USAF/AWS/AFGWC
Dr. J. T. Bradley, NOAA/NWS/OTS
Mr. S. Brand, USN/NEPRF
Dr. P. J. Breitling, AWS/USAFETAC
Mr. B. Britain, USA/ASL
Dr. F. V. Brock, NCAR
Mr. C. Brown, NASA, Marshall Space Flight Center
Mr. C. Callahan, Ocean Data Systems
Dr. S. A. Changnon, Jr., Illinois Water Survey
Lt K. Chipps, USAF/AWS/AFGWC
Mr. D. A. Chisholm, USAF/AFGL
Maj R. Christensen, USAF/AWS/AFGWC
Dr. D. S. Cooley, NOAA/NWS
Dr. J. A. Cooney, Drexel University
SSgt D. L. Coss, USAF/AWS/AFGWC
Col W. E. Cummins, USAF/AWS/5WW
Capt R. G. Cundy, USAF/AWS/AFGWC
Mr. J. A. Cunningham, NOAA/NWS/EDL
Mr. T. Czuba, USN/Naval Air Systems Command
Dr. P. C. Dalrymple, Nat'l Defense University
Mr. M. T. Decker, NOAA/ERL/WPL
Dr. F. dePercin, USA/DAEN
Dr. D. R. Dickson, University of Utah
Capt B. Diesen, USAF/AWS/2WS
Maj J. Dmytriw, USAF/AWS/12WS
Dr. A. V. Dodd, USA/Army Research Office
Mr. W. F. Donnell, TRACOR, Inc.
Mr. D. W. Downen, NOAA/NWS/EDL
Dr. L. Duncan, USA/ASL
Dr. R. L. Elsberry, USN/NPGS
Dr. O. M. Essenwanger, USA/MIRADCOM
Mr. W. A. Finley, USAF/AWS/2WS
Mr. H. P. Foltz, NOAA/NWS/Southern Region
Maj K. P. Freeman, USAF/AWS/AFGWC
Capt L. E. Freeman, USAF/AWS/12WS
Lt R. B. French, USAF/AWS/AFGWC
Capt H. E. Fresh, USAF/AWS/15WS
Dr. D. L. Gilman, NOAA/NWS/NMC
Maj F. T. Globokar, USAF/AWS/AFGWC
Mr. K. M. Glover, USAF/AFGL
Lt Col D. R. Gornell, USAF/AWS/3WW
Dr. A. K. Goroch, USN/NERPF
Col R. M. Gottuso, USAF/AWS
Mr. D. D. Grantham, USAF/AFGL
Maj V. Grocki, USAF/AWS/AFGWC
Capt C. D. Hall, USAF/AWS/AFGWC
Col J. W. Hall, USAF/AWS/2WS
Prof F. K. Hare, University of Toronto
Mr. W. Herring
Cdr W. F. Hillyard, USN/NOC
Mr. G. B. Hoidale, USA/ASL
Capt J. E. Hoke, USAF/AWS/AFGWC
Lt Col D. T. Holland, USAF/AWS/5WW
Dr. H. Holt, USA/ASL
Mr. R. S. Hughes, Northrop Corp.
Capt R. E. Hughes, USN/FNWC
Mr. R. E. Huschke, RAND Corp.
Capt G. Jensen, USAF/AWS/AFGWC
Dr. D. R. Johnson, University of Wisconsin
Lt Col W. F. Johnson, USAF/AWS
Capt W. R. Johnson, II, USAF/AWS/AFGWC
Maj G. S. Jones, USAF/AWS/5WS
BGen P. W. Kadlec, USAFR/AWS
Col A. J. Kaehn, USAF/AWS
Capt M. J. Kelly, Jr., USAF/AWS
Dr. W. H. Klein, NOAA/NWS/SDO
Mr. D. H. Lee, USN/NEPRF
Col S. R. LeMole, USAF/AWS
Dr. C. G. Little, NOAA/ERL/WPL
Mr. G. Lorenzen, GAO
Capt B. MacKay, USAF/AWS/12WS
Lt Col O. Y. Macy, USAF/AWS/5WW
Col T. D. Madigan, USAF/AWS/AFGWC
Dr. D. E. Martin, St. Louis University
Mr. W. F. Martin, USN/ONR
Dr. R. A. McClatchey, USAF/AFGL
Mr. R. G. McGrew, NOAA/NWS
Maj W. J. McKechney, USAF/AFOSR
Lt Col W. Meyer, USAF/AWS/SAMSO
Mr. D. A. R. Mettam, Canadian Forces Weather Service
Mr. B. Miers, USA/ASL
Maj J. D. Mill, AWS/USAFETAC
Dr. R. Miller, NOAA/NWS/TDL
Lt K. E. Mitchell, USAF/AWS/AFGWC
Mr. E. V. Mollichelli, Servo Corp of America
Mr. H. L. Moore, NOAA/NWS
Dr. H. S. Muench, USAF/AFGL
Dr. A. H. Murphy, NCAR
Mr. R. E. Nagle, USN/NEPRF
Maj P. Neu, AWS/USAFETAC
Capt M. A. Neyland, USAF/AWS/9WS
Capt H. E. Nicholson, USN/CNO(OP-952)
Dr. V. E. Noble, USN/NRL
Mr. J. R. Norton, Systems Applied Science, Inc.
Col J. Nou, USAF/AWS/5WW
Mr. R. O. Olsen, USA/ASL
Mr. S. A. Olson, Sandia Labs
BGen W. A. Orth, USAF/Air Force Academy
Mr. F. P. Ostby, NOAA/NWS/NSSFC
Capt J. W. Overall, USAF/AWS
Mr. G. A. Petersen, NOAA/NWS
Capt P. Petit, USN/NEPRF
Col R. M. Pfeiffer, USAF/JCS/DDO(ES)
Dr. R. G. Pinnick, USAF/ASL
Lcdr T. M. Piwowar, USN/FWC Norfolk
Mr. T. H. Pries, USA/ASL
Dr. R. R. Rapp, RAND Corp.
Lt L. C. Rawlinson, USN/FNWC
Dr. J. H. Richter, USN/NOSC
Dr. T. E. Rosmond, USN/NEPRF
Mr. D. Rottner, Bureau of Reclamation
Mr. M. J. Sanders, Jr., NOAA/NWS/EDL
Lt D. E. Sauve, USAF/AWS/AFGWC
Maj R. C. Savage, USAF/AWS/AFGWC
Cdr D. J. Schaff, USN/FNWC
CWO R. J. Scheirer, USA/ASL
Cdr W. G. Schramm, USN/NEPRF
Mr. V. Schutz, Electronic Techniques, Inc.
Lcdr O. R. Scrivener, USN/FWF Suitland
Mr. O. Singer
Mr. C. J. Stead, Nat'l Defense Headquarters
Dr. D. Stevens, Colorado State University
Dr. P. F. Twitchell, USN/ONR

Cdr K. L. Van Sickle, USN/CNO(OP-952)
Mr. W. J. Vechione, USA/ASL
Dr. A. Weinstein, USN/NEPRF
Dr. J. M. Wilcox, Stanford University
Capt M. R. Witiw, USAF/AFGWC
Lcdr F. Wooldridge, USN/Naval Space Systems Activity
Lt Col W. B. Wright, USAF/AWS
Mr. Y. P. Yee, USA/ASL
Maj J. Zak, USAF/AWS
Dr. E. J. Zipser, NCAR

OPENING REMARKS

Colonel Salvatore R. LeMole

Vice Commander Air Weather Service

On behalf of Colonel Kaehn, Commander of Air Weather Service, I welcome you to the 8th Technical Exchange Conference. As I understand it, this is the second in the revised series, and I am rather impressed with the immense turnout. I'm not sure whether we have this large a group of dedicated meteorologists or whether our setting here in the Colorado Springs area is the main attraction. I prefer to think the former.

The Technical Exchange Conferences are very important, and your presence here supports that. As you all know, we operational meteorologists look to the scientific community to provide answers to the demands our customers, civilian or military, are placing upon our services. The military continues to depend upon exploitation of technology to do the job we have to do. In the civil sector, we have industry and private business all clamboring for more support. So we have a great need for the operational community to come together with the applied meteorologists and the research community to get on with the job of exploiting technology.

The Colorado area is particularly apropos for this meeting. We have, I think, a very dynamic, scientific community in the Boulder-Denver area. Don Beran is here. I spent a week with Don at a workshop last March, on something called PROFS, Prototype Regional Observing and Forecasting Service. That type exchange, and the prime purpose of this conference, is to get the scientific community and the operational customer together to exploit technology. Not only does it do that but it gets together the scientific community in a cooperative endeavor, and I think this is very important in today's kind of limited budgets and increasingly demanding support requirements. I would also like to mention, another program, which is indication of our joint cooperative endeavors, the Joint Doppler Operational Program (JDOP) which you'll hear about later this morning. These two programs (PROFS and JDOP) typify the spirit within the Federal scientific community to get together to exploit the state-of-the-art, to exploit technology, and to move ahead in supporting our respective customers. So the conference is very important and again I think your presence here supports that.

I would like to recognize just a few representatives from the various agencies attending the conference. We have Dr. Bill Klein, from National Weather Service, Dr. Mort Barad from Air Force Geophysics Laboratory, and Capt Ron Hughes from Fleet Numerical Weather Central. Ron is representing Capt MacDonald of the Naval Oceanographic Command. Mr. Tom Pries is representing Atmospheric Sciences Lab. Col Rawlinson, Commander of ASL, unfortunately, became ill at the last moment and couldn't make the Conference. Brigadier General Paul Kadlec, the Reserve advisor to the Commander of Air Weather Service, also is here. I would like to take a minute to express Col Kaehn's regrets for not being able to attend the opening session. He's getting ready to give a presentation tomorrow to the Chief of Staff of the Air Force on why we need some new weather programs to get on with our operational support requirements. He hopes to be here on Thursday and stay through to the closing session. I'd also like to recognize Professor Don Martin from St. Louis University. Don was one of the originators of these conferences back in the mid-60's. So Don we owe this all to you as one of the founding fathers.

At this time I'd like to introduce our host who will give the welcoming address, Brigadier General William A. Orth, who is presently the Dean of the Faculty here at the Academy. I don't think we could have selected, if we had gone out deliberately to pick, a more qualified individual who represents the theme of the conference. General Orth is both an operator, with many key assignments on the tactical side of the house, as well as a scientist. He is a graduate of the Military Academy; was commissioned in the Air Force in 1954; received a Master of Mechanical Engineering Degree from Purdue University; and a Doctorate from Brown University in Applied Mathematics. He's back at the Academy for his third tour and as I said he typifies the theme of our conference, the operator and the applied scientist getting together to move forward. General Orth.

WELCOMING ADDRESS

Brigadier General William A. Orth

Dean of Faculty, United States Air Force Academy

On behalf of the Superintendent, Lieutenant General Tallman, I would like to welcome you to the Air Force Academy. We all trust that your visit here will be a pleasant one.

I was pleased to see this morning that the "ceaseless wind" had also arrived. It should make you feel at home. I was very impressed with that title for the book on Atmospheric Dynamics by Dr. Dutton from Penn State. I especially liked the poem that was inside.

I've had the opportunity at the Academy to open several conferences but I think there were very few that I feel as close to as this particular one. Before I assumed my present job I was in the Department of Physics. At that time we had the Atmospheric Science minor, which later changed to the Atmospheric Physics track in the major. Although, as Colonel LeMole said, my most recent academic background was in applied mathematics, my specialty area was in fluid dynamics, and it was actually triggered--although the results don't show it in any way--by a look at a very basic atmospheric model. So, while I was in the Department of Physics and even more recently in my PhD work, your particular field of endeavor has been of very great interest to me. Earlier, as an operator, it was obviously of very great interest. I was always pleased when the weather was as good or better than the forecast!

I know of very few areas in the scientific field which still seem to be as complex in some of their basic phenomena as yours. I believe in Fyneman's book he lists turbulence as one of the least understood areas remaining in physics, and that to my layman's impression seems to be very much tied to the studies about which you devote your time.

We, at the Academy, feel that it is very important to host such distinguished groups as this since many of our faculty and cadets are very involved and interested in the topics which are listed in your conference agenda. As you know, and as I already mentioned, the Academy has had programs in meteorology for many years. These started when General Moorman, who had been a previous Commander of Air Weather Service, was here as Superintendent, and they've continued since that time. The change to the Atmospheric Physics track occurred two years ago, and occurred in conjunction with a request for an analysis of that area by both Air Weather Service and about ten to twelve universities throughout the United States that had graduate programs in atmospheric physics.

Now obviously you're at a place where the graduates have as their operational environment the areas of your interest--the atmosphere and beyond. I will not belabor the point of the importance of Air Weather Service to the Air Force and everything that we do. I would like to mention that the Physics Department has been very fortunate in the support that it has received from Air Weather Service. We've had some very highly qualified officers from that command that have contributed greatly to the faculty during their teaching assignments. We hope that this exchange of mutual benefit to both of us will continue.

I'd encourage all of you, even though when I looked at your busy schedule I didn't see much time there, to look over our facilities, our laboratories, and to visit one of our classes. We would encourage you to talk to the faculty and the cadets that you come in contact with about weather and weather research. I know that those officers in the Department of Physics would welcome more cadets as majors in the atmospheric physics area. A strange phenomena here, or at least it seems strange to me, is that an institution with the mission of the Air Force Academy does not have more individuals who pursue this particular major. The number is relatively small. Before I arrived here, I would have guessed differently. I would have thought that in this particular environment, aeronautical engineering and atmospheric science or atmospheric physics would be very popular fields.

Please do not hesitate to call upon the conference staff here if there's anything at all that we can do for you.

We hope to handle any items of concern or problems for you so that your conference can be as pleasant and productive as possible. Again, it's been a pleasure to have this opportunity to welcome you to the Academy and I certainly give you my very best wishes for a successful and productive conference.

JOINT DOPPLER OPERATIONAL PROJECT

Kenneth M. Glover and Ralph J. Donaldson, Jr.

Air Force Geophysics Laboratory

Hanscom Air Force Base, Massachusetts 01731

and

Kenneth E. Wilk and Donald W. Burgess

National Severe Storms Laboratory

Norman, Oklahoma 73069

ABSTRACT

The Joint Doppler Operational Program (JDOP) is a cooperative effort by the National Weather Service, Air Weather Service, National Severe Storms Laboratory, Air Force Geophysics Laboratory, and the Federal Aviation Administration directed toward the evaluation of Doppler weather radar techniques and instrumentation for suitability in meeting operational weather service and aviation meteorology requirements. JDOP test results are expected to provide the basis for the definition of operational concepts and design specifications for a single Doppler radar replacement for the aging AN/FPS-77 and WSR-57 radars in the national weather radar network.

In this paper, an overview of two years of JDOP tests is presented together with a description of future efforts. It concentrates upon the tools and techniques of the JDOP meteorologist and upon the results of their use in the identification and forecasting of thunderstorm hazards. Both the rationale for and the implications of operational use of these tools and techniques are demonstrated with numerous examples. The paper concludes with a brief summary of the accomplishments of the first two years' effort and a look at objectives of the third and final year of testing.

1. INTRODUCTION

The National Weather Service (NWS), Air Weather Service (AWS), National Severe Storms Laboratory (NSSL), Air Force Geophysics Laboratory (AFGL) and the Federal Aviation Administration (FAA) have combined forces in a program directed toward the evaluation of Doppler weather radar technology for operational applications and the development of specifications for a system of advanced capability to meet the integrated requirements of the operational agencies through the year 2000 and beyond. This program is aimed toward a system flexible enough to meet the routine observational requirements of today's national network, while providing explicitly detailed measurements of the internal structure of severe thunderstorms; that is, the detection and geographical location of squall lines, tornadoes, damaging windstorms, large hail, and dangerous turbulence.

Present operational weather radars such as the WSR-57 and AN/FPS-77 measure only reflectivity, a parameter related to both the number and electrical size of the precipitation particles in the radar field of view. Maps of the reflectivity structure of thunderstorms have long been effective in providing a measure of the relative strength of the storm. In general, however, these radars cannot be used to identify those thunderstorm hazards which are associated primarily with particle motion. Tornado, gust front, and turbulence phenomena are therefore not detectable by conventional radar alone. An exception is the rare case when a large circulation effectively establishes a spiral pattern in the precipitation and thus gives rise to a hook echo.

Because of their ability to provide a measure of the motion of scatterers, Doppler radars have shown promise as an improved severe storm warning device. Doppler's potential was first demonstrated by the then U.S. Weather Bureau in 1958 when a 3-cm continuous wave Doppler radar was used to measure the wind speed in a funnel cloud (Smith and Holmes, 1961). But nearly another decade passed before pulse Doppler systems with real-time data processing equipments enabled the mapping of both the reflectivity and velocity structures of storms (Groginsky, 1965, 1972; Lhermitte, 1972; Novick and Glover, 1975; Sirmans and Bumgarner, 1975). The use of this newly-found Doppler velocity mapping capability in severe storm investigations by AFGL in Massachusetts and NSSL in Oklahoma resulted in the development of techniques for the real-time identification of velocity patterns known to be associated with

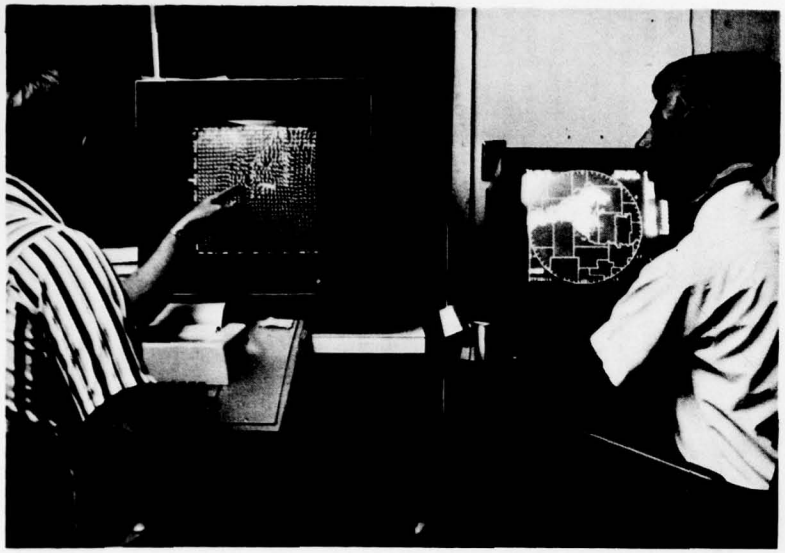

Fig. 1 The NWS Color Display (right) and the NSSL Multimoment Display (left). In the NWS display, contours of reflectivity, mean radial velocity, or velocity spectral width are presented in color on a refreshed non-fading computer terminal. Reflectivity or velocity color code appears along right side; date, time, and elevation angle show across top; and real-time commands appear along display bottom. The graphics display is a field of arrows where arrow length is proportional to intensity, arrow position to mean velocity and arrowhead size to velocity spectrum width. Arrows pointing right indicate zero radial velocity; arrows pointing up are 17 m s^{-1} (33 knots) away from the radar and bottom are 17 m s^{-1} toward the radar; arrows pointing left are at radar unambiguous velocity limit of ± 34 m s^{-1}.

Fig. 2 The AFGL Display System. Color contours of mean radial velocity are displayed on top left monitor, reflectivity at top right, and Doppler spectrum width at lower left. The color code for each parameter appears along the right side, and radar elevation angle, range marker magnitude, day of year and time (hours and minutes) appear at lower right of each screen. Scaling, centering, and contouring functions are under operator control. Screen at lower right shows results of computerized echo tracking, forecasting, and significance analysis routines.

large tornadoes and their parent mesocyclones (Donaldson, 1970; Burgess, 1976; Brown and Lemon, 1976). Statistics from five years of Doppler based severe thunderstorm observations in Oklahoma were analyzed by Burgess (1976), and it was found that 95% of all mesocyclones were associated with some type of surface damage and 62% had tornadoes. Moreover, at no time during data collection did a verified tornado occur that was not preceded by a mesocyclone signature, and the average lead time was 36 minutes.

The successful efforts by the research organizations in using pulse Doppler radar to map airflow within severe thunderstorms came at a time when the operational organizations were anticipating the replacement of the ailing WSR-57 and AN/FPS-77 network radars. Because of the close relationships among the staff of the participating organizations, the Joint Doppler Operational Project, or JDOP, developed informally within a relatively small budget. Stated simply, the project goal has been to effect the transfer of this technology from the laboratory to the operational arena.

2. TOOLS OF JDOP

The experimental Doppler facilities of NSSL served as the base of operation and were supplemented by display equipments of NWS and data processing and display equipments of AFGL. NSSL's radar is a 10-cm wavelength pulse Doppler system with a 9.2 meter diameter antenna and an advanced data processing capability. High resolution reflectivity and velocity estimates are available in real time out to ranges of 460 km (250 n mi).

JDOP forecasters viewed a variety of color and graphics displays designed to aid in the identification of severe storms. Figures 1 through 3 contain examples of the Doppler products available to the JDOP meteorologists. The NWS color display, which appears at right in Fig. 1, is analogous to present-day contoured plan-position indicators of reflectivity except that contours of mean radial velocity and velocity spectral width can also be selected. The NSSL black and white Multimoment Display shown at left is unique in that it provides multiple data types simultaneously with resolution matched to the radar output over a limited area (Burgess et al., 1976). Single-Doppler velocity shears, which are important in signature recognition, are emphasized by arrow orientations and arrowhead size. Both displays are interactive. They permit the meteorologist to view three-dimensional data selectively and then deduce the significance of the vertical distribution of reflectivity and velocity signatures.

The AFGL display system shown in Fig. 2 is a cluster of four independent displays. Mean radial velocity is continuously displayed on the top left screen; reflectivity is at top right; and Doppler spectrum width is at lower left. The display at lower right presents the results of computerized analyses of radar echo tracks and forecasts echo positions as an additional parameter. For each of the echo areas appearing on this tracking display, a listing of echo attributes is displayed on a computer alphanumeric terminal, as shown in Fig. 3.

DATE:120 TIME:1811 ELEVATION: 0.3 COLOR: 8 ZTHRES: 25

AREA	1	2	3	4	5	6	7	8	9	A	B
RANGE (KM)	58	128	104	224	216	226	146	226			
AZIMUTH (DEG)	332	323	323	307	283	294	327	298			
AREA (KM**2)	432	104	156	88	68	64	44	28			
MAX REFLCT (DBZ)	55	53	46	47	39	43	39	39			
MAX VEL (M/S)	24	22	19	27	15	12	10	10			
MAX VEL SD (M/S)	9	12	9	11	9	11	10	8			
MASS (DBZ* KM**2/10)	1600	668	500	304	244	268	160	124			
SPEED (M/S)	2	16	10	26	12	16	12	999			
DIRECTION (DEG)	315	170	100	233	243	198	206	999			

Fig. 3. AFGL Echo Track Attribute Listing

Echo numbers on this display correspond to those of the tracking display. Tabulated are the location of the centroid of the cell area exceeding 30 dBZ (range and azimuth), the motion of the centroid (speed and direction), the area of the cell, the reflectivity-weighted area of the cell, as well as the maximum reflectivity, maximum radial velocity and maximum Doppler spectrum width within the cell. The 999's appearing for echo 8 indicate that this target has not been observed long enough for the system to establish a track.

3. JDOP TECHNIQUES

Doppler radars measure only that component of motion along the radar beam; they are sensitive to the motion of precipitation particles moving toward and away from the radar but blind to motion perpendicular to the beam axis. In the absence of a mean wind field, a vortex viewed by pulse Doppler radar, appears as a couplet of closed contours of radial velocity toward and away from the radar, separated by the loci of points of 0 m sec^{-1} radial velocity. With suitable extension in height and continuity in time, this signature is unique to a vortex and is independent of viewing angle (Donaldson, 1970; Burgess, 1976).

The mesocyclone signature or couplet, usually coincident with updraft location, is observed to form in the mid-part of the storm and descend to cloud base concurrent with tornado formation. This behavior suggests the prospect of significant lead times in warnings.

A second signature, produced by the tornado itself, is the tornadic vortex signature, or TVS, a discrete region of strong shear much smaller than the mesocyclone and imbedded within it (Brown and Lemon, 1976). Experience with TVS's has demonstrated its utility for precise tornado location, usually within a kilometer

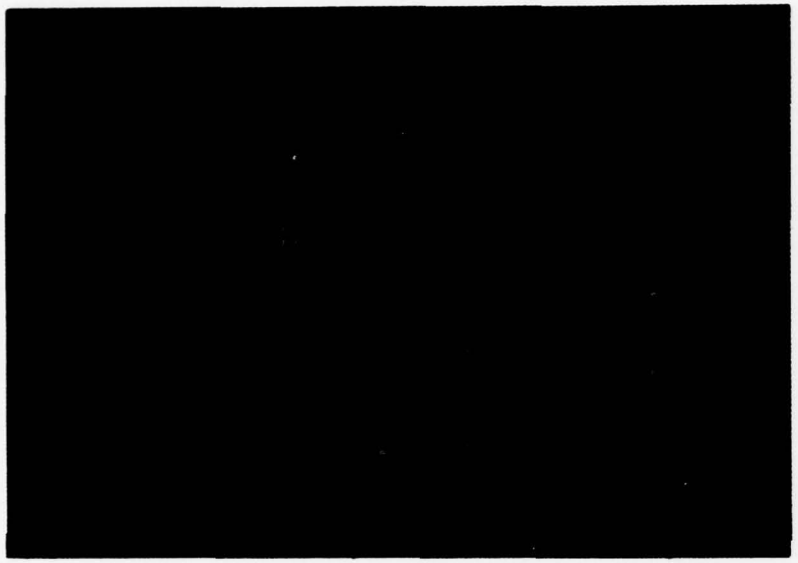

Fig. 4 Reflectivity Structure of Del City, Oklahoma Storm of 20 May 1977. The radar is sector scanning at 2° elevation toward the east. Range marks are 32 km apart. The strongest reflectivity of the storm is colored yellow.

Fig 5 Radial Velocity Structure of Del City, Oklahoma Storm of 20 May 1977. This is a classical mesocyclone couplet portrayed on a single Doppler radar. The northern velocity minimum, colored violet, indicates speeds toward the radar of 35 m sec^{-1}, while the southern velocity maximum, colored yellow and surrounded by gray and green, shows speeds of 20 m sec^{-1} away from the radar. The diameter of the mesocyclone, between peak velocities, is 3 km.

The utility of Doppler as well as conventional severe storm identification techniques is demonstrated in Fig's. 4 through 8. Fig's. 4 and 5 show the reflectivity and radial velocity structures, respectively, of a tornado in its formative embryonic stage. Eight minutes after these data were taken, a major tornado touched down in Del City, Oklahoma and inflicted damage along the eastern outskirts of Oklahoma City and into the town of Edmond. Its path length was 25 km; its maximum damage width was nearly 400 meters; and its duration was 27 minutes. A high reflectivity (yellow) hook-like protrusion is evident in the southern flank of the storm, and the tornado occurred in the relatively weak (20 to 30 dBZ) area partially enclosed by the hook. This reflectivity pattern corresponds to a height interval of 0.5 to 1 km and is typical of the reflectivity structure within the lowest 3 km of the storm.

The radial velocity structure of Fig. 5 provides the real tip-off that a tornado is imminent. This couplet of maximum (yellow) and minimum (violet) velocity, side by side and at the same range, is a classical mesocyclone signature as portrayed on a single Doppler radar. The mesocyclone at this time extended throughout a height interval of 0.8 to 3.8 km, but was most intense at the depicted height of 1.3 km. It is important to note that this mesocyclone was first recognized 36 minutes prior to the time of this photograph or 44 minutes before tornado touchdown!

A copy of the NSSL Multimoment Display taken a few seconds before the touchdown of a maxi-tornado in Piedmont, Oklahoma is shown in Figure 6.

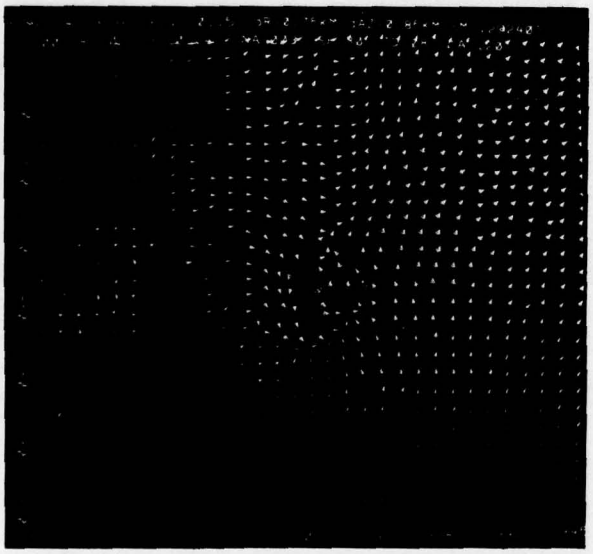

Fig. 6 Multimoment Display of 30 April 1978 Piedmont, Oklahoma Maxi-Tornado Mesocyclone and TVS Signatures. The radar is toward the bottom of the page with range (km) at left and azimuth angles below the display. Tornado and TVS signature are located near 331° azimuth and 49 km range with mesocyclone couplet visible in surrounding azimuths.

The elevation angle is 1.5°, and the radar beam is meeting the descending tornado at a height of about 1.5 kilometers. On the Multimoment Display, only the radial component of motion is displayed, and arrows should not be interpreted as streamlines of horizontal flow. A large vortex, such as a mesocyclone, is indicated by a "U" shaped pattern of arrows, and this is clearly evident. Within the "U", at 49 km range and 331° azimuth, there is a TVS indicated by two adjacent arrows pointing in opposite directions. Between these two arrows, the wind direction reverses. The Doppler is picking up motions on opposite sides of the tornado funnel.

The mesocyclone and TVS signatures of the Piedmont tornado are equally striking on the color display, as shown in Fig. 7. This photograph was taken at 1825 while the tornado was on the ground. Across the tornado funnel, the shear is so intense that the colors blend almost imperceptibly from maximum velocities toward the radar (purple) to maximum velocities away from the radar (red). The TVS is situated asymmetrically with respect to the mesocyclone; the TVS is much closer to the inbound side (blue) than it is to the outbound (red) side.

The corresponding reflectivity pattern, observed at the same time and elevation angle, is shown in Fig. 8. A comparison of Fig's 7 and 8 shows that the tornado is on the southwestern edge of the echo, but no hook is evident. There would be no way for a radar operator to suspect that a tornado was in progress, nor to locate it or to estimate its probable path.

4. OPERATIONAL TEST RESULTS

JDOP operational tests were conducted during the period April-June in both 1977 and 1978. Prior to the start of each test period, all project staff, as well as participants from other agencies, were given a thorough indoctrination on the interpretation of radar signatures, the operation and evaluation of all radar equipments, and the translation of the radar information into real time advisories to NWS and AWS facilities.

Forecasters from both NWS and AWS were assigned the responsibility for the issuance of advisories to their respective organizations; experienced radar meteorologists from NSSL and AFGL were on hand to act in an advisory role when needed. JDOP meteorologists identified, from Doppler, areas of storm rotation and possible tornado formation (mesocyclone and tornadic vortex signatures) and strong outflow winds below cloud base (gust front signatures). In addition, a measure of updraft strength and therefore hail potential was found in Doppler convergence and divergence signatures found near cloud bases and tops respectively. Through some objective and subjective interpretation, this information was transformed into severe thunderstorm and tornado advisories. National Weather Service Offices and Air Force Bases in Oklahoma, southern Kansas, northern

Fig. 7 Color Display Mesocyclone and TVS Signatures of Piedmont, Oklahoma Maxi-Tornado. The mean radial velocity scale is at right in m sec^{-1}; maximum outbound velocity is red, and maximum inbound velocity is purple. The elevation angle is 0.6° and range markers are spaced 32 km.

Fig. 8 Reflectivity Structure of Piedmont, Oklahoma Maxi-Tornado. The reflectivity scale, in dBz, is shown at right. This photograph taken at same time as that of Fig. 6. Note absence of any hook-like echo.

and panhandle Texas, and western Arkansas received the advisories by telephone.

Although some success was achieved in identifying mesocyclones at rather long ranges (to 350 km), verification of the advisories was attempted only for ranges within 230 km. Doppler based advisories were compared to public warnings issued by the Weather Service Forecast Office at Oklahoma City. Data comparisons were based upon NWS's standard method of issuance of warnings on a county by county basis. During 1978, a total of 116 advisories were issued: 106 to NWS offices and 10 to military bases. An objective analysis of the relative merits of these conventional and Doppler warnings was conducted on the basis of an evaluation of four measures of performance:

$$\text{Probability of Detection (POD)} = \frac{x}{x + z}$$

$$\text{False Alarm Ratio (FAR)} = \frac{y}{x + y}$$

$$\text{Critical Success Index (CSI)} = \frac{x}{x + y + z}$$

LT = Lead time between advisory issuance and event occurrence (in minutes).

where:

x = Forecast severe event which occurred

y = Forecast severe event which didn't occur

z = Forecast non-severe event which occurred severe

The Critical Success Index provides a measure of the overall effectiveness of a technique by giving credit for a high probability of detection and a low false alarm rate (Donaldson et al., 1975). A CSI of 1.0 indicates perfect performance and 0.0 indicates no skill. The statistical results from these tests are shown in Tables 1 and 2.

Table 1 shows the comparison of Doppler with the Oklahoma City WSFO for winds greater than 50 knots and hail equal to or greater than 3/4 inch. For these hazards, the use of Doppler

Table 1. 1978 JDOP Hail and Wind Statistics

Parameter	OKC WSFO	Doppler
POD	0.47	0.70
FAR	0.40	0.16
CSI	0.36	0.62
LT	13.6	15.4

does not significantly improve the lead time, but POD is increased and FAR is reduced. Accordingly, the CSI for the Doppler detection of these hazards is approximately twice that of conventional techniques.

A similar comparison for tornadoes observed during the two years of JDOP is shown in Table 2.

Table 2. 1977-1978 JDOP Tornado Statistics

Parameter	OKC WSFO	Doppler
POD	0.64	0.69
FAR	0.63	0.25
CSI	0.30	0.56
LT	2.2	21.4

In this case, the POD's are comparable because NWS's tornado warnings are often based upon public reports made after the tornado has started producing damage. This fact is reflected in the very low average lead time of the WSFO. Doppler based advisories did, however, show a considerably reduced FAR and a significantly improved warning time. The Doppler CSI for tornadoes, like that for hail and winds, is approximately twice that of conventional techniques.

5. IMPACT ON FORECASTING

The impact of Doppler technology on actual severe storm forecast operations can be seen

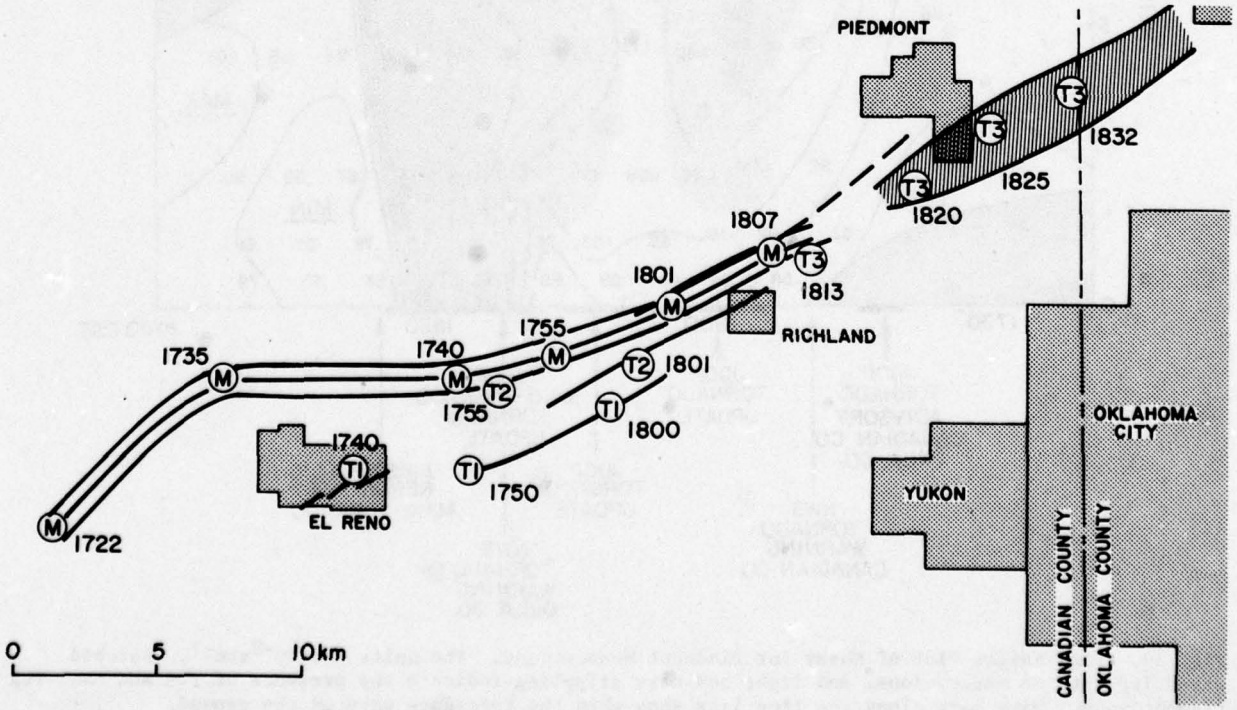

Fig. 9. Damage Path of Piedmont, Oklahoma Storm

with the aid of a few summaries of JDOP operations. A maxi-tornado which destroyed 25 homes in and near Piedmont, Oklahoma on April 30, 1978 provides an excellent example of the life-saving ability of severe storm warnings based upon Doppler radar. A multimoment view of this storm just prior to tornado touchdown has already been discussed in connection with Fig. 6, and the storm's velocity and reflectivity structure during tornado touchdown have been described in association with Fig's.7 and 8 respectively. Fig. 9 summarizes the damage path of this storm. The mesocyclone center (M) and the TVS' (T_1, T_2, and T_3) are based upon Doppler data used in real time. Doppler revealed a TVS (T_1) aloft south of the mesocyclone center, a second anticyclonic TVS (T_2) located between T_1 and the mesocyclone center where a third TVS was located. Near 1800, three tornadoes were on the ground simultaneously in conjunction with three TVS's. About 1810, cyclonic shears near the mesocyclone center intensified, and a fourth TVS (T_3) was identified. This circulation center lowered to the ground and became very strong. The Doppler signature fits closely the path of an intense tornado which was on the ground from 1820 to 1835. This tornado did F4 intensity damage along a path 2 km wide and nearly 10 km long. The initial JDOP advisory was issued at 1742 and was frequently updated. Residents in the threatened area were alerted more than a half hour before the big tornado touched down. As a result, they had plenty of time to take shelter, and there were no deaths or injuries to people.

A time-height history of the shears observed by JDOP before, during, and after the Piedmont tornado is shown in Fig. 10. The numbers indicate Doppler observed shear in units of 10^{-2}sec^{-1} (or a change in velocity in meters per second across a distance of 100 meters). At lower left and upper right (hatched areas), the shears were too small to indicate the presence of a mesocyclone. The stippled areas indicate the presence of a TVS. Note how fortunate we are that both the mesocyclone and the TVS are first

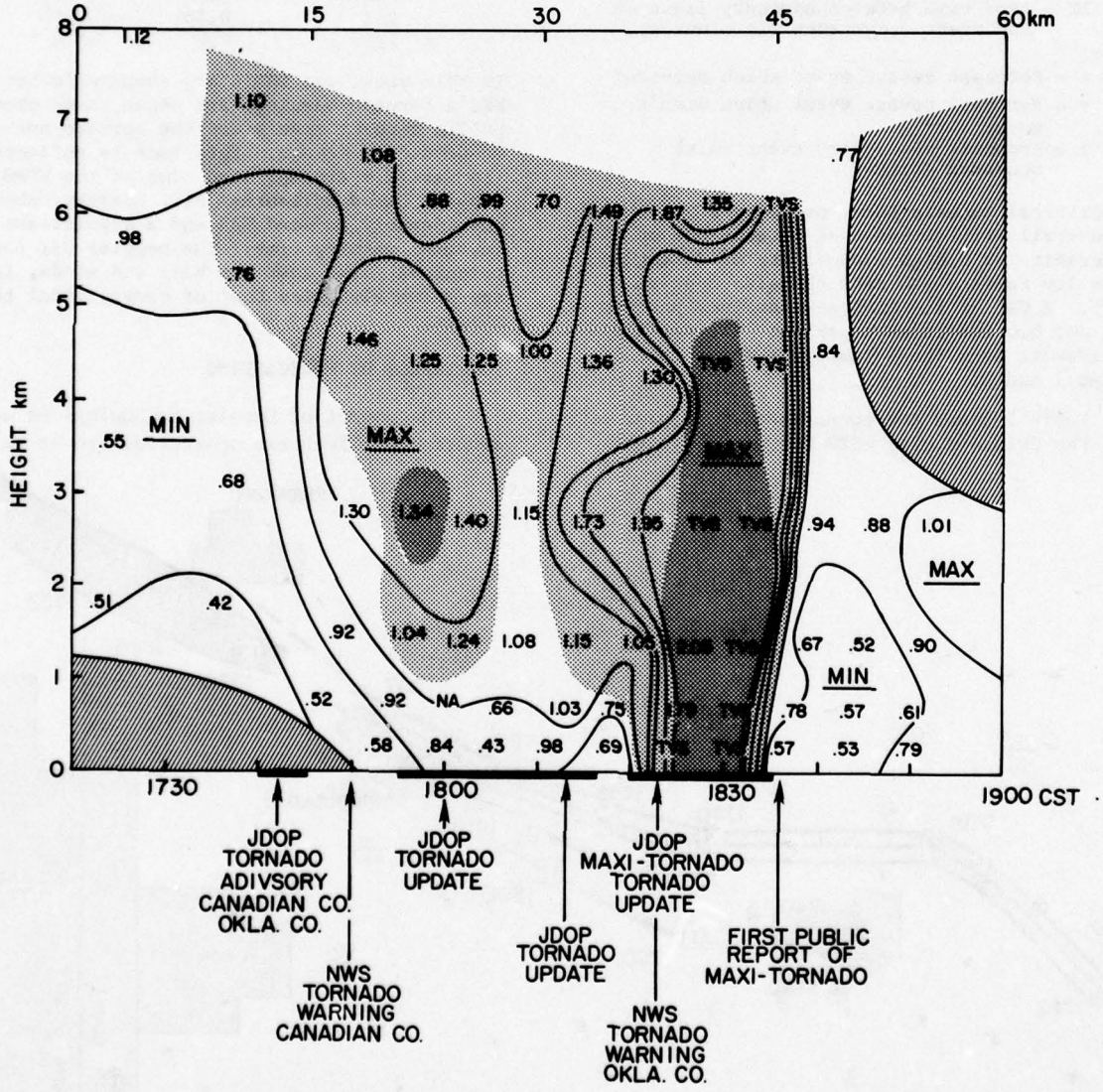

Fig. 10. Time-Height Plot of Shear for Piedmont Mesocyclone. The units are 10^{-2}sec^{-1}. Hatched areas indicate no mesocyclone, and light and dark stippling indicate the presence of TVS and maxi-TVS respectively. Dark bars along the time line show when the tornadoes were on the ground.

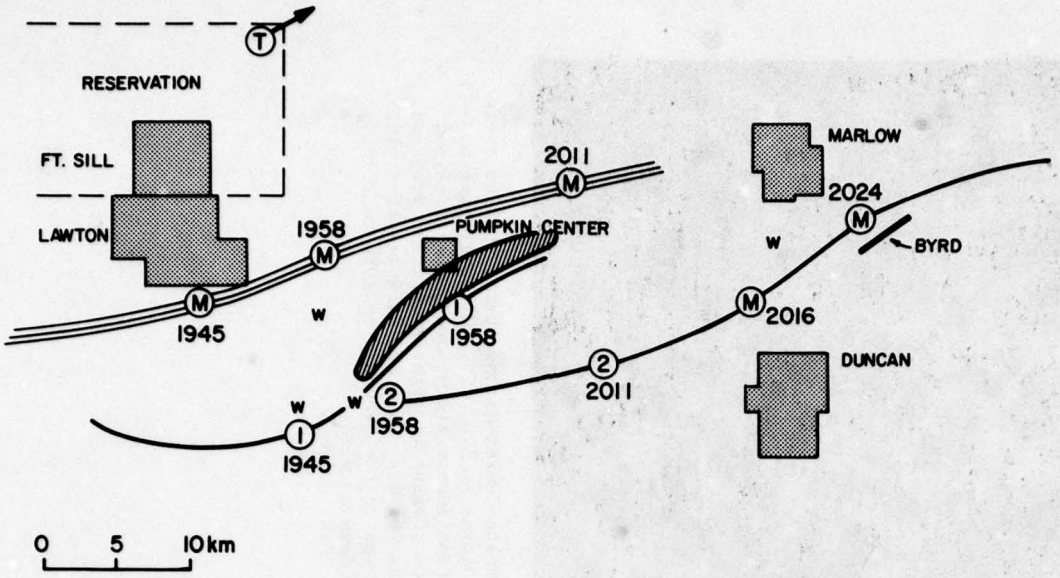

Fig. 11. Track of 5 April 1978 Pumpkin Center and Marlow Storms. Mesocyclones are denoted by (M) and two TVS's as (1) and (2). Times are CST. The Pumpkin Center tornado is hatched and the Marlow tornado is a thick line. The circled "T" indicates tornado position given in NWS warning, and W's are straight line wind damage.

detected aloft and take quite a bit of time to descend to the ground. This leisurely progression is typical of the large destructive tornadoes and provides the basis for adequate warnings with Doppler radar.

Benefits from automated storm tracking were demonstrated when a storm in southwest Oklahoma became right-moving as it started producing tornadoes. A summary track of this storm is shown in Fig. 11 and photographs of the AFGL echo tracking displays before and during this storm are shown in Fig's. 12 and 13. A tornado advisory based on a TVS south of Lawton, Oklahoma was issued at 1945 CST. The resulting NWS tornado warning was combined, erroneously, with an unverified public report of a tornado northeast of Ft. Sill. The language of the warning indicated a tornado (T) at the northeast edge of the military reservation, moving northeast. This was the same direction of movement as other cells previously detected. At NSSL, a check of the AFGL echo track display revealed an eastward storm motion. An update to OKC was therefore issued at 2000 redefining the warning based on the correct position of the mesocyclone and the correct direction of movement.

A photograph of the AFGL tracking display taken at 1938 CST, or 7 minutes before the initial tornado advisory to OKC, is shown in Fig. 12. The movement of the southernmost storm between 1906 and 1938 is clearly eastward, whereas, other cells in this line of storms are seen to move northeastward. A companion photograph, Fig. 13, shows the continuation of these storm tracks, beginning at 1952 and lasting for more than an hour after the initial tornado touchdown.

A wide tornado touched down at 1956, passed Pumpkin Center just after 2000 and dissipated near 2010. A total of 11 homes, 5 trailer houses and 21 barns were damaged or destroyed. Although the initial NWS warning (with county boundaries) covered the area of damage, residents complained of no specific warning because of the earlier reported tornado location and movement well to their north. Such confusion can be alleviated in the future through issuance of warnings to smaller areas as defined by Doppler radar capability.

A second tornado formed just southeast of Marlow, Oklahoma, at 2024. It damaged four lake cabins and a church before completely destroying the farm house of the Byrd family. The Byrds reported that they went to their storm cellar specifically because of the second NWS tornado warning which placed the tornado at Pumpkin Center, moving east.

Doppler analysis (Fig. 11) revealed the existence of two TVS's rotating around the mesocyclone but displaced as much as 10 km south of center. The mesocyclone center moved to location marked as TVS(2) location before the Marlow tornado. The mesocyclone was tracked eastward until 2200. Continued severity was verified by several reports of funnel clouds, damaging straight wind and large hail. This Marlow Pumpkin Center storm is a good illustration of Doppler's potential for providing improved severe storm forecasts. Doppler based identification and precise location of severe phenomena, when combined with an accurate motion forecast provides the best possible warning input.

6. DISCUSSION

Analyses of two seasons of weather observations taken in a real-time environment of severe storm forecasting and warning have demonstrated significant operational benefits of meteorological Doppler radar. Principal among Doppler's advantages in forecast operations are, an increased lead time for tornadoes, reduced false alarm rates for tornadoes and severe thunderstorms, and an improved probability of detection for severe thunderstorms.

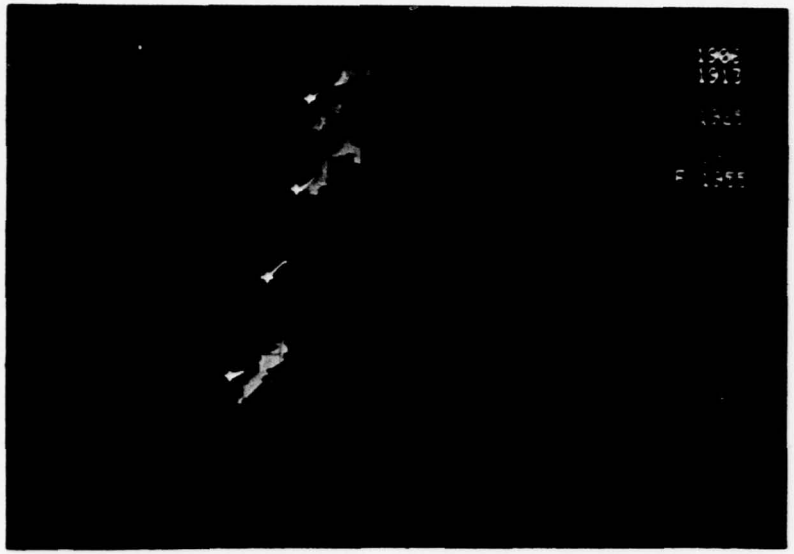

Fig. 12 Pre Tornado Track of Pumpkin Center-Marlow Storm of 5 April 1978. Shaded areas denote position of storms at 1938 CST; yellow crosses denote position of storms at 1906. Specific military bases, NWS offices, and population centers are shown as squares. Overlay is state of Oklahoma county boundaries. Note the eastward movement of the southernmost storm.

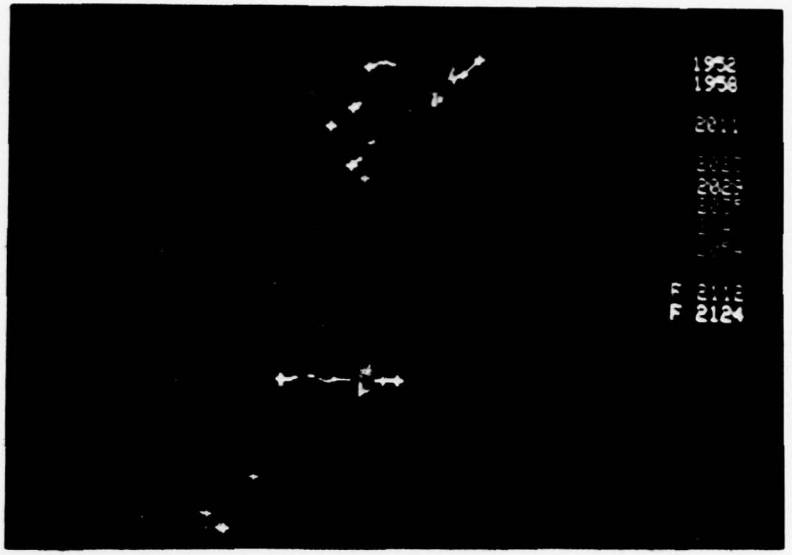

Fig. 13 Track of Pumpkin Center-Marlow Storm. Shaded areas denote positions of storms at 2100 CST; yellow crosses to left of present position denote storm location at 1952, and light green and yellow crosses to right of present position are forecast positions valid at 2112 and 2124 respectively. Pumpkin Center storm was on the ground from 1956 to 2010; Marlow storm touched down at 2024.

Doppler can be effective in distinguishing between severe and non-severe thunderstorms at long ranges (to 350 km) and can separate tornadic from non-tornadic storms at close ranges (to 230 km). Doppler radar signatures enable the identification of mesoscale vortices, tornado vortices, gust fronts, in-storm turbulence, and wind shear. Doppler signatures also enable a more precise location of the hazard and its warning area. Doppler based identification and location of severe phenomena, when combined with an accurate motion forecast, provides the best warning input that the state-of-the-art can provide.

JDOP participants agree that the next generation meteorological radar should have a Doppler capability. Moreover, radars built to a common set of specifications should suffice to provide data basic to the needs of all users, each of which would draw on the advancing technology of data systems to provide processed materials at operating centers. Thus the diversity demanded by differing responsibilities would be provided via agency-specialized computer programs, communication modules, and display systems, while the nation would benefit from the large capabilities and significant economies inherent in a single radar network.

At present, JDOP conclusions are being written into a set of recommendations for the next generation weather radar. Included are hardware specifications for an operational Doppler radar with much improved capability over present systems. Participating agencies have formed a working group under the Federal Coordinator for Meteorology to merge JDOP findings with future radar requirements into a joint Project Development Plan (PDP). A notable portion of this plan will pertain to the joint use of data from a single radar by NWS, AWS, and FAA. Initial data processing will be common, but analysis techniques and remote displays may be dissimilar. The PDP, if approved by the agencies, will be sent into the Federal Budget funding cycle. But even if final approval of funding is rapid, the nationwide deployment of a new generation radar network will be several years away.

Although basic hardware specifications for the new radar are well in hand, work is needed to complete the design of radar software, displays, and remoting techniques. Through the use of AFGL Doppler equipments and personnel, JDOP will continue during the spring of 1979 in Oklahoma in conjunction with the Severe Environmental Storms and Mesoscale Experiment (SESAME 79). SESAME 79 is a cooperative effort with intensive data collection by many groups (both university and government) interested in thunderstorm processes, and NSSL is host for the first field phase of this experiment.

Objectives for the Spring 79 JDOP involve the automation, remote transmission, and display of Doppler weather radar information. The basic objectives are:

1. To evaluate the format and effectiveness of semi-automatic data displays;
2. To evaluate one or more methods of remoting data;
3. To provide input to the warning agencies from the remote site.

In order to accomplish these objectives, AFGL display products will be transmitted once every six minutes to operational settings in central Oklahoma for use by meteorologists from the NWS, AWS, and FAA.

The computer synthesized color display planned for JDOP 79 is a combination of the salient features of the displays shown in Figs. 3 and 12 of this paper. Three reflectivity contours will be plotted: 20 dBz, 35 dBz and 55 dBz. The 20 dBz contour will represent the extent of the precipitation at the lowest elevation; the 35 dBz contour will outline the core of the cell and define the volume used in the cell track; and the 55 dBz contour will show those cores assumed to contain hail. Echo tracks and forecasts and map overlays will be similar to those of Fig. 12; however, the computer synthesized display of 1979 will also provide a coded list of echo attributes along the right hand edge. For each echo, the following parameters will be displayed:

1. Maximum reflectivity of the cell (coded);
2. Maximum velocity at lowest elevation angle;
3. Maximum velocity standard deviation observed within 30 dBz volume;
4. A two letter meteorologists' code for echo significance;
5. Azimuth angle of 30 dBz volume centroid;
6. Range of 30dBz volume centroid;
7. Cell motion (speed and direction).

An AFGL radar meteorologist will view all of the displays of Fig. 2, and will assess the Doppler fields for severe weather events. Cells associated with severe phenomena, as determined by the radar meteorologist, will be coded according to the appropriate indicator: S, strong shear; M, mesocyclone; T, tornado vortex signature; W, damaging surface winds; or B, bad data. These indicators will then become a part of the attribute listing for that cell.

Attempts have been made in the display format to provide the type of intelligence that one would expect to be generated automatically, by a computer, in the foreseeable future. The data presented will not be a final product for a new generation system, but rather an example of a computer-generated display containing as much information as can be integrated from the reflectivity, Doppler velocity and shear displays.

ACKNOWLEDGMENTS

The experiments described in this paper involved efforts and support from a rather large

group of scientists and engineers from the staffs of the National Severe Storms Laboratory, the Air Force Geophysics Laboratory, National Weather Service, Air Weather Service, and the Federal Aviation Administration. The authors also gratefully acknowledge the guidance and encouragement provided by Dr. Edwin Kessler of NSSL to the JDOP program. Thanks are also due Mrs. June Queijo for typing the manuscript.

REFERENCES

Brown, R. A., and L. R. Lemon, 1976: Single Doppler radar vortex recognition: Part 2 - Tornadic vortex signature. Preprints, 17th Radar Meteorology Conf., AMS, Boston, MA., 104-109.

Burgess, D. W., 1976: Single Doppler radar vortex recognition: Part 1 - Mesocyclone signatures. Preprints, 17th Radar Meteorology Conf., AMS, Boston, MA., 97-103.

Burgess, D. W., L. D. Hennington, R. J. Doviak, and P. S. Ray, 1976: Multimoment Doppler display for severe storm identification. J. Appl. Meteor, 15, 12, 1302-1306.

Donaldson, R. J., Jr., 1970: Vortex signature recognition by a Doppler radar. J. Appl. Meteor., 9, 661-670.

Donaldson, R. J., Jr., R. M. Dyer and M. J. Kraus, 1975: An objective evaluator of techniques for predicting severe weather events. Preprints, 9th Conf. on Severe Local Storms, AMS, Boston, MA., 321-326.

Groginsky, H. L., 1965: The coherent memory filter. Electronic Prog., Raytheon Company, 9, 3, 7-13.

Groginsky, H. L., 1972: Pulse pair estimation of Doppler spectrum parameters. Preprints, 15th Radar Meteorology Conf, AMS, Boston, MA., 233-236.

Lhermitte, R. M., 1972: Real time processing of meteorological Doppler radar signals. Preprints, 15th Conf. on Radar Meteorology, AMS, Boston, MA., 364-367.

Novick, L. R. and K. M. Glover, 1975: Spectral mean and variance processing via pulse pair processing. Preprints, 16th Conf. on Radar Meteorology, AMS, Boston, MA., 1-5.

Sirmans, D. and B. Bumgarner, 1975: Estimation of spectral density mean and variance by covariance argument techniques. Preprints, 16th Conf. on Radar Meteorology, AMS, Boston, MA, 23-28.

Smith, R. L., and D. W. Holmes, 1961: Use of Doppler radar in meteorological observations. Mon. Wea. Rev., 89, 1-7.

TECHNOLOGY TRANSFER IN PROFS

D. W. Beran and C. Gordon Little

Wave Propagation Laboratory

NOAA/ERL

Boulder, Colorado 80302

ABSTRACT

PROFS is a new NOAA initiative that has the goal of improving the nation's local scale weather services. A previous paper on this subject (Beran and Little, 1978), treated the concept of weather services from the users viewpoint. Here we discuss the role of technology in PROFS. The issues of more effective and more rapid technology transfer are addressed. Potential ways of improving this transfer through improved management, better long range planning, and more attention to the decision making process are suggested.

1. INTRODUCTION

The Prototype Regional Observing and Forecasting Service (PROFS) is a multi-faceted program that has as its long range goal the improvement of local weather services. The concept deals with the reality that a weather service is a complex technological/social system that is made up of many important elements. To improve the final service product, each of these separate elements must be optimum within itself, and be properly integrated and balanced with all other elements.

The technology within the system, and the society that is served are constantly evolving. New research results and changing user needs are external influences that make it essential for the service system to be flexible, able to accept new technology and turn to new user needs without undue disruption.

The organizational structure of both the system and the environment containing it are important. A management that encourages and is willing to accommodate positive change is essential to the vitality of a dynamic service system. External organizations which interface with the service system can also have a strong influence on the creation of optimum services. In most cases, there should be a two-way flow of information between the service system and external groups. For example, an external research group must have a clear understanding of the system's weaknesses before they can direct their efforts toward practical solutions. External groups which receive the final service products must communicate their needs before they can be served.

The PROFS Program Development Plan (PROFS, 1978) outlines a program, the schedule, and projected costs for achieving the long-range goals of improved local weather service. The need and economic justification for the program are addressed in that document. The question of need is further addressed by Beran and Little (1978), where the concept of "user scale" is introduced. The argument is made that existing meteorological services are primarily based on a synoptic scale system. The density of upper-air observations, the grid spacing of large-scale numerical prediction routines, and the dissemination process are all designed to deal primarily with synoptic scale motions. Mesoscale services are constrained by the spatial and temporal limits of this synoptic-scale system. Mesoscale services are indeed provided, but are typically merely an extrapolation downward from the synoptic-scale system. Tornado forecasts are a good example of the effect of this constraint. "Watches" are issued on the basis of synoptic or large *mesoscale* analysis. Despite the use of radar and much forecast skill, the watch area is still typically very large in relation to the actual size of the area affected by a tornado.

The "user scale" (Beran and Little, 1978) is defined as the area of interest for each individual that receives the service. In the case of a tornado warning this scale might be as small as the individual's home or the building where he is employed. The user scale is usually much smaller than the warning area. In the specific case of warnings the long range goal then becomes one of reducing the gap between the area of interest to individuals and our ability to predict the severity and timing of a weather event. Considerable economic benefit and improved safety through more precise severe storm warning could result from a reduction of this service gap. One estimate (see Appendix, PROFS, 1978) places the potential economic benefit in the Denver urban region as high as $30 million/year just for the three activities of commuting, shopping, and recreation.

In this paper we will expand further on the PROFS concept by exploring the role of new technology in achieving the goal of improved local weather services.

2. THE ROLE OF TECHNOLOGY: PROBLEMS AND OPPORTUNITIES

During the past decade, a total of almost $2 billion has been spent on meteorological research by some thirteen different federal agencies. The research has been conducted, somewhat independently, by scores of different federal laboratories and universities. Approximately one-half of this research effort has been devoted to the mesoscales. This major research effort has resulted in considerable progress across the full breadth of mesoscale research and technology. For example, major advances have been made in the ability to observe the atmosphere by satellite and ground-based remote sensors, and by automatic surface weather stations. There has been similar progress in the areas of data processing, in mesoscale numerical modeling and prediction, and in display and dissemination.

A weather service can be divided into four essential elements or functions. These are: observation, forecasting, dissemination, and communication. The first three represent a continually recurring chain of events, while the fourth is the element which binds the others into a working system. It is noteworthy that each of these elements is made to function by the actions of people who, by and large, have different backgrounds. For example, people working in the area of observations tend to be engineering oriented, forecasting is dominated by meteorologists, dissemination by broadcast journalists, and communications again by engineers. This separation by discipline is fairly consistent throughout the research-development-operations chain.

We are not implying that this separation is total, for there are some people in each area who have an interdisciplinary background. Certainly, management at successively higher levels is fully cognizant of the need to integrate the weather service elements into a working system. At the operational end of the spectrum this merging is, by necessity, effective, for the system would simply not work if this were not so. However, even here improvements could be made especially in the area of dissemination. For example, the gap between forecasters and broadcast journalists is many times the source of heated debate.

The separation of disciplines becomes even more serious in research and development. While basic researchers might argue that the freedom to explore new areas within one's own discipline might be restricted if too much emphasis were placed on how new research results were to be used, the argument rapidly becomes invalid when applied to the development phase. Here, new results must begin to pass the rigid tests of compatibility and relevance.

This lack of a mechanism for the early testing of interfaces between new technology within one element and other parts of the system can produce costly mistakes and a serious lengthening of the time required for new technologies to make a useful impact on operations. Some examples, drawn from past experience, will help to make this point more clear.

The development of weather radar was one such technological breakthrough that held great promise. In its infancy it was touted as being the ultimate nowcasting tool that would solve many problems such as severe storm tracking and warning. After many years this promise has been partially fulfilled. However, in its early stages of use little thought was given to methods of interpreting and disseminating the information. Without such interpretation and dissemination to the ultimate user, the promise of nowcasting (in near-real-time) could not be realized. If more thought had been given to the integration of this new observing tool with the forecast and dissemination elements, it might have stimulated a greater awareness of the needs at an earlier stage. This cross-disciplinary activity could have resulted in an earlier and more effective application of weather radar.

The development history of the meteorological satellite is in a sense similar to that of radar. A radically new and powerful technology was introduced into the weather service system with early hopes that "it" would permit forecasting the weather for up to two weeks in advance. The satellite has had a tremendous impact on meteorology, but one wonders how much more effective it would be today, and how much sooner this impact would have occurred, if more thought and effort had been given to the total integration of this new tool with the existing forecasting, dissemination, and communication elements of a weather service system.

It can be argued that these technological advances did not make an earlier impact simply because the supporting technologies had not yet been developed or were lagging in their evolution. This is undoubtedly true, but avoids the point that better long range planning might have helped to identify the need for the supporting technology. If this had been done it might then have been possible to accelerate certain key developments by more selectively concentrating resources in given areas. A key problem today is that much research and development activity is far too isolated from practical needs. It occurs in an environment where the researcher feels that he knows best what will be good for society, and far too little attention is paid to the broader spectrum of needs and how the individuals efforts will eventually be coordinated into a useful system. This is not to suggest that a final solution lies in either totally directed or totally undirected research. We must find a middle ground that will allow the necessary research freedom, but will also insure that priorities are known and addressed.

The radar and satellite are examples of observing technology that did not benefit from a careful early assessment of, and planning for, their future role. The area of forecasting also contains examples of this lack of broad planning and interdisciplinary communication. Highly sophisticated numerical models

are now fully operational as forecasting tools. They are by necessity tied closely to the existing twice-per-day radiosonde launches. New and improved models are also being developed, and for the most part still depend upon the twice per day data set. This is occurring despite demonstrations in the observational research community that future data sets could well be continuous in time. The elimination of the artificial 12 hour increment in observations could have a marked effect on the type of numerical prediction model that is optimum in the future, yet the absence of a close working relationship between these two research communities may well be extending the time before such new models are developed.

Similar examples of the effect of separate and somewhat isolated research and development activities are common. In many cases the problem of single discipline research is further compounded by geographical and organizational separations. For example, within NOAA we find that the Environmental Research Laboratories are organizationally and geographically far removed from the system development activity of the NWS in Washington, D.C. Further, geographical separation occurs between the individual laboratories within ERL. This situation is inevitable in any large country and organization (to attempt to centralize all research and developmental activities across NOAA into a single city and organization would certainly not be optimum, if only because of the extraordinary range of activities involved, e.g., oceanography and tornadoes), but a more conscious recognition of the problem created by geographical and organizational barriers could ameliorate the situation. The problems created by these separations need to be addressed if we are to improve our record of technology transfer.

A solution to this dilemma is proposed within the PROFS concept. The plan for an Exploratory Development Facility (EDF) addresses the need to take a broader interdisciplinary look at future systems early in the development cycle. It is seen as an organizational element that is close to the research activity in all disciplines, but is separate from the work of any given laboratory.

Staffing of the EDF will be of fundamental importance. The total staff component must cover the range of disciplines that are essential to the elements of a weather service. Further, there must be a mix of people drawn from research, development, and operations. Interdisciplinary training or experience will be emphasized, thus, helping to keep the core staff small. In order to maintain a constant flow and exchange of ideas between the research and operational communities, a portion of the staff will rotate into the EDF and back to their parent organizations on a one or two-year cycle. A similar mechanism will be encouraged with other agencies helping to ensure that new needs and ideas from outside NOAA are made part of the evolving system.

A primary function of the EDF will be systematic long range planning. Its output must be oriented toward future systems. Thus, there must be a constant analysis of needs and potential new techniques. This process will help to identify areas where research is lacking, or where there is a need to accelerate ongoing work. Such guidance will be available to upper management and policy makers in preparing long range strategy. In addition, it is planned that the PROFS EDF will have funding flexibility that will allow for the direct support of critical activities that are needed to address future needs.

As new technologies emerge from the research laboratories, the EDF will begin to assume the responsibility for testing their compatibility with other system components and their relevance to the future needs of users. The developers of the new technologies will be encouraged to transfer into the EDF during this phase where they will work with their counterparts from the operational components. This early and intimate association between developers and potential users will help to minimize the shock to the system when new technology is introduced into operations.

3. THE RATE OF CHANGE

The rate of effective technology transfer is another important aspect of the broader issue. New and improved technology is today being produced at an unprecedented rate. This rapid change is nowhere more apparent than in the area of electronic data processing. In the research community it is not uncommon to see computer systems outmoded by the time they are acquired and fully debugged. The much longer time lag that occurs before such systems can be operationally implemented results in a serious reduction in the level of service that might otherwise be possible.

Most development activity is an iterative process, whereby the creation of one new device or technique will help to stimulate development in other areas. Given this, we must seek ways of improving the rate at which such iterations take place or to overcome the built-in inertia of our existing research-development-operations cycle. New R&D management techniques must be developed and the organizational structure of government and industry must be carefully examined with an eye toward improved efficiency. This process must start by placing a new emphasis on systematic long range planning. Upper management must understand the importance of this function and be willing to direct the necessary and substantial resources toward this task.

The decision making process can be improved if solid long range plans are an integral part of the decision package. Good decisions must also be made rapidly. Bureaucracies tend to evolve with time into ever more complex organizations. Often, additional levels of management are introduced during this evolution,

with the idea that a better coordination of activities is produced. This may or may not be true, but what seems to be overlooked is the element of time in the decision making process. Each level of management feels it must see, review, and perhaps modify decision options that are introduced from below. The results of a study to determine the increased time lag introduced by each management level would be interesting. The increased time lag for each management level could well be measured in weeks or months rather than days.

Another area of real concern is the maintenance of outdated and ill-conceived regulations. A classic example of this problem can be found in the complex and time consuming procedures that are required of federal agencies purchasing automatic data processing (ADP) equipment. Judging from the regulations that control the purchase of such systems, ADP equipment must have been perceived as a mysterious and sinister device that would be used to the detriment of mankind. In reality it is an essential tool for dealing with other advanced technologies, much as the oscilloscope is an essential tool for dealing with electronic design problems. Yet, the time to purchase an oscilloscope can be measured in weeks while the purchase of standard ADP equipment sometimes takes more than a year.

If the rate of technology transfer is to be improved, a fundamental rethinking of these issues is in order. We must identify the organizational bottlenecks and carefully examine the reason for their existence. *When the need* for more rapid technology transfer outweighs other reasons for their existence we must actively work to eliminate them and to streamline the system.

4. THE PROFS PLAN

The PROFS plan calls for the creation of the research prototype of a greatly improved local weather service capability. It will integrate technological advances into a single flexible system designed to provide radically improved local weather services that are fully responsive to user needs.

A total plan leading to the eventual operational deployment of PROFS-type capabilities would be divided into the general phases of:

1) Information collection
2) Analysis and planning
3) System design
4) Development of research prototype
5) Development of engineering prototype
6) Operational implementation

The exploratory development phase covers the first four of the above steps, and will result in the demonstration (primarily within NOAA) of the feasibility of the improved services and the creation of the Exploratory Development Facility. The critical next step, the creation and evaluation of an engineering prototype, would follow completion of this exploratory development phase.

The PROFS task of integrating disparate and uncoordinated research advances in observing, forecasting, and dissemination into a single, smoothly-operated prototype local weather system may be divided into five tasks, as follows:

-- overall system design and integration
-- profiling subsystem
-- observing/nowcasting subsystem
-- extrapolation/forecasting subsystem
-- overall feasibility demonstration

These tasks are discussed in turn:

4.1 Management, System Analysis, Design, and Integration

This task provides the overall management, planning, and coordination of the multifaceted PROFS activities. PROFS must be designed as a single system whose every component contributes optimally to the goal of improved local weather services. To achieve this will require design and integration of contributions from traditionally separate areas of NOAA, such as observing and forecasting, as well as areas in which NOAA has traditionally been less strong, such as systems analysis and design, user needs *studies, and* dissemination. Therefore, this task will require the creation of a strong joint ERL, NWS, and NESS management team, supplemented by experts from other agencies, external consultants and contracts. The team will perform the necessary management and planning functions, and provide supervision of overall user needs studies, system analysis, system modeling, and system design. The efficient coordination and integration of the diverse observing, forecasting, and dissemination subsystems into a smoothly operating whole is also part of this task.

4.2 Profiler

The profiler system provides for the continuous measurement of wind, temperature, and humidity profiles. An integrated satellite/ground-based remote sensing system for the continuous measurement of the profiles of wind, temperature, and humidity will be created. (Additional information on profiles of turbulence, precipitation, and clouds should also be available). This real time profiling capability will form an essential part of the PROFS mesoscale observational system. It will be integrated with other, already developed techniques such as radar, satellites, and automated observing stations to create the PROFS observational component.

4.3 Observing/Nowcasting System

This task creates the integrated local weather observing and nowcasting system, based

on an integration of satellite and ground-based remote sensors, an array of automated in situ surface weather sensors, Doppler weather radar, cooperative observers, etc. It will also include a satellite data acquisition system, and AFOS installation, and the necessary telemetry and communication circuits. Of particular importance will be the real-time data processing, information extraction, and automatic display capabilities required for a nowcasting service.

4.4 Extrapolation/Forecasting System

This task utilizes the total available data set to prepare short term (0-3 hr) extrapolations of the local nowcasts, and mid-term (3-12 hr) forecasts of the local weather. The latter would be prepared using physical, numerical, and statistical forecasting techniques designed for each specific region, taking into account the local topography and other surface features; the former would involve a major research effort to learn how best to extrapolate the nowcast data, using physical and statistical methods.

4.5 Feasibility Demonstration

The remaining task, feasibility demonstration, involves the test and demonstration of the capability of the overall system to provide (internally within NOAA, rather than externally to the public) radically improved local weather services. This is the final step in the PROFS exploratory development phase, and tests the integration of the many subsystems, and the ability to continuously provide, in the research mode, nowcasts, extrapolations, and 3-12 hr numerical weather forecasts for the area within approximately 100 km of the Exploratory Development Facility.

REFERENCES

Beran, D. W., and C. G. Little, 1978: PROFS: A strategy to improve local weather services. Preprint Volume: AMS Conf. Wea. Forecasting and Analysis and Aviation Meteor., Oct. 16-19, 1978, Silver Spring, MD.

PROFS (Prototype Regional Observing and Forecasting Service), Program Development Plan, 1978, D. W. Beran (ed.), NOAA/ERL, Wave Propagation Lab., Boulder, CO.

THE STATUS AND PROSPECTUS OF PLANNED WEATHER MODIFICATION: 1978

Stanley A. Changnon, Jr.

Illinois State Water Survey

Urbana, Illinois

1. A WARNING ABOUT REVIEWS

Those in the field of weather modification considered sufficiently well versed to review the subject are often faced with a dilemma. No matter how they summarize the field, they are often attacked as either overly for or against weather modification. In other words, there is marked division among beliefs of atmospheric scientists. On one hand are those who believe in the potential and existing achievements of weather modification, and on the other hand are those who believe that weather modification has been a scientific hoax and that all support has been wasted. Sometimes both viewpoints are expounded in one talk (Hosler, 1977).

I am pleased to be asked to present an overview of planned weather modification. I have struggled very hard in the last 10 years to offer an unbiased view of the field. I say all this because the views of anyone addressing or reviewing the field are important in assessing what you hear or read. I must confess that my views have been critized by both the opponents and proponents of weather modification. It is very difficult to stand in the middle ground of weather modification, and yet I think it is essential. Hopefully, my views will reflect an unbiased assessment of the field, both its past and future.

2. INTRODUCTION

I think most would agree that there is clear proof that certain forms of weather can be modified under certain conditions. I also think there are now clear indications that some attainable weather changes yield useful benefits. However, I think the track record of weather modification is poor. Commercial weather modification has plowed ahead, often with little scientific basis, and the scientific experimental side of weather modification has often included ill conceived and poorly conducted experiments. Mix into this a generally poorly organized federal effort and one can understand why there has not been great scientific progress. However, I think the single greatest problem has been the extreme complexity of the subject being addressed. Modification of convective elements is dealing with the extremely complicated physics and dynamics of clouds, and when one considers how little we knew about cloud physics and cloud dynamics in 1950, one can appreciate that the achievement of significant understanding in 25 years is an unrealistic goal, even if the national effort had been well organized.

An interesting and useful way to obtain a relatively unbiased view of weather modification is through an in-depth assessment by businessmen and scientists of other disciplines. The National Weather Modification Advisory Board, which was established in 1977 as a result of Public Law 94-490, was charged with making a comprehensive assessment of weather modification and to develop a national weather modification policy and program, if needed. This Board contained a few atmospheric scientists including Roscoe Braham, Ray Booker, Bob Elliott, John Firor, Joanne Simpson, and myself. The other 10 members of the board included economists, farmers, lawyers, policy makers, environmentalists, and various national leaders. After this Board had reviewed documentation and conducted public hearings over several months, the Board members were convinced that there had been progress and there was hope for achieving useful levels of weather modification in the future. Let me quote, "The Weather Modification Advisory Board, whose mandate is to propose a national policy, thinks the indications are good that weather resources can, in time, be managed with some assurance. We conclude that it will soon be possible to influence the weather more reliably, in a much greater variety of ways, by the use of cloud seeding technologies" (WMAB, 1978).

The current status and prospects of weather modification can best be understood by a brief consideration of the history of the field.

3. THE CRITICAL HISTORY

Weather modification in the United States since the late 1950's can be characterized as having two parallel thrusts (Changnon, 1978a). One thrust has been the federally-sponsored research, generally characterized by a series of site-specific, moderately large experiments. Many of these unfortunately have been inconclusive due to inadequate planning, poor operations or inadequate funding. Experimental results have been mixed with success in some cases, with nothing modified in others and reversals in others, such as rain decreased instead of increased. The major findings after 20 years have been: 1) that clouds and rainfall are extremely complex and modification is difficult to accomplish and prove; 2) that under certain conditions rainfall or snow can be alter-

ed over small areas within certain geographical regions; and 3) a much broader more extensive research effort will be needed to make weather modification a widely useful technology.

The other thrust of the weather modification field has been in private usage of weather modification. The use of private and corporate funds to hire commercial firms to perform "operational modification projects" has brought forth hundreds of projects, largely performed in the western half of the United States. Many of these operational projects have lasted only one or two years, but a few in California have been conducted continuously for more than 20 years. Although difficult to evaluate, evaluation of certain operational projects has helped established that rainfall could be purposely modified to obtain 10 to 15% increases (NAS, 1973).

The most important point to this 2-pronged approach (research versus usage) to weather modification is that it has involved usage before the scientific basis for its usage was established. Ever growing usage of weather modification in the face of this lack of scientific proof can only be understood in light of intensive public desires to relieve losses due to weather extremes and to the low cost of cloud seeding. Typically, commercial cloud seeding projects are inexpensive to the individual, costing between 3 and 50 cents per acre depending on the size of area, type of seeding, and quality of the commercial operator employed. A general philosophy of users has been one of investing in a low cost gamble.

This 2-pronged approach involving usage without much scientific proof has led to local controversies over the effects of cloud seeding with communities becoming disenchanted and stopping projects in several instances. Sociologists who have studied the controversies related to weather modification find the prime reason for public controversy is the lack of scientific consensus about weather modification (Changnon et al., 1977).

This 2-pronged approach has helped produce the earlier mentioned division of attitudes among atmospheric scientists about weather modification. It has also led to poor relationships between those in the operational side of weather modification, and the scientific community involved in the modification research and experimentation.

4. WHERE WE STAND TODAY

The status of planned weather modification, depending upon one's view, could be classed as at a disaster point or at the apex of a new era.

On the scientific side of weather modification, the picture is reasonably gloomy although there are a few notable exceptions. On the side of commercial, operational weather modification, things are better than ever before. Let us examine these two situations.

4.1 Scientific Status

In a general way, the scientific side of weather modification has progressed slowly but notably over the last 10 years. On the atmospheric side the things that provide optimism include great improvement in cloud and precipitation sampling equipment (radars, aircraft, and aircraft instrumentation), and the ever growing expertise developed through the educational processes. There continues to be improvement in cloud and mesoscale modeling, both essential to the ultimate understanding and prediction of the outcomes of weather modification. The Weather Modification Advisory Board concluded that the field had made significant advances and was ready for growth due to its equipment development, training of people, and development of evaluation and analytical techniques. Table 1 summarizes the status of weather modification as reported by the Board (WMAB, 1978). Possibly, if judged on a scale of 0 to 100, the field stands at 10 but appears ready for rapid growth on the learning curve. However, the two major recently completed experiments must be classed as unsuccessful. That is, they failed to achieve the stated modification goals.

Table 1. Status of Weather Modification*

A. Cumulus Cloud Systems	
1. Static seeding	Results
a. Whitetop	Overall decrease in rain
b. 14 operational projects	0 to +33% increases
c. Arizona projects	Inconclusive
d. Sierra project	Favorable results
e. Necaxa Basin Mexico	21% increases
2. Dynamic seeding	
Caribbean individual clouds	Up to 200% increases
FACE, area	Encouraging, confirmation in progress
B. Warm Season Cumulus Clouds	
South Dakota ---	increases in showers, no effect in large storms
North Dakota ---	overall differences are negligible, separation on dynamic seeding conditions revealed increases
C. Downwind	
Position unclear, generally no great changes	
D. Cumuliform Clouds in Winter Cyclonic Storms	
Israel Phase I	-- 15% overall increase
Phase II	-- 13 to 15% increases
Santa Barbara Phase I	-- +50% in certain conditions
Phase II	-- increases in select areas
E. Hail Suppression	
Soviets -- 40 to 80% decrease	
Switzerland -- 66% increase suggested	
Argentina -- 34% decrease	
NHRE -- inconclusive	
North Dakota -- 4 to 21% reductions, statistically inconclusive	
Texas -- 48% reduction in loss, not statistically significant	
South Africa -- results suggest reductions	

F. Supercooled Fog and Low Stratus

Cold Fog --- can be removed
Winter stratus --- feasible, more study needed

G. Orographic Cloud Systems

Operational projects -- 10 to 15% increases
Climax I and II Experiments -- increases in certain conditions
Colorado River Basin Pilot project -- no effect
Tasmania -- 20% increases

* As summarized from the WMAB (1978) report

The National Hail Research Experiment (NHRE) after three years of field experimentation (1972-1974), ended in a scientific controversy with a claim of no evidence of hail suppression by those evaluating the experiment. Others say the effort was so poorly designed and conducted that one could not expect modification. Regardless, the launching of a major hail suppression experiment by the scientific community under the urging of bureaucrats in Washington must be considered a major strategic mistake. Decisions in the mid 1960's to go forward into a scientifically conducted hail suppression experiment at best were based on ignorance of the complexity of the hail formation in thunderstorms. One of the toughest modification problems was chosen and it is no small wonder that it failed. In my estimation, NHRE did not prove that hail could or could not be suppressed; it proved that scientists in the policy area were capable of making poor choices of problems to be attacked, and that scientific community still finds it difficult to plan and conduct a well run complex experiment.

Another experimental effort which must be classed in the failure group is the Colorado River Basin project in the San Juan Mountains of southwestern Colorado (see Table 1). The earlier experimentation with orographically-induced snow conditions in the Climax area of Colorado had shown that under certain conditions snow could be enhanced by 30%. The San Juan project was essentially designed as a "proof of concept," or confirmation experiment of the Climax findings. Unfortunately, the design and approach to this project produced a result indicating no enhancement of snowfall. There are many who would argue or explain differently the causes for failure in these two projects, but the two most recently completed major experiments in weather modification in the United States have failed, to provide any indication of a capability to modify the weather conditions they set out to change. There may have been poor choices in the weather phenomena, the site, the design, etc., but nevertheless, they failed to modify the weather.

The central feature of weather modification research in this country, of course, has been the role played by the federal government which has sponsored most of the research. The federal programs have been loosely coordinated, and the mission agencies in general have gone their separate ways: hail for NSF, rain and snow for Interior, hurricanes for Commerce, fog and stratus clouds for Defense, lightning for Agriculture, etc. The domain-protection approach of these agencies has led to a lack of attention to basic research and the long-term stable funding required to graple with the complex problems involved in weather modification. Table 2 presents the funding from FY-72 through FY-79 of the various federal agencies. Any number of interesting observations can be made. For example, agriculture, which will benefit more than any other area of endeavor from a successful weather modification in the United States (WMAB, 1978), has put particularly no money in the field over the last six years and it has now dwindled to zero. The record of Commerce reflects interesting year-to-year oscillations; note the jumps between FY-75, FY-76 and FY-77. The Department of Defense, after controversies over the use of weather modification in Vietnam, has seen their program gradually dwindle to a position of almost "getting out of weather modification." The examination of the Interior values shown in Table 2 reveals the politically inspired nature of their program with great oscillations from less than $4 million to over $8.6 million. Such vacillations between years are not conducive to the long-term stable research needed in weather modification. The National Science Foundation program, which had long been the key to stable basic research in weather modification, has dwindled to less

Table 2. The Federal Weather Modification Research Program--allocation of funding (millions of dollars).*

Department	FY 72	FY 73	FY 74	FY 75	FY 76	FY 77	FY 78	Congressional budget request FY 79
Agriculture	0.36	0.37	0.27	0.09	0.07	0.05	0.02	0.00
Commerce	3.94	3.77	3.08	2.49	4.30	2.67	3.55	2.7
Defense	1.82	1.21	0.92	1.14	1.80	2.41	3.11	0.7
Interior	6.66	6.37	3.90	4.00	4.65	6.45	7.61	8.6
Transportation	0.40	0.39	--	--	--	--	--	--
NSF	4.94	4.23	4.25	4.70	5.06	4.90	2.40	1.10
Total	18.12	16.34	12.42	12.42	15.88	16.48	16.69	13.1

* From WMAB (1978).

than $1 million after its unfortunate experience in NHRE. In summary, there are reasons for optimism due to the essential stock piling of expertise, equipment and analytical tools needed for research, but the status of the experiments and federal funding, now at one of its lowest points in history, give cause for great pessimism.

Major scientific gains of the last few years in planned weather modification have related to the gathering of good information about the societal and environmental impacts and the related institutional requirements for weather modification. For the first time, quality results from political scientists, economists, sociologists, and environmentalists have dimensionalized the impacts that successful weather modification would produce (Changnon et al., 1977). The lack of this type of quality information has previously obstructed the wise development of the field. For example, the technology assessment of hail suppression (Changnon et al., 1977) and other studies (Sonka, 1977) have pointed to the fact that agriculture has the biggest stake in weather (Table 3), and that the modification of warm season rainfall would be the most benefical weather change that could be produced, as opposed to hail suppression and modification of other weather forms. Examples of the effects of reduced hail and enhanced rain for farmers in northwestern Kansas are illustrated in Table 4. The income gain with no hail reduction and a 10% rain increase, $27.31 per acre, is comparable to a 50% hail reduction ($27.35). An example of the results of impact related research is revealed in figure 1. Here the types of impacts resulting from altered hail and rain, on the individual and community level are shown. Such in-depth analyses reveal that there will be winners and some lossers in most types of regional scale weather modification. Most importantly, these various impacts studies have helped reveal, both to the weather modification scientists and to the user community, how to deal with such problems. As Changnon (1978b) states, "Weather modification, as a scientific endeavor and an economic enterprise, can not go forward in a wise or healthy fashion without being placed in a comprehensive framework that embraces everyone potentially affected."

Table 3. Annual Weather-Caused Losses in the United States and Percent of Annual Gross Revenue[a]

Activity	Losses (millions of dollars)	Percent of annual gross revenues
Agriculture	8,240	15.5
Commercial aviation	92	1.1
Construction	998	1.0
Communications	77	0.3
Electrical power	46	.2
Energy fossil fuels	5	.1
Manufacturing	598	.2
Transportation (rail, highway, water)	96	.3
Other (e.g., general public & government)	2,532	2.0
Total	12,684	

[a]From Thompson (1976).

Table 4. Net Income Changes for Wheat Production in Northwestern Kansas Predicted from Various Degrees of Postulated Hail and Rainfall Modification[a]

Percent reduction in crop-hail damage	Percent change in growing season rainfall	Average net income per harvested acre (dollars)
0	-10	21.56
0	No change	24.58
0	+10	27.31
20	-10	22.60
20	No change	25.74
20	+10	28.47
50	-10	24.34
50	No change	27.35
50	+10	30.11
80	-10	25.98
80	No change	29.11
80	+10	31.88

[a]From Changnon, Davis et al. (1977)

It is worthy to note that there are essentially four experiments in weather modification either underway or evolving. The Bureau of Reclamation is correctly approaching the scientific study of modification of warm season convective clouds in the High Plains. Experimentation at three sites in Montana, Kansas, and Texas will soon be underway. Their major effort in Montana is using a systematic, learn as you go, approach, and if sustained should be an exemplary experiment. The Bureau of Reclamation is also moving towards another orographic snow experiment, this one located in the Sierra Mountains of California.

Another long term experiment that is nearing completion is the Florida Area Cumulus Experiment, FACE, being conducted by the NOAA in Florida. This project has been examining the seeding of convective clouds and has shown that rainfall from individual clouds can be enhanced up to 200%. An area-type confirmation experiment is still in progress, and available results are encouraging.

A new convective cloud experiment is just beginning in the Midwest, and it is labeled Precipitation Augmentation for Crops Experiment, PACE. This effort which is in its pre-experimental phase is aimed at assessing the potential for modification of midwestern summer clouds. It is designed as a 9 to 13 year effort to answer the question whether summer clouds can be modified in a manner of utility to agricultural needs.

4.2 Operational Weather Modification Status

In contrast to the many disappointments in the scientific-experimental side of weather modification, the operational side of weather

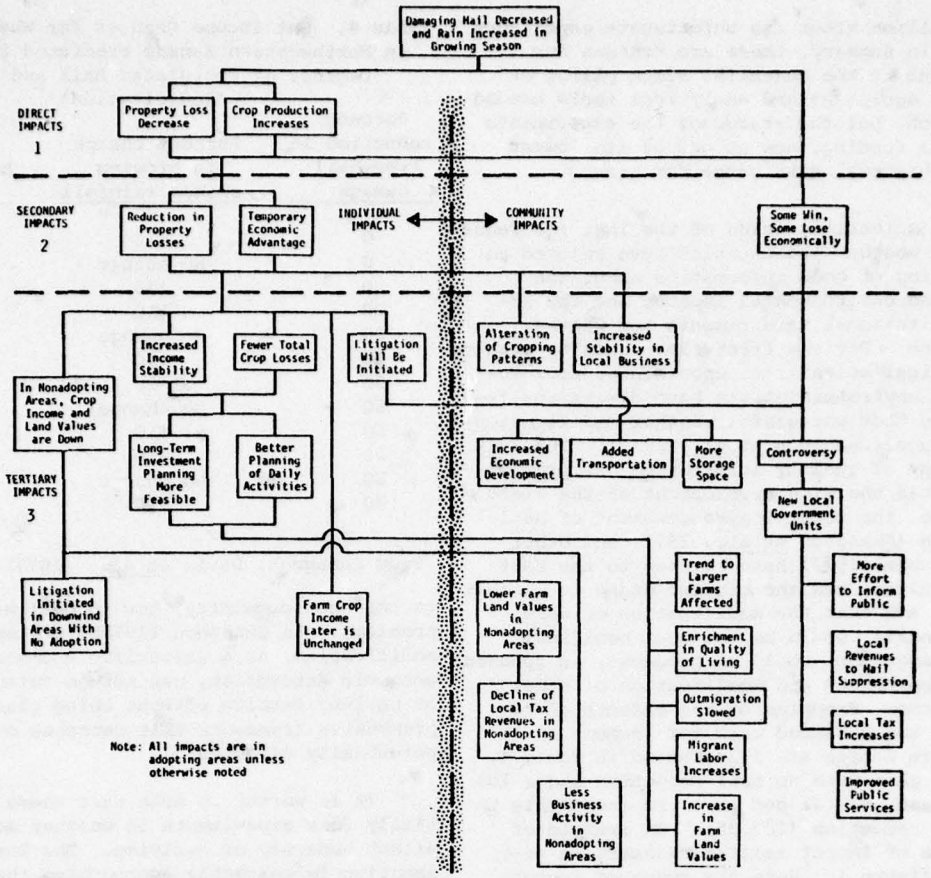

Figure 1. Possible impacts if a sizeable capacity to reduce losses from hail and increased rainfall is attained by 1995. [From Changnon et al. (1977)]

modification has been growing in recent years. The projects conducted during the last five years in the continental United States are shown in figure 2. Important has been the extension of commercial weather modification into the Midwest and eastern United States during the last three years, 1976-1978. For example, Illinois experienced its first commercial weather modification project in 1976 and by 1977, nearly 10% of the state was experiencing seeding during the summer months.

In 1972, there were 47 operational projects in the United States with modification efforts covering 85,000 square miles. The public-corporation expenditures for weather modification were approximately $4 million. The usage of weather modification has nearly doubled by 1977. In 1977 there were 88 commercial projects with weather modification being applied over 260,000 square miles. This represents 7% of the total area of the United States, and the total expenditure was $6.5 million. Thus, there has been a continuous growth in the usage of operational weather modification in the face of great scientific uncertainties.

An important part of this growth in use of operational weather modification is the evidence of maturity of the industry. For example, the Weather Modification Association (1978) has issued standards for project operations. These represent a strong industry call for the use of operational criteria and instruments systems needed for proper operations of field projects. The Weather Modification Advisory Board took a strong stand on operational weather modification efforts. The Board stated "most operational projects evaluations as currently done, are limited because quality standards have not been adhered to." The Board recommended incorporation of operational standards, federal licensing of weather modification operators, employment of sound management practices, and the use of skilled designers of field programs. Several state laws enacted in the last few years have incorporated specific operational and evaluation criteria, all of which up the standards for performing operational projects.

A third aspect of the growth in operational commercial programs concerns the growing attention to their evaluation. The technology assessment of hail suppression (Changnon et al., 1977) concludes that evaluation of operational weather modification is a key to public acceptance. The WMAB (1978) makes recommendations for development of evaluation techniques, and the statistical advisory group to the WMAB called for the use of "piggyback" research efforts on selected future operational projects (Statistical Task Force, 1978). These would be federally supported additions to certain operational projects utilizing

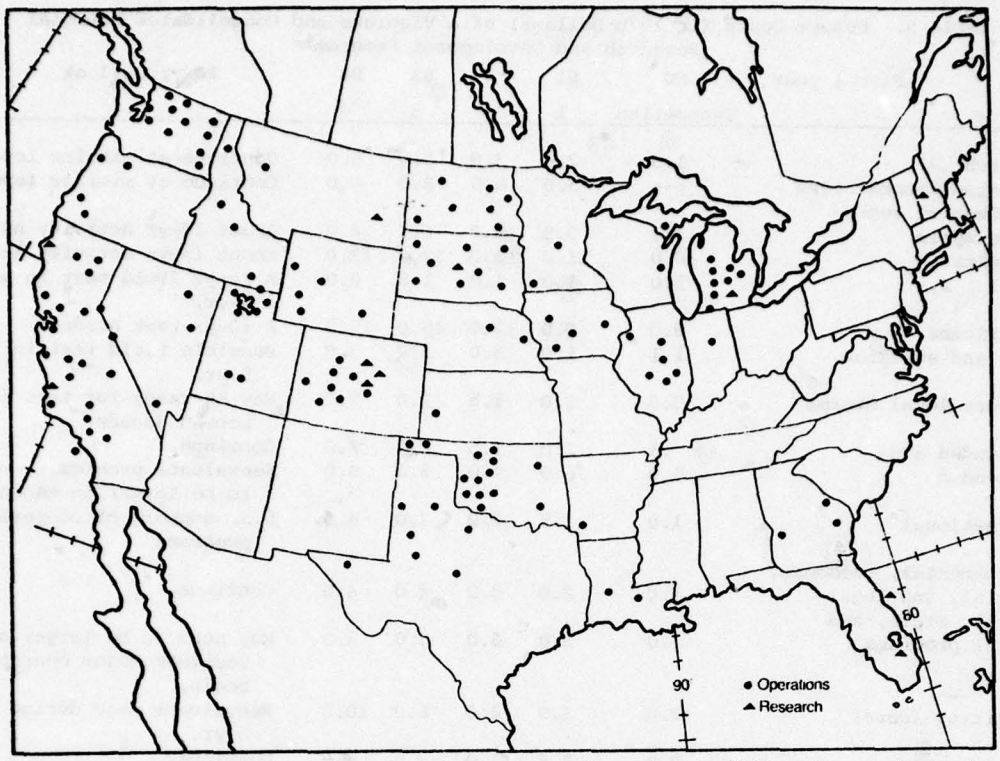

Figure 2. Locations of research and operational weather modification projects in the United States, 1973-77. Two operational projects were in south-central Alaska and no projects in Hawaii. (Courtesy of NOAA, Weather Modification Reporting Program, Rockville, MD)

some randomization and quality operations to provide scientific information while still serving the user. A project to develop evaluation techniques is in progress (Hsu et al., 1978).

5. PROSPECTUS

In my comments on my prospectus of planned weather modification, I have drawn heavily on the commentary of a recent assessment of the National Academy of Sciences and on the report of the Weather Modification Advisory Board. Having served on both of these groups, I can say that I endorse their recommendations, and they come to you as the comments of two groups of reasonably objective assessors. First, let us consider the research recommendations.

The Committee on Atmospheric Sciences of the National Academy of Sciences convened with some 70 scientists during June 1978 to assess future atmospheric research needs for the next 10 years. Recommendations for research during the next 10 years were developed by 12 groups, including one addressing planned weather modification. Although the recommendation must yet be classed in the tentative stage, the four recommendations included 1) research focusing on cloud microphysics and cloud dynamics to gain greater understanding; 2) establishment of the feasibility of selective clearing of stratiform cloud layers over areas sufficiently large to be useful for energy or agricultural purposes; 3) to proceed with 2 or more geographically separate randomized field experiments in the western mountains to confirm strong scientific evidence of a potential to enhance winter snowfall; and 4) to continue field investigations and modeling to establish the physical mechanisms associated with the concept of dynamic seeding of cumulus clouds and the role of seeding in the formulation of cloud agriculturists in meso-scale cloud systems. Projects in the Great Plains and Midwest were recommended.

The scientific recommendations of the Weather Modification Advisory Board (1978) appear in Table 5, showing the various areas of recommended research along with their recommended annual support. Excluded in this assessment is the recommendation for basic research to be conducted at the National Science Foundation, an entity not included in the envisioned consolidated national program. However, there is money for basic research and for three dedicated laboratories to be established at universities in various parts of the Nation. Several experimental tests are envisioned including two for orographic snowfall, 3 with cumulus clouds (High Plains, Midwest, and Florida), field research in hail, and major experimentation in hurricanes. Also shown are recommended efforts in the modification of winter stratiform clouds over and around cities. An important item in the recommended research picture are the "federal, state, and local programs." This is intended to include the support of well designed and operated operational projects to gather scientific information while they also attempt to provide weather modification for local sponsors. The proposed federal invest-

Table 5. Future Costs (in 1978 Dollars) of a Vigorous and Consolidated National Research and Development Program

Fiscal year	80	81	82	83	84	20-yr outlook
	Transition	1	2	3	4	
Research	1.0	2.0	3.0	5.0	5.0	Continue at similar level.
Dedicated laboratories	---	3.0	6.0	8.0	8.0	Continue at similar level.
Experimental tests						
Orographic	3.0	3.5	4.0	6.0	6.0	About 10-yr activity needed.
Cumulus	10.0	11.0	12.0	12.0	12.0	About 15-yr activity needed.
Hail	1.0	1.0	1.0	1.0	2.0	A large field test in second 5 yr.
Hurricane	8.0	8.0	12.0	15.0	15.0	A 10-yr test needed.
Fog and sunshine	1.1	1.0	3.0	3.0	3.0	Possible field test in second 5 yr.
Severe local storms	0.5	1.0	1.5	2.0	2.0	May be ready for test in second decade.
Extended area	.5	1.0	1.5	2.0	2.0	Continue.
Unintended	5.0	6.0	7.0	8.0	9.0	Reevaluate problem -- may need to be larger in second 5 yr.
International	1.0	1.5	2.0	3.0	4.0	U.S. support of cooperative programs
Environmental, economic, social, and legal	1.0	2.0	3.0	4.0	4.0	Continue.
Federal, State, and local programs	1.0	2.0	3.0	3.0	3.0	May need to be larger as well-designed major operations begin.
Facilities (core)	2.0	3.0	4.0	6.0	10.0	Reevaluate need during second 5 yr.
Administration	2.0	2.5	3.0	3.5	4.0	Continue.
Total	37.0	48.5	66.0	81.5	89.0	

ment shown in Table 5 for weather modification research and development is a part of a new national effort.

The other aspect of the future prospects relates to the reorganization of federal effort. As I have mentioned repeatedly, many of the problems in the research and development of weather modification have come from the questionable federal management of the field. As the WMAB reported, "the outstanding characteristic of the federal government's organization for weather modification is that no one is in charge." The results of fragmentation of the federal effort are clearly unsatisfactory. Weather modification has never reached a critical mass or sufficient momentum as a program of the federal government. Management and funding have been inadequate, and in general, the approach has lead to considerable waste in both research and development funds.

The Weather Modification Advisory Board calls for sweeping changes in the national program relating to weather modification. It notes that centralization and leadership are essentials and that "the lead agency" approach is not adequate. In the Board's proposal for a national program, the key management concepts are the consolidation of all the weather modification efforts of the federal government into one organization with sufficient autonomy for that organization to produce and defend its budget, and to carryout a 20-year program of research and development. The key elements of the program are shown in Table 6. A Presidentially appointed Board would be the key to this consolidated weather modification group which would be in an existing agency. If, in the federal organization plans of President Carter, a new Department of Natural Resources is formed, this new department is where the new National Weather Resources Management Program should be placed. In the meantime, the Board realized that action would have to be taken and should be placed within NOAA. Keys to this recommendation are the consolidation of the existing efforts, within an entity that has sufficient automony to move weather modification ahead.

6. SUMMARY

One might conclude that, after reviewing the Academy assessments and the WMAB assessments, that the major call in the scientific side of weather modification is "back to the drawing board." Clearly, there is a clarion call to perform basic research in cloud physics and cloud dynamics; to carry on major experiments, hopefully better designed and conducted than those in the recent past; and to perform sufficient societal, economic, environmental research in concert to discern the allied impact and institutional type problems. Another key recommendation is to conduct, as soon as possible, some demonstration type programs that will reasonably clearly define accomplishments in the field including cloud dissipation and/or orographic snowfall changes.

On the commercial operational side of weather modification there are also some key messages. First, public-corporate usage of operational weather modification should continue. However, stan-

Table 6. Elements of a National Program

The basic elements of the 20-year action program that we are recommending are these:

- A major increase in basic research focused on atmospheric processes and problems relevant to modification.
- A program of experimental tests, some operated in parallel to expedite progress.
- An increase in efforts to include the expertise available in other countries in our own enhanced national effort.
- Continuous attention to the environmental, economic, societal, and legal aspects of weather modification.
- A program of Federal aid to State or local weather modification projects that present a sound opportunity for gaining enhanced atmospheric understanding and technical aid to States.
- The development and operation by the new Federal unit of selected joint-use facilities for weather modification research.
- The support of the planning and administrative functions of the new unit.

dards for the design and operation of programs should be strengthened and tightened, both by the industry and by the government. Finally, operational weather modification projects should be evaluated to obtain proof of modification, if possible, and certain projects should be designed in a semi-experimental way to also gain scientific knowledge.

So what is the prospectus for weather modification? Legislation to develop the recommended new national weather modification effort will be introduced in Congress in 1979. I am confident that some form of new federal organization and effort will result. How well it will fair in a period of tight finances is another matter. In one sense weather modification may be standing at its last major opportunity to get going. I feel confident about the future in weather modification, not so much because of its scientific achievements, regardless of how you view these, but because there is much better understanding and solid information about the societal issues and the environmental impacts than ever existed before. Those who will make the decisions can now weigh the impacts and consider the institutional arrangements that will be necessary, and problems can be minimized as this immature science becomes a technology.

The Weather Modification Advisory Board asked a group of nationally reknowned statisticians to assess the weather modification field (Statistical Task Force, 1978), and the views of that group are very relevant in summarizing the scientific status and prospectus for weather modification. These statistical assessors interestingly described the past and present status of weather modification with this question, "why are we in this purgatory, between the heaven of conclusive success and the hell of apparent uselessness? Basically, we (statisticians) believe, because of the difficulty of the situations and the need for completely anchored, conclusions, efforts have not been taken seriously enough." In other words, the design, operations, and evaluation have not been thorough. That august group recommends, after its critical study of recent programs, "We suggest, in view of the great importance of enhancement (precipitation), if it exists, that it is quite reasonable to go forward with experimental weather modification, but only if 1) if the experiments are conducted with the greatest care, and 2) it is generally understood that the decade, not the year, is the time step in which we hope to make progress." In my words, the road ahead is long but its worth traveling if done carefully.

7. REFERENCES

Changnon, S. A., 1978a: The technical and economic aspects of weather modification: A Background for lawyers. S. Illinois Univ. Law Journal, 2, 326-358.

Changnon, S. A., 1978b: Weather Modification in a Socioeconomic Context: Its Proper Setting. Weather Modification Technology and Law, AAAS, Washington, DC, 71-79.

Changnon, S. A., R. J. Davis, B. Farhar, J. E. Haas, J. L. Ivens, M. Jones, D. Klein, D. Mann, G. M. Morgan, S. T. Sonka, E. R. Swanson, R. C. Taylor, and J. van Blokland, 1977: Hail Suppression, Impacts and Issues. Ill. State Water Survey, Urbana, 427 pp.

Hosler, C. L., 1977: Presidential Address. Bull. Amer. Meteor. Soc., 58, 402-403.

Hsu, C. F., G. Achtemeier, F. A. Huff, and S. A. Changnon, 1978: Operational Seeding Evaluation Techniques. Second Interim Report, Ill. State Water Survey, 24 pp.

National Academy of Sciences, 1973: Weather and Climate Modification. Washington, DC, 258 pp.

Sonka, S. T., 1977: Review of the Economic Case for Weather Modification. Report to the Weather Modification Advisory Board, U. S. Dept. of Commerce, Washington, DC, 116 pp.

Statistical Task Force, 1978: The Role of Statistics in Weather Resources Management. U.S. Dept. of Commerce, Washington, DC, 94 pp.

Thompson, J., 1976: Living with Climate Change: Phase II. Symposium Report, Mitre Corp., Reston, VA.

Weather Modification Advisory Board, 1978: The Management of Weather Resources, Volume 1, Proposals for a National Policy and Program. Dept. of Commerce, Washington, DC, 229 pp.

Weather Modification Association, 1978: Statement on Standards and Ethics for Weather Modification Operations. Fresno, CA, 3 pp.

GATE RESEARCH RESULTS

Edward J. Zipser

National Center for Atmospheric Research

A selection of results from the GARP Atlantic Tropical Experiment (GATE) is presented, with some emphasis on the sub-synoptic scales. Although the synoptic disturbances in the GATE area have about a 3-4 day period and about a 2500 km wavelength, the deep convection organizes into bands and clusters that have dimensions typically less than 200-300 km. Some case studies of these mesoscale events are summarized, illustrating the difference between squall lines and other types of convective bands. There were many aircraft penetrations of cumulonimbus clouds and mesoscale systems, and some results from these are summarized. Considerable progress in understanding the interactions between boundary layer fluxes and convective systems can be reported. The talk concludes with a few personal views on the significance of GATE, and some of its limitations.

A REVIEW OF GLOBAL NUMERICAL WEATHER PREDICTION

Thomas E. Rosmond

Naval Environmental Prediction Research Facility

Monterey, California 93940

ABSTRACT

The ability to model the complete circulation of the earth's atmosphere is one of the greatest challenges of modern meteorology. The complex interactions between the two hemispheres and between tropical and mid-latitude circulations are critically important to our goal of extending the period of skillful numerical forecasts, whether they be in the tropics or higher latitudes.

A summary of the history, present status, and future expectations is presented, with emphasis on general circulation modeling and medium range (3-10 day) global numerical weather prediction. Numerical aspects are reviewed with topics including finite difference and spectral techniques and the impact of increased resolution. The physics of the models is reviewed, including cumulus parameterization, radiation, and the planetary boundary layer. A summary of the global models and global objective analysis schemes around the world is given.

The impact of advances in computer technology is discussed in the context of the global prediction problem. The interaction of vector hardware and software with model dynamics and physics has many implications for the future of global numerical weather prediction.

1. INTRODUCTION

With the development of large electronic computers in the years since 1950, tremendous resources have been devoted to the science of numerical weather prediction. The potential social and economic benefits it promised in the form of improved weather forecasts was incentive enough to justify this attention. It was not until the mid 1960s, however, that computer power was adequate to allow an attempt at the ultimate problem in atmospheric modeling: the simulation of the global general circulation.

In this paper, global modeling research that has been conducted since these first experiments is reveiwed. Both general circulation studies and global numerical weather prediction are discussed. A short survey of global objective analysis and initialization is made. Some of the outstanding problems still confronting global modelers are mentioned and the prospects for the future presented.

2. HISTORICAL BACKGROUND

The first numerical experiments to model the general circulation of the atmosphere were made at the Geophysical Fluid Dynamics Laboratory (GFDL) (Manabe et al., 1965). They were successful in simulating in at least a qualitative sense most of the features of the large scale atmospheric general circulation. Soon afterward, work on a global general circulation model was begun at the National Center for Atmospheric Research (NCAR) (Kasahara and Washington, 1967) and also at the University of California, Los Angeles (UCLA) (Mintz, 1965). Global modeling studies also were begun in England (Grimmer and Shaw, 1967).

All of the above efforts were initially oriented toward modeling the general circulation of the atmosphere with a primary goal of achieving a faithful reproduction of the earth's climate by the models. The application of these models to actual global weather forecasts initialized from real data is a more recent goal of these and other groups. Among the groups that have done work in this area are the Goddard Institute of Space Studies (GISS), the National Meteorological Center (NMC), the European Center for Medium Range Weather Forecasts (ECMWF), and the U.S. Navy. Some examples of the work being done by all of these groups is presented in the next section.

3. GLOBAL MODELS: FINITE DIFFERENCE

3.1 General Circulation Models (GCM's)

This list is made up of those models which are used primarily for general circulation studies. They are also used for numerical weather prediction and data assimilation experiments. In the following sections examples are given for model resolutions. These are only to familiarize the reader with what is typically used. Many of the models are routinely run with a wide variety of resolutions as part of the research work done with them.

a. GFDL: This group has probably had more experience with global models than any other. The most frequently published model results are from their N24 and N48 models with either 9 or 18 levels. The numbers after the N's represent the number of grid intervals between a pole and the equator, so N24 has about a 4° horizontal resolution and N48 about 2°. The horizontal differencing is unstaggered. The physical parameterizations in the model are not particularly sophisticated and so are computationally efficient. This, combined with GFDL's history of always having state-of-the-art computer power, has allowed them to run with higher resolutions than any other group.

GFDL model results have been extensively published (e.g., Miyakoda, et al., 1976; Miyakoda and Sirutis, 1977), and it has been used in model comparison studies (Baede and Hansen, 1977; Arpe et al., 1976).

b. NCAR: This model's results have been extensively published and discussed. It has been run with 5° and 2.5° unstaggered horizontal resolution and either 6 or 12 vertical levels. Research done with this model includes energetics studies (Baker et al., 1978), initialization (Houghton et al., 1971), resolution sensitivity (Williamson, 1977), and model comparison (Baumhefner and Downey, 1978). The model has also been well documented (Washington and Williamson, 1977).

c. UCLA: General circulation model development at UCLA has been successfully conducted under the direction of Y. Mintz and A. Arakawa for many years. Because of lack of computer resources they have concentrated on development of the model for its own sake, instead of concentrating on applying the model to many large scale numerical experiments. The model has evolved from a 2-level model (Langlois and Kwok, 1969) to 6- and 12-level versions (Arakawa and Mintz, 1974) (Arakawa and Lamb, 1976). Horizontal resolution is 4° x 5° staggered. The present model contains a very sophisticated cumulus parameterization (Arakawa and Schubert, 1974; Lord, 1978) and planetary boundary layer (Randall, 1976). In addition, the model contains carefully designed horizontal and vertical differencing schemes to preserve important integral properties during adiabatic integration (Arakawa and Lamb, 1977).

The UCLA model has been the basis for global model research by several other groups, including GISS, RAND Corporation, and NEPRF (U.S. Navy).

d. GISS: As mentioned above, the GISS model is a derivative of the UCLA model during the early 1970's, which at that time had 3 vertical levels. The GISS model now has 9 levels and runs on a 4° x 5° staggered horizontal grid. The adiabatic parts of the model are still similar to the original UCLA model, but the physics has been extensively modified.

GISS model results have been extensively published. Numerical experiments have been conducted on extended range forecasts (Druyan et al., 1975), energetics studies (Tenenbaum, 1976), and satellite retrieved temperature impact studies (Halem et al., 1978).

e. British Meteorological Office: This model has been under development for several years and has been used for both general circulation and numerical weather prediction experiments. It runs with either 3° or 2° unstaggered horizontal differencing and 5 or 11 levels in the vertical. Corby et al. (1973) have described the results of one experiment using this model.

f. Hydrometeorological Research Center (USSR): This model is reported to run on a 4° x 5° unstaggered grid with 5 vertical levels. Results of model integrations are not known to this author, but numerical atmospheric modeling in the USSR has lagged progress in the West because of insufficient computer power.

3.2 Numerical Weather Models

A global model used exclusively for NWP applications need not be any different from a GCM. However, for short range prediction problems certain aspects of the physics can be simplified to improve computational efficiency (e.g., radiation).

a. NMC: The NMC global model (Stackpole et al., 1974) is used in a data assimilation procedure to carry data forward in time between analysis times

(either 6 or 12 hours). The model runs with a 2° unstaggered horizontal grid and 9 vertical layers.

b. U. S. Navy (FNWC): This model is the outgrowth of development work done at the Naval Postgraduate School in Monterey, California. It is designed specifically for short range prediction. It runs with a 5° x 5° staggered grid and has 5 vertical layers. Some documentation and preliminary results have been published (Mihok and Kaitala, 1976) and the model has been tested in a quasi-operational environment to evaluate its potential for mid-latitude and tropical forecast skill.

c. U.S. Navy (NEPRF): In addition to the above model, the Navy has been pursuing the goal of a medium range forecast capability (7-10 days) sometime during the 1980's. To this end the UCLA general circulation model has been adopted as the heart of this forecast system. Some data assimilation experiments using this model have been published (Barker et al., 1977), and work continues to assess the model's skill in the mid-latitudes and tropics, where its sophisticated cumulus parameterization and planetary boundary layer are hoped to provide a better simulation of the moist physics.

d. ECMWF: This group is certainly the current leader in the problems of global numerical weather prediction, specifically for medium range forecasts. The ECMWF model is 2° or 4° staggered with 9 vertical levels, with physics of a sophistication necessary for the medium range forecast problem. Preliminary results from this model have been published (Burridge and Haseler, 1977; Baede and Hansen, 1977).

ECMWF is currently scheduled to begin operational forecasting in early 1979, at which time they will be the first operational center to be fully global. The model to be run will be the one described above with about 1.5° horizontal resolution and 15 vertical layers.

4. SPECTRAL MODELS

A brief description of global spectral models is important because many groups feel that they may eventually replace finite difference models for both GCM and NWP applications. There are several theoretical and practical advantages that support this belief, such as numerical efficiency and a natural application to spherical geometry.

a. Australian Meteorological Centre: This model is based on the work of Bourke (1974). The model runs with either 15 or 21 zonal wavenumbers with rhomboidal truncation of the spherical harmonic expansions and either 7 or 9 levels. Although the model is by nature global, in the operational application only the symmetric modes about the equator are integrated, making it a hemispheric model (southern in this case). This cuts the resource requirements by a factor of 4.

A general circulation version of this model has also been tested (McAvaney et al., 1978).

b. Atmospheric Environment Service (Canada): This model is described by Daley et al. (1976) and is currently run operationally to produce Northern Hemisphere forecasts in the same manner as described for the Australian model. The model runs with 29 zonal wavenumbers (rhomboidal truncation) and 5 or 9 vertical levels. Its skill is very competitive with that of finite difference models that are run elsewhere to produce operational forecasts.

c. ECMWF: The European Center has been evaluating a high resolution (wavenumber 40, triangular truncation, 9 level) spectral model as a possible replacement for their finite difference global model described earlier in this review. It is based on the model of Hoskins and Simmons (1975). Preliminary tests indicate its skill is very competitive with the best finite difference global models (Baede and Hansen, 1977). In its operational configuration, horizontal resolutions of wavenumber 60-80 triangular truncation and 15 layers are proposed.

d. GFDL: This model is similar to the Canadian model discussed above. It is being tested as a general circulation model with the physics of GFDL's grid point GCM's. In addition it is to be the model that GFDL will use in its data assimilation system to produce the level 3-b analyses of the FGGE data sets.

5. GLOBAL ANALYSIS AND INITIALIZATION

The following is a list of those groups around the world which can routinely produce global analyses and prepare them for initializing a global model.

a. NMC: A Hough function analysis (Flattery, 1970). The resulting fields are used directly in the global model described above. Recently NMC has been testing a 3-D multivariate-optimum

interpolation objective analysis procedure as a possible replacement of the Hough analysis. In addition a normal mode initialization procedure is being proposed.

b. NCAR: A multivariate optimum interpolation analysis followed by normal mode initialization.

c. GFDL: A univariate optimum interpolation followed by direct insertion into the model (dynamic initialization).

d. U.S. Navy (NEPRF): A 3-D successive correction (Barnes technique) followed by a calculus of variations initialization using the non-linear balance equation as a strong constraint.

e. ECMWF: A 3-D multivariate optimum interpolation analysis followed by a normal mode initialization (Larsen et al., 1977).

6. PROBLEMS OF GLOBAL MODELING

Global models share many of the same problems that plague hemispheric models or other limited area models. Truncation error due to inadequate resolution, unrealistic planetary boundary layer representation, and inadequate initial data (for NWP models) are some of these. There are some problems, however, which are unique to global models or are aggravated because of the nature of global models. The following is a partial list of these problems.

a. Lack of boundary conditions: This would seem at first to be an advantage, and in an ideal situation it would be. The problem is, however, that it allows a global model extra degrees of freedom that a hemispheric model, for example, does not have. Without boundaries in the tropics, a global model with poorly designed tropical physics will not maintain a proper N-S temperature structure between poles and equator and so will develop errors in the thermal wind. For this reason global models probably need better physics than hemispheric models, especially in low latitudes.

b. Pole problems: This is a problem unique to finite difference global models which use some form of latitude-longitude grid. The poles are singular points in spherical coordinates and must be treated with care, e.g., the wind components are not defined there. Also, the convergence of the meridians toward the poles can cause restrictive time step conditions unless E-W gradients are filtered in some way to suppress the unstable short waves. This filtering is done in a variety of ways in all finite-difference global models, but all methods produce undesirable distortion of meteorological fields around the poles. One advantage of spectral models is that they do not have this problem.

c. Energy budget problems: Figure 1 shows some ECMWF results of an experimental ten day forecast (Arpe et al., 1976) comparing the UCLA GCM and GFDL's N24 and N48 GCM's. The most noticeable feature of these forecasts is the zonal nature of the flow in the two low resolution models (UCLA and N24). The N48 model has much more amplitude in its long waves and is at least qualitatively a better representation of the verifying NMC analysis. Figure 2 shows the kinetic energy (KE) as a function of time for these models for the wavenumber bands 4-9 (synoptic scale) and 1-3 (planetary scale). All these models underpredict the KE in the long waves and only the N48 can generate sufficient KE in the synoptic waves, and then only near the end of the forecast. Figure 3 shows the horizontal mean long wave KE as a function of time and pressure for these forecasts. All three models underestimate the KE, with the high resolution N48 model being the closest to reality.

Figures 4, 5, 6, and 7 show the results of another ECMWF experiment (Baede and Hansen, 1977) comparing a low resolution spectral model (T21), a high resolution spectral model (T40), and a high resolution finite-difference model (N48). Figures 4 and 5 correspond to Figures 1 and 2 with similar results being demonstrated. Only the high resolution models can recover the KE of the synoptic waves, and all models are lacking in long wave KE.

Figures 6 and 7 are latitude-pressure diagrams of the zonally averaged, synoptic scale KE for days 4.5-7.0 and 7.5-10.0. Only the N48 model can produce a jet of realistic strength, and then only at the end of the forecast. The T40 model appear to be intensifying its jet, but it lags the finite-difference model.

These results indicate that all these models suffer from lack of kinetic energy in the planetary waves. In addition, the synoptic scale waves are poorly represented during most of the forecast period. These characteristics are critical in determining the models' meridional heat transport efficiency. It is a common problem to all GCM's that their climatologies are all too cold at the poles and too warm in the tropics. This is a consequence of this inadequate meridional heat transport.

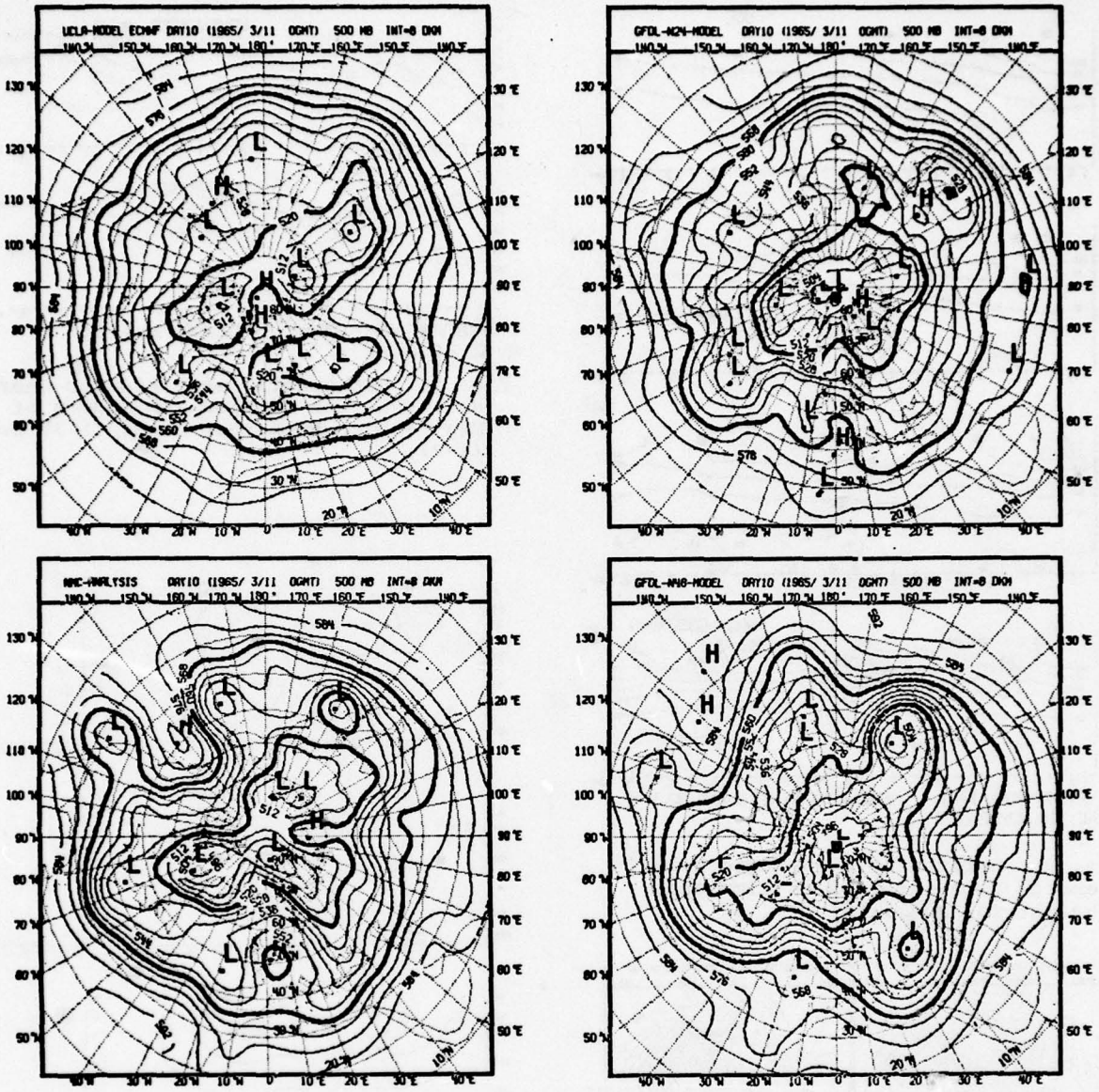

Fig. 1. 500 mb height fields for experimental 10-day forecasts by ECMWF with UCLA GCM and two GFDL GCM's, compared to verifying NMC analysis.

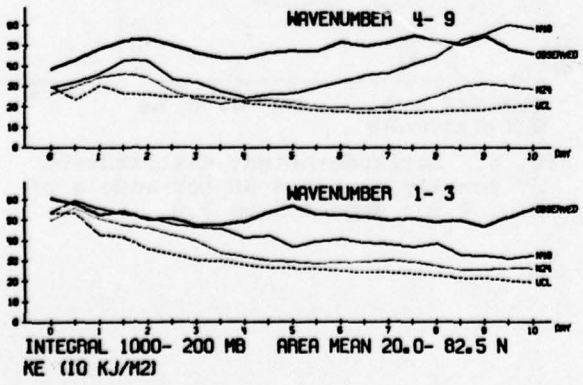

Fig. 2 (at left. Hemispheric means kinetic energy as a function of time for models of Fig. 1 for wavenumber bands (1-3) and (4-9).

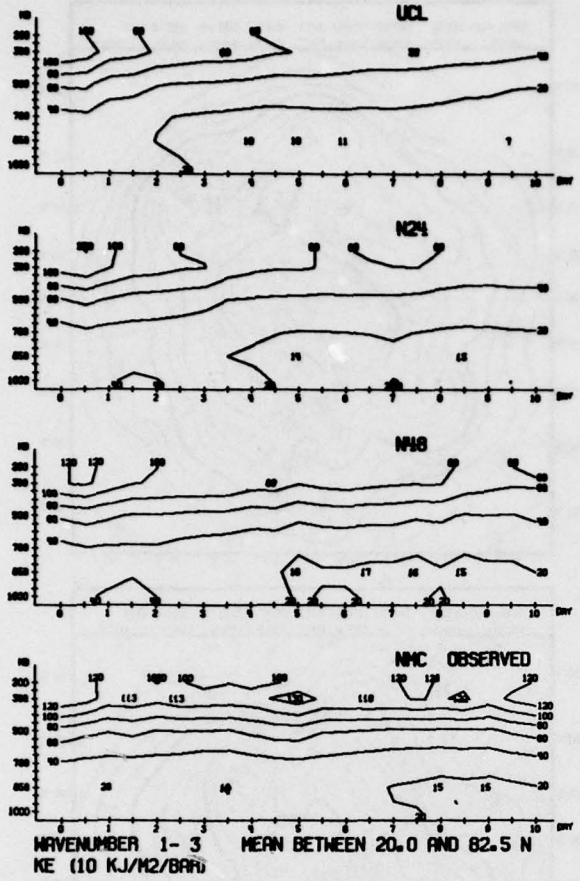

Fig. 3. Horizontally averaged kinetic energy as a function of time and height for models of Fig. 1.

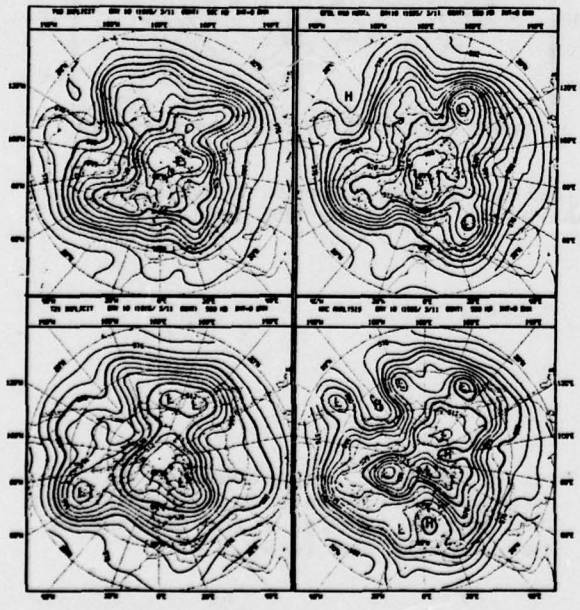

Fig. 4. 500 mb height fields for experimental 10-day forecasts by ECMWF with two spectral models and a finite difference model compared to verifying NMC analysis.

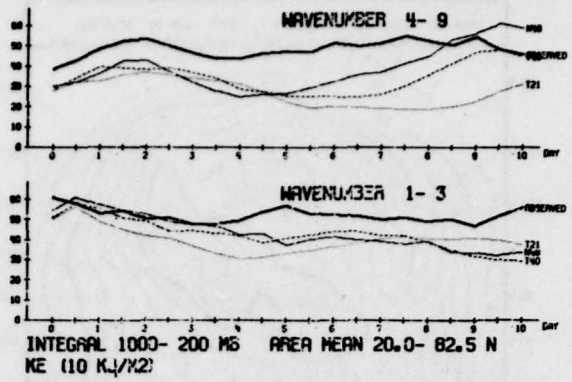

Fig. 5. Hemispheric mean kinetic energy as a function of time for models of Fig. 4 for wavenumber bands (1-3) and (4-9).

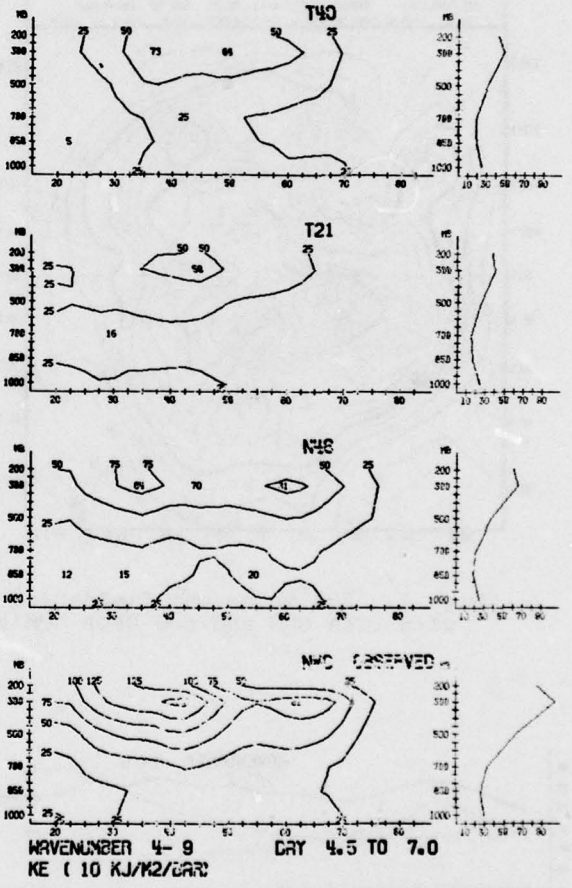

Fig. 6. Latitude-height distribution of zonally averaged KE for models of Fig. 4 for days 4.5 to 7.0.

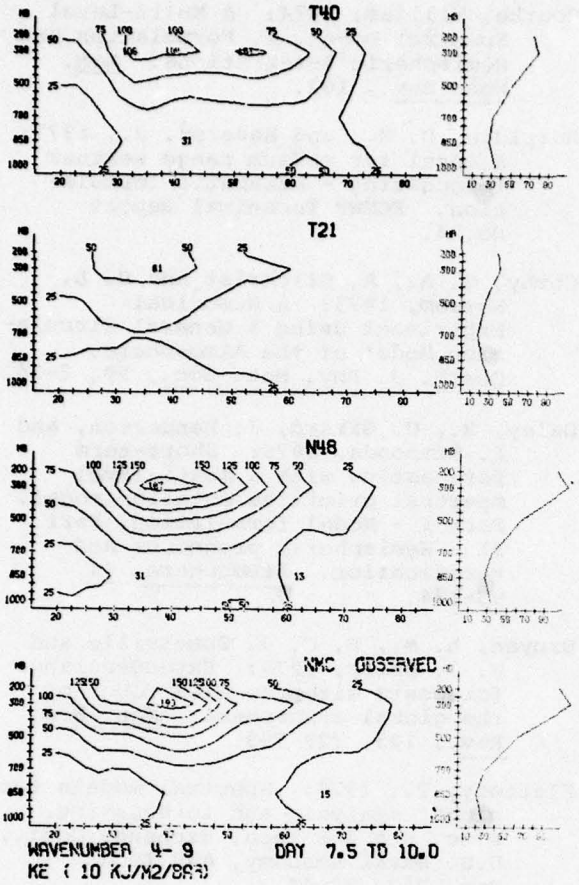

Fig. 7. Latitude-height distribution of zonally averaged KE for models of Fig. 4 for days 7.5 to 10.0.

7. SUMMARY AND CONCLUSIONS

In this review we have presented a brief summary of where global atmospheric modeling stands today. Global modeling certainly represents one of the greatest challenges to meteorologists today, either for operational application or from a research point of view. The tremendous resources required to mount an effective global modeling program means that some care must be taken in deciding if the potential benefits justify this effort. Certainly for GCM studies they are essential, since only a global model can properly represent the complex interactions that determine the general circulation. For the medium range forecast problem a global model is necessary, since tropical mid-latitude interactions are critical for proper forecasts at this range. Also, if numerical tropical forecasts are desired, a global model is probably necessary, since many important tropical meteorological events are the result of interaction with higher latitudes.

But if running a global model is a necessary condition to satisfy these goals, is it a sufficient condition? Here, there is some uncertainty. As we have seen, today's models still suffer from some systematic problems that must be solved before many of the global model requirements we have established will be satisfied. For example, can we make a skillful medium range forecast of storm track if our model cannot properly forecast planetary wave amplitude, perhaps because of poor mountain-atmospheric interaction? Can we make a useful tropical forecast (e.g., easterly wave development) if our simulation of planetary boundary layer-cumulus convection interaction is inadequate, as it probably is in all current models? Can a GCM (or a mid-range forecast model) generate a realistic climatology if the stratosphere is poorly represented, or in some models absent?

The list could go on, but these questions give an idea of what problems remain to be solved before our goals for global model application are realized. The upcoming first GARP global experiment (FGGE) will for the first time give us a complete data base with which to initialize our global models and verify the forecasts made. In addition, it will be possible to make careful diagnostic studies of the nature of the interactions between tropics and mid-latitude, from which improved parameterizations of the important physical processes can hopefully be developed. In short, for the first time we may be able to give the global models the same kind of data coverage that Northern Hemispheric models have had for years. Hopefully a significant improvement in the skill of the NWP models and realism of the GCM's will be achieved and the 1980's will be the beginning of the era of improved atmospheric modeling and forecasting on a global scale.

As a final comment, and one which is not usually a subject of a review such as this, it is appropriate to mention that global modeling from a computer programming point of view is in itself a considerable challenge. The typical global modelling system is very tightly built around a specific computer hardware and software system, so it is not very portable. Yet the expense of developing such a system makes it very desirable to be able to share software programs to minimize duplication of effort.

To achieve this end it is essential that software be made as modular as possible and that the principles of structured programming and design be followed. This will be especially true for the software developed for the new

vector processing computers now available. The difference between efficient and inefficient code on these machines is enormous, so the economic benefits of using the best techniques available are quite large. It is the future responsibility of those working in global modeling that the necessary effort be made to insure that their field does not become an economic burden too great for the possible benefits it can deliver.

8. REFERENCES

Arakawa, A., and Y. Mintz, 1974: The UCLA Atmospheric General Circulation Model. Notes distributed at the workshop, 25 March-4 April, 1974, Dept. Meteorology, UCLA, Los Angeles.

Arakawa, A. and W. H. Schubert, 1974: Interaction of a cumulus cloud ensemble with the large-scale environment, Part 1. J. Atmos. Sci., 31, 674-701.

Arakawa, A., and V. R. Lamb, 1976: Computational design of the basic dynamical processes of the UCLA general circulation model, in Methods in Computational Physics, Vol. 17, Academic Press, Inc., New York, 1976.

Arpe, K., L. Bengtsson, A. Hollingsworth and Z. Janjic, 1976: A case study of a 10 day prediction. Tech. Rep. No. 1, European Centre for Medium Range Weather Forecasts, Bracknell, England, 105 pp.

Baede, A. P. M. and A. W. Hansen, 1977: A ten-day high resolution non-adiabatic spectral integration - a comparative study. ECMWF Technical Report No. 7.

Baker, W. E., E. C. Kung and R. C. J. Somerville, 1978: An energetics analysis of forecast experiments with the NCAR GCM. Mon. Wea. Rev., 106, 311-323.

Barker, E. H., G. J. Haltiner and Y. K. Sasaki, 1977: Three-Dimensional Initialization Using Variational Analysis, Proceedings of the Third Conference on Numerical Weather Prediction, April 20-28, 1977, Omaha, NE, pp. 169-181.

Baumhefner, David, Patrick Downey, 1978: Forecast Intercomparisons from Three Numerical Weather Prediction Models. Mon. Wea. Rev., 106, 1245-1279.

Bourke, William, 1974: A Multi-Level Spectral Model. I. Formulation and Hemispheric Integrations. Mon. Wea. Rev., 102.

Burridge, D. M., and Haseler, J., 1977: A model for medium range weather forecasting - adiabatic formulation. ECMWF Technical Report No. 4.

Corby, G. A., A. Gilchrist and R. L. Newsom, 1973: A Numerical Experiment Using a General Circulation Model of the Atmosphere. Quart. J. Roy. Met. Soc., 99, 2-34.

Daley, R., C. Girard, J. Henderson, and I. Simmonds, 1976: Short-term forecasting with a multi-level spectral primitive equation model, Part I - Model formulation, Part II - Hemispheric prognoses and verification. Atmosphere, 14, 98-134.

Druyan, L. M., R. C. J. Somerville and W. J. Quirk, 1975: Extended-range forecasts with the GISS model of the global atmosphere. Mon. Wea. Rev., 103, 779-795.

Flattery, T., 1970: Spectral models for global analysis and forecasting. Proc. 6th AWS Tech. Exchange Conf., U.S. Naval Academy, AWS Tech. Rep. 242, 32-44.

Grimmer, M., and D. B. Shaw, 1967: Energy preserving integrations of the primitive equations on the sphere. Quart. J. Roy. Meteor. Soc., 93, 337-349.

Halem, M. M. Shil, R. Atlas, J. Susskind and W. J. Quirk, 1978: The GISS Sounding Temperature Impact Test. NASA Technical Memo 78063, Goddard Space Flight Center, Greenbelt, Maryland.

Houghton, D. D., D. P. Baumhefner and W. M. Washington, 1971: On the global initialization of the primitive equations. Part 2: The divergent component of the horizontal wind. J. Appl. Meteor., 10, 626-634.

Kasahara, A. and W. M. Washington, 1967: NCAR global general circulation model of the atmosphere. Mon. Wea. Rev., 95, 389-402.

Langlois, W. E., and H. C. W. Kwok, 1969: Description of the Mintz-Arakawa numerical general circulation model, Part I. Numerical simulation of weather and climate. IBM Research Laboratory, San Jose, California, 99 pp.

Larsen, G., A. Lorenc, and I. D. Rutherford, 1977: The ECMWF Analysis and Data-Assimilation Scheme - Analysis of Mass and Wind Fields. ECMWF Technical Report No. 6.

Lord, Stephen J., 1978: Development and Observational Verification of a Cumulus Cloud Parameterization. Ph.D. Thesis, UCLA, 359 pp.

McAvaney, B. J., William Bourke, and Kanal Puri, 1978: A Global Spectral Model for Simulation of the General Circulation. J. Atmos. Sci., 35, pp. 1557-1583.

Manabe, S., J. Smagorinsky, and R. F. Strickler, 1965: Simulated Climatology of a General Circulation Model with a Hydrologic Cycle. Mon. Wea. Rev., 93, 769-798.

Mihok, W. F., and J. E. Kaitala, 1976: U. S. Navy Fleet Numerical Weather Central Operational Five-Level Global Fourth-Order Primitive-Equation Model. Mon. Wea. Rev., 104.

Mintz, Y., 1965: Very long term global integration of the primitive equations of atmospheric motion. WMO Tech. Note No. 66, Geneva, 144-176.

Miyakoda, K., L. Umscheid, D. H. Lee, J. Sirutis, R. Lusen, and F. Pratte, 1976: The Near Real-Time Global Four-Dimensional Analysis Experiment During the Gate Period, Part I. J. Atmos. Sci., 33, 561-591.

Miyakoda, K. and J. Sirutis, 1977: Comparative Integrations of Global Models with Various Parameterized Processes of Subgrid Scale Vertical Transports: Descriptions of the Parameterizations. Contr. to Atmos. Phy., 50 445-487.

Randall, D. A., 1976: The Interaction of the Planetary Boundary Layer with Large-Scale Circulations. Ph.D. Thesis, UCLA, 247 pp.

Stackpole, J. D., L. W. Vanderman and F. G. Shuman, 1974: The NMC 8-layer global primitive equation model on a latitude-longitude grid. Modelling for FGGE, GARP Publ. Ser. No. 14, 79-93.

Tenenbaum, J., 1976: Spectral and spatial energetics of the GISS model atmosphere. Mon. Wea. Rev., 104, 15-30.

Washington, W., and D. L. Williamson, 1977: A description of the NCAR global circulation models. Methods in Computational Physics, Vol. 17, General Circulation Models of the Atmosphere, Academic Press, 111-172.

Williamson, David L., 1978: The Relative Importance of Resolution Accuracy and Diffusion in Short-Range Forecasts with the NCAR Global Circulation Model. Mon. Wea. Rev., 106, 69-88.

SOLAR/TERRESTRIAL METEOROLOGICAL RELATIONSHIPS

John M. Wilcox

Institute for Plasma Research
Stanford University
Stanford, California 94305

ABSTRACT

Some possible relationships are described between the solar magnetic field that is carried past the earth by the solar wind and tropospheric circulation. A minimum in the wintertime vorticity area index (area of low-pressure troughs) is observed following transits past the earth of interplanetary magnetic sector boundaries. A decline in forecast accuracy appears to be related to this minimum. Some relationships with the Lorenz energy parameters are discussed.

1. INTRODUCTION

A recent note in Nature asked "Does the troposphere respond to day-to-day changes in solar magnetic field?" (Williams & Gerety, 1978). I would like to address this question.

First, some perspective on the present status of sun-weather investigation. We may distinguish between exploratory and confirmatory investigations. In exploratory work one is trying to see what's out there. The imagination is given free reign, and it is possible to change the course of the investigation halfway through as new possibilities develop. If, as a result of an exploratory investigation, an author wishes to assert that a particular physical relationship exists, then we move to the confirmatory stage. Here the hypothesis to be tested must be carefully formulated. A considerable part of the investigation should involve random data for comparison with the purported real effect. Exquisite statistical techniques are used to analyze the results. In my opinion, sun-weather research at the present time is strictly in the exploratory stage. Some very interesting possibiliites for future investigations have been unearthed but no influence of the changing sun on the weather has been confirmed beyond the shadow of a doubt.

2. THE SOLAR AND INTERPLANETARY MAGNETIC FIELD

I will describe a structure of the solar and therefore the interplanetary magnetic field that has been extensively investigated as a possible influence on the weather. There are other possible solar influences such as transient flares that send shock waves out into the solar wind. However. we will restrict the present discussion to a quasi-stationary magnetic structure.

Figure 1 is a painting of a warped electric current sheet in the heliosphere -- i.e. the region of space in which the influence of the sun is predominant. As a first approximation the current sheet is in the plane of the sun's equator, but the next approximation is very important. The current sheet is warped north and south of the equator as shown in the painting. This structure in the heliosphere has its source in a similar large-scale structure of the sun's magnetic field. The current sheet has the property that on one side the magnetic field is directed away from the sun and on the other side the field is directed toward the sun, i.e. the current sheet reverses the direction of the field by 180^{o}.

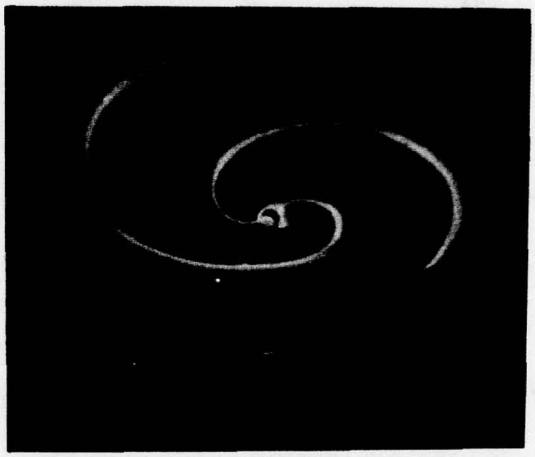

Figure 1. A painting of the warped heliospheric current sheet. At the present time the region of the heliosphere above the current sheet has interplanetary magnetic field directed away from the sun and the region below the sheet has field directed toward the sun. The entire structure rotates with the sun and sweeps past the earth in 27 days.

To aid in visualizing the geometry of the current sheet Figure 2 shows a polar cross-section and Figure 3 shows an equatorial cross-section. The entire structure rotates with the sun and therefore makes one complete rotation past the earth in about 27 days.

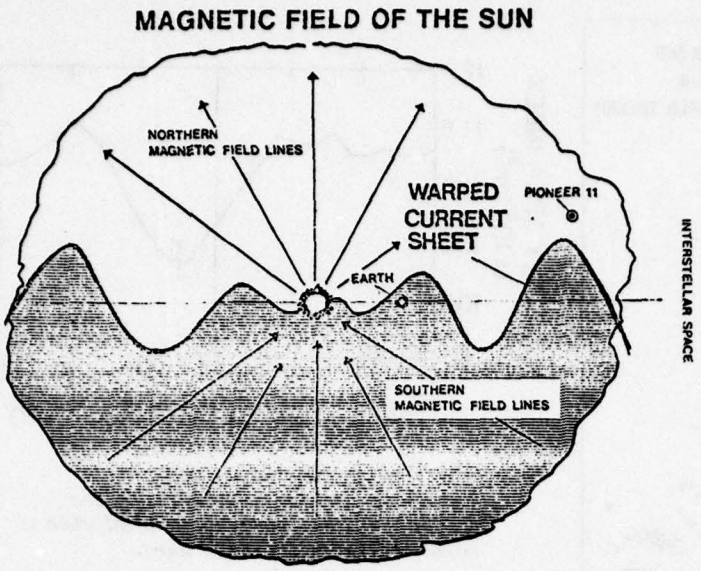

Figure 2. A polar cross-section of the warped current sheet.

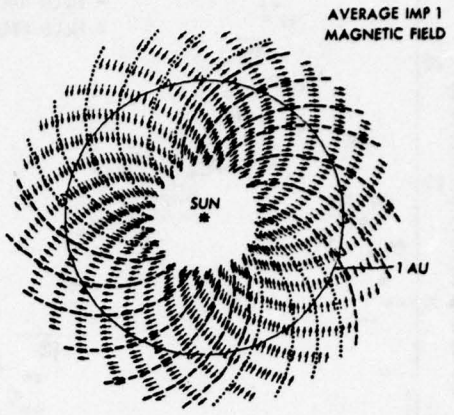

Figure 3. An equatorial cross-section of the current sheet.

The solar magnetic field that is the source of the heliospheric current sheet is observed using the Zeeman effect at several solar observatories, including our Stanford Solar Observatory. The resulting interplanetary magnetic field is observed near the earth with spacecraft so that the structure is pretty well tied down observationally.

The solar wind carries the sun's magnetic field from sun to earth in about five days. Thus, if we observe a magnetic structure on the sun then we have a forecast possibility of at least five days with regard to possible terrestrial effects of that structure.

There is some variation in the warped current sheet from one solar rotation to the next. Figure 3 shows four sectors of magnetic field that rotate past the earth. From one solar rotation to the next the size of a particular sector may change somewhat, and sometimes the warped current sheet flattens so much that only two sectors are observed at the earth. There is thus not a sharp 27-day periodicity in the sector structure observed at earth.

3. TERRESTRIAL RESPONSE TO THE SOLAR MAGNETIC FIELD

Figure 4 shows a change in geomagnetic activity associated with the sector structure that was shown in Figures 1-3. The zero time in Figure 4 is the time when the warped current sheet was observed to be carried past the earth by the solar wind. The ordinate is a measure of global geomagnetic activity -- the amount of disturbance in the earth's magnetic field. Figure 4 is a superposed epoch analysis, i.e. it is the average of many cases of boundary transits past the earth. By averaging together many cases we can emphasize structure that is physically related to the boundary transit and tend to average out structure (and noise) that is not so related.

Figure 5 is a schematic of the variation of the solar wind velocity and density after a boundary transit. The time just before a boundary transit tends to be a minimum in quantities such as solar wind velocity and density, the magnitude of the interplanetary magnetic field and geomagnetic activity. All of these quantities rise sharply at and after the boundary and reach a maximum about two days later. The intensity of galactic cosmic rays measured at earth has just the opposite variation -- a maximum before the boundary and a minimum a couple of days later. This is related to the process by which kinks in the interplanetary magnetic field moving outward in the solar wind tend to sweep galactic cosmic rays out with them. The sector structure was reviewed in Wilcox (1968).

Figure 6 shows the variation in the vorticity area index (VAI) associated with the sector structure. The zero day is when the warped current sheet was carried past the earth by the solar wind. The ordinate is the VAI computed in the northern hemisphere during the winter. It is basically a measure of the area of low-pressure troughs and is described by Roberts and Olson (1973). We see that the VAI has a minimum a day or two after the boundary transit at the time when most of the solar wind quantities discussed above are near maximum, (Wilcox, *et al.*, 1973).

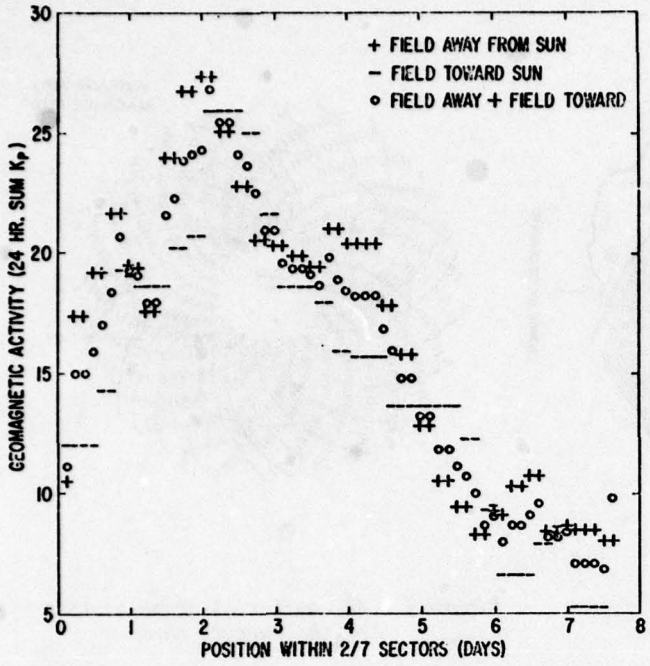

Figure 4. The average response of the geomagnetic activity index Kp associated with sector boundary transits. Zero day is when the warped current sheet shown in Fig. 1 was carried past the earth by the solar wind.

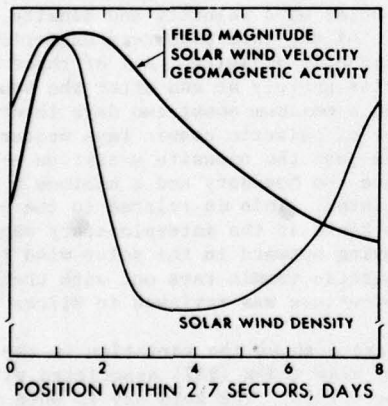

Figure 5. A schematic of the variation of the solar wind velocity and density after a sector boundary transit.

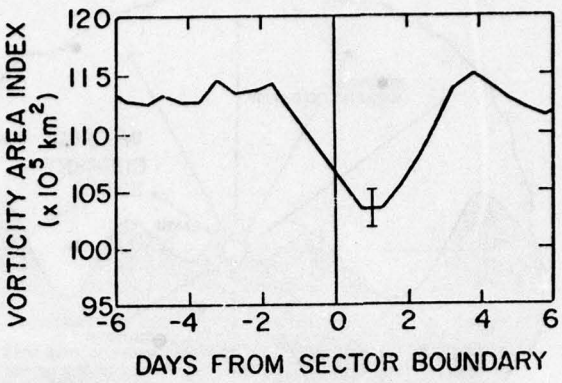

Figure 6. Average response of the vorticity area index associated with a boundary transit on day zero.

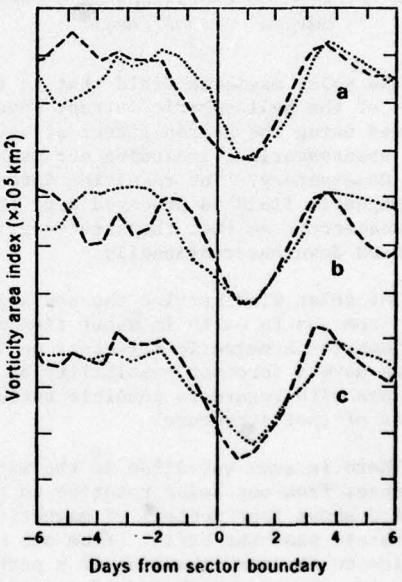

Figure 7. The same as Fig. 6 except that the list of boundary transits has been divided into three two-part groupings. 1) The magnetic polarity change at the boundary. 2) The first or last half of winter. 3) The yearly intervals 1964-66 and 1967-70.

4. SIGNIFICANCE OF THE MINIMUM IN VORTICITY AREA INDEX

How significant and meaningful is the minimum in VAI after boundary transits? We first compute the standard error of the mean of all the cases shown in Figure 6. The resulting error bar shown in Figure 6 is satisfyingly small. However, much more evidence will be needed before we begin to consider this a serious result. Figure 7 shows the result of dividing the boundary transits used in computing Figure 6 into two parts in three different ways. The minimum in VAI after boundary transit is seen to persist through this division.

Figure 8 shows an analysis of 50 boundary transits in the winters of 1964-70 and an

analysis of 81 new and independent transits in the winters of 1963-73. The VAI minimum is seen to persist in the new data.

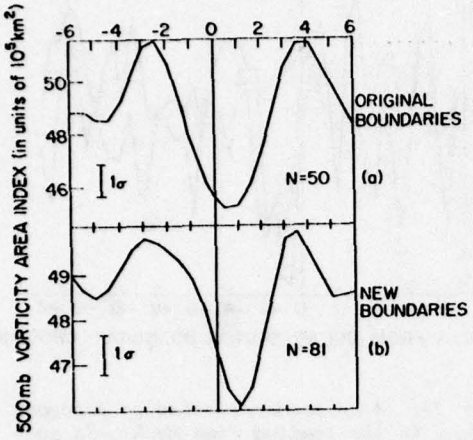

Figure 8. The same format as Fig. 6, but showing an analysis of 50 original boundary transits in the winters 1964-70 and 81 new independent boundary transits in the winters 1963-73.

In Figure 9 the northern hemisphere is divided into a latitude zone of 35°N-55°N and of 55°N-90°N. The minimum in VAI is seen to persist in both of these zones. It might be objected that the entire northern hemisphere tends to change in the same way from one day to the next so that the two latitude zones shown in Figure 9 are not independent tests. To investigate this possibility Figure 10 was constructed. We examined the VAI as a function of time in the latitude zone 35°N-55°N and selected as key times all the minima in VAI in this zone that were not near boundary transits. Figure 10 shows the average variation in the VAI associated with these key times. I emphasize that the same key times were used for both curves in Figure 10. The VAI in the zone 35°N-55°N shows a deep minimum since the key times were selected to make it do so, but the VAI in the zone 55°N-90°N shows no minimum at all. Thus, it seems that after boundary transits the VAI in both zones reached a minimum, while at other times minima in one zone were not related to minima in the other zone. I get a feeling that after boundary transits something may have grabbed the tropospheric circulation in the entire northern hemisphere. Let me repeat, however, that this is an exploratory statement and not yet a confirmatory statement.

The most important discussion of the significance of these results was by Colin Hines and Itamar Halevy. In a letter to Nature (1975) they said "Reports of short-term sun-weather correlations have been greeted with skepticism by many". They described a variety of statistical tests they had performed, and also the analysis of new

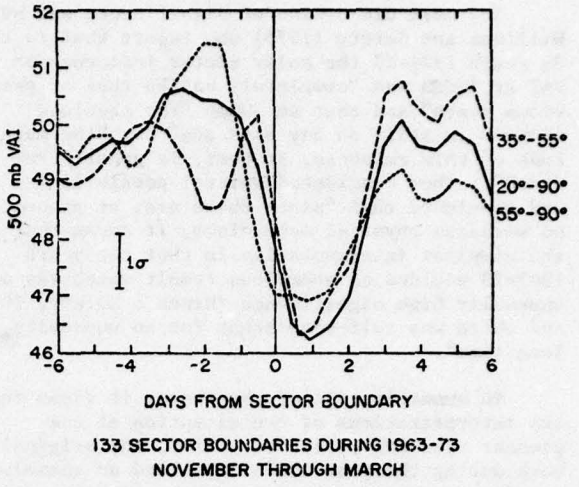

Figure 9. The same format as Fig. 6, but with the northern hemisphere divided into latitude zones 35°N-55°N and 55°N-90°N. Both zones show a minimum in VAI following boundary transits.

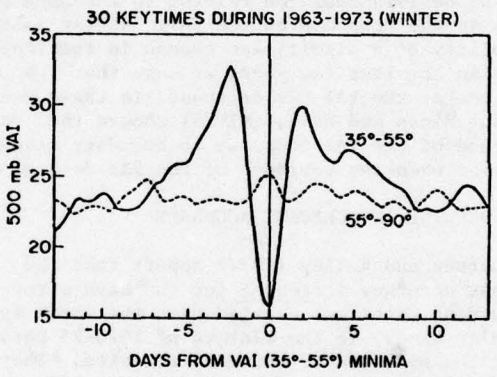

Figure 10. The same format as Fig. 9, except that zero times represent times of minimum VAI in the 35°N-55°N zone. The higher latitude zone shows no minimum VAI at this time, unlike the case following boundary transits shown in Fig. 9.

data as mentioned above. They then said "We find ourselves obliged to accept the validity of the claim by Wilcox et al. and to seek a physical explanation".

The next discussion of significance was by Larsen and Kelley in Geophysical Research Letters (1977). They used the Limited Fine Mesh grid over North America in the winters of 1973-75 and said "In this paper we report a completely independent repetition and extension of Wilcox's technique using data from a different time period and from a different source of the meteorological input. As discussed below, we have found the same decrease in vorticity area index one day following sector boundary crossings".

The next discussion of significance was by Williams and Gerety (1978) who report that in the 3½ years 1974-77 the solar sector influence on VAI at 500mb was "completely unlike that of previous years" and that at 300mb "the absolute minimum is still on day plus one" but "the magnitude of this response, at best, is greatly reduced". They considered several possibilities and concluded that "since there are, at present, no workable physical mechanisms, it seems that the simplest interpretation is that the years 1963-73 yielded an anamolous result which was of unusually high significance (Hines & Halevy, 1977) and which was self-consistent for an unusually long time".

To summarize all of the above, it seems that two interpretations of the situation at the present time are possible. First, the original work during the year 1963-73 yielded an anamolous result, or second, the troposphere probably did respond to the solar and interplanetary magnetic sector structure during 1963-73, and further analysis of that situation since that time is required. We might gain valuable information on the physical mechanism if a change in some solar, interplanetary or atmospheric quantities in the years since 1974 could be related to the apparent change in the response of the VAI. As far as the possibility of a significant change in the troposphere in the last few years we note that the magnitude of the VAI has decreased in these years, and that Hines and Halevy (1975) showed that the amplitude of the VAI response to boundary transits decreased when the variance of the VAI decreased.

5. A DECLINE IN FORECAST ACCURACY

Larsen and Kelley (1977) report that the forecast accuracy decreased for two days after the current sheet was carried past the earth by the solar wind. In the winters of 1973-75 Larsen and Kelley examined 47 boundary transits. They used the 24-hour (and 12-hour) forecast VAI on the Limited Fine Mesh grid over North America. On the 47-transit days they computed a cross-correlation between the 47 values of forecast VAI and 47 values of observed VAI. This cross-correlation is plotted on zero day in Figure 11. The exercise is repeated for several days before and after boundary transits. Figure 11 suggests that the forecast accuracy was significantly smaller in the two days following boundary transits as compared with other times. This important work should be repeated and extended to improve the statistics.

Larsen and Kelley (1977) said "A second major result of the present study is that the ability to predict the area of low-pressure deteriorates for several days after a sector boundary crossing. The decrease in accuracy at the time of the boundary crossing seems to indicate that there is an input to the atmosphere which is not included in the formulation of the model and which is not significant at other times. With the assumptions built into the model we are left with at least two alternatives. One arises

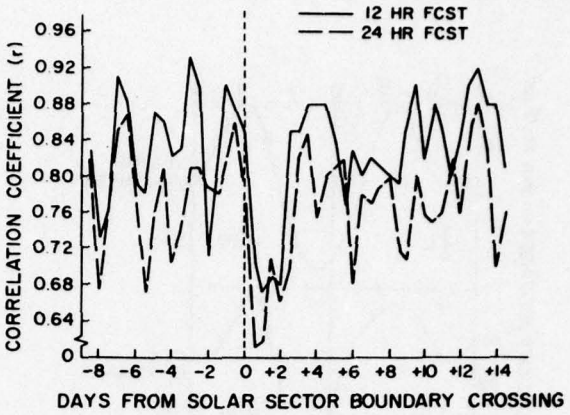

Figure 11. A cross-correlation of forecast accuracy in the Limited Fine Mesh grid over North America related to the time of sector transits. In the two days following sector transits the forecast accuracy is significantly reduced.

from the basic condition that the model does not include diabatic heating effects. This leads to the possibility that there is some form of diabatic input (which could be dissipative) between successive initialization periods leading to the decrease in the model's accuracy. Another possibility arises from the exclusion of sound waves and gravity waves from the dynamics of the model".

The study of Larsen and Kelley was only possible because Pennsylvania State University had archived the daily prognostics. In earlier attempts to do similar studies we repeatedly found that prognostics were archived only as weekly or more commonly monthly averages. It seems very important that in the future the relevant observations and prognostics be archived on a daily basis so as to permit investigations of the claimed sun-weather relationships.

6. THE LORENZ ENERGY CYCLE

It has been suggested that the VAI is too specialized, having been prepared just for sun-weather investigations, and is not in the mainstream of meteorology. The above discussion of the deterioration of forecasts after sector boundary transits certainly involves mainstream meteorology. Another link between the VAI and standard meteorological quantities is an investigation by Williams (1978) using the four components of the Lorenz energy cycle: zonal available energy, eddy available energy, zonal kinetic energy and eddy kinetic energy.

We may approach this investigation by considering five predictions that might reasonably have been made from the work described so far: 1) Of the four energy parameters, the eddy

kinetic energy would have a minimum after boundary transits, since it is the most similar to the VAI. 2) The minimum would be seen in winter but not in summer. 3) The minimum would be seen at 300 and 500mb. 4) The minimum would not be seen at 100mb. 5) The largest effect would be seen for wave numbers five or six since this would represent the same spatial scale as the troughs described by the VAI.

Let us test these predictions. 1) Williams (1978) found that the Lorenz "eddy kinetic energy displays a response which is similar in nature to but of lesser amplitude in statistical significance than the VAI response" and that "the other three (Lorenz) parameters do not show such apparently significant results". Prediction confirmed. 2) Williams (1978) reports that the sector structure influence on eddy kinetic energy "is similar to the VAI result inasmuch as it appears to be a winter phenomena". Prediction confirmed. 3) Williams (1978) reports that the sector structure influence on eddy kinetic energy "is at its greatest at 500 and 300mb". Prediction confirmed. 4) Williams (1978) reports that the sector structure influence on eddy kinetic energy "largely disappears at 100mb". Prediction confirmed. 5) The analysis of the response to the sector structure of the eddy kinetic energy for the first ten component wave numbers has not yet been done. Prediction remains to be tested.

Of the five predictions, four were confirmed and one remains to be tested.

7. POSSIBLE PHYSICAL MECHANISMS

Clues to possible physical mechanisms for the influence of the solar magnetic sector structure on the VAI may be found from reports that: 1) The magnitude of the vertical electric field at ground level (and therefore the potential of the ionosphere with respect to the earth) changes by 10 or 15% after the passage of interplanetary magnetic sector boundaries (Reiter, 1977; Park, 1976). 2) Incursions of stratospheric air into the troposphere after the passage of sector boundaries have been observed by Reiter (1977). 3) A change in solar *euv* irradiation related to the solar magnetic sector structure has been reported by Heath *et al.* (1975). 4) The cosmic ray flux detected with the Deep River neutron monitor changes with the position of the earth in the interplanetary sector structure (Wilcox & Ness, 1965). 5) Geomagnetic activity increases after the passage of the sector boundary (Wilcox & Ness, 1965). 6) Some boundaries are followed in the interplanetary medium by streams of *mev* protons that last for a few days (Wilcox & Ness, 1965; Svestka *et al.*, 1976). These boundary transits are associated with a larger response of VAI (Wilcox, 1978).

We will describe point 6) in a little more detail. Using the list of boundary transits associated with *mev* proton streams as published by Svestka *et al.* (1976), we divide all boundary transits in winters 1963-69 into those followed by *mev* proton boundaries and all other boundaries during these winters.

Figure 12 shows the response of the VAI associated with the proton boundaries (solid line) and the other boundaries (dashed line). We see that the minimum after proton boundary transits was about twice as deep as compared with the other boundary transits. In this figure the VAI was computed at 500mb for the area with vorticity $\geq 20 \times 10^{-5} s^{-1}$ plus the area with vorticity $\geq 24 \times 10^{-5} s^{-1}$.

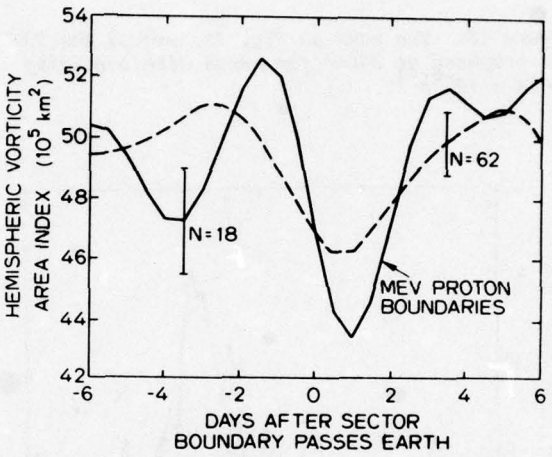

Figure 12. The change in VAI associated with mev proton boundary transits (solid line) and other boundary transits (dashed line). The VAI was computed at 500mb for areas with vorticity $\geq 20 \times 10^{-5} s^{-1}$ plus areas with vorticity $\geq 24 \times 10^{-5} s^{-1}$.

Figure 13 is the same as Figure 12 except that the VAI was computed at 300mb and for the area with vorticity $\geq 28 \times 10^{-5} s^{-1}$. Again, the minimum associated with proton boundary transits is at least twice as deep. Note that the area in Figure 13 is about ten times less than in Figure 12. A very similar response is thus seen in two rather different parts of the troposphere.

Having examined the response of the VAI to proton boundary transits, let's examine the response of geomagnetic activity. Remember that the increase of geomagnetic activity after boundary transits was first published fourteen years ago and has been repeated many times so that it is now a well-accepted result. Figure 14 shows the response of geomagnetic activity associated with proton boundary transits (solid line) and the other boundary transits (dashed line). We note that there is a large increase in geomagnetic activity after proton

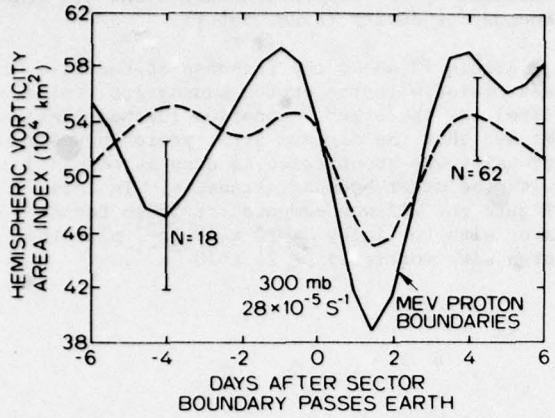

Figure 13. The same as Fig. 12, except the VAI was computed at 300mb for areas with vorticity $\geq 28 \times 10^{-5} s^{-1}$.

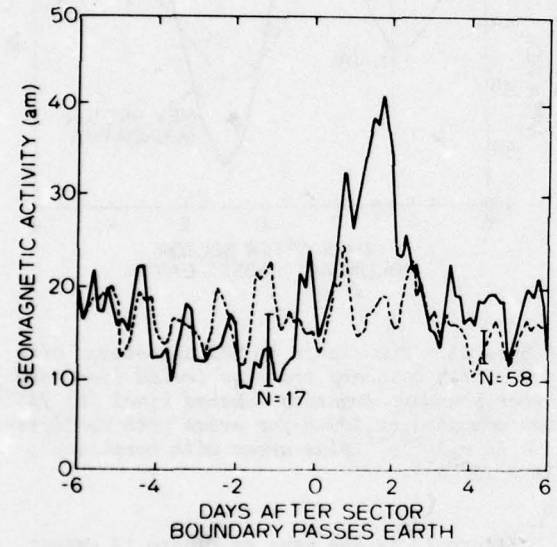

Figure 14. Change of the geomagnetic activity index am *associated with proton boundaries and with the other boundaries.*

boundary transits but not significant variation associated with the other boundary transits. Since the other boundary transits were associated with a well-defined minimum in VAI it appears that the response of the VAI to the sector structure is more persistent than the well-accepted response of geomagnetic activity.

8. CONCLUSION

To conclude I would like to quote the end of the paper by Larsen and Kelley (1977): "The present study has verified some of the results previously presented and provided possibilities for future study of the interesting and enigmatic relation between solar emissions and the tropospheric circulation. Although the mechanism for this interaction still remains a mystery, this study provides another set of clues dealing with its nature. Finally, it is hoped that this will form one more step towards the inclusion of the effects described in routine forecasting procedures".

Acknowledgements

This work was supported in part by the Office of Naval Research under Contract N00014-76-C-0207, by the National Aeronautics and Space Administration under Grant NGR 05-020-559 and Contract NAS5-24420 and by the Atmospheric Sciences Section of the National Science Foundation under Grant ATM-20580

References

Heath, D.F., J.M. Wilcox, L. Svalgaard and T.L. Duvall, 1975: Relation of the observed far ultraviolet solar irradiances to the solar magnetic sector structure. *Solar Physics*, 45, 79-82.

Hines, C., and I. Halevy, 1977: On the reality and nature of a certain sun-weather correlation. *J.Atmos.Sci.*, 34, 382-404.

_____, and _____, 1975: Reality and nature of a sun-weather correlation. *Nature*, 258, 313-314.

Larsen, M., and M. Kelley, 1977: A study of observed and forecasted meteorological index and its relation to the interplanetary magnetic field. *Geophys.Res. Lett.*, 4, 337-340.

Reiter, R., 1977: The electric potential of the ionosphere as controlled by the solar magnetic sector structure - result of a study over the period of a solar cycle. *J.Atmos.Terr.Phys.*, 39, 95.

Roberts, W.O., and R.H. Olson, 1973: New evidence for effects of variable solar corpuscular emission on the weather. *Rev. Geophys. & Space Phys.*, 11, 731-740.

Svestka, Z., L. Fritzova-Svestka, J.T. Nolte, H.W. Dodson-Prince and E.R. Hedeman, 1976: Low-energy particle events associated with sector boundaries. *Solar Physics*, 50, 491-500.

Wilcox, J.M., 1979: *Solar Terrestrial Influences on Weather and Climate*, B.M. McCormac and T.A. Seliga (eds.), D. Reidel Pub., Co., Dordrecht, Holland.

_____, P.H. Scherrer, L. Svalgaard. W.O. Roberts and R.H.Olson, 1973: Solar Magnetic Sector Structure: Relation to Circulation of the Earth's Atmosphere. *SCIENCE*, 180, 185-186.

_____, 1968: The interplanetary magnetic field, solar origin and terrestrial effects. *Space Sci. Rev.*, 8, 258.

_____, and N.F. Ness, 1965: Quasi-stationary corotating structure in the interplanetary medium. *J.Geophys.Res.*, 70, 5793-5805.

Williams, R.G., 1978: A study of the energetics of a particular sun-weather relation. *Geophys.Res.Lett.*, 5, 519-522.

_____, and E.J. Gerety, 1978: Does the troposphere respond to day-to-day changes in solar magnetic field? *Nature*, 275, 200-201.

SEVERE WEATHER FORECASTING

Frederick Ostby

NOAA/NWS/NSSFC

It has been 30 years since Fawbush and Miller made the first tornado forecast and many of their subjective techniques are still in use. The survey will discuss the present blend of subjective and objective methods. Great strides have been made in the use of model output statistics by members of the NWS's Technique Development Laboratory. With rare exceptions there has been less success in purely dynamical solutions. The survey will discuss the use made, and the limitations of weather satellites in severe weather forecasting. The survey will discuss the various types of tornadoes and their predicability as well as the limitations in the present warning systems, both from detection and dissemination.

PROBABILITY FORECASTING

Allan H. Murphy

National Center for Atmospheric Research

The rationale for probability forecasting is reviewed, and current methods of formulation probabilistic forecasts are briefly outlined. Several operational and experimental programs involving objective and subjective probability forecasting are described. Measures of the reliability, accuracy, and skill of probabilistic forecasts are defined and then used to evaluate the results of these programs. The value of probabilistic and other types of forecasts is considered within the context of specific decision-making situations. Some current problems in, and the future prospects for, probability forecasting are discussed.

APPLICATIONS OF TROPICAL CYCLONE MODELS

Russell L. Elsberry
Naval Postgraduate School
Monterey, California

ABSTRACT

The extensive research in tropical cyclone modeling during the 1960's and 1970's has resulted in a number of applications for real-time track prediction. A review of the characteristics of these three-dimensional dynamical models is given, including a discussion of procedures for initializing and for tracking the model storm. Some limited verifications of track forecasts are described. An outlook for the future is presented in terms of numerical model improvements, and for large-scale and inner-scale data required to implement the improved models.

1. INTRODUCTION

At the Sixth Technical Exchange Conference in 1970, S. Rosenthal of the National Hurricane Research Laboratory reported results from the first three-dimensional numerical model with the physical processes and horizontal resolution necessary to resolve tropical cyclones. Since that time a number of three-dimensional models have been developed--both for research purposes and for operational prediction of tropical cyclone tracks. The characteristics of these operational models, and those being tested with operational data, will be reviewed. Some of this material must be considered as interim, because several of the models to be described are in various stages of development and testing. After describing generally the characteristics of the models, we will discuss the initial fields that are required, and the methods of tracking the model tropical cyclone. An evaluation of the track forecasts will then be presented. Some of the results or conclusions based on rather limited sample sizes may have to be re-examined in the light of additional cases. The last section of this paper will be concerned with the outlook for the future and will focus on some of the data problems that are being encountered in the operational use of fine-scale, tropical cyclone models.

This survey is limited to three-dimensional models, and thus excludes a number of barotropic models that have proved very useful for tropical cyclone motion forecasts. Experience with these models has helped anticipate the types of problems that will occur during operational implementation of the more complex baroclinic models. The best known of the barotropic models is the SANBAR model, which was developed by Sanders and Burpee (1968) and subsequently modified by Pike (1972) and Sanders, Pike and Gaertner (1975). Various versions of this model have been extensively tested with Atlantic and Eastern Pacific hurricanes (Sanders et al., 1977). A balanced barotropic model for typhoon movement prediction has been run by the Japan Meteorological Agency. Similar barotropic models are also being developed in India (Singh and Saha, 1976), Taiwan (Tsay, 1977) and the Philippines. In some cases the initial fields are based on hand analyses. Until objective analysis schemes are developed and tested with the models on an operational basis, it is unlikely that these models will have a practical application.

2. GENERAL DESCRIPTION OF MODELS

A few of the physical characteristics of some selected baroclinic models are shown in Table 1. The National Meteorological Center (NMC) Movable Fine Mesh (MFM) has been used on on operational basis for several years (Hovermale and Livezey, 1977). A Tropical Cyclone Model (TCM) has been operationally tested for Pacific Ocean storms at the Fleet Numerical Weather Central (FNWC), as described by Hinsman (1977) and Mihok and Hinsman (1977). The model (Madala and Hodur, 1977) being developed jointly by the Naval Research Laboratory (NRL) and the Naval Environmental Prediction Research Facility (NEPRF) is intended to replace the FNWC-TCM after further testing with operational data. Following this, a nested grid version is to be developed and tested by NRL and NEPRF. Some limited testing of the Penn State University (PSU) mesoscale model for several western Pacific typhoon cases is being done at the Naval Postgraduate School (NPS). The primary purpose of these tests (Hacunda, 1978) is to compare the predictions with the FNWC-TCM and NRL/NEPRF models using the same input data. Anthes (1978) has shown that the PSU mesoscale model (with 60 km resolution) improved the forecasts in 32 cases over Europe and the United States. These further tests over data-sparse oceans, and with the different physics represented by typhoon circulations, will provide additional informa-

Table 1. Characteristics of several baroclinic models being applied for prediction of tropical cyclone motion based on operational data (see text for explanation).

Agency-Model	Vertical coordinate	Number of layers	Grid Size (km)	Number of points	Relocatable grid	Lateral b.c.
NMC-MFM	σ	10	60	50x50	Yes	OW
FNWC-TCM	P	3	205	32x24	No	OW
NRL/NEPRF	σ	5	60	51x51	No	OW
PSU/NPS	σ	5	120	40x40	No	OW
JMA-MNG	σ	3	291	31x31	No	OW
			145	31x31	Yes	TW
			73	31x31	Yes	TW
			36	31x31	Yes	TW

OW - One-way interaction

TW - Two-way interaction

tion regarding the applicability of these fine-mesh models. The last model listed in Table 1 is the Japanese Meteorological Agency (JMA) movable multiply-nested grid (MNG) developed by Ookochi (1978). This model has been tested on a few typhoons approaching Japan.

The entries in Table 1 suggest wide variance in model characteristics. Consequently it is not possible to evaluate directly the differences in the model predictions. The FNWC and JMA models have minimal vertical resolution with only three layers, which are able to represent the inflow, outflow and an intermediate layer of the mature typhoon circulation. Although the NRL/NEPRF and PSU/NPS models have improved resolution with five layers, only the NMC-MFM has adequate vertical resolution. However, it should be noted that the tendency for tropical observations to be distributed in two layers--near the surface and at predominately jet aircraft levels, makes initialization of a 10-layer model rather difficult.

It has been known for some time that finer spatial grids are required to predict tropical circulations than are commonly used for mid-latitude prediction models. Except for the FNWC-TCM model, each of the models in Table 1 attempts to resolve the inner structure of the tropical cyclone circulation. It is generally assumed that the primary interaction between the vortex and the steering current can be resolved on the 60 km grid used by the NMC and NRL/NEPRF models. However, to attempt intensity forecasts one must resolve the inner region of the typhoon (Elsberry, 1975; Jones, 1977a). This will require a nested grid arrangement because the entire domain cannot be covered with the approximately 10 km resolution that will be necessary for the inner-most grid. The second characteristic that will be required for intensity forecasts will be an ability to move the inner grids with the storm. The JMA model possesses both of these characteristics, although the inner grid presently has only 36 km resolution. The other models in Table 1 have a uniform grid lattice which generally covers at least 3000 km square. Even this may be inadequate for 72-h forecasts of fast-moving storms. All of the models can be positioned at the initial time to minimize the chance that the expected storm motion will bring the storm center near the boundaries. Only the NMC model has the capability of being relocated during the forecast. This relocatability feature allows one to keep the storm near the center of the domain away from adverse boundary effects, and consequently permits a smaller domain size. As the grid is relocated, some fine-mesh values along the leading edge must be interpolated from the coarse-mesh hemispheric forecast values. This introduces some additional noise in the region of the boundary.

Each of these models must be provided time-dependent values along the outer boundaries from some other prediction model. The interface boundary condition is of the one-way (OW) type (Phillips and Shukla, 1973), in that no feedback of information is provided from the tropical cyclone model to the hemispheric model. An early version (Hinsman, 1977) of the FNWC-TCM model was in a channel, and thus required no information from the larger scale model after the initial time. Hodur and Burk (1977) have demonstrated that one-way boundary conditions improve the TCM forecasts during recurvature situations. The JMA nested grid model has two-way interaction conditions for the inner grids. This requires a simultaneous integration on all grids rather than a sequential integration as in one-way integration. Various interface boundary conditions have been employed to permit mass,

momentum and energy to flow between the grids (Elsberry, 1978). Although these conditions can never be perfect because of the differences in resolvable waves with different grid lengths, it appears that acceptable numerical solutions have been obtained (see e.g. Anthes, 1976; Jones, 1977a,b; Sobel, 1976).

Note that the requirement in every case for lateral boundary conditions from a hemispheric model places an important operational constraint on these tropical cyclone forecast models. The normal procedure would be to await the completion of the hemispheric forecast model run. Allowing for the collection and analysis of the initial data, this means that the tropical model will not be initiated until 6 h or more after the map time (t_o). Consequently the model guidance may not be actually used by the forecaster until t_o +12 h. For example, Jarvinen (1977) points out that the SANBAR forecast is not available to the National Hurricane Center until t_o +4 h, and the 48-h NMC-MFM forecast appears at t_o +8 h. Likewise Mihok and Hinsman (1977) have attempted to reduce the greater than t_o +9 h lag time for the FNWC-TCM. They used a channel version of the TCM (note that this requires lateral boundary conditions only at the initial time) at t_o +4 h with initial data primarily based on a 12-h forecast. The overall average difference in forecast error between the earlier run and a later run with more complete data was only about 10 km for the small sample tested. Tests are underway at FNWC (Mihok, personal communication) to provide the necessary boundary conditions for the one-way interaction version (Hodur and Burk, 1977) of the TCM from a hemispheric forecast initiated at t_o -12 h. An 84-h hemispheric forecast would then be necessary to permit the tropical cyclone model to be run to 72 h. As a 84-h forecast is not presently available at FNWC, the boundary values in the tropical cyclone model are being held constant from 72 h to 84 h. If these tests are successful it should be possible to provide model guidance to the forecaster in time for inclusion in the t_o +6 h forecast cycle. These tests will also provide an indication of the degradation in the forecasts arising from the use of predicted boundary conditions rather than the "perfect" boundary conditions based on analyses that are used on the research models.

3. INITIAL FIELDS

It can be shown that the mass field adjusts to the wind field for low-latitude flow and for smaller scales of motion such as a tropical cyclone. Consequently, the general procedure for initializing numerical models in the tropics is to derive the mass field from the wind field. This is denoted as reverse balancing because the nonlinear balance equation is solved for the geopotential field given the stream function field, which is derived from the wind analysis. As indicated in Table 2, only the Japanese MNG model follows the normal mid-latitude approach of determining the wind field from the geopotential analysis.

Table 2. Provision of initial fields for several baroclinic tropical cyclone models (see Table 1 and text for explanation).

Agency-model	Initialization method	Storm-scale data
NMC-MFM	Reverse balance ($\psi \rightarrow \phi$)	2-d spinup
FNWC-TCM	Reverse balance	Tangential wind bogus
NRL/NEPRF	Reverse balance	Tangential wind bogus
PSU/NPS	Reverse balance	Tangential wind bogus
JMA-MNG	Balance ($\phi \rightarrow \psi$)	Pressure/temperature/radial wind bogus

The adequacy of the above initialization procedures for specifying the basic flow and the details of the tropical cyclone circulation depends on the distribution of observations. Because the rawinsonde coverage in the tropics is marginal at best, the absence or late reporting of a few key observations can have a pronounced detrimental effect. In some locations the geostationary satellite-derived cloud motion data can help fill some of the gaps. Some of the weaknesses of these cloud motion vectors include: absence of reports in clear regions and in the middle troposphere, and the inability to track cumulus cloud elements within the general region of the cirrus canopy. Better spatial resolution and a large increase in the number of clouds that may be tracked has been achieved by reducing the area that the satellite views. The images may then be received every three minutes rather than each 30 minutes, and smaller cloud elements can be followed for 15 minutes to estimate the velocities. Rodgers et al. (1978) were able to track about 6-10 times the usual number of clouds in this way, including some low-level cumulus between breaks in the cirrus overcast. This type of data helps fill the gap between the far-environment of the storm and the inner regions, which can only be sensed with aircraft reconnaissance. It is unfortunate that the number of reconnaissance flights has decreased significantly, because this has been the best source of high-resolution data. It is most encouraging that real-time transmission of observed data from some of the aircraft to the operational centers via geostationary satellites is becoming a reality. However, these advanced systems are not available on all reconnaissance aircraft.

Various alternatives have been attempted to provide finer scale data near the center of the tropical cyclone. The approach used presently for the NMC-MFM is to replace the fields in the inner region with a model storm derived by time integration of an axisymmetric version of the general model (Hovermale and Livezey, 1977). Because the two-dimensional (radius and height) version is spun-up with the same finite-difference and other physical aspects as in the general model, the addition of this model storm to the basic current tends to reduce the numerically-induced shock. Some inconsistencies remain because of the vertical shear in the general model, and because of nonlinearities in the balance equation. The virtue of this procedure is that the model storm is consistent with the numerics of the full model and that minimal information is required regarding the characteristics of the actual storm. An example of the tangential wind speed versus radius for a storm during 1975 is shown in Fig. 1. Because the model has 60-km resolution, the radius of maximum winds tends to be very large. The spun-up vortex also may be more intense than the actual storm, especially if the storm is just beginning. A consequence of these two features leads to very large wind speeds at outer radii. A more realistic variation of wind speed with radius is shown from the model of Kurihara and Tuleya (1974). Beginning in 1976, the initial vortex in the NMC-MFM was limited in speed as indicated in Fig. 1.

An alternate approach of adding a symmetrical tangential wind speed distribution to the basic current has been adopted for the FNWC-TCM, NRL/NEPRF and PSU/NPS models. This bogus is based on empirical distributions of wind speed versus radius, which are functions of the maximum wind speed and the radius of maximum winds. The mass field derived by reverse balancing then will reflect the presence of the storm. It is important that the vertical structure of wind bogus be realistic, since the initial temperature field is diagnosed from the thickness between the geopotentials at the various levels. Inclusion of only the tangential wind components, and assuming no frictional terms, the initial wind fields will be non-divergent. Consequently some time will elapse before a realistic vertical motion, and latent heat release, field will develop in the model. The JMA-MNG contains an initial symmetrical surface pressure and temperature bogus to represent the storm circulation on the inner grids. After deriving geostrophic wind fields (reduced by a factor of 0.5 to account for curvature effects) that correspond to the geopotential fields, a radial wind field is also superposed. Because of the imposed low-level convergence and upper-level divergence, and the geostrophic assumption, these initial fields will not be in balance. A period of adjustment will thus be necessary, although this would presumably be shorter than in the cases without initial divergence.

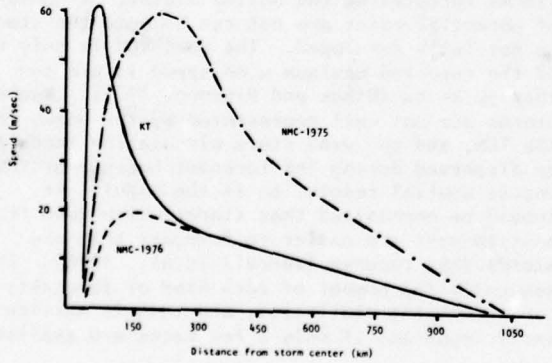

Fig. 1. Tangential wind speed versus radius from Kurihara and Tuleya (1974) model (solid line), the NMC spun-up vortex during 1975 (dash-dot line), and modified distribution used at NMC in 1976 (dashed line) from Hovermale, et al. (1977).

A superior method of minimizing the initial shock, as well as also incorporating various types of observations, is the dynamic initialization scheme of Hoke and Anthes (1976, 1977). During the pre-forecast integration period the predictive equations with all of the physical processes are supplemented by terms that drive the model atmosphere toward the observations. At the completion of the dynamic initialization phase, the terms which "nudge" the model parameters toward the observations are set to zero and the forecast proceeds. Although tested with only a single case, the dynamic initialization scheme appears to have advantages over forecasts with static initialization. The primary disadvantage is the extra computer resources that are required for the pre-forecast integration. However, this may be necessary to make optimum use of the varied types of observations, including off-time cloud motion vectors and reconnaissance data. Kurihara and Tuleya (1978) have proposed a dynamic initialization for the hurricane planetary boundary layer, which will be important for intensity forecasts.

There is some evidence that the steering flow is also not well represented by the existing observations. This is frequently revealed by a systematic bias in the predicted speed and direction. Pike (1975) has previously treated this problem for the SANBAR model by simply replacing the initial wind field within 300 n.mi. of the center by the observed storm motion. The difference between the actual and (TCM) predicted storm motion after 6 h was used by Shewchuk and Elsberry (1978) to adjust the initial wind fields near the center. A trial and error procedure was necessary to determine the relative magnitudes of the zonal and meridional components of the adjustment. Operational implementation during the 1977 typhoon season appears to have resulted in improved forecasts relative to the 1976 season (Mihok and Hinsman, 1977). The adjusted TCM forecasts based on the same map time were better than the official Joint Typhoon Warning Center forecasts in all forecast periods (see Fig. 2). If account for the nearly 12 h lag in receiving the forecasts is made by

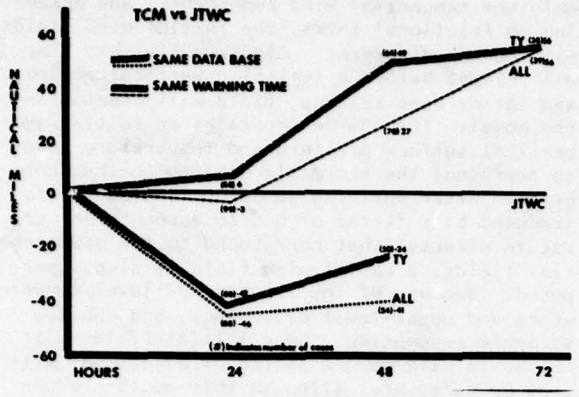

Fig. 2. Comparison of track errors between the official JTWC and the Tropical Cyclone Model (TCM) forecasts during 1977. Positive values indicate TCM errors are smaller (see text and 1977 Annual Typhoon Report for explanation of data base versus warning time comparisons).

comparing the TCM forecasts with an official forecast made 12 h later, the TCM results are only beginning to approach the official forecasts in the 72-h time frame (Annual Report, Joint Typhoon Warning Center, 1977). This emphasizes the need for improving the timeliness of the dynamical forecasts.

4. TRACKING THE MODEL TROPICAL CYCLONE

A number of observational studies (see references in Lewis and Black, 1977) have indicated oscillations along the storm path. Lewis and Black (1977) decomposed time series of radar eye positions into displacements perpendicular and parallel to a smoothed track. The cross-track oscillations had magnitudes of about $\pm$ 20 km and two dominant periods of 7-12 h and approximately 24 h. Numerical models also predict oscillatory tracks, although the mechanisms may not be the same as in nature. Jones (1977a) has shown that the vortex path is trochoidal and that the mean vortex motion is about 5° to the right of the steering current. This appears to be due to boundary layer frictional drag forces on the vortex, as suggested by Kuo (1969), because no variation in the Coriolis parameter was included in the Jones model. Therefore in each of the numerical tropical cyclone models there is a problem of determining the storm track on the basis of a few center positions at 12-h intervals. As the grid resolution improves, for example, in the JMA-MNG, the model track should show more of the trochoidal path and the center locations will have to be determined more frequently.

The methods used for estimating storm positions in the tropical cyclone models are listed in Table 3. One should recall the grid resolutions for each model (see Table 1). It is possible to interpolate quite precisely the position of all extrema in any scalar field such as

Table 3. Methods for positioning tropical cyclone centers in selected models (see Table 1 and text for explanation).

Agency-Model	
NMC-MFM	Low-level vorticity maximum
FNWC-TCM	Minimum in stream function
NRL/NEPRF	Minimum in stream function
PSU/NPS	Streamline/surface pressure centers
JMA-MNG	Surface pressure centers

vorticity, stream function or pressure. However, the asymmetries that result from representing an intense, nearly circular wind field on a rectangular grid may not justify great precision. It is possible that the location of a minimum could be displaced somewhat erratically only one or two time steps later. The surface pressure center and the vorticity maximum will not necessarily be coincident, especially for weak storms. It would seem advisable to use the vorticity center since the pressure fields tend to adjust to the wind field on these small space scales and at low latitudes. The reasoning (Shewchuk, 1977) behind the use of a stream function center in the FNWC-TCM rather than the maximum vorticity location is that the solution of the Poisson equation tends to smooth the irregularities in the field. Consequently storm positions that are more conservative in time are obtained.

5. SOME VERIFICATION STATISTICS

There are several factors which complicate the discussion of forecast errors with the dynamical tropical cyclone models. The first is the small number of cases that are available for comparison with the best track, which is determined from post-season analysis. Because the models are expensive and may cause delays in the delivery of other products, they may not be run every 12 h unless the tropical cyclone threat is imminent. For example, the primary objective of the NMC-MFM is to improve landfall forecasts of storms threatening the United States. A number of potential cases are not run because the storm is not fully developed. The FNWC-TCM is only run if the reported maximum wind speed is greater than 50 knots (Mihok and Hinsman, 1977). Weaker storms are not well represented by the bogus in the TCM, and the weak storm circulation tends to be dispersed during the forecast because of the coarse spatial resolution in the model. It should be emphasized that storms which move from east-to-west are easier to forecast than are storms that recurve (Jarrell et al., 1978). Consequently the number of each kind of forecasts can affect the statistics, and this is particularly important if only a few cases are available.

A second difficulty in establishing long-term error statistics is that these developmental models are continually being modified. Sometimes large changes are made in the models between seasons. In most cases a complete comparison between the old and the revised versions cannot

be made because the historical data are incomplete, or the necessary resources (computer and human) are not available. Such comparisons would be helpful for interpreting the effects of the model changes and improving our physical understanding of the model predictions. This is particularly important if the forecaster is to determine when to use the dynamical model guidance versus the other techniques that are available.

An example of the magnitude of track errors from the NMC-MFM for the 1976 hurricane season is given in Table 4 from Hovermale and Livezey (1977). One should note that the sample size is small, and diminishes with the forecast interval because verification data are lacking after landfall. Hovermale and Livezey treat separately the sparse data cases, which in the mean have much larger errors at 36 and 48 h. Nevertheless the total sample shows that the NMC-MFM predictions are quite good and do not decay in time as rapidly as for some other schemes. This advantage of dynamic models is evidently due to the incorporation of large-scale synoptic changes that impact the tropical cyclone at the longer time intervals. Another example (Hovermale, private communication) was the performance of the NMC-MFM model for 20 consecutive times with Hurricane Fico in the eastern Pacific during 1978. The 24- and 48-h vector errors of 73 and 157 n.mi. must be considered as very good since official 24-h forecast errors are typically 100-140 n.mi. Of course one should compare these model errors with the comparable official forecasts, because Fico was a very well behaved storm in a region with nearly continuous geostationary satellite coverage.

The use (J. Kerlin, private communication) of the NMC-MFM on selected Western Pacific typhoons during 1977 allows some preliminary comparisons with the FNWC-TCM and the official JTWC forecasts. Statistics for these (and other) forecast techniques were verified by J. Shewchuk (JTWC) on the basis of subsequent warning positions, rather than on the best track. This introduces some uncertainties but the general comparisons are not changed. The individual 24- and 48-h forecast errors are shown because the sample is so small. Note that the official forecase deteriorates rapidly from 24 h to 48 h in most of the cases. There are several cases in which the dynamical models have smaller 48-h errors than at 24 h. This probably indicates that the model tracks are somewhat irregular and cross the actual track during the period. One generally finds that the dynamical models have the same tendencies and seem to be closer to each other than to the official forecasts. It is not clear to what extent the official forecasts were guided by the FNWC-TCM (recall the nearly 12-h lag in the receipt at JTWC of the model prediction).

The FNWC-TCM predictions are not available in all periods. Mean values for a homogeneous sample of nine 24-h and eight 48-h forecasts are given at the bottom of Table 5. Considerable caution is advised in using these values because of the small sample. At most one can safely say

Table 4. Mean vector errors in nautical miles of hurricane forecasts from the MFM (NMC hurricane model) during the 1976 season (Hovermale and Livezey, 1977).

Forecast Period (hrs)	Forecasts Excluding Sparse Data Cases	(N)	Sparse Data Cases	(N)	Total Cases	(N)
12	71	(11)	62	(4)	68	(15)
24	102	(10)	135	(4)	126	(14)
36	96	(9)	250	(4)	143	(13)
48	119	(8)	365	(4)	201	(12)

Table 5. Track error (n.mi.) statistics at 24- and 48-h for selected 1977 typhoons for official (JTWC), NMC-MFM and FNWC-TCM (prepared by J. Shewchuk, JTWC).

Typhoon	Official		NMC-MFM		FNWC-TCM	
	24h	48h	24h	48h	24h	48h
Vera-1	96	58	159	156	57	60
Ivy	122	255	59	134	--	--
Dinah-1	98	420	192	302	82	154
Thelma	86	382	52	80	79	310
Jean	68	312	183	238	--	--
Dinah-2	111	236	30	208	135	146
Babe	315	---	152	478	236	--
Dinah-3	110	374	62	175	28	189
Vera-2	162	240	137	98	77	28
Gilda	131	220	99	313	54	203
Babe	103	422	117	107	106	392
Homogeneous Sample	135 (N=9)	294 (N=8)	111	180	95	185

that the dynamical models produce comparable results. It would also seem that 48-h guidance based on the dynamical models would be useful to the forecasters if it could be received on a timely fashion. Additional cases must be provided the forecaster to permit determination of the conditions for which the dynamical guidance should be accepted or discarded. When that occurs, the official forecasts will again improve on this form of guidance.

It is difficult to separate numerical model-related errors from the data-related errors. Elsberry (1977) found a correlation between cases with large model errors and initial wind fields which were ill-defined. Hovermale and Livezey (1977) also noted "sparse data" cases resulted in larger errors with the NMC-MFM. Systematic tests with improved versions of the model can illustrate some of the model-related errors. For example Hodur and Burk (1977) improved the FNWC-TCM by providing for open boundary conditions rather than a channel configuration. This model improvement resulted in a decrease of 48-h errors from 325 to 242 n.mi. (N=38) and 72-h errors from 554 to 353 n.mi.(N=28).

6. WHAT ABOUT THE FUTURE?

6.1 Improvements in numerical aspects.

We have not treated in detail the numerical aspects of the dynamical models. One of the goals for future tropical cyclone prediction models is to improve the horizontal and vertical resolution beyond that shown in Table 1. For the same domain size, an increase in horizontal resolution by a factor of two requires eight times the computer resources. In the past the improvements in computer technology have produced machines with this order of increased capability. For example, the introduction of the NMC-MFM was made possible by the acquisition of a more powerful computer. However, it is clearly not going to be possible to decrease the spatial resolution to the approximately 10 km required for representing motions on the scale of the hurricane eye by virtue of improved computers alone.

Advances in nested grid simulations of various smaller scale atmospheric phenomena have been made in recent years (Elsberry, 1978). The strategy in these nested models is to represent only the localized regions of large gradients with fine resolution, and to resolve the regions with smaller gradients on a somewhat coarser grid. The chief advantage of the nested grid model is economic. If the inner grids are permitted to move with the atmospheric phenomena of interest, the innermost grid need only cover a very small fraction of the total domain. Because of the eight-fold increase in computer time for twice the horizontal resolution, it is the inner domains which require the major fraction of the computer resources. Depending on the domain sizes, it is possible to reduce computing times by a factor of more than five over the requirements of a uniform grid model. The primary disadvantage of the nested models is the more rapid contamination of the solutions on the inner grids because the boundaries are closer to the feature of interest. Errors in the solutions at the interfaces propagate into the region, so some consideration must be given to producing the best possible solution on the outer grids as well. The research model of Jones (1977a,b) has demonstrated the feasibility of representing intense tropical cyclones on a nested grid. The streamlines and isotachs predicted on the 30 km grid of the Jones model are shown in Fig. 3. Note that the overall pattern is representative of a tropical cyclone, and that the flow crosses quite smoothly from the 30 km grid onto the 10 km grid (indicated by crosses). As noted in Table 1, the JMA-MNG model is in a quasi-operational phase, and a nested version of the NRL/NEPRF model is planned. A movable nested mesh model is also being constructed at the Geophysical Fluid Dynamics Laboratory, NOAA, to study tropical disturbances (Kurihara et al., 1977).

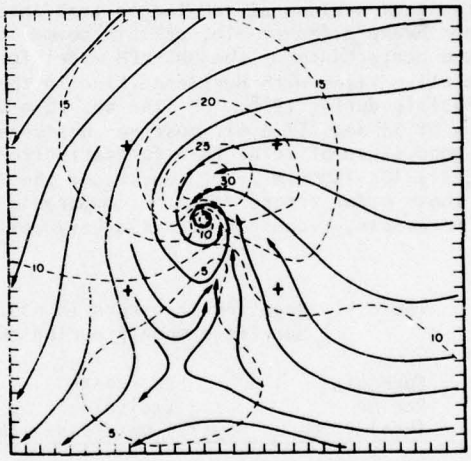

Fig. 3. Boundary layer streamlines and isotachs on 30 km grid at 24 h from the model of Jones (1977). Position of 10 km grid is denoted by four crosses.

It is also possible to use various differencing schemes to improve the efficiency of present models. Madala (1977) is using split semi-implicit techniques to increase the time step in the NRL/NEPRF model. In the split semi-implicit model, the terms governing the first few fastest moving modes in the solution are treated implicitly. The advantage gained in taking larger time steps will be lost unless an efficient direct elliptic solver is used for the two-dimensional Helmholtz equation for each implicitly treated mode. The use of the direct solver enables Madala to integrate the semi-implicit model up to six times faster than an analogous explicit model with no pressure gradient averaging. Consequently the combination of the split semi-implicit technique and a nested grid arrangement has great promise for

an efficient and more complete numerical model compared to those presently being run.

6.2 Improvements in representation of physical processes.

With the development of finer resolution models, it becomes even more important that the physical processes are well represented in the models. Because the strength of the storm depends on the rate of inflow and the air-ocean fluxes, the processes in the planetary boundary layer (PBL) are crucial. Most of the research and operational models have used a relatively crude PBL model in which the surface fluxes are determined by bulk formulae and the PBL depth is constant. Anthes and Chang (1978) have incorporated an improved PBL model with better vertical resolution and a parameterization of the vertical mixing which depends on shear and stability. This stability dependence produces a more realistic response of the hurricane model to changes in sea-surface temperature. The fluctuations in intensity in the Anthes and Chang experiments are less pronounced than in a similar model with a conventional bulk parameterization of the hurricane PBL.

Another important physical process in the tropical atmosphere is the release of latent heat. Considerable uncertainty remains as to the proper representation of the latent heat transport. Yamasaki (1977) and Rosenthal (1978) have abandoned the parameterization of the latent heat release in terms of the large scale variables. Rather they add equations which specifically treat the cloud water and rainwater. Contrary to the earlier theoretical treatments, this does not result in an unstable solution with unlimited growth on the scale of the grid interval (less than 20 km). The nonlinearity of the vertical heat redistribution during the various stages of the cloud development evidently prevents a continued growth of the cloud at the same location. Jones and Trout (1977) are utilizing this explicit treatment of the clouds on a 12-level, three-dimensional, nested tropical cyclone model.

The NMC-MFM and NRL/NEPRF models use a modified version of the Kuo (1965) scheme, whereas the PSU/NPS model uses a simplified version of the cumulus parameterization scheme of Anthes (1977). Both of the FNWC-TCM and the JMA-MNG model use an analytical heating function after Harrison (1973). Either the Kuo-type or the Anthes latent heating parameterization will be quite sensitive to the humidity distribution near the storm. This occurs because the fraction of cloud cover (and thus amount of latent heat release at the point) is proportional to the horizontal moisture convergence. Due to the lack of humidity observations, there must be a moisture bogus as well as a wind bogus for the NRL/NEPRF and PSU/NPS models. An example (Hacunda, 1978) of the convective heat release after 12 h for the PSU/NPS model with a "wet bogus" of 90% near the center in the lowest layer and 80% outside the storm is shown in Fig. 4. The central convective heating value of 75°C/day

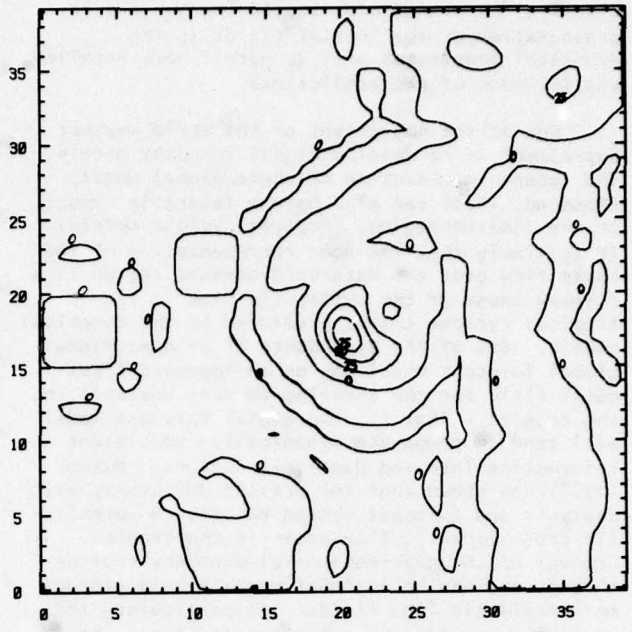

Fig. 4. Instantaneous rate of convective heating (°C/day) in the mid-troposphere after 12 h prediction based on an initial wet moisture bogus at 00GMT 09 November 1977. The axes are labeled as grid intervals with spacing of 120 km (Hacunda, 1978).

is typical of a moderate hurricane. The horizontal gradient of this heating determines the intensity of the storm, and thus the intensity depends ultimately on the amount of moisture that is available near the center of the storm. When the initial central humidity is only 85% and the environment is 80%, the heating due to convection is decreased. There is a corresponding decrease in the maximum 12-h accumulation of rainfall (both convective and large-scale saturation of lifted air) of about 25 percent. The model will eventually come into some kind of equilibrium distribution of horizontal convergence and vertical fluxes due to the PBL and latent heat parameterization schemes. However, in the early stages the initial humidity distribution will be very important and the sensitivity of the storm intensity to relatively small changes in humidity is of some concern.

6.3 Improvements in large-scale data.

The World Weather Experiment during 1979 will dramatically improve the number of observations within the tropical regions. Forty ships are to obtain vertical soundings in the 10°N to 10°S latitude belt, and additional reconnaissance flights are planned. The entire tropical belt will be covered with cloud motion vectors from five geostationary satellites. This tremendous increase in data should have a positive influence on operational forecasting of tropical cyclones.

Likewise the wind fields should improve the representation of the initial fields in the dynamical models, as well as permit more detailed verification of the predictions.

One of the objectives of the World Weather Experiment is to develop global forecast models. The recent introduction of these global models (Rosmond, 1978) can also have a favorable impact on the limited-region, tropical cyclone models. It is likely that the poor representation of the basic flow over the data-void oceanic region is a primary cause of the systematic bias in the tropical cyclone tracks predicted by the dynamical models. One of the byproducts of an operational global forecast model may be an improved first-guess field for the steering current analysis in the tropics. That is, the global forecast model will tend to propagate dynamically-consistent information into the data-void regions. Mathur (1978) has shown that the present NMC hemispheric analysis and forecast system results in unrealistic cross-isobaric flow areas in the tropics. Removal of the near-equatorial boundary regions through the use of a global model should produce more realistic flow fields. In particular, the initial guess for the subsequent analysis should be at least dynamically consistent. This is in contrast to the reversion-to-climatology feature of the present FNWC wind field analysis, which can result in unrealistic analyses in and adjacent to data-void regions.

6.4 *Improvements in fine-scale data.*

It was mentioned above that some type of bogus is necessary to define the inner regions of the tropical cyclone. Experience has shown that the resulting initial fields should not depart too significantly from real conditions (see Fig. 1). Hacunda (1978) tested two wind boguses in the PSU/NPS model described in Table 1. The initial low-level winds and pressure fields for the stronger wind bogus are shown in Fig. 5a. At first glance the wind and pressure gradients appear very realistic. However, it is important to note that only alternate gridpoints (resolution of 120 km) are plotted). Consequently the full wind barb to the east of the storm center is equivalent to 50 m s^{-1} at 240 km, and is comparable to the values in the wind bogus used in the NMC-MFM during 1975 (see Fig. 1). Note also that the areal domain of the implied cyclonic circulation associated with the typhoon is very large, with a trough extending to the northeast corner of the grid. The 24-h forecast based on the wind bogus in Fig. 5a is displayed in Fig. 5b. The initial wind maximum of 50 m s^{-1} cannot be sustained on the 120-km grid, and a marked reduction in intensity occurs. There is also a spreading of the maximum wind region which appears typically in these relatively coarse mesh models. The storm circulation at 24 h affects most of the domain. The circulation pattern in the northeast corner produced a precipitation maximum that intensified the trough and contributed to the recurvature of the storm.

A weak storm bogus as in Fig. 1 results in the initial wind and pressure fields in Fig. 6a. Note that the cyclonic area introduced by the bogus is much smaller, and the maximum winds are less than 25 m s^{-1}. Although this intensity is

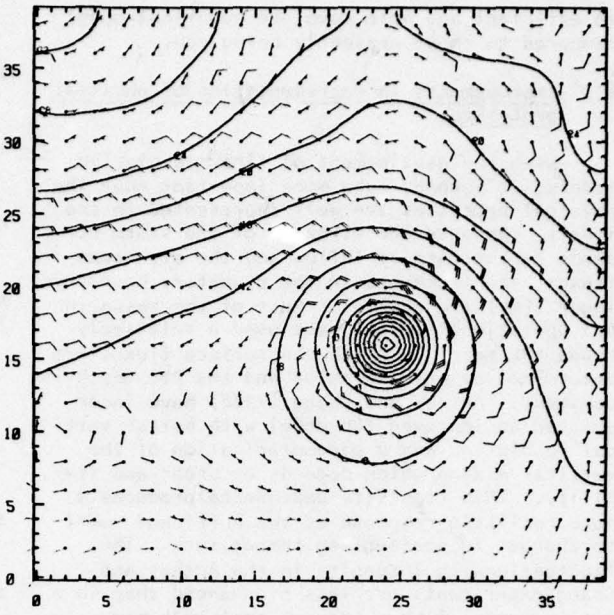

Fig. 5(a). Initial wind (full barb, 50 m s^{-1}) at σ = 0.95 and sea-level pressure minus 1000 mb for 12GMT 09 November 1977 using strong wind bogus.

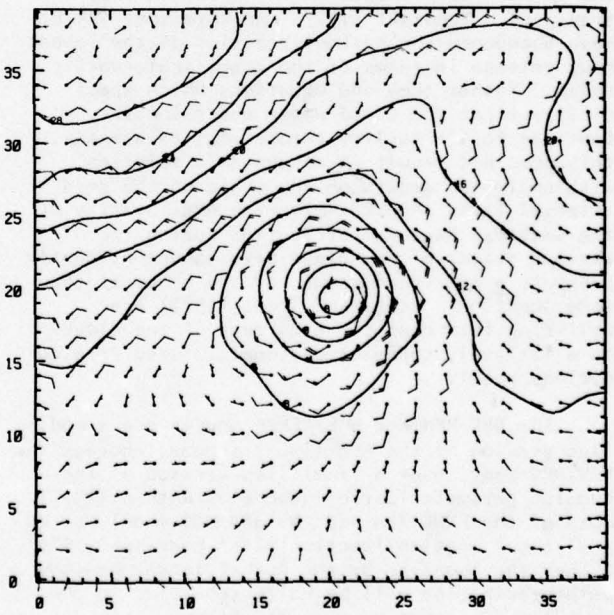

Fig. 5(b). 24-h forecast of wind at σ = 0.95 and sea-level pressure minus 1000 mb from initial field in (a).

much less than in the actual storm, it is more realistic in terms of the gradients that can be represented on the 120 km grid. Likewise the depiction of the surrounding wind field is more representative of the true flow. The 24-h forecast for the weak storm bogus is given in Fig. 6b. The maximum wind speed is now slightly in excess of 25 m s^{-1}, and it occurs at a larger radius as in Fig. 5b. After only 24 h the prediction of the storm center based on an intense vortex is about 180 km farther north than for the case with the weak vortex. Similar excessive northward displacements with strong wind boguses were found in all five cases treated by Hacunda (1978). A vortex which is too large or intense compared to the actual vortex can lead to significant westward and northward accelerations due to the variations in the Coriolis parameter (Hovermale et al., 1977). It follows that the environmental flow in the model must be as close as possible to observations, but the true interior flow cannot be realistically represented on a 60-km grid.

Not only is there a problem with how much data from the inner regions of the storm can be incorporated in the 60 km models, the distribution of these observations can have a severe impact on the initial fields. Walters (1978) tested the effect of unequal distribution of data by using an analytic representation of the vortex as in Fig. 7a. This wind field can be completely recovered by the objective analysis scheme if sufficient data are provided. However, there is lack of "observations" in the northeast quadrant of the storm. The wind field that is produced with the limited observations is shown in Fig. 7b. Whereas the large-scale aspects of the flow are reproduced, the unequal distribution of the data results in a sizable displacement of the vortex center to the southwest.

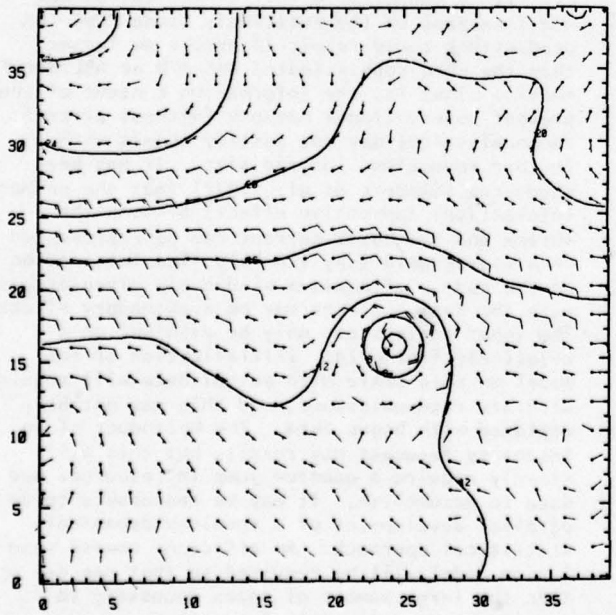

Fig. 6A.

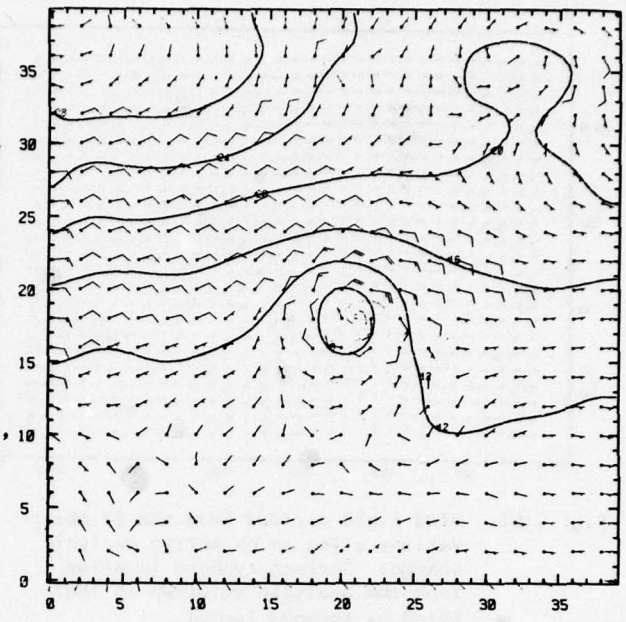

Fig. 6B.

Fig. 6. Similar to Fig. 5 except using weak wind bogus.

An unequal distribution of data is quite likely to occur during the crucial periods of landfall. An economic analysis by Neumann (1975) indicated the largest benefits are to be obtained from improved forecasts of landfall. There is normally a large difference in data coverage over the ocean relative to the land areas. Thus the dynamical models that use observations near the center may be adversely affected by the unequal distribution. Robert Burpee of the National Hurricane and Experimental Meteorology Laboratory of NOAA has proposed augmentation of the reconnaissance coverage in

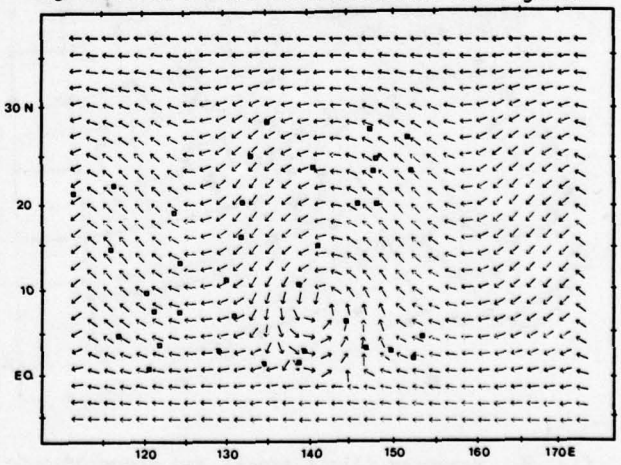

Fig. 7(a). Analytic solution of a vortex superposed on a basic current used by Walters (1978) to evalute effect of data distribution indicated by squares.

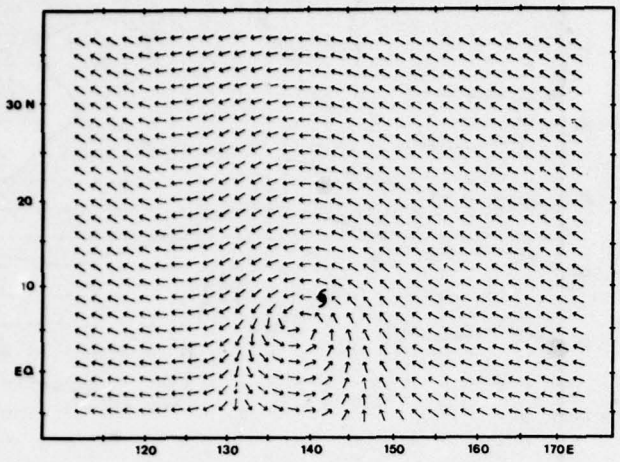

Fig. 7(b). Wind field derived from the 37 observations using an objective analysis scheme. Correct typhoon location from the analytic solution is indicated by typhoon symbol.

the area from 150-1500 km of the center. An example for a hurricane located off the Atlantic coast is shown in Fig. 8. The addition of dropwindsonde data at and below 400 mb to the existing observations would improve the specification of the atmospheric circulation patterns throughout the troposphere. Factors such as storm location, aircraft capability and dropwindsonde design must be considered in determining specific flight tracks. If dropwindsondes are made at the indicated locations, one would expect significant improvements in the wind analysis in the near-environment of the storm.

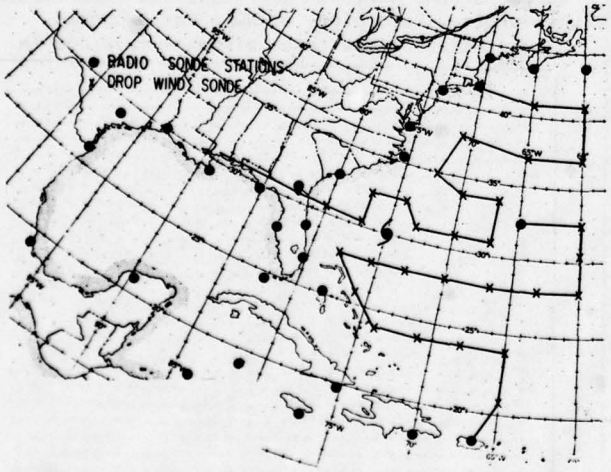

Fig. 8. Proposed flight tracks and dropwindsonde locations (x) for a hurricane located at 30°N, 75°W. Darkened circles designate locations of the regular rawinsonde network (R. Burpee, personal communication).

It appears likely that near-environmental data of the type shown in Fig. 8 are the most important for the existing dynamical models. First, it is a region in which the cyclonic envelope of the storm interacts with the basic current to determine the 12- to 36-hour track. Data coverage is generally inadequate in this domain between the center of the storm where the largest winds occur and the far environment. It is important to note that even the 60-km resolution models cannot use detailed wind profiles near the storm center. Only the center location must be known with any degree of accuracy, because the present models use some idealized (and degraded) vortex wind distributions. Additional data in the near-environment of the storm will permit a realistic blending of the bogus vortex with the large-scale flow. As indicated above, some care must be taken to assure that the data distribution does not result in a distortion of the vortex. More sophisticated models with fine resolution nested grids will require, and be able to use, more data near the center of the storm.

6.5 Statistical modification of model predictions.

One of the common features in the dynamical models has been the tendency for the track direction to be better than the speed (Hovermale et al., 1976; Shewchuk and Elsberry, 1978). In general the model displacement is too slow. If this proves to be a systematic bias, it should be possible to develop statistical regression equations to adjust the model predicted track. Work along these lines is in progress at the Naval Postgraduate School using the output of the FNWC-TCM.

It is conceivable that these statistical modifications of the relatively crude FNWC-TCM predictions could result in errors no larger than the more sophisticated NMC-MFM or NRL/NEPRF models. That is, the information content of the present observational network (without aircraft reconnaissance) may not justify models with further reductions in grid size. It has been suggested (Sanders et al., 1977) that the primary interactions (advective effect) between the vortex and the basic current can be represented on a coarse grid (say 150 km). The interaction of the radius of maximum wind scale circulations with the basic current may be a secondary effect. The inner regions can only be resolved on a relatively fine grid. Initialization of the model on this scale with actual data will require aircraft reconnaissance, and this may not be replaced with bogus data. The byproduct of an intensity forecast may result, but this will clearly require a quantum jump in resources and data to accomplish. It may be reasonable to do a parallel development of a combined dynamical-statistical approach. An efficient coarse resolution model will be required so that one can obtain the large number of cases necessary to develop stable statistical equations.

7. SUMMARY

Several three-dimensional, numerical models to predict the motion of tropical cyclones have been used operationally, or are currently being tested with operational data. Although there is a problem with the timeliness that the predictions are delivered to the forecasters, the dynamical guidance at 48- and 72-h appears superior to the official forecasts in many important cases. Further improvements in various aspects of these numerical models can be expected in the next few years, if the sophisticated research models are applied to the operational tropical cyclone track prediction problem. Specific goals include better horizontal and vertical resolution, and improved representation of the physical processes. These new dynamical models will require additional computer resources. However, nesting the grids and more efficient numerical differencing schemes will permit a better utilization of those resources.

If finer resolution (say 10 km) models are developed, one can consider intensity forecasts as well as track forecasts. A deterministic prediction of maximum wind speed appears doubtful when one considers the natural variability, and thus predictability, of these maxima. However, the general distribution of wind speed - say the radii of 50 kt and 30 kt winds in various quadrants, may be possible.

Even with a better representation of the physical processes in the models, the major limitation appears to be input data. Specification of the large-scale data for tropical cyclone forecasting should be improved during the World Weather Experiment and with the advent of the global forecast models. Cloud motion vectors from the global satellite coverage are particularly important. Additional aircraft reconnaissance will also be very beneficial, especially in those cases where the data can be transmitted directly to the forecast centers via communication satellites. The chief problem will be to provide data in the inner regions. It appears that the present models are quite sensitive to relative humidity changes of only 5% in the lowest layers. Obtaining such accurate humidity measurements may pose severe problems. Likewise the specification of the wind field is very important. Near the center of the tropical cyclone the wind can change rapidly in space and time. A good distribution of the observations with respect to the center, as well as the observations in the near-environment of the storm, must be provided. Finally, there are still important problems as to how to incorporate these data into the models and yet deliver the predictions to the tropical cyclone forecaster in a timely fashion. It seems likely that such dynamical model guidance is the best hope for improving significantly the prediction of tropical cyclone tracks beyond 24 h.

Acknowledgments. The long-term support of the Naval Air Systems Command, the Naval Environmental Prediction Research Facility and the Fleet Numerical Weather Central is gratefully acknowledged. The cooperation and assistance of numerous personnel at the latter two agencies, and at the Naval Postgraduate School, has made possible the development of the U.S. Navy Tropical Cyclone Model.

Constructive comments on this manuscript were provided by G. J. Haltiner and R. M. Hodur. The manuscript was typed by Ms. M. Marks and Ms. G. Merritt.

8. REFERENCES

Anthes, R. A., 1976: Numerical prediction of severe storms-certainty, possibility or dream? Bull. Am. Meteor. Soc., 57, 423-430.

- - - , 1977: A cumulus parameterization scheme utilizing a one-dimensional cloud model. Mon. Wea. Rev., 105, 270-286.

- - - , 1978: Tests of a mesoscale model over Europe and the United States. Naval Postgraduate School Technical Report NPS63-78004, 107 pp.

- - - , and S. W. Chang, 1978: Response of the hurricane boundary layer to changes of sea-surface temperature in a numerical model. J. Atmos. Sci., 35, 1240-1255.

Elsberry, R. L., 1975: Feasibility of an operational tropical cyclone prediction model for the western North Pacific area. Naval Postgraduate School Technical Report NPS-51Es75051, 56 pp.

- - - , 1977: Operational data tests with a tropical cyclone model. Naval Postgraduate School Technical Report NPS-63Es77031,28 pp.

- - - , 1978: Prediction of atmospheric flows on nested grids. Computational Techniques for Interface Problems. AMD-Vol.30, Am. Soc. Mech. Engr. (New York), 67-86.

Hacunda, M. R., 1978: Tests of the Penn State mesoscale model with tropical cyclones. M.S. thesis, Naval Postgraduate School, 81 pp.

Harrison, E. J., Jr., 1973: Three-dimensional numerical simulations of tropical systems utilizing nested finite grids. J. Atmos. Sci., 30, 1528-1543.

Hinsman, D. E., 1977: Preliminary results from the Fleet Numerical Weather Central tropical cyclone model. Proceedings Third Conference on Numerical Weather Prediction, Am. Meteor. Soc. (Boston), 19-34.

Hodur, R. M., and S. D. Burk, 1977: Incorporation of one-way interactive boundary conditions in the Fleet Numerical Weather Central tropical cyclone model. 11th Technical Conference on Hurricanes and Tropical Meteorology, Am. Meteor. Soc. (Boston), 116-121.

Hoke, J. E., and R. A. Anthes, 1976: Initialization of numerical models by a dynamic-initialization technique. Mon. Wea. Rev., 104, 1551-1556.

- - - , 1977: Dynamic initialization of a three-dimensional primitive-equation model of hurricane Alma of 1962. Mon. Wea. Rev., 105, 1266-1280.

Hovermale, J., 1976: First season storm movement characteristics of the NMC objective hurricane forecast model. Natl. Meteor. Center report (unpublished).

- - - , S. H. Scolnik, D. G. Marks, 1977: Performance characteristics of the NMC movable fine mesh model (MFM) pertaining to hurricane predictions during the 1976 hurricane season. Natl. Meteor. Center report (unpublished).

- - - , and R. E. Livezey, 1977: Three-year performance characteristics of the NMC hurricane model. 11th Technical Conference on Hurricanes and Tropical Meteorology. Am. Meteor. Soc. (Boston), 122-125.

Jarrell, J. D., S. Brand, and D. S. Nicklin, 1978: An analysis of western North Pacific tropical cyclone forecast errors. Mon. Wea. Rev., 106, 925-937.

Jarvinen, B. R., 1977: Comparison of initial analysis schemes on the barotropic hurricane model (SANBAR). 11th Technical Conference on Hurricanes and Tropical Meteorology. Am. Meteor. Soc. (Boston), 397-400.

Jones, R. W., 1977a: Vortex motion in a tropical cyclone model. J. Atmos. Sci., 34, 1518-1527.

- - - , 1977b: A nested grid for a three-dimensional model of a tropical cyclone. J. Atmos. Sci., 34, 1528-1553.

- - - , and J. Trout, 1977: 12-level, three-dimensional, nested grid, tropical cyclone model. Presented at 11th Technical Conference on Hurricanes and Tropical Meteorology.

Kurihara, Y., and R. E. Tuleya, 1974: Structure of a tropical cyclone developed in a three-dimensional numerical simulation model. J. Atmos. Sci., 31, 893-919.

- - - , 1978: A scheme of dynamic initialization of the boundary layer in a primitive equation model. Mon. Wea. Rev., 106, 114-123.

- - - , M. A. Bender, and G. Tripoli, 1977: A movable nested mesh primitive equation model. 11th Technical Conference on Hurricanes and Tropical Meteorology. Am. Meteor. Soc. (Boston), 99-100.

Kuo, H.-L., 1965: On formation and intensification of tropical cyclones through latent heat release by cumulus convection. J. Atmos. Sci., 22, 40-63.

- - - , 1969: Motions of vortices and circulating cylinder in shear flow with friction. J. Atmos. Sci., 26, 390-398.

Lewis, B. M., and P. G. Black, 1977: Spectral analysis of oscillations of radar-determined hurricane tracks. 11th Technical Conference on Hurricanes and Tropical Meteorology. Am. Meteor. Soc. (Boston), 484-489.

Madala, R. V., 1977: Semi-implicit and split semi-implicit integration schemes for tropical cyclone prediction models. 11th Technical Conference on Hurricanes and Tropical Meteorology. Am. Meteor. Soc. (Boston), 96-98.

- - - , and R. M. Hodur, 1977: A multi-layer nested tropical cyclone prediction model in sigma coordinates. 11th Technical Conference on Hurricanes and Tropical Meteorology. Am. Meteor. Soc. (Boston), 101-103.

Mathur, M. B., 1978: A case study of analyses and forecasts over tropics with NMC operational models. NMC Office Note 187, 15 pp plus figures.

Mihok, W. F., and D. E. Hinsman, 1977: Tropical storm forecasts during 1977 using the Fleet Numerical Weather Central Tropical Cyclone Model. 11th Technical Conference on Hurricanes and Tropical Meteorology. Am. Meteor. Soc. (Boston), 401-404.

Neumann, C. J., 1975: A statistical study of tropical cyclone positioning errors with economic applications. NOAA Tech. Memo NWS SR-82, 21 pp. [NTIS No. COM-75-11362].

Ookochi, Y., 1978: Preliminary test of typhoon forecast with a moving multi-nested grid (MNG). Japan Meteor. Agency report (unpublished).

Phillips, N. A., and J. Shukla, 1974: On the strategy of combining coarse and fine grid meshes in numerical weather prediction. J. Applied Meteor., 12, 763-770.

Pike, A. C., 1972: Improved barotropic hurricane track prediction by adjustment of the initial wind field. NOAA Tech. Memo NWS SR-66, 16 pp.

Rodgers, E., R. C. Gentry, W. Shenk and V. Oliver, 1978: Benefits of using short interval satellite images to derive winds for tropical cyclones. NASA Tech. Memo 79594, 32 pp.

Rosenthal, S. L., 1978: Numerical simulation of tropical cyclone development with latent heat release by the resolvable scales. I. Model description and preliminary results. J. Atmos. Sci., 35, 258.

Rosmond, T., 1978: A review of global numerical weather prediction. Presented at Technical Exchange Conference, Colo. Springs.

Sanders, F., and R. W. Burpee, 1968: Experiments in barotropic hurricane track forecasting. J. Applied Meteor., 7, 313-323.

- - - , A. C. Pike, and J. P. Gaertner, 1975: A barotropic model for operational prediction of tracks of tropical storms. J. Applied Meteor., 14, 265-280.

- - - , A. L. Adams, N.J.B. Gordon, W. D. Jensen, 1977: A study of forecast errors in a barotropic operational model for predicting paths of tropical storms. 11th Technical Conference on Hurricanes and Tropical Meteorology. Am. Meteor. Soc. (Boston), 389-396.

Singh, S. S., and K. Saha, 1976: Numerical experiments with a primitive equation barotropic model for the prediction of movement of monsoon depressions and tropical cyclones. J. Applied Meteor., 15, 805-810.

Shewchuk, J. D., 1977: Development of a biasing scheme to improve initial dynamical model forecasts of tropical cyclone motion. M.S. thesis, Naval Postgraduate School.

- - - , R. L. Elsberry, 1978: Improvement of short-term dynamical tropical cyclone motion prediction by initial field adjustments. Mon. Wea. Rev., 106, 713-718.

Sobel, J. P., 1976: Nested grids in numerical weather prediction and an application to a mesoscale jet streak. Ph.D. thesis, Penn State Univ.

Tsay, C.-Y., 1977: Numerical predictions of typhoon tracks in the area of Taiwan and its vicinity. 11th Technical Conference on Hurricanes and Tropical Meteorology. Am. Meteor. Soc. (Boston), 405-412.

Walters, T. P., 1978: Improvements in tropical cyclone motion prediction by incorporating DMSP wind direction estimates. M.S. thesis, Naval Postgraduate School.

Yamasaki, M., 1977: A preliminary experiment of the tropical cyclone without parameterizing the effects of cumulus convection. J. Meteor. Soc. Japan, 55, 11-30.

RECENT DEVELOPMENTS IN AUTOMATED WEATHER OBSERVING AND FORECASTING

Donald A. Chisholm

Air Force Geophysics Laboratory

Hanscom AFB, Massachusetts

ABSTRACT

The advent of microcomputer-based technology has presented to the weather observation and forecasting community the opportunity to exploit concepts of automation which heretofore were unattractive from technical, cost and system flexibility points of view. The Air Force Geophysics Laboratory (AFGL) has been exploring various aspects of airfield weather observation automation and short-range (0-3 hr) terminal forecasting. The evolution of the Modular Automated Weather System (MAWS) development will be reviewed. MAWS is a microcomputer-based airfield data acquisition, processing, dissemination and display system integral to future Air Force needs in the Automated Weather Distribution System (AWDS) era. New sensors, observational techniques and prediction techniques are being evaluated at the Otis Weather Test Facility where a high frequency of fog, low cloudiness and a wide range of precipitation forms occur. Particular attention is being given to the automated determination of slant visual range, present weather type and intensity, cloud base height, ceiling and cloud cover. Two approaches to slant visual range determination will be reviewed, offset towers using forward scatter visibility meters and a frequency doubled ruby lidar sensor. A multisensor present weather decision tree approach has been under evaluation while automation of RBC output has been the chief focus of cloud studies.

1. INTRODUCTION

The U. S. Air Force (through the Air Weather Service) has developed increasing requirements for fully-automated weather observing and short-range forecasting capabilities at both fixed and bare-based airfields. These requirements are driven by (1) the continual press for manpower reductions, (2) the emergence of technology opportunities in weather sensing, processing, communicating and display, and (3) increasing demands for weather information by DoD command, control and communications (C-cubed) and weapon systems developers and operators. The Air Force Geophysics Laboratory (AFGL) initiated a broad program dealing with various aspects of these requirements over two years ago. The foundation of this program has been the development of MAWS, which stands for Modular Automated Weather System. MAWS is a microprocessor-based system which has been configured to automatically handle the present day and future airfield weather observing and short range prediction requirements. It has been designed such that, as new sensing capabilities are automated they can be integrated into the system in a straightforward, modular fashion.

The complete development of an automated weather observing capability demands the solution of several difficult observation automation problems. These include present weather determination, cloud base height and ceiling, prevailing visibility, slant visual range and vertical profiles of temperature, moisture and winds in the lower troposphere. Efforts are underway to solve these problems at AFGL, at the Army's Atmospheric Sciences Lab, at the Equipment Development Lab and Test and Evaluation Division of the National Weather Service and at NOAA's Environmental Research Labs. There has been mixed success thus far. This paper reviews the research and development underway at AFGL and notes complementary work being accomplished in other government agencies.

2. MODULAR AUTOMATED WEATHER SYSTEM (MAWS)

The key to the design of an experimental system such as MAWS is to ensure flexibility to allow the test and evaluation of various configurations of sensing, processing, archiving and display components. The flexibility of MAWS lies in its use of microprocessing technology which is itself undergoing rapid advancements and improvements in performance, reliability and decreasing unit costs.

Figure 1 depicts major components of the MAWS Demonstration which has been undergoing test and evaluation at Scott AFB, Illinois since early 1977 in order to examine its strengths and weaknesses in a long term, real-world and

and hands-off environment. A complete description of the demonstration model can be found in Tahnk and Lynch (1978). Shown in the upper right is one of three surface observing locations placed along runway 13/31, each of which includes measurements of temperature, dewpoint, wind direction and speed, and sensor equivalent visibility obtained from a forward scatter meter (FSM). The tower, shown in the upper left, is sited 600 m south of the touchdown point of Runway 13 and has instrumentation similar to the surface locations at the 25 and 40 m levels. A digital altimeter, digital clock and operational transmissometer and rotating beam ceilometer (RBC) complete the set of sensors input to, and automatically processed by, the prototype MAWS Demonstration Model.

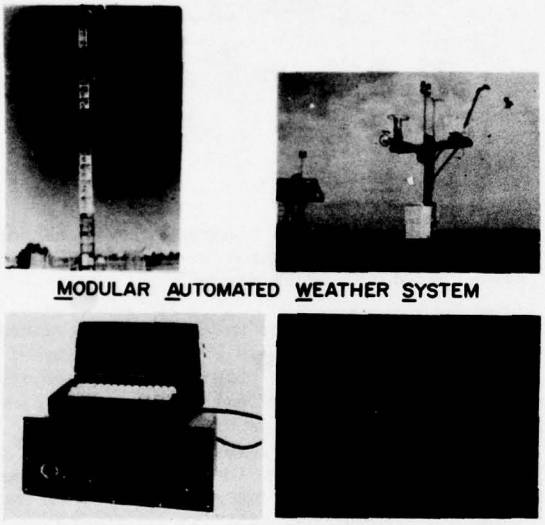

Figure 1. Modular Automated Weather System (MAWS) components: upper right, instrumented runway site; upper left, instrumented 40 m tower; lower left, microcomputer and display device; lower right, example of forecast output.

Remote and supervisory microprocessor-based data sets, illustrated in the lower left of Figure 1, are composed of central processing units, read-write and programmable memory and suitable control logic which make them easily adaptable to aviation weather requirements. Considerable flexibility exists with respect to the type and number of output devices which can be interfaced with MAWS. At Scott, the real-time display of weather data is accomplished with the Burroughs TD700 alphanumeric plasma display board, shown in the lower left. On-line printers to monitor sensor performance by on-site personnel and magnetic tape recorders for archiving and post-analysis purposes are also used.

Messages are updated every minute and sent to the alphanumeric displays located at the Scott BWS and AWS headquarters. These messages include (1) fresh observations from around the airfield, (2) comparative data from 5, 10, 15 and 30 minutes earlier, (3) "metwatch" parameters which would require the dissemination of alerts or warnings when critical values are exceeded and (4) automated probability forecasts of runway visual range and cloud base height, as shown in the lower right of Figure 1. The forecasts are generated by a single-station, single-element Markov model whose output is converted to probabilistic form, based on Gaussian assumptions, for prediction intervals of 15, 30, 60 and 180 minutes.

MAWS is viewed as a key element in the recently validated Air Force requirement for an Automated Weather Distribution System (AWDS). The conceptual relationship of MAWS to AWDS and other aspects of the Dod-wide C-cubed system is depicted in Figure 2. AWDS will encompass the total Air Force weather support system, tying together the Automated Weather Net (AWN), Global Weather Central (AFGWC), MAWS capabilities at each airfield, etc. It, in turn, will interface principally with the World-Wide Military Command and Control System (WWMCCS) and, thusly, with the rest of the DoD C-cubed system and operational units supported by the Air Weather Service.

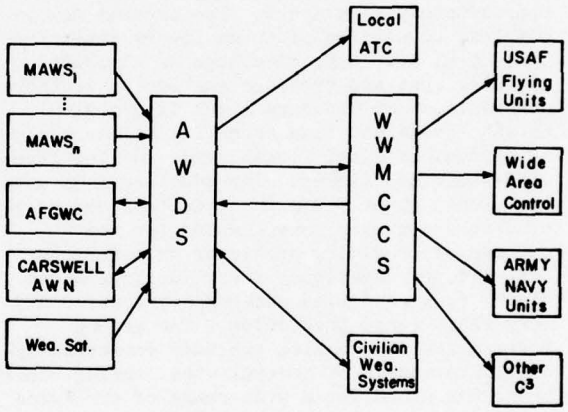

Figure 2. Conceptual relationship of MAWS to rest of DoD command, control and communications system.

3. AUTOMATION OF WEATHER OBSERVATIONS

Our efforts in the development and evaluation of new sensors, observational techniques and short-range forecasting techniques are being conducted at a Weather Test Facility (WTF) located on Otis Air Force Base, Mass. The WTF, shown schematically in Figure 3, is located on an open, flat and treeless area, well removed from the active runways at Otis and in an area frequented by considerable low cloudiness, coastal fog and the full range of precipitation forms.

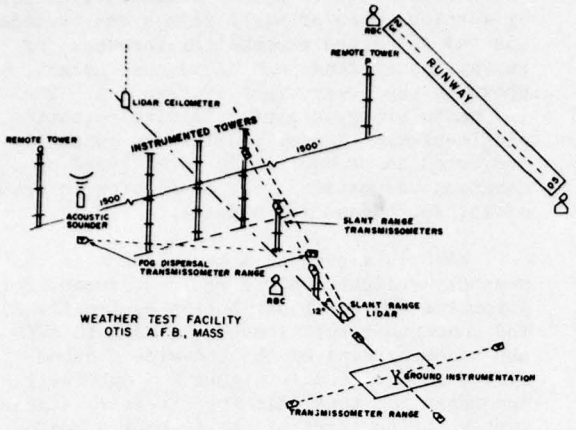

Figure 3. Schematic configuration of tower-mounted and ground-based instrumentation at the Otis Weather Test Facility.

Measurements of horizontal wind, temperature, dewpoint, and sensor equivalent visibility are made on each tower in the complex at levels approximately 17 m apart. The central tower complex, consisting of three towers extending to 5 m, 35 m, and 70 m, simulates an aircraft approach zone and provides continuous weather observations at Category I and II decision height levels and data essential to the evaluation of glideslope slant visual range and low-level wind-shear techniques. Two additional 35 m towers are placed about 500 m on opposite sides of the simulated approach zone complex for the purpose of providing predictor data for the offset tower techniques for glideslope slant visual range and wind shear specification and very short range prediction. The ground instrumentation complex includes commercially-available models of several wind sensing concepts being evaluated for a wide range of Air Force applications; several recently-developed visibility measuring devices such as forward scatter, back scatter, and total scatter meters, conventional and solid state transmissometers, and a nephelometer used in present weather determination studies; and pyranometers, sun-tracking pyrheliometers and automated rotating beam ceilometers for cloud base height, ceiling and cloud cover studies. Research prototypes of laser devices designed to measure cloud base height, weather type and obstruction to vision, slant visual range, and low level wind profiles and an acoustic wind sounder have been or will be undergoing selective testing at the WTF.

3.1 Present Weather Determination

Two fundamental approaches are being pursued herein; a high risk approach utilizing experimental laser devices at both AFGL and NWS's EDL (See Sanders, 1978) and a low risk approach described below. The availability of the array of weather sensors at the WTF and the wide range of weather phenomena common to the area provides an ideal setting for the evaluation of a decision-tree approach to the objective determination of precipitation type and intensity and the nature of the obstruction to vision. Figure 4 depicts the sensors being utilized at the Otis WTF in a MAWS context for the decision tree studies. They include both tower-mounted and ground-based temperature-dewpoint sets, wind sensors, forward scatter meter, a transmissometer, backscatter meter, nephelometer and a 0.005" tipping-bucket rain gage.

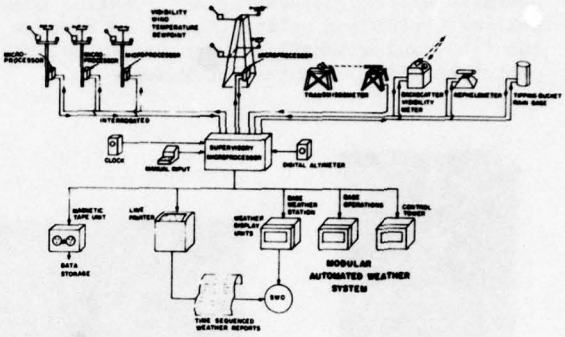

Figure 4. Functional diagram of MAWS sensor configuration for present weather decision tree technique development study.

The decision tree under initial evaluation at this time is shown in Figure 5. Some of the more obvious decision points in the approach are (a) measurement of extinction coefficient to indicate the absence or presence of an obstruction to vision, (b) rain gage measurement for precipitation intensity, (c) comparative ground and tower measurements of extinction coefficient and humidity to discriminate between fog and ground fog, and (d) the combined measurements of extinction coefficient by forward scatter and nephelometer together with temperature and humidity to distinguish between fog and haze or smoke. Comparative measurements from the forward scatter and backscatter meters along with rain gage and temperature measurements permit discrimination between rain and snow. Finally, characteristic differences between the transmissometer's output and the forward scatter meter coupled with a precipitation intensity distinguishes drizzle and rain.

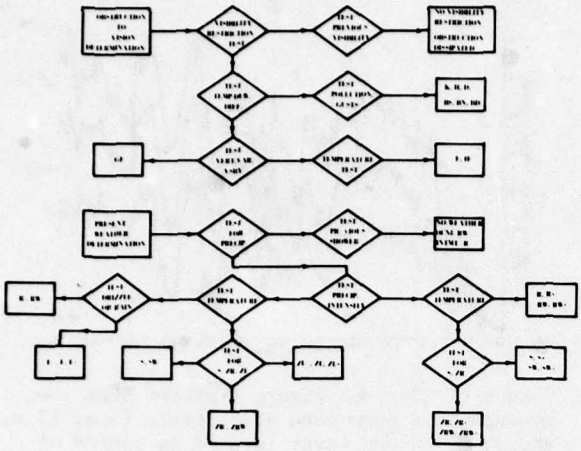

Figure 5. Flow diagram of initially developed present weather decision tree.

The model's algorithms are being evaluated on a minute-by-minute basis against the operational weather observations routinely reported for Otis AFB and taken at the FAA control tower approximately one mile south of the WTF. The technique has been found to be responsive to rapidly changing weather events and capable of properly discerning all weather events except the presence of thunder or hail. The evaluation of this technique will be completed after this winter's season.

3.2 Automation of Ceilometry

Here again there are two basic approaches being pursued by the Air Force and the NWS. Lidar devices, using a variety of laser sources, are in various stages of development, test and evaluation. AFGL's activities in this regard have diminished significantly over the past year due to the abandonment of this technology area by the sole contractor we were supporting. While we await the emergence of new corporate capabilities or interests, we have continued to pursue techniques towards the full automation of the workhorse RBC of the operational inventory.

The automation of the AN/GMQ-13 RBC has proven to be tedious, complex task of interface design and development and meticulous software logic. The rectified and filtered direct current signal from the RBC has to be acquired, processed and analyzed automatically and continuously without interfering with the standard CRT output capability of the system. The hardware design is generalized and flexible enough to be applicable to any RBC and any projector lamp. The hardware interface successfully establishes the background level from each 90 degree scan of the source lamp, filters out spurious and unwanted returns, and provides for automatic gain and offset adjustment under software control. The conditioned signal is then analyzed in real time with an Intel 8080 microprocessor software module.

The configuration of the RBC is such that there are two incandescent lamps in the projector which alternately rotate through the 90 degree scan every six seconds. The software initially evaluates the lamp intensities, selects the strongest and gathers cloud structure data from it once every 12 seconds. It identifies primary and secondary maxima from data divided into 360 distinct bins representing each 0.25 degree of elevation from 0 to 90 degrees. It then applies a rigorous averaging and filtering scheme to arrive at a representative cloud base height for each minute based on the five scans generated by the most intense projector lamp. The software logic results in a cloud base height value in one of the following forms; no reportable cloud base height, obscuration, or reportable cloud base height ranging from 15 to 1450 m (50-4800 ft) given a 152 m (500 ft) RBC baseline.

Studies have been conducted by the Test and Evaluation Division of NWS on the reliability and representativeness of one, two and three RBC's deployed around an airfield to determine cloud ceiling and cloud cover in layers up to 7000 ft AGL. Based on these studies, reported by Bradley (1978), cloud sensor configurations can be proposed for various fixed and bare-based installations.

3.3 Slant Visual Range Techniques

The requirement for accurate and timely measurements of airfield visibility have become more urgent as the operational minima for low visibility approaches and landings are reduced. Presently the operator is supplied human observer estimates of prevailing visibility and/or instrumental measurements of runway visual range (RVR) at one or more locations along the runway. Experience has shown, however, that RVR and prevailing visibility are often not representative of a pilot's visual perception while approaching decision height along the glide slope. Progress has been slow and difficult in developing sensors which can effectively measure the slant visual range (SVR) in the airspace volume, shown in Figure 6, between decision height and the runway visual segment and between the glide slope path and the cockpit cutoff angle. An experimental model of a backscatter lidar using an eye-safe, frequency doubled ruby laser has been delayed in its development due to repeated fabrication problems. This system is intended to minimize multiple scattering, provide sufficient range penetration in low visibility, be capable of identifying layers/patches of fog, and most importantly be eye-safe.

Figure 6. Depiction of landing zone slant visual range geometry and terminology.

The early work in the development of an offset tower system to specify SVR in the landing zone, see Bradley et al (1976), has been extended through tests in the marine fog environment at the WTF. There is a high degree of horizontal homogeneity in Cape Cod advection fog, as shown in Figure 7, and concurrently strong and persistent vertical gradients in fog intensity as shown in Figure 8. Drawing on this fact, techniques were formulated which use visibility observations taken on a tower 500 m (1500 ft) from the simulated landing zone, with the expectation of providing better specifications and short range predictions of glidescope SVR than would be obtained from ground-based RVR measurements. The results of this study are discussed in more detail in Hering and Geisler (1978).

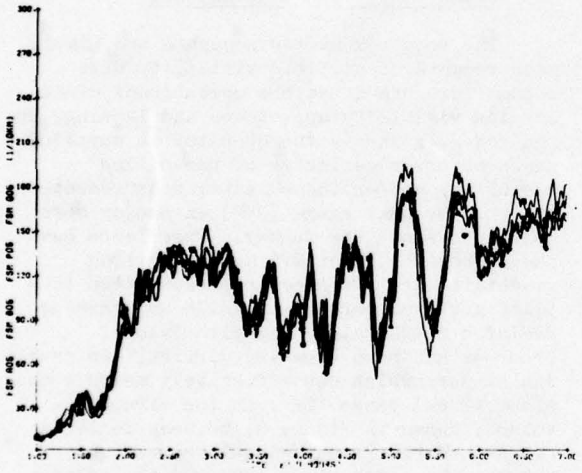

Figure 7. Atmospheric extinction coefficient measured at the WTF on 1 April 1976 at the 17 m level of 4 towers separated by up to 1 km distance. For reference, extinction coefficients corresponding to an RVR of 1600 m and 800 m, at night, would be 53 and $115 \times 10^{-4} m^{-1}$ respectively.

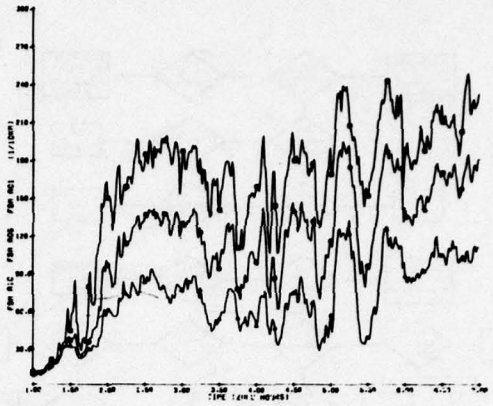

Figure 8. Same as Figure 7 except that measurements were made at 3 levels (3 m, 17 m, and 35 m) on one tower located in center of WTF.

The offset tower formulations tested thus far consist of two approaches to specifying the Category II landing zone SVR, defined by the straight-forward average of the extinction coefficient measured at the 3, 17, and 35 m levels ($\bar{A}$). The first method (Q_{100}, Q_{50}, Q_{10}) uses the simple average of extinction coefficient measured at 3 levels (3, 17, and 35 m) of tower Q (See Figure 9) while the second (Q_{50} A_{10}) tests the utility of a single sensor on a 17 m (50 ft) tower in combination with the touchdown RVR. The control technique for these tests (A_{10}) is the touchdown RVR measurement.

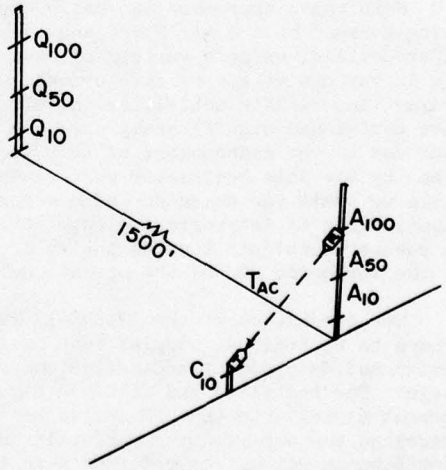

Figure 9. The configuration of tower-mounted FSM's for offset tower SVR tests.

The three methods were evaluated on four episodes of extensive fog at the WTF. The first three were advection fog episodes while the fourth was a period of intense radiation fog. Table 1 lists the percent root mean square error of estimation of $\bar{A}$ specification (lag) and very short range prediction (5 min lag). The results for the three advection fog episodes show the tower methods to be consistently better than the control technique and with a small errors of estimate.

The higher errors obtained in the radiation fog case were expected and yet the tower methods still yielded better estimates than did the control technique. When reduced to the standard categorical evaluation scores of the probability of detection (POD), false alarm ratio (FAR) and threat score (TS), one finds POD's and TS's exceeding 90% for the tower methods in advection fog with FAR's generally below 5% supporting the higher degree of horizontal homogeneity assumption of the methods.

Table 1

PERCENT RMS ERROR

0 LAG (5 MIN LAG)

EPISODE	$Q_{100}Q_{50}Q_{10}$	$Q_{50}A_{10}$	A_{10}
APR 76	11 (27)	12 (23)	43 (43)
MAY 76	19 (25)	18 (27)	33 (41)
JUL 76	17 (39)	14 (34)	34 (36)
AUG 77	42 (43)	38 (51)	114 (203)

While the utility of an offset tower system to specify SVR in coastal advection fogs has been clearly demonstrated, it must be tested in other geographical areas and under other types of fog conditions before a definitive assessment can be made of its widespread usefulness. To this end, data being gathered at Scott AFB, IL, as part of the demonstration of the prototype MAWS will provide valuable additional tests of the system. These tests will be reported at a later date.

4. MAWS DEMONSTRATION

Based on the continuing R&D program being conducted at AFGL and the Otis WTF, there are now several additional features or capabilities in the prototype MAWS at Scott AFB which were not a part of the system installed in January 1977. Horizontal and vertical wind shear algorithms based on the output of the runway and tower mounted wind sensors are now routinely computed, displayed and archieved on magnetic tape. The output of the RBC is continuously analyzed by an objective, computerized procedure and displayed. Method 2 of the offset tower SVR approach has been implemented and is undergoing evaluation. In addition, the RVR prediction model has been modified to consider the SVR observation when it (SVR) reflects a more restrictive flying condition than does the RVR.

Reflecting on our operating experience with MAWS for nearly a 24-month period, we have been generally pleased with the performance of the system given that it is based largely on commercial-grade microprocessing components and has been functioning in an experimental mode without the benefit of on-site personnel to monitor and maintain its performance. The lessons learned from the problems encountered have led to considerable redesign and reconfiguration of the system and its components although most changes are transparent to all but the most astute observers. Most of the problems have been generated by (1) variations in the AC power available to the system, (2) noise and other contaminants on the commercial-grade telephone lines, and (3) environmental factors such as nearby lightning strikes, excessive temperatures and high winds.

All of these problems point to the need, in the operational deployment of such systems, to have well-trained technicians who can maintain the full range of hardware components from weather sensors through microcomputers. Without them, no system can be expected to run continously and error-free.

5. SUMMARY

Significant strides have been made recently at AFGL and other government facilities towards developing sensing capabilities which will permit the meteorological community to step forward into the era of full automation of basic observing, on-site and real-time processing, dissemination and dynamic display of airfield weather data required by forecasters, aircraft controllers, pilots and other principal users. While some progress has been made in developing effective and reliable aviation-critical forecasts techniques for the period of 0 to say 3 hr, much remains to be done. In the meantime, the advent of inexpensive yet powerful microprocessing technology has been demonstrated to be ideally-suited for specialized applications such as automated airfield weather systems.

6. REFERENCES

Bradley, G. S., C. W. Lohkamp, and R. W. Williams, 1976: Flight Test Evaluation of Slant Visual Range/ Approach Light Contact Height (SVR/ALCH) Measurement System, Final Report Phase III, FAA-RD-76-167.

Bradley, J. and D. W. Downey, 1978: Aviation Automated Weather Observing System (AV-AWOS) Test Results and Automated Low-cost Weather Observation System (ALWOS) Development Status, Proceeding of the 8th Technical Exchange Conference, Air Force Academy.

Hering, W. S. and E. G. Geisler, 1978: Forward Scatter Meter Measurements of Slant Visual Range, AFGL-TR-78-0191, Survey in Geophysics No. 393.

Sanders, M. J., 1978: A Laser Present Weather Identifier System, Proceedings of the 8th Technical Exchange Conference, Air Force Academy.

Tahnk, W. R. and R. H. Lynch, 1978: The Development of a Fixed Base Automated Weather Sensing and Display System, AFGL-TR-78-0009, Instrumentation Paper No. 260.

AVIATION AUTOMATED WEATHER OBSERVATION SYSTEM (AV-AWOS) TEST RESULTS

AND

AUTOMATED LOW-COST WEATHER OBSERVATION SYSTEM (ALWOS) DEVELOPMENT STATUS

James T. Bradley
Test & Evaluation Division
Office of Technical Services
NOAA - National Weather Service
Sterling, Virginia

and

Douglas W. Downen
Equipment Development Laboratory
Systems Development Office
NOAA - National Weather Service
Silver Spring, Maryland

ABSTRACT

The National Weather Service (NWS) has developed the AViation Automated Weather Observation System (AV-AWOS) for the Federal Aviation Administration (FAA). The goal of the AV-AWOS development program was to develop an automated system that provides as nearly as possible the same information provided by a human weather observer. AV-AWOS was operationally test for four months during early 1978 at Patrick Henry International Airport, Newport News, Virginia. The purpose of the test was twofold--scientific evaluation and user acceptability. The scientific portion concentrated on comparing the AV-AWOS observation with manned observation made by the FAA's Flight Service Station personnel at Patrick Henry. Cloud and visibility algorithms were verified. Users of the AV-AWOS observation were querried during the test to determine their reaction/acceptance of an automated observation. Results of both aspects of the test are presented.

A follow-up program to AV-AWOS is underway for the FAA by NWS. The Automated Low-Cost Weather Observation System (ALWOS) is being developed for use at the more than 900 airports in the U.S. having standard approach procedures but having no weather observations. The development status of ALWOS is presented and plans for operationally testing are outlined.

1. INTRODUCTION

The Aviation Automated Weather Observation System (AV-AWOS) development program was conducted under an interagency agreement between the National Weather Service (NWS) and the Federal Aviation Administration (FAA). The program began with the preparation of the AV-AWOS Development Plan in 1973. The goal of the AV-AWOS program was to develop and test a system that would automate the aviation surface weather observation. Under the interagency agreement, FAA provided the funding and directed the AV-AWOS program. NWS was responsible for the technical management and administration. Assistance was provided to NWS by commercial contractors.

The development effort culminated in an operational test of the Developmental Model AV-AWOS in early 1978 at Patrick Henry International Airport, Newport News, Virginia. A similar development program is underway by NWS for FAA using microprocessor technology. The Aviation Low-Cost Weather Observation System (ALWOS) is being developed by NWS with the aid and support of the FAA. ALWOS will be demonstrated at Frederick Municipal Airport, Frederic, Maryland beginning in early 1980.

2. SYSTEM DESCRIPTION

The AV-AWOS processes meteorological sensor data for the transmission of an automated surface weather observation. Figure 1 is a block diagram of the Developmental Model AV-AWOS tested at Newport News, Virginia. Weather parameters observed, processed and transmitted by the AV-AWOS include cloud height and amount, visibility, precipitation (yes/no precipitation, thunderstorms, hail and freezing rain), sea level pressure, temperature, dew point, wind (speed, direction and gusts), altimeter setting and runway visual range. The AV-AWOS sensor information is input through interfaces to the data processor. The processor performs programmed algorithms on the sensor data for data quality and processing. The automated weather observation is then available for transmission via the media shown in Figure 1 (Service A,

CRT displays and automated voice). A sample of the AV-AWOS observation is--

PHF AWOS 15 SCT M25 BKN 1/2V P 132/60/58/ 1310G25/993/RO7VR10V25 VSBY 1/4V3/4.

The AV-AWOS is capable of updating the observation every minute. However, the system was programmed to only update the observation once every five minutes during the test at Patrick Henry.

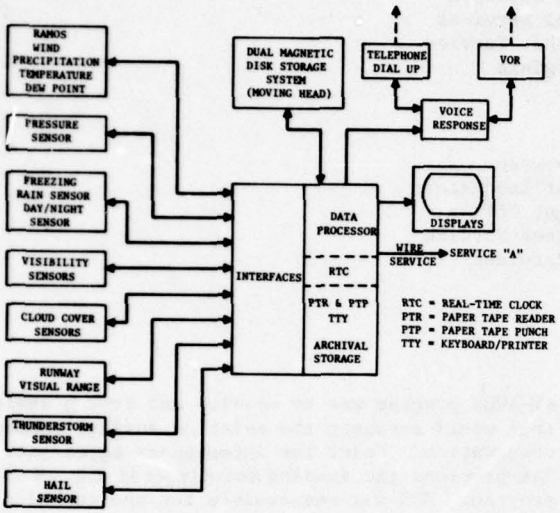

Figure 1. Block Diagram of Aviation Automated Weather Observation System (AV-AWOS)

3. OPERATIONAL TEST

The Developmental Model AV-AWOS underwent operational testing at Newport News, Virginia during a four-month period in early 1978. The test was jointly managed by NWS's Equipment Development Laboratory (EDL) and Test and Evaluation Division (T&ED). Two major areas were evaluated during the test. The first was a user assessment of the total AV-AWOS system. The second area was verification of the cloud and visibility algorithms. The latter area included testing for geographic bias in cloud height and visibility observations and evaluation of the number of cloud and visibility sensors required for an automated observation.

Certified National Weather Service observers monitored the automated observation. Their function was to prevent erroneous or unrepresentative automated observations from being transmitted. When the AV-AWOS observation was not in reasonable agreement with the human observation taken by FAA Flight Service Station personnel at Patrick Henry, the automated observation was not disseminated. This procedure was necessary for operational safety purposes.

3.1 User Assessment Plan

The purpose of the AV-AWOS assessment plan at Patrick Henry was to obtain user reaction/ acceptability of an automated observation. FAA's National Aviation Facilities Experimental Center and NWS's T&ED and EDL prepared a questionnaire for use in surveying users of the AV-AWOS observation. The questionnaire was distributed to the following user groups during the test period:

1. General Aviation Pilots
2. Air Carrier Pilots, Dispatchers and Forecasters
3. FSS Briefers
4. Air Traffic Controllers
5. NWS and Military Forecasters and Observers

Several of the unique features of the AV-AWOS were evaluated using the questionnaire. These features included the height limitation of 7,000 feet for cloud observations; visibilities greater than eight (8) miles reported as 8+; weather by computer generated voice over the telephone; no rain/snow discrimination--only precipitation yes/no reported; more frequent updating of the weather observation; no remarks on thunderstorm bearing/movement; the availability of continuous and updated weather inflight on the Harcum VOR via automated voice; the availability of weather observations locally on CRT displays; and AV-AWOS considered in its entirety.

Nearly two-hundred questionnaires were returned by users of the AV-AWOS during the test at Newport News. To determine a measure of prejudice against an automated observation, users were asked if they were bothered by the fact AV-AWOS is an automated system. Their response was--

Bothers	23%
Does Not Bother	77%

Users were querried to determine their preferred source of weather information and replied--

Human Observer	48%
Automated System	9%
Does Not Matter	43%

Users were asked to list the most desirable feature of AV-AWOS. The most frequent desirable features given were--

1. Frequent updating
2. Automated voice
3. Cloud and visibility observations

Fifty-six (56) percent of the respondees gave the frequent update capability of AV-AWOS as the most desirable feature.

The most frequent least desirable features were--

1. Precipitation type limitation
2. Automated voice intelligibility

Forty-one percent of the users gave the limitation of AV-AWOS in reporting precipitation types as the least desirable feature.

The overall suitability of AV-AWOS for widespread operational use was rated. The results were as follows--

Suitable with minor changes	82%
Unsuitable	18%

Most of the unique features of AV-AWOS were evaluated during the test at Patrick Henry. Results from some of their responses are given below.

Cloud Observation Height Limit--7,000 Feet

Desirable	20%
Neutral	41%
Undesirable	39%

Weather Observations Via TV Displays

Desirable	71%
Neutral	17%
Undesirable	12%

No Rain/Snow Discrimination

Desirable	4%
Neutral	7%
Undesirable	89%

Frequent Updating of Weather Observation

Desirable	64%
Neutral	23%
Undesirable	13%

AV-AWOS Considered in its Entirety

Desirable	48%
Neutral	24%
Undesirable	28%

No attempt is made here to interpret the users' assessment of the AV-AWOS observation. However, results from the test at Newport News are being used to refine AV-AWOS prior to operational implementation.

3.2 Scientific Test

The primary purpose of the scientific aspect of the AV-AWOS test at Patrick Henry was to verify the cloud and visibility algorithms developed by NWS's Test and Evaluation Division. These algorithms had previously undergone extensive testing at Sterling, Virginia. The test at Patrick Henry offered the opportunity to test the algorithms at a different location and under different weather regimes. The AV-AWOS used a backscatter sensor (Videograph) for measuring visibility and a rotating beam ceilometer for measuring cloud height. These sensors were in continuous operation at Newport News except for maintenance periods. Data from these sensors were recorded and underwent evaluation at T&ED.

The AV-AWOS Videographs and ceilometers were set up in a triangular network around Patrick Henry Airport. The length of each leg of the visibility triangle was about 3 miles and about 7 miles for the ceilometer triangle. Sensors were located at each vertex of the triangles. The decision to use 3-mile legs for visibility was based on the need to supply the aviation community with visibility information over a large area around an airport, yet keep within the same visibility universe. Use of three sensors was a pragmatic choice based on resources and the difficulties in obtaining sites and installing data lines across large distances.

The design length on each leg of the ceilometer triangle was about 7 miles. A basis for this configuration was the nominal amount of sky area a typical observer can view. Assuming the observer can see only to within 8° of the horizon when cloud bases are at 3,000 feet, the observer's diameter of view is about 8 miles. The AV-AWOS ceilometer network spacing, then, covers an area approximately the same size an observer could see with a cloud base at 3,000 feet. The number of ceilometers to use was a difficult choice. Although an infinite number of sensors in a network area would provide nearly perfect sampling, this approach was impractical. Instead, one ceilometer was located at each vertex of the network triangle. This decision was based on economic considerations, the availability of sensors and previous investigations.

Details on the particulars of the cloud and visibility algorithms are not presented. Copies of the algorithms can be obtained from either author.

Results from previous studies of cloud and visibility observations are included with the results obtained from Newport News. The complete results from the scientific testing are not presented for the sake of brevity. The complete test results from Newport News can be obtained from either author.

3.2.1 Results of Automated Cloud Observation Tests

An automated sky condition observation was generated by AV-AWOS each minute, but the data set is limited to the number of "record" human observations available (24 per day). This set was further restricted to the days the human observer at Patrick Henry reported the presence of clouds on several observations. The final data set totalled over 600 observations. Some comparisons are made with earlier test results obtained on T&ED's observational network at Dulles International Airport (IAD). In those tests, the data set was 100 observations.

In the following comparisons, "AV-AWOS" means the data is derived from the three ceilometer network and processed by the AV-AWOS cloud algorithms. "Two separated RBC's" means that the data from two rotating beam ceilometers are processed separately as if each were a complete and independent three-sensor ceilometer network.

Table 1 shows a comparison of cloud layers reported by various methods. In preparing this table, the number of cloud layers for each observation was put into one of four cateogries (0, 1, 2, 3 layers). The number of observations obtained by several different methods (e.g., human vs. AV-AWOS algorithm) and a 4x4 matrix formed for each pair. Agreement to $\pm$ 1 layer means, for example, that a human report of 1 layer would be compared with the number of observations in the 0, 1, and 2 layer categories of the appropriate paired sensor.

TABLE 1

NUMBER OF CLOUD LAYERS: COMPARISON OF METHODS

Methods	% Agreement $\pm$ 1 Layer
AV-AWOS/IAD Observer	74%
AV-AWOS/PHF Observer	87%
Two Separated RBC's-IAD	89%
Two Separated RBC's-PHF	92%
AV-AWOS/Separated RBC-PHF	85%

Table 1 tests our hierarchical clustering techniques. The general agreement among methods indicates that we are indeed clustering data derived from various sources in a consistent manner. The agreement between the AV-AWOS/PHF observer comparisons (87%) assures that not only are the clustering techniques consistent but the clusters themselves are similar to those reported by the human observer.

In Table 2, joint reports of ceilings occurred in upwards of about 78% of the cases regardless of the method used. The agreement between "two separated RBC's-PHF" (78%) would likely be higher in a fully operational network. In this category we suffered the loss of some data in line transmissions across our test network. As with the cloud layer comparisons, the agreements between AV-AWOS and the PHF observer give assurance that our methods are not only consistent but also in general agreement with human results.

Table 3 summarizes results of ceiling height comparisons. Agreement between methods is better at the lower, more critical cloud heights but falls off at higher cloud heights. This is probably due to the characteristics of the RBC (small errors at low altitude tend to increase with height). The AV-AWOS/PHF observer agreements have been lowered due to our experimental procedures for handling partial obscurations. During most of the PHF operational test, a -X and .6 cloudiness were added to reported cloud cover when the visibility fell below 1 1/2 miles. As a result, many scattered layers were reported as broken. This bias is reflected in these comparisons. It was also noted that many of the comparisons in which there were differences between observation methods greater than 200 feet were either nighttime observations or observations during precipitation periods.

We believe the cloud height and sky cover algorithm to be complete. This excludes partial and total obscuration for which the algorithm is inferred rather than empirical. Given a more reliable cloud sensor less prone to height and communication error, the scores in Tables 1, 2 and 3 will be still higher.

3.2.2 Results of Automated Visibility Observation Tests

FAA observers at PHF took routine visibility observations at ground level. When visibility dropped below 4 miles, observations were also taken at the airport control tower level of 45 feet, a standard procedure. In either case, distribution of visibility targets was limited by circumstance. For visibilities above 2 miles, the only adequate visibility marker was a 500-foot smokestack located 7 miles to the north of the observer. In our analyses only the visibility estimated by the ground observer was used.

The three AV-AWOS Videographs were sited to avoid local sources of moisture and fog. However, local sources of pollution, particularly automative emissions, appear to have affected one of the sites. Two of the Videographs were located on low roofs, while the third was at ground level.

For the following comparisons, both sensor and human visibility values were first rounded to the nearest mile. The number of

TABLE 2

OCCURRENCE OF CEILING REPORTS: COMPARISON OF METHODS

Methods	% of Joint Occurrence*
AV-AWOS/IAD Observer	78%
AV-AWOS/PHF Observer	82%
Two Separated RBC's-IAD	81%
Two Separated RBC's-PHF	78%
AV-AWOS/Separated RBC's-PHF	86%

*Occurrence = either method reports ceiling

TABLE 3

CEILING HEIGHT VALUES: COMPARISON OF METHODS

1. Ceiling: 100 to 1000 feet

Methods	% Agreement to ± 200 feet
AV-AWOS/IAD Observer	96%
AV-AWOS/PHF Observer	75%
Two Separated RBC's-IAD	82%
Two Separated RBC's-PHF	85%
AV-AWOS/Separated RBC-PHF	92%

2. Ceiling: 1100 to 3000 feet

Methods	% Agreement to ± 400 feet
AV-AWOS/IAD Observer	69%
AV-AWOS/PHF Observer	53%
Two Separated RBC's-IAD	82%
Two Separated RBC's-PHF	75%
AV-AWOS/Separated RBC-PHF	74%

visibility observations in each of nine categories (0, 1, ..., 7, 7+) was then computed for pairs of observations obtained by different methods (e.g., sensor vs. sensor, human vs. sensor), and a 9x9 matrix formed for each pair. Tables 4 and 5 were prepared from these matrices. In these tables, agreement to ± 1 mile means, for example, that a visibility category of 3 miles for a method based on human prevailing visibility (PV) would be compared with the observations in the 2, 3 and 4 mile range categories of the appropriate paired sensor. While a sensor PV was generated each minute (1440 per day), our data set was limited to the number of "record" human observations available (24 per day). We further limited this set to those on days which the human reported an obstruction to visibility. The final data set totaled 490 observations.

Table 4 shows the results of comparisons between totally objective sensor derived visibility observations. First, sensor observations from two of the three Videograph sites were compared with each other and level of agreement recorded. Then a sensor PV observation derived from the three-sensor network was compared with a similar observation from one arbitrarily chosen network sensor.

Results demonstrate consistently high and stable relationships between objective visibilities derived from individual sensors in the visibility network. The experiment was conducted at both IAD and PHF with almost identical effect.

The substantive results shown in Table 4, the intercomparisons of sensor derived objective visibility observations, are not duplicated when human subjective observations are introduced. Table 5 shows comparisons of objectively and subjectively derived visibility observations. Greatest agreement occurs when the observer records visibility below 5 miles. But strength of comparisons weakens for the other examples.

There appears to be the effect of a "non-linear" human/backscatter sensor relationship. Strong relationships were noted between human and Videograph derived visibility in the presence of hydrometeors. When lithometeors reduced visibility, the visibility algorithm (using Videograph measurements as input) characteristically produced lower visibilities than those reported by the human observer (Table 6). Although we believe the visibility algorithm performance to be effective, performance of the Videograph needs review.

TABLE 4

VISIBILITY OBSERVATIONS: SENSOR vs. SENSOR

Methods	Agreement ± 1 Mile
1. All Visibility Values:	
2 Separated Sensors-PHF	87%
2 Separated Sensors-IAD	89%
Sensor PV/Single Sensor-PHF	92%
2. Sensor Visibility Below 5 Miles:	
2 Separated Sensors-PHF	90%
2 Separated Sensors-IAD	90%
Sensor PV/Single Sensor-PHF	93%

TABLE 5

VISIBILITY OBSERVATIONS: HUMAN vs. SENSOR

Methods	Agreement $\pm$ 1 Mile
1. All Visibility Values:	
Sensor PV/PHF Observer	69%
Sensor PV/IAD Observer	58%
2. Observer Visibility Below 5 Miles:	
Sensor PV/PHF Observer	80%
Sensor PV/IAD Observer	72%
3. Sensor visibility Below 5 Miles:	
Sensor PV/PHF Observer	57%
Sensor PV/IAD Observer	45%

TABLE 6

VISIBILITY OBSERVATIONS: A COMPARISON OF METHODS

Methods	Agreement $\pm$ 1 Mile
1. Sensor Visibility Below 5 Miles:	
Sensor PV/PHF Observer	
- All Cases	57%
- Precip Occurring	86%
- Fog Reported by Human	88%
- No Precipitation	43%
Sensor vs. Sensor	
- All Cases	90%
2. Sensor Visibility 1 Mile or Less:	
Sensor PV/PHF Observer	
- All Cases	95%
3. All Sensor Visibility Values:	
Sensor PV/PHF Observer	
- All Cases	69%

4. AUTOMATED LOW-COST WEATHER OBSERVATION SYSTEM (ALWOS)

A follow-on development to the AV-AWOS is currently underway by NWS for the FAA. The Automated Low-Cost Weather Observation System (ALWOS) development program is being conducted under an interagency agreement between these two agencies. ALWOS is intended for use at the more than 900 public airfields in the United States where approved Standard Instrument Approaches exist and where no weather observation is available. FAA's Flight Standards has attributed numerous accidents to the lack of a weather observation at an airport prior to commencing an IFR approach.

As the name of the system implies, one of the objectives of the ALWOS design will be the lowest possible cost for production units. However, reliability and maintenance costs over the system life cycle are being considered as opposed to only initial purchase costs.

At present there is a broad spectrum of NWS projects and activities in the design and development of improved and new sensors, increased processing capabilities and efforts to develop more reliable and cost effective components for automated systems. Results from NWS activities such as ceiling, visibility and micro-processor studies are being incorporated into the ALWOS.

ALWOS is being patterned after NWS's Sensor Processor and Display (SPAD) system. SPAD has a central supervisory control microprocessor that interrogates various sensors, processes their data, performs quality control checks and provides communication sources to transmit the information.

The design and development of the Developmental Model ALWOS is being done in NWS's Equipment Development Laboratory. Figure 2 is a block diagram of the Developmental Model ALWOS. As opposed to the three ceilometer and visibility sensors in the AV-AWOS, ALWOS has only one of each. Single sensor cloud and visibility algorithms, developed by NWS's T&ED under the AV-AWOS program, will be used in ALWOS. There are three outputs of the ALWOS--local display, long lines (e.g., Service A), and computer generated voice. ALWOS can be programmed to update its observation as frequently as once per minute.

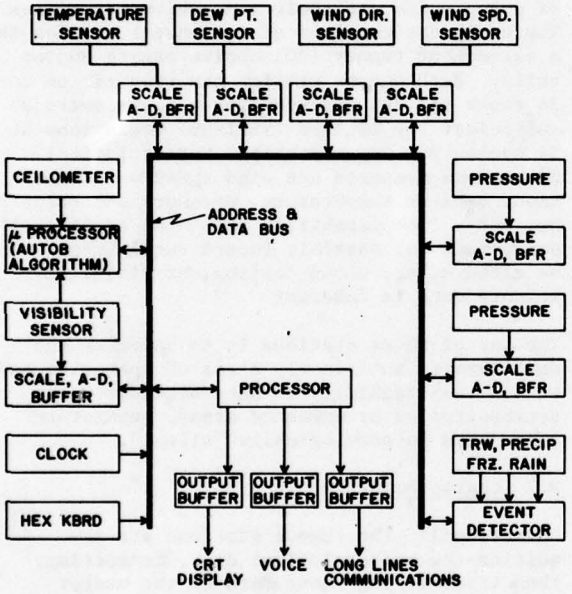

Figure 2. Developmental Model Automated Low-Cost Weather Observation System (ALWOS)

After the system has been assembled and its performance verified, it will be installed at Frederick Municipal Airport, Frederick, Maryland for an operational test. It is currently scheduled to begin the test in early 1980. Plans for the ALWOS test at Frederick have not been finalized. However, assessment of ALWOS in terms of reliability and maintainability will be of the utmost importance.

THE AUTOMATIC METEOROLOGICAL STATION, AN/TMQ-30 ( )

William J. Vechione

Atmospheric Sciences Laboratory

White Sands Missile Range, NM

ABSTRACT

The AN/TMQ-30 Automatic Meteorological Station is a system consisting of a master station and up to 20 remote sensor stations. This system is designed to supplement surface observations within an Army division's zone of responsibility. The remote stations will transmit, via digital RF link, wind speed and direction, temperature, relative humidity and pressure data to the master station. The Remotely Monitored Battlefield Sensor System (REMBASS) data transmission scheme will be incorporated into the AN/TMQ-30. Transmission times are set hourly, with a mission duration after deployment of 14 days minimum, without solar panel recharge. Microprocessor data control and processing is utilized throughout the system concept, both in the remote sensor stations and the master station. Currently, the system development is in the Advanced Development stage, with the validation hardware being manufactured. A future product improvement, by the addition of cloud base height and visibility parameter measurement capability is planned.

1. INTRODUCTION

There exists a need to obtain weather data real-time from remote areas, for applying during planning for airmobile, aviation, smoke, surveillance, and target acquisition operations. The TMQ-30 System consists of up to 20 remote sensor/data transmission stations and a master data receiving/reduction station. The remote stations provide the required meteorological surface parameter measurements in the remote, target or non-permissive (semi or noncontrolled) areas. These remote stations consist of low-cost (design-to cost of $2700 per station) items considered expendable, but can be recovered, restored and reemplaced at minimum cost. The system is capable of measuring, reporting, and displaying meteorological data with required accuracy, reliability, and timeliness. The TMQ-30 also provides observational validation of data obtained by observing systems, such as weather radars and/or meteorological satellites. Deployment is by hand emplacement.

2. DISCUSSION

2.1 Concept

The system is capable of satisfactory operation in climatic categories of wet-warm to intermediate cold (-32°C) where tactical operations can be expected, and over any type of terrain permitting line-of-sight (or relayed) operation.

The equipment will be located primarily in the forward (Brigade) areas of Division zones. The exact placement will depend on the tactical situation, operations planned, and requirements of using units and their respective priorities. The equipment consists of one master station and a maximum of twenty (20) active remote sensor units. Each sensor station can transmit up to 24 times per day and contains a power service sufficient for 14 days (minimum) operations at 24 cycles per day operation. Meteorological parameters measured are wind speed and direction, ambient temperature, pressure and relative humidity. The capability for three additional parameters for possible future requirements such as cloud cover, cloud ceiling, or visibility measurements is inherent.

The use of these stations is to increase the data density in friendly areas of operation and to add the capability of data acquisition in semicontrolled or unmanned areas, heretofore considered meteorologically "silent".

2.2 Characteristics

Operational: The remote stations are acquiring the meteorological data, formatting, then transmitting these data to the master data receiving/ reduction station. This station is capable of data reception from the sensor stations via line-of-sight or relayed radio transmission. Reduction of data received is accomplished at the master data receiving/ reduction station and the capability of generating updated meteorological data once per hour is stated as a requirement of the system. The remote stations will conform to the operations and camouflage procedure of the assigned unit, and are capable of 24 cycles per day for a total summed period of 14 days minimum. The system includes those items required to:

a. Convert observed meteorological parameter data to a meteorological format suitable for use by the supporting units.

b. Transmit data with minimum or no susceptibility to activation or response by

spurious signals.

c. Operate automatically on a predetermined time basis. Deployment of the sensor station should be accomplished by one man, with a maximum of 10 minutes deployment time.

d. The expendable sensor station will be as low in cost as possible consistent with essential requirements of accuracy, reliability and ruggedness.

e. Result in nonmutual interference with other sensor stations or other devices emanating electromagnetic radiations.

f. Assure maximum imperceptibleness to locations of sensor stations by electronic means.

g. Minimize the noise level of component parts of the system.

2.3 Physical

The components of the system are made as rugged, small, light in weight, and simple in operation as possible, consistent with the other essential characteristics.

The size and weight of the station have not been finalized, but state-of-the-art microminiaturization in circuitry design will be used to the maximum extent to limit both size and weight to the most practical unit possible. The master station, including reception equipment, interface logic, and computation capability is expected to weigh less than 40 lbs (17.9 kg). Size and weight of the remote station will remain within the constraints of 1.04 $feet^3$(0.035 m^3)(15 in X 15 in X 8 in, not including sensor package and mast), and 15 lbs (6.8 kg).

The system is designed to incorporate sufficient electronic and mechanical flexibility to permit improvements and/or design changes resulting from advancement in meteorological sensor development, communications improvement, or electronic consolidation techniques.

A high degree of durability is inherent in both the master data reduction station and the remote stations. They will be sufficiently rugged to withstand shock and vibration normally encountered in their respective operational environments.

2.4 Communications

The system utilizes a communications subsystem that has been developed for the Remotely Monitored Battlefield Sensor System (REMBASS) which is a system of remote anti-intrusion detection sensors and associated transmission, relay and reporting/display equipment to be used at Division level and below. The TMQ-30 system incorporates common communications modules, and utilizes channels in common frequency spectrum, but is not tactically associated with the REMBASS due to the different addressees of the data required.

2.5 Electronic

The master station major subcomponents are electronically based on three each RCA CDP1802 COSMAC microprocessor systems, which is a one-chip CMOS 8-bit register oriented central processing unit. This unit was selected because of its inherent temperature and voltage ranges of operation and its relatively low power consumption and noise immunity.

Two each CDP1822 256 X 4 Byte RAMS are used at the master station. 1702A EPROMS make up the resident program memories and CDP1852 programmable I/O parts are used throughout. A/D conversion of analog signals at the remote stations is accomplished via a single-chip A/D converter. The clock for the electronics is based on a temperature compensated crystal controlled oscillator. The initial operating program resident in three each 1702 EPROMS consists of 735 machine code steps. It is expected to reduce this to less than 512 steps in the AD program, thereby reducing the EPROMS to two.

2.6 Meteorological

The meteorological parameters are measured with state-of-the-art sensors. The final design/selection of these sensors has not been finalized, but it is specified that passive type sensors, due to the possible deployment sites, and constraints on site time of deployment. Orientation and verticality of the sensors accomplished readily due to the hand deployment method of emplacement.

Basic meteorological parameters of horizontal wind speed and direction, ambient air temperature, atmospheric pressure, and relative humidity are being measured. Space within the TMQ-30 will be allocated for additional sensor incorporation at a later time. It is anticipated that incorporation of a modified AN/GVS-5 laser rangefinder into the TMQ-30 sensor station will yield ceiling and visibility data. This incorporation is now being investigated as an exploratory development project.

PORTABLE AUTOMATED MESONET

Fred V. Brock

National Center for Atmospheric Research

Design highlights, system performance, and operational use of the Portable Automated Mesonet (PAM) are featured. PAM consists of a trailer-mounted base station and a network of remote sampling stations for surface mesoscale research. PAM differs from unautomated systems in that the data are sampled synchronously, averaged locally, and transmitted digitally via a telemetry link to the base station where real-time data from the entire network is displayed.

The base station uses minicomputer control for polling remotes, logging data, checking data quality, and displaying data. Displays include tabular listings, time plots, vector wind plots, and contours. Remote stations measure pressure, temperature, humidity, rain, wind speed, and wind direction and include flexibility for future expansion. A programmable microprocessor at each remote station controls communications, data sampling, and data averaging. Averaged data is reported to the base station when the base station interrogates the remote station (typically, once a minute).

A LASER WEATHER IDENTIFIER SYSTEM

Melvin J. Sanders, Jr.
NOAA - National Weather Service
Systems Development Office
Equipment Development Laboratory
Silver Spring, Maryland 20910

ABSTRACT

A Laser Weather Identifier (LWI) System has been developed to automate the surface observation of "Present Weather." This first generation design of the system deduces the type of hydrometeor passing through a collimated beam of laser light by analyzing the induced scintillation and forward scatter. In particular, the equipment automatically detects and classifies the "pure" states of fog, snow, heavy rain, rain, light rain, drizzle and clear. If a "mixture" of states occurs, then the category announced is the state detected which is highest ranked in the above hierarchical order, e.g., detected fog and rain is announced as fog. Equipment design and performance data are discussed.

1. BACKGROUND

In 1974, motivated by the desire to automate the surface observation (and, consequently, the present weather segment) the Systems Development Office (SDO) of the National Weather Service (NWS) joined with the Wave Propagation Laboratory (WPL) of the Environmental Research Laboratories to develop a research laser/optical system which "differentiates between as many hydrometeors and lithometeors as proves feasible." This decision was based on a major study (Derr et al, 1974) which summarized a voluminous quantity of research on lidar atmospheric returns. The research equipment which resulted from this venture showed, indeed, that the concept of a Laser Weather Identifier (LWI) had promise. The system (described in depth by Earnshaw and Keebaugh (1977)) was operated at the NWS Test and Evaluation Division, Sterling, Virginia, from January through August, 1976, and provided signatures of rain, snow, fog and clear events in both scintillation and forward scatter. Though the data set obtained was small, it convincingly demonstrated that, at the least, a superior "precipitation yes/no" indicator could be developed, provided that an operational equipment design was feasible and cost-effective. It also showed that these four major categories could probably be discriminated individually, but far more experimentation was required.

Concurrently, WPL developed a second research instrument (Earnshaw et al, 1978) for the Air Force Geophysics Laboratory. The design of this device was quite different from the first, overcoming many of its shortcomings. Thus, armed with the knowledge of these research instruments, the NWS Equipment Development Laboratory and Test and Evaluation Division launched a major effort to establish the feasibility of an operational equipment design, and to further evaluate the experimental concept in operational conditions. The system developed and representative results obtained from it to date are described in the following.

2. THE CONCEPT

The concept of a Laser Weather Identifier is that the "present weather" state of a volume can be determined by analyzing the interaction of laser radiation with the hydrometeors and/or lithometeors present in that volume. The first generation design of this system deduces the type of hydrometeor passing through a collimated beam of laser light by analyzing induced scintillation and forward scatter as depicted in Figure 1.

2.1 Scintillation

Scintillation, as used herein, refers to the dynamic fluctuations in power measured by a line detector, normal to the beam, caused by irregularities in the index of refraction throughout the beam, without regard to polarization. These irregularities may be classified as spatially discrete, e.g., raindrops, snowflakes, etc., or as spatially continuous, e.g., turbulance or temperature gradients. In either case, however, the irregularities must be in motion. Without motion, an irregularity will not cause a dynamic fluctuation in power.

A measurement of scintillation relates to no intrinsic quality of an object causing an irregularity, but rather relates to the motion of the object. A discrete irregularity rapidly passing normal to the beam and line detector

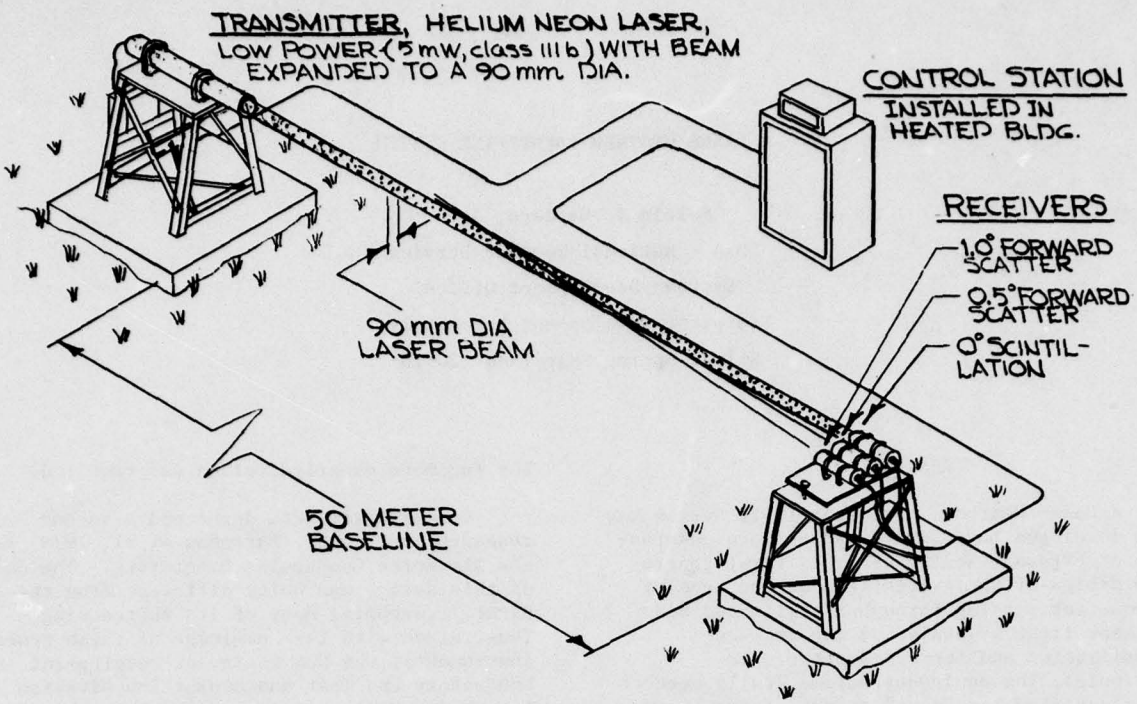

Figure 1. Laser Weather Identifier System

produces higher temporal frequency content in scintillation that does a slower moving object. Two objects having approximately the same characteristic dimensions, velocity and index of refraction produce similar scintillation signatures, though the objects themselves may be quite dissimilar.

2.2 Forward Scatter

Forward scatter, as used herein, refers to the power measured passing through a circular aperature, normal to a forward scatter direction, caused by irregularities in the index of refraction in the volume intersection of the transmit and receive beams. As with scintillation, these irregularities may be classified as spatially discrete or spatially continuous, but, unlike scintillation, the irregularities are not required to be in motion. A forward scatter measurement is an intrinsic property of the scattering object or medium.

Forward scattered power in the LWI is measured, simultaneously, in both the horizontal and vertical polarization directions with the transmitter polarization constructed as linear and vertical.

2.3 Recognition Features

For broad ranges of intensities, "pure" states of fog, snow, rain, drizzle and clear have been detected and classified using features derived from the basic measurements of scintillation and forward scatter. These features are called High-Pass Scintillation, High-Pass 0.5° Forward Scatter and Low-Pass 1.0° Forward Scatter.

High-Pass Scintillation (HPS) refers to the power contained in the scintillation temporal power spectrum above a high-pass corner frequency of 1200 Hz. This feature helps classify Heavy Rain (R+), Rain (R) and Light Rain (R-) since it is sensitive to, and increases with, the number and size of drops in the volume. HPS is also sometimes an extremely sensitive feature for Snow (S), but is not used in the recognition scheme herein due to its unreliability. In the current equipment design, driven snow often passes parallel to the horizontal line detector inducing little or no scintillation. HPS is negligible in Fog (F) and in Drizzle (L), and can be contaminated by "wind noise." Generally, however, HPS is contaminated by instrument noise.

High-Pass 0.5° Forward Scatter (HPFS) refers to the power contained in the 0.5° forward scatter temporal power spectrum above a high-pass corner frequency of 1.6 Hz. This feature helps classify Snow since it is sensitive to, and increases with, the number and size of crystals in the volume. Moreover, when measured in both the horizontal and vertical polarizations, the quotient of these measurements is an estimate of the depolarization ratio. HPFS also helps define Drizzle with a zero depolarization ratio, but is insensitive to Rain which scatters into much smaller forward angles. HPFS is insensitive to Fog, and can be contaminated (rarely) by "wind noise." Generally, however, HPFS is contaminated by instrument noise.

Low-Pass 1.0° Forward Scatter (LPFS) refers to the power contained in the 1.0° forward scatter temporal power spectrum below a low-pass corner frequency of 1/60 Hz. This feature, when measured in both polarizations, helps classify Fog due to its wide forward scatter angle and large depolarization ratio (the latter due presumably to multiple scattering). LPFS also responds to Snow, though to much less degree and much less depolarization ratio. LPFS is insensitive to Rain, Drizzle and "wind noise," and is contaminated by instrument noise.

2.4 Recognition Discriminants

The recognizer discussed herein is designed to automatically detect and classify "pure" states of Fog, Snow, Heavy Rain, Rain, Light Rain, Drizzle and Clear using the features High-Pass Scintillation, High-Pass 0.5° Forward Scatter (both polarizations) and Low-Pass 1.0° Forward Scatter (both polorizations). If a "mixture" of states occurs, then the recognizer announces the state detected which is highest ranked in the above hierarchical order.

As an aid to visualizing the performance of the recognizer, it is convenient to think in terms of feature vectors and a feature space. A feature vector $\vec{f}$, is defined to be a 5-dimensional vector with a component representation:

$$\vec{f} = \begin{bmatrix} f_1 \\ f_2 \\ f_3 \\ f_4 \\ f_5 \end{bmatrix} = \begin{bmatrix} \text{HPS} \\ \text{HPFS - Vertical Polarization} \\ \text{HPFS - Horizontal Polarization} \\ \text{LPFS - Vertical Polarization} \\ \text{LPFS - Horizontal Polarization} \end{bmatrix}$$

where $f_i \geq 0$, $i = 1, 2, 3, 4, 5$. Feature space is then reckoned as a Cartesian space containing all possible feature vectors.

Present weather categories F, S, R+, R, R-, L and C are subsets (manifolds) of feature space bounded by hyperplanes S_1, S_2, S_3, V_1, V_2, H_1, H_2, V_3 and H_3- where S_1, S_2 and S_3 are orthogonal to the HPS unit vector, V_1 and V_2 are orthogonal to the HPFS-Vertical unit vector, H_1 and H_2 are orthogonal to the HPFS-Horizontal unit vector, V_3 is orthogonal to the LPFS-Vertical unit vector and H_3 is orthogonal to the LPFS-Horizontal unit vector. Taking the hyperplane symbols as also representing the respective distances from the origin to the hyperplanes, the following ordering is also defined:

1. $0 < S_1 < S_2 < S_3$
2. $0 < V_1 < V_2$
3. $0 < H_1 < H_2$
4. $0 < V_3$
5. $0 < H_3$

The category for Fog is defined to be:

$$F = \{\vec{f} \mid f_4 > V_3 \text{ and } f_5 > H_3\}$$

which reads that the category F equals the set of all feature vectors, $\vec{f}$, such that f_4 exceeds V_3 and f_5 exceeds H_3. V_3 and H_3 are chosen such that (1) their ratio approximates the depolarization ratio in LPFS for Fog, and (2) false alarms from Snow are minimized.

The cateogry for Snow is defined to be:

$$S = \{\vec{f} \mid f_2 > V_2 \text{ and } f_3 > H_2; \text{ where } \vec{f} \notin F\}$$

which reads that the cateogry S equals the set of all feature vectors, $\vec{f}$, such that f_2 exceeds V_2 and f_3 exceeds H_2, where $\vec{f}$ is not an element in the category F. V_2 and H_2 are chosen such that (1) their ratio approximates the depolarization ratio in HPFS for Snow, and (2) false alarms from Drizzle and noise are minimized.

The cateogires for Heavy Rain, Rain and Light Rain are defined to be:

$$R+ = \{\vec{f} \mid f_1 > S_3; \text{ where } \vec{f} \notin S \text{ and } F\}$$

$$R = \{\vec{f} \mid f_1 > S_2; \text{ where } \vec{f} \notin R+, S \text{ and } F\}$$

$$R- = \{\vec{f} \mid f_1 > S_1; \text{ where } \vec{f} \notin R, R+, S \text{ and } F\}$$

S_1, S_2 and S_3 are chosen to approximate rainfall rates defined in FMH #1 (Federal Meteorological Handbook No. 1). S_1 is also chosen to minimizing false alarms from "wind noise."

The category for Drizzle is defined to be:

$$L = \{\vec{f} \mid f_2 > V_1 \text{ and } f_3 < H_1; \text{ where } f \notin R-, R, R+, S \text{ and } F\}$$

V_1 and H_1 are chosen to minimize "missed detections" for a very small depolarization ratio.

The category Clear (C) is a default category defined by:

$$C = \{\vec{f} \mid f \notin L, R-, R, R+, S \text{ and } F\}$$

3. THE EQUIPMENT

The equipment configuration of the Laser Weather Identifier is shown in Figure 1. At the transmitter, light from a low power, linearly polarized, helium-neon laser is expanded to a 90 mm. diameter, and projected along a 50 m. baseline to interact with the existing hydrometeors and lithometeors. At the receiving site are located three telescopes--one aligned coaxially with the transmitter beam measuring scintillation, while the remaining two are measuring scatter, both polarizations, at the forward angles of 0.5° and 1.0°. Interconnecting cables distribute signals and control between the transmitter and receiver sites and the control station located in a heated building.

Photographs of a transmitter installation, a receiver installation and both installations on a baseline are presented in Figures 2, 3 and 4. This installation, which is one of five currently undergoing extensive evaluation, is located atop the roof of the terminal building of the Fairbanks International Airport in

Fairbanks, Alaska. Heated shrouds seen atop the transmitter and the receiver telescopes minimize the blowing of precipitation onto the lenses. Additionally, the lenses are directly heated to minimize the effects of condensation. Also seen are sandbags which anchor the stands to the rooftop.

3.1 Transmitter

As shown in Figure 5, the transmitter consists of a helium-neon laser, an acousto-optic modulator, an expanding lens and an objective lens. The laser wavelength is .6328 micrometers, with a power of 5 milliwatts and a vertical polarization. The modulator chops the laser output with a 50% duty cycle, and at a 22.25 KHz rate. Usage of modulation serves to practically eliminate the effects of background light and the deleterious effects of DC coupled circuitry. The lens system expands the laser output from .7 mm. diameter to 90 mm.

3.2 Scintillation Receiver Channel

The scintillation receiver, as shown in Figure 6, consists of a horizontally oriented slit, 1x100 mm., which passes light through an objective lens and a 100 angstrom band-pass filter to a photovoltaic detector. The received light is detected, amplified and driven through a maximum of 150 m. of cable to processing electronics located in the control station.

The scintillation receiver processing provides as output the root-mean-square value (RMS) of both low-pass and high-pass representations of the received scintillation power. The received carrier is band-pass filtered with an 8 KHz bandwidth, and amplitude demodulated, using a 4 KHz low-pass filter, to obtain the low-pass representation. This signal is then high-pass filtered, with a 1200 Hz corner frequency, to obtain the high-pass representation. The RMS circuitry provides estimates using a 1-minute estimation interval. The RMS value of the high-pass representation is the feature f_1.

3.3 Forward Scatter Receiver Channel

The receivers used for 0.5° and 1.0° forward scatter are identical. Each receiver, as shown in Figure 7, consists of an objective lens which passes light through a beamsplitter, 100 angstrom band-pass filters and polarizers to photovoltaic detectors. The received light is detected, amplified and driven through a maximum of 150 m. of cable to processing electronics located in the control station.

The 0.5° forward scatter receiver processing provides as output, for both horizontal and vertical polarizations, a low-pass representation and the RMS value of a high-pass representation of the received 0.5° forward scatter power. The received carrier is band-pass filtered, with a 2 KHz bandwidth, and amplitude demodulated, using a 1 KHz low-pass filter, to obtain the low-pass representation.

Figure 2. Fairbanks, Alaska, transmitter installation

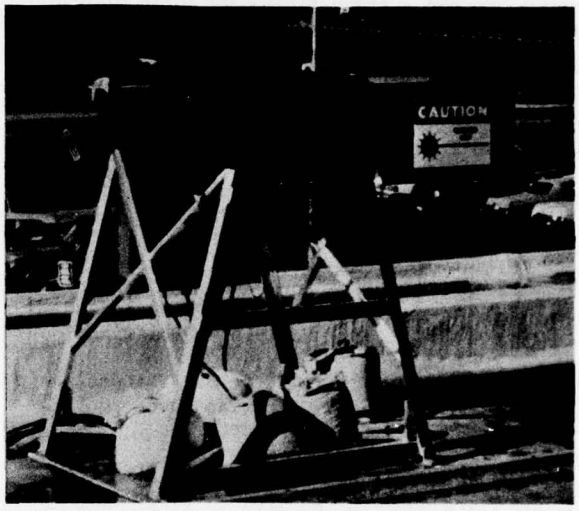

Figure 3. Fairbanks, Alaska, receiver installation

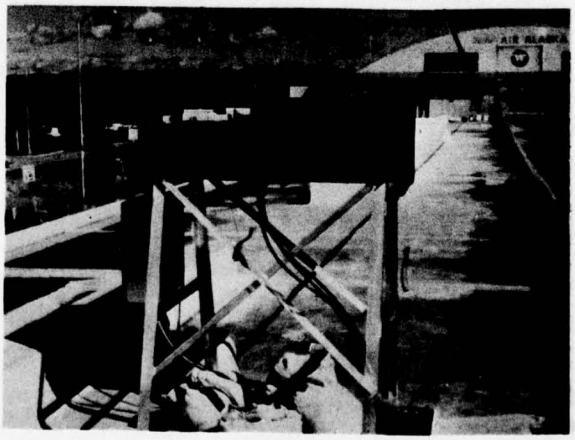

Figure 4. Complete Fairbanks, Alaska, LWI installation

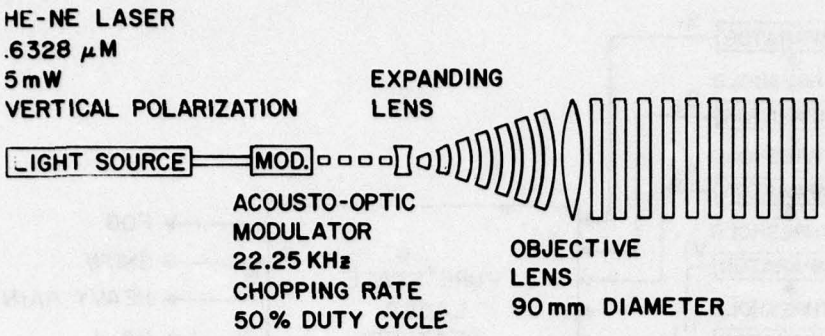

Figure 5. Transmitter functional block diagram

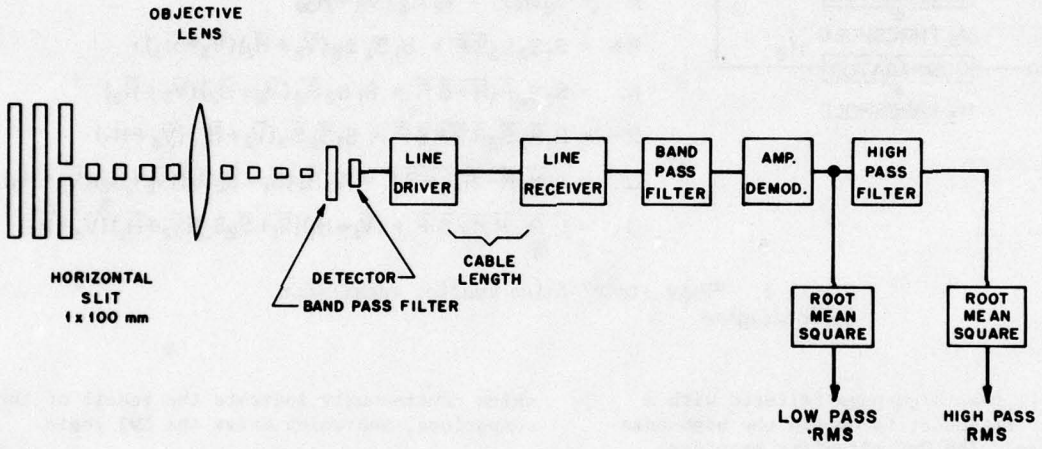

Figure 6. Scintillation receiver functional block diagram

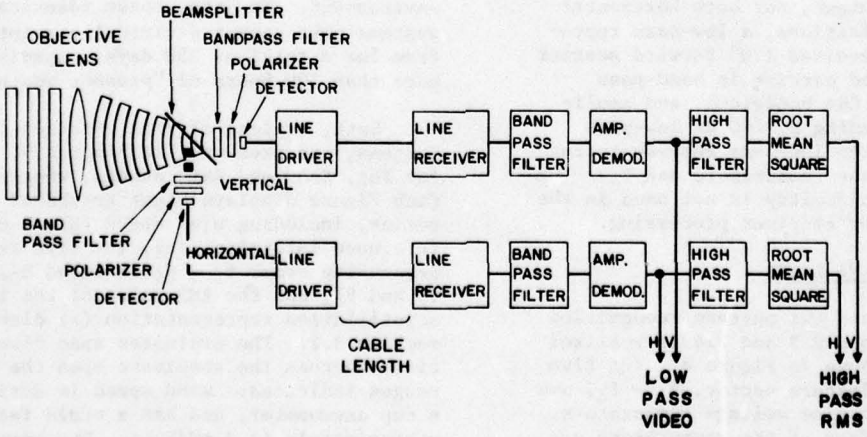

Figure 7. Forward scatter receiver functional block diagram

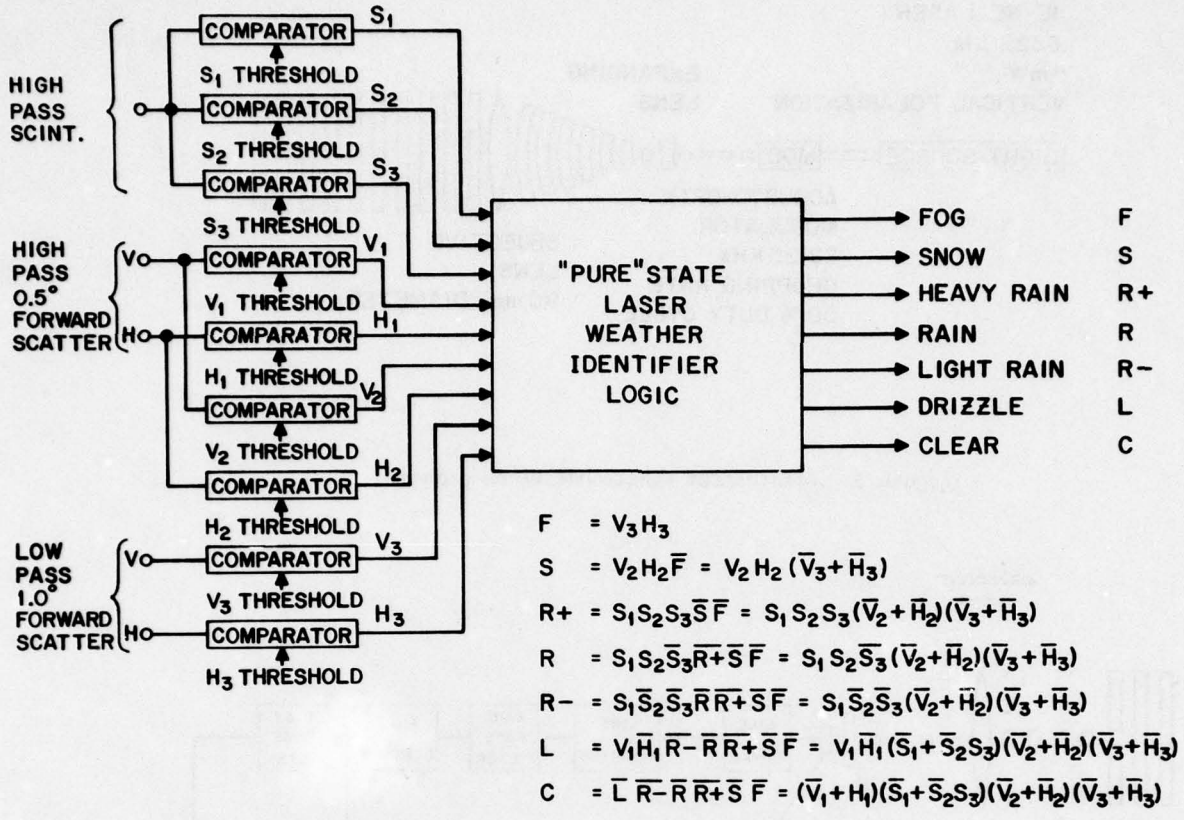

Figure 8. "Pure state" laser weather identifier logic diagram

This signal is then high-pass filtered with a 1.6 Hz corner frequency to obtain the high-pass representation. The RMS circuitry provides estimates using a 1-minute estimation interval. The RMS values of the high-pass representation are features f_2 and f_3.

The 1.0° forward scatter receiver processing provides as output, for both horizontal and vertical polarizations, a low-pass representation of the received 1.0° forward scatter power. The received carrier is band-pass filtered, with a 2 KHz bandwidth, and amplitude demodulated, using a 1/60 Hz low-pass filter, to obtain the low-pass representation. These signals are the features f_4 and f_5. The high-pass and RMS circuitry is not used in the 1.0° forward scatter receiver processing.

3.4 "Pure" State LWI Logic

The "pure" state LWI pattern recognition discussed in sections 2.3 and 2.4 is realized by the circuitry shown in Figure 8. The five components of the feature vector, f_1 - f_5, are applied as input to nine voltage comparators. The threshold voltages of the comparators are set to represent the hyperplanes. The signal output of the comparators are logic signals which continuously indicate the result of the comparison, and which drive the LWI logic.

4. SOME RESULTS

The LWI design, as presented herein, is undergoing an extensive evaluation of both the conceptual and equipment performance in a field environment. To date, three identical LWI systems have operated virtually maintenance-free for a total of 350 days, experiencing more than 500 hours of "present weather."

Data, typical of that obtained from all systems, are presented in Figures 9, 10 and 11 for Fog, Snow and Rain events, respectively. Each Figure displays eight graphs of time series, including wind speed (W), a carrier reference intensity (Io), the five features in descending order f_5 - f_1 (labeled H_3, V_3, H_2, V_2 and S), and the RMS value of the low-pass scintillation representation (X) discussed in section 3.2. The ordinates span five hours in time, whereas the abscissae span the millivolt ranges indicated. Wind speed is derived from a cup anemometer, and has a scale factor of approximately 11.5 mV/knot. The speed at the tic mark corresponds to approximately 22 knots.

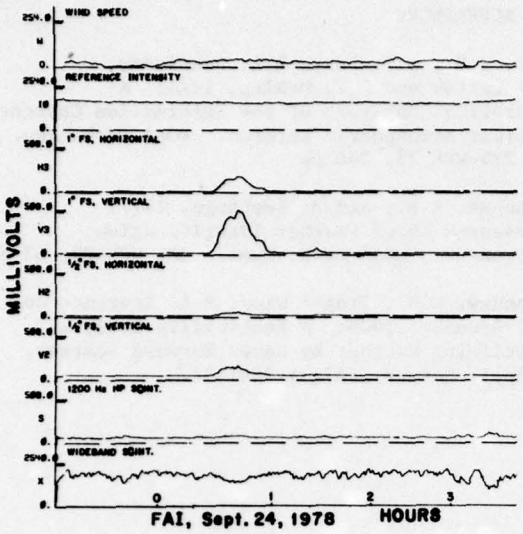

Figure 9. LWI analog signals from a Fog event

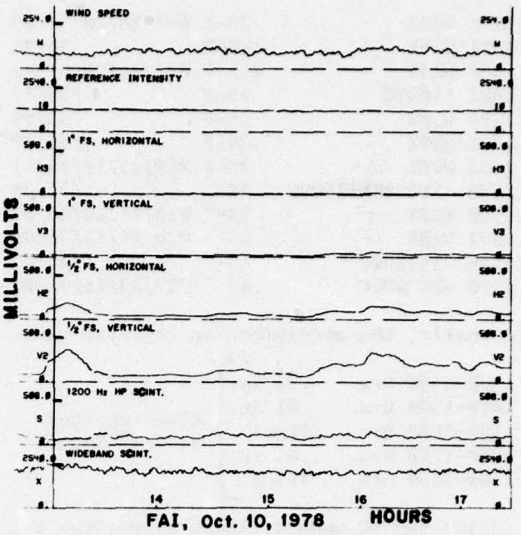

Figure 10. LWI analog signals from a Snow event

The gains for the respective channels in Figures 9, 10 and 11 are equal, allowing intercomparison with constant thresholds. Based on Fairbanks, Alaska data obtained through November 10, 1978, gains were increased by a factor of 40 for features f_5 and f_4, and by a factor of 2 for features f_3 and f_2.

To demonstrate the performance of the LWI logic, the following threshold values are assumed:

S_1 = 125 mV
S_2 = 300 mV
S_3 = 500 mV
V_2 = 60 mV
H_2 = 30 mV
V_3 = 50 mV
H_3 = 25 mV

4.1 Fog

A dense fog event, which occurred on September 24, 1978, at Fairbanks, is shown in Figure 9. The official Surface Weather Observations, taken within several hundred feet of the LWI equipment, were:

R	2252	5ØSCT1ØØSCTE2ØØBKN 7	223/31/26/ØØ/ØØ
RS	2253	3SCT 7	227/3Ø/25/36/Ø3
S	ØØ3Ø	W1X 1½F	/35/Ø5
RS	ØØ49	-X ½ F	227/30/26/35/Ø6
RS	Ø151	35SCTE14ØBKN 4 F	224/31/26/34/Ø5
S	Ø231	35SCTE14ØBKN 7	/35/Ø5
R	Ø254	E12ØOVC 7	22Ø/31/26/34/Ø5
R	Ø351	E12ØOVC 7	215/32/26/Ø4/Ø4

Using the threshold values above, there is excellent correlation of the onset of the event at ØØ3Ø. The LWI announces F continuously from approximately ØØ3Ø to Ø1ØØ, and for a few minutes around Ø125, and does not announce F when it is observed at Ø151. This event was the first F event recorded with this particular design of the LWI, and triggered a later inclusion of a gain of 40 into the 1.0° forward scatter channels.

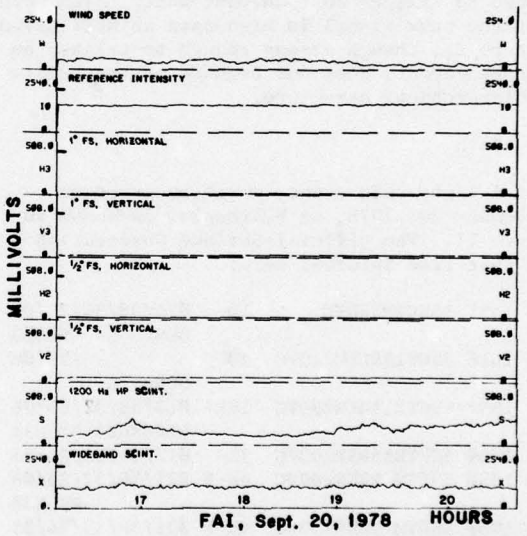

Figure 11. LWI analog signals from a Rain event

Notice that the fog signals in the 0.5° forward scatter channels, features f_3 and f_2, are strong enough to trigger an S announcement, but do not because of the built-in hierarchical structure.

4.2 Snow

A light snow event, which occurred on October 10, 1978, at Fairbanks, is shown in Figure 10. The official Surface Observations for that time interval were:

RS	1251	W2ØX	2S-F	ØØ3/26/2Ø/36/Ø9
S	1311	W15X	1½S-F	/36/Ø8
R	1354	W15X	1½S-F	ØØ7/26/2Ø/35/11
S	14Ø1	E4ØOVC	4S-F	/35/11
S	1424	W3ØX	3S-F	/35/Ø9
S	1443	W2ØX	2S-F	/35/Ø9
R	1452	W2ØX	2S-F	Ø1Ø/25/19/35/11
S	1526	-XE2OBKN11ØOVC	4S-	/36/Ø8
RS	155Ø	W2ØX	2S-	Ø13/26/18/36/Ø7
R	1651	W2ØX	2S-	Ø2Ø/24/17/36/Ø8
S	1746	-XE2ØOVC	4S-	/35/Ø7
R	175Ø	-XE2ØOVC	4S	Ø23/23/15/34/Ø7

Additionally, the precipitation reported was:

13ØØ-14ØØ Hrs.	.01 in.	Also reported as 3/4" Snow
14ØØ-15ØØ Hrs.	.01 in.	
15ØØ-16ØØ Hrs.	Trace	
16ØØ-17ØØ Hrs.	.01 in.	
17ØØ-18ØØ Hrs.	Trace	

Using the threshold values above, the LWI continuously reports S throughout the period, and reports no F throughout the period. Observe that the snow signals in the 1.0 forward scatter channels, features f_5 and f_4, are not strong enough to trigger an F announcement. Also note that the snow signal in high-pass scintillation, feature f_1, though strong enough to trigger an R-announcement, does not because of the built-in hierarchical structure.

4.3 Rain

A light rain event, which occurred on September 20, 1978, at Fairbanks, is shown in Figure 11. The official Surface Observations for that time interval were:

R	1551	15SCTM32OVC	1Ø	Ø14/38/31/23/Ø5
				OCNL L- RELBØ3
S	1616	7SCT15SCTM21OVC	1Ø	/25/Ø6
				OCNL L-
R	1652	6SCTE15BKN2ØOVC	1ØR-	Ø14/38/32/26/Ø6
				LEI8RB23 RELB3Ø
R	175Ø	5SCTE15BKN2ØOVC	7L-	Ø17/37/32/26/Ø4
RS	185Ø	5SCTM 9BKN2ØOVC	6R-F	Ø21/36/32/25/Ø6
				RELB3Ø
R	195Ø	5SCTM 9BKN15OVC	6R-F	Ø24/36/32/24/Ø5
R	2Ø51	5SCTM 9BKN15OVC	6R-F	Ø27/36/32/22/Ø5

Additionally, the precipitation reported was:

16ØØ-17ØØ	Hrs.	Trace
17ØØ-18ØØ	Hrs.	Trace
18ØØ-19ØØ	Hrs.	.01 in.
19ØØ-2ØØØ	Hrs.	.01 in.
2ØØØ-21ØØ	Hrs.	Trace

Using the threshold values above, there is excellent correlation of the onset of the event at 1623, after which the LWI announces R- continuously throughout the period except for the interval 173Ø through 184Ø. The gain of the 1.0° forward scatter channels had not, at this time, been increased by the factor of 40 discussed in section 4.1. Thus, it is not known whether the LWI would have announced F with a six mile visibility. Finally, the LWI did not have the sensitivity to observe this particular L-.

5. REFERENCES

Derr, V.E., M.J. Post, R.L. Schwiesow, R.F. Calfee and G.T. McNice, 1974: A Theoretical Analysis of the Information Content of Lidar Atmospheric Returns. NOAA Tech. Rep. ERL 296-WPL 29, 284 pp.

Earnshaw, R.B., and B. Keebaugh, 1977: A Research Laser Weather Identification Instrument. NOAA Tech. Memo. ERL WPL-23, 63 pp.

Earnshaw, K.B., Ting-i Wang, R.S. Lawrence and R.G. Greunke, 1978: A Feasibility Study of Identifying Weather By Laser Forward Scatter. J. Appl. Meteor., 17, 1476-1481.

MICROPROCESSORS IN WEATHER DATA ACQUISITION

James A. Cunningham

Equipment Development Laboratory

NOAA, National Weather Service

Silver Spring, Maryland

ABSTRACT

Microprocessors appear to be well suited to solving many of the problems of automating meteorological observations.

Due to limited time, the discussion will deal with only two aspects of totally automated stations and how the microcomputer industry has influenced the solutions.

One factor is the tremendous increase in processing capabilities for a small cost. This allows implementation of more complex sensor algorithms, on-line data quality control, and internal error checking functions required in a totally automated station.

Along with increased processing power, the microcomputer industry has produced a large number and variety of compatible peripheral sub-assemblies. These units have demonstrated good performance and reliability characteristics at a very competitive cost. These recent advancements have significantly reduced the development time and costs involved in automation projects. Therefore, the Equipment Development Laboratory of the National Weather Service has been able to direct most of its resources to the sensor development problems associated with totally automated observation systems.

1. INTRODUCTION

The rapid growth in microprocessor technology and its economic advantage appears to be a prime element in the development of totally automated weather observation stations. During the past several years the National Weather Service has developed several partial parameter automated stations. These stations automated all but the more subjective observations such as ceiling, visibility and present weather. In 1975, the Weather Service, with the support and cooperation of the FAA, began the development of a totally automated station designated AV-AWOS (AViation Automated Weather Observation System). This paper discusses the AV-AWOS experiences and the blending of microprocessor technologies to future NWS systems.

At present, the human observer serves as a filter to intercept erroneous observations. This function must also be included in future automated stations to maintain data base integrity and to gain confidence and acceptance of such systems. This paper will also discuss these functions and other features included in the development of a series of automated stations for NWS and FAA.

2. AV-AWOS EXPERIENCE

The system designated AV-AWOS is based on the centralized minicomputer concept shown in Figure 1. Many valuable experiences were gained as this project developed. A determination of the magnitude of the requirements for a totally automated system is one of the many significant contributions.

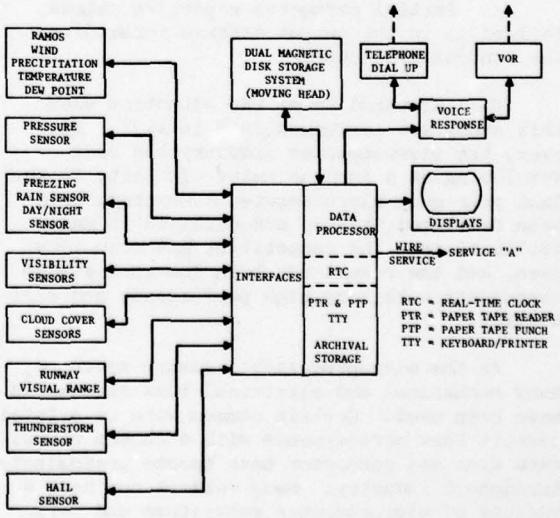

Figure 1. Aviation Automated Weather Observation System (AV-AWOS)

AD-A070 009 AIR WEATHER SERVICE SCOTT AFB IL F/G 4/2
PROCEEDINGS OF THE TECHNICAL EXCHANGE CONFERENCE 8TH AIR FORCE --ETC(U)
MAY 79

UNCLASSIFIED AWS/TR-79/001 NL

2 OF 3
AD
A070009

One of the most important objectives was the development of meteorological algorithms for the more subjective type of parameters. Our experience with the AV-AWOS system gave us a reasonable base for generating memory sizing estimates for the required software functions. Using the above experience, requirements and numbers, a trade-off study (supported by FAA and NWS) was conducted to investigate the relative advantages and disadvantages of various microprocessor configurations. Also, these different configurations were compared to the central minicomputer concept used in AV-AWOS.

Besides the expected broad flexibility and modular design advantages of a distributive microprocessor system, important factors, such as reliability and cost, were improved. The capabilities of adding independent modules for critical areas allows redundancy features to be introduced in a more economical fashion. Costs were broken into several categories and carefully analyzed. A few cost comparisons between a microprocessor distributive system and the centralized minicomputer concept are shown in Table I. (Sensors were not included since they were common to both systems.)

In addition to costs, some other advantages of the distributive system are listed below:

1. Significant improvement in reliability. It is estimated that MTBF is nearly doubled over that of a central processor system, reducing the yearly downtime to less than half.

2. Estimated ease of maintenance and less costly spares to stock.

3. Partial parameter reporting unless failure is in the output message formator or the control processor.

This appeared to be the situation when this study was performed late in 1977. However, the microcomputer industry has been developing at a furious rate. In fact, in the last year many microcomputer subsystems have been developed, tested and utilized in many applications. The competition has been very keen, and the result has been low-cost system components with very high performance and reliability.

As the microprocessor industry advanced, many mechanical and electrical buss structures have been used. Certain common wire or printed circuit buss arrangements with a chosen circuit card size and connector have become predominate throughout industry. Many vendors now have a variety of microcomputer subsystems and peripheral circuits available for these more predominate buss structures.

The Equipment Development Laboratory is now undertaking a study for the selection of a common buss structure to be used in our future automated systems. We hope to take full advantage of recent developments in the microprocessor industry. Recent estimates of the development costs now appear to be less than half of what they were a year ago if an appropriate buss structure is used.

3. NWS MICROPROCESSOR SYSTEMS

Several microprocessor systems have been designed and constructed within the Equipment Development Laboratory of the National Weather Service. These systems have had different configurations of sensors and have been used for various applications. These systems are in different phases of test and development. One system, designated ALWOS (Automated Low-Cost Weather Observation System), is being developed by the NWS with the aid and support of the Federal Aviation Agency. This system will be patterned after the NWS's Sensor Processor and Display System (SPAD). SPAD has a supervisory control microprocessor which interrogates various sensors. Depending upon the complexity of the sensor and its algorithm, other microprocessors may be used within its own interface. (Examples--ceiling and present weather.) The supervisory processor also controls various local outputs and serves as the long-line communications driver. The control processor, most of the sensors, and their respective interfaces are state-of-the-art production items. Visibility, cloud, and present weather sensors have not been developed to the point of satisfying the basic requirements. NWS, FAA and others have embarked on extensive programs to develop these particular sensors and algorithms to meet automation requirements. Results in these areas are a prerequisite to obtaining any realistic totally automated weather observation system.

TABLE I

COST TRADE-OFF STUDY BREAKDOWN

	CENTRAL MINICOMPUTER	DISTRIBUTIVE
1. NON-RECURRING DEVELOPMENT		
ENGINEERING DESIGN & TEST	$170K	$420K
SOFTWARE DEVELOPMENT-FIRMWARE	410K	730K
MANUALS	80K	100K
PROGRAM MANAGEMENT	100K	160K
	$760K	$1410K
2. RECURRING - LABOR	$15K	$20K
NON-LABOR	30K	15K
	$45K	$35K
3. RECURRING - OPERATIONAL		
MAINTENANCE	$7K/YR.	$3.5K/YR.
EXPENDABLES	1K	.5K/YR.
SPARES	15K	5K
	$23K	$9K

The ALWOS program hopes to utilize the full advantages and flexibilities of a distributive system. The sensors and their interfaces are designed on a modular basis and include internal self-checking and quality control electronic circuits.

The first phase of ALWOS is the installation of a partial system consisting of Wind, Altimeter, and Voice Equipment (WAVE) at a small municipal airport. (Figure 2). This system, which is installed at Frederick, Maryland Airport, consists of sensors that will measure wind speed, wind direction, and pressure--a processor, local display CRT, and a computer generated voice output. The system collects the information from these devices, processes it and performs quality control checks, and broadcasts the information once each minute on the FREDERICK VHF OMNI RANGE.

The processor continually performs self-checks of the system. If a fault is detected in either wind or altimeter information, the system outputs a "missing" for that parameter. To improve the reliability of altimeter setting information, the system contains two independent pressure sensors. The processor continually checks the readings of one sensor against the other to insure that altimeter setting information meets performance criteria.

During 1979 additional sensors (laser ceilometer, forward scatter visibility, etc.) are to be added to the ALWOS test station at Frederick, Maryland. This station will serve as a test bed for the latest sensor algorithms, internal checking features, and data quality control techniques.

4. INTERNAL CHECKING AND DATA QUALITY CONTROL

As stated before, the areas of self-checking and data quality control are very important parts of a totally automated station. These functions have been placed into two general categories. The first category deals with the sensor and its interface. The second category consists of data quality control which may use intra-sensor, and/or inter-sensor data checks.

The first category requires an optimum balance of hardware and software embedded in the sensor interface designs. Some of the examples used in the NWS microprocessor systems follow:

Where an analog to digital converter was required, self calibrating circuit checks were included in the interface. On Command of the control processor, the input to the A to D converter was switched from the sensor output to a predetermined voltage. The output result then compared to the correct value within allowed tolerances. Of course, if a failure occurred, then a predetermined action could be taken.

Other checks used extra data bits in data exchanges between sensor interfaces and control processor. An example is using a bit to indicate if a set of control sequences was completed since last interrogation period. Other bits were used to indicate the presence of or absence of critical voltages and voltage levels. Quite often we have experienced sliced or broken cables to our centerfield or outlying sensors at an airport. We use this technique to detect broken or deteriorated cables to our sensors.

The second category consists of data quality control which may use intra-sensor, and/or inter-sensor data checks.

Data from any one sensor can be examined from the point of view: is the data realistic? For example, does the temperature or pressure fall within acceptable limits? Another test is: are successive data falling within reasonable rules of continuity? Most sensors have a response time or a bandwidth limit; therefore, maximum data variations are predictable and can be checked.

Data from other sensors at the same site can be used to produce cross checks on data. Correlating such parameters as present weather, temperature, dewpoint, and visibility can produce realistic data boundaries for many sensors.

One of the features we have not yet capitalized on is utilization of the data quality control and electronic self-check information. There is strong support to adding such diagnostic information as an integrated part of the output observation message. This information could be used to optimize maintenance trips and to give on-line indications of the status and/or effectiveness of the data acquisition system.

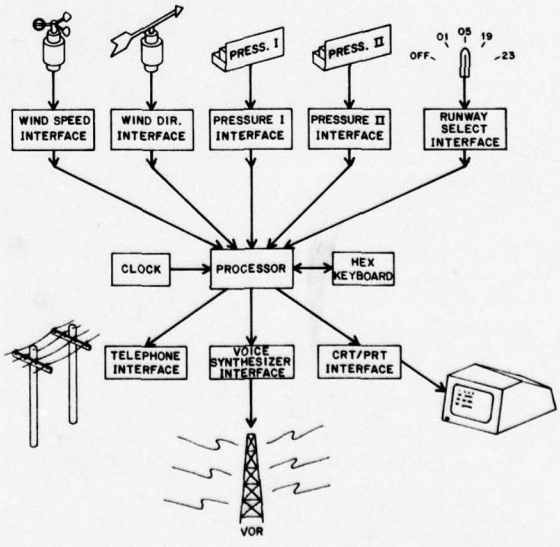

Figure 2. Wind Altimeter Voice Equipment (WAVE)

5. RESULTS AND RECOMMENDATIONS

Following is a tally of some of our experiences and results:

A. The detailed development of the requirements of totally automated stations:

B. The development of the first acceptable level of algorithms for totally automated systems.

C. An indication of the relative costs and features of a distributive microprocessor system.

D. The reliability potential of microprocessor systems.

E. The combination of electronic circuit and firmware self-checking features.

F. Data quality control techniques.

G. Design and construction experiences with microprocessors.

One of the most important conclusions that we gained from our design and construction experience is that selection of a standard mechanical and electrical buss structure is most valuable. This truly would accomplish a modular capability and allow a complete variety of sensors to be used in different stations. This is especially important due to the large and varied inventory of sensors that exist in the Weather Service system. We believe the adaption of a standard buss structure between agencies would be a significant step in assisting each group to realize the efforts of others and would provide a true and expeditious means of transferring sensor development technologies.

GROUND-BASED REMOTE SENSING OF ATMOSPHERIC PROFILES

M. T. Decker, E. E. Gossard, and E. R. Westwater

Wave Propagation Laboratory
Environmental Research Laboratories
National Oceanic and Atmospheric Administration
Boulder, Colorado 80302

ABSTRACT

Techniques for continuous remote sensing of atmospheric properties have advanced to the point that a sounder can now be designed to obtain temperature, humidity and winds as well as other derived quantities to stratospheric heights. The combination of active and passive sensors needed for such a system is discussed.

1. INTRODUCTION

Theoretical and experimental studies have shown that ground-based microwave radiometers and radars are able to measure, essentially continuously in time, profiles of atmospheric temperature and wind. Integrated values of total liquid and precipitable water vapor are also readily obtained. These instruments are almost all-weather systems in that microwave radiometric measurements are corrected for the presence of non-precipitating clouds, and Doppler radar returns for wind measurement are observed in clear air as well as in the presence of cloud or precipitation particles. The Wave Propagation Laboratory is developing a ground-based system, incorporating both the active (radar) and passive (radiometer) instruments, to provide data continuity useful for various meteorological purposes. For example, a detailed time series of these variables is believed to be especially useful for regional forecasting purposes. The ground-based measurements may also be combined with satellite measurements for improved accuracies at higher altitudes.

The ground-based system would consist of a six-channel microwave radiometer for measurement of temperature, humidity and liquid in the zenith, and a near-zenith oriented radar for measurement of wind profiles and the heights of significant temperature inversions.

2. PRECIPITABLE VAPOR AND INTEGRATED LIQUID

Vapor and liquid are measured with a two-channel microwave radiometer at frequencies of 20.6 and 31.6 GHz. Radiation at the lower frequency is more sensitive to the presence of water vapor in the antenna beam, while the higher frequency is more sensitive to liquid water. Retrieval of the integrated quantities is then equivalent to solving two simultaneous equations with two unknowns. An evaluation of the accuracy of this technique has been made by Westwater (1978a). Examples of field measurements are given by Decker et al. (1978). A radiometer of this type has been in operation at the National Weather Service Forecast Office, Denver, Co., since July 1, 1978. Over a three-month period the rms difference between the radiometer measurements of vapor and simultaneous radiosonde measurements is 1.6 mm, or about 9% of the mean value.

3. TEMPERATURE PROFILE

Unlike water vapor, oxygen is a well-mixed gas in the atmosphere, and its radiation contains information on its temperature, provided the surface pressure is known. A four-channel system operating in the 50-60 GHz oxygen absorption complex would be used in a profiling system. Various theoretical and experimental studies have been made of the capabilities of such a system (e.g., Westwater et al., 1975). Recent work (Westwater et al., 1976; Decker et al., 1978) has demonstrated that the effects of radiation from clouds may be eliminated by using data from the 20.6 and 31.6 GHz radiometers mentioned in the previous section. Further improvement in the retrieval of temperature structure (inversions) may be achieved with a knowledge of the height of this structure. An evaluation of this technique has been made by Westwater (1978b). The height of these features may be observed by active radar or acoustic systems; it is proposed that the wind-sensing radar could also provide the required data for this purpose. Results of a month-long experimental program with simultaneous active and passive systems conducted at the Boulder Atmospheric Observatory near Boulder, Colorado, in September 1978 will be published in the future.

Westwater and Grody (1979) have simulated a combined satellite- and surface-based temperature profiling system. Their results show that the combined system offers a substantial improvement over either system used alone.

4. WINDS

Wind profiles are measured by virtue of the Doppler effect. Both acoustical and radio-frequency radars have been considered, but the latter appears to demonstrate the best operational characteristics for all-weather performance, along with measurements to tropopause heights. Continuous measurement of wind profiles has been demonstrated by several Doppler radars operating at frequencies ranging from HF to microwaves. Gage and Balsley (1978) survey recent developments in the use of both VHF and UHF Doppler radars for probing the clear atmosphere and show that wind profiles are observed to heights of 20 km. Winds have also been measured with FM/CW radars as shown by Chadwick et al. (1976) and Gossard et al. (1978). The design of a wind profiler to operate over heights ranging from near the surface to the tropopause is currently under way.

5. CONCLUSION

Development of remote sensing techniques now allows the design of an atmospheric profiling system for nearly continuous measurement of water vapor, liquid, temperature, and wind. A prototype system is now in the design stage with particular attention being paid to all-weather capability and to a data-handling system that will present the observations in real time and in a format needed by the user.

6. REFERENCES

Chadwick, R. B., K. P. Moran, R. G. Strauch, G. E. Morrison and W. C. Campbell, 1976: A new radar for measuring winds. Bull. Amer. Meteor. Soc., 57, 1120-1125.

Decker, M. T., E. R. Westwater and F. O. Guiraud, 1978: Experimental evaluation of ground-based microwave radiometric sensing of atmospheric temperature and water vapor profiles. J. Appl. Meteor., 17, in press.

Gage, K. S., and B. B. Balsley, 1978: Doppler radar probing of the clear atmosphere. Bull. Amer. Meteor. Soc., 59, 1074-1093.

Gossard, E. E., R. B. Chadwick, K. P. Moran, R. G. Strauch, G. E. Morrison and W. C. Campbell, 1978: Observations of winds in the clear air using an FM/CW Doppler radar. Radio Sci., 13, 285-289.

Westwater, E. R., J. B. Snider and A. V. Carlson, 1975: Experimental determination of temperature profiles by ground-based microwave radiometry. J. Appl. Meteor., 14, 524-539.

-----, M. T. Decker and F. O. Guiraud, 1976: Feasibility of atmospheric temperature sensing from ocean data buoys by microwave radiometry. NOAA Tech. Rep. ERL 375-WPL 48, National Technical Information Service, Springfield, VA.

-----, 1978a: The accuracy of water vapor and cloud liquid determination by dual-frequency ground-based microwave radiometry. Radio Sci., 13, 677-685.

-----, 1978b: Improved determination of vertical temperature profiles of the atmosphere by a combination of radiometric and active ground-based remote sensors. Preprints, Fourth Symposium on Meteorological Observations and Instrumentation (Denver), AMS, Boston, pp 153-157.

----- and N. C. Grody, 1979: Combined satellite- and surface-based microwave temperature profile retrieval. IEEE 1979 Region 5 Conference, Space Instrumentation for Atmospheric Observation, April 1979, El Paso, TX.

STATUS OF THE NATIONAL WEATHER SERVICE AUTOMATION OF FIELD OPERATIONS AND SERVICES (AFOS) PROGRAM

Russell G. McGrew
Chief, AFOS Implementation Staff
Headquarters, National Weather Service
Silver Spring, Maryland

ABSTRACT

The National Weather Service's AFOS Program entered the implementation stage in May 1978. Field tests will begin in December 1978 with an objective of achieving full operational status by early spring, 1979. Early experience with the equipment has been encouraging; readiness for full operations, however, must be assessed in light of detailed full systems and communications tests.

1. INTRODUCTION

The principal characteristics of the National Weather Service's AFOS system (as compared to current operations) are:

- o All graphic information is communicated in vector encoded form
- o All information is transmitted over common lines
- o All routinely used displays are "soft" (CRT's)
- o Processors and digital storage are provided at all major field sites.

1.1 Communications

Weather Service Forecast Offices (WSFO) are connected by a closed-loop, full duplex voice grade line. The loop is operated at 2400 baud in a synchronous store-and-forward mode, using an Advanced Digital Communications Control Protocol (ADCCP). Most Weather Service Offices (WSO's) are spurred from their parent WSFO nodes in a "star" configuration, operated in the same modes as the closed National Distribution Circuit. Some National Centers and special installations are spurred from nodes at a 4800 baud rate. All information is transmitted in data blocks with a maximum size of 256 characters.

1.2 Site Equipment

The AFOS system incorporates the following specific equipment:

Minicomputers - Data General Eclipse (S230)
Disks - Data General (6045)
Floppy Disks - Data General (6030)
Displays - Ford Aerospace and Communications Corp.
Printers - Data General (6042)
Printer/Plotters - Versatec (PPM.1)*
A/N Terminals - Zentec (9003)*

Some representative specifications of the equipment modules are:

Minicomputers

Word size	16 bits
Priority interrupts	16
Cycle time	800 nanoseconds
Memory:	
WSFO Comm.	128K bytes
WSFO Proc.	192K bytes
WSO Combined	128K bytes
Rigid Disks	10Mb
Floppy Disks	300Kb

Graphic Display (Black/White)

Monitor	17"
Refresh	60 fps
Resolution	1024 x 768
Controls:	
Intensity lvl	Continuous
Vector gen.	Solid, dashed, dotted
ZOOM	Discrete 1:1, 4:1, 9:1, 16:1, 25:1
OFFSET	Continuous
Fields	3, independently controlled
Cursor	Trackball
Character format	7x9, 14x18 Dot matrix
" Lib.	95 ASCII; 119 Wx Symbols

Printer/Plotter

Width	11"	(20")
Speed	Print	300 lpm
	Plot	Full screen 15 sec.

*Modified to meet NWS specifications.

1.3 Processing/Peripheral Configuration

The WSFO's and WSO's are equipped with the following processing and peripheral configurations:

	WSFO	WSO
Minicomputers	2	1
Disk Drives	2	1
Floppy Disk Drives	2	2
Printer	1	1
Printer/Plotter	1	1

1.4 Display Configurations

The display consoles (work stations) are configured in a number of combinations of alphanumeric (A/N) and graphic (G) modules. The basic WSFO and WSO configurations are given below; consoles are added as staffing and responsibilities justify:

Varieties:

AK - Stand along A/N
AG - A/N + slave graphic
AAG - A/N, slave A/N, slave graphic
AGG - A/N, 2 slave graphics
AGGG - A/N, 3 " "

Basic WSFO:

AGGG
AGG
AK

Basic WSO:

AGG
AK

1.5 Software - Systems and Applications

The systems software accommodates a number of operations that are now performed in a variety of manual procedures:

- o The data base will now accommodate about 22000 individual types of reports
- o All originated information is archived automatically on floppy disks
- o Upon line or station failure, communications among surviving stations are maintained with a "dial-around" procedure.
- o Following the interruption of communications, the data base may be replenished from the central data files of the System Monitoring and Coordination Center (SMCC) in Suitland, Md.
- o Individual users may establish and change the directory of information it desires to store.

The field "user" has several software packages that may be used in routine operations. Some examples:

- o Extensive message composition and editing assists including the capability to originate preformats for the more standard messages.
- o Computer worded forecasts.
- o A capability to combine a number of operational/display commands into a single macrocommand, including a variation that generates an entire pilot briefing scenario.
- o A capability for instructing the system to sound an alert upon the receipt of certain data or products.

2. STATUS OF INSTALLATIONS

At this time equipment has been accepted at 58 sites. These include the National Meteorological Center, National Severe Storms Forecast Center, National Climatic Center, Systems Monitoring and Coordination Center, four River Forecast Centers, two River Forecast Centers-WSO Combinations, 23 WSFO's, 21 WSO's, and four unique installations, including the Air Force Global Weather Central.

All of these locations are receiving live data on a routine and a more or less continuous basis. Most sites are operating with a software package that consists of a subset of the capabilities described in 1.5. Eight of the sites are operating with a more advanced software capability, consisting of virtually all of the capabilities enumerated.

Installation is proceeding at a rate of six to eight sites per month and will continue through November of 1980. Full operation of all sites is planned for the spring of 1981.

3. ASSESSMENT OF READINESS FOR OPERATIONS

Our readiness to assume full operations with the first few stations may be assessed in a number of important aspects; others cannot really be determined until the system is subjected to the full test program. Before converting to operations we must have an extremely high confidence level that we can maintain that mode because the impact on the Weather Message Switching Center (WMSC) is major. (We define fully operational as being that point at which the input of National Weather Service sites takes place via AFOS and the SMCC-WMSC "Gateway" rather than the current teletype circuits.)

My current assessment of our readiness in several important areas of consideration follows.

3.1 Equipment Delivery

We're very optimistic concerning the basic site equipment. Adequate stockage for the depot operations is open to some question, but the situation is improving. Some unique peripherals for the River Forecast Center

operationa are not yet available, but this does not impact the first tier of sites.

3.2 Equipment Reliability

The situation with respect to the processor, storage devices and alphanumeric displays is very favorable. The graphic displays failed the first formal reliability tests; these tests must be rerun.

3.3 Communications

Precise tests of the operational reliability of the communications are about to begin. A confident projection of the performance cannot be made on the basis of our experience to date. It has been difficult to sort communications performance from software performance and the "learning" experience of operations and maintenance personnel.

3.4 SMCC/Gateway Operations

The conversion, production and entering of alphanumerics and automated graphics is in excellent shape. The production and conversion of manual graphics and the "fine-tuning" of SMCC operations will require steady and intensive attention.

3.5 Systems Software

The basic software package appears to be in good shape. The principal questions lie in the potential changes that may have to be developed to compensate for unforeseen communications performance characteristics.

3.6 Personnel

Personnel requirements are being met in a satisfactory manner. (The only unique personnel requirements are associated with maintenance and the operation of the SMCC.)

3.7 Training

The training programs for both maintenance and operator personnel has proceeded above expectations.

4. SUMMARY

The AFOS system has proceeded essentially on schedule relative to the time of formal budgeting approval. The implementation phase is well underway, and the experience to date, while not devoid of some challenging problems, has been encouraging.

OPERATING WITH NEDS

Thomas M. Piwowar

USN/FWC Norfold

The Naval Environmental Display Station (NEDS) is installed at the major operational units of the Naval Oceanography Command. It is their primary source of real-time meteorological and oceanographic data.

Each NEDS has alphanumeric and graphics display capabilities, and each operates independently with respect to the other. An environmentalist can sequence several analyses on the NEDS' graphics display, examine the historical trend and compare it to the predictive trend. Multi-color, overlay graphics capability permits viewing several data fields simultaneously. "Zoom" capability enables focusing on a particular geographic area with an expanded display of the pertinent data fields. Within seconds, the environmentalist can query the Navy's main environmental data processing computer and display the latest oceanographic and meteorological information for any area in the world. At the NEDS console, the operator can analyze the environmental situation, prepare required warnings and/or forecasts, and transmit products to fleet users.

Since NEDS is a completely new data display system, considerable education and training of operators are required to fully realize its full potential. Minor hardware and software problems normally associated with new equipment are being remedied.

NEDS represents a futuristic step in environmental product display, analysis and dissemination.

AUTOMATION OF A CONVECTIVE RAINFALL ESTIMATION TECHNIQUE USING GEOSYNCHRONOUS SATELLITE DATA

Bruce T. Miers

US Army Atmospheric Sciences Laboratory

White Sands Missile Range, New Mexico

ABSTRACT

This paper will attempt to show that by fitting particular non-linear auto- and cross-covariance functions to space time covariance values calculated from satellite data, that convective complex characteristics such as size, ellipticity, motion, growth, and decay can be determined. These modeled features then can be related to convective storm characteristics found by Scofield and Oliver (1977) which in turn are related to actual rainfall amounts. The results of this study are a first step in removing the subjectivity from current rainfall estimation techniques. Results from the 20 May 1977 storm over Texas and Oklahoma are presented.

1. INTRODUCTION

The effects of weather on the planning for and execution of combat missions have been apparent to military men as long as man has fought man. Historically, the weather has been considered to a great extent to be a natural obstacle, akin to difficult terrain, about which soldiers could do little but accept the consequences. And unlike natural obstacles, the weather often varied considerably and was difficult to predict; one had to expect and prepare for the worst.

Trafficability is of critical concern to the Army in the field. Battlefield commanders must have information on fluctuations in soil moisture content in order to make decisions concerning tactical maneuvers on the battlefield. Soil moisture conditions at a given time and place are a function of: (1) water input to the ground surface from precipitation, (2) water loss from the surface by evaporation and transpiration, and (3) changes in soil moisture storage.

In this study, our primary concern is with Item (1) above. Knowledge of where and when rain is occurring as well as the rate of rainfall will provide critical data on changes in soil moisture and thus on trafficability.

Much of the research work which is aimed at using satellite data to arrive at estimates of rainfall amounts has been very subjective in nature; that is, each person viewing the satellite imagery may interpret it in a slightly different manner, thus arriving at variations in the estimated surface rainfall amounts. The elimination of as much of this subjectivity as possible is desirable. An example of this subjective approach is Scofield and Oliver's (1977) work which made use of infrared data to make quantitative estimates of cloud heights. Rainfall estimates were made from enhanced IR satellite images based on the premise that the higher the cumulonimbus cloud top the heavier the rain. Additional information on the rate of anvil growth, the position of the cumulonimbus under the spreading anvil, merging cells, merging convective cloud lines, and overshooting tops have been used to improve the model. These factors were then incorporated into a decision tree to aid the user in determining where and how much rain has fallen (Scofield and Oliver 1977).

This study will attempt to show that by fitting particular non-linear auto- and cross-covariance functions to space time covariance values calculated from satellite data that storm characteristics such as size, ellipticity, motion, growth, and decay can be determined. These modeled characteristics then can be related to storm features found by Scofield and Oliver (1977) which in turn are related to actual rainfall amounts. The results of this study are a first step in removing the subjectivity from current rainfall estimation techniques.

2. DATA PROCESSING PROCEDURES

The Geostationary Operation Environmental Satellite (GOES) surveys the earth from a nominal altitude of 35,800 km. The GOES has a rotation speed of 100 rpm which generates a west to east scan of the earth. A stepping mirror allows the sensors to accomplish the north to south scan of the earth. Eight visible and two infrared (IR) sensors, with

resolutions of 1 km x 1 km and 4 km x 8 km, respectively, provide the data base. In one revolution of the satellite, the earth is scanned for about 18 degrees with each scan consisting of data from one IR sensor and eight visual sensors. These data are transmitted to the command station at a 28 megabit rate and then are time-stretched to fill the remaining 342 degrees of satellite rotation and retransmitted back to the satellite. GOES then retransmits the data back to earth where it is available to the users at a 2 megabit data rate.

When the satellite signal is received at the Atmospheric Sciences Laboratory's (ASL) Direct Readout Ground Station (DRGS), it is processed through the Bit Frame Synchronizer/ Sectionizer System (BFSSS). First the signal is detected and demodulated to digital baseband Non-Return to Zero-Level (NRZL) code by a demodulator. The signal is then routed to two bit synchronizers, one dedicated to infrared and the other to visible. The outputs of the bit synchronizers, each consisting of NRZL data and bit clock, are routed to the digital interface where the interface establishes synchronization on the IR signal and determines the transmission mode. Synchronization is then established on the visible signal. The digital interface is operated by a PDP 11/45 minicomputer. Through a computer program, sectors of data of interest to a researcher are stored on magnetic tape or displayed in real time.

Once the sector of interest is determined, the IR and visible data are separated into two files for further processing. Often when GOES data is viewed on a display monitor, it is obvious that entire lines of data are unacceptable for use in an analysis program; and random errors are sometimes present in the data. These errors require the use of a filtering and smoothing program to render the data acceptable for use in analysis programs. In outline form, the filtering and smoothing program handles the data in the following manner. Image positions are defined by rectangular coordinates (i,j) where i = 1,2,...,N gives the relative horizontal position (pixel) and j = 1,2...,M gives the relative position from the top of the image (line); and image intensity at point (i,j) is denoted by F(i,j). Examination of the data showed that bad isolated points were characterized by $F(i,j) > \theta_1$, or $F(i,j) < \theta_2$. For visible data, θ_1 was assigned the value 59 and θ_2 the value 4, while values of 252 and 4 were assigned to θ_1 and θ_2 for infrared data. An isolated bad point, F(i,j) is replaced by the average of its neighbors F(i-1,j) and F(i+1,j) on the same line j.

Unacceptable lines were characterized by rapid oscillation of intensities along a line and is detected by a large value of the "average slope" of the line given by Equation 1.

$$A = \frac{1}{N}\sum_{i-1}^{N-1} \left| F(i+1,j) - F(i,j) \right| \qquad (1)$$

The lines were defined as bad when A was greater than five. After examining a large number of cases, it was found that good lines have a value of A less than three and bad lines have a value of A near 20. In actual computer implementation, lines are processed first and random points next. The program also allows up to three consecutive bad lines or bad points before default of the entire data set.

For the purposes of this study, the data were segmented so that only one convective complex will appear in a data set. Tests (Eddy and Hembree, 1977), have shown that some decimation of the complete data set was possible while still producing the same covariance structure. The results of this study were derived using every fifth pixel and every second line in the IR and every 20th pixel and every 16th line in the visible.

After this facet of the data processing procedure was complete, latitude and longitude for each point of the decimated data set was calculated. The data file and the latitude-longitude file were then used to calculate the raw covariance matrices. A data processing flow chart is shown in Figure 1.

3. NAVIGATION FOR GEOSYNCHRONOUS METEOROLOGICAL SATELLITES

The navigation algorithm used by the Atmospheric Sciences Laboratory's Meteorological Analysis System (AMAS) is a modification of Phillips and Smith's (1974) work. Similar software pacakges are being used by NASA/GSFC and the Universities of Wisconsin and Colorado State.

The purpose of the navigation software is to provide the capability for accurately calculating the latitude and longitute of any point in the image data, and, conversely, for computing the position on the image of any specified earth location. The data required to perform these transformations consists of four principal components: (1) spacecraft orbital elements for computing satellite position at any specified time, (2) spacecraft spin axis attitude, specified by the right ascension and declination of the spin vector in celestial coordinates, (3) small angles of pitch, roll, and yaw that specify the misalignment between instrument optical axes and spacecraft spin axis, and (4) scan phase correction parameters for each image to which the navigation applies. These parameters (Item 4, above) are the initial offset and drift rate, in the pixel (horizontal) direction, between the center of the earth and the center of the master image.

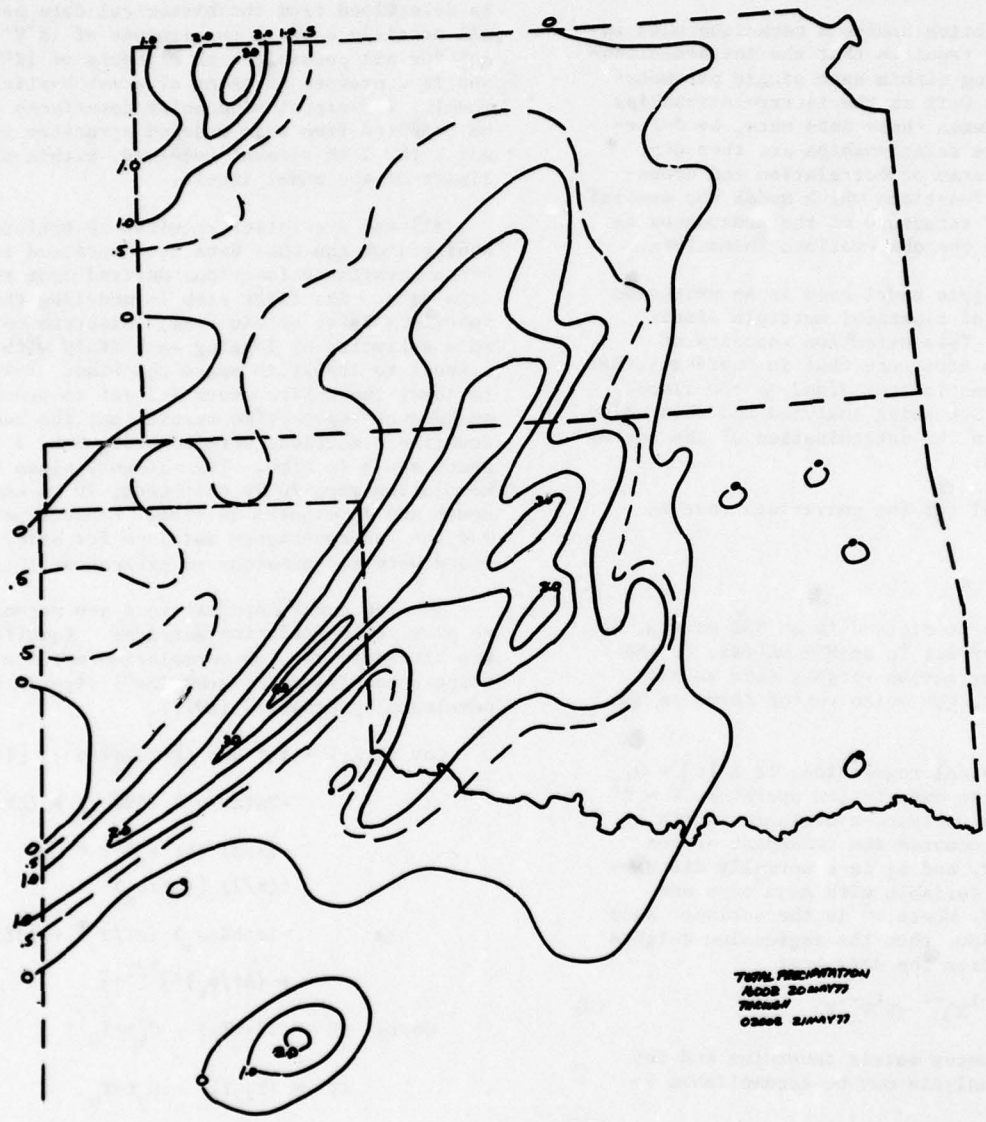

FIGURE 1 - TOTAL PRECIPITATION PATTERN FOR 20-21 MAY 77.

Three coordinate systems are used in the navigation solution; namely (1) a celestial inertial system for description of orbit and attitude, (2) a geographic system rotating with the earth for description of landmarks, and (3) a time-dependent satellite coordinate system for description of the scanning geometry. For a detailed description of this solution, consult Billingsley, et al (1977).

4. THE OBJECTIVE ANALYSIS TECHNIQUE

The objective analysis technique used in this project requires that the intrarelationships existing within each single parameter data set, as well as the interrelationships existing between these data sets, be determined. These relationships are then described in terms of correlation and cross-correlation functions which model the spatial and temporal structure of the phenomenon as reflected in the observations themselves.

The analysis model used is an extension (Eddy 1973) of classical multiple linear regression. This extension consists of modeling the structure that is representative of the information contained in the time series data set being analyzed and then using that model in the determination of the regression weights.

The model for the univariate case is given by

$$Y = X\beta + \varepsilon \tag{2}$$

where Y, the predictand is an NX1 matrix, X, the predictor set is an NXM matrix, β, the vector of regression weights form an MX1 matrix and ε, the noise vector forms an NX1 matrix.

In classical regression, if $E[\varepsilon] = 0$, where E is the expectation operator, $V = E[\varepsilon\varepsilon^t]$ is the variance-covariance matrix of ε, where ε^t denotes the transpose of the noise vector, and ε_i is a normally distributed random variable with mean zero and variance $\sigma^2 V$, where σ^2 is the variance about the regression, then the regression weights determined from the data are:

$$\hat{\beta} = (X^t V^{-1} X)^{-1} (X^t V^{-1} Y) \tag{3}$$

where -1 denotes matrix inversion and the objective analysis may be accomplished by

$$\hat{Y} = X\hat{\beta} \tag{4}$$

See Draper and Smith (1966) for details.

It can be shown that the k th, 1 th element of the matrix $X^t V^{-1} X$ is computed by

$$(X^t V^{-1} X)_{kl} = \sum_i^N \sum_j^N X_{ik} X_{jl} V_{ij}^{-1} \tag{5}$$

and that the k th element of the vector $X^t V^{-1} Y$ is computed by

$$(X^t V^{-1} Y)_k = \sum\sum X_{ik} Y_j V_{ij}^{-1} \tag{6}$$

The covariance structure function, cov(XX), is determined from the historical data set for all possible k th, 1 th elements of $(X^t V^{-1} X)$ and for all possible k th elements of $(X^t V^{-1} Y)$, and is expressed in terms of a mathematical model. The signal plus noise covariance can be computed from this modeled structure for any k th, 1 th element required, within the limits of the model itself.

All the statistics required to perform the analysis of the GOES data are contained in the cross-covariance functions derived from the data sets. The first step in modeling these functions is to obtain "raw," discrete covariance estimates by lagging each field with respect to itself in space and time. In order to cover the entire storm and yet to preserve an adequate space-time resolution, the raw covariance matrices were of order 9 by 9 in space and 4 in time. The category sizes or resolution were 70 km east-west, 70 km north-south and 15 minutes in time. Product pairs and the raw covariance matrices for selected times were too numerous to present at this time.

The raw covariance matrices are normalized to give raw correlation matrices. Equation 7 was fitted to the raw correlation matrices using a non-linear program (NLP) algorithm developed by Crawford (1977).

$$\begin{aligned} \text{Cov}(X_1X_2) = A * \exp\{&[-1/2(1-\alpha^2)]\,[(\Delta X/\sigma_x)^2 \\ &-2\alpha(\Delta X/\sigma_x)(\Delta Y/\sigma_y) + (\Delta Y/\sigma_y)^2] \\ &-(1/2)(\Delta t/\sigma_t)^2\} * \cos \\ &\{(\pi/2)\,[(\Delta X/\sigma_x)^2 \\ &-2\alpha(\Delta X/\sigma_x)(\Delta Y/\sigma_y) + (\Delta Y/\sigma_y)^2 \\ &+ (\Delta t/\sigma_t)^2]^{1/2}\}] \end{aligned} \tag{7}$$

where $\Delta X = (X_2 - X_1) - C_x t - X_o$

$\Delta Y = (Y_2 - Y_1) - C_y t - Y_o$

$\Delta t = t_2 - t_1$

X_1 = position (E-W) of variable 1

X_2 = position (E-W) of variable 2

Y_1 = position (N-S) of variable 1

Y_2 = position (N-S) of variable 2

t_1 = observation time of variable 1

t_2 = observation time of variable 2

The decision variables (NLP estimated parameters) are as follows:

A = modeled lag zero correlation coefficient. σ_x, σ_y, σ_t = modeled measures of storm size in space and time.

α = a measure of ellipticity

C_x and C_y = modeled speeds toward the east and north (positive), respectively.

An NLP algorithm maximizes or minimizes an objective function, subject to mathematical constraints. The algorithm adjusts the values of the variables until any minor change in these variables results in an improvement of the objective function of less than some small preset value. The algorithm thus converges upon values of the variables which are as good or better than any nearby values.

In the above formulation, variable 1 and variable 2 were both IR or visible thus producing an auto-covariance function.

4. SYNOPTIC SITUATION

The first case used to test the objective analysis procedures occurred on 20-21 May 1977 over the south central United States. The synoptic situation on 19 May at 1200Z showed a high pressure system centered over Kentucky with a low pressure over North Dakota. A cold front extended from this low pressure system southwestward through South Dakota, Nebraska, Western Kansas, and Oklahoma into the Texas Panhandle. Flow in advance of the front was southerly bringing warm moist air from the Gulf of Mexico in the Great Plains. Surface Temperatures in advance of the front ranged from the lower 70's in North Texas to the lower 60's in North Dakota with the dew point temperatures ranging from the mid 60's to the mid 50's.

Upper air flow at 700 mb on the 19th was characterized by a ridge over the eastern portion of the United States while a trough spanned the area from Idaho through Eastern Nevada into Southern California.

Twenty-four hours later, the surface high pressure system had moved over Pennsylvania and the cold front reached from Northwest Wisconsin to Central New Mexico. Warm moist Gulf air continued to flow into regions in advance of the cold front. The upper level trough and ridge positions had moved slowly eastward.

On the mesoscale, a line of thunderstorms had developed by 1700Z in the Texas Panhandle with the line moving southeastward and the cells in the line moving northeastward. Later in the day multiple lines had formed and thunderstorm tops to 14 km were reported. In addition, rainshowers developed around 1630Z in Central Texas and these two areas merged by 1930Z over the Red River. The greatest reported hourly rainfall amount occurred between 0000Z and 0100Z on 21 May at Geary, Oklahoma (2.00 inches). Hourly rainfall amounts in excess of 1 inch were recorded from many areas in the Texas Panhandle and Western Oklahoma between 1800Z on 20 May and 0100Z on 21 May. Total storm rainfall (see Figure 1) pattern was oriented southwest-northeast with the largest amount (4.3 inches) occurring at McLean, Texas. The three-inch isohyet ran from near Kress, Texas, northeastward to Sun City, Kansas.

5. RESULTS

The satellite data for the 20 May 77 storm produced the values shown in Part A of Tables 1 and 2. Storm features (Part B) derived from the values in Part A were computed in the following manner. The orientation (θ) is given by:

$$\theta = (1/2)\ \text{ARCTAN}\ [2\alpha\sigma_x\sigma_y/(\sigma_x^2 - \sigma_y^2)] \quad (8)$$

the major axis (a) is computed by Equation 9;

$$a^2 = \sigma_x^2\cos^2\theta + \sigma_y^2\sin^2\theta + 2\alpha\sigma_x\sigma_y\sin\theta\cos\theta \quad (9)$$

the minor axis (b) is given by;

$$b^2 = \sigma_x^2\sin^2\theta + \sigma_y^2\cos^2\theta - 2\alpha\sigma_x\sigma_y\sin\theta\cos\theta \quad (10)$$

the area is computed from Equation 11;

$$A = \pi(a)(b) \quad (11)$$

the shape by;

$$S = a/b \quad (12)$$

and the signal to noise ratio (S/N) can be inferred from the modeled lag zero correlation coefficient as follows (Equation 13)

$$S/N = \rho(0,0,0)/[(1-\rho(0,0,0)] \quad (13)$$

Also speed and direction of movement of the storm are shown in the tables.

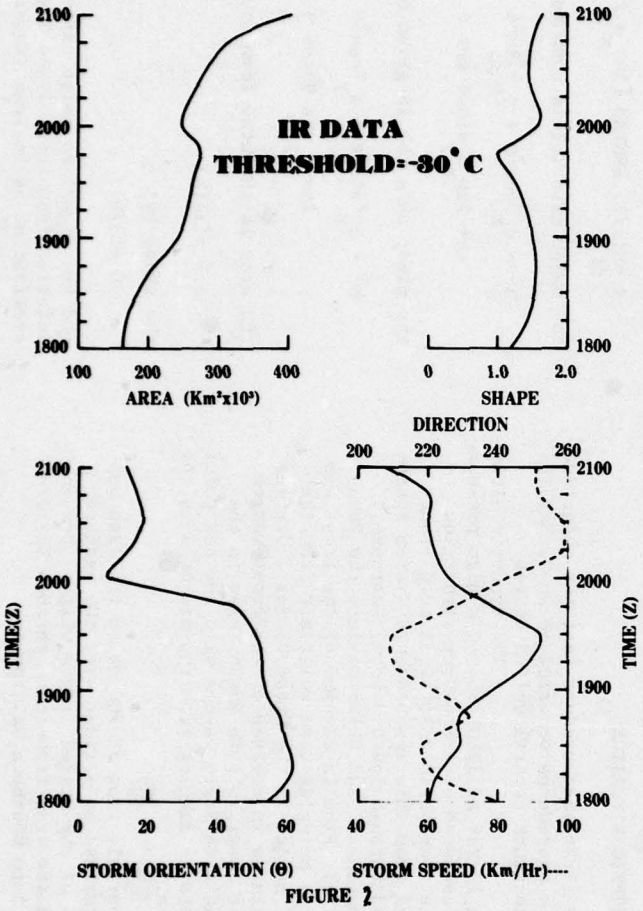

FIGURE 2

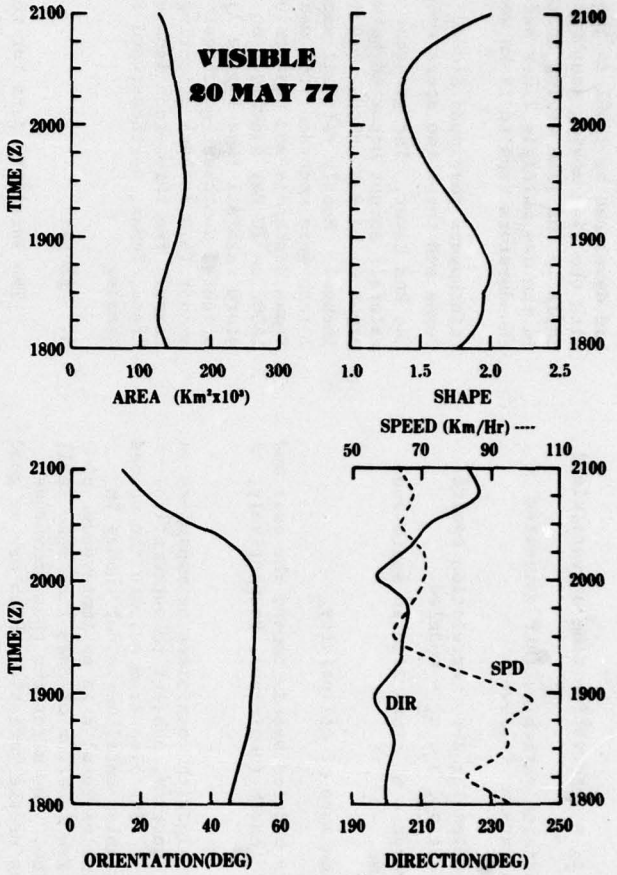

FIGURE 3

The derived storm characteristics are conservative and stable over the 1800Z to 2145Z time period. The change in orientation shown at 2000Z was due to the merging of a small cell with convective complex.

The colder IR temperatures became numerous in the southern portion of the storm during the merger thus forcing the orientation angle around to a more easterly direction; however, the direction of movement of the total storm remained about the same. Figures 2 and 3 show a plot of some of the significant parameters of the convective complex. Weather radar reports from Lubbock, Texas indicated average cell movements of 30 to 35 knots (55 to 64 km/hr) with a direction of 230 at 1800Z. Maximum observed cell speed by weather radar was 50 knots (91 km/hr) from 230. Later in the day (2030Z), the Oklahoma City weather radar reported cells moving about 25 to 30 knots (46 to 55 km/hr) from 230 to 240 degrees azimuth. A maximum speed of 35 knots with an azimuth of 230 was also recorded.

The computed storm orientation (θ) agrees well with the surface rainfall pattern up until time of cell merger.

The area shown in Tables 1 and 2 indicate that the visible cloud top is somewhat smaller and oriented a little differently than the IR cloud top. The over-shooting tops seen in the visible data (Figure 4) are pronounced and tend to line up along the direction of motion. These features tend to make the covariance algorithm deduce a smaller system.

The signal to noise ratio (S/N) increased and then decreased with time. The convective complex evolved during the period of analysis from a smooth and well defined ellipse up until the time of cell merger. Then the system became a rather flat and ragged composite of anvils produced by several embedded cells (Figure 5). One could anticipate the S/N to drop to very small values as the system ceased to produce new active rain cells.

Several inferences can be made from the results of this study; namely (1) cloud top morphology of convective complexes as deduced using the space-time covariance analysis technique is sufficiently conservative to suggest that predictions made for periods of about 1 to 2 hours could show significant skill, (2) these predictions can be objective and automated, and (3) rainfall location, movement and intensity can be associated with cloud top features of such weather systems.

6. REFERENCES

Schofield, R. A. and V. J. Oliver, 1977, "A Scheme for Estimating Convective Rainfall from Satellite Imagery," NOAA Technical Memo NESS 86

Phillips, D. R. and E. Smith, 1974, "Geosynchronous Satellite Navigation Model," U. of Wisconsin Space Sciences and Engineering Center, Internal Report.

Billignsley, J., J. Chen, C. Mottershead, A. Bellian, and T. DeMott, 1977, "AOIPS METPAK, a Meteorological Data Processing System," Computer Science Corp. Report CSC/SD-77/6084.

Eddy, A., 1973, "The Objective Analysis of Atmospheric Structure," J. Meteor. Soc. Japan, Vol 51, pp. 450-57.

Draper, N. R. and H. Smith, 1966, "Applied Regression Analysis," Wiley Press, 401 p.

Crawford, K. C., 1977, "The Design of a Multivariate Mesoscale Field Experiment," Ph.D. Dissertation, U. of Oklahoma, Department of Meteorology.

Eddy, A. and L. Hembree, 1977, "Space-Time Sampling from SMS Satellite Data Required to Define Convective Storms," Final Report Contract DAAG29-76-D-0100, US Army Research Office.

FIGURE 4 - VISIBLE IMAGE - 20 MAY 77, 1815Z

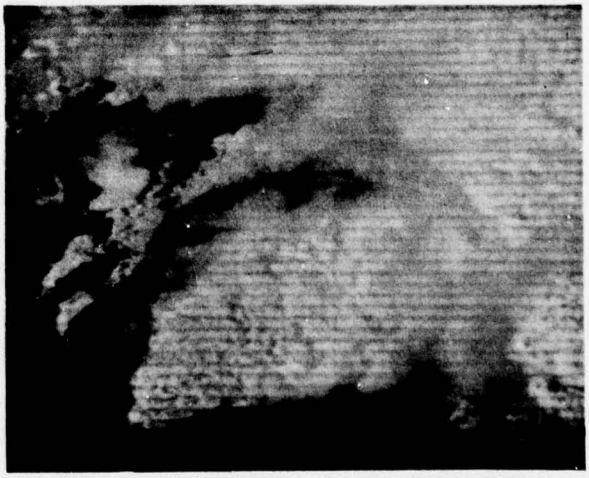

FIGURE 5 - VISIBLE IMAGE - 20 May 77, 2045Z

PART A					PART B							
σ_X KM	σ_Y KM	α	ρ	TIME (Z)	θ DEG	A KM	B KM	AREA $KM^2 \times 10^3$	SHAPE A/B	DIRECT DEG	SPEED KM/HR	S/N
199	259	.09	.61	1800-1845	54	249	211	165	1.18	220	81	1.56
197	272	.20	.62	1815-1854	61	274	195	168	1.41	223	62	1.63
195	300	.25	.63	1830-1915	60	229	196	184	1.53	229	58	1.70
195	328	.26	.65	1845-1930	58	321	206	208	1.56	229	72	1.86
191	354	.25	.66	1854-1945	55	335	223	235	1.50	234	67	1.94
191	369	.20	.66	1915-2000	53	337	243	257	1.39	249	50	1.94
197	365	.14	.66	1930-2015	51	325	258	263	1.26	252	50	1.94
211	362	.01	.65	1945-2030	45	298	295	276	1.01	239	67	1.86
226	354	-.14	.64	2000-2045	8	356	222	248	1.60	226	82	1.78
242	352	-.23	.63	2015-2100	15	360	231	261	1.56	222	99	1.70
262	356	-.25	.63	2030-2115	19	367	246	284	1.49	220	92	1.70
272	379	-.23	.61	2045-2130	17	389	258	315	1.51	221	92	1.56
295	452	-.24	.59	2100-2145	14	461	281	407	1.64	207	91	1.44

TABLE 1 - INFRARED DATA (THRESHOLD = 30°)

PART A					PART B							
σ_X KM	σ_Y KM	α	ρ	TIME (Z)	θ DEG	A KM	B KM	AREA $KM^2 \times 10^3$	SHAPE A/B	DIRECT DEG	SPEED KM/HR	S/N
224	223	.51	.60	1800-1845	45	275	156	135	1.76	200	94	1.50
214	224	.58	.61	1815-1854	47	275	142	123	1.94	200	83	1.56
216	235	.58	.60	1830-1915	49	284	146	130	1.95	202	95	1.50
221	249	.59	.60	1845-1930	51	298	149	139	2.00	201	95	1.50
225	255	.57	.64	1854-1945	51	302	156	148	1.94	197	102	1.78
228	256	.50	.67	1915-2000	52	298	170	159	1.75	204	75	2.03
228	253	.43	.68	1930-2015	52	289	180	163	1.61	205	62	2.13
221	244	.37	.68	1945-2030	53	274	183	158	1.50	206	67	2.13
216	238	.32	.67	2000-2045	53	262	186	153	1.41	198	70	2.03
219	230	.31	.64	2015-2100	49	257	186	150	1.38	206	71	1.78
231	207	.32	.63	2030-2115	36	254	179	143	1.42	213	64	1.70
253	181	.33	.61	2045-2130	22	265	163	136	1.63	227	68	1.56
273	153	.34	.58	2100-2145	15	280	140	123	2.00	224	64	1.38

TABLE 2 - VISIBLE - 20 MAY 77

AUTOMATED CLOUD-TRACKING USING GOES IMAGERY

R. E. Nagle and D. H. Lee

Naval Environmental Prediction Research Facility

Monterey, California

ABSTRACT

A research and development program for extracting information on atmospheric momentum from geosynchronous satellite data is presented. A brief description of a GOES acquisition station located at Monterey is given. The data processing and display equipment (including an array processor) to manipulate data from this system is described. The SRI ISODATA procedure for automatically tracking cloud clusters has been implemented on an interactive-graphics, minicomputer-based display system. An overview of this approach to cloud tracking is presented and examples of the resultant vectors are shown. Techniques for extracting information, including vorticity and divergence, from fields of cloud motions and blending these data with conventional observations and analyses are described. Results of studies of the optimum level to assimilate cloud motion data into objective analyses are presented.

1. INTRODUCTION

The centralization of satellite processing facilities has created a dilemma: How to disseminate the vast amounts of environmental satellite data and/or information collected at these facilities to the ultimate user, and how to do so within sufficient time to assure the currency of the data. This is a difficult and costly undertaking when considering only the contiguous United States -- when these types of data must be disseminated to Navy forces at sea and land locations worldwide, the problems become monumental. However, with the development of minicomputers and microprocessors about ten years ago, a potential solution for this dilemma began to emerge.

This new technology provided the computational power to allow consideration of acquiring the data transmitted directly from the satellites, and reducing these data in situ for local and regional use. The Man-computer Interactive Data Access System (McIDAS) (Suomi, 1975; Smith, 1975; Chatters and Suomi, 1975), developed at the University of Wisconsin, was one of the first applications of this technology to remotely sensed environmental data. Devices of this type also have been developed at SRI International (Serebreny et al., 1970), NASA (Billingsley and Hasler, 1975), and other Government agencies and universities.

The Naval Environmental Prediction Research Facility (NEPRF) has been developing the Satellite Data Processing and Display System (SPADS) since 1975. The basic objective of this research and development project is to demonstrate the utility of minicomputer-based interactive graphics display devices in processing and extracting information from data transmitted directly from environmental satellites. A major component of this effort has been directed toward data from geosynchronous satellites.

This paper presents an overview of the NEPRF geosynchronous satellite data applications program, which consists of five subelements: (1) data acquisition; (2) processing and display; (3) automated extraction of cloud motion vectors; (4) derivation of information from cloud motion vectors (CMV); and (5) assimilation of information into numerical analyses.

2. DATA ACQUISITION

The GOES Acquisition and Data Handling System (GADHS) is a stretch-mode GOES readout station, shown in functional form in Fig. 1. The 8.5 m parabolic hour-angle over declination reflector can receive data from either the eastern or western U.S. GOES satellites (but not both simultaneously). The remotely controlled antenna can be repositioned from one satellite to the other in about three minutes.

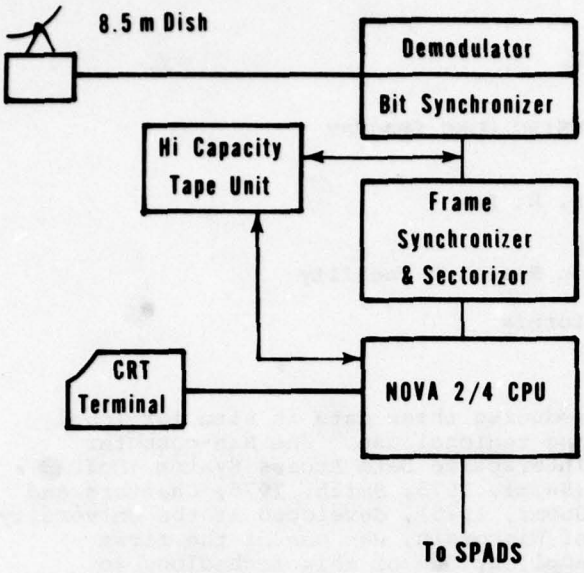

Fig. 1. Functional Diagram of GOES Acquisition and Data Handling System (GADHS).

In addition to the normal electronic components, a sectorizer is included as an integral part of the system. This subsystem extracts a 640-line by 956-element sector of data from the full-disc GOES images. The sector is selectable either under thumb-switch or automated control from the GADHS controller (a NOVA 2/4 minicomputer). Resolution options include 1.0, 2.0, 4.0, 8.0, or 16.0 km for the visible data, or 4.0, 8.0 or 16.0 km for the infrared data; simultaneous acquisition of both channels is not currently possible. The sectorizer strips-out the specified data and passes it to the NOVA 2/4 minicomputer for subsequent transfer to the Satellite Data Processing and Display System (SPADS).

A high capacity tape recorder is being added to the system to permit simultaneous bulk storage of the full resolution data and retrieval of both the visible and infrared channels. It can record up to 2.4 hours of data; playback rates of 1:1, 2:1, and 4:1 of the acquisition data rate are provided. This feature will permit the retrieval of the corresponding visible or infrared data in the twelve minutes required to recycle the satellite's telescope.

3. DATA PROCESSING AND DISPLAY

The SPADS, shown diagrammatically in Fig. 2, is a dual CPU system with one side driving a 525-line black and white CRT and the other driving a 525-line color CRT. The computers are linked together in two manners: by a hard-wired computer-to-computer channel that permits intercommunication between the two CPU's, and by a second method through the disk system. The dual disk controller has one port attached to each computer, which permits both computers to access data (but not both simultaneously) stored on the disk system.

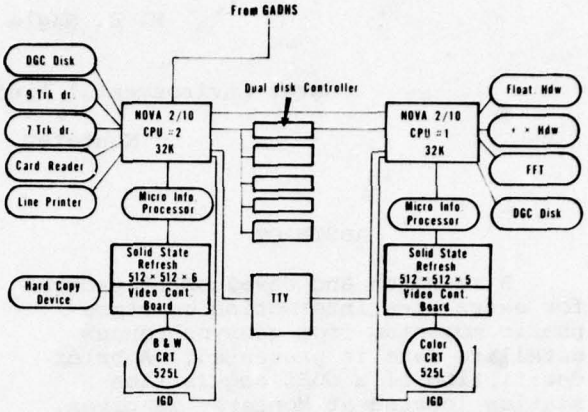

Fig. 2. Functional Diagram of Satellite Data Processing and Display System (SPADS).

The key component of the SPADS is the solid state refresh (SSR) memory; this comprises computer memory boards in which the digital imagery is stored in order to refresh the CRT's. The SPADS SSR memories are configured in different manners on the two sides of the system. The black and white SSR consists of six 512 x 512 x 1 bit planes; four planes are reserved for imagery and two are reserved for overlays. The SSR on the color CRT contains five planes, three for imagery and two for overlays.

The micro-information processor (MIP) is an essential interface between the minicomputer and the SSR. These are microprocessors with high execution cycles (150 nanoseconds). The primary function of the MIP is to perform the address computations required to load the digital imagery into the SSR as it is passed from the minicomputer.

The SPADS has a full complement of peripheral devices including 7- and 9-channel tape units, card reader, electrostatic plotter, and a hard-copy device for producing paper images (grey shades of relatively low quality). Of particular importance is the inclusion of three hard-wired special processing units: one for floating point operations, a second for multiple/divide operations, and a third for array processing operations. The latter device, which permits the execution of Fast Fourier Transforms (FFT) in hardware, is discussed further in Para. 4.2. The SPADS is shown in Fig. 3.

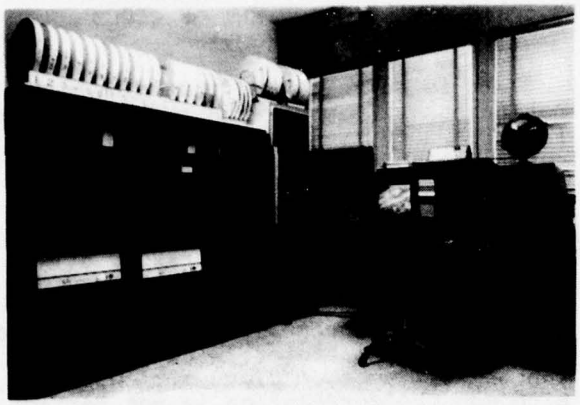

Fig. 3. Satellite Data Processing and Display System (SPADS).

When used in conjunction with the GADHS, a GOES sector is passed line-by-line to CPU-2 of the SPADS and the data are stored on the disk system. After a complete sector has been received, a 512 x 512 element subsector is extracted for display on either CRT. Successive sectors may be stored sequentially on an analog disk (not shown in Fig. 3) for later display in animated form (i.e., "movie loops").

4. AUTOMATED EXTRACTION OF CLOUD MOTION VECTORS

Manpower limitations at Navy environmental support centers preclude manual extraction of cloud motion vectors Therefore, automated techniques for extracting cloud motions have become a necessity in the operational environment. Two different automated cloud tracking techniques are currently being evaluated.

4.1 The SRI Automated Cloud Tracking System (SATS)

SRI International has developed an automated method for measuring cloud motions as shown in sequences of geosynchronous satellite images (see, for example, Endlich et al., 1971; Hall, 1977; and Wolf et al., 1977). The approach used in SATS emulates the manual tracking of clouds: clusters of clouds are identified in a sequence of digital images and the matching of clusters in successive images provides vector end points of the cloud motions.

The original SATS programs were coded for a CDC-6400, but this code has recently been converted to the NOVA 2/10's of the SPADS. The original programs contain many options: minimum size of cloud clusters, or maximum number of elements contained in a cluster, for example. Because of severe memory limitations in the NOVA 2/10's, a scaled-down version of the SATS was implemented on the SPADS. The technique is applied to successive 70 x 70 pixel arrays in order to derive motion vectors over a large geographical area.

The SATS technique is currently being evaluated to ascertain the combination of options and resolutions that produce the most acceptable results. Tests have been conducted using visible or infrared data of different resolution, and the best results obtained so far have been in the use of 8 km infrared data at a one-hour interval. The vectors derived from the infrared data for one case are shown in Fig. 4a; the vectors derived from the corresponding visible data are shown in Fig 4b. It must be noted that these are raw displacement vectors and have not been normalized for perspective or satellite motion.

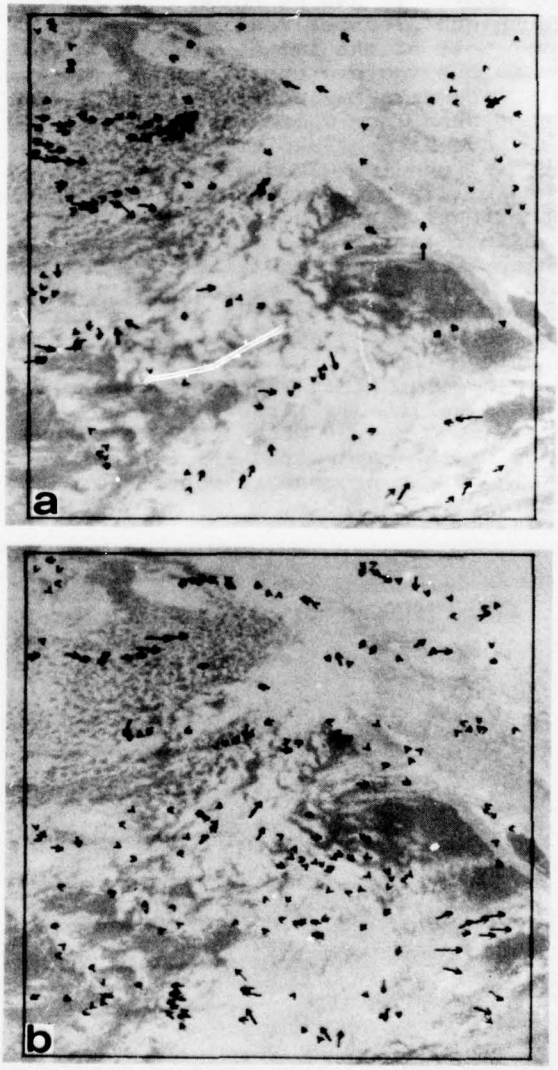

Fig. 4. Example of Cloud Motion Vectors derived from GOES Data through the Application of SATS: (a) Infrared and (b) Visible.

4.2 Cross-Covariance Technique

The application of Fourier Transform techniques for deriving cloud displacements have been discussed by Leese et al., 1971. The computational advantages of the cross-spectral density aspects of the Fourier Transform have recently been demonstrated (Arking et al., 1977). The second method being evaluated as a technique for deriving cloud displacements uses the cross-covariance feature of a two-dimensional Fast Fourier Transform (FFT) as programmed for a CYBER-175. An example of displacement vectors obtained through the application of this technique to GOES data is shown in Fig. 5.

These vectors were computed over 32 x 32 subarrays of the original 8 km resolution visible imagery; the time difference between the two images was one hour. It can be noted that this technique produces realistic vectors over most of the image, although a few anomalous vectors can be seen. These displacements may actually be real, but the clouds from which they were derived may have been at a different level than the surrounding cloud elements. The possibility also exists that they are incorrect, having been created by a manifestation of the FFT technique which limits resolvability to a maximum X or Y displacement of one-half the linear dimensions of the area to which the technique is applied. In this particular case, the limit would be a displacement of 16 elements (128 km). This algorithm is currently being programmed on the SPADS to take advantage of the hard-wired FFT capability of the array processor; results are not currently available.

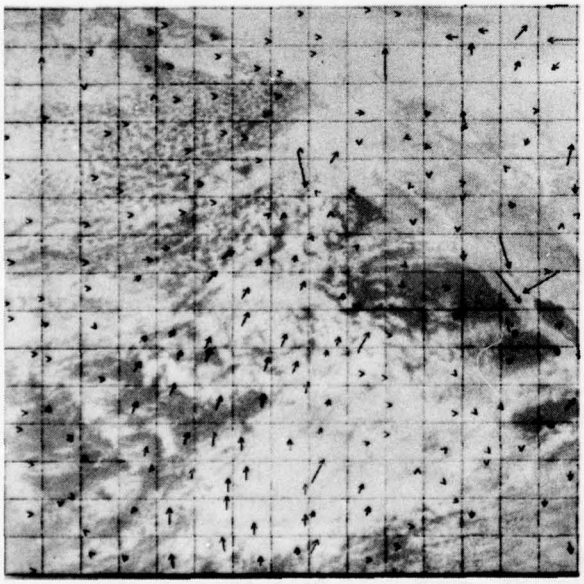

Fig. 5. Cloud Motion Vectors derived from the Cross-Covariance Technique.

5. INFORMATION CONTENT OF CLOUD MOTION VECTORS (CMV)

It is acknowledged that clouds do not necessarily move with the wind field in which they are embedded. Aircraft verification studies (Hasler, 1972; Hasler and Shenk, 1977; Hasler et al., 1977) indicate that cloud motions are best associated with the winds at the base of the clouds. Comparisons of cloud motion vectors (CMV) with radiosonde winds (Hubert and Whitney, 1971; Hasler, 1972; Suchman et al., 1975) have shown that satisfactory winds generally can be derived from cloud motions, although the correlation is not perfect.

The inconsistencies between CMV and radiosonde winds can create difficulties when these data are entered into automated analysis routines. However, advanced objective analysis techniques are capable of blending information into an objective analysis in forms other than wind speed and direction (see, for example, Gandin, 1963; Schlatter, 1975). The fields-by-information-blending (FIB) analysis procedure (Danard et al., 1968) is fully capable of blending radiosonde winds with parameters derived from wind field, cloud motion analyses and/or forecast fields.

In this context, a study conducted some years ago subjected low level CMV to independent objective analyses. The relative vorticity and divergence computed from the resulting grid-point analyses were then compared with the actual cloud patterns. An example of one case from this study is shown in Fig. 6. It can be seen that there is excellent correspondence between both the vorticity and, in this case, the divergence patterns and the corresponding cloud patterns. This study demonstrated that there was a physically consistent correspondence between the pattern of the relative vorticity field derived from CMV and the attendant cloud patterns. Although this is not an absolute verification, it clearly indicates that there is valid information, at least in the rotational component, contained in the CMV.

This concept was investigated further (Viezee et al, 1977) and attempts were made to blend the vorticity derived from cloud motions with wind speed and direction observations obtained from radiosondes into a combined analysis. Results indicated that this was a viable approach; however, little or no improvement was observed over the conventional use of CMV when the analyses were performed on a coarse mesh grid (381 km). The utility of blending the vorticity derived from CMV with radiosonde winds was clearly demonstrated for subsynoptic

scale systems and when the analyses were performed on a fine mesh. The results of this study also suggested that the divergent component of CMV was questionable.

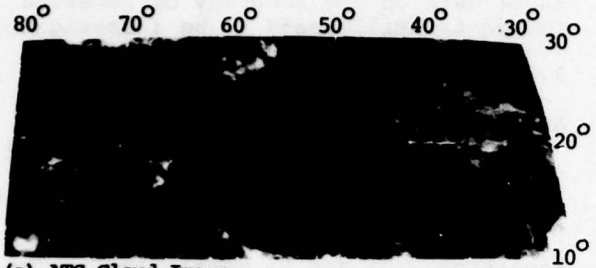

(a) ATS Cloud Image

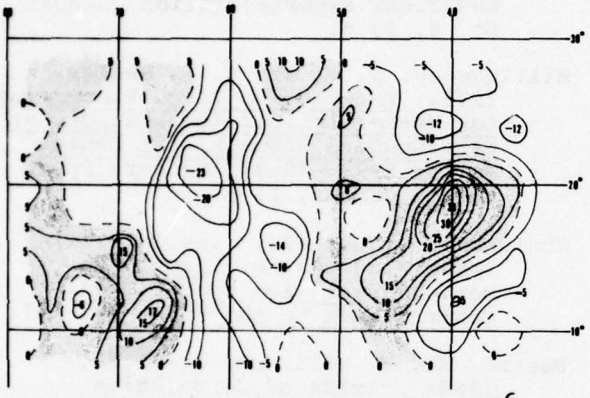

(b) Cloud Motion Relative Vorticity (x 10^{-6})

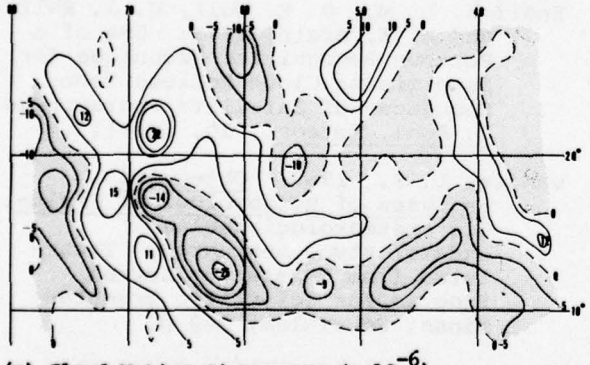

(c) Cloud Motion Divergence (x 10^{-6})

Fig. 6. Comparison between Cloud Patterns (a), Relative Vorticity (b), and Divergence (c) derived from Low-Level Cloud Motion Vectors.

6. ASSIMILATION INTO NUMERICAL MODELS

Certain problems in the data assimilation process require resolution: the derivation of valid wind information from cloud motions; the manner in which information should be extracted from CMV; and the proper method of assimilating this motion field information into a numerical analysis and prediction system. The primary utilization of CMV are for ingestion into numerical analyses for initializing numerical forecast models. The vertical resolutions of both numerical analyses and prediction models are relatively crude in comparison to those of radiosonde data. Therefore, the difficulties in the objective use of CMV are compounded because uncertainties of CMV height constitute one of the major problems in assimilating these data into numerical analyses (Bengtsson and Morel, 1974; Suchman et al., 1975).

In an attempt to minimize these uncertainties, a study was performed to investigate various methods of inserting CMV into a three-dimensional objective analysis system. Rawinsonde data and CMV derived from the SMS-2 satellite data were assimilated using the NCAR Limited Area Multivariate Statistical Objective Analysis (Schlatter, 1975); persistence was used as the first guess. The area in which the analyses were performed included both data-rich and data-sparse regions: Central and North America, and the eastern Pacific Ocean, respectively. A six-hour interval between analyses was used, and the study encompassed a three-consecutive-day period.

Except for a control experiment, four different methods of assigning the level of the CMV in the vertical (see Fig. 7) were used: (1) at the analysis level nearest the cloud-top temperature; (2) at all levels within the cloud layer as defined by the cloud-top temperature and the cloud physical thickness; (3) at the level nearest the cloud-base; and (4) at the wind-fit level, at which the CMV agreed best with the first guess wind. The cloud physical thickness was determined using the procedure described by Mosher (1974).

As in all CMV impact studies, the lack of definitive "ground-truth" was a problem in this study. Among the criteria used to assess the validity of the various insertion methods were changes produced from the first-guess and control case, and comparison with the corresponding cloud pattern as viewed in the corresponding satellite imagery.

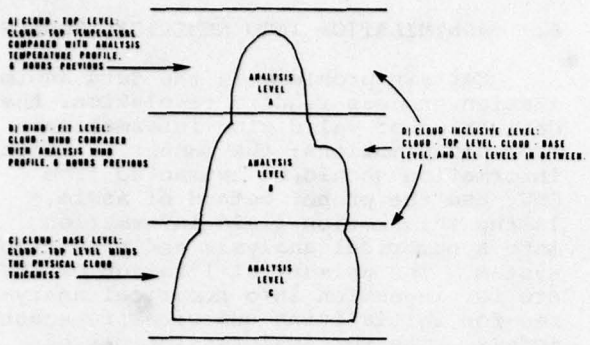

Fig. 7. Four Methods for determining the Cloud Insertion Level.

The Cloud-top and Cloud-base methods showed very similar results (see Fig. 8). However, the Cloud-base method appears to be preferable over the other methods because (1) the frequency distribution of the level at which the vectors were assimilated showed peaks at 300 mb and 900 mb, which is consistent with other research results, and (2) the resulting analyses were consistent with the attendant cloud pattern.

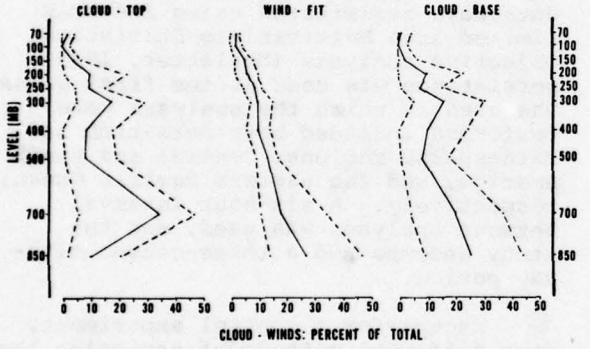

Fig. 8. Number of CMV at each Level.

7. SUMMARY

An overview of the NEPRF R&D program on the quantitative use of geosynchronous satellite data has been presented. The results of this program have demonstrated that the minicomputer-based interactive graphics display devices are fully capable of reducing geosynchronous satellite data and extracting information on the atmospheric momentum field from these data. It is clear that there is useful information in the rotational component (vorticity) of CMV; it has yet to be demonstrated that useful information on atmospheric divergence patterns can be obtained from these data.

Advanced objective analysis procedures are fully capable of using vorticity extracted from analyzed fields of CMV. This procedure greatly reduces the problem of consistent biases between CMV and radiosonde data. It would appear that the proper level to insert this information into numerical analysis systems is at the level closest to the level of the cloud base. The impact of these data on the accuracy of numerical forecasts still needs to be investigated.

8. REFERENCES

Arking, A., R. C. Lo, and A. Rosenfeld, 1977: A Fourier Approach to Cloud Motion Estimation. Report X-911-77-167, Goddard Space Flight Center, 27 p.

Bengtsson, T., and P. Morel, 1974: The Performance of Space Observing Systems for the First GARP Global Experiment. GARP Working Group on Numerical Experimentation, Report No. 6, 23 p.

Billingsley, J. B. and A. F. Hasler, 1975: Interactive Image Processing for Meteorological Applications at NASA/Goddard Space Flight Center. Report X-933-75-97, Goddard Space Flight Center, 11 p.

Chalters, G. C., 1976: The Satellite Image Wind System. Proc. Symp. Met. Observ. from Space: Their Contribution to the FGGE, 195-197.

Danard, M., M. Holl, and J. Clark, 1968: Fields of Correlation Assembly - A Numerical Analysis Technique. Mon. Wea. Rev., 96, 141-49.

Endlich, R. M., D. E. Wolf, D. J. Hall and A. E. Brain, 1971: Use of a Pattern Recognition Technique for Determining Cloud Motions from Sequences of Satellite Photographs. J. Appl. Meteor., 10, 104-117.

Gandin, L. S., 1963: Objective Analyses of Meteorological Fields. Gidrometeorologicheskae Lzdatel'stvo, Leningrad. Translated from Russian by Israel Program for Scientific Translations, Jerusalem, 242 p.

Hall, D. J., 1977: Clustering, the ISODATA Method. Computation for the Relative Perception of Similarities and Differences in Complex and Real Data. Statistical Methods for Digital Computers, Wiley-Interscience.

Hasler, A., 1972: Properties of Tropical Cloud Clusters Determined from Geosynchronous Satellite Pictures. Ph.D. thesis, Univ. of Wisconsin, 317 p.

Hasler, A. F., and W. E. Shenk, 1977: Wind Estimates from Cloud Motions: Results of an In situ Aircraft Verification Experiment. NASA Weather and Climate Program Review, NASA Conf. pub., 20-29.

Hasler, A. F., W. E. Shenk, and W. C. Skillman, 1977: Wind Estimates from Cloud Motions: Results from Phases I, II and III of an In situ Aircraft Verification Experiment. J. Appl. Meteor., 16, 812-15.

Hubert, T. F., and L. F. Whitney, Jr., 1971: Wind Estimates from Geostationary Satellite Pictures. Mon. Wea. Rev., 99, 665-72.

Leese, J. A., C. S. Novak, and B. B. Clark, 1971: An Automated Technique for Obtaining Cloud Motions from Geosynchronous Satellite Data Using Cross Correlation. J. Appl. Meteor,, 10, 118-132.

Schlatter, T. W., 1975: Some Experiments with a Multivariate Statistical Objective Analysis Scheme. Mon. Wea. Rev., 103, 246-57.

Serebreny, S. M., E. J. Weigman, R. G. Hadfield, and W. E. Evans, 1970: Electronic System for Utilization of Satellite Cloud Pictures. Bull. Amer. Meteor. Soc., 51, 848-855.

Smith, E. A., 1975: The McIDAS System. IEEE Transactions of Geoscience Electronics, GE-13 (3), 123-126.

Suchman, D., D. W. Martin, F. R. Mosher, B. Sawyer, and K. G. Bauer, 1975: Preliminary Assessment of the Cloud Tracking System at the University of Wisconsin. Space Science and Engineering Center, Univ. of Wisconsin, 77 p.

Suomi, V. E., 1975: Minicomputer Interactive Data Access System (McIDAS): Continued Development of McIDAS and Operation in the GARP Atlantic Tropical Experiment. Final Report, Contract NAS5-23296, SSEC, Univ. of Wisconsin, 255 p.

Viezee, W., D. E. Wolf, and R. M. Endlich, 1977: Evaluation of the FIB Methodology for Application to Cloud Motion Wind Data. Final Report, Contract N00228-76-C-3182, SAI International, 92 p.

Wolf, D. E., D. J. Hall, and R. M. Endlich, 1977: Experiments on Automatic Cloud Tracking Using SMS-GOES Data. J. Appl. Meteor., 16, 1219-30.

AUTOMATED SHORT-RANGE FORECASTING OF CLOUD COVER AND PRECIPITATION USING GEO-STATIONARY SATELLITE IMAGERY DATA

H. Stuart Muench and Thomas J. Keegan

Air Force Geophysics Laboratory (AFSC)

Hanscom Air Force Base, Massachusetts 01731

ABSTRACT

The geosynchronous satellite represents a vast improvement over earlier weather satellites, with more frequent images, easier navigation and digital output. However, the data rate is so high as to be overwhelming, and computer assistance is needed by the forecaster to absorb useful information. Two efforts underway at AFGL to assist the forecaster are described. The first effort is to develop algorithms to specify cloud condition and precipitation rate given satellite video and IR measurements. The second effort is to develop automated guidance forecasts through use of cloud pattern extrapolation.

1. INTRODUCTION

It was about fifteen years ago that weather satellite pictures became routinely available, and synoptic meteorologists could not help being impressed and optimistic about the future ahead. Without question, the satellite represented a means to identify and track the small weather disturbances that have always caused grief to the forecaster. However, frustration lay in the path of those developing satellite-based forecast techniques in the early days of satellite meteorology. First, synoptic meteorologists are accustomed to using numbers in making their analyses and forecasts (forever drawing isobars, isotherms, etc.) and numbers are certainly necessary to develop and test objective forecast techniques. Unfortunately, the early satellite pictures usually presented several shades of grey, with the value depending primarily on the rather arbitrary setting of the control knobs on the recorder as well as the characteristics of the paper on hand. In addition, when clouds were extensive, there was considerable uncertainty of geographical positions that lay underneath. Finally, a single satellite usually made but two passes a day, with infra-red pictures at night and video pictures by day, and forecasters must use three-hourly or even hourly charts to follow small-scale weather patterns that have short lifetimes.

2. A NEW SATELLITE AND A NEW PROBLEM

With the advent of the geo-synchronous satellite, the picture changed drastically. We now receive numbers directly from the satellite, numbers corresponding to 64 shades of grey and to 256 levels of infra-red temperature. Positioning (or "navigating") the data is more reliable because cloud-free areas are always present in the full-disk pictures. And, perhaps most important, the images are routinely updated every half hour. Certainly, the era of quantitative use of satellite data is upon us.

However, we have also come face to face with a very formidable (and unfamiliar) problem--data rate! There are perhaps ten to fifteen thousand weather stations on our world, taking anywhere from four to twenty-four regular observations per day, each observation consisting of five to twenty numbers. In addition, some thousand radio-sonde stations take two observations a day with about 200 numbers per sounding. All together, this means that one to two million numbers are transmitted each day by observers around the world. Now, a single GOES satellite transmits one to two million numbers in only seven seconds!! And, it transmits at this rate for thirty minutes of every hour during daylight.

Let us put this in a little better perspective. During a mesoscale forecast experiment at AFGL some five years ago, we had a conventional forecaster making forecasts based on hourly aviation reports. The forecaster used a map of southern New England similar to that in Figure 1, with about 34 weather stations. He could plot all the station data, analyze the mesoscale features in quite some detail and make forecasts out to three hours, and while he was not rushed, he was busy dealing with some 400 numbers each hour. For this same area, the satellite produces 378,000 video values each hour, plus 12,000 IR values! There is simply no way a person can absorb and analyze this much data this fast! The forecaster obviously needs help, if he is to use satellite information quantitatively.

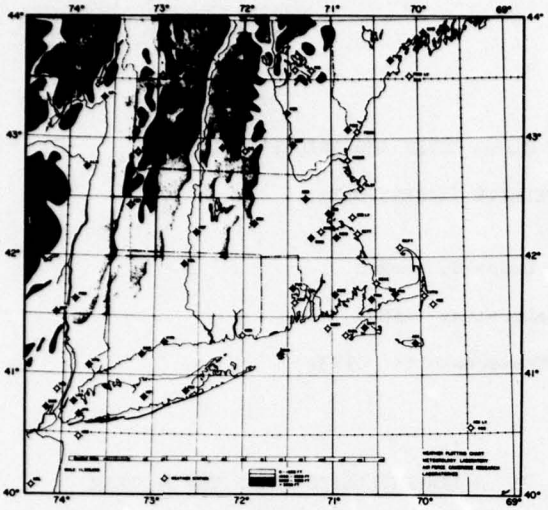

FIGURE 1. Aviation Weather Stations

3. AFGL PROGRAM

A program to help the forecaster has been set up at AFGL, and the approach is shown schematically in Figure 2.

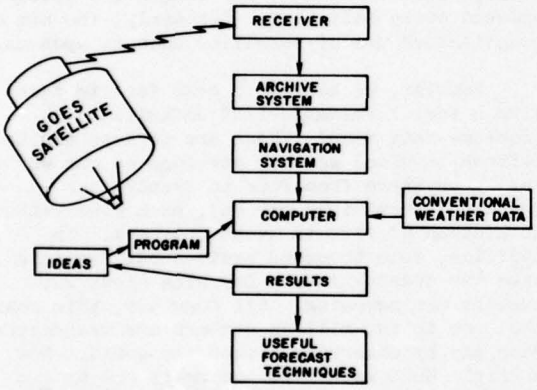

AFGL SATELLITE-BASED FORECAST TECHNIQUE DEVOPMENT

FIGURE 2

The GOES satellite in the upper left needs no introduction. On the top, we have a 7 1/2 meter dish antenna to receive the "stretched" satellite data in real time, some of which are archived on magnetic tape. Our archive system is basically a microprocessor controlled tape recorder (built by University of Wisconsin) which will accept a schedule of images to be recorded. While researchers are notorious for their capacity to acquire data, we did make compromises to keep the requirements for scheduling, tape handling and navigation within reasonable limits. A single sector is archived, running from Michigan eastward through Maine and southward to central North Carolina, with one-mile video resolution and four-mile IR resolution. Eight pictures per day are scheduled, every hour on-the-hour (to coincide with aviation weather observations) during normal working hours. For some selected days, half-hourly pictures have been recorded. Since February 1977, some 110 magnetic tapes have been filled, or about 2200 pairs of video and IR images.

Part of the problem in using satellite data is finding which point on earth corresponds with a satellite observation or, conversely, which satellite value corresponds to a weather station--a process often referred to as "navigation". On weekdays, a normal McIDAS navigation is performed, based on standard targets in Baja California, Venezuela or Peru. Using McIDAS software, row and element numbers corresponding to positions of some 18 weather stations in our archived images are placed on punch cards for use with the AFGL 6600 computer. However, we do find that the McIDAS navigation may have errors of ten to twenty miles when applied to points in New England, and thus archived tapes are run through the McIDAS display system to obtain corrections, which are probably good to $\pm$ two to three miles. Thus far, corrections for 1200 of the 2200 images have been made, hardware difficulties having slowed up the last 1000 corrections.

We are now down to the loop in Figure 2 that involves ideas, programs, computer and results. When the project was started, there was no way to tell what form of output would be most valuable to the forecaster and most beneficial to our principal client, Air Weather Service. We did know the more fully automated, the better, for Air Weather Service has been cutting back on manpower while expanding services. Thus, we are pursuing two approaches--first, the development of algorithms and procedures to specify cloud condition and precipitation rate from satellite measurements, and second, to develop automated techniques that produce guidance forecasts for the 0-6 hour period.

4. CLOUD AND PRECIPITATION SPECIFICATION

A major effort is underway to specify cloud condition given satellite imagery values. The approach has been to start with the simplest of conditions, clear sky, and progress towards the more complex. The first question to answer is what is the "normal" background seen for a clear sky? How does this normal change from hour to hour, month to month and from station to station? What is the best way to describe this normal--the average and variance over some area? What size area? A study based on the first year of data has been completed which directly addresses these questions. The results show, for example, slightly larger day-to-day variations with means of 9 points than 25, 49, 81 or 729 and slightly larger standard deviations about the means for the smallest arrays. A report on this work has been prepared and will be published in the near future.

Some clear-sky background data were extracted from this study and are shown in Figure 3 to demonstrate the quality of the satellite video data. The video data coming from the satellite are in the form of a "count", an integer from 0 through 63, which is proportional to the square-root of the albedo. In this diagram one sees plotted the space-averaged count for four clear days at points 15 miles southeast of Bedford, MA, (upper curve), over Bedford (middle curve), and 15 miles northwest of Bedford (lower curve). There is a well defined systematic difference between the backgrounds at these locations, with the darkest in the more wooded area to the northwest and the lightest in the cleared, urban areas to the southeast. The important point is that the difference between these backgrounds is only tenths of a count. Further, the reported visibility on 4/29 and 5/23 was 20 miles while only 15 miles on 5/3 and 5/12, and it is obvious that this small increase in haziness or turbidity produced an effect discernable at all three locations. Quite likely there will be a host of weak signal phenomona we will be able to identify, but to do so will require a rather precise knowledge of background as well as a stable satellite calibration.

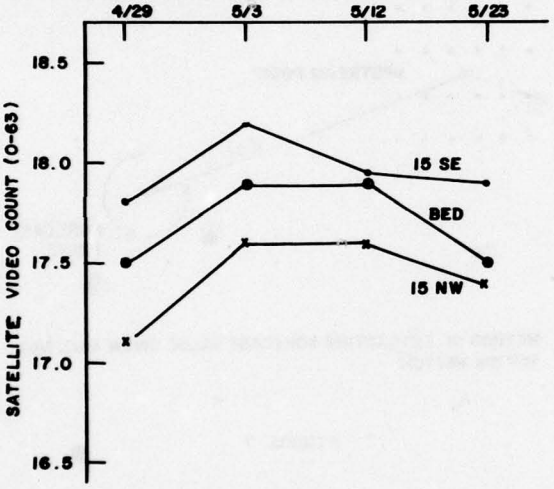

AVERAGE VIDEO COUNT (.9 row X 9 element = 1 mile video) ON FOUR CLEAR DAYS AT 1600 GMT

FIGURE 3

In the other area of specification, we are working on means to determine precipitation rate from satellite information. For this work, we have been using hourly rainfall data collected at four NWS station. Corresponding satellite video and IR values were extracted for 5x5 nautical mile areas over the stations. The video count data were converted to brightness and then normalized for sun angle. This normalization uses not only the secant of the solar zenith angle but also a factor for anisotropic scattering, which should be included because clouds, particularly liquid clouds, do not scatter uniformly in all directions (there is still much room for improvement in anisotropic scattering correction routines). Following the example of Conover and Bunting (1977) in their work on cloud water content using satellite data, the rainfall amounts were plotted against normalized brightness and IR temperatures and the resulting curves as shown in Figure 4. The rainfall during the hour that followed the satellite observation was used on the assumption that the cloud moisture seen by the satellite might take some time before it reached the ground. As one would expect, the coldest and brightest clouds are associated with the heaviest rainfall (snowstorms were excluded from the study). Also, one sees that at low IR temperature the brightness is important in specifying rainfall, so, at night when we have no video the specification of rainfall by IR alone would be poorer.

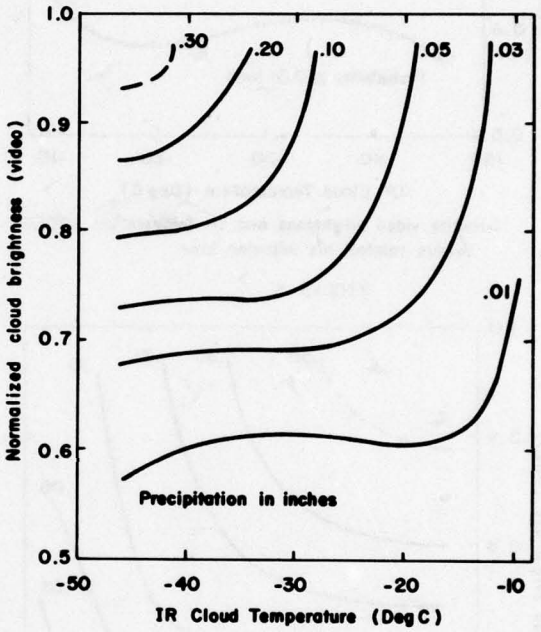

Satellite video brightness and IR Temperature (GOES) versus rainfall the following hour

FIGURE 4

Another way to present this information is a probability of exceeding a certain rainfall. In Figure 5, we have the probability of exceeding 0.01 inches in the following hour, as a function of video brightness and IR temperature. The probabilities in the upper portion are fairly high, representing a good (though not perfect) indication that either rain is falling or else soon will fall.

Figure 6 shows the probabilities for exceeding 0.10 inch in the next hour, the criterion that separates "light" rain from "moderate" rain. The probabilities are not so high, but this is a rare event and the probabilities might still be high enough for warning purposes if costs of precaution are small compared to potential loss.

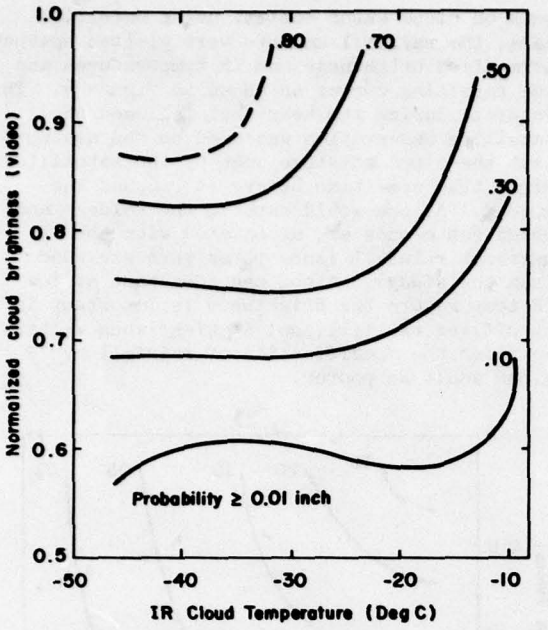

Satellite video brightness and IR Temperature (GOES) versus rainfall the following hour

FIGURE 5

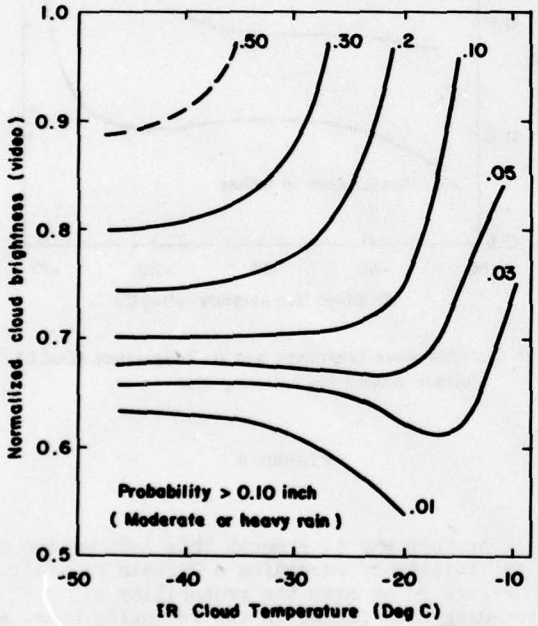

FIGURE 6

There is much more work to do on precipitation specification. More data are needed to better define the high rates--in Figure 6 the 50% line is dashed because there were only 8 values in that area. Also, we would expect improvement of specification if some measure of spatial variation of video and IR is included. And, there are questions to answer on time lag. A report describing the effort to date is being written and will be published this winter.

5. AUTOMATED FORECASTING

The last topic of this presentation is that of automated forecast technique development. If we know the direction and speed of cloud pattern motion, we can look "upstream" to see what patterns will be over us at what time. In Figure 7, we see that we must go upstream a distance t times the speed. To obtain a forecast of weather conditions, we must use algorithms such as those previously described to obtain cloud condition or precipitation rate. If we want to be more sophisticated, we consider data around the upstream point, weighing inversely by the distance r to allow for uncertainty in knowledge of speed and direction. Basically, this is merely the age-old extrapolation horizontal extrapolation technique, and versions using radar data have been programmed and used both experimentally and operationally. There is every reason to believe it will work equally as well with satellite data.

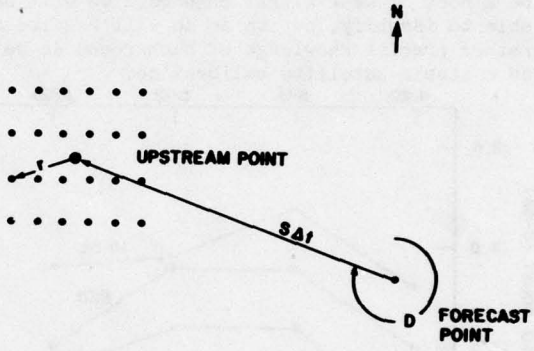

METHOD OF EXTRACTING FORECAST VALUE GIVEN TIME AND MOTION VECTOR

FIGURE 7

The biggest problem is that of obtaining motion vectors of the cloud systems automatically. Considerable work has been done on this problem by NESS (Leese et al 1971) and SRI for NEPRF (1977), for example. Presently, we are testing several motion vector procedures to see which are the most appropriate to use for determining cloud pattern motions in automated forecast routines. Included in this group are two procedures that are based on the work at SRI, and involve isolating individual clouds or clusters on two successive images and determining motion by the displacement that produces the best match between pairs of similar clouds. Two other techniques are based on cross-covariances between arrays for all potential displacements, and the displacement with the highest covariance represents the motion vector. One of these techniques uses binary arithmatic, and operates quite nicely. The other uses fast-Fourier-transforms and the programming was just completed.

Two tests of these motion vector programs have been planned. First, we have chosen some twelve video images, 256x256 arrays of 1-mile data, representing a wide variety of cloud conditions. For the test, the arrays are artificially displaced in different directions by distances which simulate 30-knot motion over a half-hour time period. When the first available programs were tested on these artificial displacements, the results were a bit disappointing--some were quite good, but some were rather bad. The primary difficulty was not hard to spot, (thanks to the generous intermediate output from the NEPRF program) and might be called the "checkerboard effect". Suppose all clouds were shaped like the pattern on a checkerboard, and between pictures the pattern moved exactly one square--you could not resolve, with a limited grid, whether the pattern moved east, west, south or north. This means that cloud features closer together than twice the distance the pattern moves between images will not likely produce useful information on the pattern motion. The solution, of course, is to smooth the pattern and an eight-row-by-sixteen-column smoothing routine does indeed improve results.

Once all of the programs are working satisfactorily and passing the artificial displacement test, we will move on to tests using specially archived half-hourly data. Since we won't know the true displacement, the test here will add upper level winds from radiosondes as potential motion vector candidates.

The first report on the automated forecast techniques will be published in the near future, and will contain program descriptions and some preliminary test results.

6. SUMMARY

To summarize briefly, we have an active program at AFGL, designed to assist the forecaster in using satellite data for short-range forecasting. Specifically, we are seeking algorithms to specify cloud cover and precipitation rate using satellite video and IR measurements, and we are developing automated guidance forecast techniques using cloud pattern extrapolation. At times the progress seems agonizingly slow, with endless hardware failures, but we are getting results and progress reports are being prepared for publication.

7. REFERENCES

Conover, J. H. and J. T. Bunting, 1977: Estimates from satellites of weather erosion parameters for reentry systems. Air Force Surveys in Geophysics No. 377, AFGL-TR-77-0260, 85 pp.

Leese, J. A., C. S. Novak, and B. B. Clark, 1971: An automated technique for obtaining cloud motion from geosynchronous satellite data using cross correlation. J. Appl. Meteor., 10, 118-132.

USE OF THE NIMBUS-G MULTI-CHANNEL MICROWAVE RADIOMETER (SMMR) TO DEDUCE ATMOSPHERIC AND SURFACE PROPERTIES

RICHARD C. SAVAGE, MAJOR, USAF

CURTIS D. HALL, CAPTAIN, USAF

AIR FORCE GLOBAL WEATHER CENTRAL

OFFUTT AIR FORCE BASE, NEBRASKA

ABSTRACT

Theoretical simulations of a variety of raining atmospheres were used to calculate the expected microwave brightness temperatures reaching the SMMR on NASA's Nimbus-G satellite. Variations of surface properties, such as temperature and moisture (and therefore reflectivity and emissivity), were included in the simulations. Matrix prediction equations incorporating the physical and radiative variables were calculated and inverted as a first step in forming remote sensing equations for the deduction of surface and atmospheric properties from SMMR data.

1. INTRODUCTION

The Scanning Multi-Channel Microwave Radiometer (SMMR) on the Nimbus-G and SEASAT satellites belongs to the third generation of microwave imaging devices. The first generation was marked by the launch, in 1972, of the Electrically Scanned Microwave Radiometer (ESMR) on Nimbus-5. At 19.35 GHz, the frequency used in the first ESMR, it was possible to detect changes in soil emissivity and radiative temperature due to changes of soil wetness and flooding. Such effects have been documented by Wilheit, et al (1976). Additionally, the increased brightness temperature due to rain over oceans has made possible the investigation of tropical storms and large scale precipitation systems, as shown in publications by Rao, Abbott and Theon (1976), by Allison (1974), and by others. The high emissivity of ice relative to water has made it possible to map oceanic ice cover, documented by Gloersen, et al (1974).

The launch of Nimbus-6, with its dual-polarized 37.0 GHz imager in 1975, made possible the investigation of rainfall effects over land surfaces. The higher frequencies (shorter wavelengths) led to a greater interaction between sensed radiation and precipitation-sized particles; the dual polarization permitted one to isolate some effects in the signal due to surface phenomena, such as wetness. Among the earlier papers on this subject were publications by Savage and Weinman (1975), and by Hall, Davies and Weinman (1978).

In the work described herein, it has been our objective to simulate the microwave brightness temperatures to be expected from a variety of rainy atmospheres, at the SMMR frequencies. From these simulated brightness temperatures, an inversion matrix was prepared for use in estimating atmospheric and surface conditions from real SMMR data, when available.

2. INSTRUMENT CHARACTERISTICS

In SMMR, we are considering an instrument with two channels (each dual-polarized) in the lower frequency part of the spectrum (6.6 and 10.7 GHz), two additional channels near a weak water vapor absorption line (18.0 and 21.0 GHz), and a channel at a frequency of relatively minimal gaseous absorption (37.0 GHz). Since we will be interested in the signatures of precipitation phenomena as well, we have indicated in Figure 1 the optical depth due to a 12,000 ft (3.67km) deep rain cloud with a

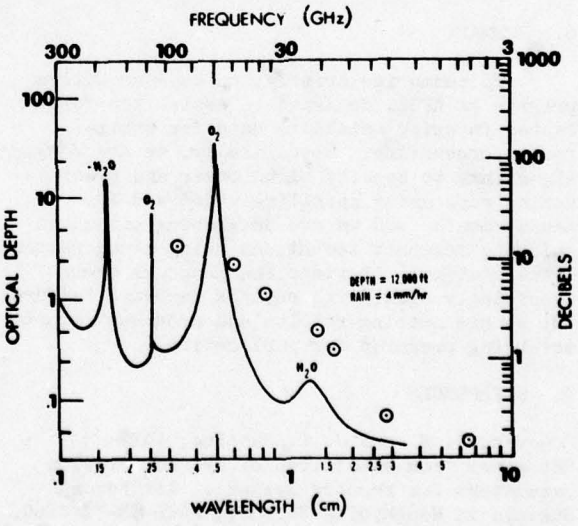

Figure 1. Optical depth and attenuation in decibels due to gaseous absorption in a maritime polar atmosphere. Circled points indicate attenuation in the presence of a 12,000 ft raincloud characterized by a Marshall-Palmer rain rate of 4 mm/hour.

Marshall-Palmer rainfall rate of 4mm/hr - a light rainfall rate. As may be seen, the optical depth or opacity of the atmosphere increases at the higher frequencies because of the interaction between precipitation particles and electromagnetic radiation with comparable sized wavelengths.

3. RADIATIVE SIMULATIONS

In order to simulate the radiative intensity (brightness temperature) to be expected, the radiative transfer equation (equation 1) must be solved. The radiative variables in equation 1 depend upon certain physical variables in this part of the spectrum.

To simulate the variation of the independent variables in the radiative transfer equation, we must vary the physical conditions in our simulation, as shown on the right of Table 1. This range of variables presents us with the computational burden of 5 x 5 x 5 x 6 = 750 simulated atmospheres, for each of which computations of upwelling radiation at 10 frequency/polarization combinations must be made.

In these computations, certain simplifying assumptions and approximations have been made. The drop size distribution, from which the ensemble extinction, absorption, scattering, and other radiative properties may be calculated by Mie theory, is based on the Marshall-

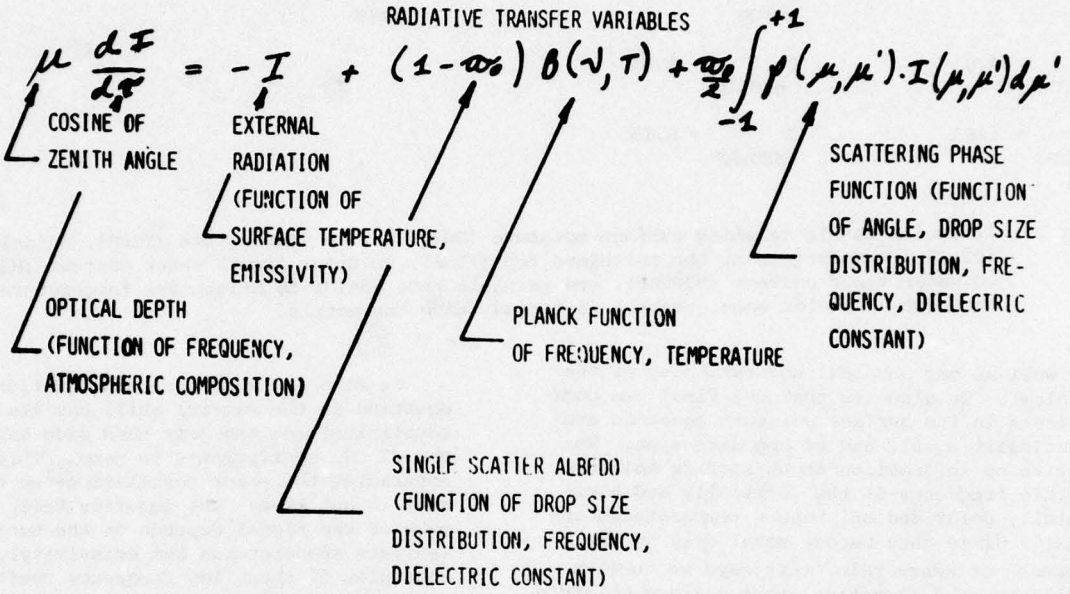

Equation 1. Variables of the radiative transfer equation and their dependence on atmospheric variables.

μ is the cosine of the zenith angle. Fortunately, only the zenith angle of 50^{o} need be considered in this case, since SMMR scans at a constant zenith angle. The optical depth, τ depends on the amount of rain and/or water vapor present; the importance of this dependence changes with frequency. The primary external source of radiation is the earth's surface, whose temperature and emissivity are both variable, the latter depending on water content, and modified by roughness and vegetation cover. As emissivity decreases, the reflection of radiation originating in the overlying atmosphere increases. This atmospheric radiation has two sources. A part arises by Planck emission from the rain cloud, which has some non-zero temperature and emissivity. Additional radiation originates in a scattering process dependent on single-scatter albedo and phase function - both dependent on drop size distribution, frequency, and material composition.

Palmer model; the techniques and numerical values may be found in Savage (1978). The M-P distribution is vertically uniform, and of liquid water species only. The soil moisture simulation, necessary to a simulation of surface emissivity and reflectivity, is based on dielectric constant values given by Burke and Paris (1975), modified by Falcone of AFGL. In an attempt to better match the muffling effect of vegetation, and the reduction of surface reflectivity due to roughness noted by Burke and Paris, we have reduced the Fresnel - calculated reflectivity by one-half. We believe this better approximates the vegetative and roughness effects empirically observed to date.

We have ignored the variations of footprint size with wave length. All SMMR frequencies share a common aperture, and are therefore focused to different resolution element size on the earth's surface. Finally, in using Chandrasekhar's (1960) discrete ordinate method, we have ignored the effect of radiation entering or leaving through the sides.

PREDICTION MATRIX

SM		1.85	-2.23	-1.01	1.30	0.0	0.0	.77	-.88	-.35	.35	T6V
TSFC		5.33	-4.78	-1.52	2.22	0.50	-1.09	0.0	0.0	-1.33	1.22	T6H
DEPTH		-1.13	.87	0.0	0.0	10.0	-6.6	-11.6	7.02	1.82	-.88	T10V
TTOP	=	2.14	-1.66	0.0	0.0	-19.0	12.5	22.1	-13.3	-3.45	1.68	T10H
H2OLIQ		.062	-.051	-.099	.081	.073	.057	-.041	.031	-.0032	-.00017	T18V
H2OVAP		0.0	0.0	-.059	.047	.40	-.29	-.47	0.32	.073	.038	T18H
RAIN		2.28	-2.09	-3.52	3.26	1.08	-1.78	0.0	1.29	-0.38	0.0	T21V

$C_{SM} = 32.8$ $C_{TTOP} = 11.2$ $C_{RAIN} = -30.3$ T21H

$C_{TSFC} = 54.0$ $C_{H2OLIQ} = 1.01$ T37V

$C_{DEPTH} = 146$ $C_{H2OVAP} = 6.15$ T37H

Table 3. Inversion matrix relating surface moisture (SM), surface temperature (TSFC), raincloud depth (DEPTH), temperature at the raincloud top (TTOP), columnar liquid water content (H2OLIQ), columnar vapor content (H2OVAP), and rainfall rate (RAIN) to brightness temperatures. The constant value for each equation is listed below the matrix.

(as well as our physical understanding of the problem). We also see that the final two coefficients in the surface moisture equation are numerically equal, and of opposite sign. We receive no information about surface moisture at this frequency if the vertically and horizontally polarized brightness temperatures are equal. Since they become equal only in the presence of heavy rain, this says we receive little or no information about surface moisture at these higher frequencies when it's raining hard - as we would expect. The 18 GHz channels give no information about surface moisture, whether it's raining or not.

We also see that the rain equation (last equation in the matrix) still has its largest coefficients on the left hand side and one of the 37 GHz coefficients is zero. This seems to contradict the prior correlations we saw, but that is not true. The equation tells us that much of the signal depends on the background (surface temperatures and emissivity); the interplay of these low frequency coefficients (note the + - alternations) is designed to remove this "background noise" and let the higher frequency atmospheric information come through.

PREDICTION IMPROVEMENT WITH MULTIPLE FREQUENCIES

	SM	TSFC	H2OVAP	H2OLIQ	RAIN
SAMPLE STANDARD ERROR	4.2%	7.1K	.14GM/CM^2	.16GM/CM^2	5.4MM/HR
INITIAL CORRELATION COEFFICIENT	-.84 (T6H)	.62 (T10V)	-.34 (T21H)	.95 (T37H)	-.88 (T37V)
INITIAL STANDARD ERROR	2.3%	5.6K	.13GM/CM^2	.050GM/CM^2	2.5MM/HR
MULTIPLE CORRELATION COEFFICIENT	.97	.96	.90	.99	.98
FINAL STANDARD ERROR	.99%	2.0K	.059GM/CM^2	.016GM/CM^2	1.1MM/HR

Table 4. Standard error of the simulation sample (first row), as estimated from the best-correlated single brightness temperature (second and third rows), and as estimated from all SMMR channels (fourth and fifth rows).

RADIATIVE VARIABLES	PHYSICAL VARIABLES
Surface Emissivity, Reflectivity	Soil Moisture (percent) (6%, 9%, 12%, 18%, 21%)
	Surface Temperature (Kelvin) (280K, 285K, 290K, 295K, 300K)
Optical Depth	Raincloud Depth (thousands of feet) 9000, 12000, 15000, 18000, 21000)
Planck Function	Rain Rate (mm/hour) (0.5, 1.0, 2.0, 4.0, 8.0, 16.0)
Single Scatter Albedo, Phase Function	Frequency & Polarization (6.6v, 6.6h, 10.7v, 10.7h, 18.0v, 18.0h, 21.0v, 21.0h, 37.0v, 37.0h)

Table 1. Simulation variables and the values used in computations.

4. SIMULATION RESULTS

The following tables present the results from this simulation effort. Because of the large number of cases (or variables) considered, at the several channels to be considered, we have resorted to the descriptive aspect of multi-variate statistics to convey the numerical results.

In Table 2 we see the correlations between all individual SMMR channels and the physical variables of the simulation sample. This table tells us something about where the information lies in the SMMR spectrum.

	SURFACE MOISTURE (SM)	SURFACE TEMPERATURE (TSFC)	RAINFALL RATE (RAIN)	COLUMNAR LIQUID CONTENT (H20LIQ)	COLUMNAR VAPOR CONTENT H20VAP)
T6V	-.76	.59	-.16	-.17	-.095
T6H	-.84	.47	.10	.10	-.029
T10V	-.72	.62	.058	.017	-.088
T10H	-.67	.42	.55	.53	.034
T18V	-.46	.47	-.55	-.46	-.26
T18H	-.58	.43	.23	.14	-.095
T21V	-.22	.28	-.81	-.90	-.33
T21H	-.41	.36	-.55	-.68	-.34
T37V	-.068	.11	-.88	-.94	-.29
T37H	-.12	-.88	-.95	-.29	

Table 2. Correlations between calculated brightness temperatures and the physical variables of the simulation.

a. For instance, surface moisture is most highly correlated (-.84) with the 6.6 GHz horizontal brightness temperature. The 37 GHz vertical brightness temperature contains least information about surface moisture per se. As may be seen in the 3rd and 4th columns, however, the 37 GHz channels give the most information about atmospheric conditions. A measure of how the information about soil moisture is "contaminated" by the atmosphere is essential to improve one's measurement of surface conditions.

b. Likewise, looking at the 37 GHz correlations with rain rate (-.88) and H20LIQ, the integrated liquid water content (-.94), we must be aware that the signal is significantly affected by surface moisture (-.12), temperature (.12), and by water vapor content (-.29).

c. We see that vapor content (H20VAP) is relatively poorly correlated with any individual channel (though 21 GHz horizontal is best).

d. Surface temperature is also poorly correlated with several low frequency channels; obviously, adding higher frequency channels is not likely to help.

The result of a stepwise multiple regression for several variables is shown in Table 3.

In quickly scanning the inversion matrix, we note the largest coefficients tend to be on the left or center of the matrix. In the top equation, for instance, the low frequencies give the most information about surface moisture; that was, perhaps, to be expected from the individual correlation values we saw earlier

5. SUMMARY

In Table 4 is summarized what can be done with a source of multispectral microwave imagery, such as SMMR.

In the first place, we're talking about automated remote sensing capabilities that don't exist with visible or infrared data.

Secondly, the multispectral nature of the instrument allows us to combine several remote sensing algorithms, with information about both surface and atmospheric conditions, in a single technique. If, for each parameter of interest, we used only the single measurement with the greatest individual correlation, we could estimate the parameters to the standard errors shown in the second line (e.g.,):

SM	TSFC	H2OVAP	H2OLIQ	RAIN
2.3%	5.6K	.13	.050	2.5

If we combine information from the several channels available, we can do better.

(1) The best final standard error is in the atmospheric liquid parameters, the integrated liquid water content and rain rate.

(2) The integrated vapor content has the lowest multiple correlation coefficient, i.e., least reduction of final standard error relative to that of the sample. On the other hand, this parameter shows the most improvement as a result of having multispectral data. A single channel of information (e.g., 21 GHz horizontal) does relatively little in the reduction of standard error.

(3) The estimate of surface parameters shows a satisfying improvement, especially under the difficult atmospheric conditions simulated.

BIBLIOGRAPHY

Allison, L. J., et al, 1974: Tropical cyclone rainfall as measured by the Nimbus-5 electrically scanned microwave radiometer. Bull. Amer. Meteor. Soc., 55, 1074-1089.

Burke, W. J. and J. F. Paris, 1975: A radiative transfer model for microwave emission from bare agricultural soils. NASA TM X-58166, NASA Johnson S.F.C., Houston, TX.

Chandrasekhar, S., 1960: Radiative Transfer. New York, Dover Publications, 393 pp.

Gloersen, P., et al, 1974: Microwave maps of the polar ice of the earth. Bull. Amer. Meteor. Soc., 55, 1442-1448, 1974.

Hall, C. D., R. Davies, and J. A. Weinman, 1978: The Distribution of Precipitation Derived from Nimbus 6 Data. Dept. of Meteorology, University of Wisc., Madison, Wisc., 25 pp.

Rao, M.S.V., et al, 1976: Satellite-derived global oceanic rainfall atlas (1973 and 1974). NASA SP-410.

Savage, R.C. and J. A. Weinman, 1975: Preliminary calculations of the upwelling radiance from rainclouds at 37.0 and 19.35 GHz. Bull. Amer. Meteor. Soc., 56, 1272-1274.

Savage, R.C., 1978: The radiative properties of hydrometeors at microwave frequencies. J. Appl. Meteor., 17, 904-911

Wilheit, T. T., et al, 1976: Meteorological Interpretations of the images from the Nimbus-5 electrically scanned microwave radiometer. J. Appl. Meteor., 15, 166-172.

TESTING OF SATELLITE UPLINKED REMOTE SURFACE WEATHER STATIONS IN THE SIERRA NEVADA

By
Donald Rottner

Bureau of Reclamation
Atmospheric Water Resources Management
Division of Research
Denver, Colorado

and

Gerald R. Price

Electronic Techniques, Inc.
Fort Collins, Colorado

1. INTRODUCTION

The Automatic Environmental Surface Observation Platforms (AESOP's) were first conceived when it became apparent that there was generally a dearth of surface weather stations at most Project Skywater* experiment sites. The stations were meant to supplement the normal surface National Weather Service and Federal Aviation Administration network in areas where the density of manned stations is very low. It was intended that they emulate manned stations in every way possible, i.e., on the hour real-time reporting, measurements of the same parameters, and similar methods of taking surface weather observations.

Originally the AESOP's were designed for remote summertime application in the High Plains Cooperative Program (HIPLEX), but with the advent of the Sierra Cooperative Pilot Project (SCPP) it was decided to test them in the sometimes severe winter conditions of the Sierra. Two manned sites were chosen for comparison of their data with AESOP's data. These two sites were the National Weather Service surface station at Blue Canyon, California and the Forest Service Central Sierra Snow Laboratory at Soda Springs, California.

This paper concerns itself with the Sierra application and test of the AESOP's, their general description, their data path through the satellite, the final computer mix of the data in the surface weather circuits, and their performance during the Sierra test.

---

* Project Skywater is the Bureau of Reclamation's precipitation management research program designed to explore, develop, and determine the feasibility of applying the technology of weather modification to meet the Nation's increasing demand for clean water. The project is concerned with developing socially acceptable technologies for enhancing snowfall from winter orographic situations and rainfall from growing season showers.

2. DESCRIPTION OF THE AESOP

The complete AESOP is made up of the Convertible Data Collection Platform (CDCP), a transmitting antenna, data sensors, power source, and interface electronics. See figure 1.

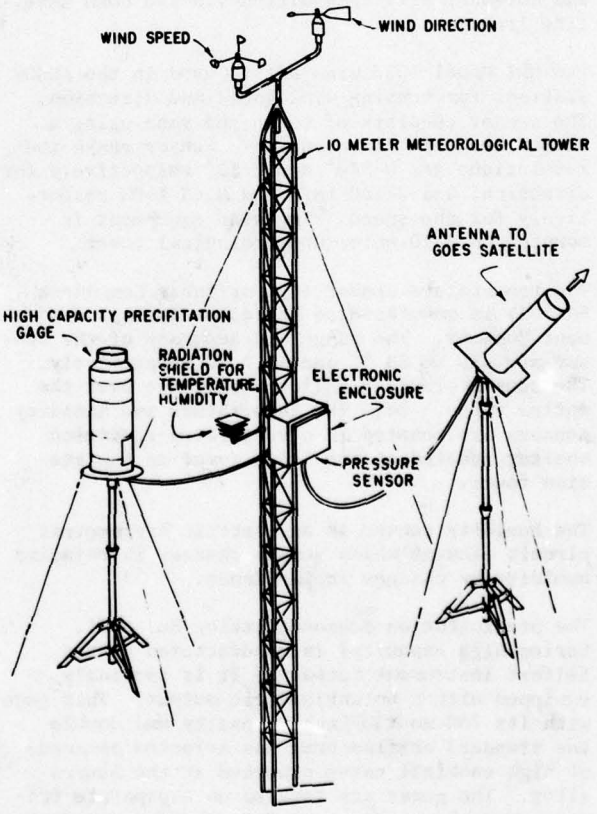

Figure 1. Automatic Environmental Surface Observation Platform (AESOP) with all components shown.

The CDCP is controlled by an internal microprocessor. All control parameters are entered into the microprocessor by means of a test set at the time a station is activated. The CDCP unit, power supplies, and sensor interface electronics are housed in a weatherproof enclosure mounted on the meteorological tower above the expected maximum snowpack. The CDCP has 256 locations of 4-bit Random Access Memory (RAM), of which 207 are dedicated to data storage. The information stored in RAM is automatically transmitted each hour to the Geostationary Operational Environmental Satellite (GOES) at 135° W. Three complete sets of hourly observations are held in memory. As new data are acquired, the oldest set of data is automatically removed from memory. The entire memory contents are transmitted during each transmission event. Therefore, three sets of hourly observations, present and past 2 hours, are transmitted each hour.

Power for AESOP stations is supplied from commercial 120 VAC with standby battery backup. For remote applications, an optional solar panel is available to provide an independent power source.

3. AESOP SENSORS

Hourly observations of wind speed, wind direction, temperature, humidity, pressure, and precipitation are automatically taken, temporarily stored, and automatically transmitted via the GOES satellite link.

The MRI Model 1022 wind set is used in the AESOP stations for sensing wind speed and direction. The sensor consists of a cup and vane using a common crossarm for mounting. Sensor range and resolutions are 0-540° and 2.11° respectively for direction; and 0-160 KmPH and 0.63 KmPH respectively for the speed. The wind equipment is mounted on a 10-meter meteorological tower.

The temperature sensor (Thermilinear Component #44203) is manufactured by Yellow Springs Instrument Company. The range and accuracy of the sensor are -30 to 50 °C and ±0.2 °C respectively. The sensor provides a linear response over the entire range. Both the temperature and humidity sensors are mounted in a ventilated radiation shelter located at the 7.5-m level on the station tower.

The humidity sensor is an electric hygrometric circuit element which senses changes in relative humidity by changes in impedance.

The precipitation sensor (Catalog No. 6071, Series high capacity) is manufactured by the Belfort Instrument Company. It is specially equipped with a potentiometric output. This gage with its 750-mm (30-inch) capacity and double the standard orifice area was selected because of high snowfall rates expected at the Sierra sites. The gages are located on a separate tripod stand placed 5 meters from the tower and elevated to a height of 4 meters above ground at the Blue Canyon site and 6 meters above ground at the Snow Lab site. The gages also have a chart recording capability which provides a direct comparison with telemetered data. Resolution of the telemetered precipitation data was limited to approximately 3.3 mm due to the 8-bit input to the CDCP.

The pressure sensor (Model 2014) is manufactured by H. E. Sostman Company. Its range and accuracy are up to 23 363 pascals (6.9 in Hg) and 0.12 percent of range respectively. However, in order to obtain high resolution and yet maintain an adequate range, the AESOP pressure sensors are presently set for 3386 pascals (1 in Hg) range which provides digital resolution to approximately 13 pascals (0.0039 in Hg). The pressure sensor is mounted in a weatherproof housing directly below the main electronics enclosure.

4. INTERFACE AND INTEGRATING ELECTRONICS

The electronic interface circuitry provides excitation to sensors, buffering to protect CDCP inputs and integrating circuits. Averaging intervals and formats conform to standards set forth in both the Federal Meteorological Handbook of Surface Observations and the design manual for the National Oceanic and Atmospheric Administration's Remote Automatic Meteorological Observation Station (RAMOS). Buffer amplifiers are provided for each input line of the CDCP to afford maximum protection from static potential buildup or nearby lightning strikes and to provide input range adjustment.

5. DATA PATH

As previously stated, the data are transmitted from the AESOP's each hour up to the GOES satellite over the equator at 135° W. The satellite then relays the data to the direct readout ground station at Wallops Island, Virginia. The data are then relayed to the World Weather Building, Camp Springs, Maryland, where the first data sort is accomplished. Next, the data are relayed to the National Meteorological Center, Suiteland, Maryland, where the data are merged with other weather data and then sent to the Bureau of Reclamation's Engineering and Research Center, Denver, Colorado. Figure 2 summarizes the AESOP data path.

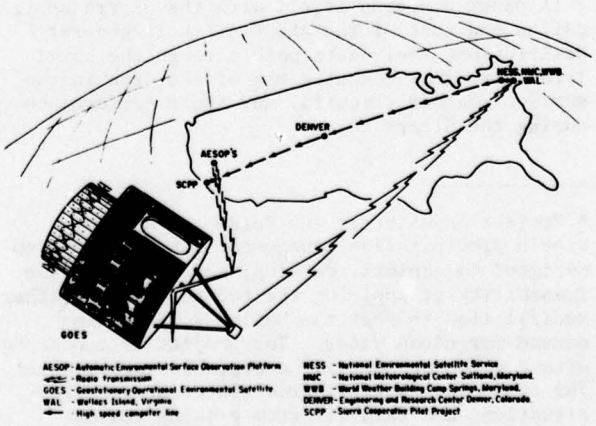

Figure 2. AESOP Data Path.

Once the data are archived in the Engineering and Research Center's computer, they are immediately available for operational use to all users of Project Skywater's *Environmental Data Network by simple timeshare access. Otherwise the data may be acquired for seasonal or long periods of record on media such as microfiche, magnetic tape, etc., by letter request from the Project Skywater Data Base Manager.

6. CALIBRATION

A detailed shop calibration is accomplished for all sensors to determine each mathematical relationship of a particular parameter as a function of voltage. The pressure sensor, however, requires additional field calibration because its range must be reset for each different site. This field calibration is accomplished by determining a climatological midscale pressure for the site and then measuring the ambient pressure. The sensor's range is approximately 3386 pascals (1 in Hg). Given the current ambient pressure and the desired midscale pressure the sensor range can be set. Next, several other ambient pressure points and their associated voltages are measured and a least squares fit is applied to the measured raw pressure voltages to provide a true raw pressure. A one-point field installation calibration is accomplished for the remaining sensors by measuring the parameter and its corresponding voltage outputs.

7. PROCESSING SOFTWARE

All of the sensor calibration equations reside in the processing software package at the Bureau of Reclamations's Engineering and Research Center (ERC) in Denver, Colorado. The data received and stored in the ERC computer are in raw hexadecimal form. When the data are accessed by the user, the date, hour and geographical group of hourly weather stations desired must be specified. The processing software then compares the date, time and location of the group of surface weather stations asked for with the AESOP data base and decides whether AESOP data are available for that time and geographical area. If the AESOP data are available the proper set of calibration equations (according to each different site) are used by the software to reduce the raw data to engineering units, the data are converted to the Aviation Weather Report format, and the hourly AESOP observation is appended to the hourly weather group of stations asked for by the user. Therefore, the software automatically mixes the AESOP data with the conventional manned surface station data whenever data are available whether the AESOP station is in the HIPLEX program in Montana during the summer or in the SCPP program in California during the winter. In this way, the user need not know the past AESOP history of application. The user may also access the AESOP data by itself, a day at a time, but this would require knowledge of the AESOP application history.

8. COMPARISON OF THE DATA

A comparison of manned observations versus AESOP's observations showed the following:

(1) Temperatures consistently compared within ±0.6 °C.

(2) Dewpoint temperatures compared within ±3 °C in moist or precipitating situations, but in the dryer situations the sensor was unacceptable.

(3) Wind speed and direction comparisons were consistently in reasonable agreement. There was, as would be expected, better correlation in the higher wind situations.

(4) Altimeter settings (pressure) compared within ±0.01 in Hg.

(5) Precipitation amounts from the AESOP data link were compared with the chart record from the AESOP gage. Figure 3 shows the very good agreement obtained from this

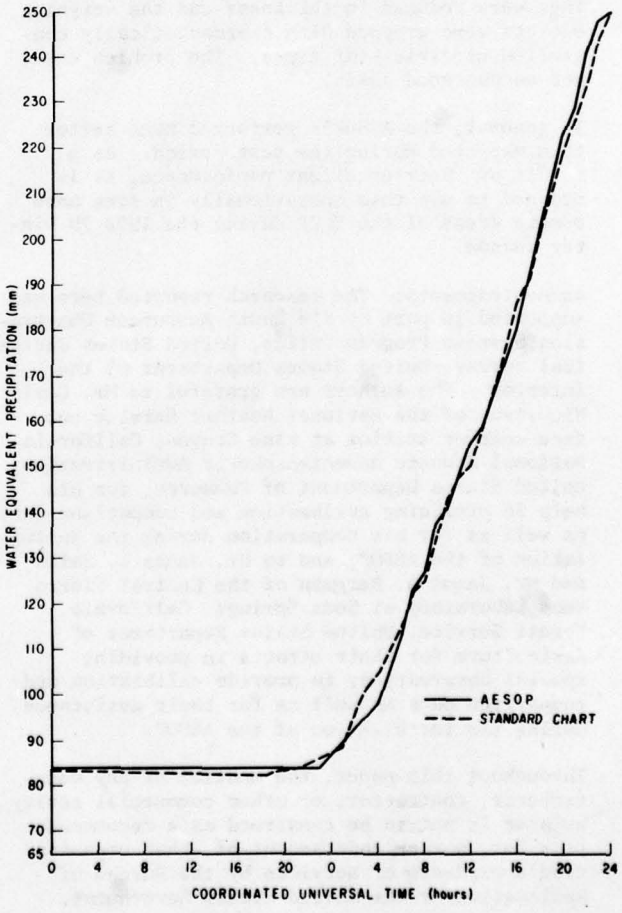

Figure 3. Comparison of AESOP reported precipitation versus standard chart precipitation.

* Project Skywater Environmental Data Network is both a real-time and post-analysis weather data base maintained by the Bureau of Reclamation in support of Project Skywater.

comparison. Note that the maximum of 8-bit resolution of the data collection platform forces a 3.3-mm (0.13-in) minimum resolution of precipitation increments from the AESOP. This would be a more serious constraint in smaller precipitation events.

9. CONCLUSION

The AESOP's have shown their reliability and ability to collect quality surface weather data in the Sierra wintertime environment. In the entire test period of 3-1/2 months during the winter of 1977-78 there were no electronic failures detected from either of the two AESOP's being tested in the Sierras. As is common with relative humidity sensors, the device used gave inordinately low readings during dry periods and seems to slowly degrade in an outdoor environment. Future tests may employ a different type of relative humidity sensor, manufactured by Vaisala. The precipitation gage had a bridging problem in some of the very-high-intensity precipitation events. This bridging could have been caused by too thick an evaporation-inhibiting oil coating on top of the ethylene glycol/methanol solution or simply because the snow rate was too high to be absorbed by the winterizing solution. Two corrective actions were taken: the oil coatings were reduced in thickness and the weighing buckets were wrapped with thermostatically controlled electric heat tapes. The problem was not encountered again.

In general, the AESOP's performed much better than expected during the test period. As a result of their excellent performance, it is planned to use them operationally in some more remote areas of the SCPP during the 1978-79 winter season.

Acknowledgments: The research reported here was supported in part by the Earth Resources Observation Systems Program Office, United States Geological Survey, United States Department of the Interior. The authors are grateful to Mr. Carl Wickstrom of the National Weather Service surface weather station at Blue Canyon, California. National Oceanic and Atmospheric Administration, United States Department of Commerce, for his help in providing calibration and comparison data as well as for his cooperation during the installation of the AESOP; and to Dr. James L. Smith and Mr. James A. Bergman of the Central Sierra Snow Laboratory at Soda Springs, California, Forest Service, United States Department of Agriculture for their efforts in providing special observations to provide calibration and comparison data as well as for their assistance during the installation of the AESOP.

Throughout this paper, the mention of any manufacturer, contractor, or other commercial entity by name is not to be construed as a recommendation for, nor an endorsement of, that organization's products or services by the Bureau of Reclamation or the United States Government.

References:

Labarge Incorporated, 1976: *Instruction Manual for the Convertible Data Collection Platform (CDCP) and Related Equipment.* Labarge Incorporated, Tulsa, Oklahoma.

Price, G. R, and V. R. Scheetz, 1977: *Automatic Environmental Surface Observation Platform (AESOP) for the High Plains Experiment (HIPLEX).* Final Report to Bureau of Reclamation, Electronic Techniques Incorporated, Fort Collins, Colorado.

Reynolds, R. R. and J. Lovkay, Jr., 1972: *Design Development of the Remote Automatic Meteorological Observation Station (RAMOS).* Equipment Development Laboratory, National Weather Service, National Oceanic and Atmospheric Administration, United States Department of Commerce, Washington, D.C.

United States Departments of Commerce, Defense and Transportation, 1975: *Federal Meteorological Handbook Number 1, Surface Observations.* United States Government Printing Office, Washington, D.C.

THE SWITCH TO A CLIMATIC PERSPECTIVE

Banquet address (abridged), 1978 Technical Exchange Conference

Air Weather Service

F. Kenneth Hare

Director, Institute for Environmental Studies, University of Toronto
Toronto, Canada

Mr. Chairman, Ladies and Gentlemen,

An invitation to visit Colorado is always welcome, even when one has to pay one's own fare as well as give a banquet speech! But I owe the U.S. so much for the support it gave to my early research that I never refuse such an invitation. Moreover I saw the names of many old friends on the program, and wanted to see them again.

My contacts with the Air Weather Service began twenty-five years ago, when the Arctic Meteorology Research Group moved from UCLA to McGill in Montreal. AWS began sending a series of excellent students up for training, especially after we started doing daily analysis at what were then the very high levels of 200, 100 and 25 mb. Our closest relations were with GRD and AFCRL -- and I hope that there is someone besides me who is old enough to remember what those acronyms mean. We owed a lot, especially, to Phil Frank, Tom Keegan and Wayne Hering, who at one time or another were our contract monitors -- and to the auditors, who were notably more understanding with us than with U.S. universities.

At the moment my waking movements -- and sometimes my dreams as well, even nightmares -- are filled with plans for the upcoming World Climatic Conference (WCC), whose chairman is to be another old GRD man -- Bob White. He and I, Jim Dooge and Juri Sedunov (of the Irish Republic and the Soviet Union) are the Bureau of this Conference, due February 12-23 1979 in Geneva, with WMO the main host. Will Kellogg of NCAR has also played a key rôle, as adviser to the Secretary-General for the World Climate Program. All the stops are out for this Conference, which marks WMO's entry on to the stage of world economic affairs. The organization's smart headquarters, on Rue Giusseppe-Motta have visibility moved nearer to the Palais des Nations since the Conference idea was launched.

Beyond the Conference lies a broader but less concrete prospect -- that of a World Climate Program (WCP), already launched by the Executive Committee, and now to be fleshed-out by the WMO Congress in April, after it gets the plan of action from the WCC. This Program has three main components: a new thrust towards research into climate variability and change; a better use of climatic data and services in support of social and economic objectives; and a study of climatic impact assessment. As with GARP, WMO will have ICSU as a partner in the research phase, and probably in the impact area too. These two activities -- WCC and WCP -- are the big news of the moment internationally. And, of course, the U.S. Congress has already legislated a U.S. climate program in support of national and world objectives. So has Canada, though in a less glamorous way. Several other countries are heading in the same direction.

Most of the people invited to the Conference will be, from our viewpoint, laymen. Three-quarters will be drawn from such fields as economics, forestry, agriculture, fisheries, health, marine mineral resources and even remoter places. Only a quarter will be atmospheric scientists. Attendance of invited experts will be about 100, though 300 more will be invited to listen to the background papers in the first week. There will be twenty-five of these papers, again written mostly by non-meteorologists. I have convened the group of authors, with the authoritative help of Will Kellogg and Pat Meade (of the United Kingdom). They have been written by experts from fourteen countries, including India, U.S., U.K., Canada, Sweden, the U.S.S.R., the People's Republic of China, Japan, Nigeria, Poland, Kenya, Argentina, Switzerland and the Federal Republic of Germany. The message comes through loud, clear and unanimous: climate has begun to matter greatly to mankind, and it is about time mankind did something about it. And that means us.

Of course, as a climatologist I agree, and am delighted to see the profession joining a club to which a few choice spirits like Helmut Landsberg have always belonged. I am especially glad to see among the writers for the Conference familiar meteorological names like Bert Bolin, Larry Gates, John Mason, Lester Machta, Ted Munn, Jimmy McQuigg, Yevgeny Fedorov and Ju.P. Izrael. But how many of you have ever heard of Ralph D'Arge? Or Wolf Weihe? Or Julius Oguntoyinbo? Or Richard Odingo? Or even of Nobel prizewinning

economist Ken Arrow, who used to be in this service? These men are as distinguished in their fields, and in their countries, as the meteorologists who have written. So are M.S. Swaminathan, and T.F. Gaskell, and H. Fukui, and F. Mattei. And all these unfamiliar names have something vital to say about climate as a factor in our lives.

What is happening is that the world has come alive to climatic impact -- and as a profession we have risen to the challenge, or to the bait, according to the way we see ourselves. The nineteen-seventies have served up a choice but indigestible diet of floods, droughts, cold, heat and damaging winds on a scale that has hurt millions, killed thousands, wrecked the economies of some young, independent nations, and awakened the media. They have also started the meteorologist himself thinking again about problems that he has constantly underestimated: what is it that determines the endlessly variable yet basically stable climate of this planet? What prompts that stability to shift to a new equilibrium? What are the limits of predictability? You all know the names of people that have attempted answers -- Ed Lorenz, Chuck Leith, G.D. Robinson, Hermann Flohn, Reid Bryson, John Kutzbach, Bill Sellers, Garth Paltridge, and a small army of others. They won't mind me saying that the job is only just begun.

But the biggest parts of this shift of perspective lie outside the traditional scope of our craft. There are two new approaches that are critical to us.

First is the recognition that climate is not an ensemble of atmospheric statistics, but an interactive system involving atmosphere, ocean, soil, biota and, increasingly, people. The carbon dioxide problem (in my student days a minor irrelevancy in the way of good, clean physics) has become the carbon cycle. Not only does the anthropogenic build-up of carbon dioxide threaten a warming of the atmosphere, it has repercussions throughout the cycle. Hence biologists have as much of a rôle to play as we do, or more, as do oceanographers; and names like Keeling, Woodwell, Revelle, Munk and Baumgartner are as important as Callendar, Plass, Machta and Kellogg. The high priest of this new approach to the climatic problem has been Bert Bolin who, after all, occupies Rossby's old niche.

The second approach is towards the organized study of climatic impact -- how, for example, the Sahelian drought affected millions in Africa, or the cold of 1976-77 affected natural gas supply in the U.S. This problem makes a meeting between meteorologists and social scientists unavoidable. And it is close to being unprecedented. The CIAP program provided a model, and involved such economists as Arrow, Raiffa and D'Arge in impact analysis. An important lead has come from the International Institute for Applied Systems Analysis at Laxenburg. The energy scenario project there, led by Wolf Haefele, has involved attention to atmospheric controls. Jill Williams, a Ph.D. graduate of the University of Colorado, and now back at NCAR, has been the key member of this team. Other leads have been given by a converted GARP official, Rolando Garcia, who is lucky enough to work with Walt Roberts, and by Mickey Glantz and his friends at NCAR. But again I'm sure that they would say that they've only just begun.

In short -- the climatic perspective has been forced on us by events, and by the interest of others. But we've risen to it, and have begun to associate with all sorts of strange bedfellows. I've name-dropped tonight, quite shamelessly. I know all the people I've named. So does Bob White, and so will Academician Yevgeny Fedorov; and so will all of us, as the world climate program unfolds. I am incurably interdisciplinary. Harlan Cleveland, a recent convert to our science, quotes two failures of interdisciplinarity. One is that in a hospital only the patients are general practitioners. The other is that in an interdisciplinary course, the professors talk about their specialisms, and only the students have to be interdisciplinary. If we as meteorologists are to make anything out of the climatic system, or of climatic impact, we'll have to avoid the trap. We'll have to learn to talk to biologists, and economists, and politicians, and managers, and ordinary people, as we haven't often done in the past.

And so Mr. Chairman, I'm very optimistic for the future. Every science goes through phases of growth, and phases of consolidation, even of stagnation. What gets us going on a new great leap forward is the infusion of new ideas. I predict -- and that's a loaded word for this audience -- that we have arrived at just such a take-off point. Rubbing shoulders with those biologists, and economists, and politicians, and managers, and ordinary people is going to be good for us -- and, I hope, for them. It is going to transform the curriculum in the universities, for example. Remember when atmospheric chemistry was a luxury we couldn't affort? Then along came air pollution, and the SST and spraycan scares, and we discovered what we should have known all along -- that atmospheric chemists are as useful as physicists and mathematicians. But that was easy. After all, learning to live with chemists isn't such a big jump. Now we've got to live with ecologists and economists, and even -- perish the thought -- with geographers. I predict that we'll survive and prosper. Maybe we'll do to them what the Chinese did to the Manchu emperors. And we'll never be the same again!

ATMOSPHERIC PROPAGATION MODELLING AND MEASUREMENT

Robert A. McClatchey

Air Force Geophysics Laboratory

Hanscom Air Force Base, Massachusetts

ABSTRACT

The AFGL Atmospheric Transmission codes (LOWTRAN and HITRAN) will be discussed with particular emphasis on their validity in the real world. The applicability of these models for horizontal and slant paths under various meteorological conditions will be discussed. This discussion will include a review of recent laboratory and field measurements which provide evidence for model validation and model improvement. The future direction of the AFGL transmission modelling efforts will be described.

1. INTRODUCTION

The calculation of the propagation characteristics of the atmosphere for visible and infrared radiation requires us to know the distributions of the atmospheric constituents and the accompanying meteorological parameters along the atmospheric path in question. Due to the complexity of molecular absorption and the requirements of different kinds of military systems, it is most appropriate to deal with this problem by two different techniques depending on spectral resolution: A high spectral resolution (or HITRAN) computation technique; and a low spectral resolution (or LOWTRAN) computation technique. The HITRAN technique involves monochromatic or degraded monochromatic calculations and is of particular pertinence to the problem of laser transmission in the atmosphere. It is also recommended that the HITRAN technique be applied to any problems requiring the computation of spectra at resolutions less than 20 cm^{-1}. There are also some problems requiring low spectral resolution, but high absolute accuracy where the HITRAN technique may be the most appropriate. The LOWTRAN code is strictly applicable to a special resolution of 20 cm^{-1} or greater. Certain approximations are inherent in the code and should be considered by the user prior to application. These codes will be described in some detail.

In addition to molecular absorption, our modelling effort must also take into account three other processes. As indicated in Equations 1a-1c, we must consider molecular scattering, σ_m, aerosol absorption, k_a, and aerosol scattering, σ_a, as well as molcular absorption, k_m.

$$\sigma = \sigma_m + \sigma_a \qquad (1a)$$

$$k = k_m + k_a \qquad (1b)$$

$$\gamma = \sigma + k \qquad (1c)$$

Although molecular absorption provides the driving force behind establishment of both the HITRAN and LOWTRAN atmospheric transmission models, the dependence of the total extinction on aerosol effects is currently the most difficult and least resolved problem area. The reason for this is related to the difficulty of measuring aerosol (particulate) effects and their great variability in the atmosphere, both in time and space. In the case of molecular absorption and scattering, the distributions of molecules and either rather well known (e.g. CO_2) or can be readily obtained from standard meteorological measurements (such as relative humidity in the case of water vapor).

Let us consider the rationale for developing such atmospheric propagation models. There are several applications which come immediately to mind: 1) A knowledge of the high resolution spectral properties of the natural atmosphere is required as a background against which the existence and abundance of trace pollutant gases can be identified. This requirement is very much of interest to the atmospheric pollution community, but is also related to a variety of specific military interests; 2) A very accurate computational capability is a necessity in the remote sensing of meteorological variables and other atmospheric or foreign constituents; 3) We want to aid in the design and predict the performance of various kinds of surveillance and weapon systems.

Table 1 is a list of atmospheric constituents, together with a representative atmospheric abundance. It is important to realize that although nitrogen and oxygen are the most abundant molecules in the atmosphere, their effect on atmospheric propagation is small due to their lack of a permanent dipole moment. The atmospheric gases of main interest here are carbon dioxide, water vapor, ozone, methane, carbon monoxide and nitrous oxide. Although with the exception of water vapor and ozone, a single mixing ratio has been listed for each molecular constituent, there is substantial evidence for variability for all species except nitrogen and oxygen. However, reasonable results can be expected in the troposphere based on the constant mixing ratios indicated in Table 1. In addition to the species listed in Table 1, recent measurements have revealed

the presence of a number of additional molecular species, some apparently of natural origin and some presumably introduced by man. As more information becomes known about such species, work will continue to introduce their spectral parameters into the HITRAN data base.

TABLE 1

ATMOSPHERIC CONSTITUENTS

Constituent	Fraction by Volume
Nitrogen (N_2)	0.78
Oxygen (O_2)	0.21
Argon (A)	0.0093
Carbon Dioxide (CO_2)	0.00033
Methane (CH_4)	1.6×10^{-6}
Nitrous Oxide (N_2O)	3.5×10^{-7}
Carbon Monoxide (CO)	7.5×10^{-8}
Ozone (O_3)	variable (10^{-8})
He, Ne, Kr	$< 10^{-4}$
Water Vapor	variable (< .03)
Aerosols	
Dust	variable
Salt	
Liquid Water	

2. THE HITRAN TRANSMISSION CODES

The HITRAN transmission codes are designed to replicate measured spectra of the kind shown in Figure 1. The spectral resolution of these measurements is about 0.5 cm^{-1} and they were taken from a balloon platform viewing the sun from the indicated altitudes and at the indicated zenith angles. Absorption features of water vapor, carbon dioxide, ozone and methane are clearly visible in the figure.

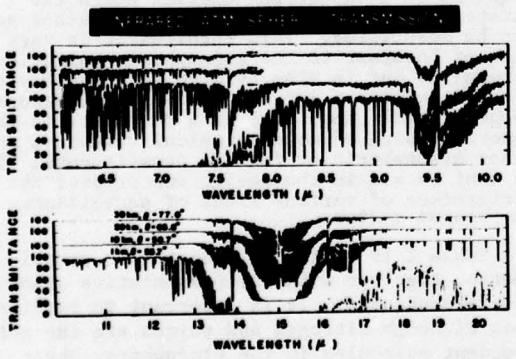

Figure 1. High Resolution Measurements of Solar Spectra made from Indicated Altitudes and Observing the Sun at the Indicated Zenith Angles.

The HITRAN computer codes are a family of special purpose codes, all utilizing a data base of molecular spectroscopic parameters known as the AFGL Atmospheric Absorption Line Parameters Compilation (McClatchey, et al, 1973). The seven molecules for which parameters are contained on this data compilation include water vapor, carbon dioxide, ozone, nitrous oxide, carbon monoxide, methane and oxygen. Calculations proceed from the description of an atmospheric model, the input spectral data from the compilation and the application of Beer's law to compute a network of monochromatic transmittances. A line shape such as the Lorentz shape indicated in Figure 2 is assumed to apply to each line of the Compilation and all line wings contributing to the absorption coefficient at a given frequency are summed as indicated in Equation 2. An integration along the atmospheric path is then performed as indicated in Equation 3 and an instrument function convolution performed as in Equation 4. For atmospheric paths at high altitudes, the Lorentz function will not be valid and Voigt or Doppler line shapes must be used. Even at lower altitudes departures from the Lorentz shape have been observed. We have taken account of these discrepancies in our propagation models by addition of molecular absorption continua in atmospheric "window" regions containing relatively few absorption lines.

$$\tau(\nu) = \exp -\left[\sum_j \sum_i k_{ji}(\nu) m_j\right] \qquad (2)$$

$$\tau(\nu) = \exp - \sum_j \left[\int \left(\sum_i k_{ji}(\nu) dm_j \right)\right] \qquad (3)$$

$$\bar{\tau}(\nu) = \frac{\int \tau(\nu) g(\nu - \nu_o) d\nu}{\int g(\nu - \nu_o) d\nu} \qquad (4)$$

The AFGL data Compilation continues to be updated and modified. Recently, a Trace Gas Tape has been made available to users (see Rothman, et al, 1978). This tape contains data on four additional trace gases (NH_3, NO, NO_2 and SO_2) not contained on the original AFGL Compilation. On the original data tape recent modifications have been made to the methane data and previously omitted data on water vapor in the visible and near infrared have now been added. A complete review of all CO_2 bands has led to some significant modifications in addition. All water vapor half-widths have been revised and additional oxygen bands at visible wavelengths have been added. The AFGL Compilation now contains parameters on more than 139,000 absorption lines in the spectral region from 0.3 to 17,880 cm^{-1}.

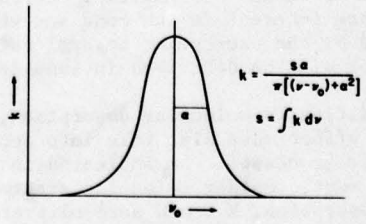

Figure 2. Lorentz Line Shape Used in Atmospheric Calculations from the Surface to 30 km.

The validation of the HITRAN models against careful measurements both in the laboratory and in the field constitutes an important continuing element of our research. Figure 3 is an example of such a comparison made with the laboratory measurements of Gryvnak, et al (1976) at a spectral resolution of 0.5 cm^{-1} in the 15 μm CO_2 band. Figure 4 shows a similar measurement compared with HITRAN calculations at lower spectral resolution (2.5 cm^{-1}). In this case a systematic discrepancy can be noted, particularly in the stronger parts of the band. This discrepancy is probably due to departures of line wings from the Lorentz shape described above. Figure 5 compares a calculation with a portion of the 1-km spectrum shown in Fig. 1. Most lines can be seen to agree favorably, although there are some discrepancies, particularly in line intensities. Figure 6 compares a calculation with measurements made by Dowling, et al (1977) in the 4 micrometer region. The results, aside from a small continuum shift are in excellent agreement. Many other workers are now making measurements and checking their results against the AFGL data compilation after performing HITRAN transmission calculations. Another example is shown in Figure 7 which is an example of a solar spectrum compared with a HITRAN calculation (see Nordstrom, et al, 1976). Aside from a continuum discrepancy, we note a line near 1208 cm^{-1} which is absent in the upper computed spectrum.

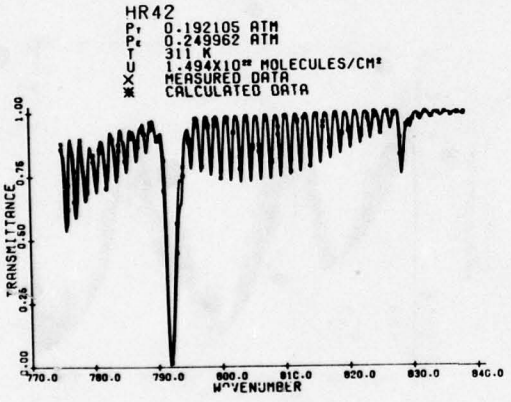

Figure 3. Comparison of High Resolution Laboratory Measurements of Gryvnak, et al (1976) and Calculations in the 15 μm Region. ($\Delta\nu$ = 0.5 cm^{-1})

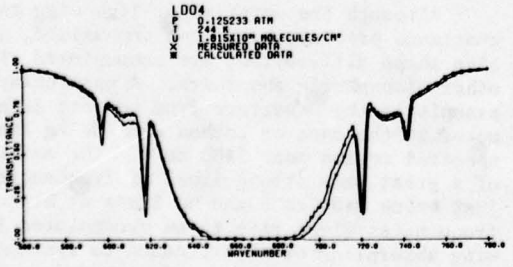

Figure 4. Comparison of Measurements of Gryvnak, et al (1976) and Calculations in the 15 μm Region. ($\Delta\nu$ = 2.5 cm^{-1}).

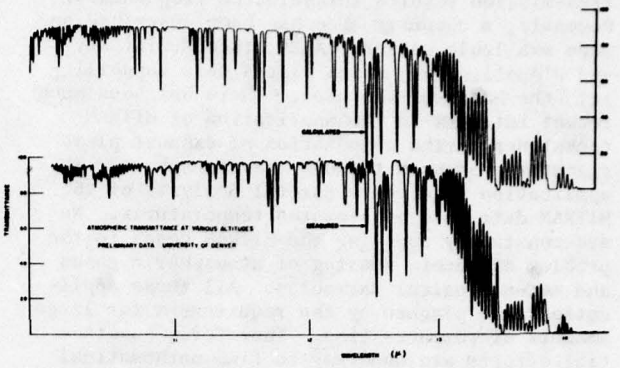

Figure 5. Comparison of University of Denver (Murcray) Measurements and HITRAN Calculation. Height of Observation = 1 km. Solar Zenith Angle = 55.7°.

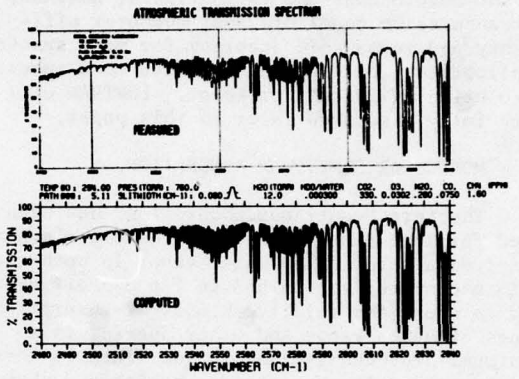

Figure 6. Comparison of NRL (Dowling, et al, 1977) Measurements and HITRAN Calculations.

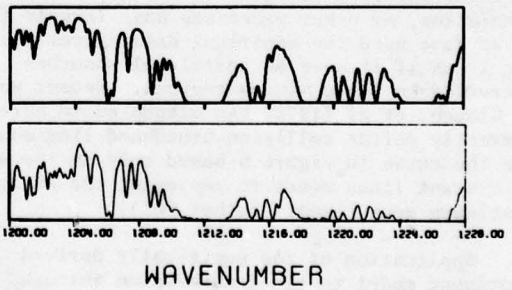

Figure 7. Comparison of High Spectral Resolution (0.125 cm^{-1}) Measured (lower curve) Solar Spectrum with Calculated (upper curve) Spectrum (from Nordstrom, et al, 1976).

The applications of HITRAN are numerous. The ability to confidently generate a high resolution synthetic spectrum is of great value in establishing the best frequencies for the operation of any kind of high resolution system. It is of particular value in generating laser

transmission results for selected frequencies. Recently, a computer code has been described and made available called, LASER, (see McClatchey and D'Agati, 1978) which places this capability into the hands of the user. There has been much recent interest in the application of HITRAN techniques to the computation of exhaust plume signatures as seen through the atmosphere. This application requires a careful analysis of the HITRAN data base at elevated temperatures. We are constantly applying the HITRAN codes to the problem of remote sensing of atmospheric gases and meteorological variables. All these applications are plagued by the requirement for large amounts of computer time. Therefore, substantial efforts are underway to find mathematical procedures to reduce this burden without substantial compromise in the resulting calculations. An example of such an effort is contained in the new HITRAN development known as FASCODE (see Smith, et al, 1978). A final application of the HITRAN calculation technique is the development and validation of LOWTRAN, a transmission model of great computer efficiency and reasonable accuracy for many systems applications, but which is limited to a spectral resolution of 20 cm^{-1} or lower. LOWTRAN will be more fully discussed later in this paper.

3. MOLECULAR CONTINUUM ABSORPTION

The term "continuum absorption" has been used for some time to describe the experimentally observed absorption by water vapor in both the 8-13 micrometer region and in the 3-5 micrometer region where the relative number of absorption lines of water vapor and other species is a minimum. Between the absorption lines in these regions there is a continuous background absorption level not accounted for by the wings of the local lines. An example of the experimental continuum measurements in the 8-13 micrometer region is given in Figure 8, where a strong temperature dependence can also be noted. Previous efforts to understand this absorption as resulting from distant line wings, water dimer absorption, or other processes have largely failed, so we have used the empirical data directly, adding it as if it were an additional absorber operating in these window regions. Recent work by Clough, et al (1978) has attempted to more correctly define collision-broadened line shapes and the curve in Figure 9 based only on the wings of distant lines seems to represent the window continuum measurements rather well.

Application of the empirically derived continuum model to the transmission through several standard atmospheres at a frequently used laser line near 10.6 micrometers and also at 4 micrometers gives the curves shown in Figure 10. Except for very dry atmospheres, the 4 micrometer continuum absorption is seen to be much smaller than the continuum in the 10 micrometer region. Another example of continuum or line wing difficulty can be observed from a study of Figures 11 and 12. Figure 11 shows the spectral location at which laser transmittance measurements were made through water vapor in the laboratory. The absorption coefficient measured near 1953 cm^{-1} is given in Figure 12 together with a calculation based on the Lorentz line shape. The calculation is seen to underestimate the measurement rather significantly. Other measurements made in closer proximity to the centers of water vapor absorption lines are in much better agreement with similar calculations. The implication is that the simple Lorentz shape describes the absorption near the line centers reasonably well, but departs as one moves further into the wing.

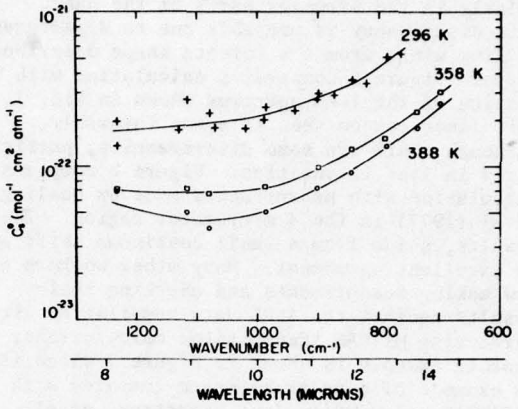

Figure 8. Measurements of the 10 μm Water Vapor Continuum Self-Broadened Absorption Coefficient (see Burch, 1970)

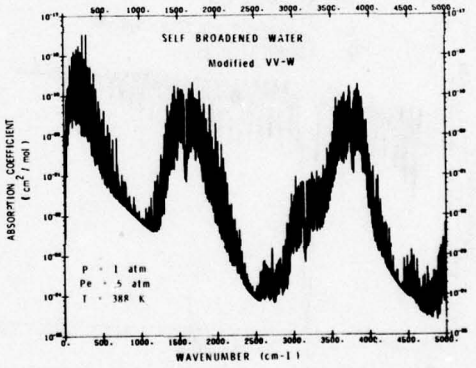

Figure 9. Computed Water Vapor Absorption Spectrum Considering All Lines Contained on AFGL Compilation (from Clough and Kneizys, 1978).

Although the water vapor line wing and continuum problem, have been emphasized, similar line shape difficulties are encountered with other atmospheric absorbers. A particular example is the departure from Lorentz lines noted in the case of carbon dioxide in the spectral region near 2400 cm^{-1}. The existence of a great many strong lines at frequencies just below 2400 cm^{-1} and no lines at higher frequencies gives rise to an accumulated line wing absorption of significance to systems operating in this region. In our models we have also included the absorption due to nitrogen near 4 micrometers and the absorption due to nitric acid in the 11 micrometer region

under the general heading of continuum absorption. These bands are not truly continuous, but are made up of a large number of closely spaced weak lines. The detailed line parameters are not available and the fact that the lines are both closely spaced and weak means that we make little error by simply including their effects as an empirical correction.

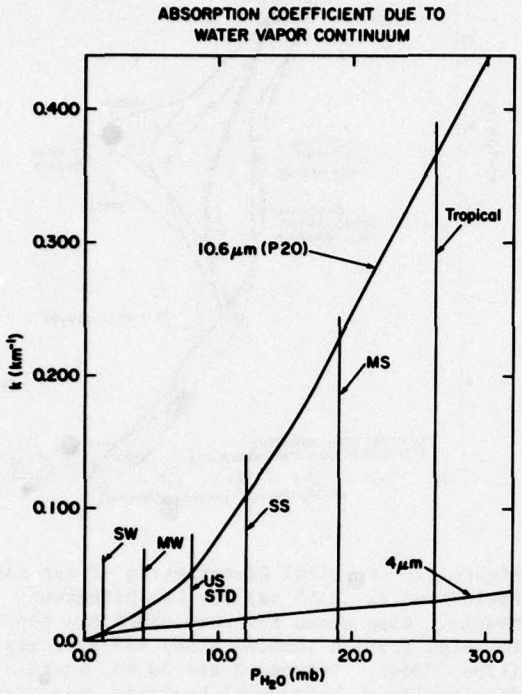

Figure 10. Absorption Coefficients Due to the Water Vapor Continuum.

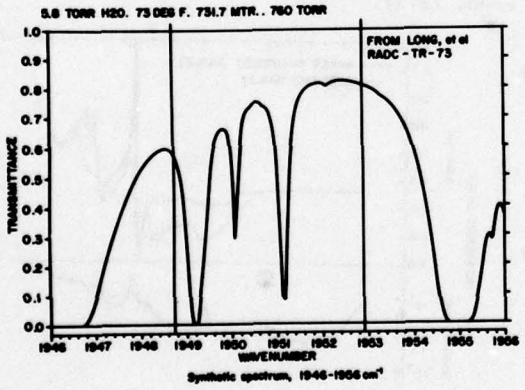

Figure 11. Spectral Location of Laser Measurements Made by Long, et al (1973), Through a Laboratory Water Vapor Path.

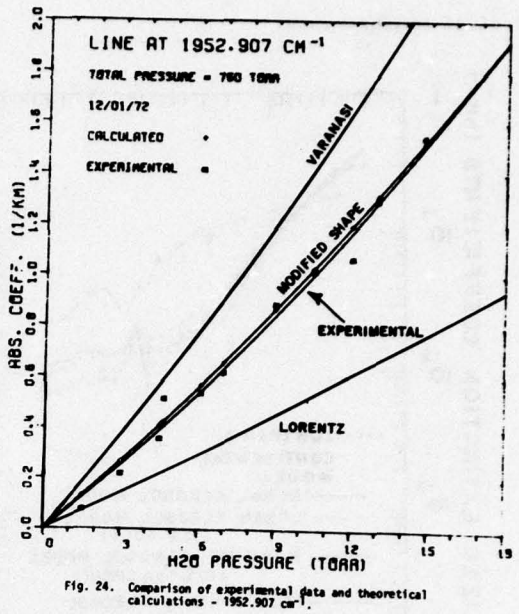

Fig. 24. Comparison of experimental data and theoretical calculations - 1952.907 cm⁻¹.

Figure 12. Comparison of Experimental Calculations and Theoretical Calculations for the CO Laser Emission Line at 1952.907. (See Long, et al, 1973).

4. AEROSOL MODELLING

As indicated in the introduction, the accurate modelling of atmospheric aerosols and their optical properties remains a very significant problem of atmospheric transmission modelling. In general a knowledge of the particle size distribution and complex index of refraction is sufficient to compute extinction coefficients. This assumes the application of Mie theory with the attendant assumption of spherical particles. The problem is that the meteorologist does not usually measure either of these quantities on a routine basis. In fact, such measurements are quite difficult and very much in the research stage. The only measured quantity directly related to the aerosol abundance is the visibility. Unfortunately, visibility is strictly related to visible wavelengths and can only be expected to have the most general relationship to extinction at longer wavelengths. Other ways must be found to extend from meteorological measurements to reasonable estimates of extinction due to aerosols at longer wavelengths.

Toward this end, several aerosol models have been developed by Shettle and Fenn (1975) based on particle size distribution and complex index of refraction measurements of many workers. The resulting aerosol models are shown in Figure 13. Although the five curves of Figure 13 are all normalized to the same extinction (visibility) at 0.55 μm, large differences can be seen at infrared wavelengths. The difficulty now is to decide which model is most appropriate for a given set of meteoro-

logical measurements.

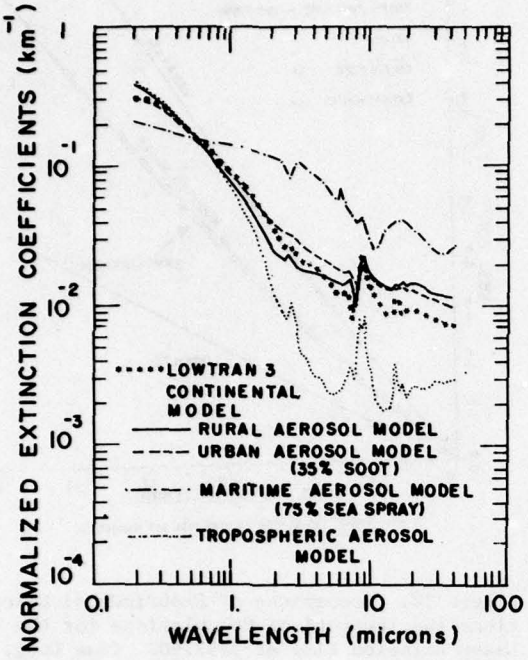

Figure 13. Extinction Coefficients for Sea Level Aerosol Models Currently Incorporated in the LOWTRAN 4 (See Selby, et al, 1978) and LASER (See McClatchey and D'Agati, 1978) Codes.

In addition to the modelling of aerosols near the surface, the whole issue of their vertical distribution is even more difficult and less understood. A number of measurements of stratospheric aerosols have been made and models based on these measurements have been produced as indicated in Figure 14 (Shettle and Fenn, (1975). The total extinction through aerosols for most paths in the stratosphere is quite small, so the indicated variations will have only a small effect on extinction predictions. However, the scattered radiation field, of importance to some systems operating in the stratosphere or in space, may be quite different for the different models indicated.

Although the complex index of refraction is a much slower varying function of wavelength than the molecular absorption coefficients, there are some significant resonances as indicated in Figure 15. The refractive index curves shown here are those used in the construction of the Rural model shown in Figure 14. Figure 16 shows the size distributions used in the construction of the Rural and Maritime models. Notice the bimodal nature of these distributions.

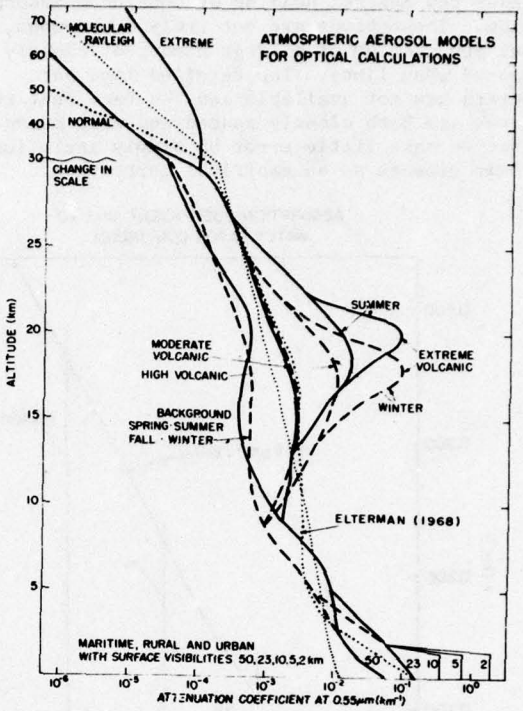

Figure 14. Vertical Distribution of Aerosol Extinction (at 0.55 μm) for the Different Models. Also shown for comparison are the Rayleigh Profile (dotted line) and Elterman's (1968) Model. Between 2 and 30 km, where a distinction on a seasonal basis is made, the Spring-Summer conditions are indicated with a solid line and Fall-Winter conditions are indicated by a dashed line. (See Shettle and Fenn, 1975).

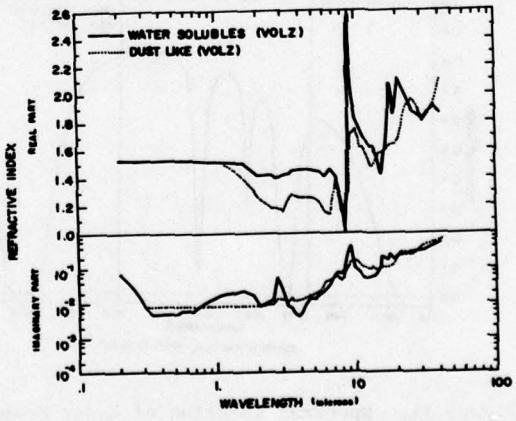

Figure 15. Refractive Index of Aerosol Material used in Construction of Rural Aerosol Model (After Volz, 1973).

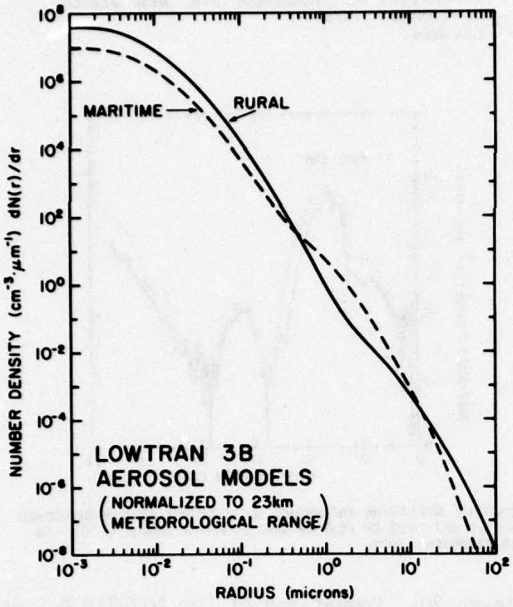

Figure 16. Aerosol Size Distributions Used in Construction of Rural and Maritime Aerosol Models (See Shettle and Fenn, 1975).

In order to properly model aerosol conditions for low visibilities, it is apparent from experimental measurements that the growth of particles with increasing relative humidity should be incorporated in our models. Following the work of Hanel (1975), a relative humidity dependence has been built into these models. An example of this very significant effect is shown in Figure 17. Notice that the extinction increases dramatically, but the wavelength dependence of that extinction also changes very significantly. The reason for this is the increasing abundance of larger particles as the relative humidity increases.

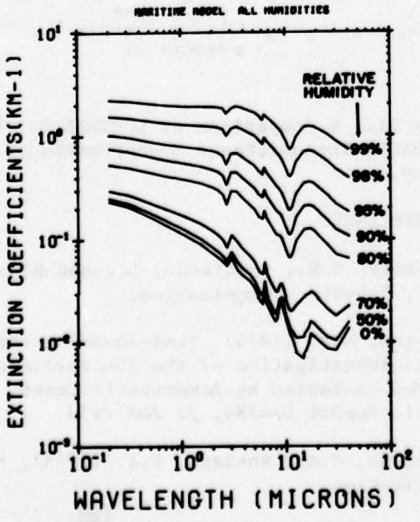

Figure 17. Relative Humidity Dependence of Extinction Coefficient for the Maritime Aerosol Model.

5. THE LOWTRAN TRANSMISSION CODE

As indicated previously, the LOWTRAN transmission code is applicable to a spectral resolution of 20 cm^{-1} or degradable to any lower spectral resolution. The primary motivation for the construction of the LOWTRAN code is computer efficiency, flexibility, and applicability to broadband systems problems. We feel that all of these goals are met with this code. It covers the spectral region from 0.25 to 28.5 micrometers and handles extinction by both molecular and aerosol atmospheric constituents. A recent modification to the code has generated the LOWTRAN 4 model, (See Selby, et al, 1978) capable of computing atmospheric thermal emission as well as transmission. The construction of such an efficient and flexible model of necessity involves some approximations. Our aim is to make the program accurate in transmission to $\pm$5% of the transmission value. Although we are close to this accuracy overall, there are certainly some spectral regions and some atmospheric conditions where this accuracy remains difficult to achieve. Problems involving molecular continuum effects and aerosol extinction continue to receive the majority of our attention. Figure 18 shows the effect of the different sea level aerosol models on the total LOWTRAN computed transmission over a 10 km sea level path. The major difficulty is to decide which of the several aerosol models to use for a given atmospheric path. Some meteorological judgement, *not currently included in the* LOWTRAN model is required in order to achieve the best results.

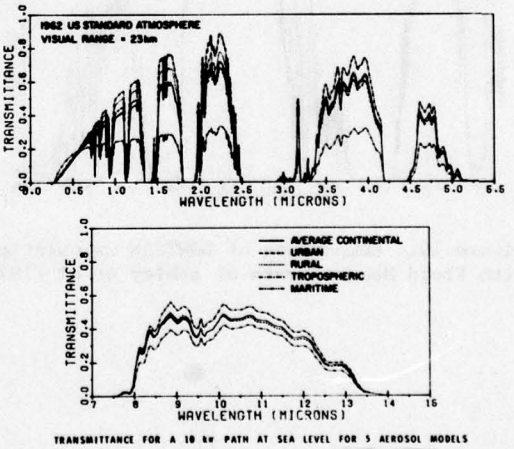

Figure 18. Transmittance for a 10 km Path at Sea Level for 5 Aerosol Models (From Selby, et al, 1978).

Efforts are continuing to validate the LOWTRAN model, particularly against field measurements. An example of a recent comparison is shown in Figure 19. These measurements made at General Dynamics by Ashley, et al (1973) were made over a 1.3 km path at sea level containing 0.72 pr. cm/km of water vapor. Figure 20 compares a LOWTRAN 4 emission result with measurements of atmospheric emission made from a balloon platform by Murcray, et al (1977).

Excellent agreement has been achieved here across this atmospheric "window" region and includes the nitric acid feature near 11 micrometers inserted for the first time into LOWTRAN 4. Other LOWTRAN validation efforts are aimed primarily at aerosol model comparisons. Figure 21 shows the time history of transmittance measurements at Meppen, Germany in the two important infrared window regions. These measurements were made as part of a NATO Program on Optical Atmospheric Quantities in Europe (OPAQUE), and have been reported by Fenn (1978). The major features in these plots are associated with the development of low visibility and fog conditions. The trends in the calculations follow rather well the trends in the measurements, but the absolute values are not in complete agreement. The rural model systematically overestimates the transmittance except in the first few days of this record. The maritime model is fairly close in the 8-12 μm region, but underestimates the transmittance in the 3.4-5 μm region. In general, the maritime model agrees better with the measurements even though the measurements are made over a continental region. This points up the need for more sophisticated aerosol model development and more sophisticated techniques for picking and choosing from among the available models.

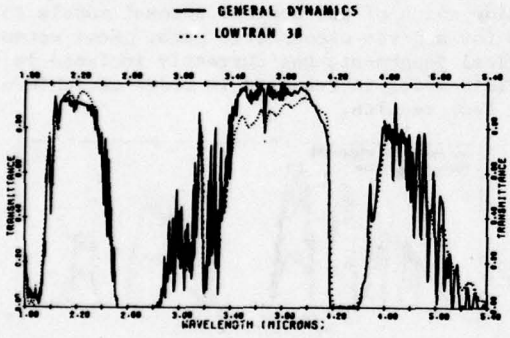

Figure 19. Comparison of LOWTRAN Calculations with Field Measurements of Ashley et al (1973).

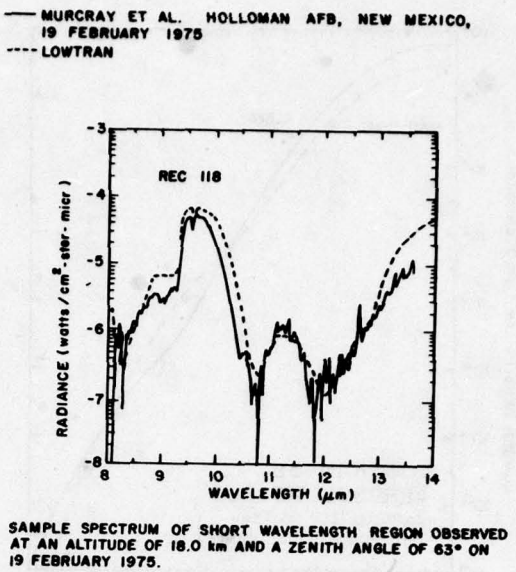

Figure 20. Comparison of the LOWTRAN 4 Code with Atmospheric Emission Measurements of Murcray, et al (1977).

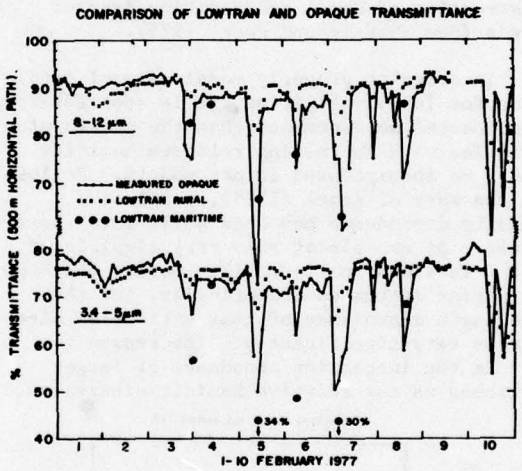

Figure 21. A Comparison of LOWTRAN Calculations and OPAQUE Transmittance Measurements at Meppen, Germany.

6. REFERENCES

Ashley, G.W., Gastineau, L., and Blay, D. (1973), Private Communication.

Burch, D.E. (1970), Semi-Annual Technical Report: Investigation of the Absorption of Infrared Radiation by Atmospheric Gases, Aeronutronic Report U-4784, 31 Jan 1970.

Clough, S.A., Kneizys, F.X. (1978), Private Communication.

Dowling, J.A., Haught, K.M., Horton, R.F., Hanley, S.T., Curcio, J.A., Garcia, D.H., Gott, C.O., and Agambar, W.L. (1977), Atmospheric Transmission Measurements Using IR Lasers, Fourier Transform Spectroscopy, and Gas Filter Correlation Techniques, Report of NRL Progress, March 1977.

Fenn, R.W. (1978), OPAQUE - A Measurement Program on Optical Atmospheric Quantities in Europe, Vol. 1 - The NATO OPAQUE Program, AFGL-TR-78-0011, 17 Jan 1978.

Gryvnak, D.A., Burch, D.E., Alt, R.L., and Zgonc, D.K. (1976), Infrared Absorption by CH_4, H_2O, and CO_2, AFGL-TR-76-0246.

Hanel, G. (1975), Properties of Atmospheric Particles as Functions of Relative Humidity at Thermodynamic Equilibrium with the Surrounding Air, Advances in Geophysics, Vol. 19, Academic Press, N.Y.

Long. R.K.. Mills, F.S., and Trusty, G.L. (1973), Experimental Absorption Coefficients for Eleven CO Laser Lines, RADC-TR-73-126.

McClatchey, R.A., Benedict, W.S., Clough, S.A., Burch, D.E., Calfee, R.F., Fox, K., Rothman, L.S., Garing, J.S. (1973), AFCRL Atmospheric Absorption Line Parameters Compilation, AFCRL-TR-73-0096, ERP No. 434.

McClatchey, R.A., and D'Agati, A.P. (1978), Atmospheric Transmission of Laser Radiation: Computer Code LASER, AFGL-TR-78-0029.

Murcray, D.G., Brooks, J.N., Goldman, A., Kosters, J.J., and Williams, W.J. (1977), Water Vapor Nitric Acid and Ozone Mixing Ratio Height Profiles Derived from Spectral Radiometric Measurements, U. of Denver, Denver, Colo. 80203, Contract Report No. 332.

Nordstrom, R.J., Shaw, J.H., Skinner, W.R., Calvert, J.G., Chan, W.H., and Uselman, W.M. (1976), A Comparison of High Resolution Observed and Computed Air Spectra Between 700 and 2300 cm^{-1}, OSU Research Foundation Technical Report RF 4221, Aug 1976.

Rothman, L.S., Clough, S.A., McClatchey, R.A., Yound, L.G., Snider, D.E., and Goldman, A. (1978), AFGL Trace Gas Compilation, Applied Optics, Vol. 17, No. 4, 15 Feb 1978.

Selby, J.E.A., Kneizys, F.X., Chetwynd, J.H., and McClatchey, R.A. (1978), Atmospheric Transmittance/Radiance: Computer Code LOWTRAN 4, AFGL-TR-78-0053.

Shettle, E.P., and Fenn, R.W. (1975), Models of the Atmospheric Aerosols, Published in Proceedings of AGARD Technical Meeting on Optical Propagation in the Atmosphere, 27-31 Oct 1975, Lyngby, Denmark.

Smith, H.J.P., Dube, D.J., Gardner, M.E., Clough, S.A., Kneizys, F.X., Rothman, L.S. (1978), FASCODE-Fast Atmospheric Signature Code (Spectral Transmittance and Radiance), AFGL-TR-78-0081.

Volz, F.E. (1973) Infrared Refractive Index of Atmospheric Aerosol Substances, Appl. Optics., 11, pp 755-759.

ELECTROMAGNETIC PROPAGATION ASSESSMENT

Juergen H. Richter, Herbert V. Hitney, Herbert G. Hughes and Robert B. Rose

EM Propagation Division

Naval Ocean Systems Center

San Diego, CA 92152

ABSTRACT

The status of electromagnetic propagation (EM) assessment systems is described. Specifically, systems for ionospheric radio, tropospheric radio, and electrooptical (EO) propagation are presented. Some of the sensing requirements of geophysical input parameters are discussed.

1. INTRODUCTION

Any system which relies on propagation of electromagnetic including electrooptic waves in the earth's environment is to some extent propagation limited. There are a number of examples. Solar disturbances affecting the ionosphere can result in complete disruption of the Navy's vital high frequency (hf) communications and surveillance network. Refractive layers in the lower atmosphere can cause "holes" in shipboard radar coverage. Oceanic ducting phenomena may be exploited for over-the-horizon detection capabilities. Aerosols (clouds) are often the limiting factors in electrooptical systems. A mere qualitative understanding of atmospheric effects on EM/EO propagation is not sufficient for optimum deployment of military systems. Therefore, the concept of real-time assessment systems useable under operational conditions has been developed. These systems are based on mini- or microcomputers with interactive graphic displays providing quantitative performance data for specific equipments and geometries under existing and, potentially, also forecast geophysical conditions. The status of assessment systems for ionospheric radio, tropospheric radio and EO propagation and sensing requirements of geophysical input parameters are discussed.

2. PROPAGATION ASSESSMENT SYSTEMS

Independent of the location within the frequency spectrum and the specific application (e.g. surveillance, communications, navigation, etc.) all propagation assessment systems have some basic features. All deal with the geophysical environment; all require a careful analysis of the sensitivity of the systems addressed to environmental parameters (which in turn defines geophysical sensing requirements); all require verified models which relate environmental conditions to systems performance; all need carefully planned operational implementations involving optimum hardware selection, man-machine interface questions, optimum displays, interface with other existing or planned equipment; and, finally, all have to demonstrate that they are affordable by either proving a quantitative pay-off through actual savings or by showing increased tactical or strategic capabilities. In recognition of the commonality of these basic features, the Navy has established an exploratory development program in "Atmospheric Effects on EM/EO Propagation" which is managed by the Naval Ocean Systems Center. A significant portion of the

Frequency Band / Implementation	Ionospheric Radio Propagation	Tropospheric Radio Propagation	EO Propagation
Exploratory Development Assessment System	PROPHET	IREPS	PREOS
Interim Operational Implementation	PROPHET CLASSIC PROPHET FOTACS	Interim E/WEPS	
Operational	Frequency Management	E/WEPS (SESC)	E/WEPS (SESC)

Table 1. Status and Plans for EM/EO Assessment Systems

effort under this program is in support of a family of assessment systems listed in Table 1. In the area of ionospheric radio propagation the PROPHET (pseudoacronym for propagation forecasting terminal) system (Richter, Rothmuller and Rose, 1977) has demonstrated its utility in initial deployments at a Naval Communications Station. CLASSIC PROPHET is a smaller desk top calculator version specifically geared to tactical applications. A limited, non real-time propagation assessment capability has been incorporated into FOTACS (Fleet Operational Telecommunications Automated Control System, Caldwell, 1978) which shortly will be installed in all Navy CAMS (Communication Area Master Station). FOTACS is a forerunner for a comprehensive frequency management system which should include all present and planned PROPHET capabiliites.

In the area of tropospheric radio propagation, the Integrated Refractive Effects Prediction System (IREPS) (Richter and Hitney, 1977) has undergone further development and a smaller version using a desk top calculator has been made available. This represents an interim version of an Environment/Weapons Effects Prediction System (E/WEPS). The operational implementation of E/WEPS may be in the frame of a Shipboard Environmental Support Center (SESC) which includes meteorological information and displays (e.g. the Naval Environmental Display Station or NEDS) and underwater acoustic propagation assessment.

Effort has started on the Prediction of Performance and Range of Electrooptical Systems (PREOS) which ultimately will be incorporated into E/WEPS and SESC.

3. IONOSPHERIC RADIO PROPAGATION ASSESSMENT

The PROPHET system described by Richter, Rothmuller and Rose (1977) has undergone initial successful testing at the Naval Communications Station at Stockton, California. PROPHET has been enthusiastically received and endorsed by operational personnel who consider it to be one of the most valuable real-time frequency prediction equipments made available to technicians since radio communications first began. During recent severe ionospheric disturbances caused by solar flares the system provided accurate disturbance warnings and provided real-time recommendations for frequency shifts to minimize communication outages. The occurrence of ionospheric disturbances is likely to increase over the next two years. Figure 1 shows Hill's (1977) sunspot number prediction (solid line) and observed monthly sunspot numbers (crosses) through October 1978. The observed sunspot numbers (and associated solar flares causing ionospheric disturbances) are well ahead of Hill's original prediction and are likely to reach the high peak forecast for the 1980-1982 time frame. It should be pointed out that this is only the second period of high solar activity for which space (satellite sensed) observations are available and that it

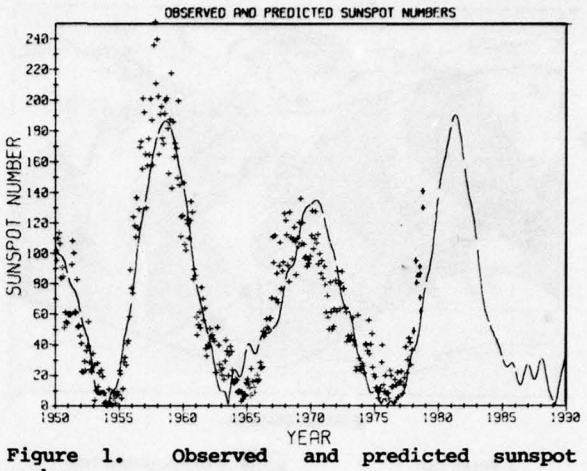

Figure 1. Observed and predicted sunspot numbers.

provides the first opportunity to verify models based on data from the previous solar maximum.

The primary emphasis with PROPHET has been on hf communications. Even though hf communications represents only a small portion of the Navy's total communications capability, the need for accurate propagation assessment will increase in the future for several reasons. First, it can be shown that sizeable electric power consumption savings can be achieved by radiating optimum power levels for respective propagation conditions and providing area coverage without redundant transmitters. Both can be done with accurate, real-time propagation assessment information. Secondly, the lesser use of the hf spectrum reduces the available number of qualified operators having long experience and good understanding of propagation phenomena. Again, PROPHET can replace this capability. Thirdly, any further reduction in available frequencies in the hf spectrum and transmission facilities will require a more efficient management of the available resources which can be achieved only by a PROPHET concept.

Besides the hf communications aspects, another potentially very important capability has been incorporated into PROPHET for correcting the Omega navigation system under

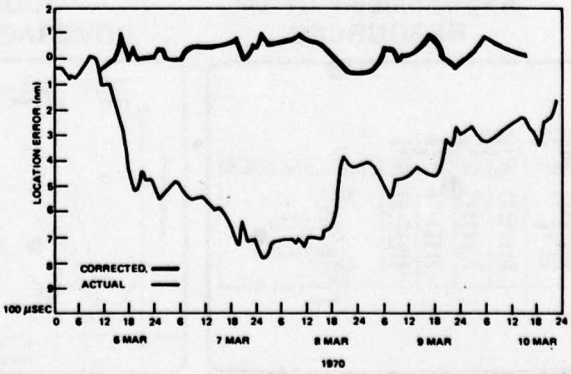

Figure 2. Omega location error for a PCA with and without corrections.

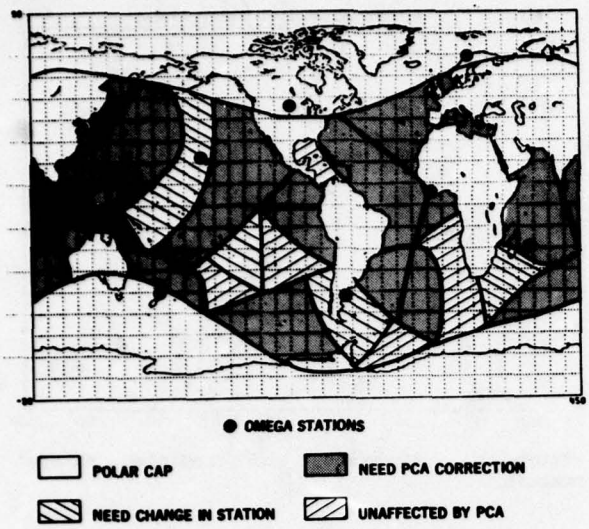

Figure 3. PCA effects on Omega coverage for oceanic areas.

disturbances of the polar ionospheres (for so-called Polar Cap Absorptions or PCAs caused by particles emitted from the sun and concentrated by the earth's magnetic field around the poles). An example of a resulting position error is shown in Figure 2 in which the actual position may be in error by as much as 7-8 nmi. Models have been developed (Argo, 1975) and implemented into PROPHET which correct for these disturbances so that Omega retains its specified accuracy of ±1 nmi. The particular example in Figure 2 is based on hyperbolic ranging using the Omega stations in Norway and Hawaii. It should be pointed out that disturbances of this kind can last for days. Figure 3 shows the oceanic areas affected by a PCA and the corrective measures required. This kind of a correction may become of increased importance should commercial air carriers replace expensive inertial navigation systems with much cheaper Omega receivers. Densely traveled routes (like the North Atlantic) most certainly require corrective measures.

A special version of PROPHET called CLASSIC PROPHET (Rose, 1976; Rose and Martin, 1977; Rose, Martin and Levine, 1978) has been developed for tactical applications using a graphics capable desk top calculator (Tektronix 4051). Figure 4 shows the information flow and examples of presentations. Unlike PROPHET which receives real-time satellite sensed environmental data, CLASSIC PROPHET requires manual input of this information. Examples of CLASSIC PROPHET products are shown on the bottom of Figure 4. For example, on the left side a display shows the hf bands that can be received by a number of stations for a given transmitter location. This information can be readily used to select a transmission frequency to eliminate or minimize reception by unwanted receivers. The other two displays on the bottom of Figure 4 show bearing quality (variance of bearing angle for direction finding) on the ordinate versus time and frequency respectively. These displays may be used to select either times of transmission or frequencies that result in either poor or good fixes for direction finding

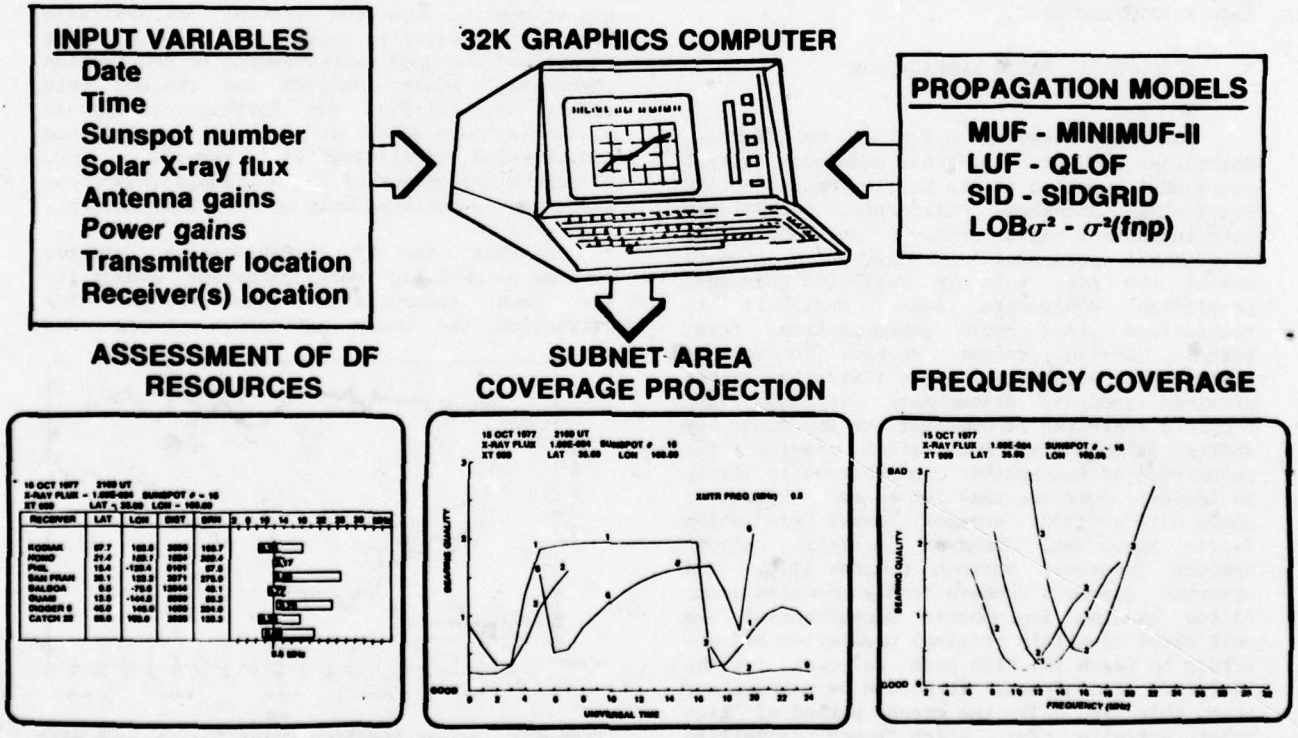

Figure 4. CLASSIC PROPHET information flow and displays.

Model	System	Action	Status	FOTACS	Pres. PROPHET	Future PROPHET
Flare detection	all hf, vlf navigation and comm	warning	operational		X	X
Flare detection	all hf, vlf nav/comm	hf comm-freq shift reroute traffic	operational		X	X
SID GRID	all hf	hf comm freq shift reroute traffic	operational	X	X	X
SPA/vlf	vlf nav Omega	phase correction factor	developed			X
SPA inversion	all hf, vlf	estimate x-ray flare size (independent of satell.) feed sid grid	in progress			X
PCA/vlf	vlf navig	phase correction factor for trans-polar circuits	developed			X
PCA/hf	all polar hf	hf comm-advice signal strength loss-freq shift	developed			X
PCA/vhf	all polar satellite	vhf comm-advice signal loss	developed			X
QLOF	all hf	hf comm-normal operations, freq management	operational	X	X	X
LOF split	covert hf systems	opt freq selection against known rcvrs	operational			X
MINIMUF	all hf	hf comm-normal ops freq. management	operational	X	X	X
15 min update to MINIMUF using auroral E fields	all hf	correct MUF est. (real time) minimize errors (to ≈1 MHz) (feeds MINIMUF)				X
Raytrace	all hf	hf comm-normal ops. antenna selection	operational		X	X
Launch angle multipath using quasi parabolic	all hf	hf comm-normal ops. antenna selection	near completion			X
Polar and auroral ionosphere	all hf vhf satellite	hf comm, auroral & polar circuits	in progress			X
Earth's magnetic field variations (ground)	ASW & any magnetically sensitive	corrections for field changes	in progress			X
Mixing shock front from auroral disturbances	all hf	hf comm-midlatitude (feeds MINIMUF)	in progress			X
Scintillation grid	vhf/uhf satellite comm	advisory-dB fade probability based on location	operational	X	X	X
Omega correction factors	Omega vlf	correction factors	operational		X	X
DMSP topside sounder ionospheric updates	hf & satellite comm	correct MUF est. (real time)	in conception			X

Table 2. Present and Future PROPHET Capabilities

applications. Initial operational use of CLASSIC PROPHET systems has convincingly demonstrated the excellent utility of such systems.

The eventual capability and configuration of the PROPHET concept has not been fully defined yet and will strongly depend on further test and evaluations in an operational environment. Table 2 lists the models, their application, their purpose and status for FOTACS, the present PROPHET and its future version. Present plans call for the deployment of three units and a test and evaluation period of approximately three years. At the end of this period decisions will be made as to which models listed in Table 2 will be used in a final operational implementation which will be part of a frequency management system.

Critical to a disturbance warning and assessment system are real-time satellite sensed data. The SOLRAD 11 program described by Richter, Rothmuller and Rose (1977) has been seriously troubled by hardware failures and is being discontinued. The PROPHET system has successfully switched to the exclusive use of NOAA satellites (SMS/GOES).

4. TROPOSPHERIC RADIO PROPAGATION ASSESSMENT

Work on the Integrated Refractive Effects Prediction System (IREPS) described by Richter and Hitney (1977) has continued primarily in the refinement of the modeling. Special attention has been given to including sea clutter effects into the models in particular under ducting conditions. An interim E/WEPS (Environment/Weapons Effects Prediction System) capability has been created in response to demands for quick deployment from the operational community. The interim E/WEPS is based on a graphics capable desk top calculator with printer (Hewlett Packard 9845). An example of a radar coverage display generated by the interim E/WEPS is shown in Figure 5. In this case a ground based duct (duct height 1000 ft) creates greatly extended detection ranges for the lower portion of the lowest lobe. The display has been slightly changed from the previous presentation (Richter and Hitney, 1977) to facilitate easier understanding by the user. The first interim E/WEPS unit has been installed and tested aboard the USS Ranger (CV 61). Within the next year all US aircraft carriers will be furnished with the same units. The final hardware configuration and implementation of E/WEPS is presently being studied. Special attention is given to a Shipboard Environmental Support Center (SESC) which is capable of handling E/WEPS, underwater acoustic propagation assessment and all information provided by the shipboard version of the Naval Environmental Display Station (NEDS).

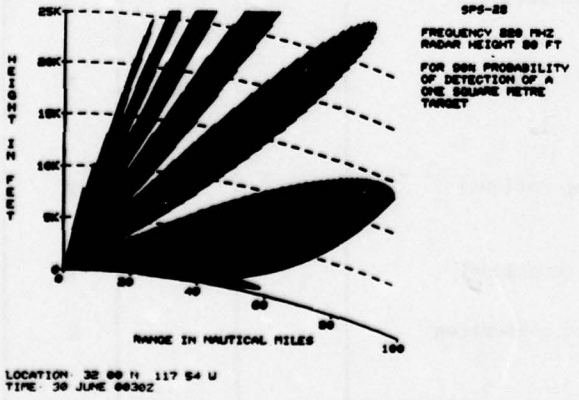

Figure 5. Radar detection range coverage for an SPS-28 radar for a ground based duct.

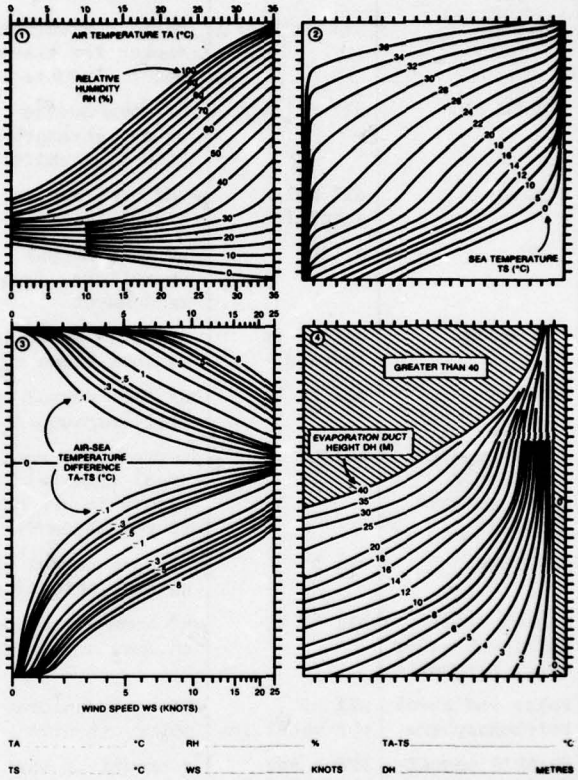

Figure 6. Evaporation duct height calculator.

An example of a quick response to an operational need for a specific propagation assessment capability is shown in Figure 6. It provides easy means for deriving evaporation duct height based on simple bulk meteorological measurements which are air temperature (TA), sea surface water temperature (TS), relative humidity (RH) and wind speed (WS). Starting at graph 1 in Figure 6, a horizontal line is drawn for the measured RH and TA values until it intersects the appropriate TS curve in graph 2. From this intersection a vertical line is drawn into graph 4 where the intersection with a horizontal line starting at the measured TA-TS

and WS values of graph 3 gives the duct height DH. Since evaporation duct height by itself does not give quantitative systems performance data additional nomograms have been developed in which the graph for duct height is replaced by, for instance, a radar detection range graph. In Figure 7 the range of detecting a 30000 m^2

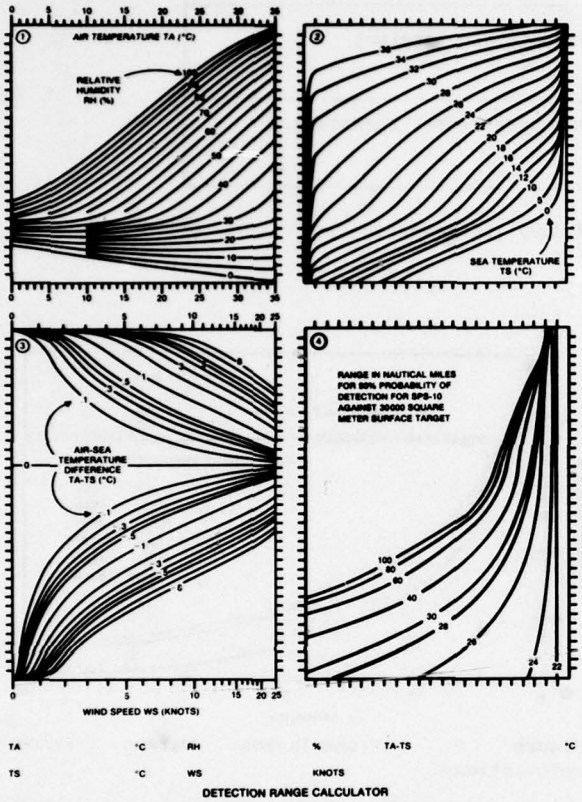

Figure 7. Detection range calculator of an SPS-10 radar against a 30000 m^2 target under evaporation ducting conditions.

target with a 90% probability using an SPS-10 radar is shown (graph 4). Besides eliminating cumbersome and lengthy calculations, Figures 6 and 7 illustrate also the sensitivity of evaporation ducting assessment to the measurement accuracy of the input parameters. For example, small changes to air-sea temperature differences values may significantly change duct heights and detection ranges. Both nomograms shown in Figures 6 and 7 are based on models and their verification described by Hitney (1975) and Richter and Hitney (1975).

In the area of sensing atmospheric refractivity, a miniaturized radiosonde carried by a 30 gram balloon has been developed specifically for shipboard refractivity measurements (Motchenbacher, 1977). In addition, a technique is being investigated to infer refractivity by monitoring satellite signals received during horizon passages (Hitney, 1976).

5. ELECTROOPTIC PROPAGATION ASSESSMENT

A significant concentrated and coordinated effort has started within the Navy to assess the performance of electrooptical systems. Table 3 lists examples of EO systems and the reasons for which they are attractive to the Navy.
The special capabilities offered for the various applications in Table 3 have to be weighed against the serious performance degradations that EO systems may experience as a result of changing environmental conditions. A Navy wide coordinated effort for EO systems performance has been described by Schefer (1977). Additional coordination and guidance has since been provided. Specifically, the Under Secretary of Defense for Research and Engineering has formulated six goals to be followed by the three different services (Army, Navy, Air Force). The goals are:

- Relate atmospheric transmission effects to sensor system performance.

- Accurately model the propagation effects of naturally-occurring and man-made aerosols.

- Relate the production, transport, and dissipation of naturally-occurring aerosols to measurable or predictable meteorological parameters.

- Accurately model the propagation effects of atmospheric molecular absorption.

- Assess the performance of weapons systems based on validated propagation models applied to historical or derived standard meteorological measurements or models.

- Develop atmospheric sensor systems to support EO systems operations.

The fundamental nature of these goals reflects the fact that much of the basic knowledge in the area of EO propagation is still missing. This coupled with the fact that there are presently no operational shipboard EO systems in the Navy results in a different emphasis on EO assessment system development than for the systems previously described. Consequently the major emphasis is presently on development and verification of models, sensitivity analyses, and sensor development.

Of the atmospheric parameters affecting EO propagation (e.g. aerosols, molecular absorption, turbulence, refraction) aerosol extinction is the key problem in the Navy's EO propagation program. For example, in Figure 8 the aerosol extinction coefficient for the 3-5μm band is plotted as a function of altitude. The solid line is calculated from dropsize distribution measurements obtained with a light scattering dropsize spectrometer (PMS ASSP-100) flown on an aircraft (Snyder and Hughes, 1978). The aerosol refractive index was assumed to be pure water. (The crosses indicate calculations for selected altitudes using the oceanic refractive index of LOWTRAN 3B.) The dashed

APPLICATION	CAPABILITY
IMAGING (e.g. low light level television, forward looking infrared system) SEARCH AND TRACK (e.g. infrared search and track system	passive surveillance (covertness), night vision, high resolution
RANGING (e.g. laser range finder) DESIGNATING (e.g. laser designator)	high pointing accuracy
COMMUNICATIONS (e.g. ship to ship, ship or satellite to submarine communication system)	covertness, water penetration

Table 3. EO Systems of Navy Interest

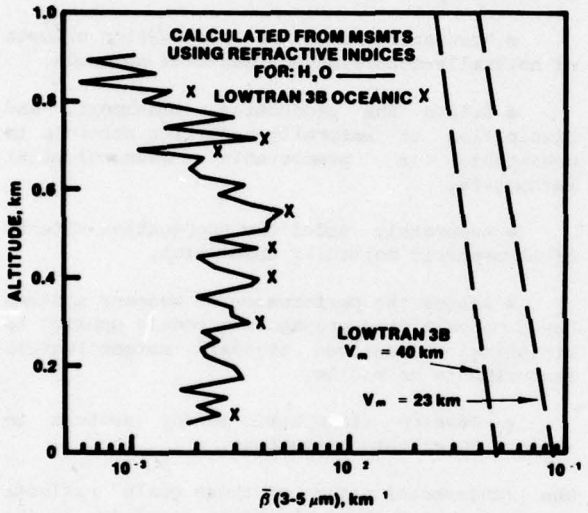

Figure 8. Aerosol extinction coefficient variations with altitude based on measured dropsize distributions and on LOWTRAN 3B.

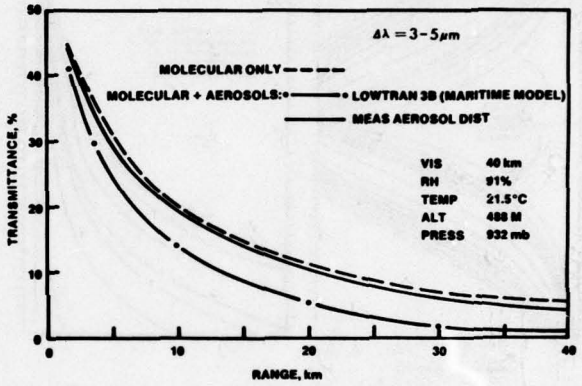

Figure 9. Transmission versus range calculations.

curves are the average aerosol extinctions based on LOWTRAN 3B for visibilities of 23 and 40 km respectively representing the range of reported visibility conditions. The extinction values based on LOWTRAN 3B decrease exponentially with height while the extinction calculated from aerosol measurements show a slight increase with altitude up the height of the convectively mixed layer (approximately 600 m) and a decrease above. The extinction calculated from LOWTRAN 3B is more than an order of magnitude greater than the extinction calculated from the measurements. To estimate what this means in terms of systems performance, transmittance was plotted against range in Figure 9 for the distributions of Figure 8. Figure 9 shows that for longer ranges there might be a serious underestimation of systems performance using the reported meteorological visibility as an input to LOWTRAN. If, for example, a value of 10% transmittance was the performance limit for a specific system, the calculations based on LOWTRAN would predict a maximum range of 14 km while the calculations based on aerosol measurements predict 22 km. This example should serve to illustrate the need for improved transmission models (in particular their marine aerosol portions) and the kind of considerations necessary to estimate the effect of a particular atmospheric parameter or modeling aspect on systems performance.

Of particular concern to a performance assessment capability for a broad range of EO systems is the number of measurements at different wavelengths necessary to characterize the entire frequency spectrum of interest (usually the visible and infrared region). Theoretical considerations and experimental data showed correlations between the total liquid water content and extinction and subsequently the possibility of scaling aerosol extinction at one wavelength to that of another (Biberman, Roberts and Seekamp, 1977). This kind of scaling was tested for marine aerosols by Hughes and Jensen (1978) and one of the results is

shown in Figure 10. A reasonable straightline correlation (in a log-log presentation) between the aerosol extinction coefficients calculated from dropsize distribution measurements between 3.5 and 10.6 μm is evident in two categories: poor and good visibilities. The dropsize spectrometer used for these data could not measure particle radii in excess of 14.7 μm. Since the aerosol measurements for the better visibilities (v > 4 km) did not show particles with radii in excess of 10 μm one can assume

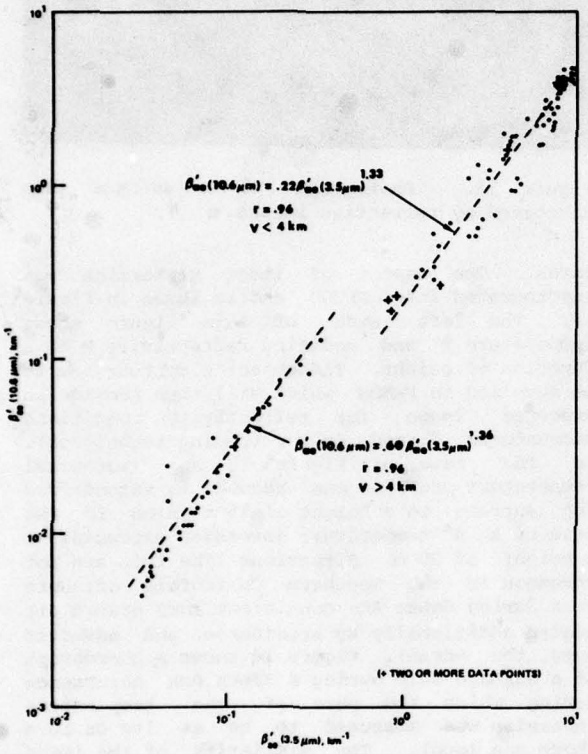

Figure 10. Calculated aerosol extinction coefficients β_{ae} for 10.6 μm vs. those for 3.5 μm.

that larger particles did not play a significant role. However, for the poor visibilities (v < 4 km) particles were measured in the largest size range and one can assume that the truncation of the distribution (by the inability to measure larger particles) would affect the results. To check this assumption the aerosol distributions for visibility ranges of less than 4 km were extrapolated to contain aerosols with maximum radii r_2 of 20, 25, and 30 μm respectively. Figure 11 shows the result of this extrapolation which causes the two regression lines to become more in agreement. The development of these scaling laws is clearly encouraging even though a number of questions need to be investigated such as aerosol refractive index changes for different air masses.

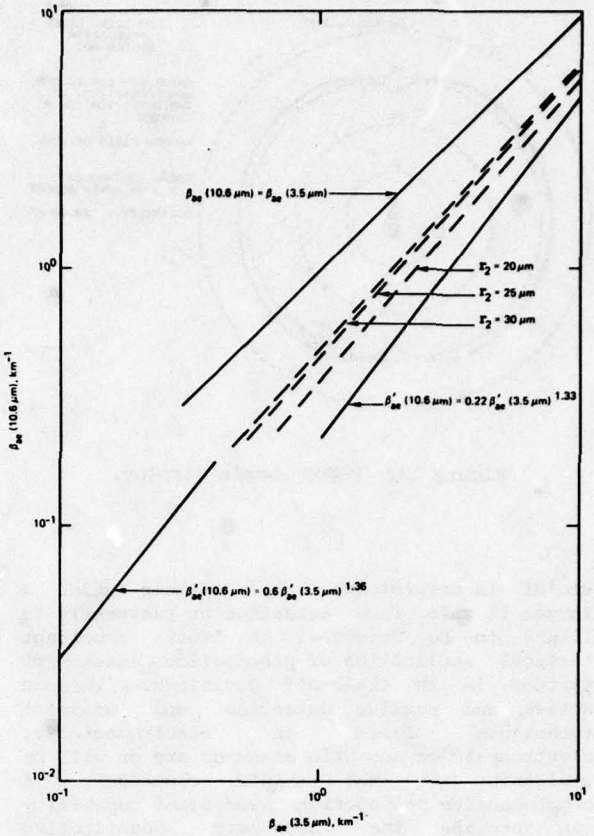

Figure 11. Increased extinction coefficients (dashed lines) for 10.6 μm vs. those at 3.5 μm for increased particle radii as indicated and compared with the regression analysis in Figure 10.

The primary effort on the development of a shipboard real time assessment system called PREOS (for prediction of performance and range for EO systems) centers presently on the selection of proper transmission models and their tailoring and incorporation into suitable hardware. The hardware is defined by E/WEPS of which PREOS is one building block. Since, as previously pointed out, there are presently no operational shipboard EO systems in the Navy, important applications of available PREOS capabilities are sensitivity analyses studies and systems performance simulation.

An example of what a PREOS display might provide is shown in Figure 12. After the operator has supplied environmental input data (such as visibility, scene luminance, etc.) and specified the system to be assessed (low light level television in this example) PREOS might give a range contour of detecting a specific target (in this case an aircraft carrier) as a function of aspect angle. This information is

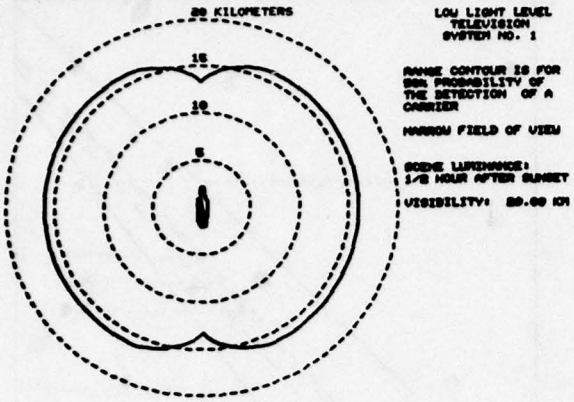

Figure 12. PREOS sample display.

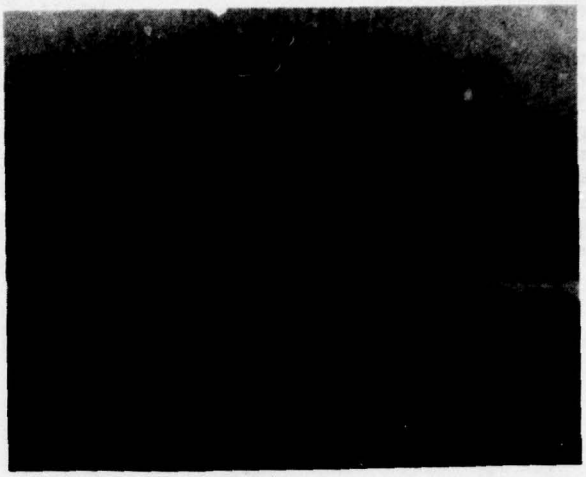

Figure 14. Photograph of a surface ship distorted by refractive layers.

useful in determining ranges within which a target is safe from detection or conversely is likely to be detected. A very important tactical application of propagation assessment systems is in trade-off decisions. Various active and passive detection and intercept techniques based on electromagnetic, electrooptic or acoustic measures are or will be available to the ship's commander. A comprehensive propagation assessment capability can provide the necessary quantitative information to optimize all available resources.

Finally, frequently observed mirages over ocean areas led to an investigation of ducting phenomena close to the water surface. The two questions of interest were range extensions or reductions and image distortions for visible and infrared imaging systems operating close to the ocean's surface. Feinberg, Hitney and Hughes (1978) found signficant range reductions for 10.6 μm propagation for superadiabatic lapse rates. One aspect of image distortion was incorporated into PREOS and is shown in Figure 13. The left side of this figure shows temperature T and modified refractivity M as a function of height. The object's contour has to be supplied to PREOS which will then provide an expected image for refractivity conditions encountered (based on ray tracing techniques). In the case of Figure 13 an isothermal temperature profile was assumed to extend from the surface to a height of 15 m which is the base of a 4° temperature inversion extending to a height of 20 m. Situations like this are not uncommon in the Southern California offshore area during Santa Ana conditions (dry desert air heated additionally by subsidence and advected over the ocean). Figure 14 shows a photograph of a surface ship during a Santa Ana occurrence during which the base of the temperature inversion was measured to be as low as 10 m above sea level. The similarity of the image provided by PREOS in Figure 13 and an observed example shown in Figure 14 is striking. An important aspect of the PREOS capability shown in Figure 13 is the possibility of reconstructing the object's true contours from a distorted image if the vertical refractivity profile is known.

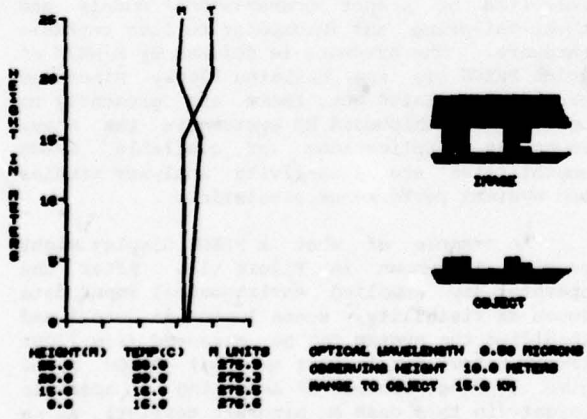

Figure 13. Image distortion analysis caused by refractive layers.

6. CONCLUSIONS

It has been demonstrated that propagation assessment systems are feasible and have proven very effective to the operational users. Their pay off reaches from actual savings, to improved understanding of sensor performance, optimization of resource allocation, and tactical exploitation of propagation phenomena. The major question is no longer if propagation assessment will be part of Naval operations but rather how to combine, integrate and implement various assessment capabilities for optimum operational utilization. In the area of ionospheric propagation a comprehensive frequency management system appears to be the proper host for real-time propagation assessment. Tropospheric radio propagation, electrooptical propagation, perhaps underwater acoustics propagation, may be best combined with oceanographic and meteorological data in a shipboard environmental support center.

7. REFERENCES

Argo, P. E., 1975: Modeling Omega PCA Phase Advances, Naval Electronics Laboratory Center Technical Report 1950.

Biberman, L. M., R. E. Roberts and L. N. Seekamp, 1977: A Comparison of Electrooptical Technologies for Target Acquisition and Guidance; part 2: Analysis of the Grafenwoehr Atmospheric Transmission Data, Institute for Defense Analysis Paper P-1218.

Caldwell, J. F., 1978: Fleet Operational Telecommunications Automated Control System (FOTACS): System Description, Naval Ocean Systems Center Technical Note 551.

Feinberg, R., H. V. Hitney and H. G. Hughes, 1978: Marine Boundary Layer Effects in the Infrared, Naval Ocean Systems Center Technical Note 555.

Hill, J. R., 1977: Long-term Solar Activity Forecasting Using High Resolution Time Spectral Analysis, Nature 266 (5598), pp 151-153.

Hitney, H. V., 1975: Propagation Modeling in the Evaporation Duct, Naval Electronics Laboratory Center Technical Report 1947.

Hitney, H. V., 1976: A Proposed Method to Infer Refractive Index Profiles by Satellite Monitoring, Naval Electronics Laboratory Center Technical Note 3108.

Hughes, H. G. and D. R. Jensen, 1978: Extinction of IR Wavelengths by Aerosols in Coastal Fog, Applied Optics, 17, pp 2138-2140.

Motchenbacher, C., 1977: Miniature Meteorological Balloonsonde, Naval Air Development Center Report NADC 76129-30.

Richter, J. H. and H. V. Hitney, 1975: The Effect of the Evaporation Duct on Microwave Propagation, Naval Electronics Laboratory Center Technical Report 1949.

Richter, J. H. and H. V. Hitney, 1977: IREPS: A Refractive Effects Assessment System, Proc. 7th Technical Exchange Conference, El Paso, TX. Published by ASL, WSMR, NM 88002, pp 72-76.

Richter, J. H., I. J. Rothmuller, and R. B. Rose, 1977: PROPHET: Real Time Propagation Forecasting Terminal, Proc. 7th Technical Exchange Conference, El Paso, TX. Published by ASL, WSMR, NM 88002, pp. 77-81.

Rose, R. B., 1976: Tactical Applications of HF Skywave Propagation Forecasts, part II, Naval Electronics Laboratory Center Technical Note 3212.

Rose, R. B. and J. N. Martin, 1977: Estimated HFDF Propagation Error Based upon the Position of the Operating Frequency in the Propagation Bandwidth, Naval Ocean Systems Center Technical Note 182.

Rose, R. B., J. N. Martin and P. H. Levine, 1978: MINIMUF-3: A Simplified HF MUF Prediction Algorithm, Naval Ocean Systems Center Technical Report 186.

Schefer, M. H., 1977: The Proposed Navy Exploratory Development Electrooptical Meteorology Project, Proc. 7th Technical Exchange Conference, El Paso, TX. Published by ASL, WSMR, NM 88002, pp 178-183.

Snyder, F. P. and H. G. Hughes, 1978: Aerosol Distributions with Altitude at Sea for High Visibilities - A Case Study, Naval Ocean Systems Center Technical Note 537.

THE ELECTRO-OPTICAL SENSOR ATMOSPHERIC EFFECTS LIBRARY

Louis D. Duncan

US Army Atmospheric Sciences Laboratory

White Sands Missile Range, New Mexico

ABSTRACT

The US Army Atmospheric Sciences Laboratory (ASL) is developing the Electro-Optical Systems Atmospheric Effects Library (E-O SAEL). The objective of this effort is the development of a library of validated user models and computer codes for simulation of the effects of the battlefield environment on the performance of electro-optical sensors and weapons systems. A interim version of E-O SAEL applicable to Europe will be completed during FY-79. In this paper we discuss (1) the models and algorithms which have been selected for the interim E-O SAEL, and (2) the basic structure of E-O SAEL.

1. INTRODUCTION AND BACKGROUND

United States and NATO military forces are increasingly relying on new sophisticated weapons systems which have greater range, accuracy, and lethality than those of previous wars. Characteristic of these systems is their dependence on electro-optical (E-O) sensors which are strongly influenced by the atmospheric environment. Therefore, it is extremely important that the effects of the atmosphere (or smoke or other obscurant) on the effectiveness of E-O sensors be clearly characterized. These effects should be analytically reproducible and permit reliable assessment through simulation of the actual E-O sensor field performance.

In November 1977, General Kerwin issued his now familiar directive in which he stated "I am concerned that despite the great strides that have been made to inject realism into our material development and training process, there are still too many individuals and agencies who treat the environmental conditions of continuous combat, full ECM, smoke, aerosols, rain, fog, haze, dust, etc., as unusual occurrences. Unless we take positive action to routinely include these vital factors in all facets of our material acquisition process and our training and evaluation programs, the Army will find itself unable to fight, survive, and win on the modern battlefield".[1] This strongly worded, clear statement formally recognized the seriousness of environmental effects on all aspects of military (Army) performance and ushered in a dedicated attack on the problem of low visibility environments.

Figure 1 depicts the major sources of obscuration on performance degradation together with the atmospheric and optics effects which must be considered. In the clear atmosphere case most Army E-O devices perform admirably well; however, when the visibility becomes limited (5 km or less) performance can be seriously degraded. Low clouds can limit the performance of airborne systems such as Copperhead, Hellfire, and airborne E-O surveillance systems. Fog, haze, rain, and snow are major attenuators of electromagnetic energy and, hence, seriously degrade the performance of a number of E-O and near millimeter wave (NMMW) devices. Several additional problems are caused by battlefield induced contamination (BIC). The major sources of contamination include: screening smokes, dust generated by artillery explosions and vehicular activity, fire products, and the incidental gases resulting from battlefield activity.

2. THE ELECTRO-OPTICAL SYSTEM ATMOSPHERIC EFFECTS LIBRARY (E-O SAEL)

E-O SAEL addresses the major environmental effects that affect Army systems performance (Figure 2). The E-O SAEL strategy involves the development of an interim E-O SAEL which will be available this year. The interim version will adopt existing codes which are applicable and supplement these codes with empirical codes developed from atmospheric measurements. The interim E-O SAEL will be applicable to the frequency ranges shown in Figure 3. The E-O SAEL codes will be modular, simple and understandable, adaptive, easy to control, and easy to communicate with. They will bridge the gap between the specialist in atmospheric optics and the operational user of these techniques.

The models which have been selected for inclusion into interim E-O SAEL will be discussed below.

3. GASEOUS ABSORPTION

The three codes used for computing gaseous absorption are the Lowtran Code[2], the SAI laser code[3,4], and the NMMW code[5]. The Lowtran code is used for computing gaseous absorption for the spectral bands. Since this code is well known it will not be discussed in any detail. It should be mentioned, however, that the original computer code

has been separated into a number of subroutines. This should make the code more flexible and easier to update. A contractor report on this modification will be published in the near future. In addition those portions of Lowtran not applicable to the spectral bands of interest have been removed in order to reduce computer core requirements.

The SAI laser code was obtained by fitting a polynomial to absorption coefficients computed by line-by-line calculations. This resulted in a polynomial of the form

$$\alpha = A_o + A_1T + A_2P + A_3TP + A_4P^2 + A_5TP^2,$$

where T is the temperature in degrees K and P is the partial pressure of water vapor, in torr. For the P(20) line of the CO_2 laser it was necessary to add the following terms

$$A_6T^2 + A_7T^2P + A_8T^2P^2.$$

Gaseous absorption in the millimeter wave domain is dominated by the water vapor (H_2O) and oxygen (O_2) molecules. Interim E-O SAEL will include this absorption at three frequencies of primary interest: 94 GHz, 140 GHz and 220 GHz. The absorption coefficients, in units of dB/Km, will be given as functions of temperature in ^oK, pressure in torr, and absolute humidity in gm/m^3.

Oxygen absorption was calculated using line by line procedures for the 60 GHz band and the 118 GHz line. Included in the calculation were the effects of line overlapping modeled by the use of an empirically reduced line width, and the contribution of the nonresonant absorption. This method provided the following expression:

$$a = A(\nu)(T/298)^{-3.4}\ (P/760)^2,$$

where A(94 GHz) = 0.05 dB/Km, A(140) = 0.04 dB/Km, A(220) = 0.025 dB/Km and $275^oK \leq T \leq 320\ ^oK$, 400 torr $\leq P \leq$ 800 torr.

The water vapor absorption was modeled by a line by line calculation based upon a modified Kinetic line profile which attempts to account for the effects of impact theory broadening of the line core, and statistical broadening of the line wings. No empirical "continuum" was found necessary to fit the data. This gave the following result:

$$a = A\ (\nu)(T/298)^{-1.7}(P/760)^{0.9}(\rho/7.5),$$

where A(94) = 0.32, A(140) = 0.77, A(220) = 2.05 and $295^oK \leq T \leq 320^oK$, 200 torr $\leq P \leq$ 800 torr, and 0.5 $gm/m^3 \leq \rho \leq$ 20 gm/m^3.

4. NATURAL AEROSOL EXTINCTION MODULE

Adverse weather which produces low visibility conditions can severly limit the usefulness of E-O weapons systems. Fog, haze, rain, and snow attenuate electromagnetic propagation through both scattering and absorption. Under controlled conditions it is possible to measure the composition and size distribution of atmospheric aerosols and then use this information with radiative transfer calculations to determine atmospheric transmission characteristics for spectral wavelengths or bands of interest. Unfortunately size distribution and composition are not routine meteorological observations. Until techniques are developed to predict composition and size distribution from standard meteorological measurements it is necessary to adopt a model which does not depend upon aerosol microphysical data.

The aerosol module for treatment of fog and haze in interim E-O SAEL is based upon Beer's Law

$$T_\lambda(R) = \exp(-K_\lambda R),$$

where $T_\lambda(R)$ is transmittance at range R and wavelength λ and K_λ is attenuation coefficient. Empirical algorithms which accept standard input, e.g., visibility, will be used to determine the attenuation coefficient.

Although there are several ongoing studies to develop models which relate attenuation coefficients, at various infrared wavelengths, to measurable meteorological parameters, few models have, at this time, been proposed. From those which are available, it has been decided that the GAP model[6] developed by the Night Vision and Electro-Optics Laboratory (NV&EOL) is the most appropriate model for inclusion into interim E-O SAEL. The GAP model was developed from measurements of transmission data taken over horizontal paths. Data from measurements taken at Grafenwohr, GE, Baumholder, GE, and Ft A.P. Hill, VA, were used in the model development. The model is developed in the form of scaling laws which use visible extinction coefficient (visibility or visible range) as the independent variable. The generic form for the model is

$$\log y = a + b \log x + c \log^2 x,$$

where x is extinction coefficient in the visible, y is extinction coefficient in the desired spectral band and a, b, and c are coefficients. x is related to visibility through Koshmeider's relation

$$x = V/3.912.$$

The GAP model provides predictions for the 3-5 μm, 8-12 μm, and 1.06 μm regions. It is assumed that the aerosol attenuation is invariant within each of the regions. Although this is not strictly true, as is easily shown by MIE calculations, the errors in such an assumption are relatively small and the current state of knowledge does not seem to warrant more precise modeling.

During the collection of the data used in the development of the GAP model, the NV&EOL personnel observed that during some of the observational periods moisture condensed upon objects which were exposed while at other times such objects remained dry. The terms "wet" and "dry" fog were used to describe the conditions. During the analysis of the data and development of the model it was discovered that attenuation at infrared wavelengths was quite different for the two different "types" of fogs. Consequently separate scaling laws were developed for the "wet" and "dry" data. The coefficients for these scaling laws, together with those developed for the combined data set are shown in Table 1. Recent analysis[7] of preliminary OPAQUE data from the Netherlands indicates that the GAP "wet" model correlates well with data where the airmass was analyzed as being of maritime origin while the "dry" model correlates well with continental air mass data.

For the NMMW wavelengths of 94, 140, and 220 GHz the aerosol module of interim E-O SAEL addresses the attenuation due to rain and fog. The attenuation for rain is taken from the work of Olsen et. al.[8] The attenuation in dB/Km is given by the equation

$$A = aR^b,$$

here A is attenuation in dB/Km, R is rain rate in mm/hr and a and b are frequency dependent coefficients. Two rain models are included, the thunderstorm (J-T) which is representative of the rain expected during summertime convective activity in Germany and the drizzle (J-D) which is typical of the rain expected during spring, fall, and winter in Germany. The a and b coefficients for these two models are shown in Table 2.

Although the attenuation of NMMW's by fog is not nearly as severe as the attenuation at IR frequencies, it can still be significant for heavy fogs. Since the drop size is small compared to the wavelength, the Rayleigh approximation is valid. This gives

$$A = 81.86\ \mathrm{Im}(-K)\ M/\lambda,$$

where A is the attenuation in dB/Km, K is the index of refraction, M is the liquid water content of the fog in gm m^{-3} and λ is wavelength in mm. If M is not available for input it will be computed from visibility using the equation[9]

$$K_{.55} = 93M^{.638}$$

5. CONTRAST

The contrast between an object (or target) and the background may be expressed in a number of ways. The more commonly used expression, and the one used in interim E-O SAEL is the contrast ratio

$$C = (L^T - L^B)/L^B,$$

where C is contrast, L is radiance*, and the superscripts T and B indicate target and background respectively. The apparent contrast of an object located at a distance R is given by:

$$C_R = (L_R^T - L_R^B)/L_R^B,$$

where the subscript R has been added to denote distance. With this notation the contrast at zero distance, usually called the inherent contrast, is C_o.

There are two factors which prevail to reduce the inherent contrast to the value C_R. These are: (1) the attenuation of the radiation by absorption and scattering, and (2) the contribution to the observed radiation resulting from both emission by the molecules and aerosols contained in the optical path and radiation scattered or reflected into the path. This second factor is usually called path radiance and is difficult to obtain experimentally.

Let T and L_p represent the atmospheric transmission and path radiance respectively. Then

$$L_R^T = TL_o^T + L_p,$$

with a similar equation for L_R^B. Thus, the ratio of the apparent to the inherent contrast, called the atmospheric contrast transmission, is given by

$$T_c = C_R/C_o = (1 + L_p/TL_o^B)^{-1}.$$

Following the work of Dunlley[10] and others, T_c can be expressed in the form

$$T_c = (1 + g\,(e^{\beta R} - 1))^{-1},$$

where β is the visible extinction coefficient and g is the so-called sky-to-ground ratio. The con-

*Sometimes referred to as luminence in the visible region of the spectra.

trast transmission model for interim E-O SAEL uses this formulation. The model was developed by Huschke[11] from radiometric measurements made in Southern Germany and results from Monte Carlo calculations.

The major contribution from Huschke's developments is a series of algorithms which estimate the sky-to-ground ratio from surface albedo, α, solar elevation angle, ε, and visbility, V. The value of g is derived from

$$g = F_\delta \, (g_\alpha + g_\varepsilon + g_V)/3 \text{ where,}$$

$$g_\alpha = \exp (1.15 \ln \alpha - 0.75),$$

$$g_\varepsilon = \exp (-3.4 \sin \varepsilon + 2.7),$$

$$g_V = \exp (-.5 \ln V + 1.5).$$

The factor F_δ is determined by a complicated rule based upon α, ε, V, and δ which is the receiver depression angle.

The user of interim E-O SAEL will have the option of specifying g as an input in lieu of using the Huschke algorithms. The user's guide will contain a tabulation of values appropriate for various scenarios.

6. SMOKE OBSCURATION MODEL

The smoke obscuration model which has been selected for inclusion into interim E-O SAEL was developed for the Night Vision and Electro-Optics Laboratories (NV&EOL) by General Research Corporation. This model, which we refer to as the NVL/GRC model has been validated for WP smoke and has been incorporated into CARMONETTE. ASL is currently extending the model, in cooperation with the NV&EOL, to provide a model which is also validated for HC and fog oil smokes.

7. DUST OBSCURATION MODULE

During the past 18 months a considerable amount of data has become available for investigation of the obscuration effects of dust generated by artillery shell explosions. Data has been obtained by the PM Smoke during Smoke Weeks I and II plus the Ft. Sill tests. Data has also been obtained by the NV&EOL at Grafenwohr II and by ASL during DIRT I. ASL, with contractor support, is developing a semi-empirical dust obscuration model for inclusion into E-O SAEL.

8. CLIMATOLOGY MODEL

The gaseous absorption and natural aerosol extinction modules of E-O SAEL will enable the user to obtain the atmospheric effects information required to evaluate an E-O systems performance for a given or postulated atmospheric condition. For detailed analysis and evaluation of a system the probabilistic variations in the weather must be taken in to account to obtain an effective performance of the system. Such an effectiveness measure should give probabilistic estimates of the percentage of time the system will perform in a specific geographical area. A well defined climatological data base is required for such an analysis. Since it is well known that adverse weather which degrades E-O system performance is more prevalent during certain months and even certain periods of the day, the data base must be capable of pinpointing, in a probabilistic sense, those times which are both favorable and unfavorable for system performance.

The Atmospheric Sciences Laboratory has obtained historical weather records for a large number of stations in Central Europe. This data was obtained from the Air Force Environmental Tactical Applications Center (ETAC) and contains hourly observations for an eleven year period of routine surface meteorological data. This data is being analyzed to construct a climatological data base for E-O SAEL. Probability of occurrence for various parameters will be included in the E-O SAEL data base.

Several of the parameters for the analysis of E-O systems effectiveness analysis are not included in the standard meteorological analysis. These include transmission at various IR wavelengths, precipitation rate, type of fog, and liquid water content. Scaling laws are being used to extend the data to include estimates of transmission. In addition a scheme has been developed by Essenwanger and Stewart[12] to differentiate between radiation and non-radiation fog.

9. REFERENCES

1. Kerwin Sends, 22 Nov 77.

2. Selby, J.E.A., F.X. Kneizys, J.H. Chetneynd, Jr., R.A. McClatchey, "Atmospheric Transmittance/Radiance Computer Code LOWTRAN 4,", AFGL-TR-78-0053, Feb 78.

3. Woods, D.R., S.L. Manning, P.G. Eitner, D.H. Leslie, R.E. Meredith, "CO Laser Atmospheric Absorption Coefficient Modeling," SAI-78-004-AA, Mar 78.

4. Thompson, B.D., F.G. Gebhard, "Polynomial Expression for CO_2 and DF Laser Molecular Absorption Coefficients," SAI, Ann Arbor Memo[2], IM 78-097-127, June 78.

5. Woods, D., ASL. Preriate Communication, Jan 79.

6. Shields, F.J., "NV&EOL G/AP Aerosol Atmospheric Models," DF to Director, Vesionics, NV&EOL, Sep 78.

7. Gebhart, F.G., J.L. Manning, R.E. Meredith, S.M. Singer, F.G. Smith, R.E. Turner, and P.C. Voura, "Model Development for E-O SAEL: Natural Aerosol Contract, Laser Transmission and Turbulence," SAI-78-008-AA, Dec 78.

8. Olsen, R.L., D.V. Rodgers, and D.R. Hodge, "The aR^b Relation in the Calculation of Rain Attenuation," IEEE Trans on Atennas and Propagation, Vol AP-26, No. 2, Mar 78.

9. Low, R.D.H., "A Theoretical Investigation of Cloud/Fog, Optical Properties and Their Spectral Correlations," Atmospheric Sciences Laboratory, ASL-TR-0024, Feb 79.

10. Duntly, S.Q., "The Reduction of Apparent Contract by the Atmosphere," J.Opt. Soc. Am., Vol 38, 179, 1948.

11. Huschke, R.E., "Atmospheric Visual and Infrared Transmission Deduced from Surface Weather Observations: Weather and Warplanes VI," Rand Corp. R-2016-PR, Oct 76.

12. Essenwanger, O.K., D.A. Stewart, "Fog and Haze in Europe and Thier Effect on Performance of Electro-Optical Systems," US Army MIRADCOM, Proceedings 1978 Army Science Conference.

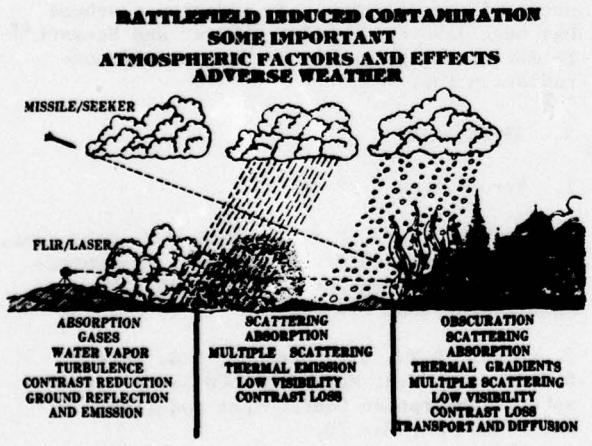

Figure 1. Major Sources of Obscuration.

E - O SAEL

NATURAL ATMOSPHERIC EFFECTS MODELED

- GASEOUS ABSORPTION
- AEROSOL ATTENUATION DUE TO FOG, HAZE, RAIN, SNOW
- CONTRAST DEGRADATION
- TURBULENCE
- FREQUENCE OF OCCURRENCE OF ADVERSE WEATHER

BATTLEFIELD INDUCED CONTAMINATION

- ATTENUATION DUE TO DUST FROM H.E EXPLOSIONS
- ATTENUATION DUE TO DUST FROM TANKS, TRUCKS, ETC.
- ABSORPTION CAUSED BY DUST AND INCIDENTAL GASES
- OBSCURATION CAUSED BY SCREENING SMOKES
- CONTRAST LOSS
- TRANSPORT AND DIFUSSION

Figure 2. Weather and Obscuration Effects Modeled in E-O SAEL.

E - O SAEL

SPECTRAL BANDS TREATED

VISIBLE, 3-5 μm, 8-12 μm

LASER FREQUENCIES TREATED

0.9 μm, 1.06 μm, 3.8 μm, 10.6 μm, HF-DF (3-5 μm)

NEAR MILLIMETER WAVELENGTHS

94 GHz, 140 GHz, 220GHz

Figure 3. Frequency Range Covered by E-O SAEL.

TABLE 1: Coefficients for GAP Model

		A	B	C
		FOG & HAZE		
3-5	"ALL"	-1.002	2.406	-.512
3-5	"WET"	-1.029	2.568	-.623
3-5	"DRY"	-2.026	3.308	-.512
8-12	"ALL"	-1.002	1.896	-.234
8-12	"WET"	-1.042	2.095	-.362
8-12	"DRY"	-2.541	3.169	-.142
1.06		-.230	1.042	.183
		RAIN		
3-5		-.108	1.120	0
8-12		.037	1.040	0
		SNOW		
3-5		.021	1.050	0
8-12		.114	.992	0

TABLE 2: Coefficients for NMMW Rain Attenuation

FREQ GHz	J-T		J-D	
	a	b	a	b
94	.837	.695	1.10	.945
140	1.05	.610	1.65	.895
220	1.02	.609	2.33	.722

A COMPARISON OF THE AFGL FLASH, DRAPER DART AND AWS HAZE MODELS WITH THE RAND WETTA MODEL FOR CALCULATING ATMOSPHERIC CONTRAST REDUCTION

Dr Patrick J. Breitling, USAF Environmental
Technical Applications Center
Scott Air Force Base, Illinois

Abstract

In 1975 USAFETAC was tasked to develop a model to calculate the lock-on range for TV guided PGMs. Investigation revealed the availability of several models for calculating contrast reduction by the atmosphere. These models, listed in the title, were compared with one another using the same input data. The FLASH Monte Carlo model was assumed as the standard for the comparison. Visible (.55 m) contrast transmission values were computed for all models for a TV sensor at 12,000 feet AGL, for two mixing depths (200m and 1500m), two visibilities (5 and 23Km), three solar zenith angles (20°, 60°, 85°), three albedos (.06, .18, .80) and seven dive angles (85°, 70°, 50°, 30°, 20°, 10°, 7°). If one accounts for the difference in optical depths which results from Huschke's stair step treatment of vertical extinction coefficients, his model does an acceptable job of approximating FLASH contrast transmission values for a visibility of 23Km. When the visibility is 5Km, the agreement was not as good due to a combination of mathematical and geometrical factors.

I. INTRODUCTION

In 1975, the Electromagnetic Propagation Section of the Aerospace Sciences Branch of USAFETAC (USAFETAC/DNE) was tasked by Air Weather Service (AWS) to develop a technique to forecast the loss in contrast that T.V. guided missiles suffer in air-to-ground operations. DNE culled from the scientific literature a variety of atmospheric models which simulate the loss of visible light contrast between a ground target and an airborne TV sensor. Initially these models included the AFGL FLASH Monte Carlo Model, the Draper Lab's DART model and the AWS Haze Model. In late 1976, Mr R.E. Huschke published his RAND WETTA model (Huschke, 1976). Since this model held the possibility of answering DNE's search for an appropriate forecast model, a study was undertaken to compare the output from this basically empirical model under similar meteorological and geometrical conditions with that from the more complex models mentioned above.

While the WETTA model and the others share some basic elementary assumptions and equations, each model treats the vertical structure of the atmosphere and other input variables in a different manner, complicating the comparison process. These differences include:

1. The WETTA model treats the atmosphere as being composed of two layers; a lower layer with the surface visibility extending to the top of the mixing layer and an upper layer extending from there to the top of the atmosphere with a visibility of 80Km. The other models assume an exponentially decreasing extinction coefficient from a surface value based on the surface visibility. Figure 1 contrasts these two profiles for a visibility of 23Km.

2. The WETTA model computes contrast transmission (T_c) for the entire visible spectrum while the others compute T_c for individual narrow intervals within that region. Due to limited computer time and since computed T_c values for .55 microns approximate those for the entire visible, WETTA model values were compared with computed T_c values from the other models at .55 microns.

3. The WETTA model does not take into account the sun-target-sensor azimuthal angle variation of computed contrast transmission, while the other models do. For certain sun and dive angles, this differrence can be considerable. The lack of acceptable weighting factors necessitated the use of the arithmetic mean of the T_c values for azimuthal angles of 0°, 90°, and 180° in comparing the other models with WETTA.

4. The Huschke model uses the equation B=3.352/visibility to compute visible extinction coefficients while the others use B=3.912/visibility. This results in WETTA inferred values being about 15 percent lower than the other models.

5. The other important input variables, dive or depression angle, solar elevation or zenith angle, surface background albedo and visibiity were the same for all models. However, Huschke treats specific values of these variables as belonging to a particular category as input to an algorithm to compute the sky-ground ratio, while the other models employ the values directly as input.

The study compared computed contrast transmission values from the WETTA, FLASH, DART and AWS models for clear sky conditions and

a. One sensor altitude, 12,000 feet AGL.

b. Two mixing depth, 200 and 1500m.

c. Two visibilities, 5 and 23Km.

d. Three solar zenith angles, 20°, 60°, 85°.

e. Three albedos, .06, .18, .80.

f. Seven dive angles, 85°, 70°, 50°, 30°, 20°, 10°, and 7° (90° is nadir)

The .55 micron extinction coefficient profiles were taken from (Elterman, 1968) and (Elterman, 1970).

2. CONTRAST TRANSMISSION COMPARISON FOR 23Km VISIBILITY

A common notation is used in all the figures which follow. FL denotes the FLASH model, DT the DART model, H1 is the Huschke model with a mixing depth of 200 meters, H2 for a mixing depth of 1500 meters. A1 refers to the results of the AWS model with an exponentially decreasing B profile while A2 is for a stair step profile with a mixing depth of 1500 meters.

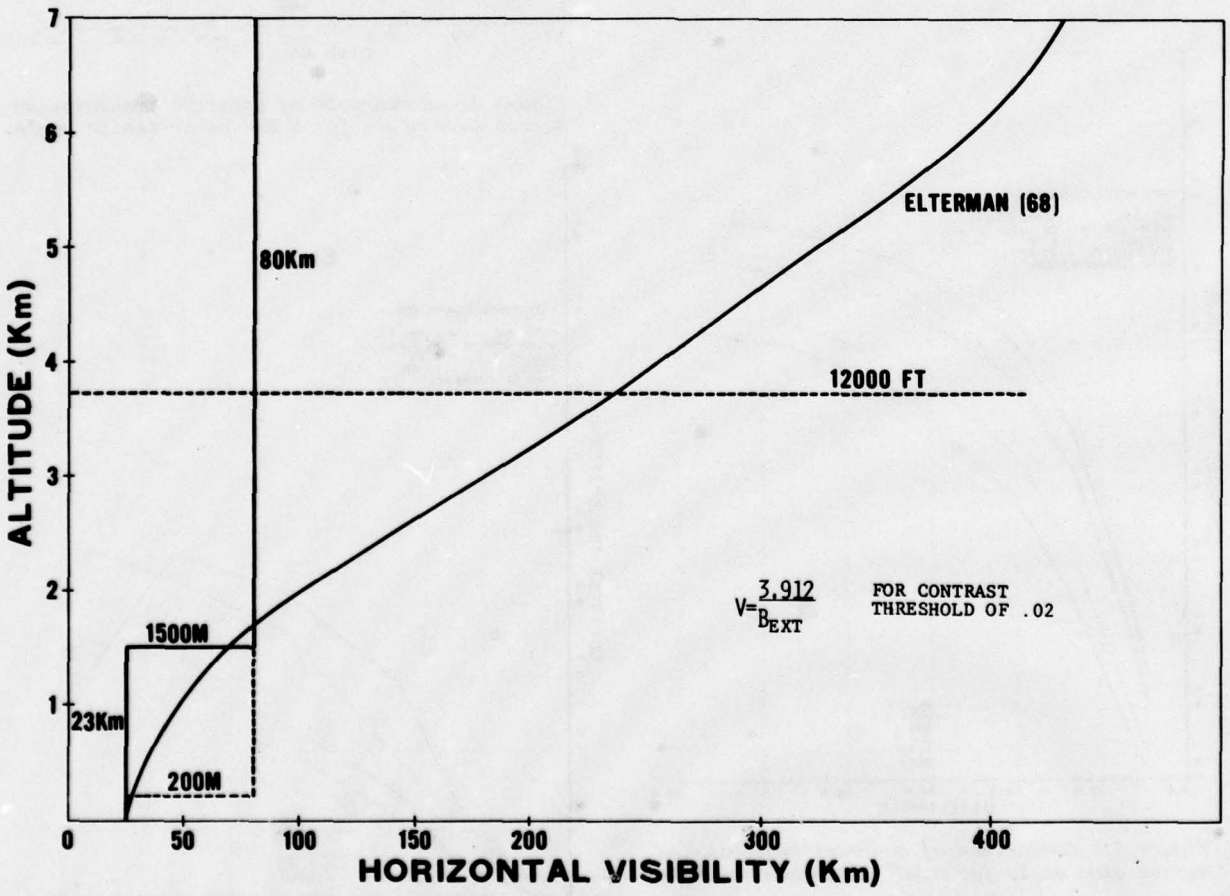

FIGURE 1. Comparison of exponential and stair-step extinction coefficient profiles.

Figures 2, 3, and 4 depict the variation of computed contrast transmission for the various models for an albedo of .18 and solar zenith angles of 20°, 60°, and 85° respectively. A feature common to these three figures and most of those which follow is that the Huschke WETTA model values (H1 and H2) bracket nearly all the values for the other models. H1, with the smallest total opitcal depth below the sensor, is nearly always the most optimistic while H2, with the largest optical depth, is generally the most pessimistic. A discrepancy in the WETTA model is apparent in Figures 3 and 4. At nearly vertical dive angles (85°) the model predicts T_c values that are considerably less than for a 70° dive angle. This aspect of the WETTA model is not shared by the other models, or previous conceptions of the variation of contrast loss with look angle.

Figures 5 and 6 demonstrate more clearly the differences between the various models. Plotted are the percent differences:

$$((T_c^1 - T_c^2)/T_c^1)) \times 100 \qquad (1)$$

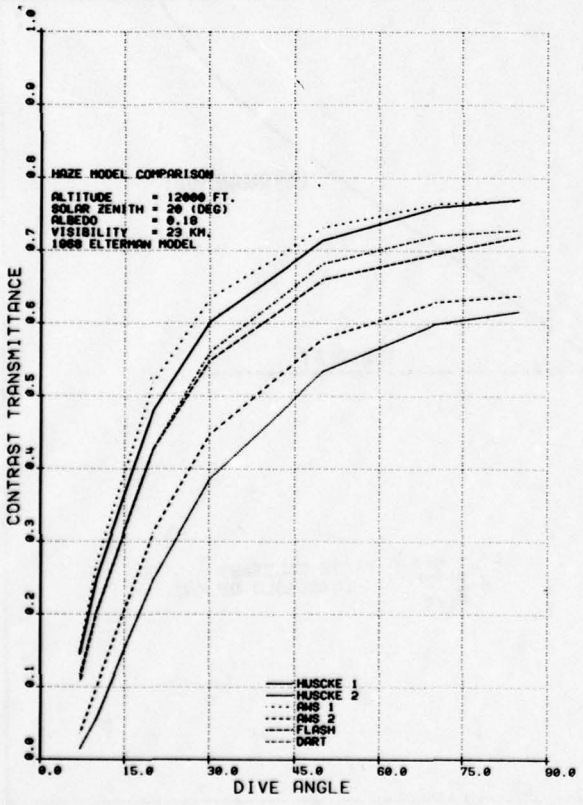

Figure 2. Comparison of contrast transmission versus dive angle for a 20° solar zenith angle.

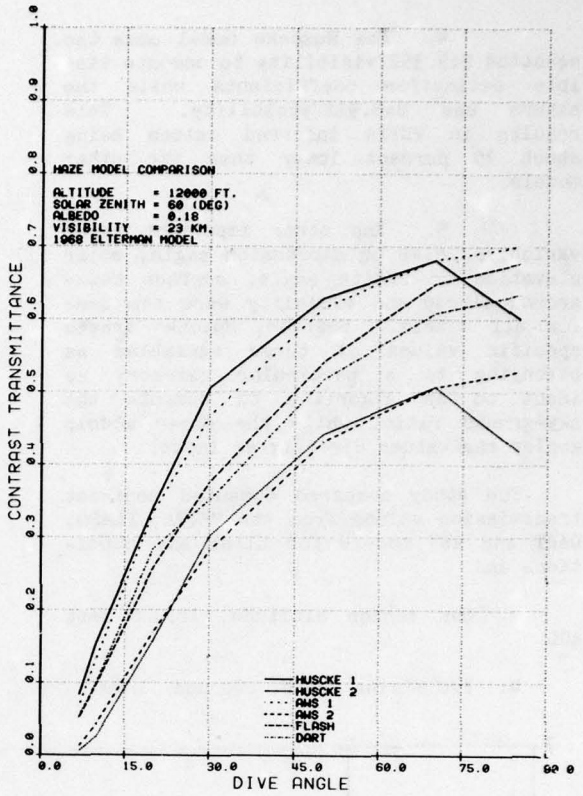

Figure 3. Comparison of contrast transmission versus dive angle for a 60° solar zenith angle.

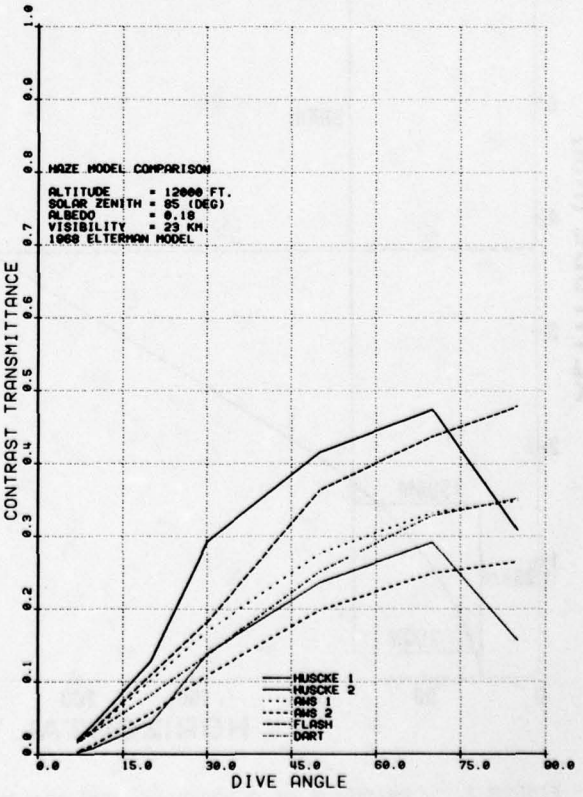

Figure 4. Comparison of contrast transmission versus dive angle for a 85° solar zenith angle.

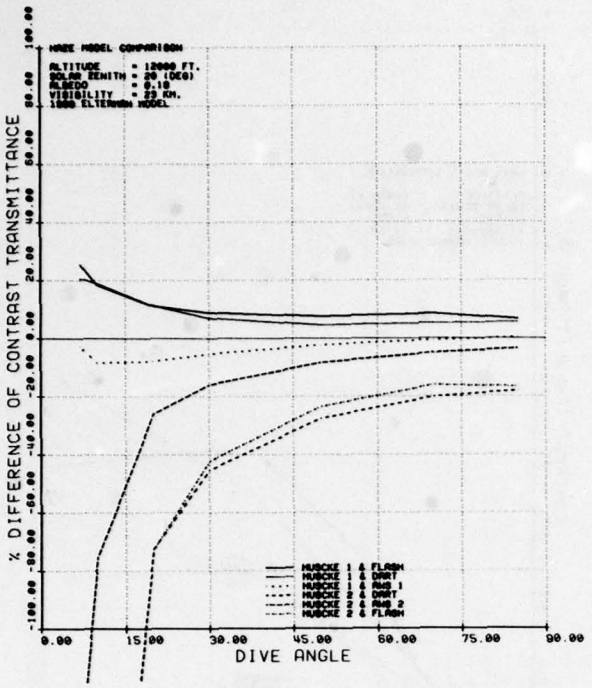

Figure 5. Percent difference of contrast transmission between pairs of models.

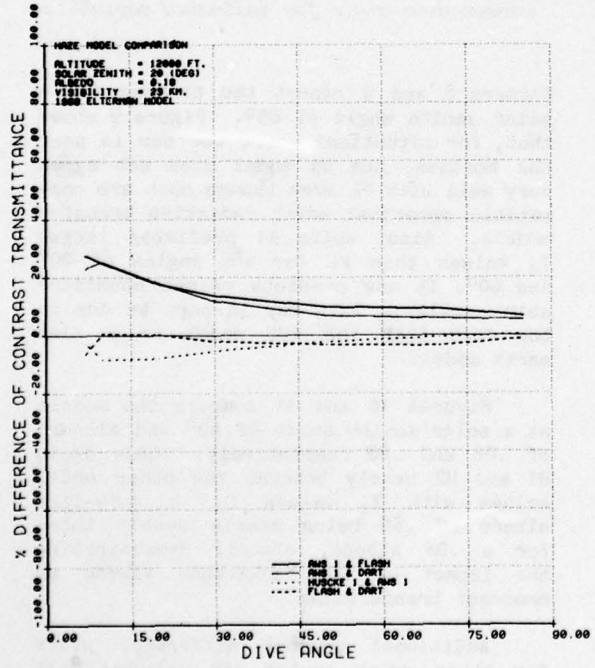

Figure 6. Percent difference of contrast transmission between pairs of models.

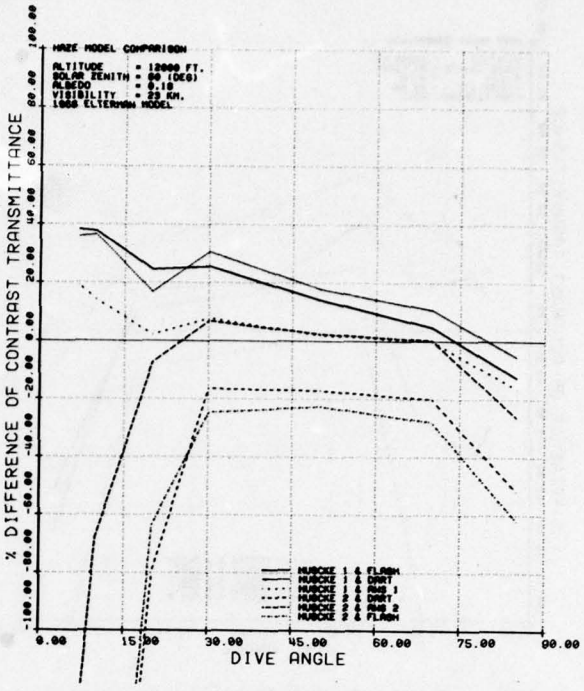

Figure 7. Percent difference of contrast transmission between pairs of models.

between T_c values for each of several dive angles. The WETTA H1 model agrees best with A1 and quite well with FL and DT, with a gradual fall off in agreement as one approaches near horizon dive angles. H1 shows T_c values that are consistently higher than FL as one would expect since its surface-to-sensor optical depth is smaller. On the other hand, there is no apparent reason why A1 with the same optical depth and aerosol model as FL should show consistently higher T_c values than FL. H2 compares less favorably with FL, especially at dive angles less than 30°. Figure 5 shows that the percent difference between H2, FL and DT gradually increases with decreasing dive angle. Figure 6 demonstrates that, as the dive angle decreases, A1 compares less favorably with both FL and DT.

Figure 7 compares the percent differences between the two WETTA outputs and the other models for a solar zenith angle of 60°. Once again A1 compares best with H1 and the H2FL and H1DT model comparisons show differences of less than 30 percent. H2 compares less favorably with FL and DT for dive angles less than 30° showing differences of over 100 percent for dive angles less than 20°. The consistent negative difference for an 85° dive angle again points up a possible problem with the WETTA model at near nadir dive angles.

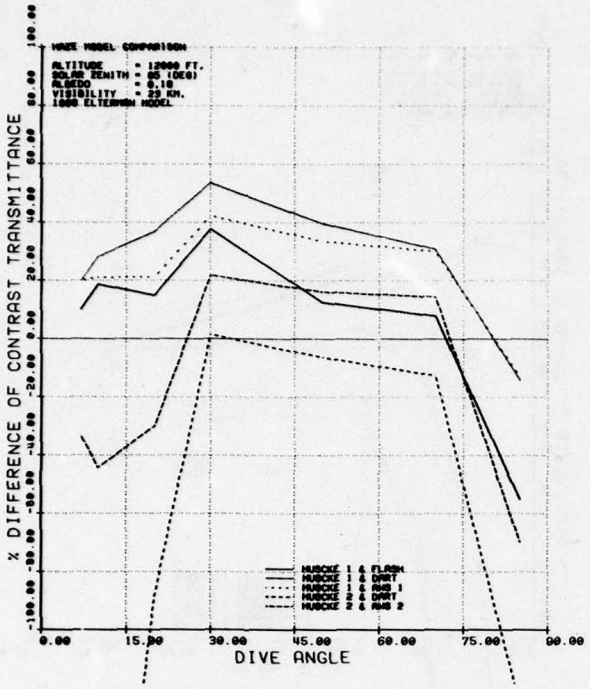

Figure 8. Percent difference of contrast transmission between pairs of models.

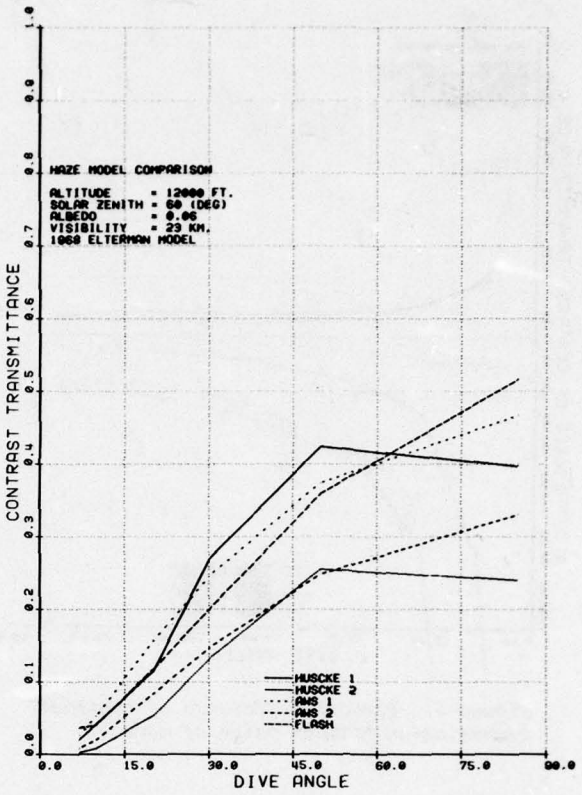

Figure 10. Comparison of contrast transmission versus dive angle for indicated variables.

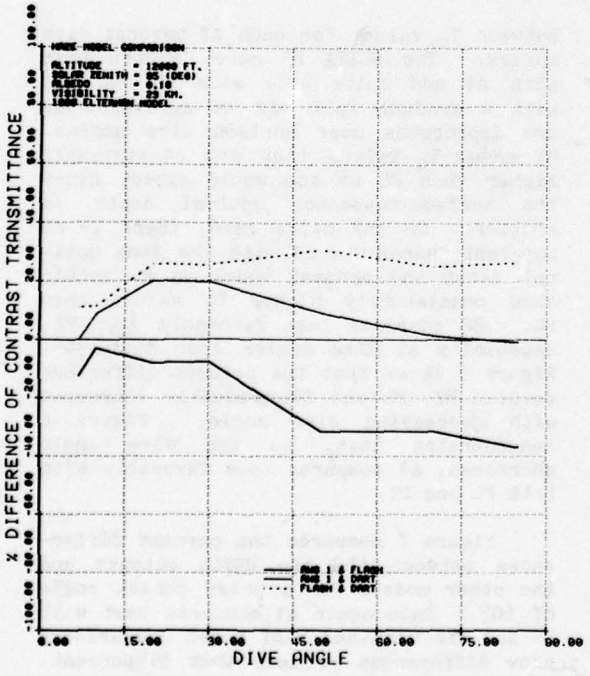

Figure 9. Percent difference of contrast transmission between pairs of models.

Figures 8 and 9 repeat the process for a solar zenith angle of 85°. Figure 9 shows that, for situations where the sun is near the horizon, the DT model does not agree very well with FL even though both are compatible spherical earth radiative transfer models. Also, while A1 predicted larger T_c values than FL for sun angles of 20° and 60°, it now predicts values considerably smaller. This may in part be due to the fact that the AWS model is a flat earth model.

Figures 10 and 11 compare the models at a solar zenith angle of 60° and albedos of .06 and .80 respectively. Once again H1 and H2 nearly bracket the other model values with T_c values for a snow-like albedo of .80 being nearly double those for a .06 albedo, clearly demonstrating the impact of the background albedo on contrast transmission.

Additional percent difference plots for other solar angles and albedos will not be included because they would be repetitious.

Figure 12 compares all models with each other through the mean of the summed, squared differences between T_c values for all seven dive angles. The model comparison with the smallest root-mean-squared-error (RMSE) value represents the best overall intercomparison. Lines connecting similar comparisons demonstrate the sun angle effect.

Overall, both the WETTA and AWS models do a fair job of approximating FLASH contrast transmission values when the visibility is good (23Km). The inherent limitations imposed by comparing models with different optical depths probably account for some of the discrepancies. Figure 13 shows that the total optical depth below the aircraft for the three exponentially decreasing models FL, ET, and A1 (.230) falls between the values for H1 (.203) and H2 (.361).

3. CONTRAST TRANSMISSION COMPARISON FOR 5Km VISIBILITY

A 5Km surface visibility was chosen for this study because it is much more representative of central Europe and probably approaches the lower limit of visibilities

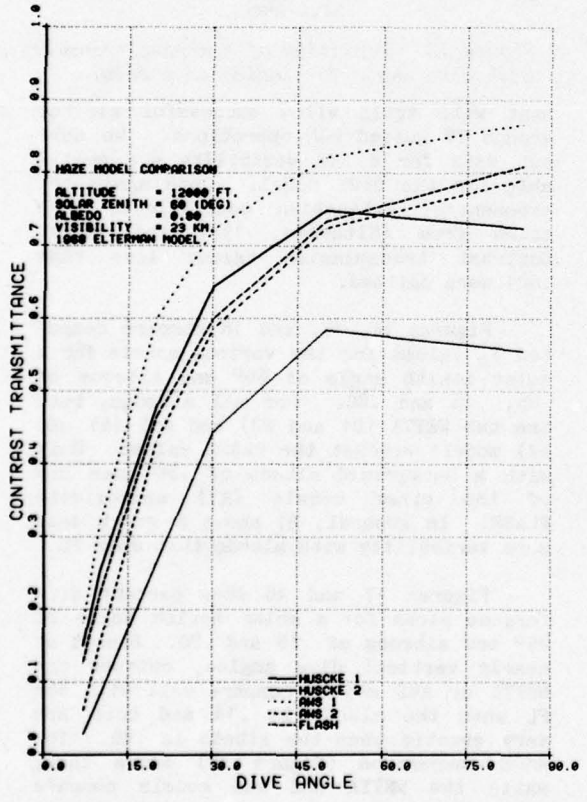

Figure 11. Compairson of contrast transmission versus dive angle for indicated variables.

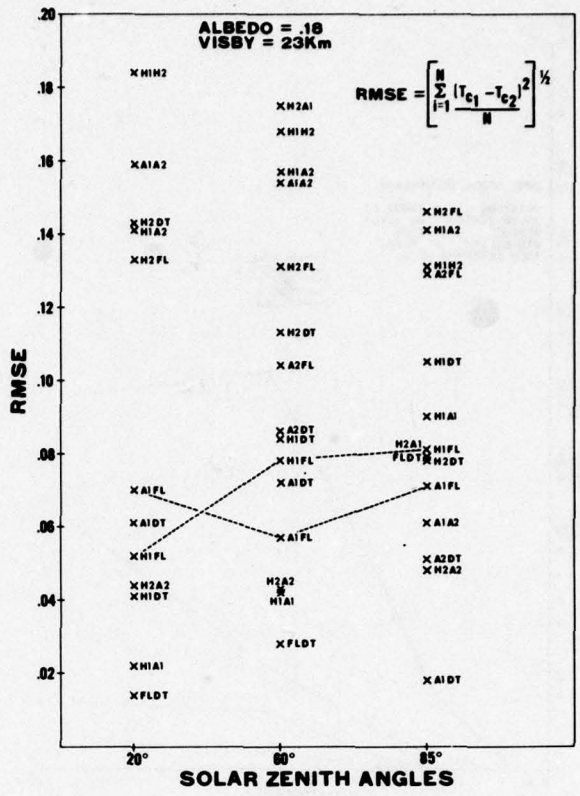

Figure 12. Comparison of RMSE differences for all Dive angles for pairs of models.

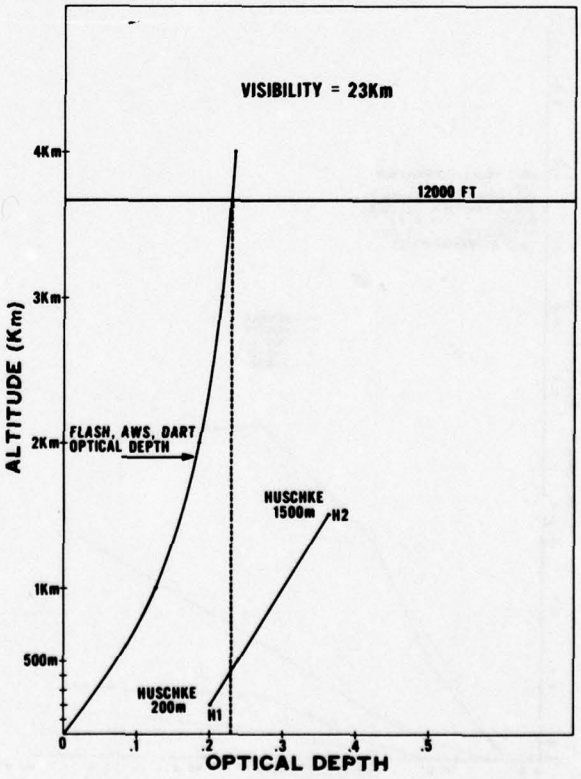

Figure 13. Comparison of the optical depths for the Huschke versus the other models.

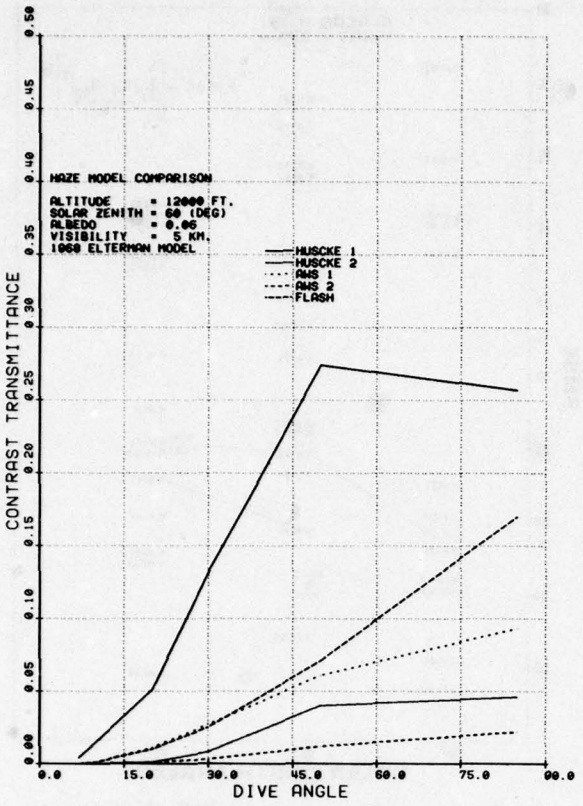

Figure 14. Variation of contrast transmission with dive angle for indicated models.

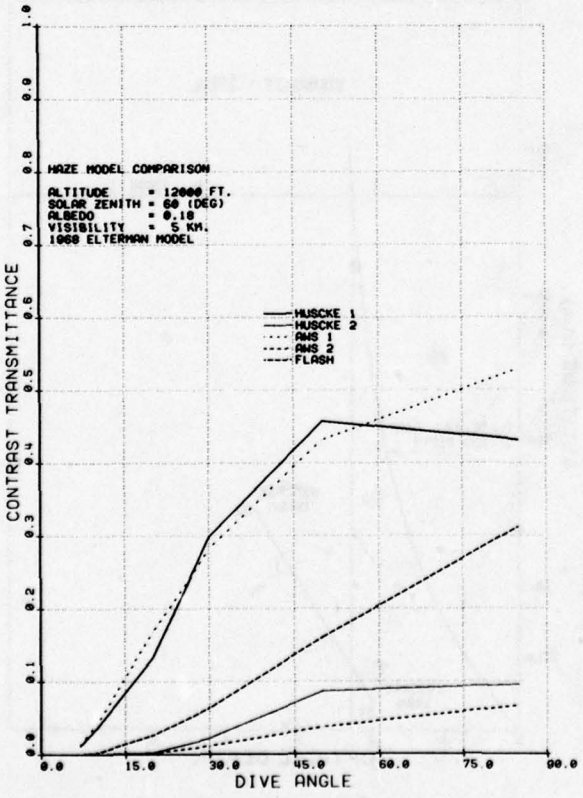

Figure 15. Variation of contrast transmission with dive angle for indicated models.

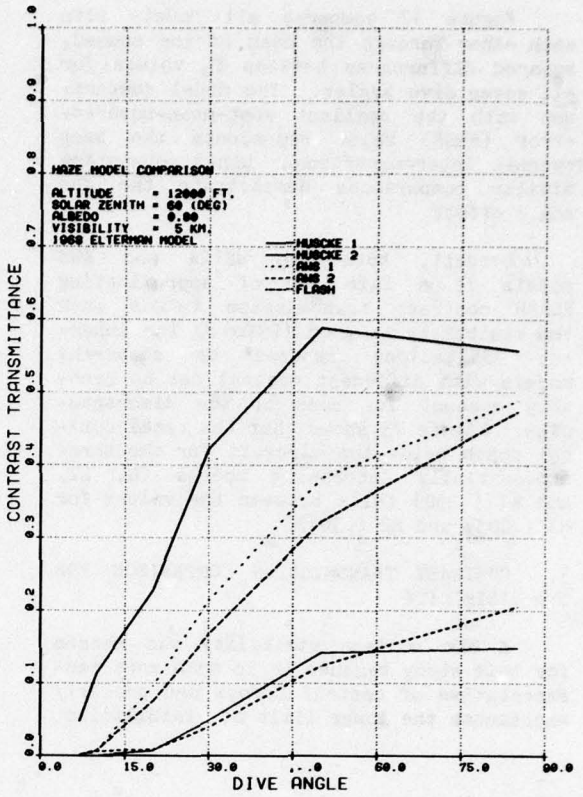

Figure 16. Variation of contrast transmission with dive angle for indicated models.

that will still allow successful air-to-ground TV guided PGM operations. No output data for a 5Km visibility was available for the DART model. Once again the exponential extinction coefficients were taken from (Elterman, 1968 and 1970). Contrast transmission values less than .001 were omitted.

Figures 14, 15, and 16 compare computed T_c values for the various models for a solar zenith angle of 60° and albedos of .06, .18 and .80. For all albedos, both the two WETTA (H1 and H2) and AWS (A1 and A2) models bracket the FLASH values. Only with a background albedo of .80 does any of the other models (A1) approximate FLASH. In general, H1 shows a great deal more variability with albedo than does FL.

Figures 17 and 18 show percent difference plots for a solar zenith angle of 85° and albedos of .18 and .80. Except at nearly vertical dive angles, neither the WETTA or AWS models compare well with the FL when the albedo is .18 and both are very erratic when the albedo is .80. The RMSE comparison (Figure 19) shows that, while the WETTA and AWS models compare well with each other, they do not compare as well with FLASH.

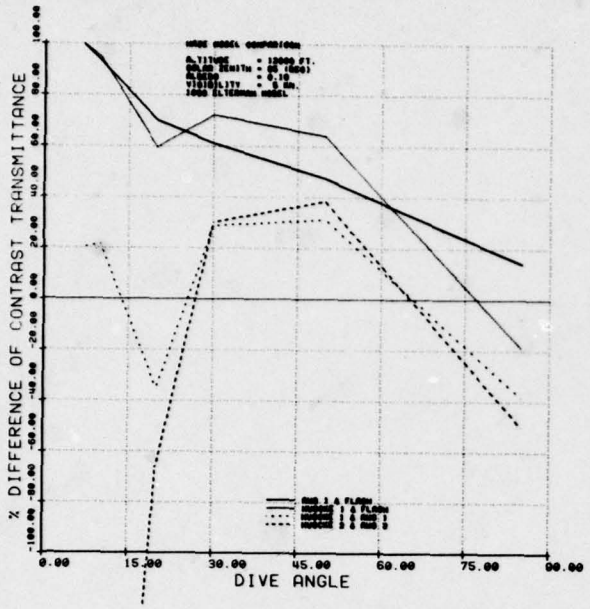

Figure 17. Percent difference of contrast transmission versus dive angle of indicated model pairs.

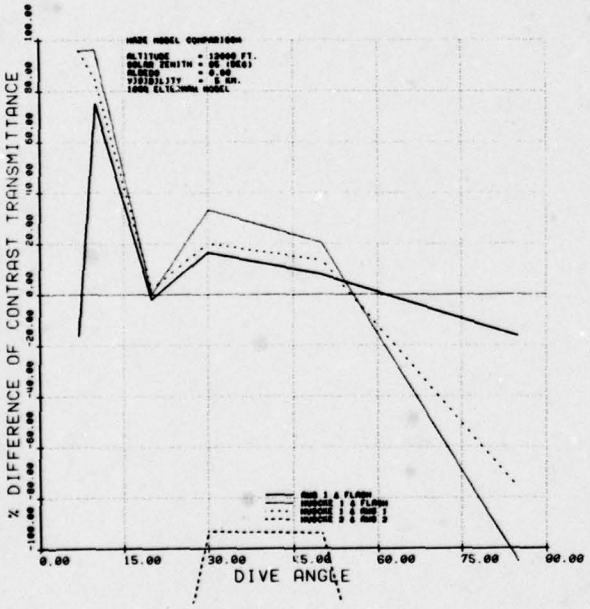

Figure 18. Percent difference of contrast transmission versus dive angle of indicated model pairs.

Figure 20 shows that, when the surface visibility is 5Km, the total optical depth for the FLASH and AWS models (.780) lies about halfway between that for H1 (.325) and H2 (1.28).

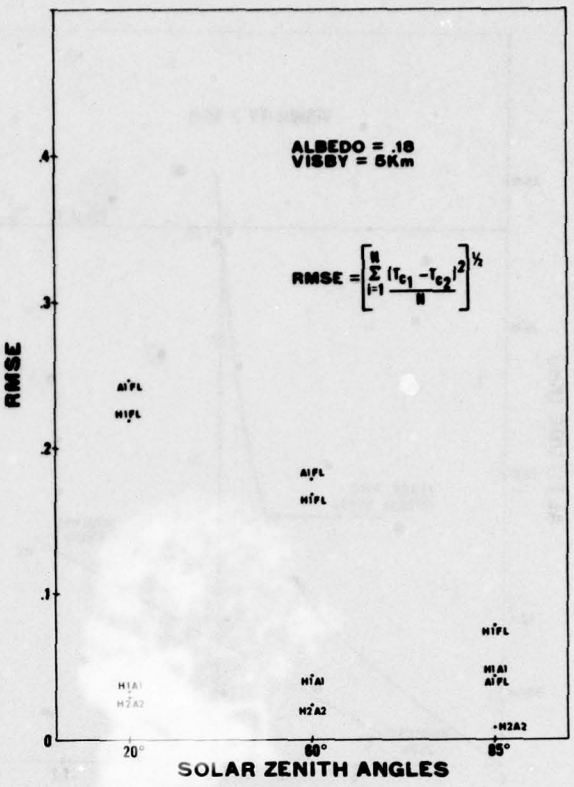

Figure 19. Comparison of RMSE for pairs of models for all dive angles.

4. CONCLUSIONS

Within the constraints imposed by comparing models with different optical depths, the Huschke WETTA model does a good to fair job of approximating FLASH contrast transmission. If one computes T_c values for cases where the FLASH and WETTA profile optical depths are equal, the WETTA values approach FLASH values and sometimes fall within the range of FLASH T_c values for 0°, 90°, and 180° azimuthal angles. Since the three most important input variables (mixing depth, visibility, albedo) to both models are based on unproven forecasting techniques a simple model such as WETTA holds the promise of competing with complex models like FLASH in supporting TV guided PGM operations.

5. REFERENCES

Huschke, R.E., 1976: Atmospheric Visual and Infrared Transmission Deduced from Surface Weather Observations: Weather and Warplanes VI, R-2016-PR.

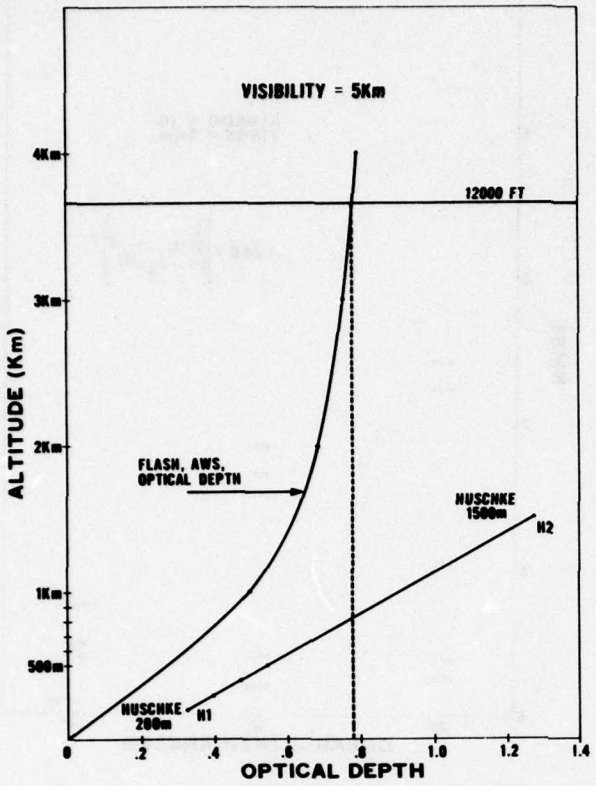

Figure 20. Comparison of optical depths for Huschke versus the FLASH and AWS models.

Elterman, L., 1968: UV, Visible, and IR Attenuation for Altitudes to 50Km, AFCRL Environmental Research Papers No 285, AFCRL - 68-0153.

Elterman, L., 1970: Vertical Attenuation Model with Eight Surface Meteorological Ranges 2 to 13 Kilometers, Tech. Report AFCRL-70-0200.

RESPONSE CHARACTERISTICS OF KNOLLENBERG LIGHT-SCATTERING AEROSOL COUNTERS

R. G. Pinnick and H. J. Auvermann
US Army Atmospheric Sciences Laboratory
White Sands Missile Range, New Mexico 88002

ABSTRACT

Response calculations are presented for four commercially available "Knollenberg" light-scattering aerosol counters: the classical scattering aerosol spectrometer probe (CSASP), the active scattering aerosol spectrometer probe (ASASP), the forward scattering spectrometer probe (FSSP) and the axially scattering spectrometer probe (ASSP). The results show sensitivity of the response to aerosol refractive index for values of indexes characteristic of atmospheric aerosols, and for a particular index, multivalued response for particles in the 0.5-4μm radius range. The response calculations have been validated for two of these instruments (the CSASP and ASASP) by measurement of monodisperse spherical particles. The size resolution of these two instruments is significantly less than advertised by the manufacturer and measurement of irregular particles causes additional loss of resolution.

1. INTRODUCTION

Light-scattering aerosol counters are used for determination of size distribution and number concentration of aerosol particles. These devices work on the principle that as aerosol flows through an illuminated volume, light scattered by a single particle into a particular solid angle is measured and used to determine particle size by electronically classifying response pulses according to their magnitude. Determination of particle size from the response is indirect because of the dependence of the response on factors other than particle size; namely, particle shape and complex index of refraction, lens geometry of the counter optical system and for broadband sources, phototube spectral sensitivity. A number of theoretical and experimental studies of response characteristics of light scattering counters have been done for several commercially available instruments (Cooke and Kerker, 1975; Liu et al., 1974; Quenzel, 1969, 1970; Whitby and Vomela, 1967) and those of special design (Pinnick et al., 1973; Hodkinson and Greenfield, 1965; Oeseburg, 1972; Bakhanova and Ivanchenko, 1973; Gravatt, 1973; Lioy et al., 1975; Heyder et al., 1971; Gebhart et al., 1970; Jacobi et al., 1968). In this paper we investigate the response characteristics of four models of "Knollenberg" (after R. G. Knollenberg, the developer) light scattering counters that have recently become commercially available [Particle Measurement Systems (PMS), Boulder, Colorado]. These instruments are widely used for aerosol measurement, perhaps indiscriminately and without adequate understanding of their response characteristics and limitations. An understanding of these factors is needed to assess errors in measurements made with them. In this paper we attempt to gain this understanding.

Measurements of known monodisperse aerosols are highly desirable for investigating counter response. Thus, in Section 2, a brief account is given of techniques used for generations of both spherical and irregular monodisperse aerosols. In Section 3, a general description of the optical systems of the four Knollenberg counters is given: the classical scattering aerosol spectrometer probe (CSASP), the active scattering aerosol spectrometer probe (ASASP), the forward scattering spectrometer probe (FSSP) and the axially scattering spectrometer probe (ASSP). In Section 4, the theoretical methods used for calculation of these counters' response for spherical particles is given, followed in Section 5, by comparison of theoretical and experimental results for the CSASP and ASASP using both monodisperse spherical and irregular particles. Finally, theoretical response calculations of all of the instruments are presented for spherical particles with refractive indexes representative of atmospheric aerosol constituents.

2. GENERATION OF MONODISPERSE AEROSOLS

To definitively measure the response characteristics of aerosol counters one must be able to generate aerosols of uniform size and different composition (or refractive index). For these studies uniform particles of nigrosin dye, sodium chloride and potassium chlorate were generated by the vibrating orifice technique described earlier (Pinnick et al., 1973). In this technique, the aerosol material is dissolved in a volatile solvent (water) and the resulting solution is forced at high pressure through a small (5-20μm dia.) orifice. A transducer is attached to the orifice and at certain resonant frequencies the jet of solution squirting through the orifice breaks under the action of surface tension into droplets of uniform size. The volatile component of the droplets evaporate

leaving the residual aerosol. The size of the aerosol depends on the concentration of material in solution, orifice size, orifice pressure, viscosity of the solvent used and resonant frequency. For example, one part per thousand nigrosin dissolved in water forced through a 10μm orifice at 20 lb/in.^{2} results in a resonance at 163 kHz and generation of aerosol of 2.12μm radius following evaporation of the solvent. An aerosol particle is generated for each complete vibration of the orifice. The standard deviation in particle size of aerosol made with this technique is on the order of 2% of the mean diameter, not counting particles that coalesce before drying, forming particles two, three and four times larger in volume. This aerosol generation technique is essentially the same as that of Bergland and Liu (1973). In fact, a modified Bergland and Liu generator (commercially available for Thermal Systems, Inc., Minneapolis, Minnesota) was used. The modification consisted of replacing the syringe pump with a compressed air source held at constant pressure.

Monodisperse spherical aerosols of polystyrene, polyvinyltoluene and styrene divinylbenzene latexes, available from Dow Chemical in the hydrosol, were generated by nebulizing hydrosol samples diluted with distilled water. Also, nearly monodisperse crown glass beads, available from Particle Information Services, were generated by simply shaking the beads from their vial container. A summary of monodisperse aerosols utilized in this study is shown in Table 1.

3. THE PARTICLE COUNTERS

A schematic of the CSASP optical system modified from a drawing supplied by the manufacturer is shown in Fig. 1. The instrument is essentially a dark-field microscope with silicon photodiodes used as the detectors. Air containing aerosol being sampled is drawn through the focal point of the collecting optics where individual particles scatter light into the microscope and photodetectors. The source of illumination is a 5 mW He Ne laser tuned to a high order random mode. The optical system has axial symmetry with respect to the direction of the laser source and permits collection of light scattered 4-22° from the direction of forward scattering.

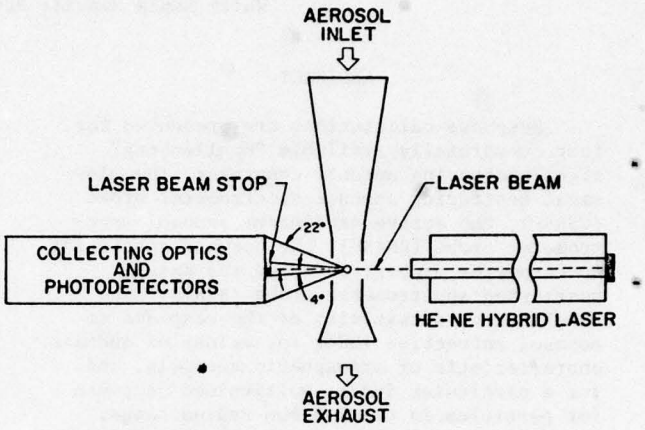

Figure 1. Schematic of the Knollenberg CSASP light scattering aerosol counter.

The output of the photodetector is a measure of the intensity of light scattered by single particles and is fed into a 15-channel pulse-height analyzer. A typical CSASP spectrum for monodisperse aerosol of nigrosin dye is shown in Fig. 2, together with a scanning electron microscope micrograph of several of these particles collected onto a nuclepore

TABLE 1. MONODISPERSE AEROSOLS USED IN THE CSASP AND ASASP RESPONSE MEASUREMENT STUDIES

Type	Shape	Isotropic or Anisotropic	Complex Refractive Index	Sizes(s)	Size Determination	Source
Polystyrene latex	Spherical	Isotropic	1.592-0i*	6 sizes, 0.12-0.545 μm in radius	Manufacturer	Dow Chemical Midland, Michigan
Polyvinyltoluene latex	Spherical	Isotropic	1.581-0i*	1 size, 1.01 μm radius	Manufacturer	Dow Chemical Midland, Michigan
Styrene divinylbenzene latex	Spherical	Isotropic	1.587-0i†	1 size, 2.85 μm mean radius	Manufacturer	Dow Chemical Midland, Michigan
Sodalime crown glass beads	Spherical	Isotropic	1.51-0i*	2 sizes, 5.5 and 10 μm mean radii	Manufacturer ‡	Particle Information Service, Inc., Grants Pass, Oregon
Nigrosin dye	Spherical	Isotropic	1.67-0.26i†	13 sizes, 0.20-3.4 μm in radius	Scanning electron microscope (SEM)	Vibrating Orifice Generator
Sodium chloride	Cubes or assemblies of cubes with hollow centers	Isotropic	1.544-0i*	17 sizes, 0.34-6.54 μm equivalent radius	SEM	Vibrating Orifice Generator
Potassium chlorate	Ellipsoids with hollow centers	Anisotropic	1.52-0i ordinary ray* 1.409-0i extraordinary ray*	20 sizes, 0.25-4.2 μm equivalent radius	SEM	Vibrating Orifice Generator

* Measured at λ = 0.5893 μm (sodium light)

† Measured at λ = 0.6328 μm (He Ne laser light)

‡ Measured at λ = 0.5400 μm

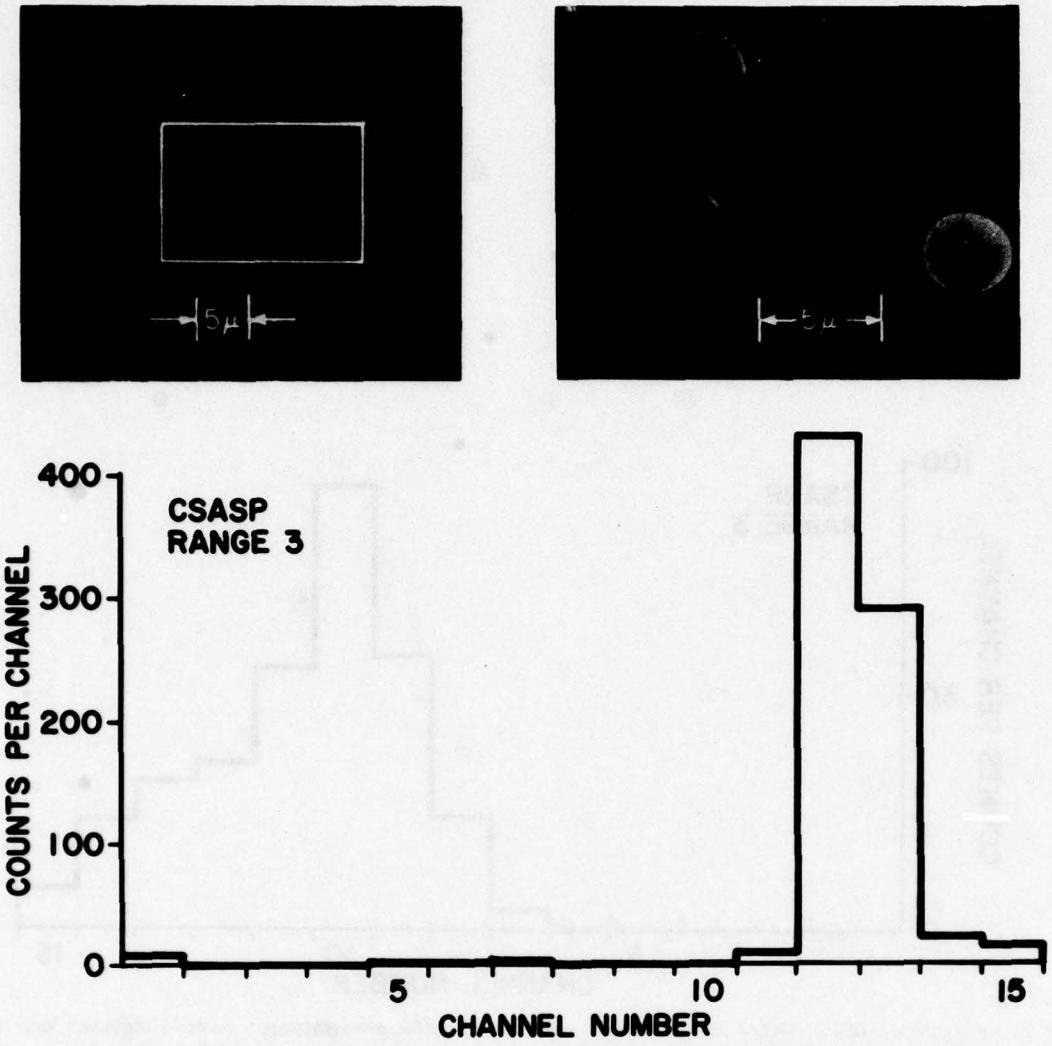

Figure 2. A typical CSAS pulse-height spectrum for monodisperse aerosol. This particular spectrum is for solid particles of nigrosin dye with mean radius 1.78μm; a scanning electron microscope micrograph of several of these particles collected onto a Nuclepore filter is also shown. The black circles are holes in the filter substrate.

filter. The peak in channel 12 corresponds to the most frequently occurring scattered intensity for this aerosol and its position is proportional to the counter response. The spread in the peak is caused by statistical broadening, nonuniform illumination of the sample volume and variation in aerosol size. For irregular particles a broader spectrum of pulse heights is measured, as different particle orientations result in distinctly different response pulses, even for particles nearly identical in shape. The spectrum in Fig. 3 shows this effect for uniform slightly irregular particles of sodium chloride; a micrograph of typical salt particles corresponding to this spectrum is also shown in the figure. This spectrum would be more nearly Gaussian if pulse height were plotted on the abscissa rather than channel number, as the channels are not of equal width. The size resolution of the instrument is obviously degraded for irregular particles.

The light-collecting optics of the ASASP instrument is identical to that of the CSASP, but in this case the particle illumination source is the intra-cavity standing wave radiation of a hybrid 2 mW He-Ne laser (Schuster and Knollenberg, 1972). An advantage of utilizing the open-cavity source is the high energy density available (about 1 kW/cm^2 according to PMS), permitting measurement of particles down to about 0.1μm radius. Pulse height spectra for monodisperse spherical and irregular particles for this instrument are similar to those for the CSASP.

Only a small fraction of the particles which pass through the relatively large intakes of the CSASP and ASASP instruments, which consist of a conical horn with minimum diameter 3.3 cm, is counted. The relatively small volume through which particles must pass before they are counted is determined opto-electronically. Signals which derive from particles that do not

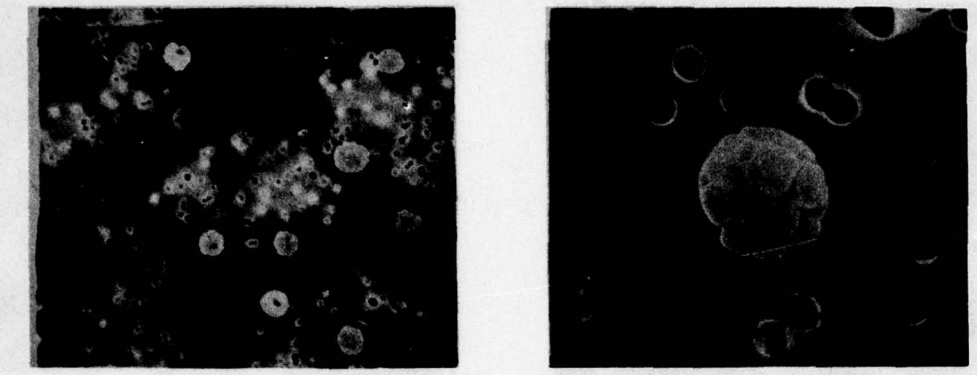

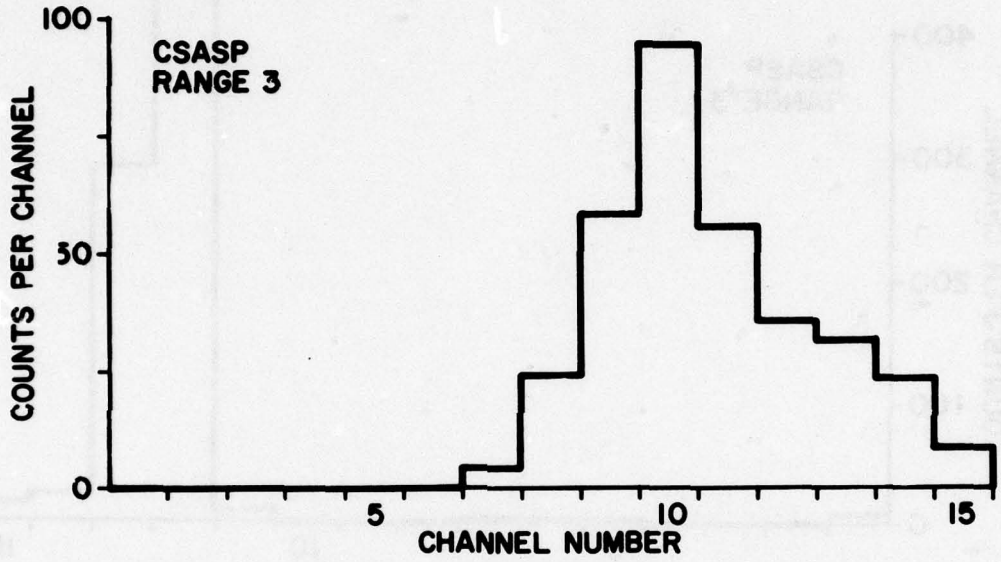

Figure 3. A typical CSASP pulse height spectrum for monodisperse aerosol particles that are irregular in shape. This spectrum is for sodium cloride particles with mean equivalent radius 1.53μm (in the sense of spheres of equal cross-sectional area); a micrograph of several of these particles collected onto a Nuclepore filter is also shown.

flow through a particular volume which is within a sufficiently uniformly illuminated part of the laser are out-of-focus and electronically rejected.

Both FSSP and ASSP instruments are similar to the CSASP in that they are forward-scattering instruments and the illumination source is a He Ne laser. The optical systems permit collection of light scattered 3-13° (for the FSSP) and 5.3-12.4 (for the ASSP) from the direction of forward scattering. In both instruments the coincidence scheme for particle detection involves a time-of-flight measurement of single particles traversing the laser beam and subsequent rejection of particles passing through the beam edges.

The characteristics of the light-scattering counters are summarized in Table 2.

TABLE 2. CHARACTERISTICS OF KNOLLENBERG LIGHT SCATTERING AEROSOL COUNTERS

Instrument	Light Source	Light-collecting Optics* α,β	Flow Rate of Active Area
CSASP	5 mW He Ne laser	4-22	0.15 cm^3/sec
ASASP	2 mW He Ne laser (intra-cavity)	4-22	0.1 cm^3/sec
FSSP	5 mW He Ne laser	3-13	0.25 mm^2†
ASSP‡†	5 mW He Ne laser	5.3-12.4	0.4 mm^2†

* All instruments have axial symmetry with respect to the direction of the laser source and the polar angles α,β refer to a cone subtending angles α through β from the direction of forward scattering.

† Flow rate can be determined from active area by multiplying by the speed at which air (containing aerosol) passes through the instrument.

‡ The manufacturer has produced two models of the ASSP having different optics, but only one of these has been studied here. The other collects light scattered 6.7-14.4° from the direction of forward scattering.

4. *THEORETICAL RESPONSE CALCULATIONS*

In this section the theoretical methods used for calculating particle counter response are outlined using Mie theory for the CSASP, FSSP and ASSP instruments, and using a solution for scattering of standing wave radiation by a spherical particle for the ASASP.

From Mie theory for a polarized plane wave having wavenumber k incident on a sphere

with radius r the scattering cross-section (in cm^2 per particle) for radiation scattered into a solid angle having axial symmetry with respect to the direction of the light source is:

$$R = \frac{\pi}{k^2} \int_{\Omega} \{|S_1|^2 + |S_2|^2\} \sin\theta \, d\theta. \qquad (1)$$

where $S_1(x,m,\theta)$ and $S_2(x,m,\theta)$ are the Mie scattering amplitude functions corresponding to light polarized with electric vector perpendicular and parallel to the plane of scattering. They depend on the particle size parameter $x = kr$, the refractive index m, and the scattering angle θ. The angular integration is over the solid angle Ω subtended by the light-collecting optics.

Because the scattering for the ASASP is for a particle in a standing wave, we calculate the scattering amplitude S' by adding the Mie scattering amplitudes for plane waves traveling in opposite directions: $S'(\theta) = S(\theta) + S(\pi - \theta)$. The response for the ASASP is then

$$R = \frac{\pi}{k^2} \int_{\Omega} \{|S_1(\theta) + S_1(\pi - \theta)|^2 + |S_2(\theta) + S_2(\pi - \theta)|^2\} \sin\theta \, d\theta. \qquad (2)$$

5. RESULTS

Measurements of the CSASP and ASASP response to monodisperse spherical latex and nigrosin dye aerosols are presented in Figs. 4 and 5 as open and solid circles. The radii of the latex particles are those advertized by Dow Chemical; those for nigrosin were measured by scanning electron microscope. The error in radius is not more than the width of the circles marking the measurements.

The measured response is expressed in cross-section per particle normalized to the computer calculated theoretical results (solid-line curves) for best fit to the theoretical response for latex Aerosols. This single normalization was used for all experimental results for each instrument. Polystyrene, polyvinyltoluene and styrene divinylbenzene latex aerosols actually have three similar but distinct indexes of refraction (see Table 1); however, the response curves for these indexes are not significantly different and therefore only the response curve for polystyrene latex with index 1.592-0i is shown. Error in measurement of response is due to the finite width of the instrument pulse height channels and instrument drift. Repeated measurement of polystyrene latex particles showed instrument drift to be ±10% in pulse height over a period of one month.

Also shown in Fig. 4 is the CSASP response to relatively narrow polydispersions of glass beads having refractive index 1.51-0i. The measured response is denoted by the squares and the theoretical response by the broken curve. The standard deviation in particle size of the

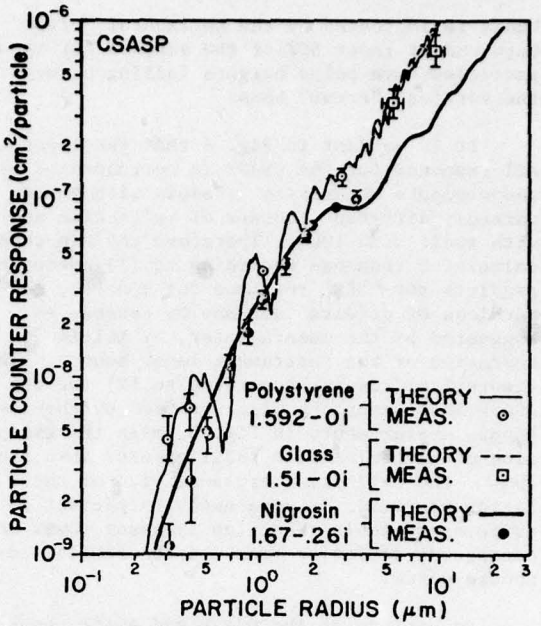

Figure 4. Knollenberg CSASP response: measured (circles and squares) and calculated using Mie scattering theory (curves) for single spherical particles versus particle size. The measurements have been normalized for best fit to the calculated response for polystyrene latex particles with refractive index m = 1.592-0i. The theoretical curve for glass beads with refractive index 1.51-0i extends down only to about 5μm radius.

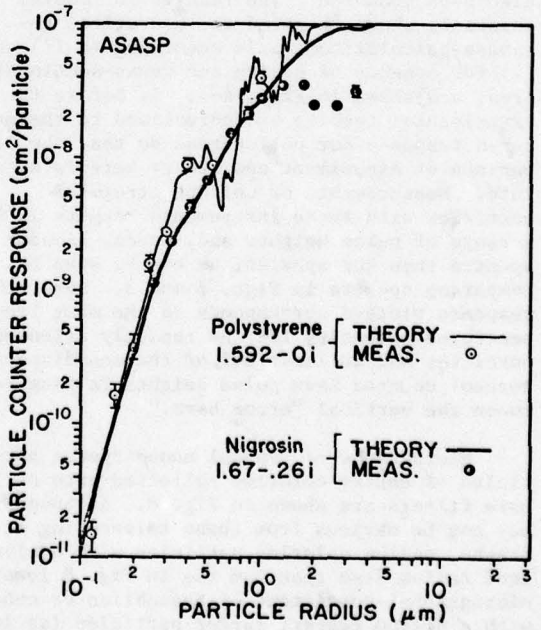

Figure 5. Knollenberg ASASP response: measured (circles) and calculated using a solution for particle scattering in a standing wave (curves) for single spherical particles versus particle size. The measurements have been normalized for best fit to the calculated response for polystyrene latex particles with refractive index km = 1.592-0i.

beads is indicated by the horizontal "error" bars and at least 68% of the signals for these particles have pulse heights falling between the vertical "error" bars.

It is evident in Fig. 4 that the theoretical response for the CSASP is corroborated by measurements on uniform aerosols with three markedly different indexes of refraction and with radii 0.30-10μm. Therefore the Mie theory calculated response according to (1) adequately predicts the CSASP response for spheres, regardless of effects that may be caused, as suggested by the manufacturer, by multimode operation of the instrument laser source. The theoretical results according to (2) for the ASASP instrument are also verified by the response measurements in Fig. 5, with the exception of particles with radii greater than about 1μm. The extinction cross-section of these larger particles is apparently sufficient to cause appreciable reduction in laser power and consequent deviation from the theoretical response curve.

Comparison of the CSASP and ASASP theoretical response curves for both absorbing and nonabsorbing aerosols show they are quite similar, the ASASP having high frequency wiggles in its response for particles in the resonance region (i.e., in the region where particles have sizes comparable to the wavelength) which are not found in the CSASP response.

The CSASP and ASASP response to slightly irregular randomly oriented uniform particles of sodium chloride and potassium chlorate have also been measured. The results for sodium chloride, shown compared to theoretical response calculations again according to (1) and (2) for spheres of equivalent cross-sectional area, are shown in Figs. 6-7. As before the experimental results are normalized to the measured response for polystyrene so that the comparison of experiment and theory here is absolute. Measurements of uniform irregular particles with these instruments results in a range of pulse heights and, hence, broader spectra than for spheres, as can be seen by comparing spectra in Figs. 2 and 3. Here, the response plotted corresponds to the most frescattered intensity for the randomly oriented particles and at least 68% of the monodisperse aerosol counted have pulse heights falling between the vertical "error bars."

Micrographs of typical monodisperse particles of sodium chloride collected onto nuclepore filters are shown in Fig. 8. Although it may not be obvious from these telescoping micrographs, sodium chloride particles with equivalent radius less than 3μm (as in Fig. 8 lower micrographs) consistent of assemblies of cubes with a hollow center; larger particles (as in Fig. 8 upper micrographs) have five flat sides and one rounded side with a hole in the center.

For the CSASP both the sodium chloride and potassium chlorate results show: (1) rough agreement of measurement and theory for equivalent radii $1.5\mu m < r < 4\mu m$, (2) the resonance behavior in the calculated response is not evident in the measured response, (3)

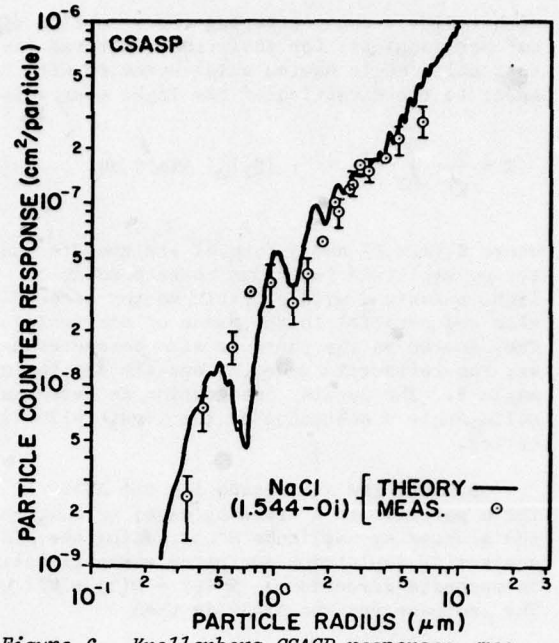

Figure 6. Knollenberg CSASP response: measured for irregular particles of sodium chloride (circles) and calculated for spheres of equal cross-sectional area using Mie scattering theory (curve) for single particles versus particle size. The measurements are relative to the polystyrene measurements which have been normalized for best fit to the calculated response for those particles (see Fig. 4).

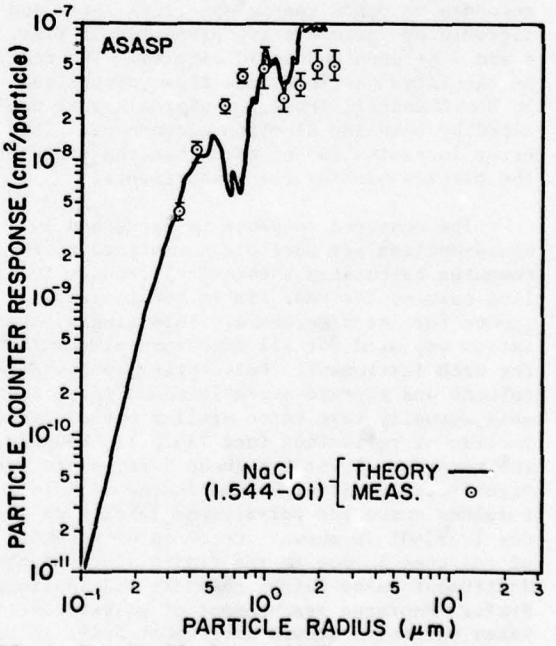

Figure 7. Knollenberg ASASP response: measured for irregular particles of sodium chloride (circles) and calculated for spheres of equal cross-sectional area using the theory for particle scattering in a standing wave (curve) for single particles versus particle size. The measurements are relative to the polystyrene measurements which have been normalized for best fit to the calculated response for those particles (see Fig. 5).

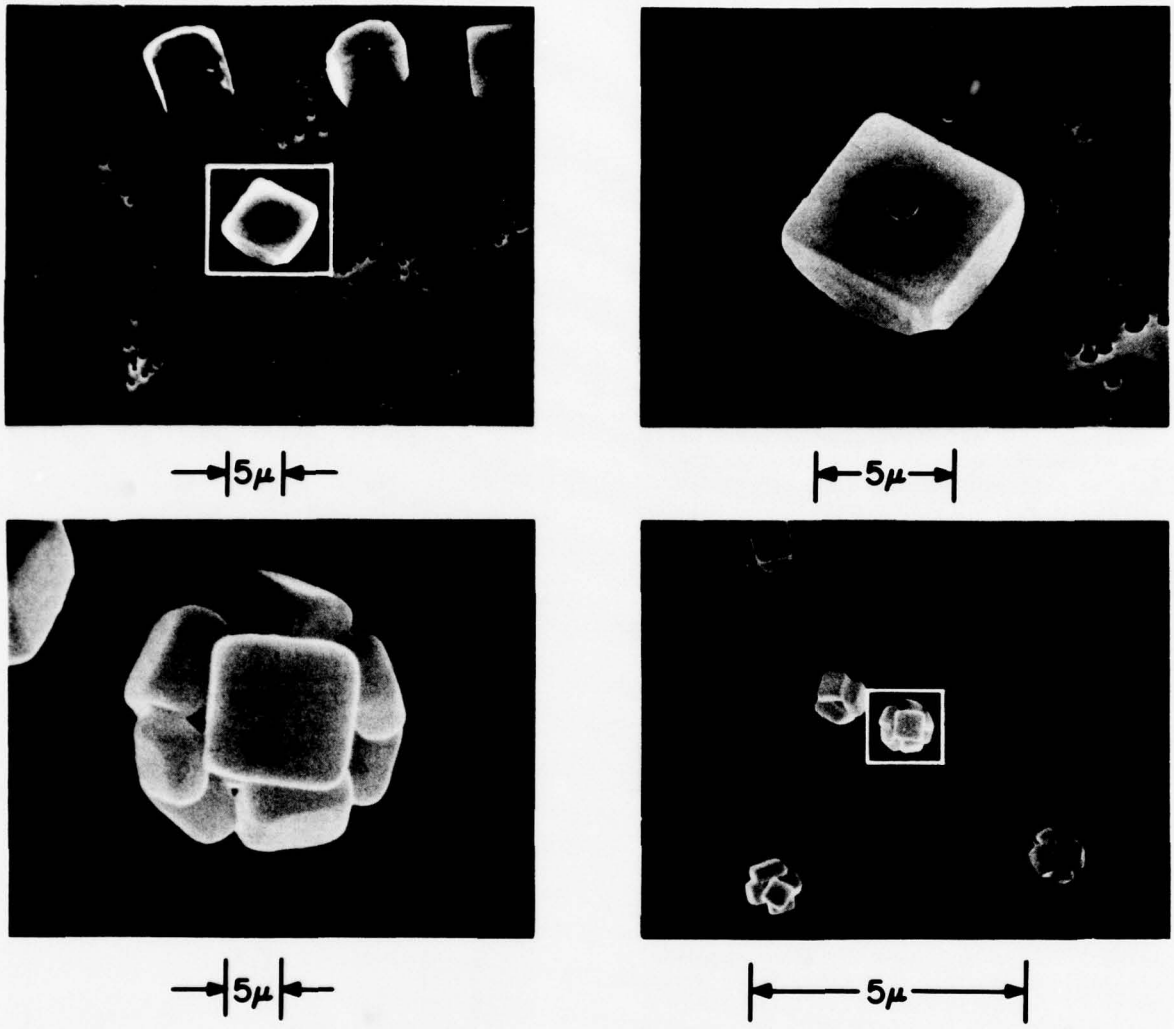

Figure 8. Scanning electron micrographs of typical monodisperse particles of sodium chloride used to measure the CSASP and ASASP response characteristics.

slightly smaller response measured than predicted for particles with equivalent radius $\tilde{>}$ 4μm and (4) a resonance in the measured response for particles with equivalent radius 0.8μm which we speculate may be a consequence of the shell-like structure of the particles.

The following geometrical optics argument is offered to explain the general agreement of the measured response for irregular particles and that predicted for spheres of equal cross-sectional area, providing equivalent radii are between 1.5μm and about 4μm. First, particles must have equivalent radii $r \tilde{>} 1.5\mu m$ (or size parameters $x > 15$) for geometric optics to apply. Thus, if particles have $r \tilde{>} 1.5\mu m$ and if light scattered within the forward lobe is sensed, diffraction is dominant and to the first order only the projected area of the particle is important. Thus, low-angle scattering constitutes a somewhat reliable measure of particle projected area for particles of irregular shape, providing they are sufficiently large ($r \tilde{>} 1.5\mu m$). On the other hand, they cannot be too large, since if light scattered primarily outside the forward lobe is sensed, as it is for particles with equivalent radius $r \tilde{>} 4\mu m$, reflection and refraction contributions are liable to produce a response which deviates considerably from that of a sphere of equal area, as the measurements show in Fig. 6. These measurements suggest that the CSASP response to even larger ($\tilde{>}$ 6μm equivalent radius) irregular particles might result in significant underestimation of particle sizes. Response measurements for more irregular and larger particles is an obvious deficiency of this work.

For the ASASP the irregular particle measurements show agreement of measured and theoretical response for particles with equivalent radius $r \tilde{<} 0.5\mu m$, but disagreement for larger sizes and virtually no size resolution for particles with $r \tilde{>} 0.5\mu$.

For the special case of spherical particles the measurements corroborate the theoretical response curves for both the CSASP and ASASP, with the exception of particles having radius $\tilde{>}$ 1μm for the ASASP, which apparently

cause significant reduction in laser power. Confidence can, thus, be placed in response calculations for materials with refractive indexes different from those studied here. Response calculations for refractive indexes typical of atmospheric constituents at λ = 6328 Å ranging from that of water (m = 1.33-0i) to carbon (m = 1.95-0.66i) were consequently carried out and are presented in Figs. 9 (CSASP) and 10 (ASASP). The pulse height discriminator levels, as set by the manufacturer for our particular models of these instruments, are shown by the tick marks in these figures. There are 15 particle size channels for each "range" of the instruments; channels 1, 5, 10, and 15 are labeled between the appropriate tick marks. Changing range is merely an adjustment of amplifier gain for the CSASP (for the ASASP both amplifier gain and discriminator level settings are different for each range) and has the effect of shifting the size range of sensitivity.

We warn the user of these counters that discriminator levels for different CSASP and ASASP instruments are not necessarily set as shown in Figs. 9 and 10, as the manufacturer has a number of different schemes for setting these levels. Nevertheless, the manufacturer utilizes several sizes of polystyrene, polyvinyltoluene and styrene divinylbenzene latex particles and glass beads in the factory "calibration," identified according to what channel they are counted as per the instrument manual supplied with each instrument. This information enables the user to infer positions of discriminator level settings relative to the theoretical results presented here.

It is hardly necessary, in light of these results, to stress the fact that for spherical particles both the CSASP and ASASP response is sensitive to aerosol refractive index over the range of realistic values for these indexes. For example, for the CSASP (Fig. 9), water particles (m = 1.33-0i) with radii 5μm have identical response to dust particles (m = 1.50-0.005i) with radii 10μm. Even for aerosol of known composition there are, on some ranges of the instruments, discriminator levels set in regions of multivalued response. Thus, for the CSASP, water particles with radii 0.63, 0.94 and 1.3μm all have the same response. Nevertheless, size distribution information for a polydispersion of homogeneous particles can be determined by reducing the number of channels to avoid these regions.

For example, if the CSASP is used to measure fog droplets the channels can be grouped according to the response curve for water to avoid regions of multivalued response. This channel grouping is indicated by the heavy tick marks in Fig. 9. The channels are grouped with less size resolution than the response curve dictates because, in practice, statistical spectra broadening effects result in some channel cross sensitivity. As was pointed out previously, even measurement of monodisperse spherical aerosol results in a range of pulse heights and identical particles are not counted entirely in one particle size channel. Therefore, use of discriminator levels set near regions of multivalued response has been avoided.

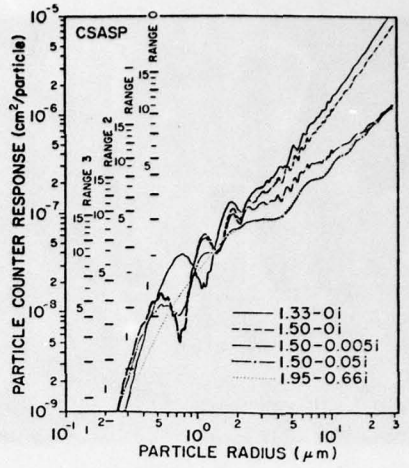

Figure 9. Mie theory response calculations for the Knollenberg CSASP particle counter for water particles with refractive index 1.33-0i, ammonium sulfate with approximate index 1.5-0i, atmospheric dust with indexes 1.50-0.005i and 1.5-05i, and carbon with index 1.95-066i. The tick marks indicate the pulse-height discriminator levels as set by the manufacturer for the counter. Channels 1, 5, 10 and 15 are labeled between the appropriate tick marks for the different ranges of the instrument. The heavy tick marks indicate the pulse-height discriminator levels used to avoid regions of multivalued response under the assumption that particles are water.

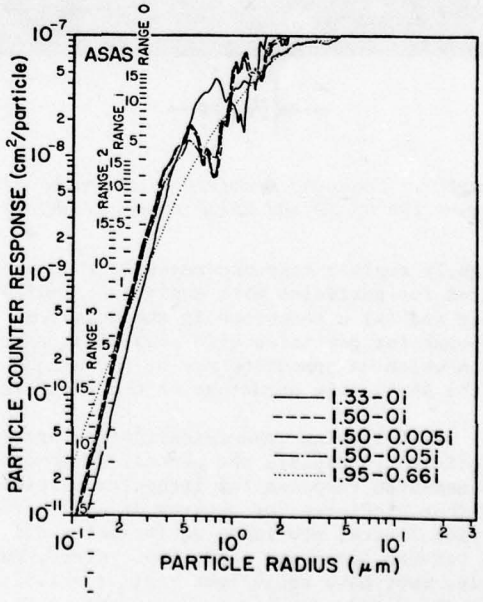

Figure 10. Response calculations for the Knollenberg ASASP particle counter using a solution for particle scattering in a standing wave for particles with refractive indexes as in Figure 9. The tick marks indicate the pulse height discriminator levels as set by the manufacturer for the counter. Channels 1, 5, 10 and 15 are labeled between the appropriate tick marks for the different ranges of the instrument.

This scheme reduces the number of size channels for each range from 15 to 8. Specific channel size limits for the different ranges of the instrument can be determined from Fig. 9 by noting at what radii on the water response curve the appropriate heavy tick marks correspond. Measurements of spherical particles having refractive indexes different from water would, of course, require different channel groupings and size definitions.

If the manufacturer's calibration is used in determination of size distribution of polydispersions of spherical particles, artificial knees or bumps in the distribution will appear in regions of multivalued response. The reason is that in these regions particles with a relatively large range of sizes produce response pulses in a small range of pulse heights; whereas, between regions of multivalued response, particles with a relatively narrow range of sizes produce response pulses in a comparable range of pulse heights. We have seen the resulting artifacts in the manufacturer calibration-derived distribution for our CSASP both in measurements of atmospheric fog and in measurements of laboratory generated polydispersions of oil droplets. The positions of these knees in the distributions are of course different for particles with different refractive index. We note recently reported measurements of atmospheric aerosols by Livingston (1978) with the Knollenberg ASASP show knees in the distribution in the region of multivalued response for water droplets (as per Fig. 10) which, we suggest, are simply artifacts of the instrument response and not real.

The FSSP and ASSP light scattering counters are similar to the CSASP; the essential difference being geometry of their light-collecting optics (see Table 2). Theoretical response calculations for these instruments, again according to (1), are presented in Figs. 11 and 12. Like the CSASP, the response is sensitive to particle refractive index over a range of indexes characteristic of atmospheric aerosols; the ASSP has particularly poor resolution in the 1-4μm radius range. These instruments utilize near-forward scattering and as argued previously should offer a somewhat reliable measure of particle cross-section for irregular particles less than a certain size. Otherwise, measurement of their response to known irregular particles is needed.

A terse summary of our findings for the four Knollenberg light scattering counters is given in Table 3. For the CSASP and ASASP instruments, the manufacturer generally specifies more particle size channels than can be justified, particularly for particles with radii greater than 0.5μm. The theoretical results suggest the same is true for the FSSP and ASSP, although we do not have information on the discriminator level settings for these instruments.

Finally, although we did not address the question of the counting efficiency of these light scattering counters in this paper, we are aware of two potential problems with the CSASP instrument that might be important for

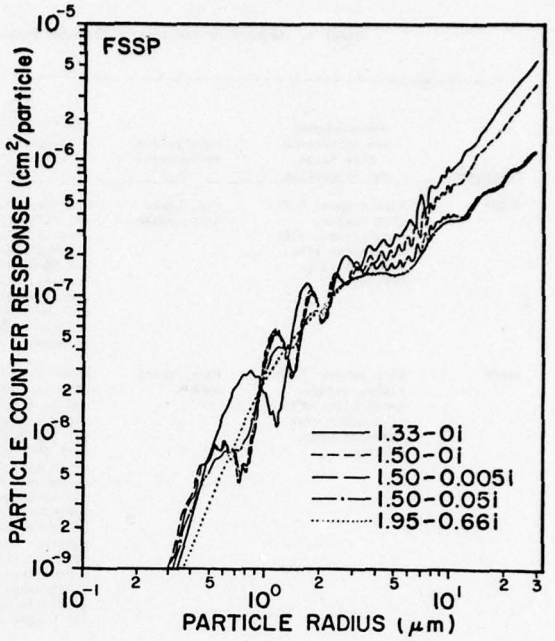

Figure 11. Mie theory response calculations for the Knollenberg FSSP particle counter for particles with refractive indexes as in Fig. 9.

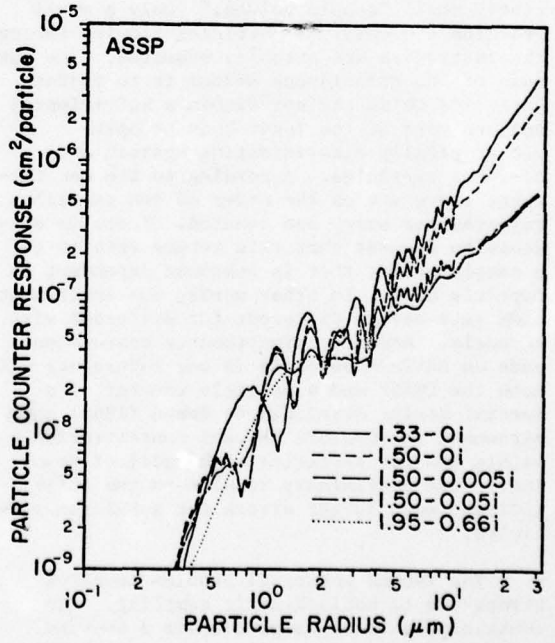

Figure 12. Mie theory response calculations for the Knollenberg ASSP particle counter for particles with refractive indexes as in Figure 12.

TABLE 3. SUMMARY OF FINDINGS OF RESPONSE CHARACTERISTICS OF KNOLLENBERG LIGHT-SCATTERING AEROSOL COUNTERS

Instrument	Manufacturer Specifications Size Range and Resolution	Manufacturer Recommended Use*	Findings (this work): Size Range and Resolution		
			Homogeneous Spherical Aerosols of Uniform Composition	Homogeneous Spherical Aerosols of Mixed and Unknown Composition	Irregular Particles
CSASP	Size range: 0.22-16μm radius. Resolution: ±5% of maximum size for each range setting.	Fog, haze, dust, smoke.	Size range depends on aerosol refractive index: for water droplets (m = 1.33-0i) 0.23-14μm, for dust (m = 1.50-0.005i) 0.21-50μm radius. Resolution less than advertised; channels must be grouped to avoid regions of multivalued response.	Size range: 0.20-50μm radius. Resolution severely degraded for particles with radius greater than 0.5μm.	Size range unknown; however, slightly irregular particles have response comparable to spheres of equal area, providing equivalent radii are between 1.5 and 4μm.
ASASP	Size range: 0.085-1.50μm radius. Resolution: ±5% of maximum size for each range setting.	Haze, dust, smoke.	Lower size limit depends on aerosol refractive index and is 0.096μm radius for water droplets (m = 1.33-0i) and 0.080μm radius for dust (m = 1.50-0.005i). Upper size limit about 1-1.5μm radius; however, particles larger than 1.0μm apparently cause reduction of laser power and some are counted. Good size resolution for particles with radius less than 0.5μm; multivalued response and generally poor resolution for larger sizes.	Size range: 0.05μm to about 1-1.5μm radius; see previous comment concerning particles larger than 1.0μm radius. Relatively good resolution for particles with radius less than 0.5μm; poor resolution for larger sizes.	Size range for slightly irregular particles about the same as for spheres of equal area. Spectra broadening significantly degrades resolution.
FSSP and ASSP	Size range: 0.22-22μm radius. Resolution: ±5% of maximum size for each range setting.)	Fog, clouds, dust.	Size range and resolution depends on aerosol refractive index. Multivalued response for particles with radii greater than 0.5μm. Resolution comparable to CSASP.	Resolution severely degraded for particles with radii greater than 0.5μm.	Unknown.

* Manufacturer comments that caution should be exercised in measurement of high aerosol concentrations for all probes.

the other instruments too. The first concerns the coincidence scheme utilized in the CSASP to reject or accept particles depending on whether or not they pass through the relatively small "sample volume." Only a small fraction (~0.003%) of particles flowing through the instrument are actually measured. The purpose of the coincidence scheme is to reject particles which are not within a sufficiently uniform part of the laser beam by opto-electronically discriminating against out-of-focus particles. According to the manufacturer there are on the order of ten particles rejected for every one counted. There is evidence to suggest that this scheme results in a sample volume that is somewhat dependent on particle size. In other words, the instrument flow rate may be different for different size channels. However, simultaneous measurements made on uniform aerosols in our laboratory with both the CSASP and a particle counter of a special design developed by Rosen (1968) show agreement in absolute aerosol concentration to within 30% for particles with radii of about 1μm. Some preliminary results on the ASASP indicate much larger errors for submicron particles.

The second potential problem concerns errors due to nonisokinetic sampling. Air containing aerosol sampled under a no-wind condition with our particular aspirated CSASP flows at 340 l/min through a conical intake tube 45 cm long with maximum diameter 10 cm and minimum diameter 3.3 cm. The fraction of particles lost in this tube due to gravitational settling depends strongly on size and is estimated 7% for 15μm radius particles, increasing to 18% for 25μm radius particles, under the assumption particle density is 1 gcm^{-3}. The magnitude of errors due to nonisokinetic sampling during windy conditions is unknown.

6. CONCLUSIONS

Theoretical response calculations for two models of Knollenberg light scattering aerosol counters (the CSASP and ASASP) have been compared to measurements of monodisperse aerosols of different size and refractive index. The theoretical predictions for the CSASP, which are based on Mie theory, are verified by the measurements on spherical particles with radii 0.3-10μm. The ASASP predictions are derived from a solution for scattering by a sphere in a standing wave and are also validated by measurements on spherical particles with radii 0.12-1μm. Particles larger than 1μm radius, which is near the upper limit of detectability for the ASASP, apparently have sufficiently large extinction cross-section to cause significant reduction in laser power and disagreement of predicted and measured response results. In any case both instruments show sensitivity of response to aerosol refractive index over the range of values of indexes realistic for atmospheric aerosol. This results in poorer size resolution than advertised for these counters, as two aerosol particles differing in size by as much as a factor three may be counted in the same size channel. For aerosol of known composition size resolution is much improved, although not as good as advertised, since size channels must be grouped to avoid regions of

multivalued response. As might be expected, measurement of irregular particles causes further degadation in resolution, because of the importance of particle orientation.

For the Knollenberg FSSP and ASSP light scattering counters the theoretical predictions of response for spheres again show sensitivity to aerosol refractive index and the attending loss of size resolution.

7. REFERENCES

Bakhanova, R. A., and L. V. Ivanchenko, 1973: *J. Aerosol Sci.*, 4, 485.

Bergland, R. N., and B. Y. H. Liu, 1973: *Envir. Sci. Techn.*, 7, 147.

Cooke, D. D., and M. Kerker, 1975: *Appl. Opt.*, 14, 734.

Gebhart, J., J. Bol, W. Heinze, and W. Letschert, 1970, *Staub.*, 30, 5.

Gravatt, G. C., 1973: *J. A. P. C. A.*, 23, 1035.

Heyder, J., C. Roth, and W. Stahlhofen, 1971: *J. Aerosol Sci.*, 2, 341.

Hodkinson, J. R., and J. R. Greenfield, 1965: *Appl. Opt.*, 4, 1463.

Jacobi, W., J. Eichler, and N. Stolterfont, 1968: *Staub*, 28, 314.

Lioy, P. J., D. Rimberg, and F. J. Haughey, 1975: *J. Aerosol Sci.*, 6, 183.

Liu, B. Y. H, R. N. Bergland, and J. K. Agarwal, 1974: *Atmos. Environ.*, 8, 717.

Livingston, P. M., 1978: *Appl. Opt.*, 17, 818.

Oeseburg F., 1972: *J. Aerosol Sci.*, 3, 307.

Pinnick, R. G., J. M. Rosen, and D. J. Hofmann, 1973: *Appl. Opt.*, 12, 37.

Quenzel, H., 1969: *Appl. Opt.*, 8, 165.

____, 1970: *Appl. Opt.*, 9, 1931.

Rosen, J. M., 1968: *J. Geophys. Res.*, 73, 479.

Schuster, B. G., and R. Knollenberg, 1972: *Appl. Opt.*, 11, 1515.

Whitby, K. T., and R. A. Vomela, 1967: *Envir. Sci. Techn.*, 1, 801.

SENSITIVITY ANALYSIS AND PARAMETERIZATION OF IR CONTRAST TRANSMISSION

Major Kenneth P. Freeman

Air Force Global Weather Central

Offutt Air Force Base, Nebraska

ABSTRACT

The transmission of infrared contrast through the atmosphere is modeled with the use of the AF Geophysics Laboratory computer code LOWTRAN 4 to compute transmittance and radiance along atmospheric slant paths. A sensitivity analysis of apparent contrast is conducted, and the results used in an attempt to model lock-on range using a multiple regression technique.

1. INTRODUCTION

The advent of electro-optical sensors in the field of military weapons systems has brought about a growing requirement for highly specialized meteorological support, particularly to precision guided munitions. Infrared and visible light sensors such as IR contrast seekers, laser designators, and TV guided munitions, demand quantitative forecasts of the propagation of radiation through an atmosphere laden with a variety of energy absorbing, emitting, and scattering constituents.

Direct radiative transfer computations are costly and complex and, therefore, not satisfactory for operational employment either in the field or in meteorological forecast centers. The great temporal and spatial variability of the atmosphere and the global responsibilities of the military meteorological services drive the demand for a simplified approach to computation of meteorological parameters of importance to electro-optical sensors. This paper is a report on a rather simple empirical approach to parameterizing, or modelling, the contrast transmission through the atmosphere, based on an analysis of the sensitivity of contrast transmission to atmospheric and external factors.

For the sake of simplicity, this study has been restricted to the infrared spectrum, specifically the 8 to 12 micrometer "window". This choice of spectral interval eliminates most considerations of scattering and target or background reflectivity and illumination angle. By ignoring the optical and electronic properties of sensors, the study can be reduced to one of atmospheric effects only.

A stepwise multiple regression technique was used in an attempt to model contrast transmission and lock-on range (LOR). Only modest success was achieved in this initial attempt to derive a predictive equation for LOR based on input parameters which may be easily measured or inferred. The statistical approach to LOR forecasting is reasonable, however, and may warrant further work.

2. CONTRAST TRANSMISSION AND LOCK-ON RANGE

The infrared inherent contrast, C_o, between a target and its background is a function of the temperature difference between the two surfaces, and is given by the equation

$$C_o = \frac{N_{o,t} - N_{o,b}}{N_{o,b}} \qquad (1)$$

where N_o is the blackbody radiance from the surfaces and the subscripts $\underline{t}$ and $\underline{b}$ refer to the target and background, respectively.

Apparent contrast, C_R, is the "sensed" contrast or contrast remaining between target and background after passage of the emitted radiation through the atmosphere to a range R. Apparent contrast is given by the relation

$$C_R = \frac{(N_{R,t} + N_{R,a}) - (N_{R,b} + N_{R,a})}{N_{R,b} + N_{R,a}}$$

or

$$C_R = \frac{N_{R,t} - N_{R,b}}{N_{R,b} + N_{R,a}} \qquad (2)$$

where N_R is the radiance arriving at the sensor from the surface and the subscript $\underline{a}$ refers to the atmospheric contribution, that is, the radiation emitted by the atmosphere intervening between the target-background scene ar the sensor. Since the atmospheric contri-

butions to the numerator of Eq. (2) are cancelled by the subtraction, the effect of the atmospheric term is to reduce the apparent contrast and, in turn, the contrast transmission, T_c, which is given by

$$T_c = \frac{C_R}{C_o} \qquad (3)$$

For the purposes of this study and for modelling lock-on range, the apparent contrast will be used instead of the more commonly calculated contrast transmission. It is the apparent contrast which is of importance to a sensor.

3. MODELLING AND SENSITIVITY ANALYSIS

Modelling of the apparent contrast was performed with the AFGL program LOWTRAN 4 (Selby, et al, 1978). LOWTRAN 4 was used to compute transmittance and radiance for atmospheric slant paths. By varying the surface temperatures input to LOWTRAN, radiances from the background (temperature = T) and target (temperature = T + ΔT) were simulated for a given path geometry and atmospheric type.

Data used in the modelling and sensitivity analysis included five atmospheric profiles of temperature and water vapor, shown in Figs. (1) and (2). These were the tropical, mid-latitude winter and summer, and sub-arctic winter and summer standard atmospheres compiled by McClatchey, et al (1972) at AFGL. They provide a wide range of atmospheric temperature and absorber profiles to allow a sensitivity analysis over a broad span of atmospheric conditions.

Three target-to-background temperature contrasts (ΔT) were utilized in the study: 2, 5, and 10°C. The "sensor" was maintained at a constant altitude of 500 meters and by varying the zenith angle from sensor to surface, the slant range was varied from 1 km to 47 km. The spectral range of the model was from 833 to 1250 cm^{-1}, with a spectral resolution of 25 cm^{-1}.

From LOWTRAN 4 were obtained values of averaged path transmittance and integrated radiance for every temperature/atmosphere combination at every range. From the values of integrated radiance, apparent contrast was then computed for a given ΔT from the equation

$$C_R = \frac{N_R(T + \Delta T) - N_R(T)}{N_R(T)}$$

Note that the output radiance from LOWTRAN 4 includes the atmospheric emission contribution.

In modelling lock-on range, it was assumed that LOR could be defined as the maximum range for which C_R exceeded some threshold value, below which "lock-on" could not occur. All instrumental effects were modelled only by considering the threshold C_R. No considerations

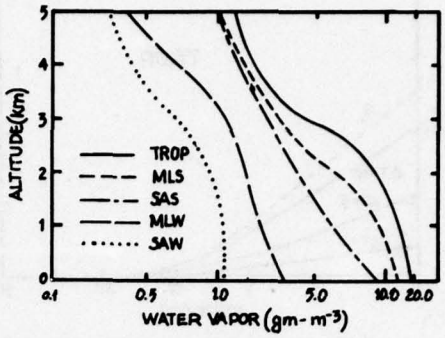

Fig. 1. Water vapor profiles of AFGL standard atmospheres.

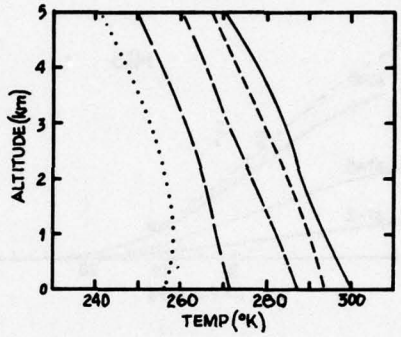

Fig. 2. Temperature structure of AFGL standard atmospheres.

for target size or instrument field of view were made, and both the target and background were considered to be blackbodies.

The basic results of the sensitivity analysis are plotted as a series of curves showing the variation of apparent contrast with range for different values of ΔT, and for the 5 different atmospheric types. Examples of this output are shown in Figs. (3) through (7). The plots show a strong dependence of C_R on atmospheric type. In Fig. (3), for a warm, moist tropical atmosphere, the values of C_R are reduced greatly from the values demonstrated in a dry, cold atmosphere, such as that shown in Fig. (7). The primary quantities influencing the differences in C_R between the atmospheric types are variations in water vapor content and atmospheric temperature. Also plotted in these figures are values of averaged spectral band transmittance as functions of range. As can be seen in the figures, the plots of C_R for $\Delta T = 10°C$ follow the plots of $\bar{\tau}$ closely. The apparent contrast is strongly dependent upon atmospheric transmittance, as might be expected.

Figures (8a) and (8b) are plots of the apparent contrast as a function of averaged path transmittance for the model atmospheres

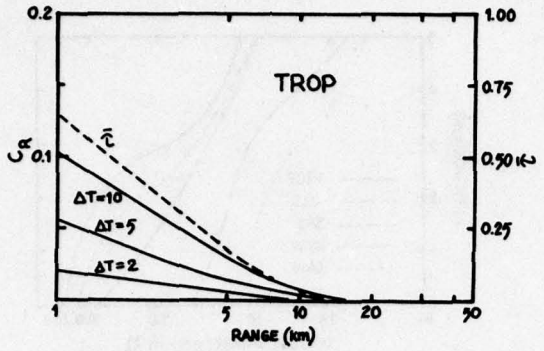

Fig. 3. Apparent contrast, C_R, as a function of range for the TROPICAL atmosphere.

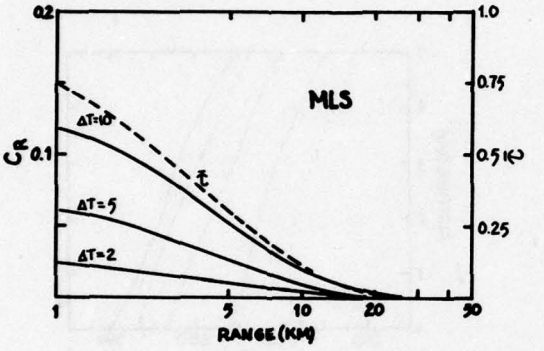

Fig. 4. Apparent contrast, C_R, as a function of range for the MID-LATITUDE SUMMER case.

indicated. Most of the plotted values fall very nearly in straight lines, indicating strong linear relationships between apparent contrast and transmittance. Nonlinearity is accounted for, in part, by the atmospheric emission contribution.

The apparent contrast, or lock-on range, is also strongly dependent upon the initial thermal contrast, ΔT, between target and background, especially at short ranges. This is demonstrated in Fig. (9) where LOR is plotted against ΔT for two values of threshold contrast. The strong dependence of LOR upon atmospheric type is also exhibited by these curves. The extreme values of LOR shown in the figure (LOR > 40 km.) are for illustrative purposes only. Note that the values for lock-on range for a given value of ΔT are generally greater for the lower value of threshold C_R, but that there is no uniform relationship between the two plots.

The strong dependence of LOR or C_R upon ΔT can be modelled quite simply, as shown in Fig. (10). The value of C_R at a given range for $\Delta T = 10^{\circ}C$ is approximately twice that for $\Delta T = 5^{\circ}C$ and five times greater than that for a target-background temperature difference of $2^{\circ}C$. It can be seen that there is a strong, nearly linear relationship between values of

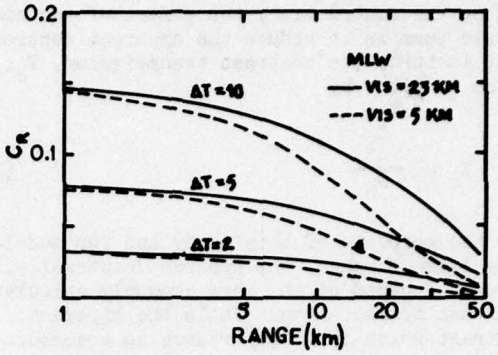

Fig. 5. Apparent contrast, C_R, as a function of range for the MID-LATITUDE WINTER case.

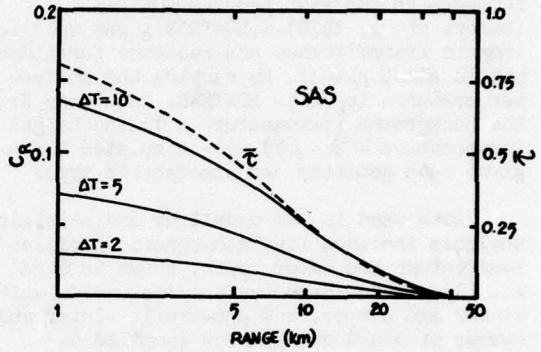

Fig. 6. Apparent contrast, C_R, as a function of range for the SUB-ARCTIC SUMMER case.

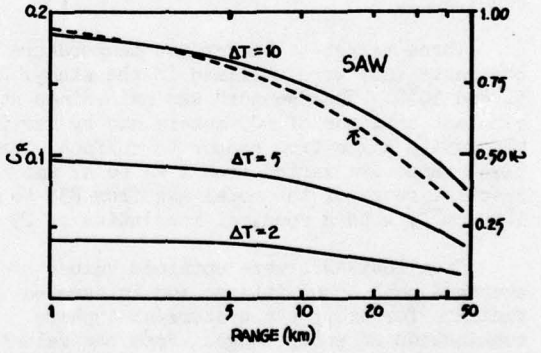

Fig. 7. Apparent contrast, C_R, as a function of range for the SUB-ARCTIC WINTER case.

C_R and the ratios of the ΔTs. This fact can considerably simplify the modelling of LOR in an operational sense, because only one value of ΔT need be used in computations of LOR. Figure (10) shows the comparison between values of C_R at $\Delta T = 5^{\circ}$ and 2° computed from LOWTRAN 4 (solid lines) and the values calculated from the case for $\Delta T = 10^{\circ}$ by using the ratio of temperature contrasts. The calculation can be illustrated by the expression

$$C_R(T=5) \doteq \frac{C_R(T=10)}{2}$$

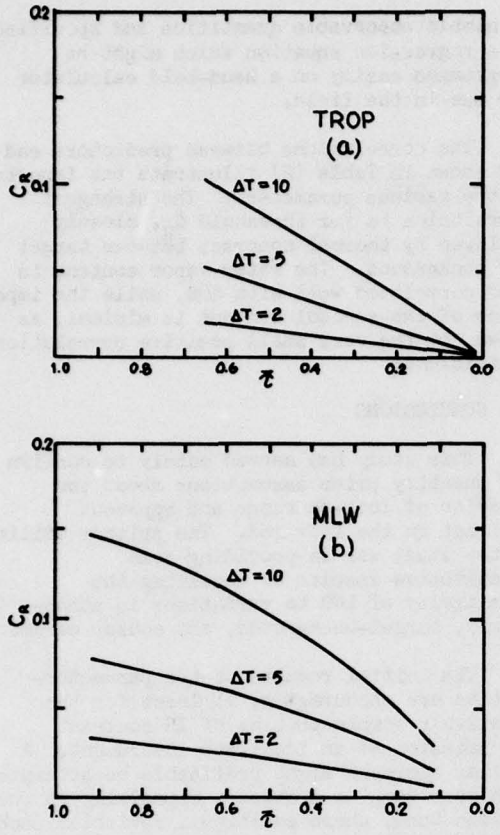

Fig. 8. Apparent contrast as a function of averaged transmittance, . (a) TROP, (b) MLW cases.

The dependence of C_R on aerosol content of the atmosphere is illustrated in Fig. (5) where the solid lines are computed values for an aerosol case giving a surface visibility of approximately 23 km (McClatchey, et al, 1972) and the broken lines represent the plots of C_R versus range for an aerosol model yielding a surface visibility of approximately 5 km. The aerosol dependence is only important for moderate to extreme ranges, beyond abour 15 km. The reduction in C_R caused by the added aerosol loading is also dependent upon the ratio of temperature contrasts of target and background.

This sensitivity analysis demonstrates the variability of apparent contrast with variations in atmospheric type, target-to-background contrast, sensor threshold C_R, and aerosol loading of the atmosphere. It is difficult to assess the relative importance of each variable however, because of their complex interrelationships. In the attempt to parameterize the LOR, however, the relative importance of each variable can be assessed through an examination of the correlations between the independent variables and the LOR.

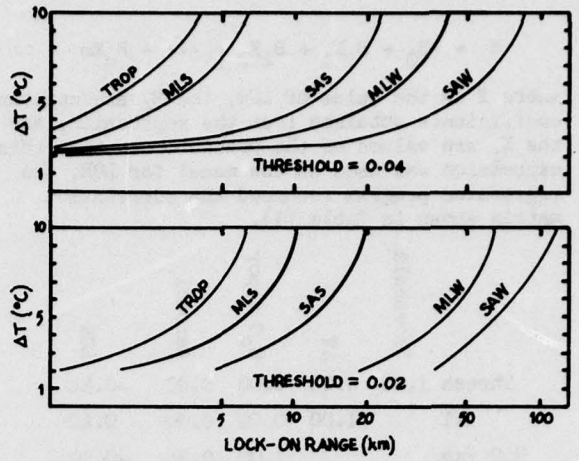

Fig. 9. Lock-on range, LOR, as a function of for different atmospheres and different values of threshold T.

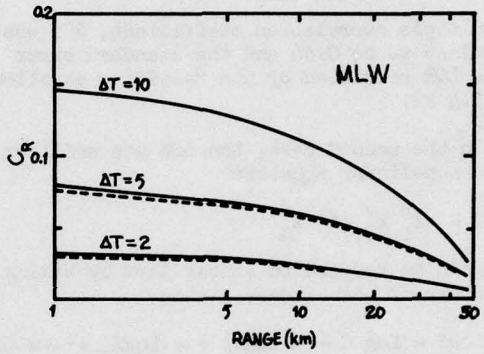

Fig. 10. Apparent contrast as a function of range as computed from LOWTRAN 4 (solid line) and as computed from the ratio of Ts (broken line).

4. PARAMETERIZATION OF LOCK-ON RANGE

Parameterization of the lock-on ranges computed from the sensitivity analysis model was attempted using a stepwise multiple regression technique to derive a predictive equation for LOR. The multiple regression computer program used was the UNIVAC Statistical Package subroutine RESTEM. Input predictors used in the parameterization were water vapor content per kilometer of path length, the aerosol content per kilometer of path length, the target-background contrast temperature difference, ΔT, and the threshold value of C_R. Fifty-four sets of independent variables (predictors) and their corresponding values of lock-on range as determined from the LOWTRAN output were used in the regression.

Two cases were considered. In the first case, the variables were considered to be related in a linear manner expressed by the equation

$$Y = B_0 + B_1X_1 + B_2X_2 + \cdots + B_mXm$$

where Y is the value of LOR, the B_i are constant coefficients obtained from the regression, and the X_i are values of the predictors. When this expression was used as the model for LOR, the regression program returned the correlation matrix shown in Table (1).

	Threshold	ΔT	H_2O vapor	Aerosol	LOR
Thresh	1.00	0.00	0.00	0.00	-0.34
ΔT		1.00	0.00	0.00	0.42
H_2O vap			1.00	-0.34	-0.50
Aerosol				1.00	-0.05

Table 1. Correlation matrix for the linear case.

The multiple correlation coefficient, R~, was determined to be 0.56 and the standard error of the LOR predicted by the resulting equation was 15.4 km.

In the second case, the LOR was modelled by the non-linear equation

$$Y = cX_1^u X_2^v \cdots X_m^w$$

which can be reduced to linear form by taking logarithms of both sides, giving

$$\text{Log}Y = \text{Log } C + u \text{ Log}X_1 + v \text{ Log}X_2 + \cdots + w \text{ Log}X_m$$

where Y is again LOR, c, u, v, and w are constants returned by the regression, and the X_i are values of the predictors. The results obtained from this case were somewhat better than those for the linear case. The correlation matrix then became that shown in Table (2).

	Threshold	ΔT	H_2O vapor	Aerosol	LOR
Thresh	1.00	0.00	0.00	0.00	-0.50
ΔT		1.00	0.00	0.00	0.64
H_2O vap			1.00	-0.24	-0.30
Aerosol				1.00	0.02

Table 2. Correlation matrix for the logarithmic case.

In this case, $R^2 = 0.74$ and the standard error of the predicted LOR was reduced to 7.9 km. This reduction in error and the stronger correlation are hopeful signs that the LOR, by choosing a suitable equation, can be modelled to within acceptable tolerances by simple observable quantities and specified by a regression equation which might be programmed easily on a hand-held calculator for use in the field.

The correlations between predictors and LOR shown in Table (2) illustrate the importance of the various parameters. The strongest correltaion is for threshold C_R, closely followed by thermal contrast between target and background. The water vapor content is also correlated well with LOR, while the importance of the aerosol content is minimal, as shown by the very small positive correlation coefficient.

6. CONCLUSIONS

This study has served mainly to confirm and quantify prior assumptions about the behavior of lock-on range and apparent contrast in the infrared. The primary utility of the study was in providing some quantitative results of modelling the sensitivity of LOR to variations in atmospheric, target-background, and sensor parameters.

The initial results of the parameterization are encouraging, at least for the relatively simple problem of IR contrast transmission to an idealized instrument. A similar approach might profitable be attempted with more complex problems, especially in the visible band, where additional variables such as illumination, target reflectance, and atmospheric scattering must be considered.

7. REFERENCES

McClatchey, R.A., R.W. Fenn, J.E.A. Selby, F.E. Volz, and J.S. Garing, 1972: Optical Properties of the Atmosphere (3rd Ed). AFCRL-72-0497, Environmental Research Papers, no. 411, 108 pp.

Selby, J.E.A., F.X. Kneizys, J.H. Chetwynd, and R.A. McClatchey, 1978: Atmospheric Transmittance/Radiance: Computer Code LOWTRAN 4. AFGL-TR-78-0053, Environmental Research Papers, no. 626, 100 pp.

Sperry Rand Corporation, 1970: UNIVAC Stat-Pack Programmers Reference. Sperry Rand Corp. UP-7502 Rev. 1, pp 9-1 to 9-11.

IN SITU MEASUREMENTS OF GASEOUS AND AEROSOL ABSORPTION

Young Paul Yee, Charles W. Bruce, John Corriveau, Ronald G. Pinnick, and Ralph J. Brewer*

US Army Atmospheric Sciences Laboratory

White Sands Missile Range, New Mexico 88002

1. INTRODUCTION

In light of recent DOD electro-optical (EO) and high energy laser (HEL) systems, new atmospheric measurements must be made in addition to the standard meteorological measurements. Atmospheric parameters such as gaseous/particulate concentrations, identification of natural and/or anthropomorphic constituents, and gas/particulate absorption and scattering are important to the effective operation of these systems.

2. CATEGORY OF POTENTIAL USERS

2.1 EO Systems

Target ranging, laser guidance, target designation, and forward looking infrared devices are highly dependent upon the transmission losses due to atmospheric gaseous and particulate constituents (Wallace, 1972).

2.2 HEL Systems

Depending upon the media through which the beam is being transmitted (for instance, fog, dust, haze, or smoke environment), absorption of radiation can be extremely variable. Atmospheric conditions may result in complete or partial obscuration of the emitted laser wavelength (Jacobs et al., 1974). The spectrophone alone measures absorption relatively directly. The thermal blooming calculations are, of course, based on absorption.

2.3 Radiative Transfer Processes

Radiative models of the atmosphere need valuable input concerning the interaction between common gases and particles in the air and radiation, whether it be shortwave or infrared. Much of this information is unavailable at the present.

2.4 Monitoring of Gas Concentrations

Knowing the absorption coefficients of the constituent gases as a function of wavelength, even discrete wavelengths, one can work backward and determine concentration values of important gases such as ozone, water vapor, and various pollutants.

Military users have a definite need to know absorption coefficients under either natural or battlefield conditions.

3. SPECTROPHONE ABSORPTION MEASUREMENT AND TECHNIQUE PROGRAM

The major goals of this work effort are outlined as follows:

a. Measure absorption in situ of known atmospheric gases and particulates.

b. Design and use spectrophone systems for real-time field measurements of gaseous and/or particulate absorption in atmospheric windows.

These goals are being accomplished by laboratory in situ measurements in conjunction with field measurements taken at Arky Site and Obscura Peak on the White Sands Missile Range.

Some approaches to the problem are summarized:

a. Measure absorption properties of known atmospheric gases and aerosols (wet, dry, smoke, and dust) measured in laboratory controlled environmental chambers.

b. Develop the differential resonant spectrophone to distinguish gaseous absorption from particulate absorption.

c. Correlate spectrophone absorption measurements with particle number density instruments (Knollenberg counter), gas concentration, total water content, electron micrographs, spectrophotometer, meteorological parameters for laboratory and field programs.

d. Add data acquisition system base to assimilate, store, and reduce data from multiple sources.

e. Construct real-time, in situ field systems and integrate into field program.

4. BASIC SPECTROPHONE DESIGNS

The typical spectrophone is composed primarily of a very sensitive capacitance microphone. The capacitance of the longitudinal mode systems vary from approximately one to two nanofarads and the voltage potential is about 300

*Science Applications, Inc., 15 Research Drive, Ann Arbor, Michigan 48103

volts. The production of acoustical sound waves by an illuminated absorbing medium was first observed by Bell (1880). The molecules within a gas, solid, or liquid substance are excited by an intense light source through the medium being studied. After these molecules absorb the radiant energy, they experience a change in temperature and pressure. An acoustical signal in the resonant cavity of a spectrophone is thus produced when the light intensity is modulated. The guiding idea has not changed over the decades, but many innovations and developments have been introduced in designing specific spectrophones. Kerr and Attwood (1968) were the first to employ laser light sources in their gaseous spectrophone systems with the added advantages of high power densities and high spectral resolution. Using laser sources (Rosencwaig, 1973; Harshbarger and Robin, 1973) have made measurements of liquids and solids. At the Atmmospheric Sciences Laboratory specialized flow-through spectrophone systems measure particle absorption, and pulsed laser sourced systems are used to produce very high sensitivities. Later spectrophones may be designated to measure the more efficient, radially acoustical modes.

The microphone shown in Fig. 1 utilizes radially acoustical waves into which longitudinal resonant modes are generated.

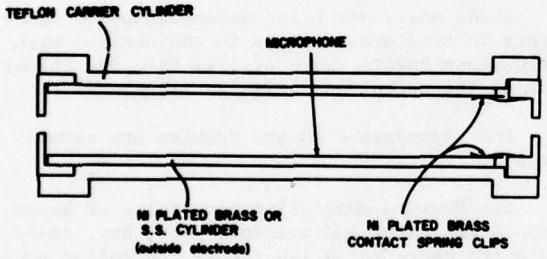

Figure 1. Components of a typical longitudinal acoustical mode microphone. Newer designs have laminar airflow through cavities and gold-plated contact clips.

The diaphragm is an aluminum (or gold) coated mylar sheet with connecting gold-plated contact clips for the inner electrode. There are mylar spacers between the diaphragm and the outside electrode, the Ni plated brass or stainless steel cylinder.

The teflon cylindrical holder provides acoustical and electrical isolation from extraneous noises. Further noise isolation is provided by conical teflon spacers placed at both ends of the microphone to damp out outside interferences. Design characteristics of other spectrophone types are described by Bruce (1976).

The major advantage of the spectrophone system is that a priori knowledge of the particle size, shape, number density, or complex refractive indices is not required as it is in formulating Lorenz-Mie calculations. The only requirement of the spectrophone is to calibrate the instrument. The linear spectrophone constant can be found by using as a reference the strong water vapor absorption line at 10 micrometers R-20 line or by applying a known concentration of a particular gas (10-20 ppm of ethylene, for instance). The absorption coefficient is then simply the product of the calibration factor for a particular spectrophone and the normalized amplitude of the acoustical signal. The amplitude of the acoustical signal as measured by a Honeywell chart recorder is multiplied by the chart recorder scale factor and the Dynatrac Lock-In Analyzer scale factor. The signal is divided by the electrical gain due to an HP 450A amplifier and a Rockland 852 bandpass filter centered between 600 Hz and 1000 Hz. The scaled signal then must be normalized to the laser output power as measured by a Coherent Radiation 201 calorimeter. A simplified schematic of the cw source spectrophone electrical circuit is shown in Fig. 2. By applying the above system, the sensitivity of the measured acoustical signal can be as low as one thousandth of an inverse kilometer for absorption.

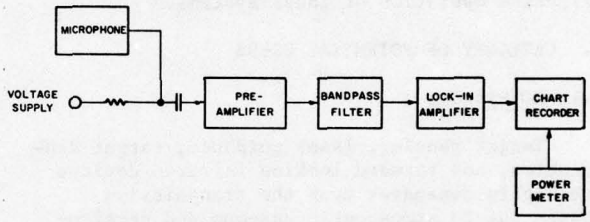

Figure 2. The electrical circuit of a cw laser sourced spectrophone.

For the measurements to be discussed here, either a Sylvania 950 cw CO_2 laser source or a deuterium fluoride (DF) laser source is used. The CO_2 laser can be tuned to 80 spectral lines somewhere between the 9- to 11-micrometer window region. The DF laser has a total of about 30 fixed lines tunable from 3.5 to 4.1 micrometers. Various atmospheric gases and the more common types of particles found in the national atmosphere were studied. A brief review of quartz, calcite, and ammonium sulfate are presented.

5. ENVIRONMENTAL CHAMBER ANALYSIS OF KNOWN DUST PARTICLES

a. First, the particles were finely grounded and sifted using a mortar and pestle. This process was repeated numerous times under a heat lamp to prevent particle dumping.

b. The particles were dispersed into a 0.5-cubic-meter chamber as illustrated in Fig. 3.

c. As the finely grounded dust settles down through the dust spectrophone, measurements are taken at several laser lines, for example at 9 micrometers R-24 and 10 micrometers R-24 lines.

d. Filter samples were taken at various time intervals to determine number size densities. Histograms of the number density of particles versus mean radii were compiled from electron micrographs reproduced at magnification of 200X, 500X, 1000X, and 2000X.

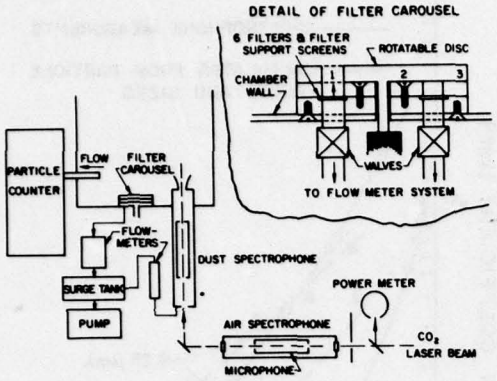

Figure 3. Schematic arrangement of spectrophone and particle sampling apparatus showing light scattering particle counter, six filter particle collectors, and spectrophone cutaway. The insert depicts a cross-sectional view of the filter carousel. To obtain a filter sample, the top disk is rotated to expose a filter, and the appropriate valve to the flowmeter is opened.

e. The absorption contribution due only to the ambient gas in the chamber as measured by the gas spectrophone was subtracted from the total gas/particle absorption as measured by the dust spectrophone.

f. Finally, the spectrophone measured absorptions are correlated with Lorenz-Mie absorption calculations, spectrophotometer measurements, met data, White cell measurements, or other alternate sources of information.

5.1 Quartz

Figure 4 shows spectrophone absorption of quartz (SiO_2) as compared to Lorenz-Mie calculations at 9.4 and 10.3 micrometers as a function of time after the dust was introduced into the environmental chamber (Bruce and Pinnick, 1977). The time interval between measurements was approximately 25 minutes. The results show very good agreement considering the experimental uncertainties involved such as unknown particle shapes and sizes and inhomogeneous particle density. For the theoretical calculations, the particles were assumed to be spherical; but as seen by Fig. 5, the shapes were highly irregular.

5.2 Calcite

Calcite ($CaCO_3$) was dispersed into the environmental dust chamber, but since it proved to be a very weak absorber in the 9- to 11-micrometer wavelength region, it was not studied further. Figure 6 demonstrates good relative correlation with low resolution spectrophotometer measurements using the potassium bromide pellet technique. The actual particle absorption values were near the gaseous absorption levels, which accounts for some of the random scatter in the spectrophone measurements.

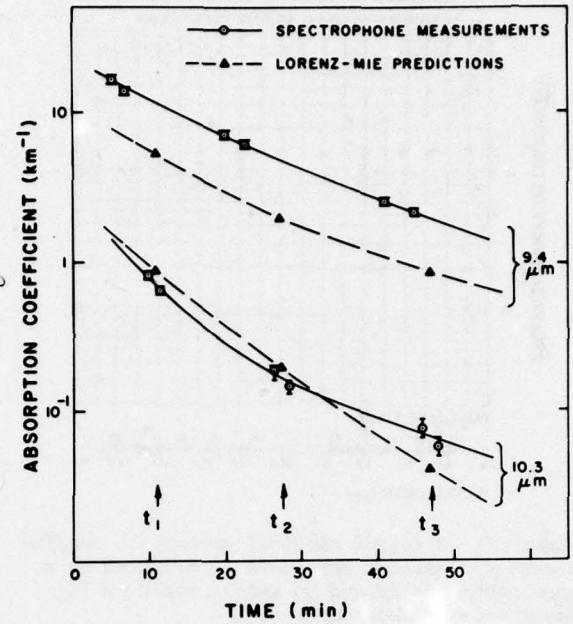

Figure 4. Absorption coefficients of quartz dust as a function of the time after the dust was dispersed in the holding chamber, as predicted by Lorenz-Mie theory, and as measured with a spectrophone for two wavelengths. The predictions are based on particle size distributions measured at times t_1, t_2, and t_3.

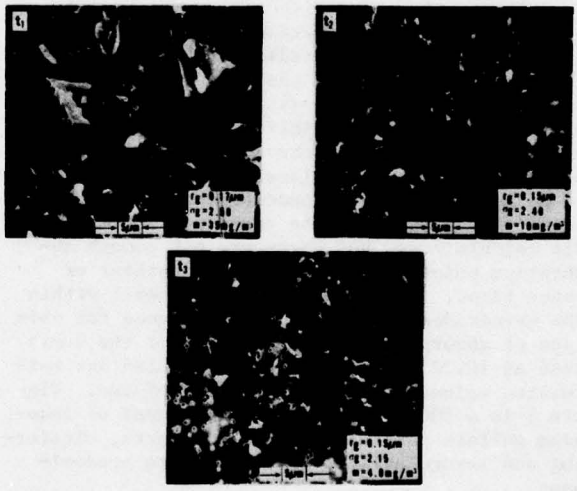

Figure 5. Photographic electron microscope enlargements of quartz dust collected onto Nuclepore filters. The particle samples were taken at times t_1, t_2, and t_3 corresponding to Fig. 4. Each photograph contains the geometric mean radius r_g and geometric standard deviation σ_g for lognormal size distributions obtained by determining the radii of spheres of equivalent cross sections from SEM photomicrographs. Also shown are the corresponding aerosol mass loading m, as determined from the lognormal size distribution parameters by using a quartz density of 2.6 g cm^{-3}. The dark circles are holes in the Nuclepore filter substrate.

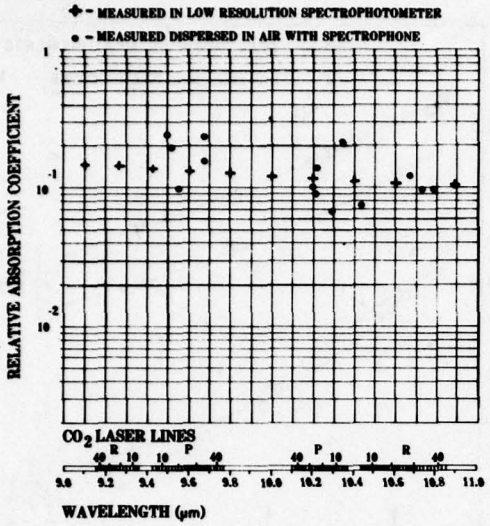

Figure 6. Relative spectral absorption coefficients for calcium carbonate as measured by a spectrophotometer and an uncalibrated cw CO_2 laser sourced spectrophone.

5.3 Ammonium Sulfate

Like quartz, ammonium sulfate is a strong absorber in the 9- to 11-micrometer region. The methodology was similar to the previous cases; and filter samples were taken 4, 9, 14, 20, and 33 minutes after dust dispersal. The peak integral absorption contribution came from approximately 1 micrometer in radius. Eighty percent of the total absorption was from particles 1.2 to 6.3 micrometers in radius. In Fig. 7 spectrophone measurements (solid lines) are plotted with time at 9 micrometers R-24 laser line and at 10 micrometers R-24 laser line. There seems to be more spectral dependence for the spectrophone values than for the corresponding Lorenz-Mie calculations, but there are not enough absorption points to extrapolate to earlier or later times. The results correlate well within the magnitudes that are considered good for this type of absorption measurements. For the worse case at 10.22 micrometers, the measured and calculated values are within a factor of two. Figure 8 is a 2000X micrograph enlargement of ammonium sulfate particles and as in quartz, clustering and irregularity of particles are predominant.

6. LABORATORY MEASUREMENTS OF ATMOSPHERIC GASES

Various known atmospheric gases were studied under controlled laboratory conditions. From the absorption characteristics of these gases at a sufficiently large number of laser lines, it is possible to obtain enough spectral information to identify specific gases as well as concentrations.

6.1 Ozone

The optical setup for ozone (O_3 measurements is shown in Fig. 9 where the He-Ne laser beam is used to align the CO_2 laser beam through

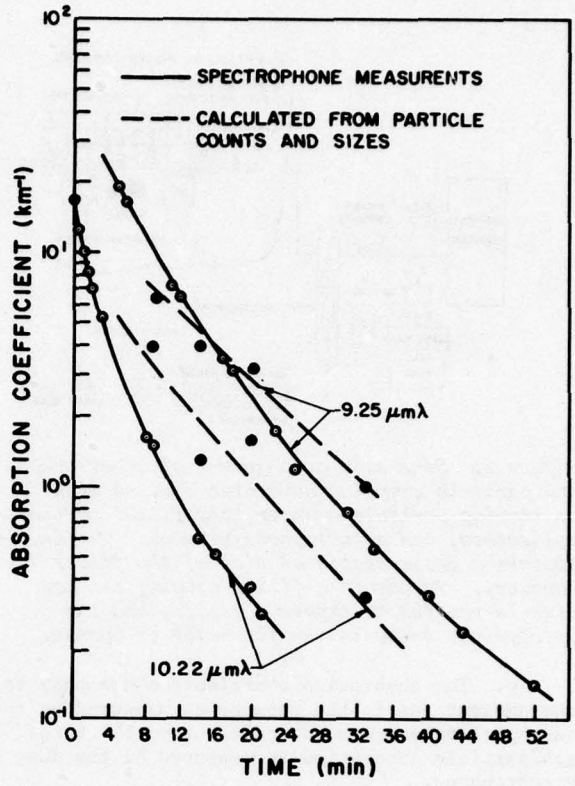

Figure 7. Absorption coefficients of ammonium sulfate dust as a function of time after dispersal, as predicted by theory and measured by a spectrophone for 9.25- and 10.22-micrometer wavelengths.

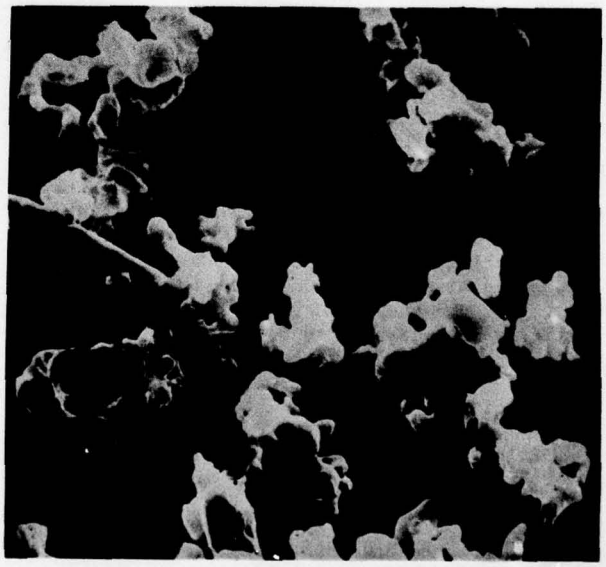

Figure 8. A 2000X photographic enlargement using a scanning electron microscope for ammonium sulfate particles.

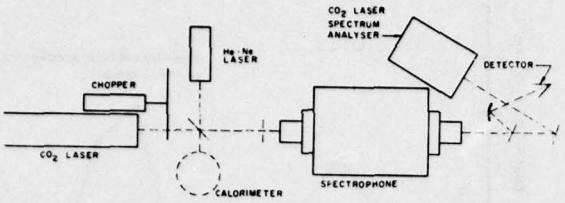

Figure 9. Optical diagram for spectrophone gas analysis of ozone at CO_2 laser wavelengths.

the spectrophone. The laser power is read in from the calorimeter and the box enclosing the spectrophone is insulated to cool down the ozone to -70°C. Table 1 compares ASL spectrophone absorption coefficients with the AFCRL (currently AFGL), Patty, and/or JPL values (km^{-1}/ppm) for 9-micrometer laser lines at T = 300°K and T = 210°K for various pressures. For a majority of the CO_2 laser lines, the ASL spectrophone values were slightly higher than the other corresponding values (Bruce, submitted for publication).

6.2 Methane

At DF laser lines, methane absorption patterns from a pulsed source spectrophone (Bruce et al., 1976) are consistent with ASL's Watkins (1976) and Spencer (1974) White cell results and with AFWL and AFCRL's McClatchey et al. (1973) predictions (Fig. 10). Differences of the normalized values ranged from 3 percent to 13 percent with no apparent trends with amplitude of absorption value or frequency. The AFCRL line-by-line values were generally much lower than the other referenced values.

6.3 Other gases

Photoacoustical spectroscopy of ammonia (NH_3) has just been completed for 9- and 10-micrometer laser wavelengths (Brewer and Bruce, to be published). The ammonia was buffered with N_2 to 1 atmosphere at 295°K and its concentration varied from 30 to 200 ppm. The absorption coefficients at 77 laser lines and their probable errors were tabulated.

TABLE 1. OZONE ABSORPTION COEFFICIENTS FOR ASL SPECTROPHONE MEASUREMENTS, AFCRL LINE-BY-LINE PREDICTIONS, PATTY'S VALUES, AND/OR JPL VALUES AT 9-MICROMETER CO_2 LASER LINES.

(a) Absorption values at T = 300°K for pressures of 1.0, 0.35, and 0.18 atm.

OZONE ABSORPTION COEFFICIENTS

T = 300°K

CO_2 Lines	p=1.0 atm					p=0.35 atm		p=0.18 atm	
	ASL	AFCRL	Patty	JPL	norm	ASL	AFCRL	ASL	AFCRL
P-6		0.811					0.200		0.063
P-8		1.09					0.455		0.298
P-10		0.624		0.63			0.134		0.044
P-12	1.24	0.953	1.22	1.17		0.511	0.423		0.297
P-14	1.20	1.09	1.27	1.24		0.352	0.296	0.146	0.101
P-16	0.934	0.771	0.90	0.87		0.192	0.203	0.0556	0.065
P-18	0.642	0.514	0.64	0.57		0.259	0.193	0.146	0.0957
P-20	0.479	0.365	0.55	0.42		0.160	0.101	0.0569	0.0412
P-22	0.201	0.228	0.18	0.16		0.0454	0.0435	0.0101	0.0135
P-24	0.074	0.066	0.07	0.03		0.0226	0.0167	0.0081	0.0070
P-26	0.626	0.527	0.60			0.142	0.150	0.0351	0.0595
P-28	0.945	0.713	0.94			0.344	0.293	0.157	0.153
P-30	0.644	0.551	0.64			0.236	0.217	0.177	0.126
P-32	0.565	0.468	0.59			0.158	0.168	0.0546	0.0848
P-34	0.369	0.339	0.30			0.101	0.088	0.0719	0.0483
P-36	0.742	0.550	0.67			0.320	0.266	0.114	0.170
P-38		0.632				0.429	0.345		0.283
P-40		0.496					0.125		0.049

Patty, et.al. (P(14)-P(34))

(b) Absorption values at T = 210°K for pressures of 1.0, 0.35, and 0.18 atm.

T = 210°K

CO_2 Lines	p=1.0 atm		p=0.35 atm		p=0.18 atm	
	ASL	AFCRL	ASL	AFCRL	ASL	AFCRL
P-6	1.25	1.05		0.292		0.0825
P-8	1.74	1.59		0.635		0.398
P-10	1.03	1.01		0.216		0.0675
P-12	2.03	1.65	0.763	0.702		0.466
P-14	2.28	1.99	0.709	0.560	0.209	0.198
P-16	1.68	1.57	0.495	0.460	0.0721	0.162
P-18	1.09	1.00	0.526	0.363	0.295	0.182
P-20	0.815	0.749	0.280	0.213	0.065	0.0910
P-22	0.360	0.489	0.0936	0.0937	0.0289	0.0285
P-24	0.116	0.108	0.0375	0.0256	0.0211	0.0106
P-26	1.11	1.11	0.386	0.332	0.135	0.142
P-28	1.46	1.19	0.699	0.513	0.274	0.223
P-30	0.911	0.826	0.362	0.290	0.429	0.167
P-32	0.847	0.694	0.249	0.217	0.0863	0.0955
P-34	0.587	0.625	0.128	0.127	0.0751	0.0543
P-36	1.05	1.00	0.516	0.485	0.286	0.285
P-38	1.43	1.14		0.625		0.510
P-40	0.973	0.913		0.218		0.0835

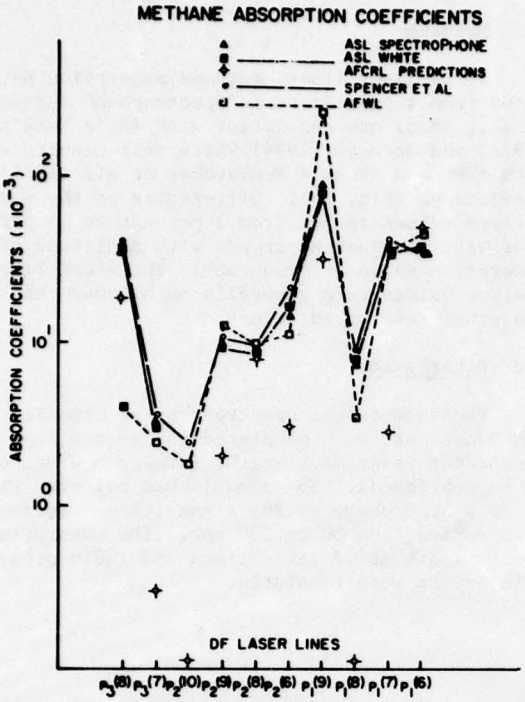

Figure 10. Methane absorption coefficients versus DF laser wavelengths.

For water vapor measurements, a 1-cubic-meter environmental chamber was designed similar to the dust chamber described previously. A water content meter is being constructed and a commercial "Knollenberg" particle counter is used to measure the water droplet distribution. This work is currently in progress.

7. OFF-LINE GAS ANALYSIS

The first off-line gas analysis was attempted at Obscura Peak on the Army's White Sands Missile Range (Samuel et al., 1978). The purpose of this analysis was to determine atmospheric absorption spectra and gas concentrations at field sites. The sampling bottles were made of stainless steel and were pumped and baked to insure a high degree of purity. Before and during the sampling period, the tanks were cooled down with liquid nitrogen so that a positive pressure differential would exist when the tanks warmed to ambient temperatures. The field sifted gas then could be valved into a spectrophone cell for laboratory measurements. To determine its composition, a deconvolution program using iterative computer calculations was used to identify specific gases. The average absorption at DF laser lines is plotted in Fig. 11, and the residual absorption represents the unidentifiable gases and impurities within the system. A summary of concentrations of known constituents for nine gas samples is tabulated in Table 2. Nitrous oxide and methane gas concentrations were measured approximately two times higher than the standard values. The water vapor concentrations varied with meteorological measurements (taken with sling psychrometers and not necessarily at the same location), but generally the correlation

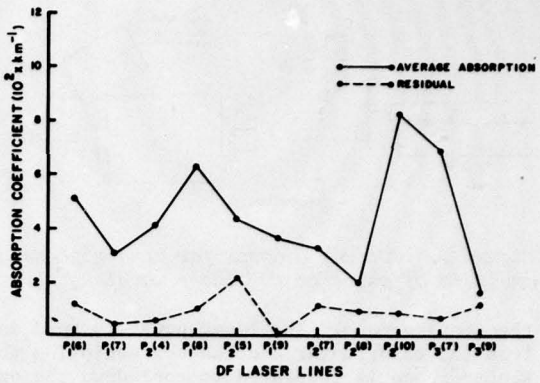

Figure 11. Remote field site's average initial and residual absorption for eight gas samples at DF laser wavelengths.

TABLE 2. OFF-LINE GAS CONCENTRATION ANALYSIS FOR EIGHT REMOTE SITE SAMPLES AT DF LASER WAVELENGTHS.

CONCENTRATIONS (OR PARTIAL PRESSURES) OF KNOWN CONSTITUENTS
* CALCULATED FROM SPECTROPHONE MEASUREMENTS
** OBTAINED FROM METEOROLOGICAL SOURCES (SLING PSYCHROMETERS)
*** ASSUMED

Sample Identification	Water Vapor (torr) *	Water Vapor (torr) **	H_2O (ppm) *	CH_4 (ppm) *	N_2 (torr) ***	CO_2 (ppm) ***
1622-2	4.75	----	0.462	18.2	600	330
RSDF-3	3.60	3.20	0.397	4.75	550	330
RSDF-4	3.57	3.61	0.398	4.26	560	330
RSDF-5	3.87	2.69	0.748	5.46	500	330
RSDF-6	2.69	2.69	0.760	4.41	610	330
RSDF-7	3.53	3.78	0.554	5.49	600	330
RSDF-8	7.06	5.59	0.472	3.54	600	330
RSDF-9	5.36	6.20	0.340	3.84	600	330
RSDF-10	5.04	3.94	0.346	3.79	600	330

was good. The feasibility of the off-line gas sampling technique at DF laser wavelengths is very encouraging.

8. FIELD EXPERIMENTS

The culminative efforts of previous spectrophone results are directly applicable to the in situ field experiments now under way at the Arky Site on the White Sands Missile Range. A series of dust tests conducted during March through June 1978 represented the first in situ field measurements of particulate absorption using a flow-through spectrophone system. The basic design of the optics is outlined in Fig. 12. The CO_2 laser beam passes through a mechanical chopper at a frequency of 880 Hz; and after several beam splitter and mirror deflections, the beam enters a horizontal gas spectrophone and a vertical total absorption spectrophone. A schematic (Fig. 13) of the vertical spectrophone shows an aluminum intake bell (to damp out undesirable wind gusts, reduce particle velocities, and provide laminar flow through the spectrophone), a microphone casing which consists of acoustic wave absorbers and a teflon isolated microphone, a calorimeter, and an outlet valve from which the dust particles are drawn through the spectrophone's cavity by means of an air pump. The laser power output is also recorded along with the dew point hygrometer readings. The acoustical signal is processed in the same manner as previously mentioned.

AD-A070 009 AIR WEATHER SERVICE SCOTT AFB IL F/G 4/2
PROCEEDINGS OF THE TECHNICAL EXCHANGE CONFERENCE 8TH AIR FORCE --ETC(U)
MAY 79

UNCLASSIFIED AWS/TR-79/001 NL

3 OF 3
AD A070009

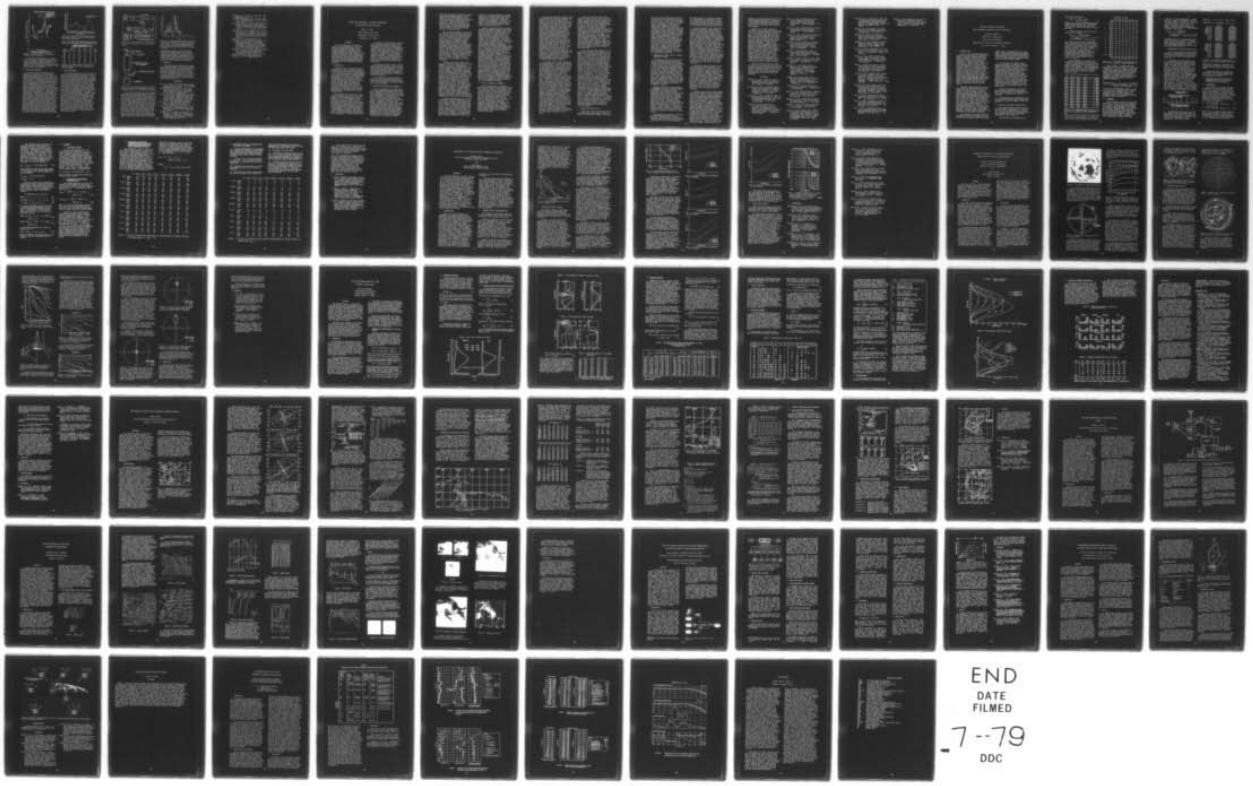

END
DATE FILMED
7-79
DDC

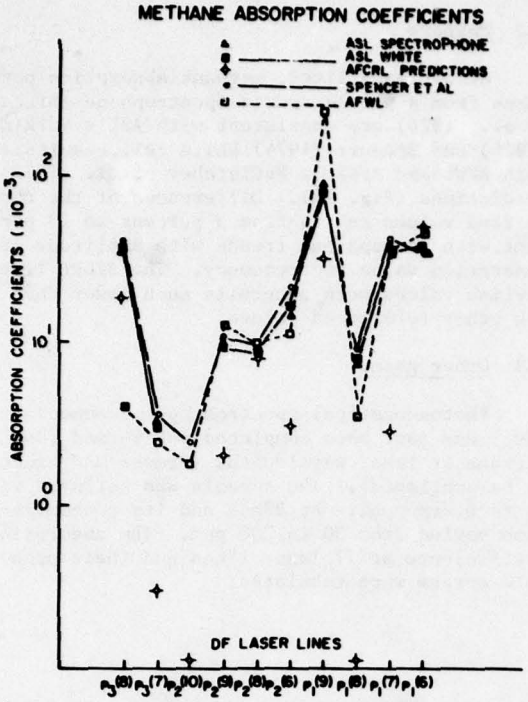

Figure 10. Methane absorption coefficients versus DF laser wavelengths.

For water vapor measurements, a 1-cubic-meter environmental chamber was designed similar to the dust chamber described previously. A water content meter is being constructed and a commercial "Knollenberg" particle counter is used to measure the water droplet distribution. This work is currently in progress.

7. OFF-LINE GAS ANALYSIS

The first off-line gas analysis was attempted at Obscura Peak on the Army's White Sands Missile Range (Samuel et al., 1978). The purpose of this analysis was to determine atmospheric absorption spectra and gas concentrations at field sites. The sampling bottles were made of stainless steel and were pumped and baked to insure a high degree of purity. Before and during the sampling period, the tanks were cooled down with liquid nitrogen so that a positive pressure differential would exist when the tanks warmed to ambient temperatures. The field sifted gas then could be valved into a spectrophone cell for laboratory measurements. To determine its composition, a deconvolution program using iterative computer calculations was used to identify specific gases. The average absorption at DF laser lines is plotted in Fig. 11, and the residual absorption represents the unidentifiable gases and impurities within the system. A summary of concentrations of known constituents for nine gas samples is tabulated in Table 2. Nitrous oxide and methane gas concentrations were measured approximately two times higher than the standard values. The water vapor concentrations varied with meteorological measurements (taken with sling psychrometers and not necessarily at the same location), but generally the correlation

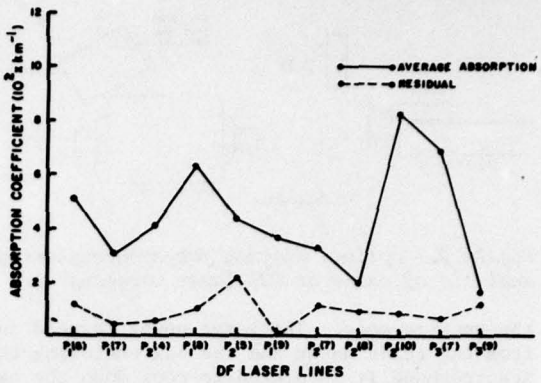

Figure 11. Remote field site's average initial and residual absorption for eight gas samples at DF laser wavelengths.

TABLE 2. OFF-LINE GAS CONCENTRATION ANALYSIS FOR EIGHT REMOTE SITE SAMPLES AT DF LASER WAVELENGTHS.

CONCENTRATIONS (OR PARTIAL PRESSURES) OF KNOWN CONSTITUENTS
* CALCULATED FROM SPECTROPHONE MEASUREMENTS
** OBTAINED FROM METEOROLOGICAL SOURCES (SLING PSYCHROMETERS)
*** ASSUMED

Sample Identification	Water Vapor (torr) *	Water Vapor (torr) **	H_2O (ppm) *	CH_4 (ppm) *	N_2 (torr) ***	CO_2 (ppm) ***
1622-2	4.75	----	0.462	18.2	600	330
RSDF-3	3.60	3.20	0.397	4.75	550	330
RSDF-4	3.57	3.61	0.398	4.26	560	330
RSDF-5	3.87	2.69	0.748	5.46	500	330
RSDF-6	2.69	2.69	0.760	4.41	610	330
RSDF-7	3.53	3.78	0.554	5.49	600	330
RSDF-8	7.06	5.59	0.472	3.54	600	330
RSDF-9	5.36	6.20	0.340	3.84	600	330
RSDF-10	5.04	3.94	0.346	3.79	600	330

was good. The feasibility of the off-line gas sampling technique at DF laser wavelengths is very encouraging.

8. FIELD EXPERIMENTS

The culminative efforts of previous spectrophone results are directly applicable to the in situ field experiments now under way at the Arky Site on the White Sands Missile Range. A series of dust tests conducted during March through June 1978 represented the first in situ field measurements of particulate absorption using a flow-through spectrophone system. The basic design of the optics is outlined in Fig. 12. The CO_2 laser beam passes through a mechanical chopper at a frequency of 880 Hz; and after several beam splitter and mirror deflections, the beam enters a horizontal gas spectrophone and a vertical total absorption spectrophone. A schematic (Fig. 13) of the vertical spectrophone shows an aluminum intake bell (to damp out undesirable wind gusts, reduce particle velocities, and provide laminar flow through the spectrophone), a microphone casing which consists of acoustic wave absorbers and a teflon isolated microphone, a calorimeter, and an outlet valve from which the dust particles are drawn through the spectrophone's cavity by means of an air pump. The laser power output is also recorded along with the dew point hygrometer readings. The acoustical signal is processed in the same manner as previously mentioned.

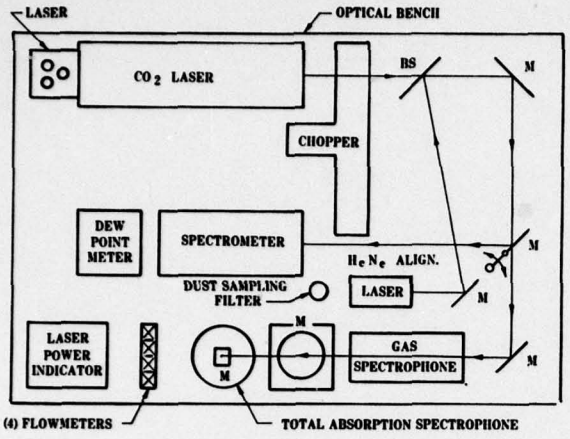

Figure 12. Optical design of the field spectrophone system as mounted on top of an optical bench.

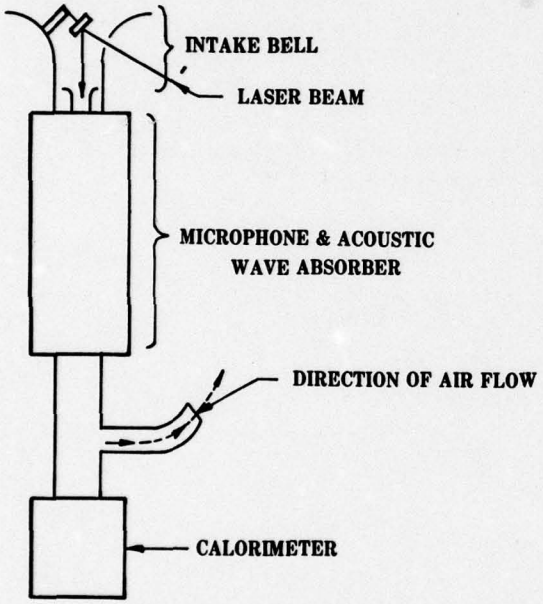

Figure 13. The vertically mounted total absorption spectrophone with an aluminum intake bell, microphone casing, and a detachable calorimeter.

An Army 3/4-ton vehicle was used to generate the required dust conditions that may be present under real battlefield environments or under adverse climatic dust storms. The desert terrain was relatively flat although existing winds frequently changed speed and direction. To correlate the spectrophone-measured absorption coefficients, a PMS "Knollenberg" particle counter was positioned within 2 meters from the spectrophone probe. Preliminary results (Fig. 14) indicate good pattern correlation although the relative absorption values varied significantly, a maximum of about 150 km^{-1} for the Lorenz-Mie calculations and of about 50 km^{-1} for the spectrophone. As the dust clouds swept over the individual probes it was noticed that there was substantial spatial variation of the dust density.

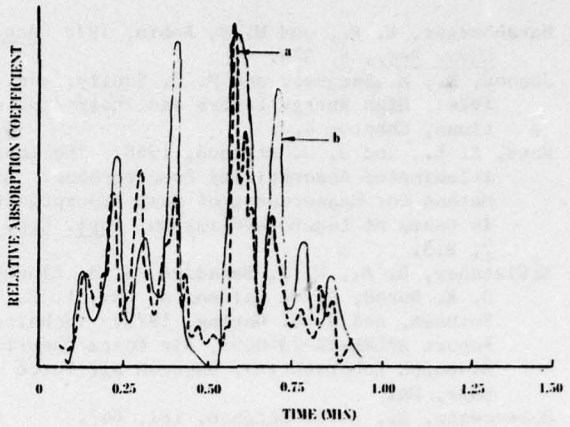

Figure 14. A sample dust run taken 19 May 1978, showing relative absorption patterns as a function of time: (a) is the uncalibrated spectrophone curve, and (b) is the PMS "Knollenberg" particle density calculations taken in 5-second intervals.

The horizontal position of the PMS particle counter made it more sensitive to the larger, crosswind particles than the vertical total absorption spectrophone. Uncertainties in the dust's complex index of refraction and the PMS reliability under heavy dust loading can also contribute to these amplitude discrepancies.

9. CONCLUSION

In the near future, newer and more compact spectrophone systems will be designed and tested under fog, dust, smoke, and haze environments. The electronics will be considerably condensed such that one functional unit can be easily carried to designated field sites. The addition of a data acquisition system to record, store, and manipulate analog and digital signals will automatically monitor ambient levels of gaseous particulate absorption.

REFERENCES

Bell, A. G., 1880: On the Production and Reproduction of Sound by Light. Proc. Am. Assoc. Advancement Sci., 29, 115.

Brewer, R. J., and C. W. Bruce: Photoacoustic Spectroscopy of NH_3 at the 9 Micrometer and 10 Micrometer CO_2 Laser Wavelengths. (to be published in Appl. Opt.).

Bruce, C. W., 1976: Development of Spectrophones for CW and Pulsed Radiation Sources, R&D Technical Report, ECOM-5802, US Army Electronics Command, Atmospheric Sciences Laboratory, White Sands Missile Range, NM.

Bruce, C. W.: Ozone Absorption Measurements Using a CW CO_2 Laser Sourced Spectrophone. (submitted for publication)

Bruce, C. W., and R. G. Pinnick, 1977: In Situ Measurements of Aerosol Absorption with a Resonant CW Laser Spectrophone, Appl. Opt., 16, 1762-65.

Bruce, C. W., B. Z. Sojka, B. G. Hurd, W. R. Watkins, K. O. White, and Z. Derzko, 1976: Application of Pulsed-Source Spectrophone to Absorption by Methane at DF Laser Wavelengths, Appl. Opt., 15, 2970.

Harshbarger, W. R., and M. B. Robin, 197: Acc. Chem. Res., 6, 329.
Jacobs, S., M. Sargent, and M. O. Scully, eds., 1974: High Energy Lasers and Their Applications, Chapter 4.3.
Kerr, E. L., and J. G. Attwood, 1968: The Laser Illuminated Absorptivity Spectrophone: A Method for Measurement of Weak Absorptivity in Gases at Laser Wavelengths, Appl. Opt., 7, 915.
McClatchey, R. A., W. S. Benedict, S. A. Clough, D. E. Burch, R. F. Calfee, K. Fox, L. S. Rothman, and J. S. Garing, 1973: Technical Report AFCRL-TR-73-0096, Air Force Cambridge Research Laboratories, Hanscom Air Force Base, MA.
Rosencwaig, A., 1973: Science, 181, 657.
Samuel, D., C. W. Bruce, and R. J. Brewer, 1978: Spectrophone Analysis of Gas Samples Obtained at Field Site, Technical Report ASL-TR-0009, US Army Research and Development Command, Atmospheric Sciences Laboratory, White Sands Missile Range, NM.
Spencer, D. J., G. C. DeNault, and H. H. Tahimoto, 1974: Technical Report SAMSO-TR-74-7, Space and Missile Systems Organization, Los Angeles Air Force Station, CA.
Wallace, J., 1972: J. Opt. Soc. Am., 62, 373.
Watkins, W. R., 1976: Appl. Opt., 15, 16.

GENERAL CIRCULATION MODELS, SEA-SURFACE TEMPERATURES, AND SHORT-TERM CLIMATE PREDICTION

Donald L. Gilman

Climate Analysis Center, NMC

NOAA National Weather Service

Washington, D.C. 20233

ABSTRACT

This review describes the principal results of nine experiments in which fixed sea-surface temperature anomalies were imposed as boundary conditions on general circulation models of the atmosphere and allowed to modify those models' behavior in extended integrations. Some inferences about the future of theoretically-based modeling and prediction of short-term climate fluctuations are drawn from these experiments and from several studies on predictability and on statistical prediction of seasonal weather anomalies.

1. INTRODUCTION

During the 1970's a new type of research became dominant in the field of long-range forecasting--or short term climate prediction, as it is coming to be called. Several general circulation models (GCM's) had been developed to the point of being able to simulate fairly effectively many of the climatic averages of the atmosphere, and researchers began to believe that the models could now be applied to start testing ideas that Namias and Bjerknes had been advocating during the previous decade: namely, that anomalies of sea-surface temperatures (SST's) at mid-latitudes or in the tropics should influence the evolution of atmospheric anomalies over several months in a consistent or at least predictable way.

Nine different sets of GCM tests, often called "sensitivity tests", have so far been completed in the United States and Great Britain. In each, the response of a model to the imposition of one or more fixed SST anomalies has been calculated and compared to the outcomes of various control runs. Being performed without observed initial data and without either observed time-varying SST data or calculations of an interactive feedback of the atmosphere on the sea, these cannot be called prediction experiments, but they constitute a relevant and necessary preparation for such experiments. Why are they necessary? The essence of the ideas being tested is that anomalies in the upper layers of the ocean change more slowly and perhaps more predictably than do those in the atmosphere, and that over times of a month, a season, or several seasons they might act to force some changes in the atmosphere. Unless a GCM could first be made to show significant and convincing responses to strong, fixed SST anomalies, therefore, one would hesitate to employ it for more complex experiments with real initial data, weak and variable SST anomalies, and interactively coupled upper-ocean models.

This paper will offer a brief, critical review of the GCM sensitivity tests that have been conducted in the United States and Great Britain with imposed SST anomalies. It will also describe some implications of several other studies for the future of theoretically-based modeling and prediction of short-term climate fluctuations.

It is convenient to separate the sensitivity tests into two groups, according to whether they deal with effects of mid-latitude or tropical SST anomalies. We begin with the mid-latitude SST group.

2. EFFECTS OF MID-LATITUDE SST ANOMALIES

First to be applied to the mid-latitude SST case was the Mintz-Arakawa 2-level global model, independently by Spar (1973 a,b,c) and Gates (unpublished, but see Stidd et al, 1973). Spar superimposed a 6°C warm pool on the annual normal SST pattern of the eastern North Pacific, first for winter conditions, then summer. He repeated the winter trial with the warm pool switched to the eastern South Pacific. Gates placed a 5°C warm pool in the wintertime eastern North Pacific. Each investigator made control runs with normal SST's from unchanged initial conditions, and each produced further control runs with perturbed conditions, Gates deliberately with random temperature errors in the atmosphere and Spar inadvertently by a change in a calculating algorithm and by an SST anomaly that ended after one month. What was the outcome?

Except for some effects near the SST anomaly, the differences between anomaly runs and normal runs, although substantial, were neither steady nor on average larger than the differences between perturbed runs and the normal runs. These results dashed any expectation that once the GCM physics had evolved sufficiently questions about hypothetical oceanic effects on the atmosphere could be settled by straightforward comparisons of a few model runs.

The principal and almost only conclusion to be drawn from Spar and Gates' efforts was that the GCM's own natural variability would have to be allowed for in sensitivity tests in order to judge the statistical significance--that is, the credibility--of any apparent effects on the model's behavior. Direct estimates of variances for GCM parameters would have to be calculated--at considerable extra expense--and a deliberate experimental design worked out in advance to assure a reasonable likelihood that some conclusions could be drawn at the end of any desired test. "Sensitivity testing" had been shown to require something beyond theoretical and computational techniques: namely, experimental technique. The subsequent history of this line of work is largely a story of gradual, painful accommodation to the new requirement.

The NCAR 6-layer global model was the next one brought to the mid-latitude SST case. Houghton et al (1974), following up on Ratcliffe and Murray's (1970) empirical study of the influence of North Atlantic SST's on European weather, placed warm and cold pools (± 2°C) alternately in the model's Northwest Atlantic near Newfoundland--the area believed to be critical--under winter conditions. The outcome of the trials was disappointing: poor simulation of observed effects, failure to achieve climate steadiness, lack of storm tracks over the critical area, and effects that were weak in comparison to observed atmospheric variability. (The model's own natural variability was still largely unknown and therefore unavailable for evaluating the significance of effects.) Why were these problems encountered? It appears that the start-up run was probably too short for the model's climate to have reached an equilibrium, that the model's storm climatology was inadequate to the task, and that there was no adequate statistical design for the experiments.

A southern hemisphere version of the GFDL 9-level model followed the NCAR model to the mid-latitude SST scene. Under autumn conditions, Simpson and Downey (1975) twice placed a 4°C warm pool in the model's central South Pacific. The first trial began 40 days after a start-up from real initial conditions, the second, 50 days after the same initial conditions. The outcomes of the two 50-day runs were radically different. In one case some apparent local responses were substantially larger than an estimated noise level; in the other, not. The great dependence of outcome on conditions at precisely the time the SST anomalies were inserted casts doubt on the attribution of any special or consistent effects to those anomalies. Furthermore, the absence of true ensemble estimates of the model's long-term variability precluded any rigorous significance testing.

Chervin and Schneider (1976 a,b) finally overcame this obstacle to proper significance testing by collecting ensemble variances over five different runs of the NCAR model. The model was promptly re-applied to the mid-latitude winter SST case by Chervin et al (1976), this time treating the North Pacific instead of the North Atlantic. They first imposed a pair of opposite 4°C SST anomalies, warm east of cold, then repeated the test with triple-strength anomalies of 12°C. Only the super anomalies produced significant, realistic local response in temperatures above the surface layers. Downstream responses were weak. If these results can be translated to the real atmosphere, they imply that typical SST anomalies at mid-latitudes would not generate a predictable atmospheric response, but whether the mode;'s behavior was sufficiently realistic for such a translation remains questionable. Some of the questions were highlighted by the follow-up analyses of Kutzbach et al (1976), who studied the same tests and then switched warm and cold pools and re-ran the calculations. They noted that the control-case conditions generated by the model were not representative of typical mid-winter atmospheric conditions over the North Pacific, particularly as to storm tracks and pressure patterns. Whether the control case conditions were also unrepresentative of the model's winter climate remains unknown, as does the closeness of correspondence between the model's variance and covariance fields and those of the atmosphere. These are questions that could be answered as more model simulations are generated and analyzed.

3. EFFECTS OF TROPICAL SST ANOMALIES

Tests of the effects of tropical SST anomalies on GCM behavior began somewhat before Spar and Gates' studies at mid-latitudes. The first model applied to the tropical SST case was GFDL's 9-level northern hemisphere version. Rowntree (1972) used it to run two separate pairings of warm versus the more normal cold SST's in the eastern equatorial Pacific, imposing a difference of 3.5°C each time. The model's responses were strong: convective rain near the warm water, pronounced meridional overturning, and increases of the subtropical upper westerlies. Although no randomly perturbed cases were run for comparison, the strength of the two outcomes and the consistency between them implied truly forced responses, just about as Bjerknes (1966) had postulated.

Questions have been raised, however, about some of the links in Bjerknes' hypothesis and about the fitness of this model for the tropical test. Doberitz (1968) found that the variation of central equatorial Pacific rainfall supposed by Bjerknes to be caused by the introduction of warm water had tended to precede the water temperature rises by several weeks instead. Krueger and Gray (1969) noted that widespread warmth of equatorial waters in the winter of 1965-66 was not accompanied by widespread convective cloudiness as the Bjerknes mechanism would have suggested, and Ramage (1975) obtained a similar result for the winter of 1972-73. Concentrating on one key record, that of Canton Island, Ramage (1977) concluded from synoptic and statistical evidence that the local air-sea heat exchange, another link in the Bjerknes mechanism, was not directly related to SST or rainfall. Earlier, Ramage and Murakami (1973) had argued that the model's strong circulation responses to change of SST was an artifact produced by the proximity of its equatorial boundary wall and by an overly strong convective mechanism. Certainly the model was able to simulate Bjerknes concept quite well; whether either it or the concept was describing nature sufficiently well remains uncertain.

An equatorial wall no longer figured in the next application of a GCM to the tropical SST anomaly problem. Shukla (1975) chose the 11-level global version of the GFDL model to calculate the effect of temperatures in the western Arabian Sea on the summer monsoon of the Indian Ocean and India. Replacing the normal temperatures east of the Horn of Africa by values up to 3°C colder, he obtained a downstream reduction of almost half in the general rainfall rate for thirty days, averaged over India and adjacent ocean areas. This result appeared to be significant in comparison to an estimate of model variability determined from the control run, but Chervin and Schneider (1976) pointed out that such estimates cannot replace estimates derived from an ensemble of model runs in a strict test of significance; the interpretation of the experiment's outcome therefore remains in some doubt. An exchange between Shukla and Sikka and Raghavan (1976) and comments by Ramage (1977) established clearly that the model's simulation of rainfall and circulation could not delineate detail on the scale of the Indian peninsula or of the Arabian Sea, where the effects of orography and of an east-west vertical circulation cell dominate the actual water vapor and rainfall balance. The scale problem may explain why Shukla and Misra (1977) empirically found only modest, though positive, correlations between SST anomalies over the central Arabian Sea in July and rainfall over Central and western India in August.

The focus was turned to the tropical Atlantic in the next set of trials. Rowntree (1976) introduced a new family of models, three closely related 5-level northern hemisphere GCM's developed in the British Meteorological Office. His principal trials imposed on two of the models a 2°C warm pool near Africa, centered on about 18°N, that resembled January 1963. Averaged outcomes for days 41-80 differed according to which model was employed and whether initial atmospheric conditions were made isothermal or real. The largest differences, however, were found when random temperature perturbations were added to the real atmospheric conditions. Only one of the three principal trials produced a North Atlantic pressure field with any resemblance to the marked Icelandic blocking pattern that dominated the winter of 1962-63. Clearly the model's own natural variability overwhelmed any signal produced by the SST variations in these experiments.

In the most recent GCM simulations of sea-temperature influence on the atmosphere, the NCAR 6-layer global model was given its third outing. Julian and Chervin (1978) used it to follow up on the first of all such experiments, Rowntree's (1972) study of the tropical East Pacific case. They now had the advantage of not having to account for an equatorial wall and of being able to set up proper significance tests based on the NCAR model variance estimates compiled by Chervin and Schneider (1976). Two SST anomaly fields were separately imposed: an extensive warm pool of central value +5°C in the Southeast Pacific between Easter Island and Peru and a warm strip of +2°C in the equatorial East Pacific, centered on 5°S. The outcomes of the two trials were very encouraging. Within the tropics and subtropics, the model atmosphere responded by producing many of the features of the Walker Circulation and fair agreement with the shifts of its pressure-field counterpart, the Southern Oscillation. Some of these changes were statistically significant. Low and high level winds in the East Pacific changed significantly and in accord with Bjerknes' (1966) hypothesis and Rowntree's (1972) earlier simulation. Convection and precipitation were not carried far enough downstream to the west, however. At higher latitudes, no greater areas of significant change occurred than might have been expected from the 95% criterion used in the tests. Pressure falls in the North Pacific, though not significant, did generally conform to Bjerknes' expected pattern. Overall, the trials may be described as the first adequately modeled, properly designed SST sensitivity experiment to have obtained a successful outcome.

4. CONCLUSIONS FROM THE TESTS

Some general lessons may be drawn from the published accounts and critiques of the SST sensitivity experiments reviewed in this paper.

First, it cannot be assumed that the GCM's now available are each suited to any kind of sensitivity test. Several of the experiments so far have come to grief because the model's physics, climatology, or spatial resolving power were not adequate to the demand. Second, proper experimental design must include both rigorous significance tests and a format that gives a reasonable chance that true effects can pass those tests. Although test protocols have been developed by Chervin and Schneider (1976) and Laurmann and Gates (1977), only the NCAR model has so far been made to generate preliminary and rather uncertain versions of the estimates of its own natural variability that these protocols require. Because of the multiple computer runs involved in establishing a model's variability, performing experiments along these lines is going to prove very costly. And third, it appears that pinning down predictable SST anomaly effects in the middle and higher latitudes of GCM's, where their variability is greatest, is going to be a particularly arduous task.

5. PREDICTABILITY STUDIES AND THE FUTURE OF SENSITIVITY TESTING

The idea that costly sensitivity tests of the kind described here are relevant and necessary for the development of short-term climate prediction rests on three assumptions: (1) that they will help tell whether a persisting, non-atmospheric anomalous component of the climate system has important effects on atmospheric climate fluctuations; (2) that they will predict the location and even the magnitude of those effects better than will empirical analyses of the available observations; and (3) that they will help point the way to useful predictive models in which the "external" components interact with the atmosphere in a fully-coupled simulation of short-term climate fluctuations. Some recent work on predictability places each of these assumptions in jeopardy.

Robinson (1978) has critically examined the fundamental equations of dynamical large-scale weather and climate prediction, concluding that the derivations are not theoretically sound and that therefore results from the equations are not to be accepted until they have been empirically validated. Furthermore, results need not be superior to those of statistical techniques based on observations alone. Particularly on the matter of calculating credible predictions of human impacts on climate, the implications of Robinson's argument are very serious and should be closely examined. For shorter-term problems, such as interannual prediction of natural fluctuations, many kinds of validation should be possible. None will be quick or easy.

The assumption of the superior efficiency of theoretically-based models against empirically oriented analysis in evaluating "external" effects has also been questioned by Leith (1975). He invoked the fluctuation-dissipation theories of statistical mechanics in a form adapted to two-dimensional turbulence theory to suggest that the consequences of the less external perturbations, such as mid-latitude SST anomalies, could be estimated as well from data as from model simulations.

The third assumption, that sensitivity to a persisting perturbation implies predictability in an interacting climate system, has received a blow from calculations run with something much simpler than a GCM: Lorenz's classic two-level, global, truncated spectral model. Salmon and Hendershott (1976) equipped it with an underlying "ocean" that could store and release heat, but not move. Continents and mountains were omitted, as were all of the spherical harmonics of wind and temperature except 3 meridional and 5 longitudinal ones and their combinations. The model's free parameters were adjusted to tune its energetics to realistic values known from observation. An array of 6 fixed mid-latitude SST anomalies around each hemisphere, alternating +4 and -4°C produced an apparently significant set of effects over a year's worth of constant winter conditions. When, however, thermal interaction with the atmosphere was allowed to modify the SST values in a shallow "mixed layer" during a second run, all significance of the new results vanished in the noise of the model's variability.

One might be tempted to generalize from Salmon and Hendershott's experiment to the real atmosphere, to all seasons of the year and other latitudes, and to a conclusion that allowing interactive feedback between air and sea must destroy any atmospheric predictability associated with a constant SST pattern. Indeed, an observational study by Davis (1976) of the statistical relationships between SST's and sea level pressures in the North Pacific mid-latitudes appeared to support this line of reasoning. He concluded that the only evidence of a predictable forcing influence suggested in these statistical relationships was one where the SST field responded to anomalies of sea level pressure, and not vice-versa.

Subsequent work by Namias (1976), however, suggested that summer SST's near the Aleutians could in fact be used to predict subsequent sea level mean pressures there in autumn; this result was supported and extended by Davis (1978) to include prediction of winter mean pressure from autumn SST. Davis' earlier treatment of all seasons together had masked these relationships. Predictions of about the same quality and several months greater range based on pressures instead of SST's also emerged from Davis' second analysis. Best predictions were obtained by combinations of SST and pressure; no good predictions for spring or summer came from either field. Davis concluded that unless the initial SST's and pressures were responding to some common influence, predictability of ensuing pressures was the result of dynamical interactions between the two fields and not of action by either field alone. These conclusions, unanticipated by anyone relying on Salmon and

Hendershott's model experiment, require us to go slowly in generalizing from it. Interactive air-sea feedback may destroy predictability, or it may not. As Robinson (1978) stressed, empirical verification holds the key to any valid judgment.

Particularly in light of Robinson's strictures, I believe that future sensitivity tests of the kind described here should be run in a truly predictive--and thus verifiable--mode. In this mode, model-generated initial conditions would be replaced by real ones; fixed, arbitrary SST anomalies, by evolving real ones. Verification, skipping over the period of dynamical predictability, would begin after two weeks. It would be as intensive as possible, perhaps treating many statistically independent principal components of the atmospheric fields simultaneously in order to shorten the computer runs and reduce the "noise" in the observed data. The model's variability would be estimated with respect to random perturbations of the SST field as well as the initial atmospheric conditions. Careful thought would be given to any possible further refinements of experimental design: cost would be a severe limiting factor and inconclusive results no longer tolerable.

When SST sensitivity tests with GCM's are first put in a predictive mode, Leith and Robinson's conjecture about the equal validity of linear statistical estimates of SST effects should if possible be tested in parallel on the same cases. The results may determine whether any further tests with GCM's are justified.

REFERENCES

Bjerknes, J., 1966: A possible response of the atmospheric Hadley circulation to equatorial anomalies of ocean temperature. Tellus, v. 18, 820-829.

Chervin, R.M., and S.H. Schneider, 1976a: A study of the response of the NCAR GCM climatological statistics to random perturbations: Estimating noise levels. J. Atmos. Sci., v. 33, 391-404.

Chervin, R.M., and S.H. Schneider, 1976b: On determining the statistical significance of climate experiments with general circulation models. J. Atmos. Sci., v. 33, 405-412.

Chervin, R.M., W.M. Washington and S.H. Schneider, 1976: Testing the statistical significance of the response of the NCAR general circulation model to North Pacific ocean surface temperature anomalies. J. Atmos. Sci., v. 33, 413-423.

Davis, R.E., 1976: Predictability of sea surface temperature and sea level pressure anomalies over the North Pacific Ocean. J. Phys. Oceanogr., v. 6, 249-266.

Davis, R.E., 1978: Predictability of sea level pressure anomalies over the North Pacific Ocean. J. Phys. Oceanogr., v. 8, 233-246.

Doberitz, R., 1968: Cross spectrum analysis of rainfall and sea temperature at the equatorial Pacific Ocean. Bonner Meteor. Abhand., No. 8.

Houghton, D.D., J.E. Kutzbach, M. McClintock and D. Suchman, 1974: Response of a general circulation model to a sea temperature perturbation. J. Atmos. Sci., v. 31, 857-868.

Julian, P.R., and R.M. Chervin, 1978: A study of the Southern Oscillation and Walker Circulation phenomenon. Mon. Wea. Rev., v. 106, 1433-1451.

Krueger, A.F. and T.I. Gray, Jr., 1969: Long-term variations in equatorial circulation and rainfall. Mon. Wea. Rev., v. 97, 700-711.

Kutzbach, J.E., R.M. Chervin and D.D. Houghton, 1977: Response of the NCAR general circulation model to prescribed changes in ocean surface temperature, Part I: mid-latitude changes. J. Atmos. Sci., v. 34, 1200-1213.

Laurmann, J.A., and W.L. Gates, 1977: Statistical considerations in the evaluation of climatic experiments with atmospheric general circulation models. J. Atmos. Sci., v. 34, 1187-1199.

Leith, C.E., 1975: Climate response and fluctuation dissipation. J. Atmos. Sci., v. 32, 2022-2026.

Namias, J., 1976: Negative ocean-air feedback systems over the North Pacific in the transition from warm to cold seasons. Mon. Wea. Rev., v. 104, 1107-1121.

Ramage, C.S., 1975: Preliminary discussion of the meteorology of the 1972-73 El Niño. Bull. Amer. Meteor. Soc., v. 56, 234-242.

Ramage, C.S., 1977: Sea surface temperature and local weather. Mon. Wea. Rev., v. 105, 540-544.

Ramage, C.S. and T. Murakami, 1973: Comment on the paper by P.R. Rowntree: The influence of tropical East Pacific ocean temperatures on the atmosphere. Quart. J. Roy. Meteor. Soc., v. 99, 393-394. P.R. Rowntree, 1973: Reply. Ibid, p. 394-395.

Ratcliffe, R.A.S., and R. Murray, 1970: New lag associations between North Atlantic sea temperature and European pressure applied to long-range weather forecasting. Quart. J. Roy. Meteor. Soc., v. 96, 226-246.

Robinson, G.D., 1978: Weather and Climate forecasting as problems in hydrodynamics. Mon. Wea. Rev., v. 106, 448-457.

Rowntree, P.R., 1972: The influence of tropical East Pacific ocean temperatures on the atmosphere. Quart. J. Roy. Meteor. Soc., v. 98, 290-321.

Rowntree, P.R., 1976: Response of the atmosphere to a tropical Atlantic ocean temperature anomaly. Quart. J. Roy. Meteor. Soc., v. 102, 607-625.

Salmon, R., and M.C. Hendershott, 1976: Large scale air-sea interactions with a simple general circulation model. Tellus, v. 28, 228-242.

Shukla, J., 1975: Effect of Arabian sea-surface temperature anomaly on Indian summer monsoon: a numerical experiment with the GFDL model. J. Atmos. Sci., v. 32, 503-511.

Shukla, J., and B.M. Misra, 1977: Relationships between sea surface temperature and wind speed over the central Arabian Sea, and monsoon rainfall over India. Mon. Wea. Rev., v. 105, 998-1002.

Sikka, D.R., and K. Raghavan, 1976: Comments on "Effects of Arabian sea-surface temperature anomaly on Indian summer monsoon: a numerical experiment with the GFDL model. J. Atmos. Sci., v. 33, 2252-2253. J. Shukla, 1976: Reply. Ibid., 2253-2255.

Simpson, R. W. and W.K. Downey, 1975: The effect of a warm mid-latitude sea surface temperature anomaly on a numerical simulation of the general circulation of the southern hemisphere. Quart. J. Roy. Meteor. Soc., v. 101, 847-867.

Spar, J., 1973a: Some effects of surface anomalies in a global general circulation model. Mon. Wea. Rev., v. 101, 91-100.

Spar, J., 1973b: Transequatorial effects of sea-surface temperature anomalies in a global general circulation model. Mon. Wea. Rev., v. 101, 554-563.

Spar, J. 1973c: Supplementary notes on sea-surface temperature anomalies and model-generated meteorological histories. Mon. Wea. Rev., v. 101, 767-773.

Stidd, C.K., W.H. Berger, R.M. Born and J.C.K. Huang, 1973: Conference summary of "Climatic changes on time scales ranging from a month to millenia" Bull. Amer. Meteor. Soc., v. 54, 425-432.

CLIMATIC MODELS FOR PLANNING AND SUPPORTING WEATHER SENSITIVE OPERATIONS

Donald E. Martin

Director of Meteorology

Saint Louis University

Department of Earth and Atmospheric Sciences

St. Louis, Missouri 63103

1. INTRODUCTION

Each of the formulae developed by Saint Louis University pertaining to Climatic Mission Success Indicators ($CMSI_t$) requires unconditional probability values for ceiling and/or visibility. These are available primarily in "book" form at ETAC and its Climatic Center at Asheville. A stated objective of the Air Weather Services (AWS) is to compact this information for on-line computer operations. Saint Louis University has proceeded toward that goal in two steps: 1) $CMSI_t$ for joint ceiling and visibility categories for a given location and time have been analytically modeled using Russwo margin data, and 2) the margin data have been compacted in a form suitable for computer processing and for making hand calculations should the need arise.

Computer tapes containing ceiling and visibility observations were obtained from ETAC and processed for a number of station pairs. Analytic functions were then devised for estimating data dependencies which involve time elapses and separation distances. This greatly expands the utility of the Russwo data by tying the statistics for a given hour and station together with those of a later hour and by tying the occurrence probabilities of one location together with those of a neighboring location. In other words, the Russwo data now has the increased dimension of being able to provide climatic mission success indicator and conditional probability estimates.

The problem of providing climatic estimates for data void areas was investigated using West German and United States data. Interpolations (or analyses) based upon peripheral data worked well in those areas where the mesoscale elevations were relatively homogeneous. This procedure, however, produced large errors in the mountain areas.

Our research with German data, where the terrain is rather irregular, showed that comparisons between a station's elevation (E) and its space mean elevation ($\bar{E}$) provided a means of objectively delineating weather sensitive variations on the basis of topography and topographical slopes. Hence, elevation data were acquired from ETAC and processed by Saint Louis University (SLU) to provide a hemispheric fine-scale grid of space mean elevations. The space means were computed by averaging elevations on the circumference of a circle of 20 kilometer radius circumscribed about each grid point.

Various combinations of E and $\bar{E}$ were studied to devise an objective method of describing the mesoscale terrain slope characteristics about a station.

(An elaboration on the materials in this article is being published by AFGL in Scientific Report Number 2 early in 1979.)

2. Modeling the Russwo Margin Data

The Russwo format presents ceiling probabilities irrespective of visibility, visibility probabilities irrespective of ceiling and joint probabilities for various ceiling and visibility combinations, see figure 1.

The formula for determining the

joint probabilities is

$$CMSI_t = 1_o - P_{cig} - P_{vis} + P_{cig} \wedge P_{vis} \quad (1)$$

where P_{cig} is the unconditional probability that ceilings will be observed below a given height and P_{vis} that visibilities will be less than a given distance.

Values of $CMSI_t$ can also be estimated by the formula

$$CMSI_t = 1_o - \frac{P_{cig} + P_{vis}}{2} + \sqrt{\left(\frac{P_{cig}+P_{vis}}{2}\right)^2 - K(P_{vis})(P_{cig})} \quad (2)$$

This expression generates reasonable $CMSI_t$ estimates for any desired ceiling and visiblity combination on a given Russwo page providing the corresponding K-value is known. For most United States locations, the value of K = .87 will suffice. However, certain European stations exhibit a lesser magnitude for this coefficient. A simple scheme for determining the K-value from Russwo margin data is shown in Figure 2.

The procedure is to enter the unconditional probability of ceilings $\geq$ 1000' on the abscissa and the unconditional probability of visibilities $\geq$ 1 mile on the ordinate. The corresponding K-value is read off at the intersection. This K-value can be used to generate $CMSI_t$'s for that particular station, month and hour.

≥ 5	≥ 3	≥ 1	≥0	
63.7	67.2	69.3	70.3	≥ 5000
65.7	69.3	71.7	72.6	≥ 4500
67.5	71.3	73.6	74.6	≥ 4000
69.8	73.8	76.2	77.2	≥ 3500
71.6	75.7	78.4	79.4	≥ 3000
72.8	77.2	80.1	81.2	≥ 2500
74.2	78.9	82.1	83.2	≥ 2000
74.4	79.2	82.4	83.6	≥ 1800
75.2	80.3	83.8	84.9	≥ 1500
75.6	81.0	84.8	85.9	≥ 1200
76.2	81.5	85.6	86.8	≥ 1000
76.5	81.9	86.1	87.4	≥ 900
76.5	82.3	86.8	88.2	≥ 800
76.6	82.5	87.2	88.8	≥ 700
76.7	83.0	88.3	89.9	≥ 600
77.0	83.7	90.2	91.9	≥ 500
77.1	83.8	91.4	93.6	≥ 400
77.1	83.9	92.3	94.8	≥ 300
77.1	84.1	93.2	96.4	≥ 200
77.1	84.1	93.4	98.0	≥ 100
77.1	84.1	93.4	100.0	≥ 0
≥ 5	≥ 3	≥ 1	≥ 0	

Figure 1. A condensed representation of the McGuire Russwo for Feb. 0300-0500 LST.

Note: The values in figures 1 and 2 are expressed in percentages. The probabilities in the various equations which use these values are expressed as decimals.

CEILINGS ≥ 1000'

VISIBILITY	98	96	94	92	90	88	86	84
66	94	92	92	90	88	87	87	85
68	95	94	92	91	88	87	87	86
70	97	96	94	91	90	89	88	87
72	98	98	96	94	92	90	89	88
74	97	97	97	96	94	93	90	89
76	95	96	96	96	94	93	91	90
78	93	94	94	94	94	93	91	90
80	92	92	92	92	91	90	89	89
82	91	90	89	88	88	88	88	88
84	90	88	86	86	85	85	85	85
86	86	83	82	81	81	81	82	82
88	82	80	78	76	76	77	78	79
90	80	76	73	72	72	74	77	79
92	76	72	70	69	72	75	78	82
≥ 94	74	68	70	74	78	81	84	86
96	68	72	76	81	84	86	88	89
98	72	76	80	84	86	88	89	90
	98	96	94	92	90	88	86	84

VISIBILITY: ≥ 1 mi

Figure 2. A condensed representation of the K-value graph for use in equation 2.

The ≥ 1000'/ ≥ 1 combination was selected for figure 2 since it tunes the coefficient, K, to the lower ceiling and visibility categories without seriously jeopardizing the accuracy of the higher ceiling and visibility combinations. The data for Figure 2 was obtained by processing over 200 Russwo stations for randomly selected hours and months. Computed values of

$$K = \frac{(1_o - CMSI_t)/\bar{P}_{vis<1\ mi} + P_{cig<1000'} - (1_o - CMSI_t)/}{(P_{vis<1\ mi})(P_{cig<1000'})} \quad (3)$$

were obtained where $CMSI_t$ refers to the ≥ 1000'/ ≥ 1 mi category in this case, and plotted on a common graph. The composite plot was then analyzed as a universal field and transposed into the gridded values of figure 2.

2.1 Examples

Figure 1 shows a value of 86.8% for ceilings ≥ 1000' and 93.4% for visibility ≥ 1 mile. When these probabilities are entered into the matrix in Figure 2, a K-factor of approximately .82 results. This K-value inserted into equation 2 will provide $CMSI_t$ estimates for any desired ceiling/visibility combination for McGuire AFB in February during the 03-05 time period (LST). Suppose a $CMSI_t$ magnitude is desired for the

≥ 5000'/ ≥ 3 mile combination. Referring to figure 1, a value of .297 for ceilings < 5000' is obtained. Similarly, the visibility value from the Russwo margin is .159 for P_{vis} <3 miles. Inserting these values into equation 2 along with the corresponding K-value of .82 gives:

$$CMSI_t = 1. - \left(\frac{.297+.159}{2}\right) - \sqrt{\left(\frac{.297+.159^2}{2}\right) - (.82)(.297)(.159)} \quad (4)$$

or $CMSI_t$ = 65.7%. This estimate compares favorably with the 67.2% magnitude given in the Russwo. In contrast, the independent assumption would grossly underestimate the Russwo value by giving $CMSI_i$ = 59.1%.

3. COMPACTING THE RUSSWO MARGIN DATA

Saint Louis University has devised methods for compressing probabilities of ceiling and visibility occurrences with a minimal loss of accuracy, see figure 3.

Note that the ceiling and visibility categories are cumulative and range from very restrictive to essentially non-restrictive weather conditions. A nine digit number is aligned with each category and month. The first digit is the multiplier to be applied to each of the following 8 digits in order to reproduce the diurnal profile for the corresponding category and month. The second through ninth digits of the nine-digit number are the coded probabilities for the time intervals 0-2, 3-5, 6-8, 9-11, 12-14, 15-17, 18-20 and 21-23 LST respectively. To reproduce the original diurnal profile, simply multiply the factor (first digit) by each of the following eight digits. As an example, the following sequence applies to the <1000' category in Figure 3 for January.

9-digit number
246764334

compacted diurnal profile
ceilings <1000'

hr	0	3	6	9	12	15	18	21
	2	5	8	11	14	17	20	23
	8	12	14	12	8	6	6	8

diurnal profile given by the original Russwo

9	11	13	12	8	6	6	7

The accuracy with which the nine-digit number will approximate the unconditional Russwo or "D" summary data (from which the original data for compaction were extracted) is ≤½% x multiplier. The role of this multiplier, therefore, is merely to restrict each diurnal profile to nine digits and to minimize the round off error.

WEBB AFB LAT = 32.2 LONG = 101.5

ELEVATION (E) 781 meters E/$\bar{E}$ = _____

	DEC	JAN
500 FT	167863334	233542222
<1000 FT	256764334	246764334
<3000 FT	356765444	356665434
<5000 FT	367775545	366765445
<10000 FT	367886655	378886656
<.5 MI	112321111	123431112
<1 MI	133431211	134653222
<3 MI	155765433	156986544
<5 MI	234544322	234554432
<6 MI	244554423	234655533

	FEB	MAR
<500 FT	234542112	123421112
<1000 FT	256774334	146874333
<3000 FT	367886444	345664322
<5000 FT	367887555	346763433
<10000 FT	466776544	367876545
<.5 MI	123311111	101100000
<1 MI	145532212	112222211
<3 MI	168986555	133566543
<5 MI	245665433	222443432
<6 MI	245776544	233456543

Figure 3. An extract from the compacted Russwo data for Webb AFB, Texas.

Other benefits to be gained by presenting the compacted Russwo data in the form of diurnal profiles will be discussed in Section 4.

4. MODELING $CMSI_t$ FOR CEILING AND VISIBILITY WHEN TIME AND SPACE DIFFERENTIALS ARE INVOLVED

4.1 Discussion

Equations 5 and 6 were employed to model the joint probability term, $P_1 \wedge P_2$, as a function of time and distance differentials. These equations, together with the Russwo margin data such as that found in figure 3, provide $CMSI_t$ and persistency estimates for a specific location as well as joint probability estimates when more than one station is involved.

$$r^2 = \frac{P_1 \wedge P_2 - (P_1)(P_2)}{P_2 - (P_1)(P_2)} \quad \text{where } P_1 > P_2 \quad (5)$$

$$r^2 = \frac{P_1 \wedge P_2 - (P_1)(P_2)}{P_1 - (P_1)(P_2)} \quad \text{where } P_1 < P_2 \quad (6)$$

Here P_1 is the unconditional probability of either ceiling or visibility (whichever variable is being studied) at the starting hour and location and P_2 the unconditional probability of

that same variable at the ending hour and/or location. The value of r computed by this formula closely approximates the correlation coefficient needed to model $P_1 \wedge P_2$ using the U.S. Bureau of Standard's bivariate normal tables. The numerator on the right hand side of equations 5 and 6 represents the "actual" joint relationship between P_1 and P_2 in excess of chance. The denominator represents the maximum value that $P_1 \wedge P_2$ could possibly attain in excess of chance.

Computer tapes from ETAC (Asheville, N.C.) provided the raw data for computing r^2 as a function of distance and time differentials. A comprehensive discussion on how the r^2-values were obtained is found in [17].

To limit the data handling, three ceiling and three visibility categories were selected, i.e., cig <1000', <500', <200' and visibility <3 mi, <1 mi, <½mi for each of these routes and their return trips (Mildenhall to Lakenheath and Lakenheath to Mildenhall, for example). Time lags of 0, 3, and 6 hours were chosen for months representative of the four seasons of the year. Calculated r^2-values were aligned by month and distance to provide arrays such as that in Figure 4.

Equations for modeling the r^2-values are presented in Figure 5. The decay rates for r^2-values with separation distances in excess of 20 kilometers generally, follow different exponential curves than for r^2-values ranging between 0 and 20 kilometers. Hence, the equations are formulated about the 20 kilometer value with zero time lag. They exhibit the properties of logarithmic decay functions with respect to distance and time from that starting point. For distances less than 20 km, a linear interpolation between the 20 km and 0 km r^2-values best fits the data.

For illustration purposes, consider the equations in Figure 5 for <1000'.

Jan: $r^2 = \exp - [.13 + .07t + .003 (S-20) \exp - .13t]$ (7)

April: $r^2 = \exp - [.24 + .07t + .0045 (S-20) \exp - .07t]$ (8)

The first term in the exponent of each equation sets the starting point by specifying the power to which the exponent, e, must be raised to give r^2 at 20 km if no time lag is involved. I.e., $e^{-.13} = .88$ and $e^{-.24} = .79$, which correspond with the magnitudes found in Figure 4 at 20 km for 0-time lag during January and April, respectively.

r^2 Values for Ceilings <1000' with 0-Hr Time Differential Route Distance in Air Kilometers

	0	20	40	60	80	100	120	140
Jan.	1.00	.88	.83	.78	.73	.69	.65	.61
Feb.	1.00	.87	.82	.76	.71	.67	.63	.59
Mar.	1.00	.83	.77	.72	.66	.62	.57	.53
Apr.	1.00	.79	.72	.66	.60	.55	.50	.46
May	1.00	.75	.67	.60	.54	.48	.43	.39
June	1.00	.71	.62	.56	.49	.43	.37	.33
July	1.00	.70	.61	.54	.47	.41	.35	.31
Aug.	1.00	.71	.62	.56	.49	.43	.37	.33
Sept.	1.00	.75	.67	.60	.54	.48	.43	.39
Oct.	1.00	.79	.72	.66	.60	.55	.50	.46
Nov.	1.00	.83	.77	.72	.66	.62	.57	.53
Dec.	1.00	.87	.82	.76	.71	.67	.63	.59

r^2 Values for Ceilings <1000' with 3-Hr Time Differential Route Distance in Air Kilometers

	0	20	40	60	80	100	120	140
Jan.	.74	.71	.68	.66	.63	.61	.58	.56
Feb.	.73	.70	.67	.65	.61	.59	.56	.54
Mar.	.71	.67	.64	.61	.57	.55	.51	.49
Apr.	.69	.64	.59	.55	.51	.48	.44	.41
May	.67	.61	.55	.49	.45	.42	.37	.33
June	.66	.59	.51	.45	.41	.37	.32	.28
July	.64	.57	.50	.44	.39	.35	.30	.26
Aug.	.66	.59	.51	.45	.41	.37	.32	.28
Sept.	.67	.61	.55	.49	.45	.42	.37	.33
Oct.	.69	.64	.59	.55	.51	.48	.44	.41
Nov.	.71	.67	.64	.61	.57	.55	.51	.49
Dec.	.73	.70	.67	.65	.61	.59	.56	.54

r^2 Values for Ceilings <1000' with 6-Hr Time Differential Route Distance in Air Kilometers

	0	20	40	60	80	100	120	140
Jan.	.60	.58	.56	.55	.53	.52	.50	.49
Feb.	.60	.57	.55	.54	.52	.51	.48	.47
Mar.	.58	.55	.52	.50	.48	.46	.44	.42
Apr.	.56	.52	.49	.46	.43	.41	.38	.36
May	.54	.49	.45	.42	.38	.35	.32	.30
June	.51	.47	.43	.38	.34	.31	.28	.25
July	.51	.46	.42	.37	.33	.30	.26	.23
Aug.	.51	.47	.43	.38	.34	.31	.28	.25
Sept.	.54	.49	.45	.42	.38	.35	.32	.30
Oct.	.56	.52	.49	.46	.43	.41	.38	.36
Nov.	.58	.55	.52	.50	.48	.46	.44	.42
Dec.	.60	.57	.55	.54	.52	.51	.48	.47

Figure 4. An extract of the r^2-value graph of [17] for determining joint relationships of ceilings <1000' separated by distance and time.

Category	Formulae
Ceilings < 1000'	
January:	$r^2 = e^{-[.13 + .07t + .003(S-20)\, e^{-.13t}]}$
April or October:	$r^2 = e^{-[.24 + .07t + .0045(S-20)\, e^{-.07t}]}$
Ceilings < 500'	
January:	$r^2 = e^{-[.21 + .09t + .004(S-20)\, e^{-.12t}]}$
April or October:	$r^2 = e^{-[.26 + .13t + .007(S-20)\, e^{-.06t}]}$
Ceilings < 200'	
January:	$r^2 = e^{-[.26 + .12t + .0067(S-20)\, e^{-.07t}]}$
April or October:	$r^2 = e^{-[.40 + .16t + .011(S-20)\, e^{-.04t}]}$
Visibility < 3 Miles	
January:	$r^2 = e^{-[.25 + .06t + .0034(S-20)\, e^{-.05t}]}$
April or October:	$r^2 = e^{-[.29 + .11t + .0044(S-20)\, e^{-.03t}]}$
Visibility < 1 Mile	
January:	$r^2 = e^{-[.33 + .12t + .0045(S-20)\, e^{-.04t}]}$
April or October:	$r^2 = e^{-[.45 + .19t + .0075(S-20)\, e^{-.02t}]}$
Visibility < ½ Mile	
January:	$r^2 = e^{-[.42 + .12t + .006(S-20)\, e^{-.03t}]}$
April or October:	$r^2 = e^{-[.53 + .19t + .014(S-20)\, e^{-.01t}]}$

Figure 5. Analytic formulation of r^2-values for ceiling and visibility.

The next term in each of these equations adjusts r^2 to account for time differences. For example, at 20 km and 3-hr time lag, exp - (.13+.21) = exp -34 = .71 in January and r^2 = exp - (.24+.21) = exp -45 = .64 in April (see Figure 4 for verification).

Finally r^2 is adjusted for distances other than 20 km by the last term in the equation. For a separation distance of 140 km and 3-hr time lag, our example would show exp - [.13+.21 +(.003)(120) exp - .39] = exp -.58 =.56 in January and exp - [.24+.21+.0045(120) exp -21] = exp - [89] = .41 in April as indicated by Figure 4.

In a previous report, (see bibliography reference [2], Billiken factors were calculated for numerous stations for all months of the year using statistics from a dense data base provided by ETAC. It was found that the Billiken factors varied exponentially with distance and periodically with month. The r^2-values can be expected to behave likewise since the two are closely related.

I.e, the Billiken factor can be expressed in terms of r^2 by the equation

$$r^2 = 1_o - \beta(1-P_L) \qquad (9)$$

where P_L is the larger of the two ceiling or visibility unconditional probabilities involved.

The Billiken factor research experience provided the insight for representing the r^2-values by a combination of exponentials and cosine functions. The equations in Figure 5, for January and April, contain sufficient information to generate r^2-values for each month of the year. The procedure for doing this is to first determine the January and April r^2-values. The difference between January and April's r^2-values defines the amplitude (A) for the function.

$$r^2_M = r^2_{April} + A \cos \left[(M-1) \frac{\pi}{6} \right]. \qquad (10)$$

Here M refers to the given month under consideration where January begins with 1. For example, r^2 for the month of March would be

$$r^2_{April} + A \cos \left[(3-1) \frac{\pi}{6} \right] =$$

$$r^2_{April} + .5A.$$

Various "conditional" probability estimates and $CMSI_t$ calculations can be readily made using statistics such as those shown in figure 4 or their equivalent in figure 5 and the compacted Russwo margin values illustrated in Figure 3.

In equations 11, 12 and 13;

$$CMSI_t = 1_o - P_1 - P_2 + P_1 \wedge P_2 \qquad (11)$$

$$\text{and } CMSI_i = 1_o - P_1 - P_2 + P_1 P_2 \qquad (12)$$

$$\text{or } CMSI_i = (1_o - P_1)(1_o - P_2) \qquad (13)$$

P_1 and P_2 represent a pair of ceiling or visibility unconditionals for locations separated by distance and/or time. When equation 5 or 6 is substituted into (11), the following expressions result:

$$CMSI_t = 1_o - P_1 - P_2 + P_1 P_2 + r^2 P_2 (1_o - P_1) \qquad (14)$$

where $P_1 > P_2$

$$CMSI_t = 1_o - P_1 - P_2 + P_1 P_2 + r^2 P_1 (1_o - P_2) \qquad (15)$$

when $P_2 > P_1$

An alternate expression in terms of equation 12 is

$$CMSI_t = CMSI_i + r^2 P_S (1_o - P_L) \qquad (16)$$

where P_S denotes the smaller and P_L the larger of the two unconditionals involved.

4.2 Examples

1. Calculating $CMSI_t$

Suppose the probability of observing ceilings below 500 ft. at a given station at 00 LST in January is 10%. Assume a neighboring station located 60 kilometers away for January at 03 LST, has odds of 15%. What are the chances of making this flight when ceiling conditions below 500 ft. constitute the deciding criterion? Figure 5 indicates an r^2-value of .55 for this time and space differential. From equation 13, $CMSI_i = (1.00 - .15)(1.00 - .10) = 76.5\%$. The magnitude of the second term in equation 16 is

$$r^2 P_S (1_o - P_L) = .55 (.10) (.85) = 4.7\%$$

Thus the odds of making the flight are $76.5\% + 4.7\% = 81.2\%$

2. Calculating Persistency Probabilities

The probability that an event will persist can be modeled by using the r^2-values in Figures 5 and the compacted data of Figure 3. The equations that apply are:

$$P_{(2|1)} = \frac{P_1 \wedge P_2}{P_1} = r^2 + (1.00 - r^2) P_2$$

when $P_1 < P_2$ (17)

$$\text{and } P_{(2|1)} = r^2 \frac{P_2}{P_1} + (1.00 - r^2) P_2$$

when $P_1 > P_2$ (18)

Here P_1 is the unconditional probability at the hour that the forecast is made and P_2 the unconditional probability at a later time, say 3 hours later.

Consider a 3-hour persistency forecast of ceilings < 1000' at Webb AFB in January made during the 06-08 Local Standard Time interval. The unconditional ceiling probabilities from Figure 3 are .14 for P_1 and .12 for P_2. An r^2-value of .74 is obtained from the center array in Figure 4. From equation 18, $(P_{2|1}) = .74 \left(\frac{.12}{.14}\right) + (.26)\ .12 = 66.5\%$. Had the unconditional probabilities been reversed so that formula 17 were to apply, then $(P_{2|1})$ would have been 78%. This example indicates how the slope of the diurnal unconditional profile for a given ceiling or visibility event influences the persistency of that event.

3. Estimating Conditional Probabilities for Locations Separated by Distances and Events Separated by Time

The probability that a ceiling or visibility event occuring at station A will also be observed at station B at the same or some subsequent time can be determined from the corresponding r^2-value provided by Figure 5, the unconditional probability at station A at the time that the forecast is made, and the unconditional probability at station B at the verifying time. These values inserted into either equation 17 or 18 (whichever applies) will provide the desired conditional probability. For example, suppose that ceilings <1000' are occurring at station A at 0400 LST in January. What is the probability that this event will occur at station B located some 60 km away at 0700 LST? Figure 4 gives the r^2-value of .66. Let us suppose that the respective unconditionals were found to be .20 for station A and .25 for station B. Here equation

$$P_{2|1} = r^2 + (1. - r^2)\, P_2,$$

applies since $P_2 > P_1$.

Hence,

$$P_{2|1} = .66 + (.34)(.25) = 74.5\%$$

	Hr	0-2	3-5	6-8	9-11	12-14	15-17	18-20	21-23
<500	Sept.	36	41	42	33	30	22	17	19
	Oct.	70	72	72	74	69	66	63	64
	Nov.	65	57	54	48	47	51	52	54
<1,000	Sept.	39	42	44	39	38	30	25	28
	Oct.	72	74	75	74	74	72	70	68
	Nov.	58	60	57	52	52	57	58	58
<3,000	Sept.	45	46	47	46	45	41	38	34
	Oct.	73	75	76	78	76	74	42	36
	Nov.	70	62	59	56	56	60	62	62
<5,000	Sept.	47	49	49	48	46	43	41	38
	Oct.	70	76	76	79	76	76	43	37
	Nov.	70	62	60	56	58	62	62	62
<10,000	Sept.	48	50	51	50	48	44	42	42
	Oct.	75	77	78	80	77	77	44	38
	Nov.	71	63	61	58	60	63	64	63
<½ mi.	Sept.	34	40	54	31	27	16	14	15
	Oct.	65	72	73	72	69	60	59	61
	Nov.	61	64	60	60	55	57	57	60
<1 mi.	Sept.	35	41	55	33	29	19	15	17
	Oct.	72	73	74	74	70	61	61	63
	Nov.	64	66	62	62	59	60	60	62
<3 mi.	Sept.	43	44	60	39	37	27	20	21
	Oct.	74	76	77	77	63	67	65	67
	Nov.	67	68	63	65	64	64	64	65
<5 mi.	Sept.	50	50	67	46	45	34	27	28
	Oct.	76	68	68	80	76	71	69	70
	Nov.	68	70	64	69	67	67	68	68
<6 mi.	Sept.	51	51	70	49	49	38	30	31
	Oct.	77	78	79	81	77	73	70	71
	Nov.	69	70	65	70	69	69	69	68

Figure 6. Ceiling and visibility occurrences in percentages for mountain stations in Germany where $2.5 < \frac{E}{E} < 3.5$.

5. ESTIMATING CLIMATIC PROBABILITIES FOR DATA VOID AREAS

In the introduction it was stated that comparisons between the elevation at a station and the space mean of the elevations about the station offered insights into varying climatic probabilities.

Figures 6 and 7 provide evidence of this fact. Our preliminary recommendations for treating the data void areas are:

(a) Determine the elevation (E) from topographical maps for the location involved.

(b) Calculate an $\overline{E}$ value by averaging the terrain heights for a number of equally-spaced points on the circumferences of a 20 kilometer radius circle circumscribed about that point.

(c) Calculate the ratio $E/\overline{E}$.

(d) If $E/\overline{E}$ has a magnitude close to one or if the altitude is less than 300 meters analyze the probability values at the neighboring stations and interpolate to the location under consideration.

(e) If $E/\overline{E}$ varies more than ± 10% from unity and the elevation exceeds 300 m seek out a neighboring station(s) having an $E/\overline{E}$ value that most closely matches that computed in Step 3. Use the climatic data for the selected analogue as a direct substitute for the data-sparse location.

		Hr. 0-2	3-5	6-8	9-11	12-14	15-17	18-20	21-23
<500	Sept.	2	4	6	2	1	0	0	1
	Oct.	4	7	12	7	2	1	1	4
	Nov.	4	6	7	5	3	3	3	5
<1,000	Sept.	3	6	9	6	3	2	2	2
	Oct.	6	10	18	16	8	5	4	8
	Nov.	10	13	16	16	11	11	10	9
<3,000	Sept.	13	18	23	23	21	15	11	11
	Oct.	27	34	40	39	34	26	21	26
	Nov.	42	43	48	49	48	43	40	40
<5,000	Sept.	21	28	36	34	34	28	22	19
	Oct.	38	43	51	49	44	39	33	36
	Nov.	53	57	65	65	61	58	51	52
<10,000	Sept.	34	40	49	46	46	40	37	28
	Oct.	47	49	58	57	52	48	42	46
	Nov.	66	69	74	74	70	68	66	64
<½ mi.	Sept.	2	7	9	2	0	0	0	1
	Oct.	5	8	13	6	1	0	1	4
	Nov.	2	4	5	4	1	1	2	2
<1 mi.	Sept.	4	11	14	4	0	0	0	2
	Oct.	7	13	20	11	3	1	2	6
	Nov.	9	9	11	9	4	4	6	8
<3 mi.	Sept.	14	29	35	21	8	5	5	8
	Oct.	26	33	43	36	17	11	16	24
	Nov.	31	33	37	36	23	23	26	29
<5 mi.	Sept.	32	45	52	36	18	12	14	22
	Oct.	53	60	68	55	32	26	35	46
	Nov.	53	54	57	55	41	42	45	52
<6 mi.	Sept.	46	57	61	44	23	17	22	32
	Oct.	67	72	75	64	42	35	46	57
	Nov.	65	65	66	63	51	52	55	60

Figure 7. Ceiling and visibility occurrences in percentages for valley stations in Germany where $\frac{E}{\overline{E}} < .7$.

Since $E/\bar{E}$ does not distinguish the sign of terrain slope, care must be exercised to confine the search to those stations lying on the same side of mountain ranges or other pronounced topographical features.

(f) If no reasonable analogue can be found, investigate the elevation (E), the space mean elevation, ($\bar{E}$), and the climatic probabilities for neighboring stations to uncover relationships between terrain features and the local climatology of that area. Once terrain-based relationships are established for a given data-void location, climatic estimates can be made since the values of E and $\bar{E}$ are known for the data void region.

6. REFERENCES

1. Martin, Donald E. and Myers, Eloise M., "Climatic Models that Will Provide Timely Mission Success Indicators for Planning and Supporting Weather Sensitive Operations," AFGL-TR-77-258, Hanscom AFB, Mass. 1977.

2. Martin, Donald E., "Research to Develop Improved Models of Climatology that Will Assist the Meteorologist in the Timely Operations of the Air Force Weather Detachments," AFGL-TR-76-0249, Hanscom AFB, Mass., 1976.

3. Martin, Donald E. and Myers, Eloise M., "Climatic Models that Will Provide Timely Mission Success Indicators for Planning and Supporting Weather Sensitive Operations, "Scientific Report Number 2, to be published in 1979 by AFGL.

DEVELOPMENT OF AN ELECTRO-OPTICAL PARAMETER CLIMATOLOGY

Andreas Goroch
Naval Environmental Prediction Research Facility
Monterey, California 93940

and

Barry Katz
Naval Surface Weapons Center
Silver Spring, Maryland 20910

ABSTRACT

The requirements of an EO climatology are that it provide expected values of electro-optical system parameters (a) to system analysts to specify range and variability of system performance and (b) to operational users to provide expected systems performance under operational conditions. The ability to satisfy these requirements is limited by the accuracy of available models. The EO system model used in the present development is composed of an integrated group of aerosol, molecular, and extinction occurrence algorithms. It was compared to a set of independent measurements, and agreement was found to be satisfactory. Data from ocean station vessels (OSV) were used to calculate the frequency of occurrence of extinction at several visible and infrared frequencies. Examples of calculations for data from ocean station vessel JULIET are shown.

1. INTRODUCTION

The use of an EO system as a component of a weapons system suite requires an adequate understanding of the advantages and limitations of the EO system in an operational environment. A climatology of marine environmental effects on such systems is being developed to satisfy these needs for two user communities: systems designers and operational users. The designer must know the frequency of occurrence of environmental effects on EO systems; for this purpose, a summary of frequencies of occurrence of such parameters as optical extinction and turbulence is sufficient. The operational user must have this same information, but an additional requirement is knowledge of persistence, i.e., how long these conditions are expected to continue. The present or planned deployment of several hundred types of EO systems makes the need for a climatology that provides such information increasingly pressing.

The most important requirement of such a climatology is that it describe the actual physical situation correctly. This places a constraint on the model being used, and on the data to which the model is applied. For example, we cannot apply a physical model to the climatological means of meteorological variables in order to infer the expected value of extinction of an EO signal. Extinction is found to be related to both wind speed and ambient relative humidity, and these variables are not correlated; consequently, the resultant extinctions may not be the mean value of extinction. In fact, the model must be applied to each set of simultaneous wind and relative humidity records, and then the extinctions must be averaged in order to produce an accurate picture of the occurrences.

2. GENERAL MODEL CHARACTERISTICS

The model we have chosen consists of three segments: molecular absorption, turbulence, and aerosol extinction.

Molecular extinction of the optical signal is calculated by using a linear fit to the LOWTRAN IIIB computer code, the characteristics of which are described by Selby et al. (1976). Turbulence effects are described by a model proposed by Davidson (1975), based on parameterizations of heat and flux profiles. The present work discusses the aerosol extinction, outlining problem areas and options for resolution as well as our choice of aerosol submodels for use in the climatology.

Before the model is discussed, it is important that the difference between aerosol extinction in the visible and infrared wavelength bands be understood. Figure 1 shows the contribution of segments of a marine aerosol size

distribution at visible (0.55 μm) and infrared (1.06, 3.8, 10.6 μm) wavelengths. Most extinction at each wavelength is due to particles about a wavelength in diameter. Thus, most extinction at visible wavelengths is due to submicron particles with little contribution by the relatively rare large aerosols. At the longer wavelengths, large particles (although rare) account for most of the extinction. This point underscores the importance of knowing the correct concentrations of large sea-salt aerosols, which constitute most of the large marine aerosols.

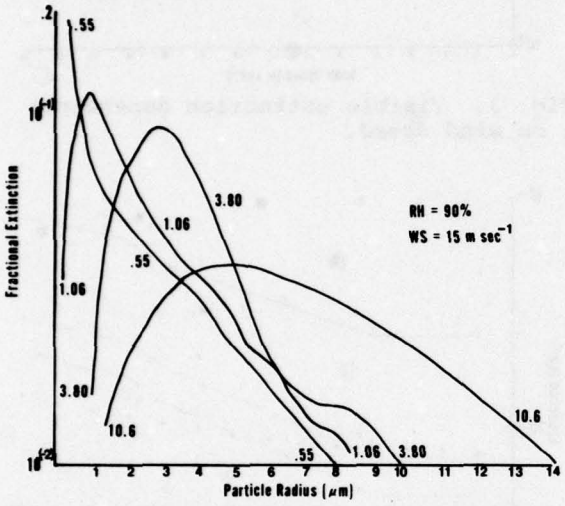

Fig. 1. Aerosol fractional contribution to extinction.

3. AVAILABLE AEROSOL MODELS

The aerosol model is separated into two parts: one describing the growth of particles with relative humidity, and the other describing the wind-dependent concentration of marine aerosols.

Probably the best understood component is the relationship of aerosol size and relative humidity; comprehensive reviews of the subject have been developed by Fitzgerald (1978) and Hänel (1976). Their conclusions are similar, although Hänel describes a more precise treatment of the behavior of sea-salt aerosols, including hysteresis of the aerosol growth curve between 40% and 70% relative humidity. It is questionable that this state of double values actually will be observed under atmospheric conditions, because of the latent variability of atmospheric humidity and aerosol composition. The relationship of aerosol size to humidity used in the present model is that of Fitzgerald (1978).

The wind-speed dependence of aerosol concentrations has been treated in a range of models by evaluating wind-speed-dependent coefficients of aerosol size distributions from measured data. Perhaps the most straightforward model is that of Fitzgerald (1976), which determines the constants of a logarithmic Junge distribution (Junge, 1963) as polynomials of wind speed. An alternative approach -- proposed by Barnhardt and Streete (1970) and used by Wells, Gall and Munn (1977) and Katz (1976) -- considers the aerosol distribution to have a background component independent of wind, and a maritime component generated by wind/wave interaction; the large sea-salt aerosols are accounted for by the maritime component.

Chaen (1973) proposed a different theory relating aerosol distribution to the degree of wave breaking. This formulation has the advantage of using not only wind-speed information, but also other influences including sea state and atmospheric stability.

The models of the dependence of aerosol distribution on wind speed can be chosen from a variety of available treatments. The main characteristic of the available models is that, to a large extent, they are empirical fits to a particular data set. Hence the optimal model should not only fit its own data well, as all models do, but should be amenable to modification for a wide range of conditions that includes type of air mass under consideration, proximity of land and surf aerosol sources, and varying sea surface compositions. In this regard, the two component models of Wells, Gall and Munn (1977) and Katz (1976) show an advantage since such flexibility is inherent in their formulations. In addition, concentrations of maritime aerosols have been shown to fit a modified gamma function rather than a logarithmic function in this distribution.

The model of Chaen (1978) is quite attractive in that it includes several clearly important parameters such as sea state and stability. The derivation of this model is based on data lacking an adequate consideration of the effects of relative humidity on size distributions and hence is not used here.

The predictions of the various models are evaluated for a relative humidity value of 85% and a wind speed of 4.4 m/sec (Fig. 2). The models exhibit a good agreement over the range of aerosol sizes. In general, the model of Chaen seems to predict a smaller concentration of aerosols in the size range below 1 μm.

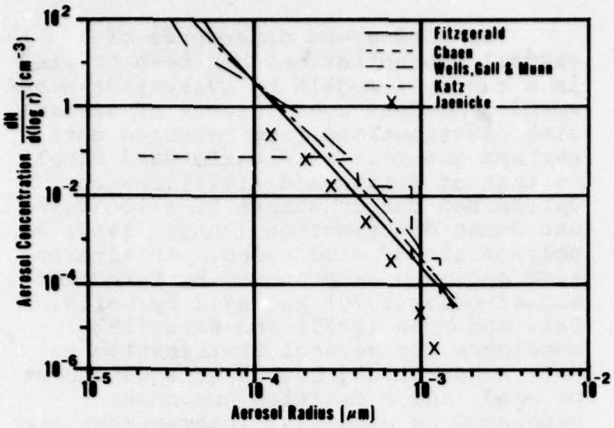

Fig. 2. Comparison of aerosol size distributions: RH=85% and WS=4.4 m/s.

Independent measurements of aerosol size distribution were made during a cruise of the research vessel METEOR in the northern and central Atlantic (Jaenicke et al., 1970). The data were obtained using a combination of diffusion batteries, impactors, and an optical particle counter. There is agreement in most values of the concentrations. The measured data show smaller concentrations of large particles (greater than 10 μm) than the model results.

The main application of the aerosol concentrations is for extinction calculations. The aerosol concentration data of Jaenicke et al. (1970) were fitted to a smooth curve, and were used to calculate extinction coefficients for the three wind speeds of the data, assuming a relative humidity of 85%. This was compared to the extinction coefficient calculated by using the Katz aerosol model for a range of wind speeds from 0.5 to 25 m/sec and relative humidities of 75%, 85%, and 95%.

The wind-speed dependence of aerosol mass concentration of Lovett (1978) was also compared to the latter results. A low wind aerosol distribution of Jaenicke was assumed for the basic size distribution. Distributions at higher wind speeds were inferred by multiplying concentration of each size by the Lovett wind dependence function.

The Katz model shows a good agreement with the Jaenicke data at wind speeds less than 8 m/sec for all wavelengths (Fig. 3-6). As the wind increases, the model predicts a larger concentration of aerosols and consequently a smaller extinction coefficient. This discrepancy increases with increasing wavelength. Although this discrepancy is not yet explained, it is in basic agreement with preliminary CEWCOM-78 analyses.

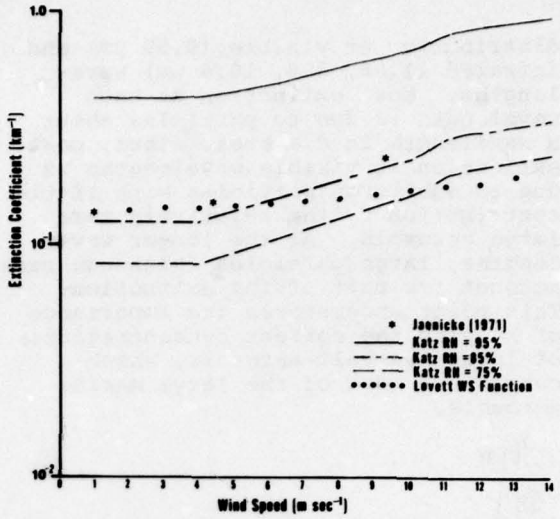

Fig. 3. Visible extinction dependence on wind speed.

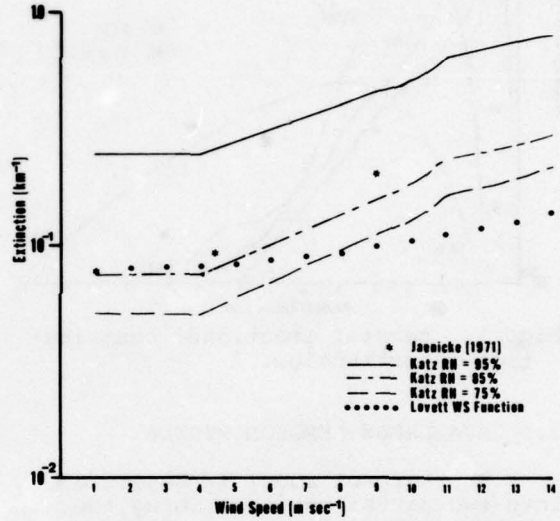

Fig. 4. 1.06 μm extinction dependence on wind speed.

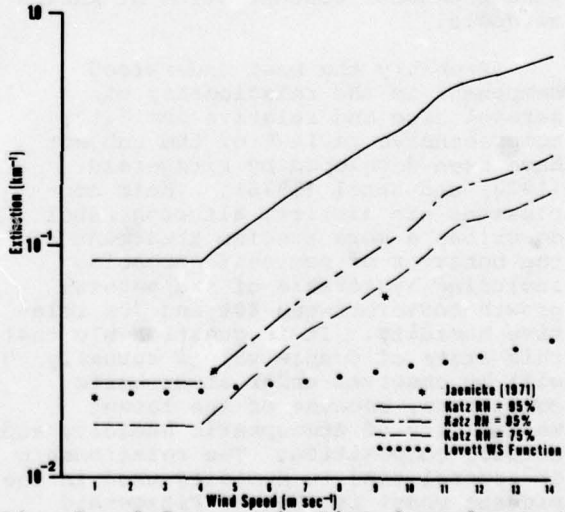

Fig. 5. 3.8 μm extinction dependence on wind speed.

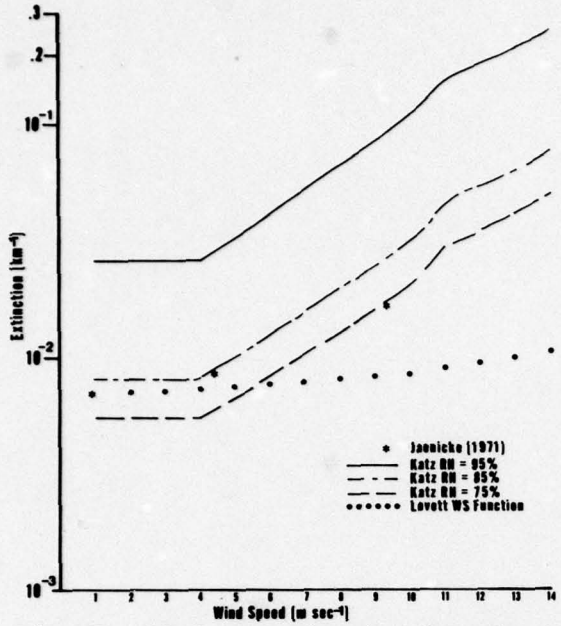

Fig. 6. 10.6 μm extinction dependence on wind speed.

The Lovett wind speed function does not provide good agreement with the measurements or the model. It is probable that the aerosol distribution is not uniformly affected by the wind. Rather, concentrations of large particles are affected by wind more than are concentrations of small particles.

4. MODEL APPLICATION

The aerosol extinction model was used with the other component models to calculate some initial distributions of extinction at relevant wavelengths.

Meteorological records for ocean station vessel JULIET and area 2 in the Mediterranean were evaluated to provide frequencies of occurrence of extinction coefficients in the 8-12 μm and 3-4 μm wavelength bands. Figure 7 shows the seasonal distribution of the total extinction coefficient in the 8-12 μm band for the vessel (52°30'N 2°W) and the Mediterranean area (2-Tangier). These calculations indicate that the total extinction is not strongly dependent on season in the North Atlantic, while there is a seasonal distribution in the Mediterranean. Overall, the probability of large extinctions (equivalently short ranges) is zero in the Mediterranean, while being non-zero in the North Atlantic. These results are being extended to other areas of the Atlantic.

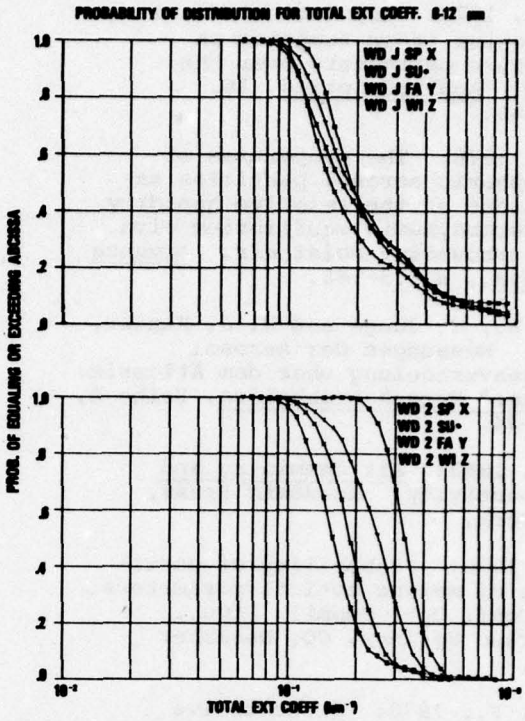

Fig. 7. Seasonal statistics for ocean station vessel JULIET (top) and Mediterranean area 2 (bottom). Season symbols: x - spring, * - summer, Y - fall, Z - winter.

5. REFERENCES

Barnhardt, E., and J. Streete, 1970: A method for predicting atmospheric aerosol scattering coefficients in the infrared. Applied Optics, 9, No. 6, 1337-1344.

Chaen, M., 1973: Studies on the production of sea-salt particles on the sea surface. Mem. Fac. Fish, Kagoshima University, 22, No. 2, 49-107.

Davidson, K. L., C. Fairall, T. Houlihan, G. Schacher and D. Hinsman, 1975: Description of optically relevant turbulence parameters. Unpublished memorandum.

Davidson, K. L., T. M. Houlihan, C. W. Fairall and G. E. Schacher, 1978: Observations of the temperature structure function parameter, C_T^2, over the ocean. To be published.

Fitzgerald, J., 1978: On the growth of aerosol particles with relative humidity. NRL Memorandum Report 3847.

Friehe, C., 1977: Estimation of the refractive index temperature structure parameters over the ocean. Applied Optics, 16, 334-340.

Hänel, G., 1976: The properties of atmospheric aerosol particles as functions of the relative humidity at thermodynamic equilibrium with the surrounding moist air. Advance Geophys., 8, 73-188.

Jaenicke, R., C. Junge and H. J. Kanter, 1971: Messungen der Aerosol Grossenverteelung uber dem Atlantik. "Meteor" Forsch-Ergebnisse, Reihe B, 7, 1-54.

Junge, C., 1963: Air Chemistry and Radioactivity. Academic Press, New York.

Katz, B., 1976: Probability of occurrence of marine optical parameters. DoD Conf. Opt. Submil. Prop., Colorado Springs, CO, December 1976.

Lovett, R. F., 1978: Quantitative measurements of airborne sea-salt in the North Atlantic. Tellus, 30, 358-364.

Selby, J. E. A., E. P. Shettle, and R. A. McClatchey 1976: Atmospheric Transmittance from 0.25 to 28.5 μm: Supplement LOWTRAN 3B (1976) AFGL Report No. AFGL-TR-76-0258.

Wells, W.C., G. Gall, and M. W. Munn, ,, 1977: Aerosol distributions in maritime air and predicted scattering coefficients in the infrared. Applied Optics, 16, No. 3, 654-659.

ESTIMATING THE PROBABILITY OF CLOUD-FREE FIELDS-OF-VIEW BETWEEN EARTH AND AIRBORNE OR SPACE PLATFORMS

Donald D. Grantham and Iver A. Lund
Air Force Geophysics Laboratory
Hanscom Air Force Base, Massachusetts

and

Richard E. Davis
NASA, Langley Research Center
Hampton, Virginia

ABSTRACT

More than three years of whole-sky photographs and simultaneous sky cover observations were used to develop a method for estimating probabilities of cloud-free fields-of-view (CFFOV) as a function of sky cover and elevation angle. This paper will describe how the model was developed for opaque cloud cover and how it can be applied to problems of viewing objects in space from the earth's surface or viewing the earth's surface from space.

1. INTRODUCTION

For almost 15 years the Air Force Geophysics Laboratory, has been investigating the problem of seeing through the atmosphere. In these studies we have used sunshine observations, aircraft inflight reports and whole-sky photographs as sources of information for determining cloud-free line-of-sight (CFLOS) probabilities. These probabilities are required to estimate the utility of a wide variety of electro/optical systems. However, an instantaneous CFLOS is often not sufficient for acquiring and tracking a target, or for estimating the probability of detecting a target when there is an opportunity to search for favorable cloud conditions. Therefore, probability distributions of cloud-free areas or fields-of-view (FOV) are needed.

The National Aeronautics and Space Administration also needs cloud-free field-of-view (CFFOV) information for the design and operation of several proposed satellite systems. For NASA satellite missions devoted to such research areas as the remote sensing of earth resources or atmospheric pollution, a class of sensors having wide fields-of-view and/or long integration times is coming into being. These requirements stem from the need to integrate very weak signals, for example, as from trace constituents or pollutants, over large areas or non-instantaneous periods in order to obtain an acceptable signal for constituent identification. The requirement for larger fields-of-view makes cloud contamination effects of more consequence than for narrow FOV or LOS sensors. Therefore, in support of Air Force and NASA requirements AFGL has engaged in a joint study with NASA Langley Research Center to investigate the FOV problem by re-evaluating the whole-sky photographs taken for the line-of-sight studies. These investigations are not complete, but this paper will describe the progress to date. As an introduction to the FOV endeavor, a brief review of the CFLOS history will be given.

2. CFLOS REVIEW

In order to have a data base which could be used to estimate more accurately the probability of CFLOS, AFGL contracted with the University of Missouri (Shanklin and Landwehr, 1971) to take photographs of the whole sky from the National Weather Service observing site at the airport in Columbia, Missouri. A Nikon F, 35-mm camera with a 180 degree (fisheye) lens and infrared film was used to take high contrast photographs of the whole sky every daylight hour, synoptic with the National Weather Service's surface observations. This combination of whole-sky photographs and concomitant surface weather observations were taken for a period of more than three years.

An example of a whole-sky photograph is shown in Figure 1. This is a cumulus-type of cloud cover showing good contrast. However, when stratus conditions existed, the contrast between the cloudy and cloud-free areas was not as distinct as shown on this picture. It was often difficult to distinguish clouds near the sunshield, and to distinguish between clouds and haze overhead. From our recent study of these photographs it now appears that the CFLOS probabilities which have been published in the past are somewhat higher than they should be.

Figure 1. An example of a whole-sky photograph.

Figure 2 depicts the template that was used to locate azimuth and elevation angles on the photographs. This template was placed over each photograph and two students independently examined the center of each of the 33 circles for the presence of clouds. These 33 line-of-sight points were recorded as either cloudy or cloud-free. (Most of the haze conditions were included among the cloud-free cases since infrared wave lengths penetrate most haze.)

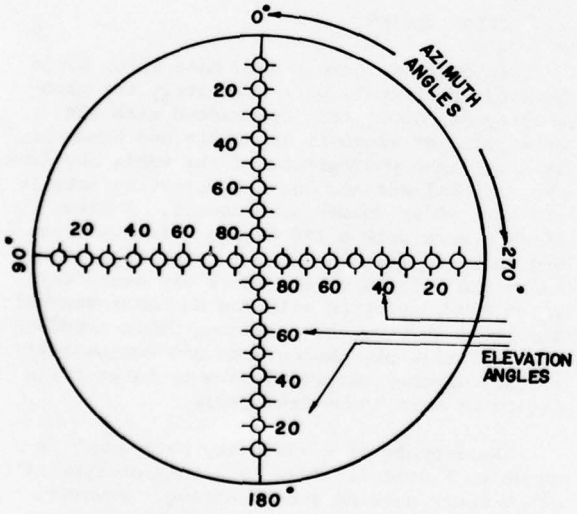

Figure 2. Template used to determine azimuth and elevation angles.

Methods for estimating cloud-free line-of-sight probabilities from the whole-sky photograph statistics were published by Lund and Shanklin (1972). Figure 3 depicts relative frequencies of CFLOS as a function of elevation angle and total sky cover, as determined from the photographs. The curves for each 10th of cloudiness are shown without any smoothing. The relative frequencies consistently increase with decreasing cloudiness. With but few exceptions, probabilities of CFLOS increase as the zenith angle is approached. Failure to increase consistently is most likely due to minor sampling instabilities.

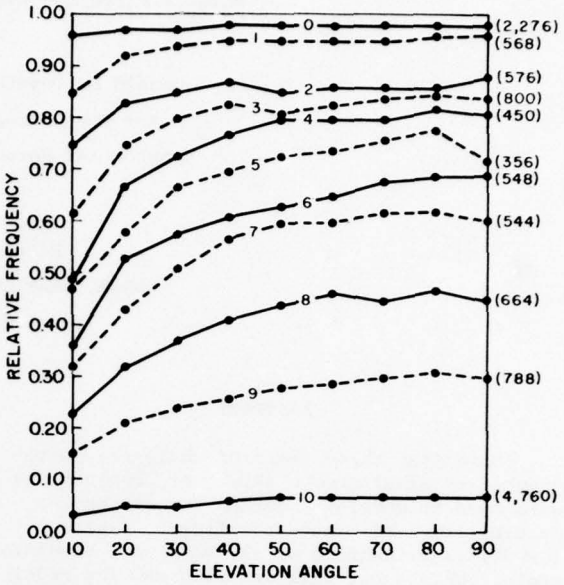

Figure 3. Relative frequencies of CFLOS as a function of elevation angle and observed total sky cover, in tenths. Each point is based on the number of observations shown at the end of the line.

After the lines shown in Figure 3 were subjectively smoothed, they were used as a model to estimate probabilities of CFLOS as a function of elevation angle and sky cover. Publications are available, Lund and Shanklin (1973), that describe how these curves can be used to estimate CFLOS probabilities for any location that has a long record of sky cover observations.

This model has been applied to climatic sky cover statistics for more than a thousand weather stations over the northern hemisphere. From these data, atlases have been prepared for Germany, the USSR, the USA and Europe. A sample page from the atlas for the USSR (Lund, et al, 1976) is shown in Figure 4. This shows the probability of having a cloud-free line-of-sight in January at 1200 to 1400 local standard time at a 90° elevation angle. This atlas is based on more than 10 years of record at the 97 stations shown by the dots on Figure 4. Maps in each of the atlases are presented for the 4 mid-season months, 4 periods of the day and 3 elevation angles, 10°, 30°, and 90°.

The Lund CFLOS model has been modified by Rapp and his associates at Rand Corp. for use in estimating probabilities as a function of altitude. In order to apply that model, it is necessary to know the frequency of occurrence of each category of sky cover as a function of

altitude. This adaptation of the CFLOS model is currently available, on computer, at the Air Weather Service's Environmental and Technical Applications Center.

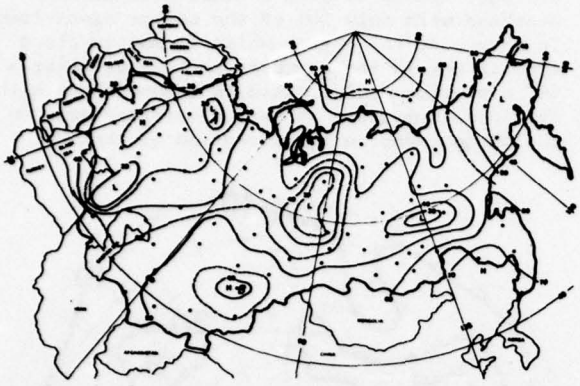

Figure 4. Sample page from CFLOS Atlas for USSR showing CFLOS probabilities for January, 1200-1400 LST, 90° elevation angle.

3. CLOUD-FREE FIELDS-OF-VIEW

As stated in the introduction, there are times when probabilities of a CFFOV, or the areal coverage of clouds, are more useful than probabilities along lines of sight. We have turned again to the whole-sky photographs taken at Columbia, Missouri to obtain statistics on FOV. Because many thin clouds did not appear on the photographs, we have started our study by considering only those times when the total sky cover equals the total opaque sky cover, that is when no thin clouds are reported.

The CFFOV study will be extended to include all clouds but difficulty may be encountered because the pictures are not as distinct as expected.

Figure 5 depicts the template used to study CFFOV. This template was printed on a 24-inch diameter screen on which each picture, taken at 0900, 1200 and 1500 local time, was projected. An estimate was then made of the eighths of cloudiness in each of the 185 sectors shown on the template.

The average cloud-free area in each sector when 2/10 opaque cloudiness is observed is shown in Figure 6. The averages are based on the 70 photographs taken when the observer reported 2/10 opaque cloudiness and 0/10 thin clouds. Clearly, the average cloud-free area decreases as we go from the center, that is from directly overhead, to low elevation angles at the edges of the picture. (No attempt was made to estimate cloudiness within 5° of the horizon.) The maxima (highs) are not exactly centered at the zenith, i.e., the center of the picture, as one would expect. The failure of the isolines to be symmetric about the center of this and the next three figures is certainly due in part to sampling variability. However, other studies of the photographs have suggested that sun angle or local effects, perhaps from the city of Columbia, may also contribute to the lack of symmetry.

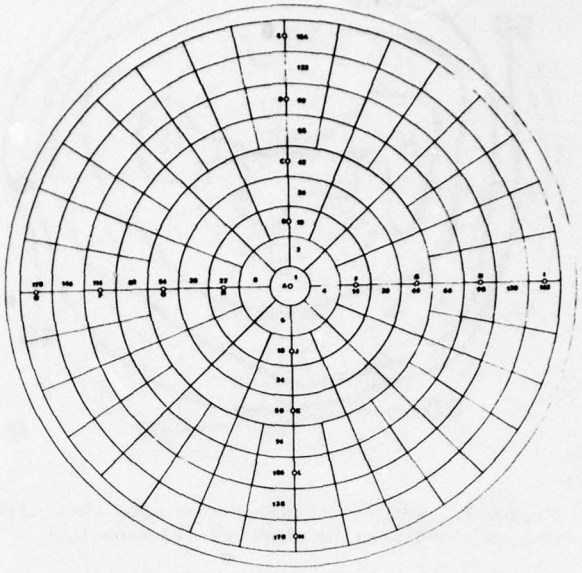

Figure 5. Template used to determine cloud-free areas in each of 185 areas.

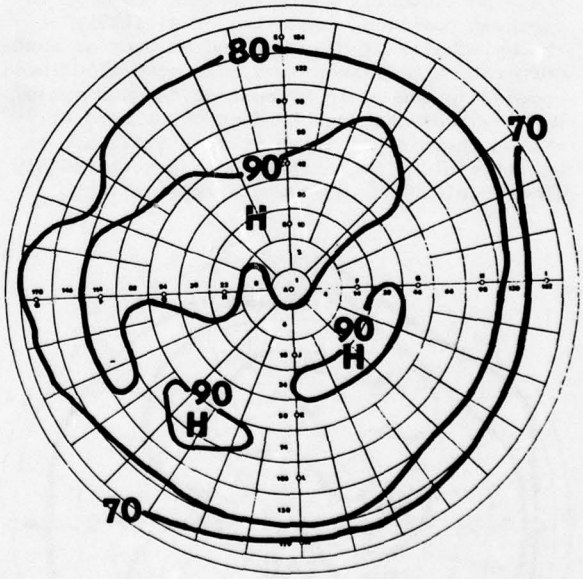

Figure 6. Percent of cloud-free area when 2/10 opaque cloudiness is observed (70 cases).

Figure 7 is based on the 49 photographs when 4/10 opaque and 0/10 thin cloudiness was reported. Here the isolines are more nearly symmetric about the overhead position, i.e., the center of the picture. More than 80% of the center area is, on the average, cloud-free. Along the horizon about 40% of each sector is cloud free.

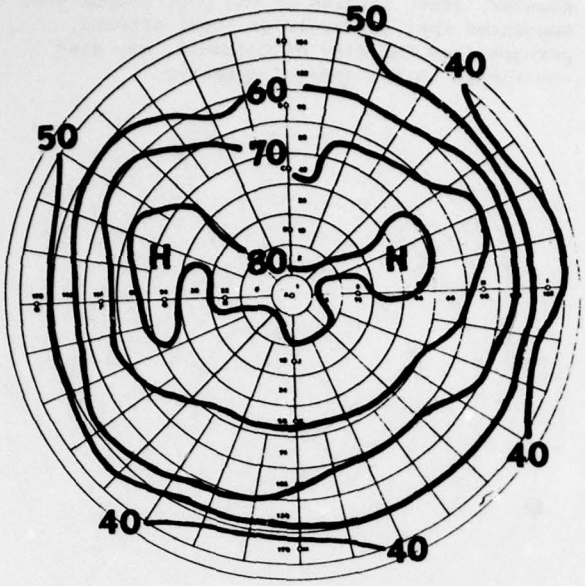

Figure 7. Percent of cloud-free area when 4/10 opaque cloudiness is observed (49 cases).

Figure 8 is based on the 52 photographs when the observer recorded 6/10 opaque clouds and no thin clouds. At higher elevation angles the variability increases with most of the high cloud-free values to the north of the overhead position. Shanklin et al (1971) at the University of Missouri and Delaney at Rand Corporation have suggested that more cloudiness appears in the south because of the sun angle. We know that the sunshield obscures some of the southern area making it more difficult to estimate cloudiness but we have not thoroughly investigated these sun angle implications.

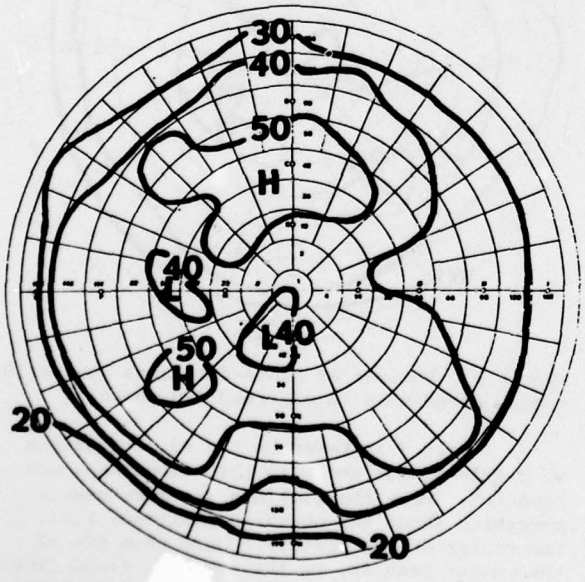

Figure 8. Percent of cloud-free area when 6/10 opaque cloudiness is observed (52 cases).

Figure 9 is based on the 83 photographs when the observer recorded 8/10 opaque cloudiness and no thin clouds. Near the horizon about 10% of each sector is cloud-free, on the average. There is also a small area almost overhead with only 10% of the sector cloud-free. In this case the region which is mostly cloud free is now in the southern sectors at about a 50° elevation angle. This is inconsistent with the idea that there is more cloudiness seen on the photographs in the direction of the sun.

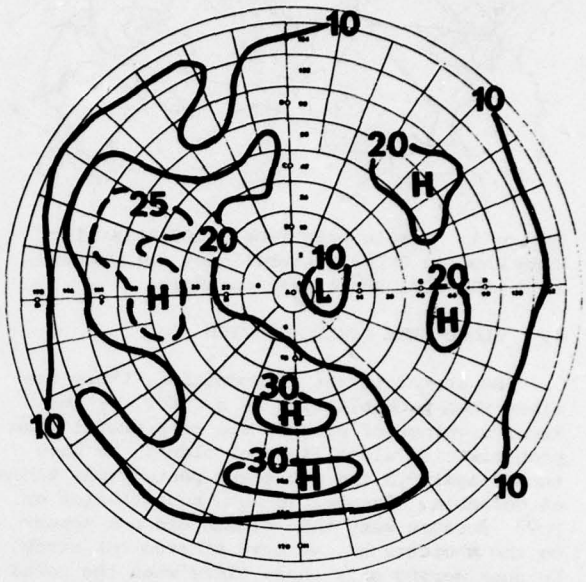

Figure 9. Percent of cloud-free area when 8/10 opaque cloudiness is observed (83 cases).

Again these are cases when only opaque clouds are reported. The sun angle effect may be more important when thin clouds are observed.

3.1 CFFOV from Ground Perspective

Next, circular fields-of-view centered at a ground observers zenith were investigated. The circles with angular diameters of 10, 50, 90, 130 and 170 degrees, illustrated in Figure 10, were used with the whole-sky photographs to estimate cumulative probability distributions of the percentage of these areas that are cloud-free. Because the probability distributions are functions of the sky cover, they were stratified on that basis.

Figure 11 is an example of how the distributions appear when the observer reports 5/10 opaque sky cover. Let us assume a requirement that at least 30% of a viewing area must be cloud free. Curve A on this figure shows that for the small 10° circular area there is about a 66% chance that at least 30% of the area will be cloud-free. Curve C shows that for the 50° area the probability increases to a 71% chance and to almost 100% for the large 170° area, shown by Curve I. If, however, the requirement is that at

least 70% of the area must be cloud-free, the probability will be near zero for the large 170° area and will increase to 53% for the small 10° area. This is an example of the type of information that is being extracted from the whole-sky photographs.

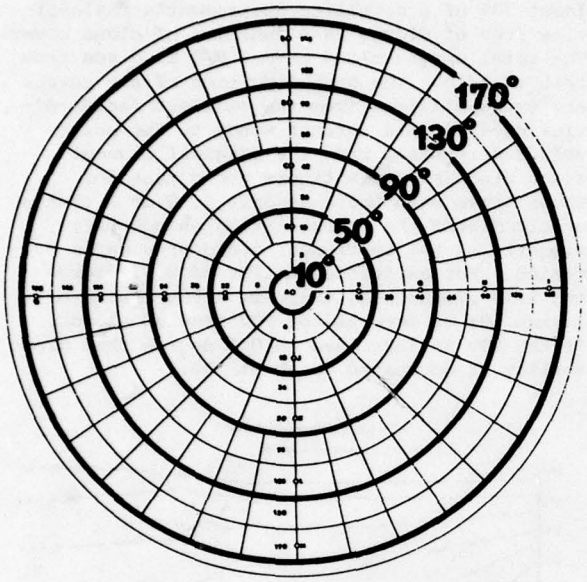

Figure 10. Circular fields-of-view with angular diameters of 10, 50, 90, 130, and 170 degrees centered at a ground observer's zenith.

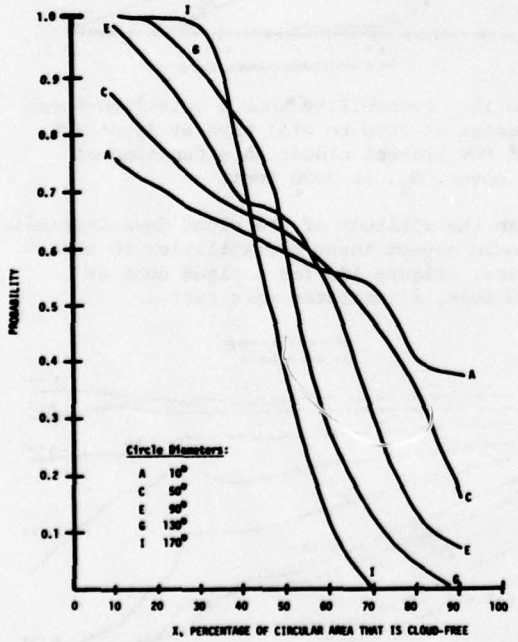

Figure 11. Probability that selected circular areas at zenith are at least x percent cloud-free when 5/10 opaque cloudiness is observed.

Another way to depict this information is shown in Figure 12. This shows cumulative frequency distributions of the percent of cloud-free area in the small 10° circle at zenith for 1/10 through 9/10 sky cover. (The lines are drawn without smoothing from the data points.) It shows, for example, that if one wants to be 90% sure that at least 30% of the area is cloud-free he can only operate when it is $\leq$ 4/10 cloud cover shown by the top 4 curves. If he wants to be 90% sure that at least 80% of the area is cloud-free he can only operate when clear or 1/10 cloudiness is reported.

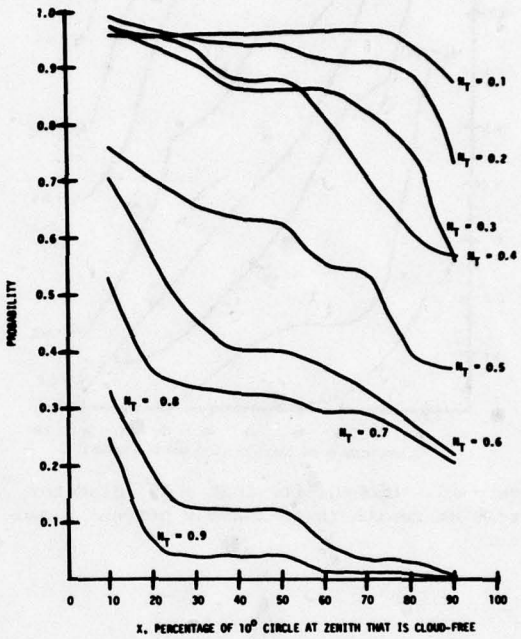

Figure 12. Probability that a 10° diameter circle at zenith is at least x percent cloud-free.

Figure 13 shows the same information except it is for a 70° diameter circle from the ground observer's zenith. The slopes of the lines are steeper, i.e., the probabilities change more rapidly with increasing percentages of the area. For example, when 6/10 cloudiness is reported (NT = 0.6) the probability is almost one that at least 10% of the area will be cloud-free but the probability is near zero that at least 90% of the area will be cloud-free.

3.2 CFFOV from Space Perspective

Up to this point in the paper, only fields-of-view from a ground observers perspective have been considered. The geometry for the case of a satellite or aircraft-borne sensor viewing at nadir is shown in Figure 14. Without going into the specifics of the transformation geometry, it is sufficient to say that by specifying the altitude of the satellite, HS, the field of view of a satellite-borne instrument, Ω, and the altitudes of cloud decks in the observer's locality, then the angles, α, can be defined for a FOV analysis in the ground observer's

frame of reference. Thus, the input data for the satellite studies can be taken directly from the elevation angles determined from the whole-sky photographs. This concept can be extended to FOV's with different shapes, such as squares or ellipses.

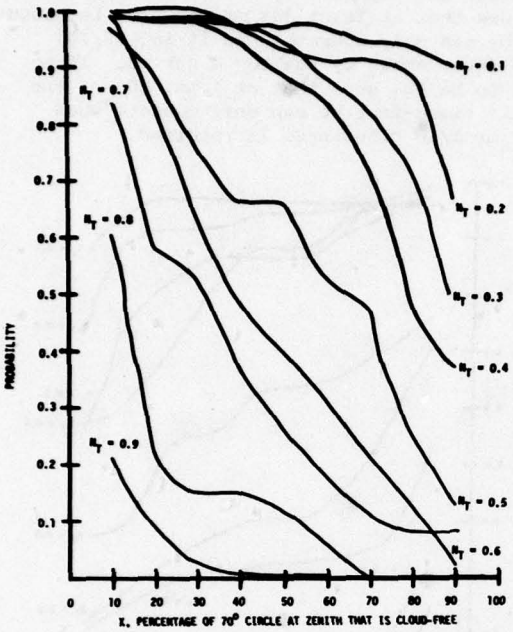

Figure 13. Probability that a 70° diameter circle at zenith is at least x percent cloud-free.

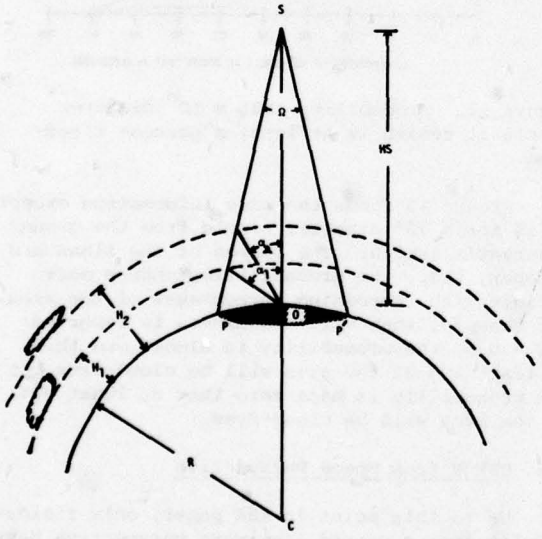

Figure 14. Geometry relating FOV, Ω, of a satellite-borne instrument to equivalent circle (radius α) at ground observers zenith.

An analysis has been performed for circular fields-of-view to show the functional relationships between instrument FOV, sky cover and the probability of varying percentages of the FOV being cloud-free.

Figure 15 presents an application of this approach assuming a satellite at an altitude of 1000 km and a cloud height of 3000 ft (.91 km). This graph shows the probability of having at least 70% of a satellite instrument's field-of-view free of clouds as a function of cloud cover. The total opaque cloud cover, N_T, is given from 1/10 to 9/10. The dashed portion of the curves are extrapolations from the smallest fields-of-view used in this current study to the point values determined from the original line-of-sight studies. This figure shows that for those times when there is only 1, 2 or 3 tenths of cloudiness the probabilities change only slightly as the instrument field-of-view is varied. For an instrument FOV of 0.01 degree and 5/10 cloudiness, there is a 55% chance of having 70% or more of the FOV free of clouds. If the FOV is increased to 0.1 degree that probability is decreased to about 30%.

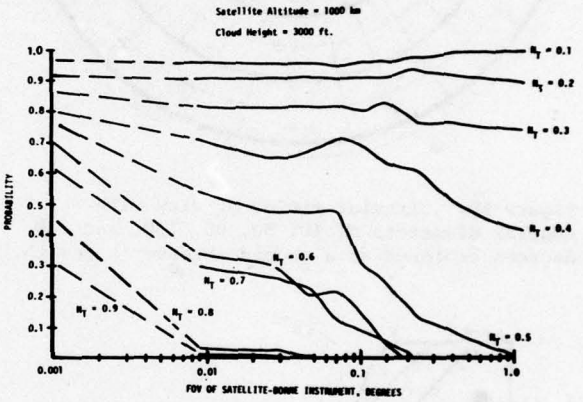

Figure 15. Probability that a satellite-borne instrument at 1000 km will have at least 70% of its FOV free of clouds as a function of cloud cover, N_T, at 3000 feet.

As the altitude of the cloud deck increases, one would expect these probabilities to also increase. Figure 16, for a cloud deck at 18,000 feet, illustrates this fact.

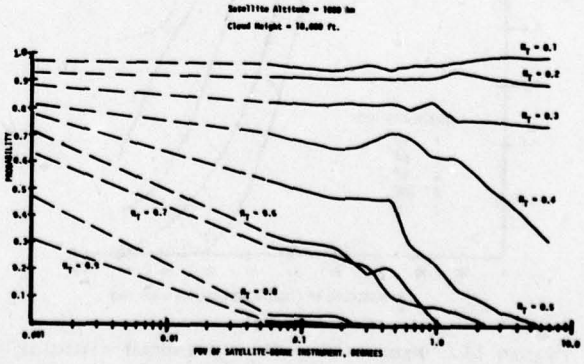

Figure 16. Same as Figure 15 except for cloud cover, N_T, at 18,000 feet.

Now, for 5/10 cloudiness, the probability for a 0.01 degree FOV has risen from 55% to about 66% and for a 0.1 degree FOV, the probability increased from 30% to 50%.

When a satellite scans off nadir, the circufield of view becomes a quasi-elliptical footprint. The next 3 figures are presented to show how the footprints on the ground observer's sky dome change in size and shape as cloud height and nadir angle are varied. This footprint may be regarded as a cloud-free window, i.e., an area that must be cloud free on the observer's sky dome if the satellite instrument's FOV is to be free of clouds.

Figure 17 illustrates the case for a satellite at 250 km, a nadir angle of zero degrees (corresponding to a ground observer's elevation angle of 90 degrees) and an instrument field-of-view of 0.1 degree. The size of the footprint for a cloud-free window required for a cloud height at 4000 feet (1.21 km) is shown by the outer ring identified by the small circle. At an 8000-foot cloud height (2.43 km) the foot print is shown by the middle ring, identified by the small square, and at a 25,000-foot cloud height (7.61 km) the footprint becomes the tiny center ring, identified by the small diamond. This figure shows that for a given instrument FOV, as the cloud height increases, the size of the required cloud-free window decreases.

In Figure 18 the nadir angle was increased to 42.9°, corresponding to a 45° elevation angle. Here the footprints at cloud height have increased in size slightly but have remained essentially circular.

In Figure 19 the nadir angle has been further increased to 73.5 degrees, corresponding to a 5° elevation angle. In this case the footprints at cloud-height have changed significantly.

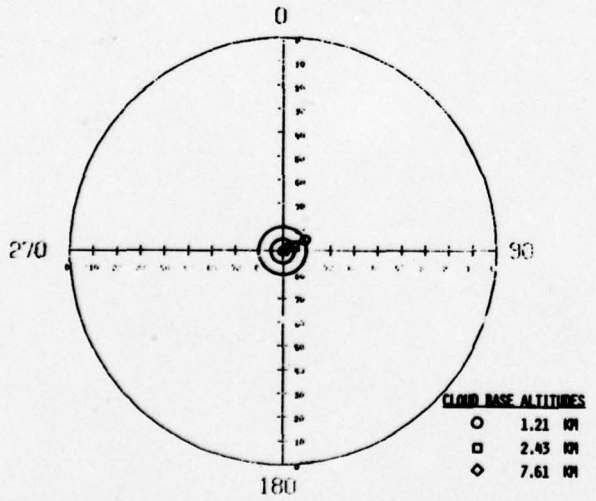

Figure 17. The footprint (area) that must be cloud free on an observer's sky dome if a satellite instrument's field of view (IFOV) is to be cloud free. Satellite altitude = 250 km; IFOV = 0.1 degree; cloud base altitudes: 4000 feet (1.21 km), 8000 feet (2.43 km) and 25000 feet (7.61 km). Satellite instrument viewing at 0 degrees nadir (ground observer's elevation angle of 90 degrees).

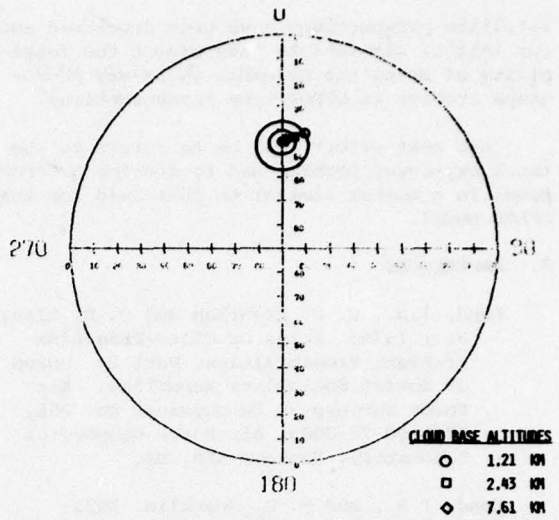

Figure 18. Same as Figure 17 except satellite viewing at 42.9 degree nadir angle (ground observer's elevation angle of 45 degrees).

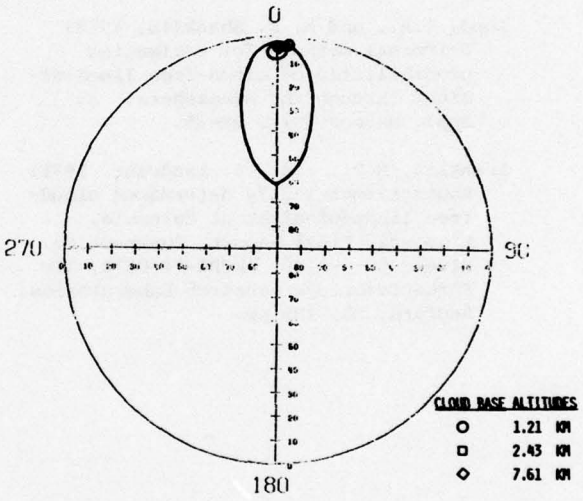

Figure 19. Same as Figure 17 except satellite viewing at 73.5 degree nadir angle (ground observer's elevation angle of 5 degrees).

At this time, pending resolution of the total vs opaque cloud cover question, we have not analyzed the whole-sky photographs to determine cloud-free probabilities for oblique-angle footprints, but the computer software for doing so has been developed.

4. CONCLUSIONS

Thus far our FOV study, using the Columbia whole-sky photographs, have been confined to only opaque sky cover. This condition is primarily of interest for those systems which can penetrate haze and thin clouds. The problem in modeling this condition is that opaque cloudiness is not normally archived and therefore cannot be directly used as a variable. Nevertheless, algorithms and software for computing CFFOV statistics from both ground observer and

satellite perspectives have been developed and our initial simulations have proven the feasibility of using the Columbia whole-sky photograph archive in CFFOV-type investigations.

Our next effort will be to return to the total sky-cover problem and to develop a CFFOV model in a manner similar to that used for the CFLOS model.

5. REFERENCES

Lund, I.A., D. D. Grantham and C. B. Elam, Jr., 1976: Atlas of Cloud-Free Line-of-Sight Probabilities, Part 2: Union of Soviet Socialists Republics. Air Force Surveys in Geophysics, No. 358, AFGL-TR-77-0005, Air Force Geophysics Laboratory, Hanscom AFB, MA.

Lund, I.A., and M. D. Shanklin, 1972: Photogrammetrically determined cloud-free lines-of-sight through the atmosphere. J. Appl. Meteor. 11, 773-782.

Lund, I.A., and M. D. Shanklin, 1973: Universal methods for estimating probabilities of cloud-free lines-of-sight through the atmosphere. J. Appl. Meteor., 12, 28-35.

Shanklin, M.D., and J.B. Landwehr, 1971: Photogrammetrically determined cloud-free lines-of-sight at Columbia, Missouri, Final Report, Contract No. F19628-68-C-0140, AFCRL-71-0273, Air Force Cambridge Research Laboratories, Bedford, MA, 185 pp.

WIND PROFILE MODELS (SURFACE TO 25 KM)

IN VARIOUS CLIMATIC ZONES

Oskar M. Essenwanger
Missile Research Directorate
US Army Missile R&D Command
Redstone Arsenal, AL 35809

ABSTRACT

The vertical structure of the wind profile from surface to 25 km is examined in terms of empirical polynomials (eigenvectors) and by standard functions. Modelling of the wind speed profile from surface to 25 km is then attempted based on a Fourier Series representation. Five wind profile groups, or a total of 14 types, are deduced. The number of subtypes depends on the chosen tolerance of dispersion from the best prototype. These subtypes differ in number and altitude occurrence of the wind maxima. In this study 49 models were selected.

About 85% of the profiles in midlatitudes and subtropics exhibit a single wave pattern with a maximum close to the tropopause (jet stream). This group drops to 65 and 40% in the polar and tropical zone, respectively, and is replaced by a type whose maximum is above 20 km. The remaining profiles disclose a double wave pattern with maxima in the troposphere and stratosphere. The profile structure is interpreted in terms of the general circulation.

1. INTRODUCTION

The derivation of global design criteria for the wind profile is a difficult task because the wind velocity is a vector quantity and the altitude dependency must be taken into consideration. Therefore, the first objective is a mathematical description of the wind profile under inclusion of the vertical structure. This task is rendered even more difficult by the added condition that the models must enable us to assess an exceedance probability.

Several approaches have been taken in the past. Synthetic wind profiles (see Handbook of Geophysics, 1960, chapter 5 or Handbook of Geophysics and Space Environment, 1965, chapter 4) stress the exceedance probability while the vertical structure is only partially considered. Correlation matrices of wind components by altitude include a vertical structure but it is difficult to derive a probability of exceedance from them. In fact, the exceedance probability has only a simple definition for a one dimensional (one parameter) system.

The author has attempted to parameterize the wind profile in order to derive a one parameter description. As a by-product a system of wind models evolved which permits us to study the vertical wind structure in individual geographic zones while in most climatological studies the consideration of the vertical association is neglected in favor of the horizontal field.

Five wind profile groups or a total of 14 different prototypes can be found. These major groups may be subdivided. The number of subtypes depends largely on the error tolerance between subtypes. Because the adoption of an error tolerance is a subjective decision, no specific number of subtypes can be given without reference to the tolerance limit.

2. MATHEMATICAL REPRESENTATION OF THE WIND PROFILE

Although two dimensional systems for the mathematical representation of the wind velocity could be based on a calculation of eigenvectors for complex variates, of primary importance for missile design is the wind speed. Consequently, the author decided to split the wind vector into components of wind speed and wind direction. Mathematical modelling then requires a solution to:

$$V(h) = A_o + A_1P_1 + A_2P_2 + \ldots A_nP_n = V_h \qquad (1)$$

$$D(h) = B_o + B_1Q_1 + B_2Q_2 + \ldots B_nQ_n = D_h \qquad (2)$$

where A_j and B_j are coefficients which vary by season and location and P_j, Q_j are suitable functions ($j = 1,\ldots,n_j$). If the system can be reduced to a one-parameter variable x, the exceedance probability can be written simply as:

$$F(x) = 1 - \exp(-[(x-\gamma)/\theta]^{\beta}) \qquad (3)$$

where the cumulative frequency distribution F(x) is expressed by a Weibull distribution (see Essenwanger, 1976a, p. 119). Other suitable models could be substituted for F(x). Eqn. (3) can be solved for a given threshold $x = x_{th}$, or x_{th} can be calculated for a given probability F(x). (See Stewart and Essenwanger, 1978).

2.1 Eigenvector Solution

Several mathematical tools are available for a solution of Eqns. (1) and (2). They depend on the specific goals which are intended. If our primary concern is a representation where the first term should include a maximum of information an eigenvector system (also called empirical polynomial system) is appropriate. The calculation requires a solution of:

$$M_\phi^{-1} M_v M_\phi = M_\lambda \qquad (4)$$

were M_v is a correlation or covariance matrix of the wind speed, and M_ϕ and M_λ are matrices of eigenvectors and eigenvalues, respectively. Then $P_j \equiv \phi_j$, both being a function of altitude, i.e., $\phi_j(h)$.

Today eigenvectors and eigenvalues can be found relatively quickly by electronic data processing. The details of the process have been described previously by the author (1976a, 1975). An example for the structure of the first 3 eigenvectors is exhibited (Figure 1) for the radiosonde data of Montgomery, Alabama (period of record 1956-1964) for an altitude range of surface to 24 km. The eigenvectors have been scaled in agreement with their contribution to the total variance (see section 2.2).

The structure of the first eigenvector for 4 stations from different climatic regimes is depicted in Figure 2 (wind speed) and Figure 3 (wind direction). While this structure shows a relatively simple pattern for the eigenvectors of the wind speed, the eigenvectors for the wind direction have a more entangled shape. For more details see Essenwanger (1975, 1978).

2.2 Residual Variance and Percentage Reduction

Two measurements which indicate the goodness of representation are customary. We designate by σ^2 the total variance of the wind profile about the vertical average and by $\sigma^2_{\phi_j}$ the variance of the individual term. Thus:

$$\sigma^2 = \sum_{h=1}^{n_h} (V_h - \bar{V})^2 / n_h \qquad (5)$$

where $\bar{V} = \Sigma V_h$ over the altitude range $h = 1,\ldots,n_h$, and:

$$\sigma^2_{\phi_j} = \sum_{h=1}^{n_h} (\phi_{jh} - \bar{\phi}_j)^2 / n_h. \qquad (6)$$

In an orthogonal system $\bar{\phi}_j = 0$, and:

$$\sigma^2 = \sum_{j=1}^{n} \sigma^2_{\phi_j} \qquad (7)$$

Consequently, the residual variance is defined by:

$$\sigma^2_{R_j} = \sigma^2 - \sum_{j=1}^{n_j} \sigma^2_{\phi_j}, \quad n_j < n \qquad (8)$$

In a non-orthogonal system the residual variance must be calculated from a matrix (see Essenwanger, 1976a, p. 217).

Figure 1. First Three Eigenvectors (Scaled)

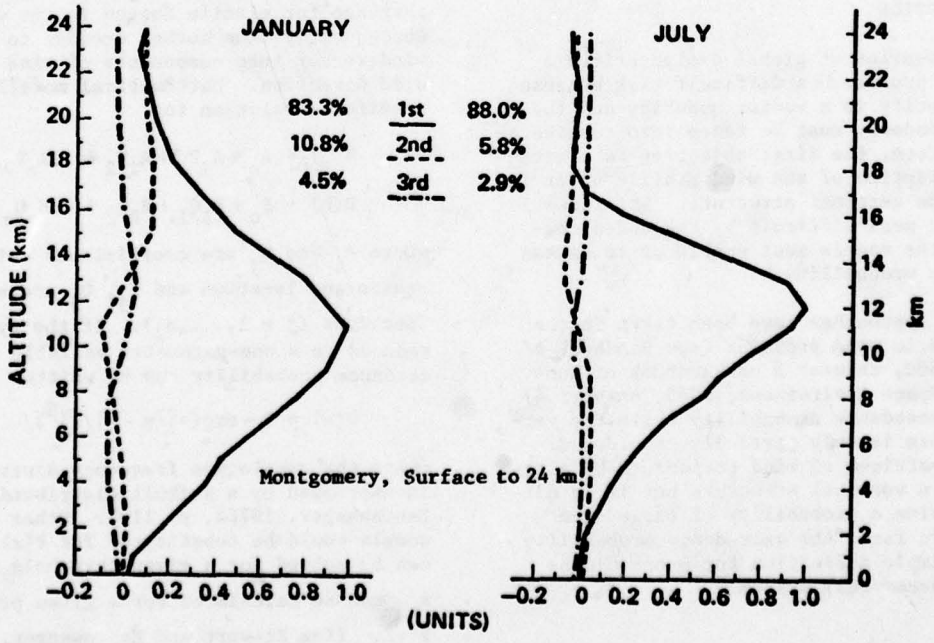

Figure 2. First Eigenvector Structure (Surface to 24 km)

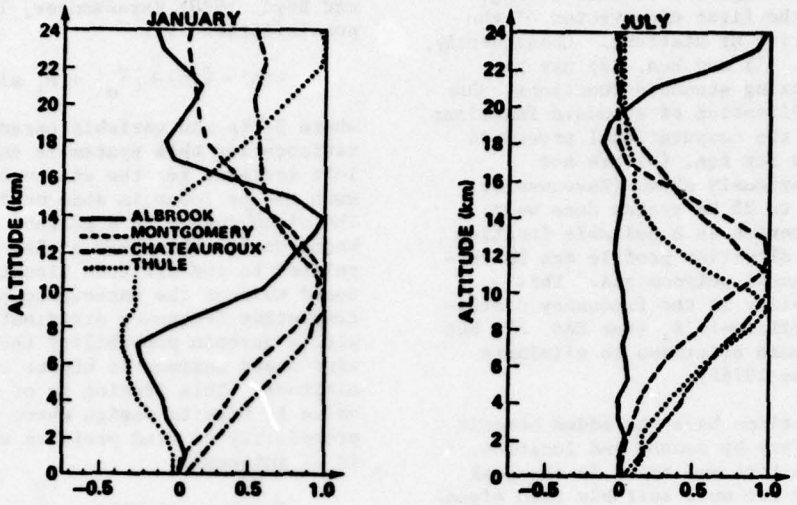

Figure 3. First Eigenvectors, Wind Direction

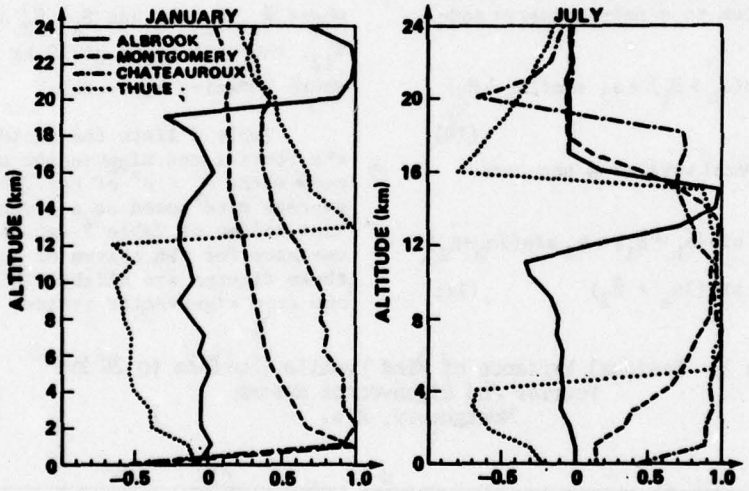

The percentage reduction is defined as:

$$PR_j = (1 - \sigma^2_{R_j})/\sigma^2 \qquad (9)$$

Table 1 exhibits PR_1 for the first eigenvector at 4 stations. We learn that the first eigenvector for the subtropical and midlatitude station serves well as a single parameter but Albrook and Thule display some months where the first eigenvector furnishes a relatively low contribution to the total variance. It must be added, however, that in these cases the total variance is small. Consequently, the absolute amount of $\sigma^2_{R_1}$ would be small.

Table 1. Percentage Reduction of the Largest Eigenvector

	A	M	CH	TH
JAN	64.3	83.2	77.6	57.2
FEB	63.1	92.6	76.7	88.0
MAR	56.8	92.9	94.6	82.8
APR	70.3	97.7	94.1	65.1
MAY	71.8	95.5	98.1	92.8
JUN	71.8	95.4	98.1	94.3
JUL	72.7	88.0	97.6	94.3
AUG	92.6	95.0	98.0	97.0
SEP	92.5	95.8	98.0	89.3
OCT	91.4	97.6	97.5	84.0
NOV	57.7	94.4	95.5	61.4
DEC	60.2	93.6	85.5	95.6

A = Albrook (Canal Zone) TH = Thule (Greenland)
M = Montgomery (AL) CH = Chateauroux (France)

2.3 Standard Functions

Examination of Figure 1 reveals a single wave pattern for the first eigenvector of the speed at the majority of stations. Consequently, solutions for Eqn. (1) and Eqn. (2) may be attempted by utilizing standard functions. One benefit of the utilization of standard functions is a reduction of the computational procedure since calculations for Eqn. (4) are not necessary. As previously shown (Essenwanger, 1977) the surface to 25 km system does well with the Fourier series as a suitable function for P_1. The wind direction profile can be represented by orthogonal polynomials. This generated a bimodality in the frequency distribution of the coefficients B_1 (see Eqn. 2), but the author found some solutions to eliminate the bimodality (see 1976b).

Standard functions have the added benefit that they do not vary by season and location. If a comparison in time and space is the goal standard functions are more suitable than eigenvectors in many cases.

Standard functions have one other advantageous property: The coefficients are not orthogonal although the functional terms can be orthogonal. This property is important for the reduction of the system to a one-parameter model. Thus, the system:

$$V(h) = a_o + a_1 \sin(\alpha_h + \beta_1) + a_2 \sin(2\alpha_h + \beta_2) + \ldots \quad (10)$$

can be reduced in several ways to a one-parameter model. First:

$$V(h) = a_o\left[1 + k_1 \sin(\alpha_h + \bar{\beta}_1) + k_2 \sin(2\alpha_h + \bar{\beta}_2) + k_3 \sin(3\alpha_h + \bar{\beta}_3)\right] \quad (11)$$

where k_1, k_2, k_3, $\bar{\beta}_1$, $\bar{\beta}_2$, $\bar{\beta}_3$ are constants varying with season or location (see Essenwanger and Boyd, 1970; Essenwanger, 1964). Other possibilities are:

$$V(h) = \bar{V}(h) + |\bar{a}_o| + \bar{a}_1 \sin(\alpha_n + \beta_1) \quad (12)$$

where β_1 is the variable parameter. The left variance for this system is equivalent to the left variance for the eigenvector system and even can be lower in some months and stations. The disadvantage is a probability of exceedance based on β_1, the phase angle. Because β_1 is related to the altitude (location) of the wind speed maximum the exceedance probability of the cumulative frequency distribution means that with a certain probability the altitude of the wind speed maximum is higher than the threshold altitude. This finding is of little practical value in missile design where the exceedance probability of wind profiles with strong winds is of interest.

Another suitable one-parameter system can be based on:

$$V(h) = k_o + k_1 \sin(\alpha_h + \beta_1) + k_2 \sin(2\alpha_h + \beta_2) \quad (13)$$

where k_o, k_1, k_2 and β_1, β_2 are functions of V_{12}, the wind speed at 12 km altitude, or V_H, where H varies by month.

Table 2 lists the residual variance for the Fourier and Eigenvector system for Montgomery where $\sigma^2 \equiv \sigma^2$ of Eqn. (5), and $\bar{V}_h$ is the average wind speed at a given altitude. The last column of Table 2 exhibits the residual variance for the system of Eqn. (13). Although these figures are slightly higher than for the one term eigenvector system, they are statis-

Table 2. Residual Variance of Wind Profile (Surface to 25 km)
Fourier and Eigenvector System
Montgomery, Ala.

	$y_h = V_h - \bar{V}_h$				$y_h = V_h$				Cov 1 Eigenvector			Eqn. 13
	σ^2	1 Term	2 Terms	3 Terms	σ^2	1 Term	2 Terms	3 Terms	1 Term	2 Terms	3 Terms	One parameter
JAN	56.41	24.34	15.05	10.65	234.5	31.9	17.7	12.7	44.8	28.9	18.6	52.2
FEB	61.26	23.09	14.80	9.52	255.8	29.0	15.4	10.4	38.5	24.7	17.7	42.4
MAR	50.77	23.42	15.12	11.64	267.3	31.0	16.6	12.6	35.1	24.3	19.0	39.2
APR	52.37	17.55	11.00	7.96	180.7	23.9	12.2	8.4	26.1	16.9	12.2	28.3
MAY	28.44	11.38	6.51	4.59	66.6	15.1	7.4	4.9	15.3	10.5	7.8	17.9
JUN	23.38	9.56	5.38	3.65	33.8	15.2	7.8	4.6	12.0	8.7	6.6	22.1
JUL	14.45	7.25	4.41	3.06	25.4	16.8	8.9	5.8	9.8	7.4	5.7	17.7
AUG	17.53	8.10	4.75	3.30	30.5	19.9	9.0	5.9	9.6	7.6	5.8	18.7
SEP	25.08	10.06	5.49	3.67	41.1	16.8	7.3	4.5	12.5	9.2	7.2	18.6
OCT	32.65	11.91	6.69	4.75	93.6	19.0	7.8	5.1	17.0	11.6	8.3	19.2
NOV	48.81	18.17	10.89	7.88	151.9	25.6	12.7	9.1	29.6	20.5	13.6	34.4
DEC	58.50	21.48	13.86	9.67	182.3	30.6	18.0	12.4	36.7	23.8	16.6	47.7

Cov 1 = $(x - \bar{x})(y - \bar{y})/N$

Unit: $(m/sec)^2$

tically not signifcantly different except for some summer months where the residual variance is small. More details may be found in the author's 1977 article.

3. CLIMATIC MODELLING

Conventional climatic studies are based on the horizontal fields of the meteorological elements. The vertical structure is less frequently utilized but vertical cross sections have been analyzed in the past, e.g., Flohn (1952), Faust (1967), Stewart (1967). One can also find mean values as functions of altitude, such as in the US Standard Atmosphere (1976) or the US Standard Atmosphere Supplements (1966), but they do not include mean wind profiles. The development of individual prototypes for the wind speed is of recent origin (Essenwanger 1971, 1973). Some details may be reiterated in the subsequent sections.

3.1 Wind Profile Models

It was previously stated that one primary concern was the assessment of an exceedance probability for the wind speed profiles. Consequently, the wind vector was split into magnitude and direction. This type of breakdown into components is equivalent to a hodograph analysis (see Essenwanger, 1962; Schwerdtfeger et. al 1959, 1970). Prototypes are subsequently developed for the wind speed from surface to 25 km, and the wind direction can be correlated with the wind speed profile (e.g., as given in Figure 3).

The advantages of utilizing standard functions for wind speed models have already been discussed. It was decided to base the modelling on the Fourier Series, but to introduce a slightly modified version of Eqn. (11):

$$V_h = C_o\left[1 + C_1\{k_1 \sin(\alpha_h + \bar{\beta}_1) + k_2 \sin(2\alpha_h + \bar{\beta}_2) + k_3 \sin(3\alpha_h + \bar{\beta}_3)\}\right] \quad (14)$$

For $C_1 = 1$ Eqn. (14) is identical with Eqn. (11).

In order to derive prototypes the k_j coefficients with $C_1 = 1.0$ were computed for 4 stations of different climatic regimes. These are the same stations as listed in Figure 2 or Table 1. The coefficients are given in the author's 1973 reference and are not repeated here because the primary concern here is the discussion of prototypes. A careful examination of the percentage reduction represented by these coefficients led to a system of profiles with the basic definition:

$$\sum_{j=1}^{3} k_j^2 = c^2 \quad (15)$$

$c^2 = 1.0$ for prototypes one through 4, and 0.75 for type five. This deviation in the latter case does not affect the percentage reduction for the individual profiles which is:

$$PR_j = k_j^2 / \sum_1^3 k_j^2 \quad (16)$$

For type five $PR_j = 33\%$ each. The selected coefficients and resulting prototypes are given in Table 3.

The coefficients k_j are related to sine waves. Thus, the combination $k_1 = 1$, $k_2 = 0$ and

Table 3. Configuration of Models Based on Eqn. (14)

MODEL	C_1	β_1	β_2	β_3	K_1	K_2	K_3	C_o = 6	12.5	19.5	27	35	40 m/sec
GROUP								MODEL NUMBER					
11	1.0	240	–	–	1.0	–	–	1	2	3	4		
12	1.0	300	–	–	1.0	–	–	–	–	5	6	7	
10	0.6	300	–	–	1.0	–	–	8	9	10	11	12	13
21	1.0	–	200	–	–	1.0	–	14	15	16			
22	1.0	–	300	–	–	1.0	–	17	18				
31	1.0	300	280	–	0.7	0.7	–	–	19	20	21		
32	1.0	340	210	–	0.7	0.7	–	–	22	23	24		
41	1.0	330	210	240	0.9	0.3	0.3	–	25	26	27		
42	1.0	300	90	240	0.9	0.3	0.3	–	28	29	30	31	
43	1.0	270	90	240	0.9	0.3	0.3	–	32	33	34	35	
45	1.0	0	240	240	0.75	0.35	0.35	36	37	38			
51	1.0	240	210	230	0.5	0.5	0.5	–	39	40	41		
50	0.6	160	210	230	0.5	0.5	0.5	–	42	43	44	45	
52	1.0	160	150	230	0.5	0.5	0.5	–	46	47	48		

. CALM, $C_o = 0$ MODEL 49

$k_3 = 0$ provides a single wave pattern where β_1 defines the altitude of the maximum wind speed. The closer the β_1 is to 360° the lower is the altitude of the maximum. Because C_1 only affects the relationship between C_o and k_1 the percentage reduction is unaffected by $C_1 \neq 1$.

Table 3 illustrates 5 major groups which are identified by the first digit in the group number. The second digit indicates a further subdivision, resulting in 14 prototypes. Finally, these prototypes can be stratified by classes of C_o. The class width depends on a chosen tolerance between individual models and empirical profiles. First the difference:

$$\varepsilon^2_{s,t} = \sum_{h=1}^{n_h} [\bar{V}_s(h) - V_t(h)]^2 / n_h \qquad (17)$$

has been calculated. The subscripts s and t designate the individual permutations, s = 1, ...,$n_s - 1$ and t = 1,...,n_s; n_s is the number of possible models for the prototypes and classes of C_o. Then $\varepsilon^2_{s,t} > \varepsilon^2_T$ was required where ε^2_T is a preselected threshold. E.g., the profiles with s = 1, t = 2 differ in amplitude only (see Table 3). In this case the difference is simple to calculate:

$$\varepsilon^2_{1,2} = (C^2_{0,1} - C^2_{0,2})/2 = (156.25 - 36)/2 \sim 60 \qquad (18)$$

As reflected in Table 3, ε^2 is calculated for the 14 prototypes and 6 classes of C_o. All models with $\varepsilon^2_{s,t} < 50$ were discarded which left 48 models as numbered in the last columns of Table 3. A final model $C_o = 0$ was added. Although this condition is not rigorously fulfilled, some empirical profiles with very weak winds fall into this model class.

The system of models was used to derive an empirical error threshold for every model V_m:

$$\varepsilon^2_m = \sum_{h=1}^{n_h} [\bar{V}_m(h) - V(h)]^2 / n_h \qquad (19)$$

The model number with the minimum ε^2_m, m=r, was assigned to fit the empirical profile best, e.g., model r has ε^2_r, then $\varepsilon^2_r \leq \varepsilon^2_m$, m = 1,...,49. Thus, r is the assigned model number for the empirical wind profile.

In the system of 49 models the average $\bar{\varepsilon}^2_r$ was 10. Since this error is of the same magnitude as the instrumental error the system of 49 models was considered to be sufficient. It is evident that a condition for the average error $\bar{\varepsilon}^2_r < 5$ requires smaller classes of C_o and more models but a relaxation to $\bar{\varepsilon}^2_r = 25$ can reduce the number of models.

3.2 Model Examples

For many readers Table 3 may mean little because it is difficult to visualize patterns of the wind speed profile for mixture of waves. Table 4 was prepared to summarize in non-mathematical terms the characteristics of the 14 prototypes. Figures 4 and 5 further illustrate the meaning of prototypes and individual models. More details can be found in the author's articles of 1971 and 1973, and only 2 graphs have been included here.

Table 4. Description of Wind Profile Groups

	Group 1, Single Wave
11	Wind Maximum at 14 km
12	Wind Maximum at 10 km
10	Shift of C_1, Wind Max at 10 km
	Group 2, Double Wave
21	First Wind Maximum at 10 km
22	First Wind Maximum at 6 km
	Group 3, Mixture Equal Single + Double Wave
31	First Maximum at 10 km (peak speed narrow spread)
32	First Maximum at 8 km (peak speed narrow spread)
	Group 4, Mixture Dominant Single Wave
41	Maximum at 7 km (peak speed wide spread)
42	First Maximum at 5 km Main Maximum 13 km
45	Main Maximum at 13 km
45	Main Maximum at 5 km
	Group 5, Mixture Three Equal Waves, Triple Max.
51	Main Peak at 14 km
52	Main Peak at 25 km
50	Main Peak at 25 km, shift of C_1

Figure 4 depicts a single wave pattern with two different β_1 values. Thus, the altitude of the wind speed maximum appears at 10 and 14 km. The models resulting from dividing C_o into classes are illustrated by inclusion of all wind models for types 11 and 12.

Figure 5 exhibits the differences within 6 of the prototypes. We learn that the single wave pattern 12 and 31 differ by the narrowing of the maximum from 12 to 31. This contraction is accomplished mathematically by mixing two waves such as 12 and 21. A dominant single wave pattern is disclosed for group 4, and the two examples from 42 and 45 give an insight into the complex structure of some of the wind speed profiles. Finally, the mixture of 3 waves is illustrated by one model from group 5.

Figure 4. Family of Models in Group 11 and 12

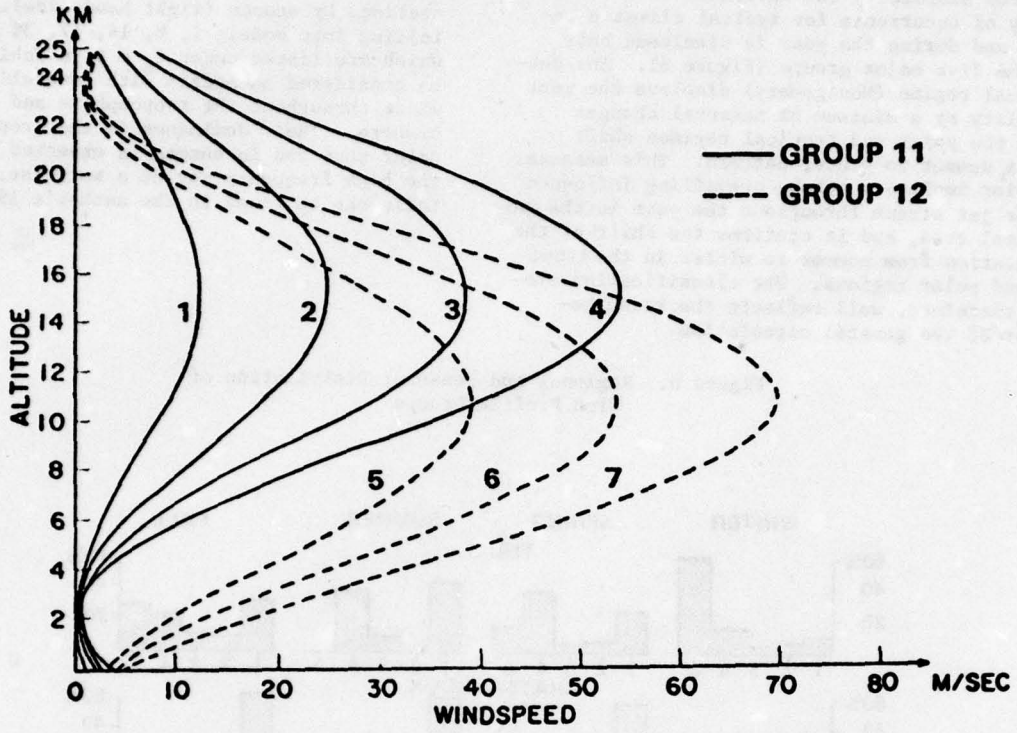

Figure 5. Typical Models of Wind Profile Groups

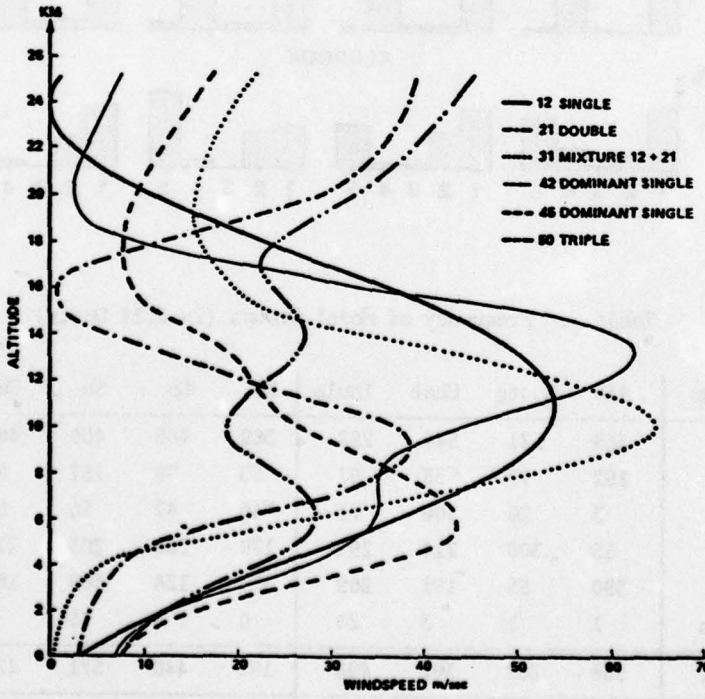

3.3 Seasonal and Regional Distribution

For simplicity the variation of the frequency of occurrence for typical climatic regimes and during the year is disclosed only for the five major groups (Figure 6). The subtropical regime (Montgomery) displays the most stability by a minimum of seasonal changes while the polar and tropical regimes shift from a summer to winter pattern. This seasonal behavior implies a strong prevailing influence of the jet stream throughout the year in the subtropical area, and it confirms the shift of the circulation from summer to winter in the tropical and polar regions. The classification system, therefore, well reflects the known behavior of the general circulation.

Table 5 provides a summary of the frequency for the entire year at an individual station (left hand side), and a combination of all stations by season (right hand side). Profiles falling into models 1, 8, 14, 17, 36 and 49, which are listed under C_o = 6 in Table 3, can be considered as models with generally weak winds throughout the troposphere and lower stratosphere. Their dominance in the tropical and polar zone and in summer is expected although the high frequency may be a surprise. More details can be found in the author's 1973 article.

Figure 6. Regional and Seasonal Distribution of Wind Profile Groups

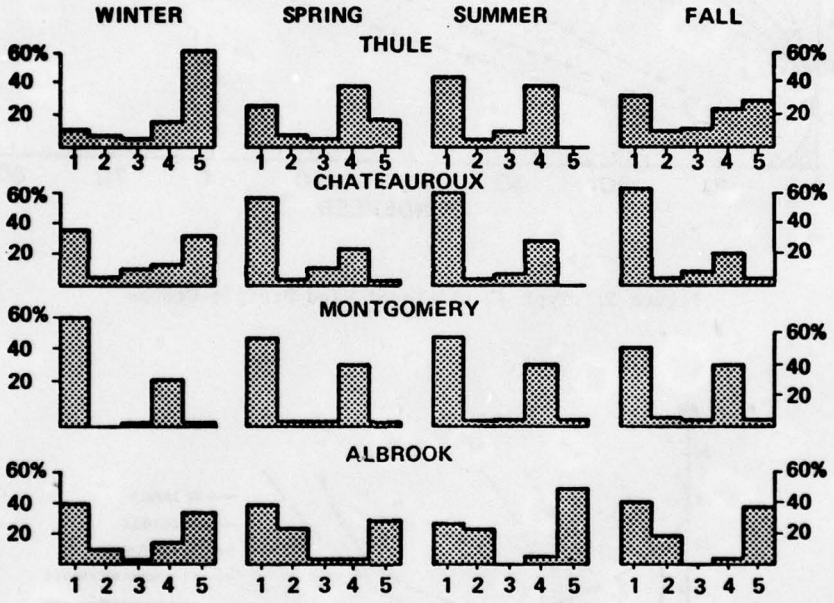

Table 5. Frequency of Model Groups (in 0.1% Units)

Group	Alb	Montg	Chat	Thule	Wi	Sp	Su	Fa	Total
1	369	521	544	288	389	465	400	467	431
2	192	97	38	57	53	90	157	85	96
3	3	26	100	71	46	47	56	52	50
4	55	300	214	291	179	266	203	212	205
5	380	55	101	269	333	124	169	180	201
Calm	1	1	3	24	0	8	15	4	7
Weak	558	269	302	498	193	440	571	424	407

(weak = profiles in first models with 6 m/sec amplitude of C_o, and model 49)

4. CONCLUSION

The advantage of empirical polynomials (eigenvectors) over standard function was examined. It was confirmed that empirical polynomials permit us to approximate the total variance of the empirical wind profiles by a mathematical expression whose first order term provides an optimum fitting. Standard functions are more suitable, however, for a geographical and seasonal comparison and offer advantages for statistical modelling.

The wind speed profile from surface to 25 km has been approximated by a Fourier Series. Based on this mathematical background five wind profile groups or a total of 14 prototypes have been deduced. The groups are robust to reasonable model variations. The number of subtypes depends on the spacing of C_o, which in turn affects the average dispersion from the profile models. Forty-nine models have been found to be sufficient so that the average dispersion of the empirical profiles from the models is of the same magnitude as the instrumental error.

The main groups display a typical structure of the wind profile in various climatic zones. About 85% of the profiles in the mid-latitudes and subtropics exhibit a single wave pattern with a maximum close to the tropospause (jet stream) while this percentage drops to 65 and 40% in the polar and tropical zones, respectively. This group is replaced by a type whose maximum is situated in the stratosphere above 20 km, with 40% and 25% frequency in the tropics and polar region, respectively. The remaining profiles essentially follow a double wave pattern with maxima in the troposphere and stratosphere. This structure of the profiles can be readily interpreted in terms of the general circulation.

The shift from the summer to the winter pattern, as known from the general circulation, is reflected by a change of the wind speed groups from summer to winter in the tropical and polar latitude stations. The weaker circulation in summer and in the polar and tropical regions is illustrated by the association of a majority of empirical profiles with models with weak wind speeds (see Table 5). This fact is not new, but a quantitative assessment has not been given in the past.

Some readers may ask whether modelling with four stations considers enough variety of the wind speed profile to provide all necessary models. The author has meanwhile added other stations but no evidence has been found that the other stations contributed either to an expansion of models or to added knowledge about the general circulation which could not have been obtained from the derived prototypes. Admittedly, the frequency of occurrence deviates slightly from the amounts as shown for the stations in Figure 6 but the essential features depicted by the 4 different wind regimes remain.

ACKNOWLEDGEMENT: The author appreciates the assistance given by Mrs. C. Brooks who diligently typed and assembled the manuscript. Mrs. H. Boyd deserves the credit for her critical review of the text.

REFERENCES CITED

Essenwanger, O. M., 1962: The Wind Profile from Surface Through 30 km in Atmospheric Ballistic Problems. Geofisica pura e applicata, Vol. 53, No. III, p. 189-197.

____, 1964: Mathematical Characteristics of Individual Wind Profiles. US Army Missile Command, RR-TR-64-12, pp 41.

____, 1971: Characteristic Coefficients, Probability and Classification of Wind Profiles (Surface to 25 km). ARO-D Report 71-3, p. 163-184.

____, 1973: The Structure of the Wind Profile From Surface to 25 km in Various Climatic Zones. in. Klimatologische Forschung, Ferd. Dummler, Bonn, Bonner Meteorol. Abh. Heft 17, p. 523-539.

____ 1975: Eigenvector Representation of Wind Profiles. Fourth Conf. on Probab. and Statistics in Atmospheric Sciences. Publ. by Am. Meteorol. Soc., Boston, p. 206-210.

____, 1976a: Applied Statistics in Atmospheric Sciences, Part A: Frequencies and Curve Fitting, Elsevier, pp 412.

____, 1976b: On Some Practical Aspects of Statistical Analysis as Exemplied by Parameterized Daily Radiosonde Profiles. Revue belge de statistique et de Reserche operationelle, Vol. 15, #3, 15-36.

____, 1977: Eigenvector Analysis of Empirical Data versus Utilization of Standard Functions. ARO-D Report 77-2, p. 165-175.

____ 1978: Wind Profiles and Wind Shear for Evaluation of Missile Designs. Proceedings of the 3rd Annual Free Flight Rocket Workshop, 10-12 Oct 78, MIRADCOM Tech. Report, in publication.

Essenwanger, O. M., and H. Boyd, 1970: On Methods to Establish a Set of Global Characteristic Wind Profiles. US Army Missile Command, RR-TR-70-25, pp 35.

Handbook of Geophysics, 1960: MacMillan, pp 657.

Handbook of Geophysics and Space Environment, 1965: McGraw Hill, pp 639.

Faust, H., 1967: Interaction between different layers of the homosphere. Archiv Meteor. Geoph. Bioklim. A. Vol. 16, p. 12-30.

Flohn, H., 1952: Probleme der grossräumigen Synoptik. Ber. Dtsch. Wetterd. US-Zone, No. 35, p. 12-23.

Schwerdtfeger, W., and Radok, W., 1959: Hodograph Analysis as Applied in the Occurrence of Clear-Air Turbulence. Journ. Meteor., Vol. 16, No. 5, p. 588-592.

Schwerdtfeger, W. and Mahrt, L. M., 1970: Ekman Spirals for Exponential Thermal Wind. Boundary Layer Meteor., Vol. 1, p. 137-145.

Stewart, D., 1967: Interrelationships Between Thermodynamic Variations in the Troposphere and the Lower Stratosphere. US Army Missile Command Report No. RR-TR-67-14.

Stewart, D. A., and O. M. Essenwanger, 1978: Frequency Distributions of Wind Speed. Journ. Appl. Meteoro. Vol. 17, #11, p. 1638-1642.

DEVELOPMENT OF SINGLE STATION AND AREA STATISTICAL SHORT-RANGE FORECAST TECHNIQUES

Captain Michael J. Kelly

Headquarters Air Weather Service

Scott Air Force Base, Illinois 62225

ABSTRACT

Many military scenarios require that a forecast be made without weather teletype, facsimile, satellite, and radar data. An objective method for providing weather support under these limitations has been developed. REEP regression equations were used to generate three and six hour probability forecasts. The regression predictors are all available from a surface weather observation or known geophysical features. A programmable calculator was used to simplify field use of the equations. Computer verification and a field evaluation are discussed.

1. INTRODUCTION

The work discussed in this paper is an extension of an earlier project described by Miller (1977). The raison d'etre is the same: crisis/contingency weather support can be greatly different from peacetime weather support. An unpublished Headquarters Air Weather Service (HQ AWS) report, The Korean Short War Study, recognizes the weather communications problems in Korea. A similar study describes potential weather communications problems in the European theater. The 2nd Weather Wing, the European arm of AWS, devoted their August 1977 Technical Bulletin to limited data forecasting techniques.

In a contingency, many levels of degraded weather support are possible. Earlier weather charts and teletype bulletins may be available. The forecaster may be familiar with the local climatology. If the forecaster has been stationary for a period of time, continuity may help. Our goal was to provide a "last resort" forecast capability for Korea.

We assume that the only weather information available to the forecaster is what he can determine by using simple instruments and his eyes, i.e., a local surface observation. We wanted a completely objective, short-range technique. Finally, unlike most climatological aids, the method should be applicable to any location throughout Korea.

2. METHOD

REEP was the statistical approach used (Miller, 1964). The regression predictors were all binary. The types of predictors and corresponding number of binaries are given in Table 1.

Table 1. Predictors

Predictor Type	Number of Binaries
Month	12
Hour	8
Latitude	4
Longitude	3
Elevation	5
Region of Country	4
Wind Direction	5
Wind Speed	7
Temperature	17
Dewpoint Depression	8
Sky Cover	5
Visibility	12
Present Weather	5
Cloud Amount below 500'	4
Cloud Amount below 1000'	6
Cloud Amount below 3000'	6
Ceiling	14
Cloud Type	3
TOTAL	128

Including geophysical predictors such as elevation and region of the country is an attempt to make the REEP equations applicable to any location in Korea. Statistical equations that are applicable throughout different times of the year and at different geographical locations are know as generalized operators. (Harris, et al, 1963)

The effects of geophysical features on weather and climate are not well known. Pielke and Mehring (1977) used elevation to improve climatological maps of mean monthly temperature. Boehm (1976) has described modelling the climatology of ceiling and visibility by a cubic polynomial. The coefficients of the polynomial are defined by geophysical features. The derivation of generalized operator techniques using geophysical-weather relationships is an important concept for military weather support. Objective target forecasts will require generalized operators. HQ AWS has forwarded a Geophysical Requirement to the Air Force Geophysics Laboratory asking their assistance in this area.

Observations from 31 stations scattered throughout Korea were used to develop the REEP regression equations. These data are from 1953 to 1956. Over 80,000 observations are included in both the three and six hour data sets.

3. VERIFICATION

The REEP equations were used to make forecasts for Uijongbu and Osan AB. These are independent data comparisons since these months and stations were not part of the development data. The Brier Score, and the Brier Score using the observed sample probabilities (Brier and Allen, 1951) are given in Table 2.

Table 2. Verification Results

Station	Forecast Length(HR)	Type Equation	Category	POR	Number Of Forecasts	Brier Score	Brier Score Using Obsvrd Probs
UIJONGBU	3	G/O	CIG $\geq$ 3000'	12/51-02/52	605	.09	.15
UIJONGBU	3	G/O	VIS $\geq$ 3 mi	12/51-02/52	605	.06	.07
UIJONGBU	6	G/O	CIG 3000'	12/57-02/58	718	.19	.28
UIJONGBU	6	G/O	VIS 3 mi	12/57-02/58	718	.12	.12
UIJONGBU	6	Persistence	CIG 3000'	12/57-02/58	718	.29	.28
OSAN	3	G/O	CIG 3000'	12/57-05/58	1455	.14	.25
OSAN	3	G/O	VIS 3 mi	12/57-05/58	1455	.13	.17
OSAN	6	G/O	CIG 3000'	12/57-05/58	1454	.18	.25
OSAN	6	G/O	VIS 3 mi	12/57-05/58	1454	.16	.17
OSAN	6	OSAN DATA	CIG 3000'	12/57-05/58	1454	.18	.25
OSAN	6	OSAN DATA	VIS 3 mi	12/57-05/58	1454	.16	.17

The REEP regression technique has been tested many times; the fact that even these simple forecast equations have skill is not surprising. Although this is not an exhaustive analysis, the strength of the generalized operator equations vis-a-vis those based solely on Osan data is an encouraging surprise. There are factors influencing these results in addition to the use of geophysical predictors. Seven times more data was used to develop the generalized operator equations. Also, the short-range nature of the forecasts minimizes the advantage of a localized data base.

4. TEAM SPIRIT EVALUATION

A field evaluation of the single station forecasts was conducted in Korea during the TEAM SPIRIT 78 exercise. A programmable calculator and its magnetic cards were used to store a computation program and forecast coefficients. Using a calculator eases the workload on a forecaster and helps to minimize computational errors. Although it is simple to use a programmable calculator in this manner, this is, nevertheless, an important concept. There is an established trend towards smaller, more powerful, and less expensive microcomputers. Their use in field meteorology should increase as this trend continues.

The single station equations were compared with conditional climatology, forecasts made by the Osan AB Weather Support Unit, and forecasts

made at the Air Force Global Weather Central. Sound conclusions regarding the skill of the single station method cannot be reached from the TEAM SPIRIT evaluation data for the following reasons:

a. There were too few forecasts.

b. The date/times of the forecasts is not the same for the different forecast methods.

c. The coefficients stored on at least one magnetic card were erroneous.

d. The single station results have unexplainable anomalies indicating some forecasts were incorrectly calculated.

Obtaining an estimate of skill was not the primary reason for the TEAM SPIRIT 78 evaluation. Valuable information was gained by using the single station method in an operational mode. We found that the calculator worked well throughout the evaluation. However, the computation program took too much time to produce a forecast. Finally, current programmable calculators are not quite powerful enough for our needs. Consequently, we believe all AWS forecasters would not be able to effectively use today's calculators without extensive training. This is a temporary problem since there are sure to be further dramatic advances in microcomputer technology.

5. CONCLUSION

Statistical forecast techniques can be used to provide crisis weather support to military decision-makers. Progress in microcomputer technology will allow widespread use of this approach. Further research is needed to better understand the relationships between terrain features and climatology, and to develop more sophisticated single station predictors.

6. ACKNOWLEDGEMENT

The author wishes to express his appreciation to 1WW's Captain Ron Rodney for his help in organizing and accomplishing the TEAM SPIRIT 78 evaluation.

7. REFERENCES

BOEHM, A. R., 1976: Optimal Decisions Through Mission Success Indicators. Proc. of 7th Tech. Exchange Conf., Atmos. Sciences Lab., White Sands Missile Range, New Mexico, 17-25.

BRIER, G. E., and ALLEN, R. A., 1951: Verification of Weather Forecasts. Compendium of Meteorology, Am. Meteor. Soc., Boston, Massachusetts, 841-848.

HARRIS, R. G., BRYAN, J. G., MACMONEGLE, J. E., 1963: Terminal Weather Prediction Studies. System 433L, Tech. Note 3, The Travelers Research Center Inc., Hartford, Connecticut, 264 pp.

MILLER, R.G., 1964: Regression Estimation of Event Probabilities. Tech Rpt 7411-121, Contract Cwb - 10704, The Travelers Research Center Inc., Hartford, Connecticut, 153 pp.

-----, WHITON, R.C., KELLY, M.J., 1977: Results of a Single Station Forecasting Experiment. Fifth Conf. on Prob. and Stat. in Atmos. Sciences, Am. Meteor. Soc., Boston, Massachusetts, 37-40.

PIELKE, R. A. and MEHRING, P., 1977: Use of Mesoscale Climatology in Mountainous Terrain to Improve the Spatial Representation of Mean Monthly Temperatures. Mon. Wea. Rev., VOL 105-No. 1, Am. Meteor. Soc., Boston, Massachusetts, 108-112.

THE TROPICAL CYCLONE STRIKE PROBABILITY PROGRAM (STRIKP)

Samson Brand

Naval Environmental Prediction Research Facility

Monterey, California 93940

ABSTRACT

In a previous study, statistical techniques were used to analyze 10 years of western North Pacific tropical cyclone forecast errors. The results of this analysis were used as a basis for the development of the tropical cyclone strike probability program. Strike probability is a method for determining probabilities up through 72 hours that a tropical cyclone will come within specified distances around geographic points of interest to the user. This program can be used as an aid for operational decisions associated with tropical cyclone evasion, evacuation and base preparedness. The experimental version of the strike probability program currently operational at Fleet Numerical Weather Central will be discussed.

1. INTRODUCTION

The Commander in Chief, U.S. Pacific Fleet (CINCPACFLT), in a letter to the Joint Chiefs of Staff in June 1976, requested an analysis of tropical cyclone forecast errors in the western North Pacific. The request indicated that operational decision makers routinely use information concerning average forecast position errors of tropical cyclones in order to determine actions required to evade or protect against tropical cyclones. This information is readily available from the Annual Typhoon Reports issued by the U.S. Fleet Weather Central/Joint Typhoon Warning Center, Guam (FWC/JTWC). Other verification information which could be of significant value, if available, includes an analysis of variations in forecast performance for different geographical areas and for storms having recognizably different characteristics. In this same letter, CINCPACFLT stated such an analysis could be conducted by the Naval Environmental Prediction Research Facility (NEPRF) and in addition a parallel effort could be conducted to determine the optimum method of applying these results in decision making. Following this request, NEPRF channeled an effort to meet these goals.

The first step was a statistical analysis of the JTWC official forecast errors for the period 1966-1975. (This was performed in conjunction with a thesis student at the Naval Postgraduate School, Capt. Don S. Nicklin, USAF, and advised by CDR Jerry D. Jarrell, USN.) Figure 1, which shows the geographic variations of mean 24-hour forecast errors, dramatically demonstrates the differences between tropical cyclone forecast errors for tropical cyclones affecting the Philippines versus those affecting the Japan/Korea area.

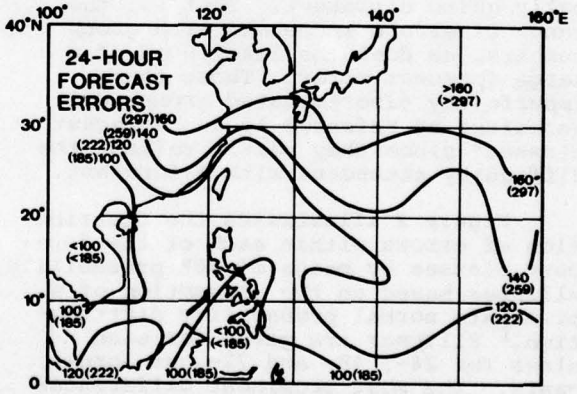

Fig. 1. Geographic distribution of mean 24-hour forecast errors for western North Pacific tropical cyclones. Errors are based on 1966-1975 data and relate to mean forecasts from initial positions. Values are given in km ( ) and n mi.

Other parameters that relate to forecast error are maximum wind, tropical cyclone movement, and number of tropical cyclones in progress (see Jarrell et al., 1978). These parameters were used to discriminate between large error forecasts and small error forecasts. The forecast cases were first stratified into three groups according to their known errors. Group 1 consisted of cases where the magnitude of the error was less than the median in both west-east and south-north components. Group 2 had one component above the median and one below the median, and Group 3 had both components above the median.

Typically, Group 1 was characterized by well developed or intense tropical cyclones in the western part of the region at low latitudes and moving generally west. A typical Group 3 forecast was during or after recurvature and included the total spectrum of tropical cyclone intensities. Group 2 included many low-latitude weak depressions, or tropical cyclones of all intensities at or near typical recurvature latitudes but not as yet exhibiting recurvature. Also included in Group 2 were many otherwise Group-1 cases in multiple storm situations.

By discriminant analysis, functions were derived to separate forecasts into these three groups. The functions were then applied to the dependent data, and the groups that emerged were statistically quite different. That is, the range of errors increased with group numbers, as does the likelihood of a large forecast error. These three imperfectly discriminated groups will hereafter be referred to as "forecast classes" since they partly reflect the difficulty attendant with a forecast.

Figure 2 illustrates the distribution of errors within each of the forecast classes by means of 40% probability ellipses based on the assumption of a bivariate normal probability distribution.[1] Ellipses are given for each class for 24-, 48- and 72-hour forecasts. The most prominent differences in the three sets of ellipses are their sizes. The area within each of the class 1 ellipses is roughly half that of the corresponding class 3 ellipses. The orientation of the major axis is similar for all three classes.

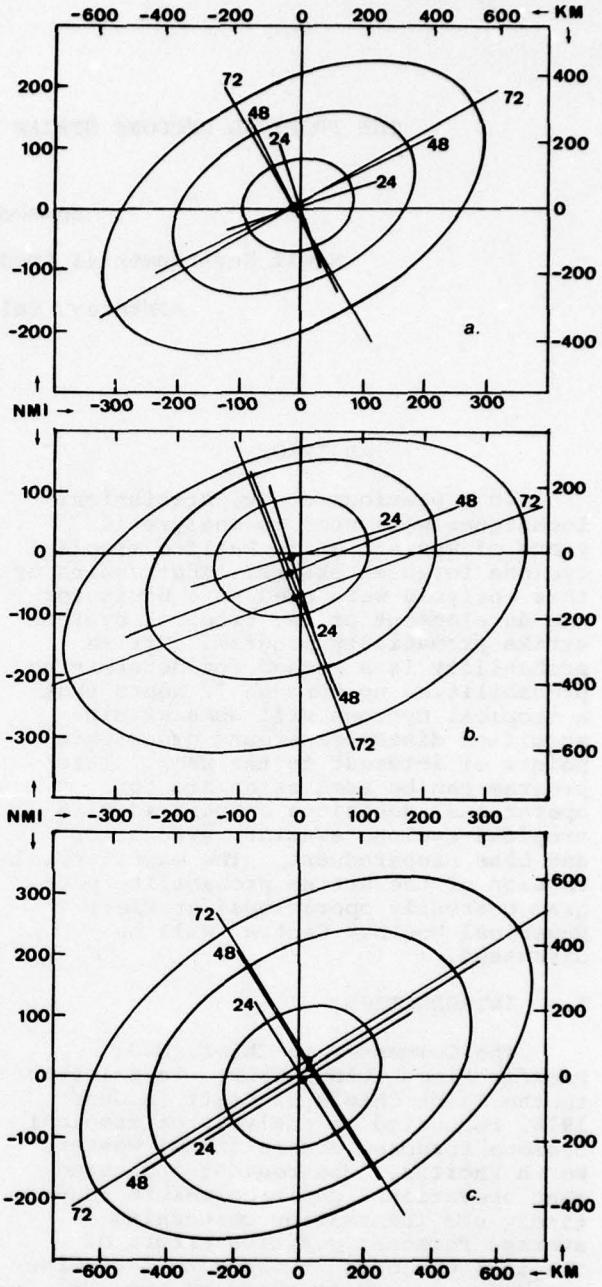

Fig. 2. The 40% probability ellipses for each forecast interval for (a) Class 1; (b) Class 2; and (c) Class 3 forecasts. The origin is the forecast position with each ellipse center the average verifying position relative to forecast position.

Given knowledge of the forecast error distributions associated with tropical cyclones, it is possible to apply this information in decision-making. One application is to derive "threat" or "strike" probabilities for specific locations in the western North Pacific. For example, Fig. 3 gives the probability integrated over an area 75 n mi to the left and 50 n mi to the right of Kadena Air Base, Okinawa, relative to the forecast track of

[1] To convert to 70% and 90% ellipses, the lengths of the axis shown in Fig. 2 should be increased by factors of 1.55 and 2.15, respectively.

Typhoon Fran. The integration is also performed over time from an initial time of 1800 GMT, 7 Sept 1976, to time 12, 24, 48, and 72 hours later. These time-integrated values (within hours) are larger than the instantaneous values at specified times (at hours) after the initial warning time. Both the time-integrated and the instantaneous strike probabilities could be of use to tropical cyclone decision makers.

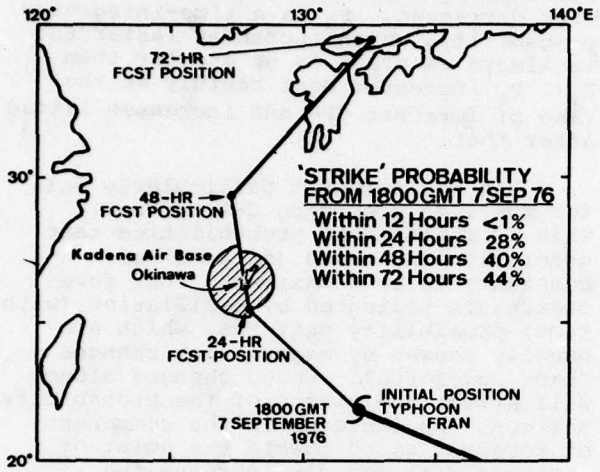

Fig. 3. The "strike" probability of Typhoon Fran (1800 GMT, 6 Sep 1976) passing through the shaded area relative to Kadena Air Base, Okinawa. The probabilities are based on the forecast track and the error distributions for this type of tropical cyclone. Typhoon Fran did in fact miss the shaded area as the storm passed to the east of Okinawa.

The forecasts for the 1976 tropical cyclone season were used to test the accuracy of the strike probabilities (Jarrell, 1978). Forty geographical points in the western North Pacific were selected for the test. If a tropical cyclone had a closest point of approach (CPA) within 500 n mi of one of the points, all forecasts made within four days before and three days after CPA were saved and considered. The test area was defined as a circle of radius 62.5 n mi offset 12.5 n mi left of the test point relative to forecast direction of motion.

Table 1 summarizes the results of the instantaneous strike probability test. The predicted strike probabilities were classed into the 5% class intervals listed on the left. Entries in the body of the table give the verifying average strike probability and number of cases for each class. The verifying average was tested for significance (5% level) assuming a binomial distribution of strikes, with the probability of a strike given by the upper class limit, then the lower class limit.

Table 1. Frequency of verifying strikes (%) as function of predicted strike probability. Number of cases shown in (). (A) is any value significantly above lower class limit, (↓) any value significantly below upper class limit. (From Jarrell, 1978.)

Predicted Strike Probability	Frequency of verifying strikes					
	12-hours	24-hours	36-hours	48-hours	60-hours	72-hours
0- 4.5	0.1(5524)↓	0.3(4703)↓	0.7(3976)	0.9(3516)	1.5(2943)	2.0(2373)
4.5- 9.5	4.4(123)	8.7(210)^{A}	6.7(320)	9.1(182)	6.6(47)	
9.5-14.5	8.0(53)	10.0(112)	8.8(51)			
14.5-19.5	19.4(40)	12.5(56)	23.2(4)			
19.5-24.5	27.6(33)	15.1(18)				
24.5-29.5	29.7(34)	26.2(13)				
29.5-34.5	30.2(18)					
34.5-39.5	54.7(4)					
39.5-44.5	35.3(6)					
44.5-49.5	57.9(5)					
49.5-54.5	42.8(4)					
>54.5	89.2(4)					

The mean of the first group (0-4.5%) was not tested against the lower boundary (0%) since any non-zero average outcome would appear to be significant. The symbol (↓) means the average value was significantly lower than the upper class limit, while (A) means the average value was significantly above the lower class limit. There were no cases where the average value was significantly either above the upper limit or below the lower limit. Note: The over 55% group at 12 hours was tested against the single mean predicted strike probability (60.0%).

A similar test was designed for the time probability summation. The same data were used as in the previous test, but now the time-summed probabilities for time intervals in multiples of 12 hours (i.e., 0-12, 0-24, .., 0-72 hours) were estimated. The verifying probability was taken to be the maximum probability of the cyclone being within the area at any of the subsequent warning times (at six hourly intervals) within the interval being considered. Figure 4 illustrates the results of this test.

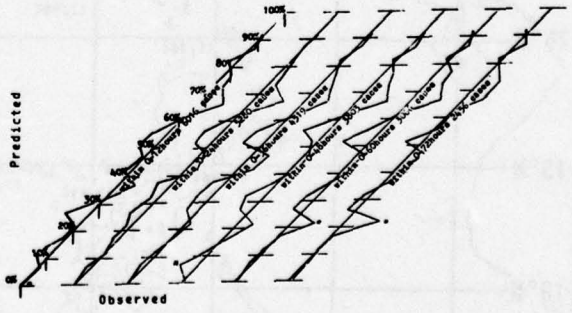

Fig. 4. Comparison between observed strike frequency and predicted strike probability. 45° line represents the "expected" for each of 6 progressively wider time intervals. (*) indicates differences in forecast probability and observed frequency significant at 5% level. (From Jarrell, 1978.)

The predicted probabilities were classed into cells of 0 to 4.5%, 4.5% to 9.5%, etc., up to 89.5% to 94.5% (no probabilities >94.5% were forecast). The mean predicted probability and the mean observed frequency of strikes are shown for each time interval. The differences between observed and predicted mean values were tested (same binomial test as before) for statistical significance. A total of 114 such tests were conducted (six time intervals vs 19 cells); of these, only four differences were found to be significant at the 5% level.

2. OPERATIONAL EXAMPLES AND PRODUCTS

To illustrate strike probability, the program (STRIKP) was run on all the forecasts for Typhoon Kim (6-17 Nov 1977). A plot of the warning positions is shown in Fig. 5. The arrow at each warning position gives the forecast direction (16 points) of motion and the number above each position relates to the forecast class, either 1, 2 or 3.

Table 2 gives strike probabilities for Guam, defined in three different ways: Typhoon Kim will pass Guam (1) within a 50 n mi radius circle; (2) within 75 n mi on the left side or 50 n mi on the right side relative to forecast track; or (3) within a 100 n mi radius circle. Columns are headed by times 12-72 hours in 12-hour steps. The column entries are two numbers separated by a slash (/): the first is (P_I), the probability (%) of a "strike" at the given number of hours after warning time; and the second (P_S) is the probability (%) of a strike at any time within the given number of hours after warning time. Notice that P_I (the instantaneous probability) increases approaching the time of forecast CPA and then decreases. P_S is a time-integrated probability, which increases faster and is always as great as or greater than P_I. P_S increases most rapidly at the time of forecast CPA and increases little after that.

Kim was forecast particularly well for the time preceding CPA to Guam. This is revealed in probabilities that generally increased (or remained constant) up to a maximum. Poor forecasting is indicated by oscillating (with time) probability patterns, which are usually caused by major track changes (back and forth). Speed changes alone will affect the timing of the probability maximum. An increase in the component of forecast speed toward the point of interest will rapidly increase the strike probabilities, while a decrease in that component may show little change in probability, since forecast CPA in hours after warning will change little.

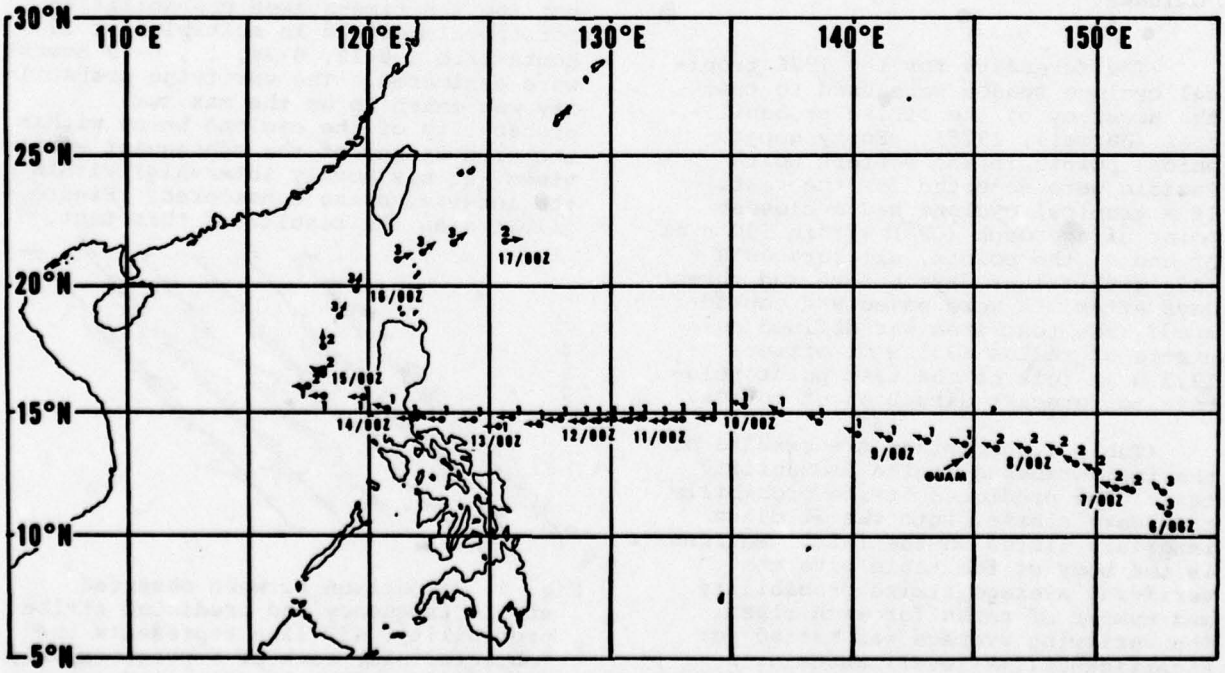

Fig. 5. Warning positions for Typhoon Kim (6-17 Nov 1977).

Table 2. Forecast strike probabilities (P_I/P_S) of Typhoon Kim being within a defined area about Guam. h is hours after warning time (left column). P_I is the instantaneous probability for time = warning time + h. P_S is the probability that Kim will be in the area at some time within the interval h-hours after warning time. Closest Point of Approach occurred at about 08/1100Z.

within 50 n mi radius of Guam

h / Time	12 P_I/P_S	24 P_I/P_S	36 P_I/P_S	48 P_I/P_S	60 P_I/P_S	72 P_I/P_S
6/06Z	0/0	0/0	3/6	3/10	2/12	1/12
6/12Z	0/0	0/0	2/6	3/9	2/11	1/12
6/18Z	0/0	2/2	5/11	4/14	2/15	1/16
7/00Z	0/0	1/2	5/11	4/14	2/15	1/16
7/06Z	0/0	8/14	6/18	3/19	1/19	1/19
7/12Z	3/3	11/19	5/21	2/21	1/22	1/22
7/18Z	6/8	12/22	5/23	2/23	1/23	0/24
8/00Z	29/37	7/37	2/37	0/37	0/37	0/37
8/06Z	14/62	1/62	0/62	0/62	0/62	0/62
8/12Z	0/82	0/82	0/82	0/82	0/82	0/82
8/18Z	0/3	0/3	0/3	0/3	0/3	0/3

within a 75 n mi radius to the left and 50 n mi radius to the right of Guam relative to forecast track

h / Time	12 P_I/P_S	24 P_I/P_S	36 P_I/P_S	48 P_I/P_S	60 P_I/P_S	72 P_I/P_S
6/06Z	0/0	1/1	4/9	4/13	2/14	1/15
6/12Z	0/0	0/1	4/8	4/12	3/14	2/15
6/18Z	0/0	2/4	8/14	5/17	3/18	2/19
7/00Z	0/0	2/3	8/14	5/17	3/18	2/19
7/06Z	0/1	12/18	9/21	4/22	2/22	1/23
7/12Z	4/5	16/23	7/25	3/25	1/25	1/25
7/18Z	9/11	17/26	7/27	3/27	1/27	1/28
8/00Z	39/45	11/45	2/45	1/45	0/45	0/45
8/06Z	20/69	2/69	0/69	0/60	0/69	0/69
8/12Z	0/90	0/90	0/90	0/90	0/90	0/90
8/18Z	0/7	0/7	0/7	0/7	0/7	0/7

within 100 n mi radius of Guam

h / Time	12 P_I/P_S	24 P_I/P_S	36 P_I/P_S	48 P_I/P_S	60 P_I/P_S	72 P_I/P_S
6/06Z	0/0	2/3	11/16	10/19	6/21	3/22
6/12Z	0/0	2/2	9/14	10/18	7/20	4/21
6/18Z	0/0	7/10	18/23	14/25	8/26	5/26
7/00Z	0/0	6/9	18/23	13/25	7/26	4/26
7/06Z	3/3	29/32	22/34	11/34	5/34	3/34
7/12Z	15/18	37/40	19/40	8/40	4/40	2/40
7/18Z	27/31	39/45	17/45	7/45	3/45	2/45
8/00Z	74/74	26/74	6/74	2/74	1/74	1/74
8/06Z	49/95	5/95	1/95	0/95	0/95	0/95
8/12Z	4/99	0/99	0/99	0/99	0/99	0/99
8/18Z	0/51	0/51	0/51	0/51	0/51	0/51

Forecast confidence can be defined as the probability that a tropical cyclone will be within a circle of given radius at a particular time. The strike probability concept provides the estimation of these confidence values and was developed at the request of the Joint Typhoon Warning Center. The forecast confidences for some selected radii about forecast points given in three different Typhoon Kim (1977) warnings are shown in Table 3. These particular forecasts were selected because they were the first of forecast class 1 (8 Nov 1200Z), class 2 (6 Nov 1800Z), and class 3 (6 Nov 0600Z). Since these are instantaneous forecasts (i.e., no time integration involved), these values are functions only of forecast class, time after forecast, and radius of circle. Therefore, the values given in Table 3 under column heading 8 Nov 1200Z are always valid for a class 1 forecast; and those in the next two columns are valid for class 2 and 3 forecasts.

Table 3. Forecast confidences for three warnings of Typhoon Kim (1977).

	8 Nov 1200Z Class 1	6 Nov 1800Z Class 2	6 Nov 0600Z Class 3
24 hour			
Within 100 n mi	61%	42%	34%
Between 100-150 n mi	26%	28%	26%
Outside 150 n mi	13%	30%	40%
48 hour			
Within 200 n mi	57%	44%	36%
Between 200-300 n mi	26%	28%	27%
Outside 300 n mi	17%	28%	37%
72 hour			
Within 300 n mi	55%	45%	41%
Between 300-450 n mi	26%	27%	27%
Outside 450 n mi	19%	28%	32%

Three distinct strike probability products will be available on an experimental basis during the 1978 typhoon season:

Product 1. Tropical cyclone strike probabilities for preselected points.

Product 2. JTWC forecast confidence estimates (available with product 1 only).

Product 3. Individual user requests for tropical cyclone strike probabilities via Automated Product Request (APR) System [AUTODIN or Naval Environmental Data Network (NEDN)].

Products 1 and 2 can be generated together automatically by FNWC upon receipt of the JTWC digital warning every six hours. Product 1 gives the probabilities of a particular tropical cyclone being within 75 n mi (left) or 50 n mi (right) relative to forecast track of nine preselected points of interest to major commands. As designated by CINCPACFLT, the preselected points are: Anderson AFB, Guam; Apra Harbor, Guam; Clark AB, RP; Subic Bay, RP; Kadena AB, Okinawa; Yokota AB, Japan; Yokosuka NS, Japan; Hong Kong; and Keelung, Taiwan.

The strike probabilities, computed upon receipt of each six-hourly JTWC warning and given at 12-hour intervals after warning time, are presented in

two forms. The first is the instantaneous probability, valid at a single instant of time only. The second is a time-integrated probability -- the probability that a strike will occur at some time between the effective time of the warning and multiples of 12 hours thereafter.

Product 2 lists the probabilities of forecast errors falling within certain preselected, time-dependent limits. It is intended for JTWC use and is always provided with product 1.

Product 3 is run only upon request. The user makes his request to Fleet Numerical Weather Central (FLENUMWEACEN) via AUTODIN (or NEDN). He includes information sufficient to identify the tropical cyclone, the point of concern (latitude/longitude), and the radii about that point describing the area considered to constitute a strike. The output is in a format similar to that of product 1 (i.e., instantaneous and time-integrated strike probabilities at 12-hour intervals after warning time).

The following example will provide some insight into what user input is required and how the output will appear. The example is Tropical Storm Olive on 21 April 1978 at 0600 GMT. Olive was located about 125 n mi southwest of Manila and forecast to move west to west-northwest at 10 kt with center winds of 50 kt and some intensification to a minimal typhoon expected in the next 48 hours (see Fig. 6). Two strike probability program (STRIKP) runs are discussed.

Run 1 is a FLENUMWEACEN-originated run. Input required is effective date/time of latest warning, name, and approximate latitude/longitude of the tropical cyclone. The latter is used as a backup in the event the cyclone warning cannot be found by name (e.g., misspelled name or changed name because of up- or downgrading). The latitude/longitude can be an estimate (within 2°).

Run 2 is in response to a hypothetical user specifying a point (15°N, 115°E) in the South China Sea. The request will go to FLENUMWEACEN via AUTODIN (or NEDN) message as an APR formatted message (see Table 4). Required input is the same as that for Run 1 above (/STM line), and at least one Area of Concern (/AOC) line which defines the area of concern by means of a point (lat/long) and radii to the left and right of that point (relative to forecast motion).

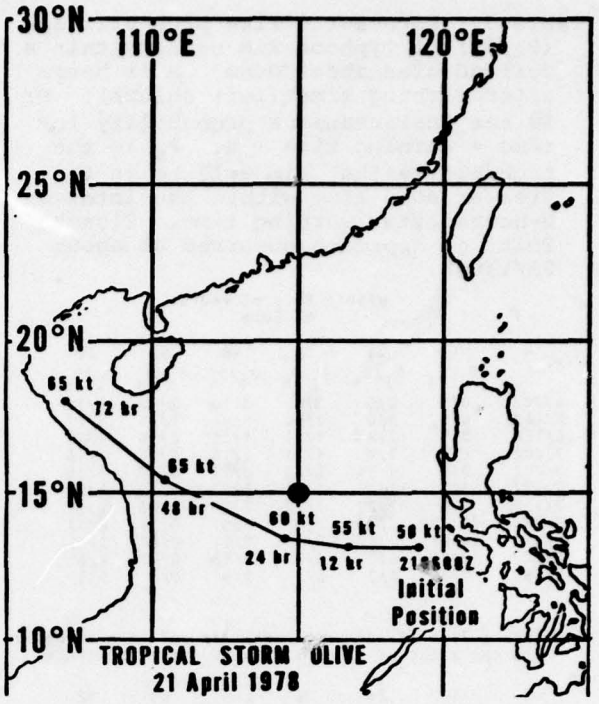

Fig. 6. Initial position of Tropical Storm Olive, 0600 GMT, 21 Apr 1978, and forecast positions out to 72 hours.

Table 4. Sample Automated Product Request (APR) System message.

```
BT
UNCLAS//N03160//
TROPICAL CYCLONE STRIKE PROBABILITY REQUEST
Q92X0001
/APR,AP(STKP),(other entries on this line as required/
/STM,NM(OLIVE),LA(130N),LO(1190E),DH(2106)/
/AOC,LA(150N),LO(1150E),RL(75),RR(50)/
  .
    (as many AOC lines as needed)
  .
/AAD,
 etc.  (as needed)
/PARA,
/ERK/  (required end)
BT
```

/STM: Storm line
- NM: Name of cyclone.
- LA: Latitude of cyclone, approx. LA(130N)=13.0° north.
- LO: Longitude of cyclone, approx. LO(1190E)=119.0° east.
- DH: Effective Date/time of warning. DH(2106)=210600Z (Day 21 hour 0600 GMT)

/AOC: Area of concern line
- LA: Latitude of point of concern. LA(150N)=15.0° north.
- LO: Longitude of point of concern. LO(1150E)=115.0° east.
- RL: Radius of area of concern to left of storms track.
- RR: Radius of area of concern to right of storms track.

Usually RL is greater than RR. Default values of 75/50nm will be used if both RL and RR are blank or missing. If only one is missing, it will default to zero.

Note: One input record will be written for each /AOC (continuing storm info). If no /AOC lines, APR system will put zeros in unfilled positions on input record, and program STRIKP will use internal list of areas. Request message format in accordance with FLENUMWEACEN, 1977: ASWOCAS Request Procedures Manual, Vol 2.

Tables 5 and 6 illustrate the output from Runs 1 and 2, respectively. All three tables also contain some descriptive information.

Table 5. Output from run (1).

```
Run 1 Output (Products 1 and 2) (No  /AOC lines in request)

OLIVE    210600Z

SUBIC BAY  000101  12 IN01  24 IN01  36 IN01  48 IN01  60 IN01  72 IN01
CLARK AB   00IN1N  12 IN1N  24 IN1N  36 IN1N  48 IN1N  60 IN1N  72 IN1N
APRA GUAM  00IN1N  12 IN1N  24 IN1N  36 IN1N  48 IN1N  60 IN1N  72 IN1N
ANDERSEN   00IN1N  12 IN1N  24 IN1N  36 IN1N  48 IN1N  60 IN1N  72 IN1N
KADENA AB  00IN1N  12 IN1N  24 IN1N  36 IN1N  48 IN1N  60 IN1N  72 IN1N
YOKOSUKA   00IN1N  12 IN1N  24 IN1N  36 IN1N  48 IN1N  60 IN1N  72 IN1N
KEELUNG    00IN1N  12 IN1N  24 IN1N  36 IN1N  48 IN1N  60 IN1N  72 IN1N
YOKOTA AB  00IN1N  12 IN1N  24 IN1N  36 IN1N  48 IN1N  60 IN1N  72 IN1N
HONG KONG  00IN1N  12 IN1N  24 IN1N  36 IN1N  48 IN1N  60 0102  72 0105

(Preselected
 Points)              (See Run 2 output for explanation)

For JTWC 24H61/100/26/150/13  48H57/200/26/300/17  72H55/300/26/450/19
```

Prob that 24 hr forecast error, E_{24} > 150 n mi = 13%.

Prob that 24 hr forecast error is between 100 and 150 n mi = 26%

Prob that 24 hr forecast error, E_{24} < 100 n mi = 61%

```
INPUT WARNING DATA

001311188050  121321167055  241351145060  481541103065  721801072065

FORECASTS:  Time 12 hr  Latitude 13.2N  Longitude 116.7E  Max Wind 55 kt
```

LAT/LONG of preselected points are stored within program. Strike is predefined to occur if tropical cyclone passes within 75 n mi radius (left) or 50 n mi radius (right) of points of interest. Right/left are with respect to forecast track of tropical cyclone.

Table 6. Output from run (2).

```
Run 2 Output (Product 3) (Using  /AOC line in request)

STRIKE PROBLTY OF TROP CYCLONE OLIVEΔΔΔ FROM 210600Z WITHIN Δ50 NM

RIGHT AND Δ75 NM LEFT ABOUT 15.0N 115.0E INPUT WARNING DATA USED:

001311188050  121321167055  241351145060  481541103065  721801072065
              (See Run 1 output)

PROBS - 00IN1N  12IN1N  240307  360313  480114  60IN14  72IN14
```

PROB (%) that OLIVE will be in area at some time between 210600Z and 220600Z (24-hr period) was 7%

PROB that OLIVE will be in area at 220600Z was 3% (Warning Time + 24 hr)

Time

ABBREVIATIONS:

Number 01-99; strike probability in %

IN = insignificant; p<0.5% Prevents representation of 0% and 100% which occur only as an approximation.

ST = strike; p>99.5%

NF = No Forecast; for example, when tropical cyclone is forecast to go overland, longer range forecasts will be missing.

The input forecast data is error checked only in that the tropical cyclone forecast motion is computed between forecast points. If vector motion deviates substantially from the climatological mean, the following warning message will appear in all products:

*** UNUSUAL MOTION NOTED -- CHECK WARNING ***

The strike probability products described in the preceding discussion are being evaluated during the 1978 typhoon season.

3. FUTURE OPERATIONAL APPLICATIONS

3.1 Wind Threat Probabilities

To illustrate the potential for operational applications of the strike probability concept, an example concerning Typhoon Fran (1976) is examined.

On 7 September 1976, Supertyphoon Fran with winds in excess of 130 kt was moving across the Philippine Sea on a pre-recurvature track toward Okinawa. Fran was an enormous storm having gale force winds out nearly 300 n mi from the center.

The forecast considered in this example was made at 1800 GMT and had Fran passing over Okinawa in about 30 hours and then recurving over Kyushu and Honshu within the three-day forecast period.

The extent of Fran's winds was not exactly known, but it was assumed that hurricane force winds extended to 75 n mi on her right side and 50 n mi on her left side, and that 50 kt winds extended 150 n mi on her right side and 125 n mi on her left side. The latter were one-half the extent of 30 kt winds given in the 1800 GMT forecast, which were assumed to be correct. It was further assumed that this wind distribution would remain the same for the following three days.

Figure 7 illustrates these wind radii inverted about Okinawa. The inversion exists because winds generally extend farther on the right side, hence the same effect occurs with the typhoon farther away on the left than on the right. If the assumptions are correct and the typhoon passes within the inner shaded area, the point (Buckner Bay) receives at least 65 kt winds. If the typhoon passes within the 50 kt limits (which also includes the inner area), then the point receives at least 50 kt winds. Similarly, if the typhoon passes within the outer ring, Buckner Bay receives at least 30 kt winds.

The first inset table of Fig. 7 shows the instantaneous probability of Fran being within either the 65, 50 or 30 kt wind areas at forecast time and at 12-hour intervals thereafter to 72 hours.

The second inset table shows the time-integrated probability of Fran being inside the wind areas at any time between 1800 GMT 7 September 1976 and some later time given in 12-hour intervals. For example, the probability of 65 kt winds at Buckner Bay within 48 hours is about 40%, which is much larger than the probability of 65 kt at 48 hours after forecast time (only 3%). This is due to the fact that

"within 48 hours" includes not only 0, 12, 24, 36 and 48 hours, but also all the in-between times.

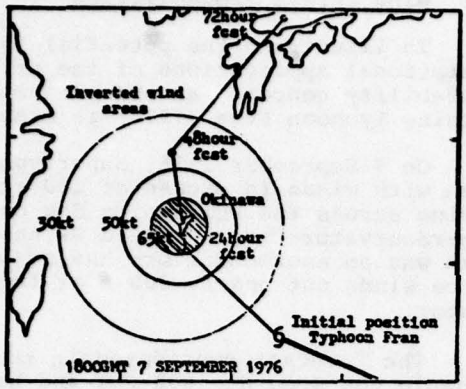

Inset Table 1

time (hours)	65kt wind threat	50kt wind threat	30kt wind threat
0	<.5%	<.5%	<.5%
12	<.5	2	40
24	25	75	99
36	11	43	89
48	5	18	46
60	1	6	25
72	<.5	2	10

Inset Table 2

within time (hours)	65kt wind threat	50kt wind threat	30kt wind threat
0	<.5%	<.5%	<.5%
12	<.5	8	55
24	28	82	99
36	37	88	>99.5
48	40	94	>99.5
60	42	96	>99.5
72	44	97	>99.5

Fig. 7. Illustration of actual forecast, Typhoon Fran, 1800 GMT, 7 Sep 1976. Nested offset circles represent 65 kt area of concern (inner), 50 kt area, and 30 kt area (outer) about Buckner Bay, Okinawa. Inset tables show estimated threats of 65, 50, 30 kt winds at specific hours (multiples of 12) after forecast time, Inset Table 1; and during a time period beginning at forecast time and ending some hours (multiple of 12) later, Inset Table 2 (after Jarrell, 1978).

3.2 Conditions of Readiness

Conditions of readiness indicate that the probability of winds of a certain force occurring within a specified time interval will reach some critical value. Western Pacific commanders commonly use either 50 kt or 65 kt as the wind force which limits their most serious readiness condition. These are referenced here as Severe Storm (SS) or Typhoon (T) conditions. Commanders also use a sequence of numbers determined by probability within a time period:

Condition 4: SS or T force winds possible within 72 hours
Condition 3: SS or T force winds possible within 48 hours
Condition 2: SS or T force winds anticipated within 24 hours
Condition 1: SS or T force winds anticipated within 12 hours

Since possible and anticipated are vague terms, it may be better to have a quantitative assessment of the apparent threat and relate this to the decision-makers. For example, Fig. 8 defines the contour of at least a 5% probability of typhoon force winds within 72 hours as Condition 4 or T4. Fig. 8 also represents the same type information for 10%, 20% and 33% for T3, T2 and T1 respectively. These represent overwarning factors of 20, 10, 5 and 3.

An overwarning factor of 3 means a particular point would brace itself for 65 kt winds three times and only observe the occurrence once. The factor of 3 is considered to be the overwarning factor used by the National Weather Service for Atlantic hurricane warnings (Sugg, 1967). Private communication with National Hurricane Center forecasters indicate 5 to 6 is the approximate overwarning factor used for setting hurricane watches.

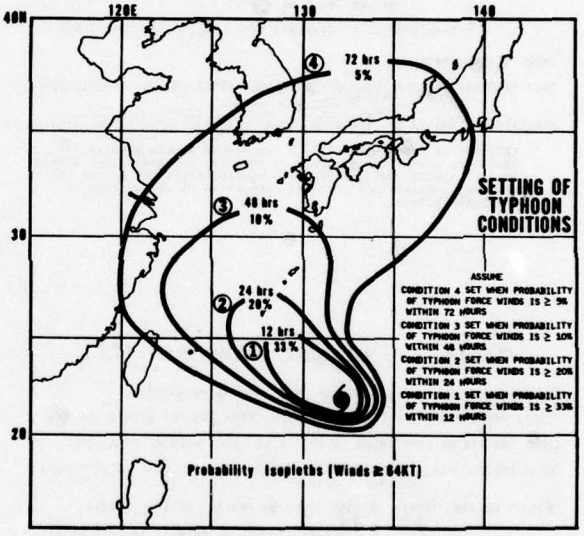

Fig. 8. Probability isopleths of typhoon conditions for Typhoon Fran (1976).

3.3 Ship Routing

Again using the example of Typhoon Fran, assume that 50 kt winds and the seas that accompany such winds are the upper limit for safe ship operating conditions. Assume also, that the ship router wants to be 95% confident of staying out of 50 kt winds. To provide guidance for the ship router for decision making, Fig. 9 gives contours of 5% probability of 50 kt (or greater) winds at 12-hour intervals from 0 to 72 hours. For example, if a ship was heading from Korean waters to the east of Japan via the route south of Kyushu, it would have to do so within 24 hours and certainly before 36 hours from the current time.

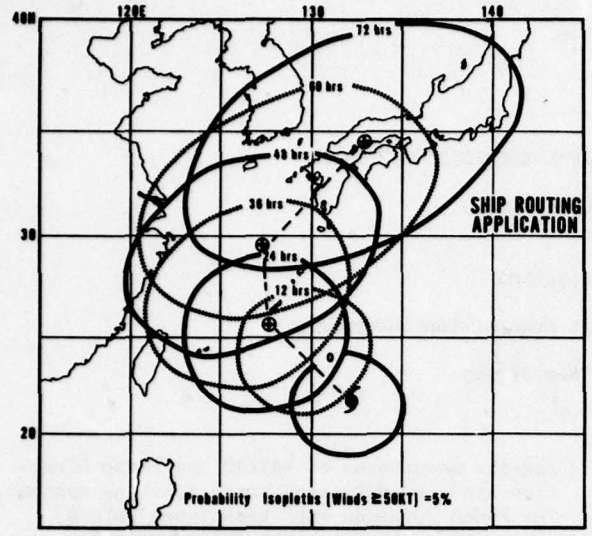

Fig. 9. Probability isopleths, ship routing applications, Typhoon Fran (1976).

The ship router might also be interested in the probability of specified sea heights surrounding tropical cyclones. A NEPRF program, TYWAVES (Brand et al., 1977), uses the JTWC warning information and predicts the storm-generated seas about the moving cyclone center. One or more contours of this pattern can be described by a series of ranges and bearings from the cyclone center. Thus a particular height of seas is expressible relative to the storm center. See, for example, the 24 hour tropical cyclone $\geq$ 12 foot ($H_{1/3}$) sea probability for Typhoon Fran as shown in Fig. 10.

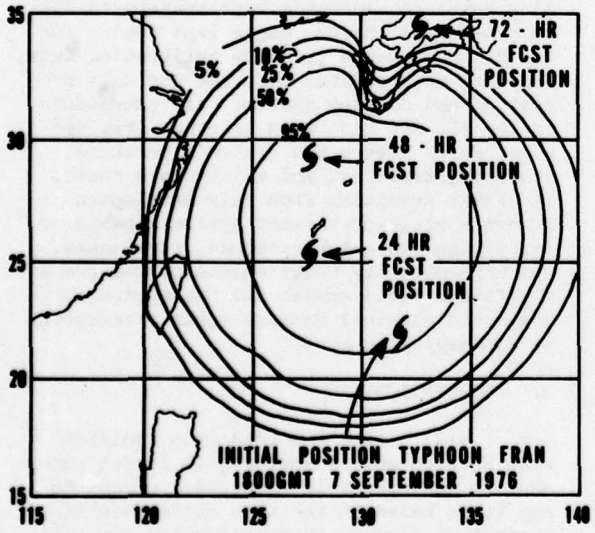

Fig. 10. Twenty-four hour $\geq$12 ft sea probability for Typhoon Fran (1976).

4. SUMMARY

The tropical cyclone strike probability program has been described and several examples and applications have been demonstrated. As the program evolves from an experimental version to a more operationally available product, user feedback will ultimately determine the direction for further development. If found to be a successful aid to operational decisionmakers, the strike probability concepts may well expand to additional ocean areas other than the western North Pacific.

5. REFERENCES

Brand, S., K. Rabe and T. Laevastu, 1977: Parameterization characteristics of a wind wave tropical cyclone model for the western North Pacific Ocean. J. Phys. Ocean., Vol. 7, No. 5, 739-746.

Jarrell, J. D., 1978: Tropical cyclone strike probability forecasting. NAVENVPREDRSCHFAC Cntrctr. Rept. CR 78-01 (SAI-79-782-WA).

Jarrell, J. D., S. Brand and D. S. Nicklin, 1978: An analysis of western North Pacific tropical cyclone forecast errors. Mon. Wea. Rev., 106, 7, 925-937.

Sugg, A. L., 1967: Economic aspects of hurricanes. Mon. Wea. Rev., 95, 143-146.

FIELD ARTILLERY METEOROLOGICAL ACQUISITION SYSTEM

(FAMAS)

Raymond L. Robbiani

Combat Surveillance and Target Acquisition Laboratory

Fort Monmouth, New Jersey

ABSTRACT

The FAMAS described is the newest type equipment that provides accuracies, capabilities, flexibility and features not available in other sounding systems. The FAMAS is being designed for the Army in support of artillery fire. The purpose of the FAMAS is to give the artillery sections the capability of first round hits by providing reliable, fresh (hourly), and comprehensive meteorological data. These data are obtained through the available passive techniques of NAVAID and RDF radiosonde tracking systems. The FAMAS combines both techniques into a small system in which the fully automatic ground receiving, computing, display and transmitting equipment are housed in a S-250 shelter and the RDF antenna/pedestal is on a 3/4 ton trailer. The radiosonde is being designed with the unique capability that will permit pressure levels to be identified during flight and also identified immediately upon the return of interrupted telemetry data. The NAVAID capability includes the use of four different available techniques; LORAN C and D, Navy VLF communications, and OMEGA. Accuracy tests of these NAVAID techniques, using a FPS-16 Radar Set at Wallops Island for comparison, will be presented, as well as accuracy comparisons of various size RDF antenna when low elevation angles were encountered.

1. INTRODUCTION

Atmospheric sounding systems have become important meteorological tools for both the civilian and military communities. The Field Artillery Meteorological Acquisition System (FAMAS) provides accuracies, capabilities, flexibility and features not available in other sounding systems. The FAMAS is being designed for the Army to support artillery fire. The purpose of the FAMAS is to give the artillery sections the capability of first round hits, even in areas obscured from observers, by providing reliable, fresh (hourly), and comprehensive meteorological data. These data are obtained through the passive techniques of NAVAID and Radio Direction Finding (RDF) radiosonde tracking systems. The FAMAS combines both techniques into a small system in which the fully automatic ground receiving, computing, display and transmitting equipment are housed in a S-250 shelter (1-1/4 ton) and the RDF antenna/pedestal is located on a 3/4 ton trailer. The NAVAID capability includes the use of four different NAVAID systems; LORAN C and D, Navy VLF communications, and OMEGA. The system also has the capability of using a mix of OMEGA and VLF signals. The system therefore actually has an option of using any one of six radiosonde positioning techniques.

All meteorological data is fed to a single computer (AN/UYK-19) that converts the data to any one of eleven meteorological messages. Direct communications with the user and with TACFIRE (via a direct TACFIRE interface) makes the system a truly fully automated system. The plasma display, system controlling keyboard, magnetic tape transports for computer programming, paper tape reader for insertion of sonde pressure calibration data, and hard copy printer comprise the data processing and display system. All components of the ADP are also used in other Army systems, which lowers the system's purchase, logistic, training, and maintenance costs. The FAMAS resulting from this development offers a state-of-the-art system capable of satisfying the quick response, ruggedness, and high mobility requirements of the present and future field armies and the accuracies and meteorological message formats necessary to satisfy all users.

2. DESCRIPTION

I will assume the reader is familiar with NAVAIDS and, therefore, it is not necessary to describe this technique, except to say it is based on the time difference of arrival of signals from calibrated transmitters.

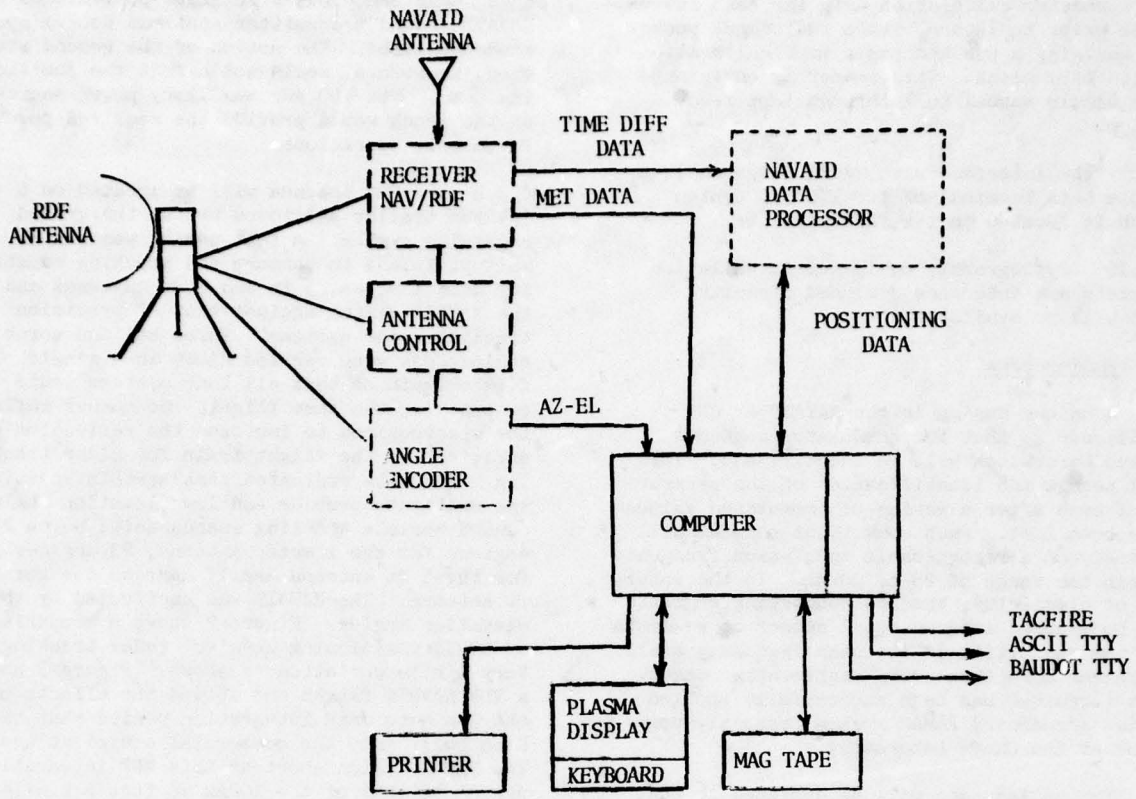

Figure 1. Field Artillery Meteorological Acquisition System

2.1 Figure 1 is a block diagram of the system. The solid lined blocks represent the data processing components, the dotted lined blocks the NAVAID positioning components and the dashed lined blocks the RDF related components. The meteorological data being transmitted from the radiosonde enters either the RDF (1680 MHz) or the NAVAID (403 MHz) antenna.

2.1.1 The common receiver with dual front ends (400 or 1680 MHz) separates the meteorological data from the positioning data and channels the data to the appropriate components. Meteorological data (NAVAID or RDF) is channeled directly to meteorological data unit for conversion and format, and entry into the control processor.

2.1.2 Under NAVAID operations, the NAVAID data (LORAN, VLF or OMEGA) are directed to the appropriate NAVAID data unit where the time differences are converted to X and Y positioning data prior to entering the central processor for storage and meteorological message computations.

2.1.3 Under RDF operations the antenna azimuth and elevation data generated by the antenna tracking assembly are encoded and fed to the antenna data unit for conversion into X and Y data prior to entering the central processor for met message computations.

2.1.4 The central processor stores the significant levels of the meteorological and positioning data. At the command of the operator, the desired message is computed, formatted and transmitted to the user in less than one minute after flight termination. Both Baudot and ASCII codes are available.

2.1.5 The operator instructs and controls the ADP components (Rolm 1602B) (UYK-19) through the keyboard of the Plasma Display Unit (AN/UYQ-10). The operator controls such activities as the positioning technique (NAVAID/RDF) to be used, message format to be generated, when messages are to be transmitted, what NAVAID technique to use, what display data is desired, diagnostics, etc.

2.1.6 A magnetic cassette tape recorder, AN/UYH-1, is used for system programming, for raw flight data storage, and for diagnostic inputs for maintenance.

2.1.7 A line printer (TT-708) is used to log outgoing and incoming messages and raw data if desired for historic purposes after the flight is completed.

2.1.8 The paper tape reader is used to enter the barometer calibration data for each radiosonde prior to launch. Each radiosonde package contains a punched paper tape calibration of its baroswitch. This reader is envisioned as a simple manual pull through tape read device.

2.1.9 The interface with TACFIRE system is a Remote Data Terminal of the TACFIRE system which is located in the FAMAS shelter.

2.1.10 Cryptographic equipment installation brackets and interface designed circuitry also will be available.

2.2 Radiosondes

A unique design in the NAVAID or RDF radiosonde is that the commutator segments of the baroswitch will be identifiable. This will permit the identification of the pressure level even after a series of commutated values have been lost. Each commutator segment will be assigned a recognizable modulation frequency within the range of 25 to 90 Hz. In the interest of simplicity, the 180 conducting segments may be grouped into an equal number of segments but the repetition of the same frequency shall not occur more than every eighteenth contact. This technique has been successfully applied to the breadboard FAMAS system presently operating at the CS&TA Laboratory.

The radiosondes will be designed so that the optional receivers and transmitters can be inserted into a common met sensor radiosonde. The choice of component is dependent on the NAVAID or RDF mode to be used. the NAVAID technique can be used on either 403 or 1680 MHz. The RDF can only operate using the 1680 MHz signal since the RDF requires a tracking antenna for azimuth and elevation angular data.

2.3 Antenna

2.3.1 The NAVAID telemetry antenna (400 MHz) permits the system to be highly flexible. For ranges below 75 KM, which will provide data within the range of most artillery required altitudes (11 Km), a simple omnidirectional dipole is required. For ranges beyond 75 Km, a corner reflector with at least a 45 degree beamwidth is available. The dipole provides the system with the capability of releasing the balloon remote from the ground system. Since the antenna is omnidirectional and will detect radiosonde signal from whatever direction or range the sonde is released, position data will be recorded as soon as detectable signals are available. Remote releases up to 12 Km have been accomplished at Fort Hood, Texas. The omnidirectional antenna and NAVAID technique also raises the possibility of the ground system moving toward a new location while recording flight data. Since the propagation path from the sonde to the ground station is always equal for all sonde generated data, only the sonde's relative position to the NAVAID ground transmitter stations determines sonde position. The motion of the ground station, therefore, would not affect the positioning data. The 100 AMP auxillary power source of the truck would provide the required power for mobile operations.

2.3.2 The RDF antenna will be located on a 3/4 ton trailer and towed behind the ground receiving system. A test series was run at Wallops Island to compare the tracking capability of a 1 meter, 5 ft and 7 ft antennas and the NAVAID system against that of precision tracking radar systems. Three balloon borne radiosondes were carried aloft in a single flight train so that all four systems would be tracking the same flight. No corner reflector was required to increase the reflection coefficient of the flight train for radar tracking. The data indicated that at this location the multipath problem and low elevation angles caused serious tracking inaccuracies below 28 degrees for the 1 meter antenna, 23 degrees for the 5 ft antenna and 17 degrees for the 7 ft antenna. The NAVAID was uneffected by the elevation angles. Figure 2 shows a comparison of LORAN positioning data vs. radar tracking. Very little deviation is shown. Figure 3 shows a VLF NAVAID flight and showed the effects of the 3-minute data integration period that had been built into the commercial equipment used. The FAMAS design shortens this VLF integration period to that of the LORAN so that a similar tracking capability as the LORAN is anticipated.

2.4 Messages

Eleven meteorological messages will be available to the users. Approximately 1 minute after flight termination any one of the eleven can be transmitting or all messages can be transmitted serially. Any message can be made available at any time during the flight without interfering with the data accumulation for the full flight.

2.5 Advantages of a Dual System

Lightweight-small size (S-250 shelter, 1-1/4 T) (RDF-NAVAID)
No ground radiating source (Passive) (NAVAID-RDF)
Minimum personnel (6) (NAVAID-RDF)
Fully Automatic System (NAVAID-RDF)
Omnidirectional antenna (NAVAID)
Remote antenna location (NAVAID)
Remote balloon release (NAVAID)
Multisonde capability (NAVAID)
Ten minute set up time (NAVAID)
No orientation or leveling (NAVAID)
Meteorological data collection while ground system is in motion (NAVAID)
No moving parts (NAVAID)
Redundancy in data collection technique (RDF-NAVAID)

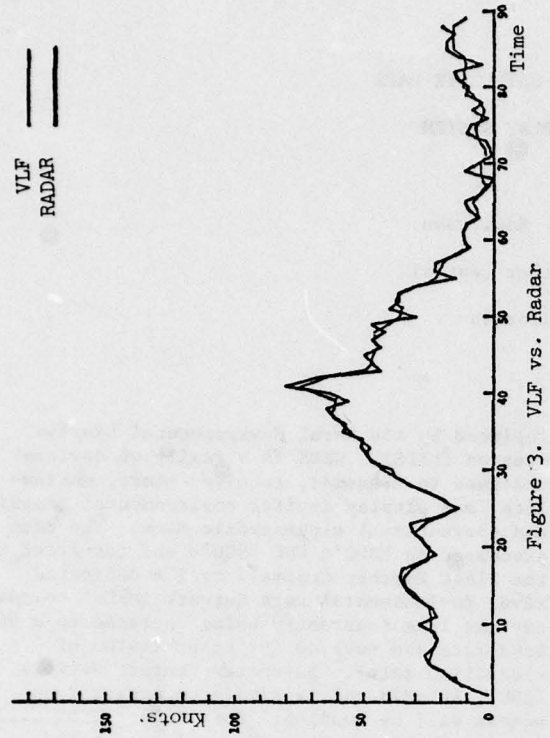

Figure 3. VLF vs. Radar

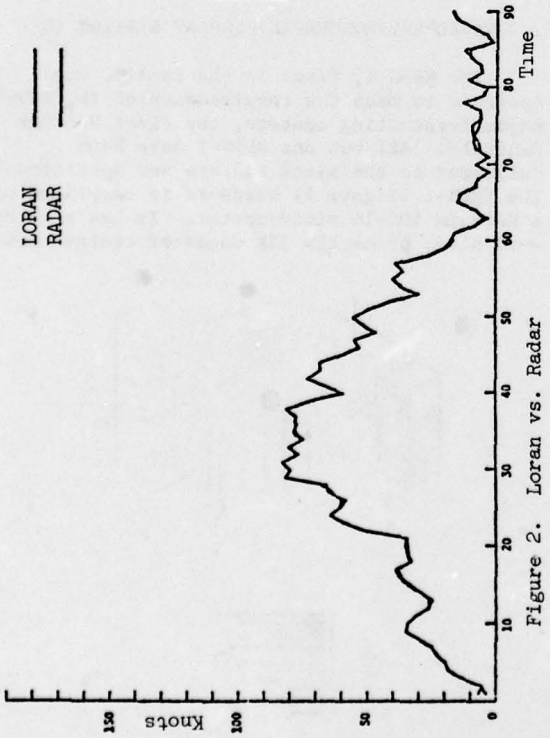

Figure 2. Loran vs. Radar

Autonomous Operation (RDF)
Irrelevance of low elevation tracking angles (NAVAID)

2.6 Conclusions

The FAMAS offers a very flexible tactical type system well suited to provide required meteorological data from the forward area of operations. In the civilian sector, where redundancy of RDF and NAVAID techniques are not required to counter potential enemy jamming efforts, the user may elect to choose either the all NAVAID or all RDF automatic sounding system. The location of the fixed station operation, high wind potential which may cause low elevation angles, cost and maintenance requirements, etc. will all effect the choice of system for a specific application. NAVAID operations are relatively simple; LORAN, VLF and OMEGA transmitted data generally are always available, and are there for the taking. When available the users will have a variety of sounding techniques from which they can choose in order to tailor their operations for specific locations or applications.

2.7 Acknowledgment

I would like to extend my thanks to CWO Ronald Scheirer of the Atmospheric Sciences Laboratory, White Sands Missile Range, for making the presentation of the system on very short notice because of a last minute commitment that prevented my attendence.

A REAL-TIME INTERACTIVE SATELLITE DATA PROCESSING AND DISPLAY SYSTEM

Lieutenant Linda C. Rawlinson

Fleet Numerical Weather Central

Monterey, California

ABSTRACT

A Satellite Quick-look Interactive Display System (SQIDS) device is under development at Fleet Numerical Weather Central (FNWC), Monterey, California. This powerful quality control tool will be used to interactively view processed visual and infrared (IR) Defense Meteorological Satellite Program (DMSP) data on a color monitor and to selectively extract data and modify environmental contours/fields for use in the Primary Environmental Prediction System (PEPS). In order to conserve resources, minimize development time, and maximize compatibility with the Naval Environmental Display Station (NEDS), a NEDS-1 device is being modified to meet the specific requirements of SQIDS. The major difference will be enhanced graphic capabilities by use of the Programmable Graphics Processor (PGP) in place of the Memory Interface Processor (MIP). Data modification by use of the graph pen will permit reanalysis of data fields within PEPS without the manual drudgery currently involved with weather chart bogussing. Utilization of SQIDS will mean improved accuracy in the environmental products provided to the users, thus, increasing their confidence in FNWC products. The result will be increased customer satisfaction which is FNWC's goal.

1. INTRODUCTION

Fleet Numerical Weather Central (FNWC), situated on California's scenic Monterey Peninsula, is the primary U.S. Navy center for computer modeling of the environment. FNWC is tasked with providing on an operational basis oceanographic and meteorological products unique to the Department of the Navy. To meet this requirement, FNWC provides on a continual basis oceanographic and atmospheric numerical analyses and prediction services to the fleet in support of worldwide Naval operations.

Until 1978, FNWC's walls were covered by countless charts, analyses and bathythermographs. But a new age is dawning for the Navy environmentalist. The charts are being replaced by the Naval Environmental Display Station (NEDS). NEDS is a family of devices designed to transmit, receive, store, manipulate, and display digital environmental graphics and conventional alphanumeric data. The data is processed on FNWC's CDC 6500's and forwarded to the Fleet Weather Centrals over a dedicated Naval Environmental Data Network (NEDN) communications line (currently being upgraded to a 9600 baud rate and covered for transmission of classified data). Automated Weather Network (AWN), Autodin and facsimile communications access will be available thru NEDS. NEDS will eventually become the primary forecast and briefing tool in use at all Navy environmental forecast activities.

2. NAVAL ENVIRONMENTAL DISPLAY STATION (NEDS-1)

The NEDS-1, first in the family, was designed to meet the requirements of the Navy's major forecasting centers, the Fleet Weather Centrals. All but one NEDS-1 have been delivered to the sites and are now operational. The NEDS-1 (figure 1) hardware is comprised of a Keronix IDS-16 minicomputer. It has a 16 bit word size, presently 32K words of central memory

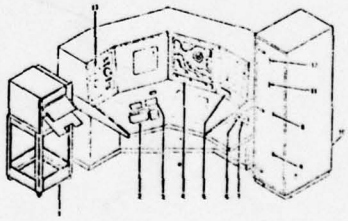

Figure 1: NEDS-1 Device

to be expanded to 64K, and an access time of one microsec. The mass storage device is a Media III top loading removable disk system. It provides a random access storage capability of 320,000,000 bits (An average graphic requires 20K bits/chart) with an access time of 55 milliseconds per 36,000,000 bits transfered. Communications is handled by an Educational Data Systems, EDS-8 multiplexer providing synchronous and asynchronous ports. Other components include: alphanumeric and graphic (color) monitors and keyboards, a Talos graph pen and tablet, and a Versatec electrostatic printer/plotter capable of displaying 8 gray shades. The Keronix has been modified to include a video generator, three refresh memory planes, and a Memory Interface Processor to control graphic display.

A new software operating system with supporting application software is under development for SQIDS which will be implemented in all NEDS-1 units, providing enhancements to the current capabilities. One of the major capabilities is the display of color graphics as dictated by the operator. Graphics may be scrolled (up, down, right, left), zoomed, time sequenced and overlayed. Black and White depictions of color graphics are inadequate to demonstrate the color variations available on a color monitor. The product examples shown are the same as the hardcopy provided from the Versatec printer. Figure 2 demonstrates the overlay features. It shows the surface pressure analysis for 11 Dec 78 overlayed on the station models of western Europe.

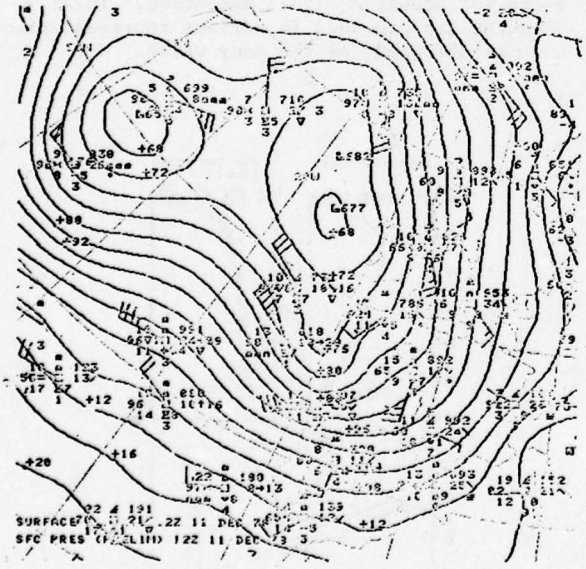

Figure 2: Overlay Example

A variety of environmental products which are provided to the fleet are available on the NEDS-1.

A few of the meteorological products include pressure and wind analyses, the indispensable Skew-T diagram, figure 3, and station models figure 4.

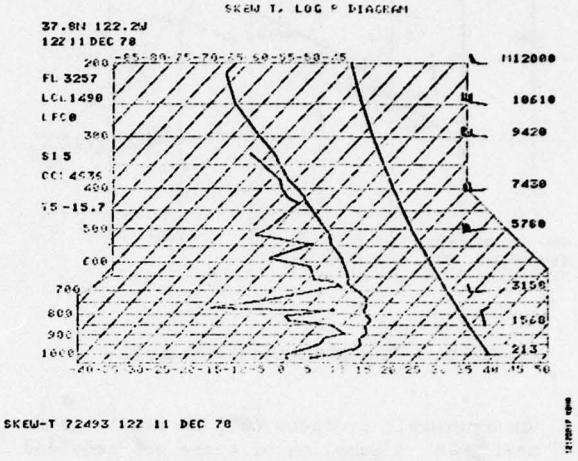

Figure 3: Skew-T Example

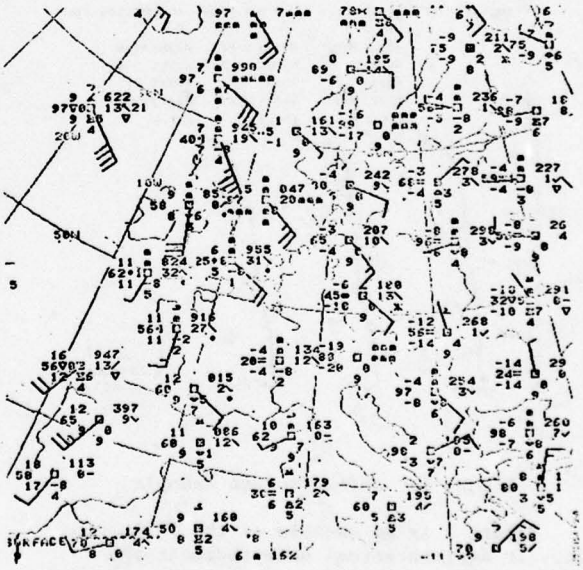

Figure 4: Station Models Example

FNWC has also developed a ship positioning product, figure 5, which shows the projection of a ship's ocean track for a maximum of 4 days. Each days progress is shown as a different color on the monitor.

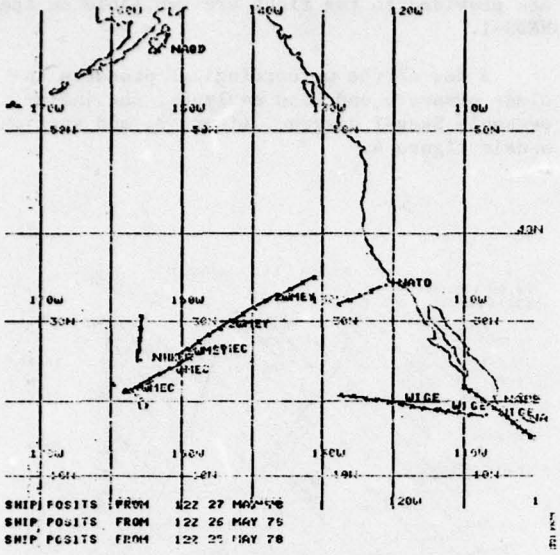

Figure 5: Ship Positioning Example

Oceanographic products will be available on NEDS next year. A sampling of these are provided to demonstrate the versatility of NEDS-1.

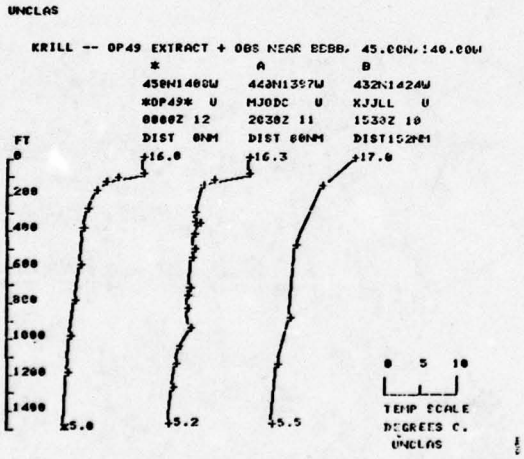

Figure 6: KRILL Product Example

Figure 6 is an example of the KRILL product. It depicts actual bathythermographs (bathys A & B) received as input data to the acoustic model within the last 72 hours, which contributed to the composite synoptic bathy (*) within a 600 nautical mile radius of a user specified postion (BBB, 45.0N 140.0W). The reported bathy's positions, the reporting unit identifier i.e. MJODC, classification i.e. U for unclassified, the time and date the bathy was taken, and the distance in nautical miles from the user specified position are also provided.

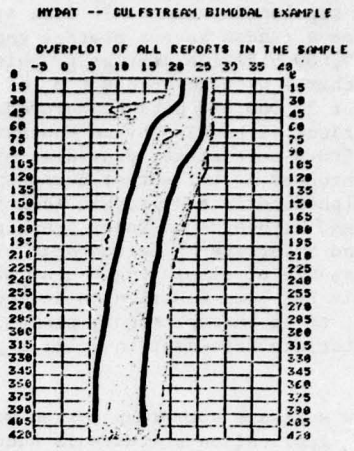

Figure 7: HYDAT Example

HYDAT, figure 7, is a statistical analysis of historical bathy data to deduce a typical profile. This product is particularly useful in the southern hemisphere where bathy collection is limited and in regions such as the Gulf Stream where variations are common. All bathys for a selected region are shown with the typical bathy highlighted in a different color. In this example there are two typical profiles.

The Antisubmarine Warfare (ASW) forces are provided with propagation loss (PROPLOSS) products for acoustic signal detection. These products are provided in various representations to meet the needs of the many users.

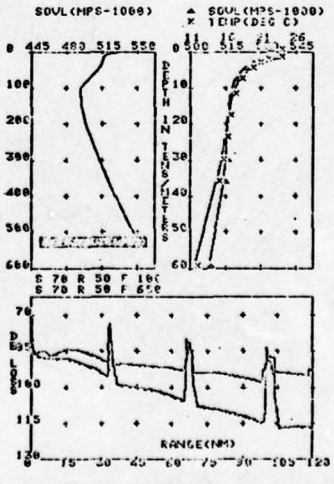

Figure 8: TCPLOT Example

The TCPLOT product, figure 8, is temperature and sound velocity profiles with PROPLOSS. It consists of three plots: the upper right displays the sound velocity, indicated by s, and bathy, indicated by the Xs, for the first 600 meters; the upper left shows the sound velocity profile to the bottom, shown at approximately 5000 meters; and the lower plot depicts the decibel, dB, loss verses range in nautical miles for a source signal at 70 feet and a receiver at 50 feet for various frequencies. This is a high resolution PROPLOSS.

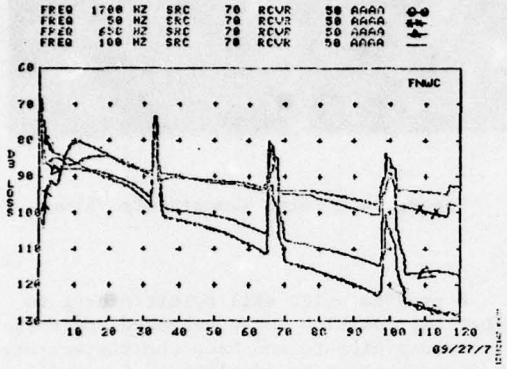

Figure 9: PRAP Example

A low resolution PROPLOSS, figure 9, the passive acoustic sensor range prediction product known as PRAP, consists of just the dB verses range PROPLOSS curves for low frequency sensors. A maximum of four frequencies may be displayed at one time. The TCPLOT and PRAP products are based on FNWC's acoustic model which assumes horizontal topography.

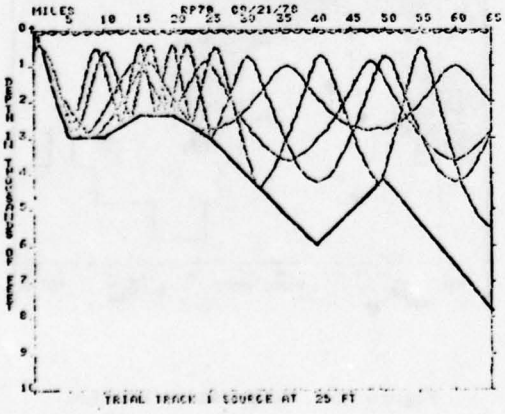

Figure 10: Variable Topography Example

Another product, Bottom Value (BOTVAL) provides for a variable bottom topography along a specific track which is combined with the RAY-TRACE product which depicts the path of sound rays in relation to depth and range. Figure 10 shows these products for a signal source at 25 feet.

3. SQIDS

The Satellite Quick Look Interactive Display System consists of software programs resident on FNWC's Satellite Processing Computer (SPC), a Control Data Corporation Cyber 175, and a modified NEDS-1 known affectionately at FNWC as SID. This device will provide a powerful quality control tool to:

Interactively view processed visual and infrared Defense Meteorological Satellite Program (DMSP) data on a color monitor

and

Selectively extract data and modify environmental contours/fields for use in the Primary Environmental Prediction System (PEPS).

A modified NEDS-1 was chosen as the SQIDS device in order to maximize compatibility with NEDS and to reduce the cost and development time.

The major hardware differences between SID and a NEDS-1 are a hard copy device (to be determined) which generates 16 gray shades and the Programmable Graphic Processor (PGP) to replace the Memory Interface Processor of the NEDS-1. The PGP permits the display of 64 color variations and incorporates the scroll and zoom software features of the NEDS-1 into its hardware.

The major software differences will be in the application packages. SQIDS will have enhanced satellite data display and manipulation capabilities. The following capabilities, currently available on the Satellite Processing and Display Station (SPADS) are projected to be available on SQIDS next year.

A satellite orbit tracking program which indicates the orbits of the various satellites allows viewing of a user defined region with the calibrated positions on the track indicated.

Figure 11: Orbit Tracking Example

IR Visual

Results

Figure 12: Threshold Example

A temperature enhancement program which color codes various temperature ranges as indicated by the user to enhance the temperature variations of visual data.

Figure 13: Enhanced Sea Surface Temperature

A threshold program to determine clear ocean areas for sea surface temperature extraction by comparing infrared and visual data.

Figure 14: Point Temperature Values

A program which will permit a user to select any position on an enhanced sea surface temperature picture and have the temperature for that position be displayed. Also will permit the display of a temperature profile between two user selected points.

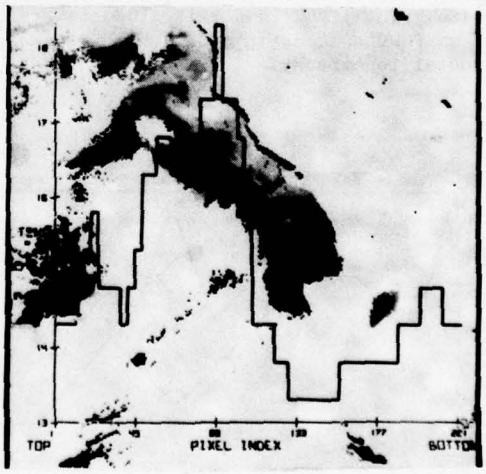

Figure 15: Temperature Profile

A program designed to overlay contour data such as sea surface temperatuers on satellite imagery. Will also provide gridding of backgrounds features on satellite imagery.

SQIDS will also provide a re-analysis capability of environmental fields/contours for PEPS input by use of the graph pen. The modification will include any vertical changes required as input to PEPS to insure the vertical consistency of the analysis is maintained.

4. Conclusion

The NEDS-1 device is only the first in a family of devices, each one being configured to meet the requirements of its individual sites mission. Development of the NEDS-1A/1R devices is nearing completion. These devices will be located typically at shorebased Naval and Marine Corps environmental activities. Cost on 1A is estimated at 50K and varies for the 1R depending on options, approx $30K average. A shipboard version, NEDS-2 is in the design stage at FNWC.

When completed, SQIDS and the NEDS family of devices will provide enhanced environmental products to the field of greater usefulness and faster than is currently possible. Greater satisfaction and utilization of these products is expected by FNWC customers. FNWC's goal is to provide accurate, timely, and useful environmental products tailored to the needs of the customer. With the coming of SQIDS and NEDS, this goal is in reach.

A MODEL FOR PRODUCING CLIMATOLOGICAL AND REAL-TIME PREDICTIONS OF CLEAR LINE-OF-SIGHT FOR TV PRECISION GUIDED MUNITIONS

Majors Lawrence D. Mendenhall* and John D. Mill,

Capt Donald F. Woolley, Dr Patrick J. Breitling, and Major Paul H. Neu

USAF Environmental Technical Applications Center

Scott Air Force Base, Illinois

ABSTRACT

A model has been developed at the USAFETAC to estimate the probability of a clear line-of-sight for TV precision guided munitions (PGM), using the USAF Environmental Technical Applications Center (USAFETAC) climatological data base or the Air Force Global Weather Central (AFGWC) operational data base. The model consists of a contrast transmission module based on the RAND WETTA (Huschke) technique, a cloud-free line-of-sight (CFLOS) module using the Lund-Shanklin tables, an illuminance module, and a sun angle module. The user specifies latitude, longitude, date/time, background albedo, surface visibility and mixing depth. The output consists of two range vs height cross sections. The first gives the contrast transmittance at specified altitudes and dive angles. The second cross section gives the probability of a CFLOS for the same geometry. From these, the user can infer maximum lock-on range for a given scenario, knowing inherent target to background contrast and sensor threshold.

1. INTRODUCTION

Over the last decade, several variations of a new type of tactical weapon have been introduced into the DOD inventory. They use some form of electro-optical (E-O) terminal guidance for increased accuracy, and are known generically as precision guided munitions (PGM). Several of these PGMs and some associated target acquisition systems operate in the visible portion of the spectrum, using small TV cameras and associated logic to lock on to a target. Examples of these passive, visibile systems include the TV maverick (AGM-65A/B) and the GBU-15 glide bomb. Like all other weapon systems, they have certain critical environmental sensitivities which limit their effectiveness. The light level (illuminance) in the target area must exceed the sensor threshold. In addition, the line of sight to the target must be unobstructed by terrain or clouds. Finally, the contrast between the target and the background, as seen by the sensor, must exceed a given threshold. There are other limitations to employment of these weapons unrelated to environmental contraints, but they will not be considered here.

Forecasts of these limiting environmental factors are needed for upload and employment decisions, while climatological estimates of weapon effectiveness are very useful for production and stockpiling decisions. A computer model, the TV Maverick clear line-of-sight (CLOS) model, has been developed at the USAF Environmental Technical Applications Center (USAFETAC) to produce these estimates.

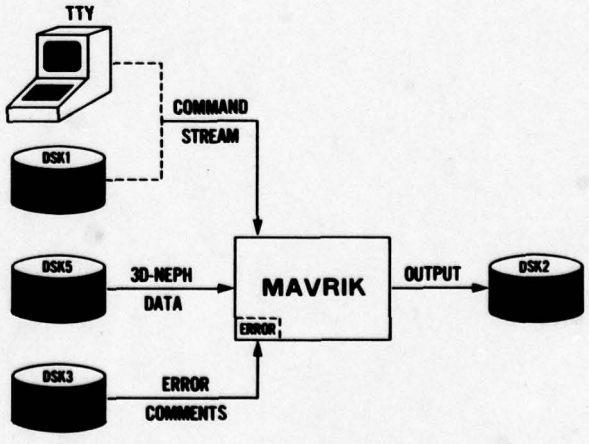

Figure 1. Basic File structure for the CLOS model.

*Now with the 2nd Weather Wing, Kapaun AS, Germany

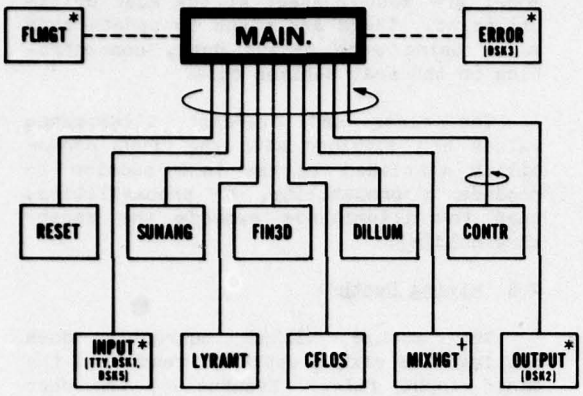

Figure 2. CLOS model basic program structure, showing the major modules. Those with an asterisk (*) are system dependent. The mixing height module (+) is presently stubbed and reads from TTY or DSK1.

2. OVERALL MODEL STRUCTURE

The CLOS model is written in a highly modular, structured manner to facilitate design and testing, to ensure maximum transportability and to ensure that updates of major modules will have minimum impact on the rest of the model. The required files and their relationships are shown in figure 1. The top level structure is shown in figure 2. The system dependent modules are FILMGT (file management) and INPUT; and, to a lesser extent, ERROR (the error handler), OUTPUT, and READ3D (submodule of INPUT which reads 3-D Nephanalysis[8] data).

Two modules are presently incomplete. GE03D, part of INPUT, when in production mode will read a data base of average surface elevations for the 3-D Neph grid points. For testing purposes, it reads from the basic input file. MIXHGT, which will calculate the mixing depth, also reads from the basic input file. In the production mode at AFGWC it will interface with their boundary layer model.

RESET zeros selected memory locations in preparation for subsequent cases. The remaining major modules will be discussed below.

3. REQUIRED INPUTS

There are two types of inputs, those supplied by the user and those extracted from existing data bases at the AFGWC and the USAFETAC.

The basic inputs supplied by the user are latitude and longitude of the target, the date and time for which a prediction is required and the sensor type (or illuminance threshold). Additional inputs which may be required from the user are the background (surface) albedo and the maximum range for which results are desired. In the operational mode, the albedo may be taken from a data base and the maximum range set to a standard value.

In the operational mode, the basic meteorological variables will be taken from existing data bases. The cloud depiction will come from the 3-D Neph data base or, in the forecast mode at AFGWC, the High Resolution Cloud Prognosis (HRCP). The visibility in the mixing layer will come from surface observations or forecasts. The depth of the mixing layer is currently read from the basic input file, but future updates will allow the user to choose one of several sources. These will include heights based on stability criteria calculated from either surface or upper air data, or predicted by the AFGWC boundary layer model (BLM).

4. MODEL CALCULATIONS

4.1 Solar Elevation and Azimuth Angles

The SUNANG module accepts the latitude, longitude and Greenwich Mean (ZULU) time and returns the solar elevation and azimuth angles, uncorrected for refraction. This module was adapted from a program developed by Goldsmith (1977) of USAFETAC, based on the work of Citrynell (1976). Semi-empirical equations are used to calculate the solar declination and Greenwich hour angle. The solar elevation and azimuth angles are then calculated using spherical geometry. Accuracy is said to be (Goldsmith, 1977) 0.1 degree when compared to the nautical almanac.

4.2 Cloud Layers and Cloud Types

The module LYRAMT resolves the fifteen 3-D Neph layers into low, middle and high clouds, using the conventions of the 3-D Neph data base (Feddes, 1974), and the ADDCLD routine developed by Major Ingle of USAFETAC. It returns low, middle and high cloud amounts to the nearest five percent.

FIN3D accepts these results, and the low, middle and high cloud type codes and present weather code available in the 3-D Neph data base. It checks for consistency between cloud amounts and types in the three layers and determines a single dominant cloud type using an empirical algorithm. This dominant cloud type is required by the DILLUM module.

The empirical procedure is based on meteorological judgement and resolves conflicts in favor of "darker" clouds (less illuminance). In order of increasing

[8]The 3-D Nephanalysis (3-D Neph) data base is described in Feddes (1974) and Fye (1978).

illuminance, the types are stratus, nimbostratus, stratocumulus, altostratus, altocumulus, cirostratus and cirrus. These are grouped by low, middle, high categories except for nimbostratus/stratocumulus. This conflict, and the convention of calling certain precipitating low clouds nimbostratus, leads to a requirement to treat a combination of low and middle clouds in a slightly different way from other combinations.

Single layers are resolved using the above order. For multiple layers, if one amount is greater than the rest by a fixed percentage (currently 20%), it is considered the dominant layer. If this condition is not met, the precedence low, middle, high is used unless there are both low and middle clouds. In that case, nimbostratus takes precedence over stratocumulus.

4.3 Cloud-Free Line-of-Sight

The CFLOS module accepts a maximum elevation angle and an angle increment (5 or 10 degrees) and returns a matrix of static cloud-free line-of-sight (CFLOS) probabilities for thirteen standard levels corresponding, essentially, to the 3-D Neph data levels. The 3-D Neph data are summarized from the surface to each level by the ADDCLD routine. The resultant cloud cover values, and the set of elevation angles, point to a table of the universal CFLOS probabilities of Lund and Shanklin (1973). This module also accepts the solar elevation angle and determines the probability that the target will be sunlit. This probability is used later by the illuminance module.

4.4 Illuminance

The inputs to the illuminance module DILLUM are solar elevation angle, dominant cloud type, and up to ten sensor illuminance thresholds. The clear sky illuminance on a horizontal surface is determined by a table look-up of data extracted from the work of Brown (1952). Illuminance for overcast skies (E) is calculated from the equation of Haurwitz (1948):

$$E=E_o \frac{a}{94.4} \exp\left[-(b-0.059)m\right]$$

Where E_o is the clear sky illuminance in foot candles, a and b are empirically derived constants which depend on cloud type, and m is the airmass.

Haurwitz determined the constants a and b from a data set which included few observations at solar elevation angles less than about 15 degrees. Unfortunately, typical sensor thresholds correspond to elevation angles near zero. Consequently, the corrections for overcast skies in this model are most suspect at the most critical point. There are plans to update this model using more recent data, concentrating on the near horizon case.

The clear and overcast illuminance values are combined with the CFLOS probability mentioned in the last section to produce a probability, or probabilities, that the illuminance exceeds the sensor threshold(s).

4.5 Mixing Depth

The module MIXHGT currently does nothing; the mixing depth is read from the basic input file. Eventually, the user will be given a choice of algorithms for calculating the mixing height. At the USAFETAC, the choices will include: a method based on the work of Holzworth (1972), using radiosonde data; and a scheme developed at the USAFETAC which uses surface observations. The latter calculates the thermal turbulence and the mechanical turbulence and takes an average of the two weighed by a function of the Pasquill stability class. At the AFGWC, the mixing depth will normally be taken from their boundary layer model.

4.6 Contrast Transmittance

The third major environmental factor affecting weapon performance, loss of contrast due to scattering by aerosols, is estimated in the module CONTR. The technique used is essentially that of Huschke (1976). The method is described in a companion paper (Breitling, 1978) and will not be repeated here. Although the WETTA model, as it is called, shows some discrepancies compared with a monte-carlo model, it gives reasonably good results. Also, it is much faster than other available models. Since the three most important model inputs (visibility, cloud cover and mixing depth) are difficult to forecast, or even to observe in most cases, it was felt that the WETTA model introduces less error than do the input data. Consequently, the WETTA model was chosen in the interest of efficiency.

5. MODEL OUTPUT

The model output consists of three pages per case. The first page repeats the input data in both metric and English units, summarizes the cloud data, and prints the illuminance probabilities. In addition, if there have been any errors during execution, the 3-D Neph data are dumped, the appropriate error comments are printed, and the CFLOS and CONTR output is dumped in tabular form on a separate (extra) page.

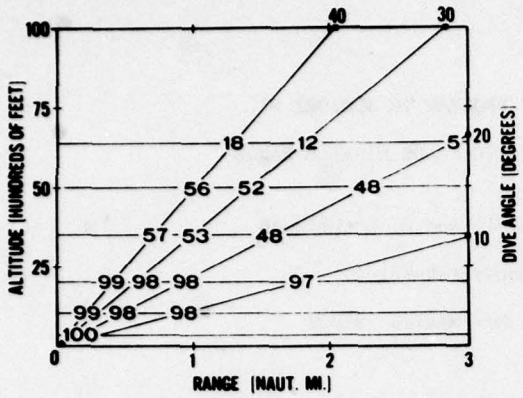

Figure 3. A schematic of the range vs height cross section on which the CFLOS and contrast transmittance values are plotted. The interior horizontal and oblique lines are not on the actual printer plot, but are included here for clarity.

The second page is a printer plot of a range/height cross section of CFLOS values. Reduction problems preclude showing this graph here, but figure 3 shows an abbreviated schematic of this plot. The third page is a printer plot, in the same format, of the contrast transmittance values. These general results can be tailored by the user (normally a staff weather officer) to a particular mission, given the inherent target to background contrast and the contrast threshold of the sensor.

For an inherent contrast of C_o and a threshold contrast of C_t, the maximum lock on range (due only to environmental factors) is the locus of points where the contrast transmittance is equal to the critical value $T_c=C_t/C_o$. Isopleth(s) of critical T_c may be drawn and transferred to the CFLOS graph. The clear line-of-sight (CLOS) probability for a given scenario is equal to the CFLOS probability within the maximum lock on range. It is zero elsewhere.

6. SUMMARY

The model described here will provide the capability to produce assessments of the environmental factors affecting the performance of sensors which operate in the visible portion of the spectrum. It can predict these factors using forecasts of clouds, visibility and mixing depth provided by the AFGWC forecast models. It can also assess the frequency of occurrence of these factors using the historical data base of the USAFETAC. With minor modification, it could assess the influence of the environment on the probability of mission success for classes of missions.

The model will be implemented at AFGWC in the near future for test and evaluation. The decision to declare it operational at either the AFGWC or the USAFETAC awaits the results of that evaluation and the necessary resources.

7. *REFERENCES*

Breitling, P.J., 1978: A Comparison of the AFGL FLASH, Draper DART, and AWS Haze Models with the RAND WETTA Model for Calculating Atmospheric Contrast Reduction. Paper elsewhere in this volume.

Brown, D.R.E., 1952: Natural Illumination Charts, Navy Dept., Bureau of Ships, Wash., D.C.

Citrynell, H.; 1976: Planetary Motion Calculation Method. Indian J. Meteorol. Hydrol. Geophys., 27, 185-186.

Feddes, R.G., 1974: Development of a Gridded Data Base, USAFETAC TN 74-2, Scott AFB, IL, April 1974.

Fye, F.K., 1978: The AFGWC Automated Cloud Analysis Model, AFGWC TM 78-002, HQ AFGWC, Offutt AFB NE, June 1978.

Goldsmith, R.A., 1977: Computation of Solar Declination, the Solar Azimuth Angle, and the Equation of Time, USAFETAC TN 77-5, Scott AFB IL, Sep 1977.

Haurwitz, B., 1948: Insolation in Relation to Cloud Type. J. Meteorol., 5, 110-113.

Holzworth, G.C., 1972: Mixing Heights, Wind Speeds, and Potential for Urban Air Pollution Throughout the Contiguous United States, EPA, Office of Air Programs, Research Triangle Park, NC, Jan 1972.

Huschke, R.E., 1976: Atmospheric Visual and Infrared Transmission Deduced from Surface Weather Observations: Weather and Warplanes VI, Report R-2016-PR, RAND Corp., Santa Monica CA, Oct 1976.

Lund, I.A., and M.D. Shanklin, 1973: Universal Methods for Estimating Probabilities of CFLOS Through the Atmosphere. J. Appl. Meteorol., 12, 28-35.

MICROMETEOROLOGICAL MEASUREMENT PROGRAM IN SUPPORT OF HIGH ENERGY LASER FACILITIES AT WHITE SANDS MISSILE RANGE

G. Hoidale, E. Fawbush, K. Kunkel, and D. McCullough

US Army Atmospheric Sciences Laboratory

White Sands Missile Range, New Mexico 88002

ABSTRACT

Department of Defense High Energy Laser facilities are being established at White Sands Missile Range, New Mexico. In support of these facilities, the Atmospheric Sciences Laboratory is responsible for data base measurements and the interpretation of these measurements.

The data base measurement program covers optical turbulence, crosswind, gases and particulates and was initially keyed to converge on diurnal and seasonal variability of these atmospheric elements so as to establish "operational windows." The optimum window was provisionally determined to be late afternoon and early evening in the spring. Serving to molify this window is the decoupling of the boundary layer from the free atmosphere. This decoupling may result in the development of local air masses. It has been found that passage of these small-scale systems often results in intense short-term (ca. 15-20 min) perturbations in the optical turbulence, wind, and temperature fields.

1. INTRODUCTION

The Department of Defense High Energy Laser System Test Facility (HELSTF) is being established at White Sands Missile Range (WSMR), New Mexico. In support of the HELSTF the US Army Atmospheric Sciences Laboratory (ASL) is responsible for the development and interpretation of a data base of atmospheric conditions. The data base in turn is used to identify atmospheric operational windows and to develop forecasting techniques applicable over time scales ranging from hours to seconds.

In an operational mode the overall beam quality of the HEL systems will be degraded by the atmosphere. This degradation consists of linear and nonlinear effects. The main linear effects are due to optical turbulence and molecular and aerosol extinction. Optical turbulence is a random process whereby small-scale fluctuations of density change the index of refraction, thereby rendering the atmosphere nonhomogeneous and nonisotropic and resulting in scintillation, spot dancing, beam bending and consequently beam spreading. Absorption and scattering of photons by gases and by liquid and solid particles also contribute in a linear fashion.

Among the nonlinear effects is thermal blooming. Thermal blooming results from absorption of energy in the laser beam by the medium (gas, liquid, solid). The absorption raises the temperature of the absorbing medium and hence lowers its density. Part of the energy is refracted out of the original beam path, thus reducing the beam quality. Since thermal blooming depends on the heat absorbed in the atmosphere, the magnitude of the effect is inversely proportional to the motion of the medium across the beam, i.e., the so-called crosswind.

At the Seventh Technical Exchange Conference in El Paso, Texas, Watkins et al. (1976) discussed the measurements required for prediction of high energy laser transmission through the atmosphere and presented some preliminary data applicable to the HELSTF. More extensive data on the propagation conditions at WSMR were documented by Norton et al. (1978) and presented by Walters (1976), Hoidale et al. (1976), Norton and Walters (1977), and Pinnick et al. (1977).

The primary purposes of this paper are: (1) to present selected aspects of the data base measurements of optical turbulence, crosswind, gases, and particulates at the HELSTF with respect to operational windows and (2) to outline the operational meteorological support system which evolved out of the data base measurements.

2. HELSTF

The HELSTF area is located near the southwestern corner of the White Sands National Monument on the WSMR in the Tularosa Basin of south-central New Mexico. Although the HELSTF is situated on nearly level semidesert terrain, marked atmosphere variability may be induced by proximity to: (1) the San Andres Mountains to the west, (2) the high albedo gypsum sands of the White Sands National Monument to the north, and (3) the occasionally water-filled Lake Lucero to the northwest.

The facility itself is in the design stage. Completion of the design is scheduled for December 1978. Construction is targeted to commence in May 1979, with completion of the facility scheduled for March 1982.

With respect to meteorological support at the HELSTF, the ASL program is divided into three phases. The ongoing Phase I began in 1976 and is focussed on establishment of a data base of natural atmospheric conditions at the HELSTF. These atmospheric conditions include optical turbulence, crosswind, gas concentrations, and particulate extinction coefficient. Phase II is keyed to examination of the effect of the facility itself on atmospheric conditions (mainly optical turbulence and wind) in the vicinity of the HEL pointer/tracker(s). During Phase III, direct support for testing of HEL will be provided.

3. MEASUREMENT PROGRAM

The near-surface data base for the natural background at the HELSTF encompasses optical turbulence, crosswind, gases, and particulates. The instrumentation used to provide the measurements is summarized in Table 1 together with an indication of whether the measurement is point or integrated path.

TABLE 1. ATMOSPHERIC MEASUREMENTS AT THE HELSTF

Element	Unit	Point (P) Integrated Path (I)
Optical Turbulence	Spatial Temperature Probe (In House)	P
	Scintillometer	I (hor)
	Acoustic Sounder	I (ver)
Wind Velocity	R. M. Young U-V-W	P
	AN/GMQ-11 or WS-101	P
Gases (Concentration)		
H_2O	General Eastern Dewpoint 1200 AP	P
O_3	Dasibi 1003 AH	P
THC/Methane	Horiba FIA-21	P
N_2O	Miran II	P
CO_2	Horiba AIA-23	P
Particulates		
Size Distribution	Particle Measuring Systems	P
Mass Concentration	GCA Mass Monitor	P
Scattering Coefficient	Meteorology Research Inc. Scattering Nephelometer	P
Gases and/or Particulate (Absorption Coefficient)		
CO_2 & DF laser spectrophone	In House	P

Measurements of optical turbulence and crosswind are made at the 9-m and 34-m tower levels at the Laser Systems Test Center (LSTC) and Apache Site (Fig. 1) located 5.5 km west of the LSTC. Gases are monitored at the 4-m level at the LSTC and particulates at the 5-m level at the Arky Site (2.2 km northwest of the LSTC). The turbulence, wind, and gas data are sampled at a frequency of 1 Hz. These values are arithmetically averaged over 10 sec and the 10 sec averages recorded on magnetic tape. Subsequently the 10 sec samples are arithmetically averaged over 15 min. Measurements of particulate size distribution are cumulative over periods of 10 to 15 min.

To probe heights above the reach of the towers and acoustic sounder, the ASL has enlisted the support of the Wave Propagation Laboratory, Environmental Research Laboratories, NOAA, and Airborne Research Associates for aircraft measurements of optical turbulence and water vapor and of the University of Wyoming for balloon measurements of particulate size distribution.

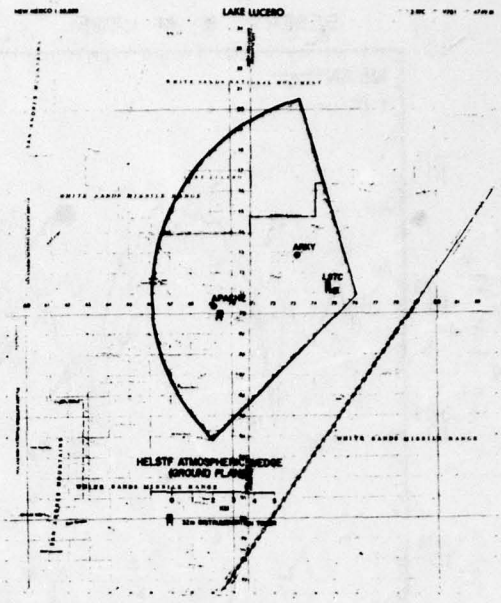

Figure 1. Surface-based atmospheric data base measurement sites, High Energy Laser Systems Test Facility, White Sands Missile Range, New Mexico.

The ASL data were generally acquired over periods of 48 to 72 consecutive hours on a once per month basis.

4. OPERATIONAL WINDOWS

The optimum atmospheric window for operational testing of HEL at the HELSTF would have minimum optical turbulence, minimum extinction coefficient (gas and particulate), and maximum crosswind. In general at the HELSTF, optical turbulence is at a minimum around sunrise and sunset and shows little seasonal dependence. Water vapor, the main gaseous absorber, is at a minimum in the afternoon but is strongly seasonally dependent with minimum values usually associated with winter and spring. Particulate effects are strongest in spring and weakest in fall and winter. The crosswind is strongest in spring and weakest in the summer.

Based on a limited data base, the optimum operational window for HEL firings at the HELSTF was provisionally accepted to be late in the afternoon in spring. Late in the afternoon would enable the users of the facility to take advantage of the minimum in optical turbulence (Fig. 2) and minimum in water vapor (Fig 3) which usually occur at that time. Spring would afford the advantage of the prevailing moderate-to-strong southwesterly flow which, for a northwest-southeast oriented firing line, would serve to mitigate the effects of thermal blooming.

However, strong southwesterly flow over WSMR in spring is often associated with blowing dust or dust storms, conditions which could increase the extinction coefficient to an unacceptable level. An example of the particulate extinction

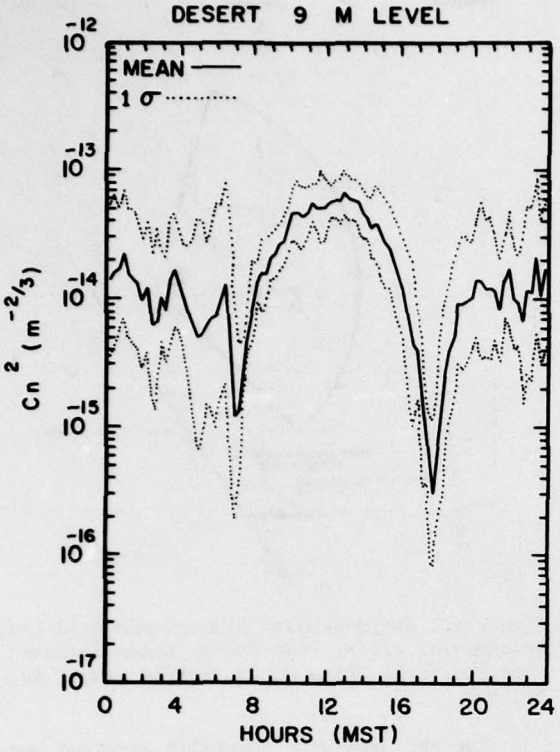

Figure 2. Diurnal variation of the mean and 1 σ of the refractive index structure parameter at the 9-m tower level at the LSTC, 24 March to 8 April 1977, White Sands Missile Range, New Mexico.

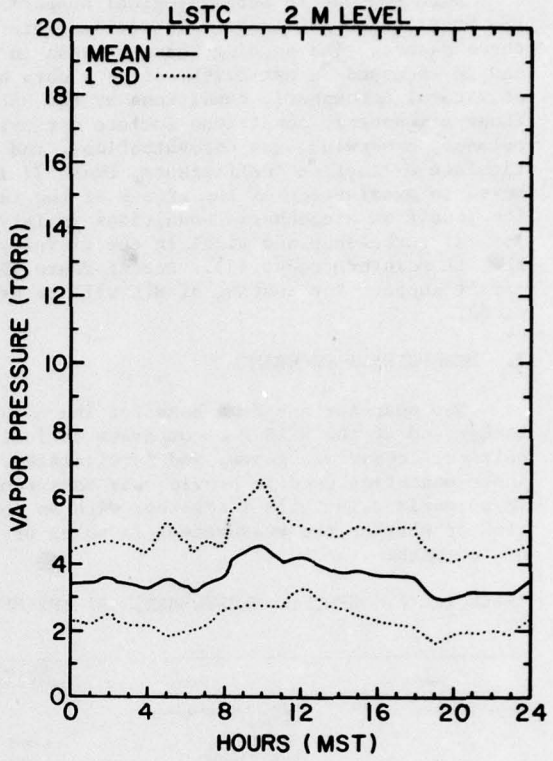

Figure 3. Diurnal variation of the mean and 1 σ of the water vapor pressure, LSTC, 24 March to 8 April 1977, White Sands Missile Range, New Mexico.

actually exceeding the gaseous (H_2O, CO_2, N_2O, CO, CH_4) absorption in the extinction of the $P_2(10)$ line of a DF laser is shown in Fig. 4. The horizontal dashed lines represent the extremes of gaseous extinction for the absolute range of vapor pressure observed at WSMR, the horizontal solid lines the mean dry season and wet season range, and the intermediate line which ends about 1800 MST the track of gaseous extinction for that particular day. An analysis of 300 hours of particulate data taken in the spring of 1977 revealed that during only 3 percent of the time was the particulate extinction significant, i.e., over 0.1 km^{-1}.

Another factor relative to the late afternoon and evening period at the HELSTF is the formation and subsequent movement of air masses of subsynoptic, i.e., local, scale. The formation of these so-called transitory air masses is related to a decoupling of the surface layer from the synoptic-scale atmospheric pressure gradients which generally dominate the surface wind patterns during the daylight hours and occasionally at night if the gradients are sufficiently intense.

The transitory air masses appear to form over the surrounding mountain slopes to the west; the high albedo White Sands National Monument to the north; the generally dry, but high water table Lake Lucero to the northwest; and over the HELSTF area itself. The air

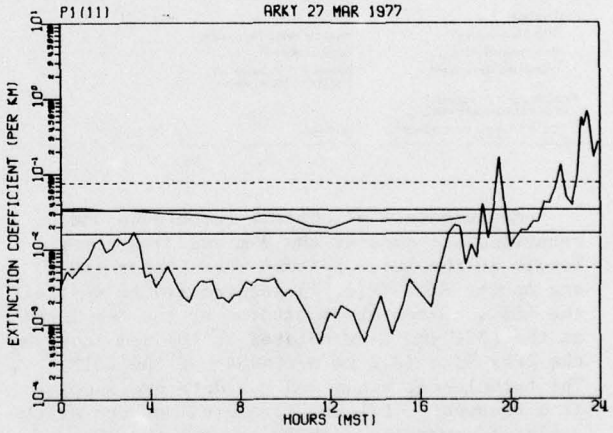

Figure 4. Comparison of particulate (sharply irregular curve) and gaseous (slightly irregular curve) extinction for the $P_2(10)$ DF laser line, Arky Site, 27 March 1977. Horizontal lines represent gaseous extinction based on absolute extreme water vapor conditions (---) and mean dry and wet season water vapor conditions (——) as observed at White Sands Missile Range, New Mexico.

masses assume properties characteristic of the source region and begin to shift after the decoupling. Passage of a transitory air mass at the HELSTF is accompanied by changes in wind

speed, wind direction, temperature, and occasionally by marked changes in optical turbulence. Figure 5 shows an artist's concept of the transitory air masses.

5. OPERATIONAL METEOROLOGICAL SUPPORT SYSTEM

The meteorological support system depicted in Fig. 6 was conceived as a result of the data base measurements at the HELSTF. Measurements will be made at fixed sites (firm power) along the centerline of the HEL firing corridor and from a network of mobile sites (battery/solar power). The former measurements will be made at four locations: (1) 0 km Test Cell Complex, (2) 500-m Receiver/Target Site, (3) 1 km site, and (4) 2 km site. A 16-m bulwark sensor platform and a 32-m tower will be located at the 0 km Test Cell Complex. A gas/aerosol van and a 32-m tower are to be located at the 500-m Receiver/Target Site. A single 32-m tower will be located at each of the 1 km and 2 km sites. Measurements from the surrounding area will be made from six portable 16-m towers. Data stations at each of the 12 sites will electronically transfer information to the High Energy Laser Meteorological Data Analysis System (HEL-MDAS) in the LSTC. The HEL-MDAS handles the final data managing, archiving, and modeling. The system is to provide operational support by 1982.

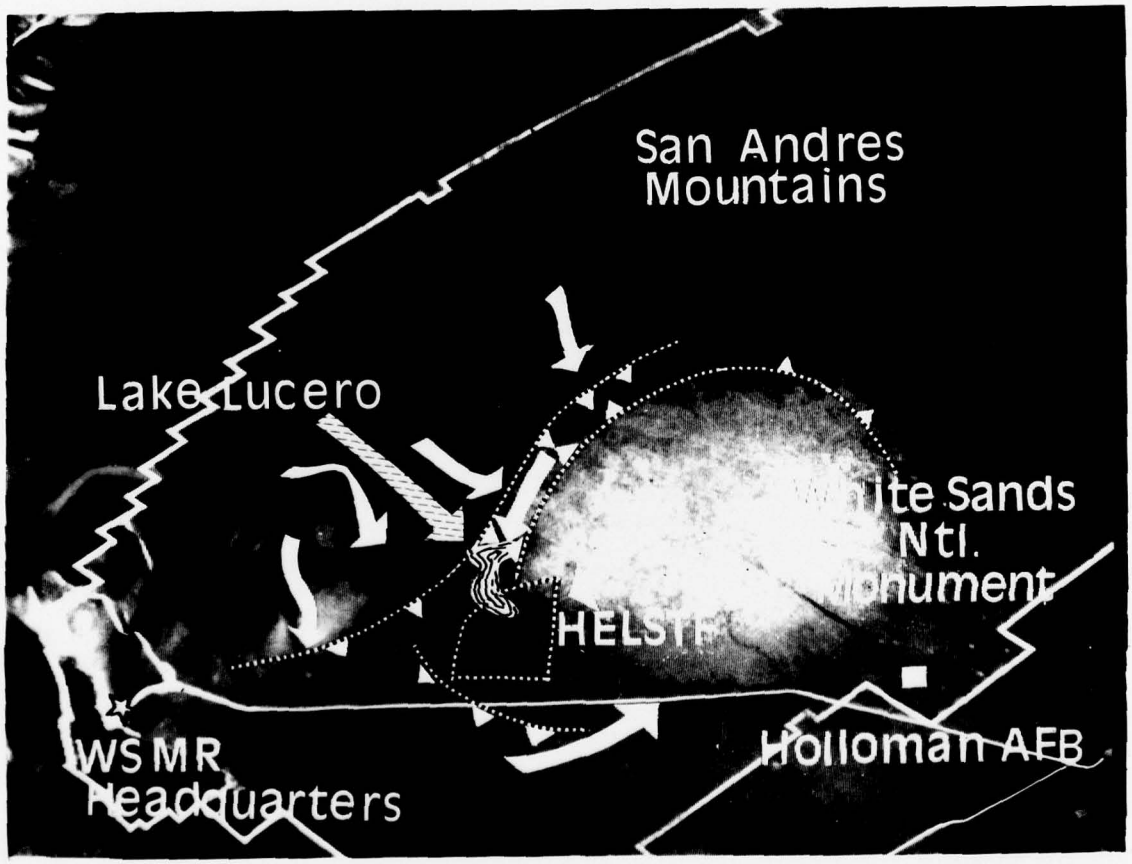

Figure 5. Artist's concept of the movement of transitory air masses at the High Energy Laser System Test Facility, White Sands Missile Range, New Mexico.

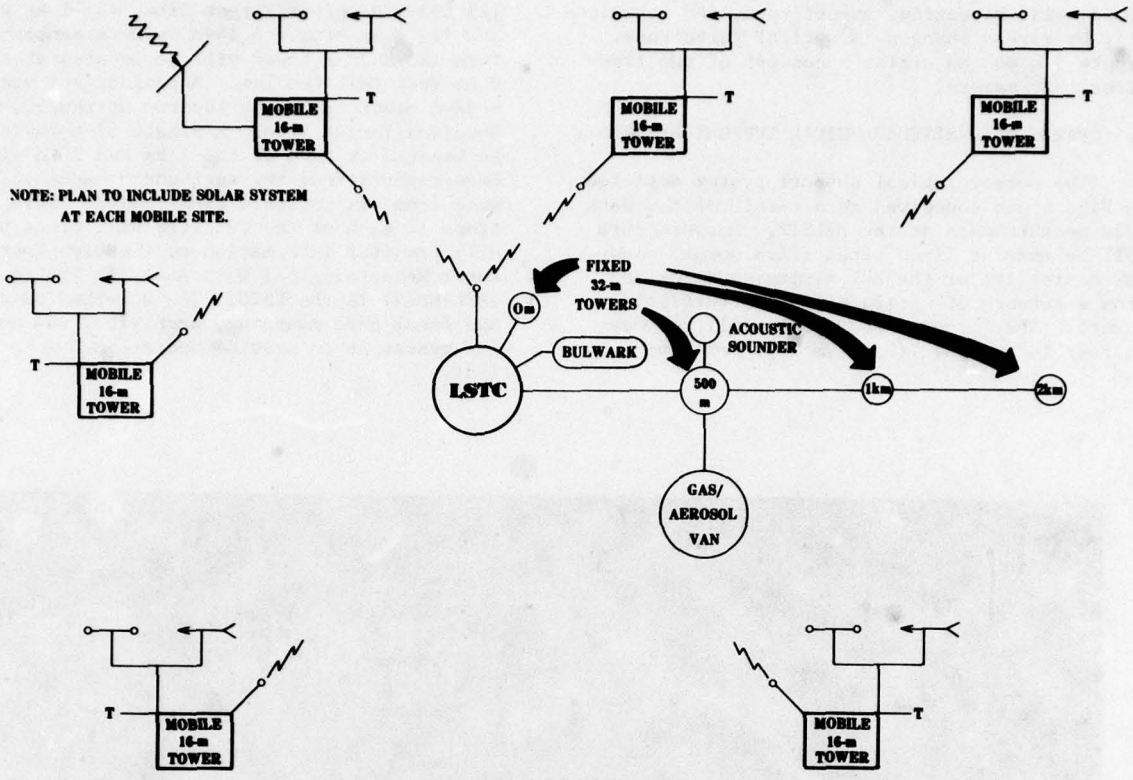

Figure 6. Conceptual HELMET Support System for the High Energy Laser System Test Facility, White Sands Missile Range, New Mexico.

ACKNOWLEDGMENTS

The authors wish to thank W. Hatch for development of the data processing system used in the acquisition of the data base.

REFERENCES

Hoidale, G. B., D. L. Walters, C. L. Norton, and T. H. Pries, 1976: Micrometeorological Measurements for Electro-Optical Propagation Tests at White Sands Missile Range. ODDR&E Electro-Optical/Submillimeter Propagation Workshop, Colorado Springs, CO.

Norton, C. L., and D. L. Walters, 1977: Statistics of Thermal Turbulence at White Sands Missile Range. Paper presented at the Topical Meeting on Optical Propagation thru Turbulence, Rain, and Fog, University of Colorado, Boulder, CO.

Norton, C., D. Walters, G. Hoidale, J. Hines, W. Hatch, D. Favier, M. Hamiter, R. Pinnick, G. Fernandez, E. Huth, and C. White, 1978: Atmospheric Conditions at the High Energy Laser Systems Test Facility (HELSTF), White Sands Missile Range (WSMR), New Mexico - 24 March to 8 April 1977, Data Report, ASL-DR-0001, Atmospheric Sciences Laboratory, US Army Electronics R&D Command, White Sands Missile Range, NM, 465 pp (AD A055 028)

Pinnick, R. G., G. Fernandez, G. B. Hoidale, and B. D. Hinds, 1977: Near-Surface Desert Aerosol Measurements at White Sands Missile Range, New Mexico, and Their Effects on IR Extinction. Paper presented at the Tri-Service Panel on Environmental Research, Air Force Geophysics Laboratory, Hanscom AFB, MA.

Walters, D. L., 1976: High Energy Laser Propagation Conditions at White Sands Missile Range (U). Proceedings of the Second High Energy Laser Conference, US Air Force Academy, Colorado Springs, CO.

Watkins, W. R., K. O. White, C. W. Bruce, D. L. Walters, and J. D. Lindberg, 1976: Measurements Required for Prediction of High Energy Laser Transmission. Proceedings of the Seventh Technical Exchange Conference, El Paso, TX.

OPTIMUM PATH AIRCRAFT ROUTING SYSTEM (OPARS)

William G. Schramm

USN/FNWC

OPARS is a system of software programs being implemented at the Fleet Numerical Weather Central in Monterey, CA, that will provide naval air crews with optimum route, altitude, fuel management and environmental information. The optimum route, depending on flight requirements, may be the most economical in terms of fuel, the quickest of the route that avoids severe weather conditions. Data bases, to support OPARS, will be maintained for aircraft characteristics, global air route structure and environmental data. Aircraft characteristics will be used to compute fuel consumptions, determine air speeds, climb rates, etc., from formulas for each specific aircraft type. The air route structure data base will contain detailed descriptions of enroute airways, checkpoints, airports and pre-determined tracks. The environmental data, such as winds, temperature, severe weather, etc., will be extracted from the Fleet Numerical Weather Central global, synoptic data base. The optimum route as calculated by OPARS, may be along airways, direct, pre-determined track or a combination of the above. The user will have the option of limitations on route selection. OPARS service will be provided over three primary communications links. The first is the Naval Telecommunications system wherein both the request and the route will be in standard "message" format. The second link will be using the Naval Environmental Display Station network which will allow for graphics. The third link will be by means of remote, portable, dial-up telephone terminals.

THE DETERMINATION OF VEHICLE FLIGHT ENVIRONMENT FOR REENTRY ANALYSIS STUDIES

Robert O. Olsen and Bruce W. Kennedy
US Army Atmospheric Sciences Laboratory
White Sands Missile Range, New Mexico 88002

E. T. Fletcher and T. Hanrahan
Xonics, Inc.
6151 West Century Blvd.
Los Angeles, California 90045

1. INTRODUCTION

The Technology Development Vehicle Program conducted by the Air Force Space and Missile Systems Organization/Advanced Ballistic Reentry Systems (SAMSO/ABRES) involved the launch of a Minuteman ICBM from Vandenberg AFB, CA, with reentry and impact occurring at Kwajalein Missile Range (KMR). To evaluate various test and vehicle performance parameters, the reentry vehicle was tracked by an array of ground-based radars and optical sensors located at various sites throughout the Kwajalein atoll. In addition to the ground-based sensors, onboard instrumentation provided data and information on various test functions required for reentry analysis studies.

Important inputs to the performance analysis of accurate reentry vehicle systems are the flight test environment data. These data are used in the evaluation of reentry miss contributors, the calculation of reentry vehicle aerodynamic parameters and the correction of tracking data for refraction effects. This paper describes the types of data and related accuracies which are being attained at KMR. Comparisons to KMR upper atmosphere wind and density measurements in the 160 kft to 340 kft altitude interval using Robin inflatable falling spheres (Luers, 1970) are also described. Flight environment data obtained in conjunction with the recent SAMSO/ABRES TDV-3 flight are utilized to illustrate the application of flight test environment to reentry vehicle performance analyses.

2. METEOROLOGICAL MEASUREMENTS

Table 1 summarizes the TDV-3 impact area meteorological measurements. Rawinsonde measurements of density, temperature, pressure, and winds were obtained from the surface to approximately 100 kft. Rocketsondes provided similar data over the altitude interval of approximately 70 kft to 230 kft and Robin falling spheres provided data from 160 kft to 340 kft. A radar-tracked Jimsphere (Scoggins, 1963) was used to measure winds from 15 kft to 60 kft. The purpose of the multiple measurements is to be able to assess atmospheric conditions encountered by the vehicle during the reentry phase. The measurements before and after vehicle impact define the variability of the atmosphere both in space and time. Figure 1 consists of wind and density measurements plotted with the Kwajalein Standard Atmosphere (KSA) from the surface to 120 kft. Figure 2 consists of similar data over the altitude interval of 120 kft to 340 kft. Information on spatial and temporal variability are contained in Figure 1, which includes data from simultaneous rawinsonde releases with approximately 70 km separation. The upper atmospheric measurements shown in Figure 2 presents data only on the temporal variability. As expected, both sets of data indicate increasing variability between individual measurements as altitude increases. Figures 3 and 4 provide estimates of the TDV-3 wind and density measurement temporal and spatial variability. The solid line function given on these graphs connects the rms variability estimate for the two measurements closest in time and space to the reentry vehicle. Hence, these functions provide an indication of measurement accuracy including sensor error and temporal/spatial extrapolation effects. The dashed line curve given on the temporal variability of the measurement closest in time and space to the reentry vehicle is compared to the Kwajalein November monthly IRIG model atmosphere data from the surface to 86 kft and the Kwajalein Standard Annual Atmosphere model from 87 kft to 394 kft). Comparison of the dashed and solid curve provides an indication of the accuracy improvement which is obtained using actual flight environment measurements, as opposed to model data.

3. CONCLUSIONS

An application of the flight environment data to reentry vehicle performance is illustrated by Figure 5. This figure gives the miss contribution due to winds for the TDV-3 trajectory and vehicle parameters. Data are presented in terms of downrange and crossrange impact miss as functions of altitude. Cases are included for the flight test atmosphere

TABLE 1

SUMMARY OF TDV-3 IMPACT AREA METEOROLOGICAL MEASUREMENTS

	RELEASE OR LAUNCH TIME HRS:MIN (G.M.T.)	KMR IDENTIFIER(S)	SENSOR	LAUNCH/ RELEASE LOCATION	DATA INTERVAL (KFT)	COMMENTS
	3:54	K412	Rawinsonde	Kwaj. Island	.1–86	Simultaneous measurements. Roi 59 tracked (for winds) by MPS-36 S/N 4 (15-60 kft)
	3:58	R59	Rawinsonde	Roi-Namur	.1–82	
	5:30	OP No. 2051 (77-198)	Rocketsonde	Meck	69–257	
	6:04	OP No. 2052	ROBIN Sphere	Meck	165–208, 274–340	Tracks by ALCOR & TPQ-18 (in daylight); ALCOR lost track approx. 240–264 kft
	7:35	OP No. 2053	ROBIN Sphere	Meck	164–231, 260–240	Tracks by ALCOR & TPQ-18, proper inflation of sphere questionable, , hence only wind data obtained; ALCOR lost track approx. 249-256 kft.
	7:47	R60	Rawinsonde	Roi-Namur	.1–96	Simultaneous measurements. Roi 60 tracked (for winds) by MPS-36 S/N 4 (15-60 kft) & TRADEX (59-87 kft)
	7:48	K413	Rawinsonde	Kwaj. Island	.1–87	
TDV IMPACT PRE	8:15	-----	JIMSPHERE	Gagan	15–60	Wind speed and direction data, track by MPS-36 S/N 3(15-60 kft)
TDV IMPACT POST	9:19	OP No. 2054	ROBIN Sphere	Meck	163–340	Tracks by ALCOR & TPQ-18
	9:51	OP No. 2055	ROBIN Sphere	Meck	163–340	Tracks by ALCOR & TPQ-18
	10:20	OP No. 2056 (77-199)	Rocketsonde	Meck	70–220	
	10:45	K414	Rawinsonde	Kwaj. Island	.1–105	
	11:40	R61	Rawinsonde	Roi-Namur	.1–108	
	12:45	OP No. 2057 (77-200)	R ocketsonde	Meck	69–195	

which is based on the measurements closest in time and space to the trajectory as well as for all of the other available measurements made in the vicinity of the vehicle impact within an 8-hour period. The approximate 10-foot spread in the impact dispersion estimates for the different measurement cases provides an indication of the uncertainty in determining the reentry miss contribution due to winds. The dashed curve shown on Figure 5 corresponds to the Kwajalein November IRIG wind model data. Comparison of the dispersion estimates for the model data with the flight test measurement cases shows that large errors in excees of 40 feet in the crossrange and downrange dispersion estimates would result if the model, as opposed to flight test measurements were used to estimate wind dispersion effects. Recent work by Fletcher and Hanrahan (1978) in support of the TDV program has demonstrated that ballistic reentry trajectory reconstruction accuracies on the order of 10 feet in position can be achieved for optimal radar and optical coverage at Kwajalein. Given these results it is apparent that uncertainties in the flight test environment data are important error contributors in the evaluation of reentry vehicle performance.

4. REFERENCES

Fletcher, E. T., and T. Hanrahan, 1978: TDV-3 Multi Sensor Best Estimate Trajectory and Meteorological Data Summary, Xonics, Inc.

Luers, J. K., 1970: A Method of Computing Winds, Temperature, Pressure, and Their Associated Errors from High Altitude Robinsphere Using an Optimum Filter, AFCRL-70-0366.

Scogginns, J. R., 1963: An Evaluation of Detail Wind Data as Measured by the FPS-16 Radar/Jimsphere Balloon Technique, NASA TM D-1572, NASA Marshall Space Flight Center.

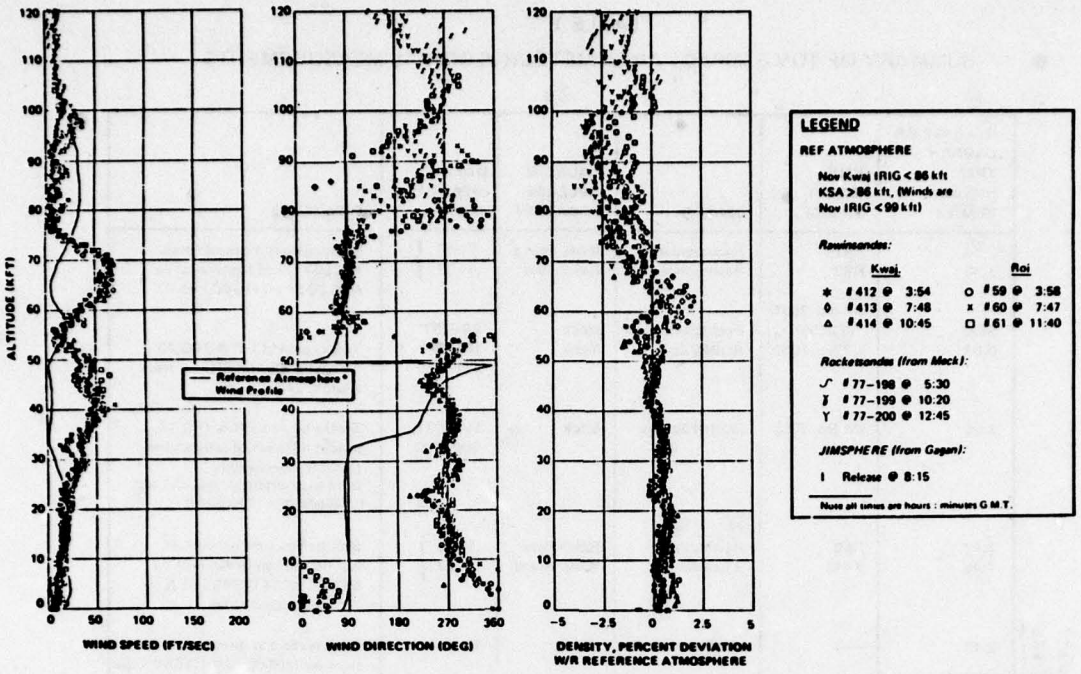

FIGURE 1 SUMMARY OF TDV-3 RAWINSONDE, ROCKETSONDE, JIMSPHERE AND ROBIN SPHERE METEOROLOGICAL MEASUREMENTS, 0–120 KFT

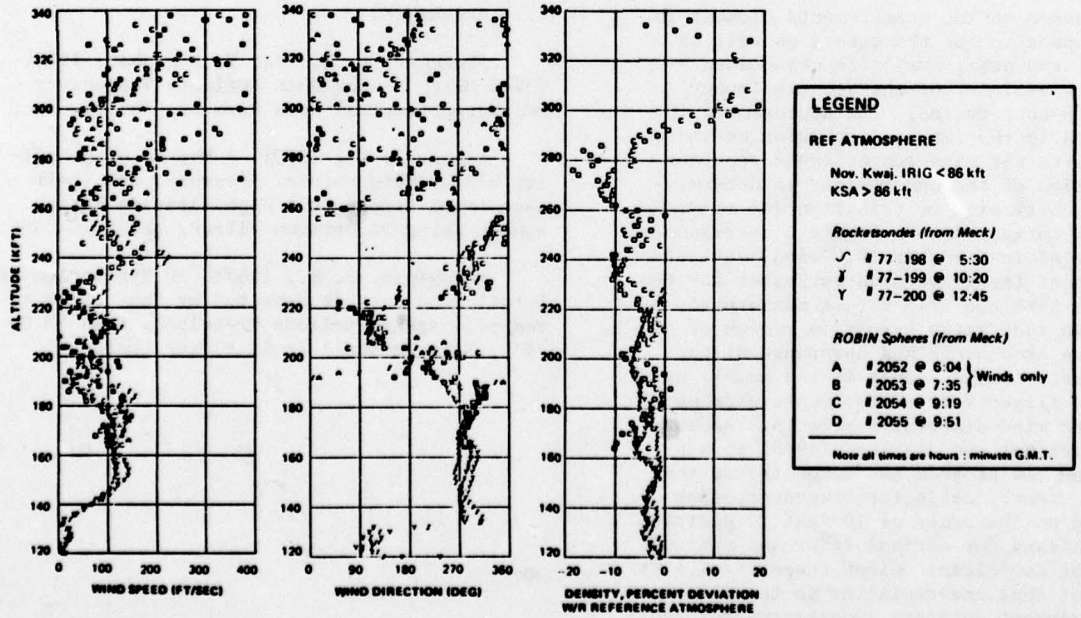

FIGURE 2 SUMMARY OF TDV-3 ROCKETSONDE AND ROBIN SPHERE METEOROLOGICAL MEASUREMENTS, 120–340 KFT

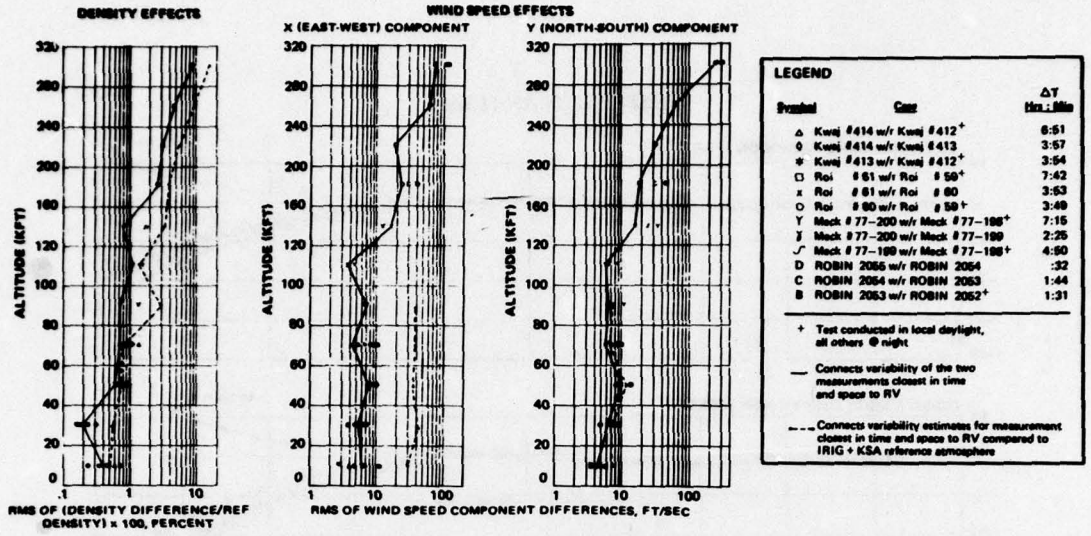

FIGURE 3 TEMPORAL VARIABILITY OF TDV-3 IMPACT AREA DENSITY AND WIND MEASUREMENTS

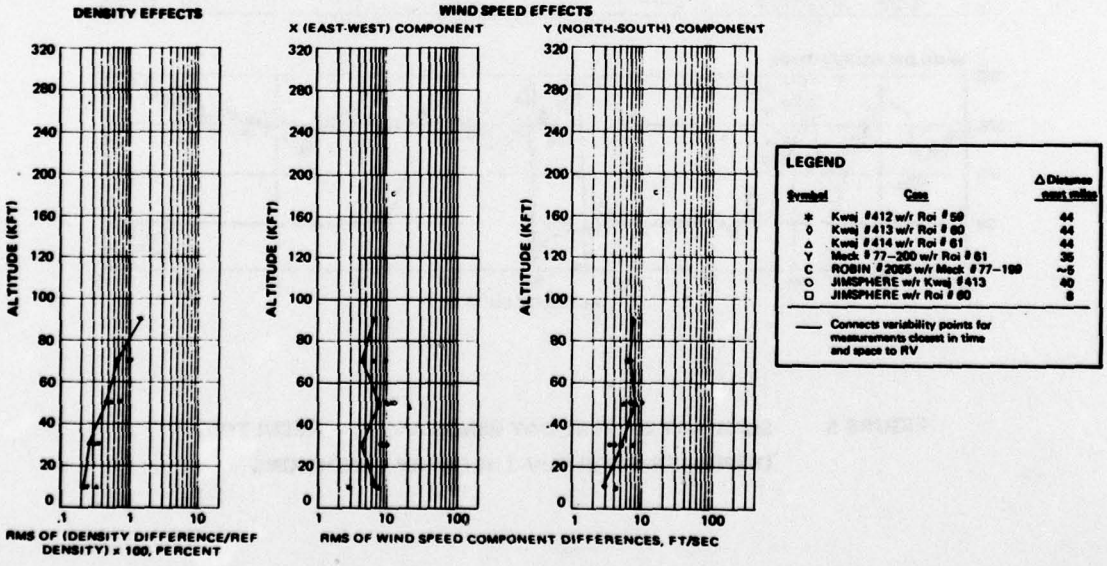

FIGURE 4 SPATIAL VARIABILITY OF TDV-3 IMPACT AREA DENSITY AND WIND MEASUREMENTS

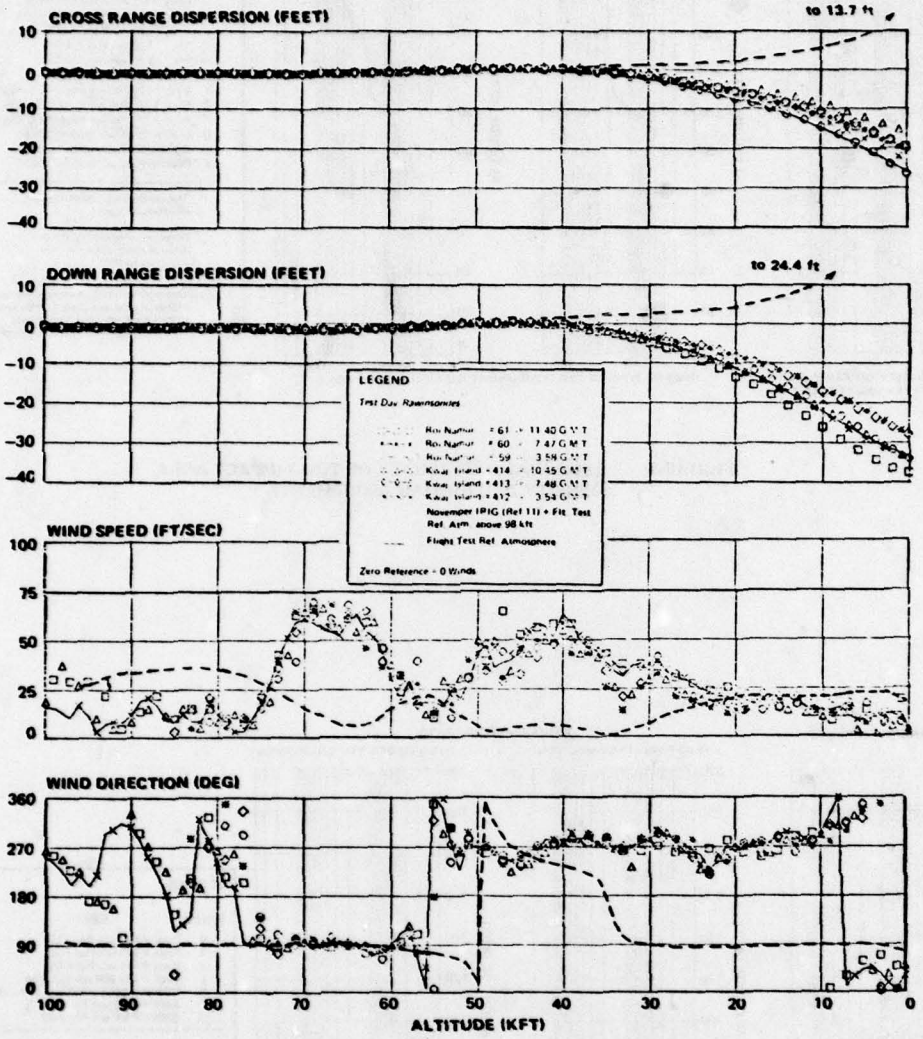

FIGURE 5 SUMMARY OF TEST DAY WINDS AND THE RESULTING DISPERSIONS FOR TDV-3 REENTRY CONDITIONS

CLOSING REMARKS

Colonel Albert J. Kaehn, Jr.

Commander Air Weather Service

I extend my apology for not attending the opening of this Conference, but the press of business in Washington kept me from being here. I'm happy that Col Sal LeMole had an opportunity to come out and open the Conference. Reports I've had indicate that it has been an extremely successful conference and it's been the Air Weather Service's pleasure to sponsor this activity. We do have a need to get together. It's interesting for me to come back to these conferences now on the other side of the fence because I used to interact a great deal with the R&D people. We broke a lot of glass together in three years, and swept it up together, I guess. It's interesting to be on the other side and watch what's coming out of those efforts. We're still waiting at the bottom of the pipe for anything you can give us. It's good to see that kind of dedicated effort going on in the R&D community because certainly for those of us in the operational business, that's what we thrive on. There is a distinct need because, as you pointed out, Ron (Capt Hughes, USN), there are a number of agencies that are looking at what we are doing in the environmental sciences business and the environmental services. I think that some of the efforts we have under way help us in that regard and I would hope that they would continue: specifically, the Joint Doppler Operational Program at Norman that involves a number of agencies and people; the work we're doing by interacting with the Techniques Development Laboratory in Washington with the National Weather Service, keeping us abreast of techniques and things that are happening there; and a good bit of work that's going on in the way in which we acquire, process, and apply meteorological satellite data. Those are the kinds of things that I think give us the in road to do more. We need to do more because there are a lot of people watching what it is we do.

I'd be remiss if we didn't leave here today with some recognition of the people who made this all happen. We ought to recognize them publicly because they had a great deal to do with this being a very successful conference. First as the Chairman of the Joint Steering Committee, Col Gary Atkinson. Steering Committee members Captain Jim Overall and Dr. Bob Miller. I don't know how many of you knew but Wayne Hering, from AFGL was a very important guy in this. He has retired, and his place was taken on the Steering Committee by Mr. Don Chisholm, who has departed because of travel arrangements. Also I would like to include at this point Mr. Tom Pries from the Atmospheric Sciences Laboratories who is also gone but I think we should recognize in absentia those folks with a round of applause. Commander Bill Hillyard, also a very important part of the Steering Committee. There have been some very key people here in the Colorado Springs area, specifically here at the Academy, who made this all happen and first and foremost I think we want to congratulate and thank the very kind young lady, Capt Cheryl Gillespie, who's made it all come together. Not to be forgotten, our guy in the booth, SSgt Steve Milligan, recent winner of $7,000 on the show "The Price is Right." Next time I think about buying a calculator I'm going to give this guy a call. We would ask you, Cheryl, please, to convey to the people in the billeting area and the Club our sincere appreciation for their services and their facilities which have just been super. I think we should all recognize that the success of a meeting like this has a great deal to do with the way in which the people who chair the various sessions do their business. I think a round of applause is due each of those fellows. So, for the session chairman. I would like you all to know that we were able to get over very quickly and I made a courtesy call on Lt Gen Tallman, Superintendent of the Academy, and conveyed on behalf of all of us here our sincere appreciation due him for making the facilities available, and to the Academy Staff for the support that they've provided us. So that expression of appreciation has been conveyed. Now, plans for the future. We should continue the TEC and we'll have to sift and sort and see when the best time is, and collectively put our heads together and decide on a place and the time. Certainly the agenda, I would imagine, would be full of promising things like this one has been. I'd like to let everyone know about the conference proceedings; we expect we'll be able to have them published and in your hands some time in late spring, probably late April or early May. I guess my next official act is to wish all of you a very happy holiday season, wish you all a safe trip home, and officially declare this conference closed. Have a good ride back. Good seeing you.

ORGANIZATION ACRONYMS

AFGL	Air Force Geophysics Laboratory
AFGWC	Air Force Global Weather Central
AFOSR	Air Force Office of Scientific Research
ASL	Atmospheric Sciences Laboratory
AWS	Air Weather Service
CNO	Chief of Naval Operations
DA	Department of the Army
DDO(ES)	Deputy Director Operations (Environmental Services)
EDL	Equipment Development Laboratory
ERL	Environmental Research Laboratories
FNWC	Fleet Numerical Weather Central
FWC	Fleet Weather Central
FWF	Fleet Weather Facility
GAO	General Accounting Office
JCS	Joint Chiefs of Staff
MIRADCOM	Missile Research and Development Command
NEPRF	Naval Environmental Prediction Research Facility
NCAR	National Center for Atmospheric Research
NOAA	National Oceanic and Atmospheric Administration
NOC	Naval Oceanography Command
NOSC	Naval Ocean Systems Center
NPGS	Naval Post Graduate School
NSSFC	National Severe Storms Forecast Center
NWS	National Weather Service
ONR	Office of Naval Research
SAMSO	Space and Missile Systems Organization
SDO	Systems Development Office
USA	United States Army
USAF	United States Air Force
USAFETAC	USAF Environmental Technical Application Center
USN	United States Navy
WPL	Wave Propagation Laboratory
WS	Weather Squadron
WW	Weather Wing